



UNIVERSITAT DE  
BARCELONA

## Screening and biological evaluation of novel anticancer agents and lipid profiling of autophagy-related proteins

Mireia Quintana Agustí

**ADVERTIMENT.** La consulta d'aquesta tesi queda condicionada a l'acceptació de les següents condicions d'ús: La difusió d'aquesta tesi per mitjà del servei TDX ([www.tdx.cat](http://www.tdx.cat)) i a través del Dipòsit Digital de la UB ([diposit.ub.edu](http://diposit.ub.edu)) ha estat autoritzada pels titulars dels drets de propietat intel·lectual únicament per a usos privats emmarcats en activitats d'investigació i docència. No s'autoritza la seva reproducció amb finalitats de lucre ni la seva difusió i posada a disposició des d'un lloc aliè al servei TDX ni al Dipòsit Digital de la UB. No s'autoritza la presentació del seu contingut en una finestra o marc aliè a TDX o al Dipòsit Digital de la UB (framing). Aquesta reserva de drets afecta tant al resum de presentació de la tesi com als seus continguts. En la utilització o cita de parts de la tesi és obligat indicar el nom de la persona autora.

**ADVERTENCIA.** La consulta de esta tesis queda condicionada a la aceptación de las siguientes condiciones de uso: La difusión de esta tesis por medio del servicio TDR ([www.tdx.cat](http://www.tdx.cat)) y a través del Repositorio Digital de la UB ([diposit.ub.edu](http://diposit.ub.edu)) ha sido autorizada por los titulares de los derechos de propiedad intelectual únicamente para usos privados enmarcados en actividades de investigación y docencia. No se autoriza su reproducción con finalidades de lucro ni su difusión y puesta a disposición desde un sitio ajeno al servicio TDR o al Repositorio Digital de la UB. No se autoriza la presentación de su contenido en una ventana o marco ajeno a TDR o al Repositorio Digital de la UB (framing). Esta reserva de derechos afecta tanto al resumen de presentación de la tesis como a sus contenidos. En la utilización o cita de partes de la tesis es obligado indicar el nombre de la persona autora.

**WARNING.** On having consulted this thesis you're accepting the following use conditions: Spreading this thesis by the TDX ([www.tdx.cat](http://www.tdx.cat)) service and by the UB Digital Repository ([diposit.ub.edu](http://diposit.ub.edu)) has been authorized by the titular of the intellectual property rights only for private uses placed in investigation and teaching activities. Reproduction with lucrative aims is not authorized nor its spreading and availability from a site foreign to the TDX service or to the UB Digital Repository. Introducing its content in a window or frame foreign to the TDX service or to the UB Digital Repository is not authorized (framing). Those rights affect to the presentation summary of the thesis as well as to its contents. In the using or citation of parts of the thesis it's obliged to indicate the name of the author.



UNIVERSITAT DE BARCELONA

FACULTAT DE FARMÀCIA I CIÈNCIES DE L'ALIMENTACIÓ

Institut de Química Avançada de Catalunya (IQAC)  
Consejo Superior de Investigaciones Científicas (CSIC)

Programa de Biotecnologia

**SCREENING AND BIOLOGICAL EVALUATION OF NOVEL  
ANTICANCER AGENTS AND LIPID PROFILING OF  
AUTOPHAGY-RELATED PROTEINS**

MIREIA QUINTANA AGUSTÍ

2019



UNIVERSITAT DE BARCELONA

FACULTAT DE FARMÀCIA I CIÈNCIES DE L'ALIMENTACIÓ

DOCTORAT EN BIOTECNOLOGIA

**SCREENING AND BIOLOGICAL EVALUATION OF NOVEL  
ANTICANCER AGENTS AND LIPID PROFILING OF  
AUTOPHAGY-RELATED PROTEINS**

Memòria presentada per Mireia Quintana Agustí per optar al títol de  
doctora per la Universitat de Barcelona

Directora

Dra. Gemma Triola Guillem

Tutora

Dra. Josefa Badia Palacín

MIREIA QUINTANA AGUSTÍ

2019





# ABSTRACT

The efficiency of R&D models of the pharmaceutical companies (new medicines launched/monetary investment) has declined since decades. Consequently, the identification of new biomarkers and the development of new strategies to detect and treat pathological disorders is an emerging field of research. These approaches may provide a greater understanding of the mechanism of disease progression as well as the identification of novel targets for therapeutic intervention.

This thesis addresses three different subjects closely related. First, a **phenotypic screening** measuring cytotoxicity in the gastric cancer cell line HGC-27 is reported. Next, a **targeted-based assay** measuring the activity of the autophagy-related protein Atg4B is developed and employed to identify small-molecules inhibiting this protein. Finally, a **basic research study** is carried out in order to gain knowledge of the molecular mechanisms that control autophagy, with special emphasis on the role of C-terminal lipidation of LC3B. The three topics will be discussed in more detail.

Squaramates and squaramides present a unique structure owning two hydrogen bond acceptors that makes them interesting for the development of novel active and selective compounds. The **first chapter** of this thesis covers the study of a variety of squaramates and squaramides and their cytotoxic activity in different cancer cell lines. Among the studied compounds, the squaramide **34** showed a potent and selective cytotoxicity against the human gastric cancer cell line HGC-27. Studies directed to elucidate the mechanism of induced cell death were performed. Cell cycle distribution analysis and cell death studies showed that compound **34** induces cell cycle arrest at the  $G_0/G_1$  phase and caspase-dependent apoptosis implicating the intrinsic pathway and mitochondrial membrane depolarization. In conclusion, squaramide **34** can be considered a potential anticancer agent for gastric carcinoma.

Cancer therapy is mainly based on selective cancer cell death induction. However, drug resistance is a major issue in oncology and a limiting factor for anticancer drug efficacy. Autophagy induction as a response for nutrient and oxygen deprivation is employed by cancer cells as a survival mechanism. Therefore, the employment of autophagy inhibitors as adjuvant treatment could increase the anticancer drug efficacy. Consequently, the identification of novel autophagy inhibitors is an emerging field of research. In this context, the **second chapter** of this thesis is focused on the development of a novel AlphaScreen-based HTS assay and a mass spectrometry-based counter screen to identify Atg4B inhibitors, which is a specific enzyme in charge of the synthesis of the autophagy marker LC3. A high-throughput virtual screening performed with the library of National Cancer Institute Open Database and

subsequent evaluation of 250 selected compounds allowed the identification of three potential inhibitors (**NSC83713**, **NSC126353** and **NSC611216**). Derivatives of **NSC126353** and **NSC611216** were synthesised in the group and their characterization by both techniques allowed the discovery of most active compounds **54**, **55**, **56** and **57**. Compound **57** was chosen for additional characterization based on its high potency, a 10-fold improved activity, and good cytotoxicity profile on cell lines. Moreover, inhibition of the autophagic flux was maintained, as measured by LC3-II and p62 protein levels. Finally, the synergistic effect of **57** combined with oxaliplatin resulted in an enhanced cell death in the human colorectal adenocarcinoma cell line HT-29. In conclusion, the aminobenzo[*cd*]indol-2-[1*H*]-one scaffold represents a novel chemotype for the development of small molecule inhibitors of Atg4B. These results will contribute to expand the toolbox used to study autophagy in mammal cells and to unravel the role of Atg4B in cancer treatment.

Understanding the molecular mechanism regulating biological and pathological processes is key for the development of new therapeutic strategies. The conjugation of a phosphatidylethanolamine (PE) unit at the C-terminus of LC3 is essential for the autophagy regulation. Despite the high variability described in cellular lipids, and more particularly, in glycerophospholipids (polar head, fatty acids length and unsaturation degree), a potential role of heterogenous lipidation on protein activity has not been considered. Hence, the **third chapter** of this thesis is focussed on the development of a lipidomic approach for the study of the PE species conjugated to LC3/GABARAP. The method relies on the enzymatic release of the protein-bound lipids mediated by Atg4B incubation. The strategy is applied to the whole proteome and proteins isolated by immunoaffinity techniques. Preliminary results could not succeed in the analysis of the lipid bound proteins.

# SYMBOLS, ABBREVIATIONS AND ACRONYMS

<b>[M+H]<sup>+</sup></b>	Positive mode analysis
<b>[M-H]<sup>-</sup></b>	Negative mode analysis
<b>3-MA</b>	3-methyladenine
<b>Ab</b>	Antibody
<b>ABL1</b>	Abelson murine leukaemia viral oncogene
<b>ACD</b>	Autophagic cell death
<b>Akt</b>	Protein kinase B
<b>AlphaScreen</b>	Amplified luminescent proximity homogeneous assay screen
<b>ALR</b>	Autophagic lysosome reformation
<b>AMPK</b>	AMP-activated protein kinase
<b>Annexin V-FITC</b>	Recombinant Annexin V conjugated to fluorescein isothiocyanate
<b>ATG/Atg</b>	Autophagy related genes/proteins
<b>ATP</b>	Adenosine triphosphate
<b>Bcl-2</b>	B-cell lymphoma 2
<b>BECN1</b>	Bcl2-interacting protein
<b>BNIP3</b>	BCL2 interacting protein 3
<b>BSA</b>	Bovine serum albumin
<b>C</b>	Control sample
<b>C17</b>	Heptadecanoic acid
<b>Calcd.</b>	calculated
<b>Cath. Inh.</b>	Cathepsin inhibitor III
<b>CDK4</b>	Cyclin-dependent kinase 4
<b>CDP-choline</b>	Cytidine 5'-diphosphocholine
<b>CDP-ethanolamine</b>	Cytidine 5'-diphosphoethanolamine
<b>CE</b>	Cholesteryl ester
<b>Cer</b>	Ceramide
<b>CHK1</b>	Checkpoint kinase 1
<b>CI</b>	Confidence interval
<b>CL</b>	Cardiolipin
<b>CMA</b>	Chaperone-mediated autophagy

c-MET	Receptor tyrosine kinase MET
CML	Chronic myelogenous leukaemia
CPE	Cloud-point extraction
CPS	Counts per second
CQ	Chloroquine
CRS	Cytokine-release syndrome
CSCs	Cancer stem cells
CSIC	Consejo Superior de Investigaciones Científicas
Cvt	Cytoplasm-to-vacuole targeting
CW	Channel wavelength
DAG	Diacylglycerol
DCF	Dichlorofluorescein
DCFH-DA	2',7'-Dichlorofluorescein diacetate
DHA	Docosahexaenoic acid
DMPE	1,2-Dimyristoyl- <i>sn</i> -glycero-3-phosphoethanolamine
DMSO	Dimethyl sulfoxide
DNA	Deoxyribonucleic acid
DOPE	1,2-Dioleoyl- <i>sn</i> -glycero-3-phosphoethanolamine
DPPE	1,2-Dipalmitoyl- <i>sn</i> -glycero-3-phosphoethanolamine
DSPE	1,2-Distearoyl- <i>sn</i> -glycero-3-phosphoethanolamine
DTT	Dithiothreitol
EBSS	Earle's balanced salt solution
EDTA	Ethylenediaminetetraacetic acid
EGFR	Epidermal growth factor receptor
EICs	Extracted ion chromatograms
eIF4E	Eukaryotic translation initiation factor 4E
p300	Histone acetyltransferase p300
ER	Endoplasmic reticulum
ERES	ER exit sites
ESI	Electrospray ionization
FA	Fatty acid
FasL	Fas ligand
FasR	Fas receptor
FDA	Food and drug administration
FGFR	Fibroblast growth factor receptor
FIP200	Focal adhesion kinase family interacting protein of 200 kDa
FP	Fluorescence polarisation

<b>FRET</b>	Fluorescence resonance energy transfer
<b>FUNDC1</b>	FUN14 domain containing 1
<b>FYCO1</b>	FYVE and coiled-coil domain-containing 1
<b>GABARAP</b>	GABA type A receptor-associated protein
<b>GABARAPL1</b>	GABA type A receptor associated protein like 1
<b>GABARAPL2</b>	GABA type A receptor associated protein like 2
<b>GATE-16</b>	Golgi-associated ATPase enhancer of 16 kDa
<b>GC</b>	Gas chromatography
<b>GFP</b>	Green fluorescent protein
<b>Gp78</b>	Tumour autocrine motility factor receptor
<b>GPI</b>	Glycosylphosphatidylinositol
<b>GPLs</b>	Glycerophospholipids
<b>GST</b>	Glutathione S-transferase
<b>GTP</b>	Guanosine-5'-triphosphate
<b>HCQ</b>	Hydroxychloroquine
<b>HCT-116</b>	Human colon tumour cell line 116
<b>HDAC6</b>	Histone deacetylase 6
<b>HEK293</b>	Human embryonic kidney 293 cell line
<b>HeLa</b>	Henrietta Lacks cell line
<b>HER2</b>	Human epidermal growth factor 2
<b>HGC-27</b>	Human gastric cells 27
<b>Hh</b>	Hedgehog
<b>HIV-1 Tat</b>	Human immunodeficiency virus trans-activating regulatory protein
<b>HRMS</b>	High resolution mass spectrometry
<b>Hsc70</b>	Heat shock cognate 70
<b>HSV-1</b>	Herpes simplex virus type 1
<b>HT-29</b>	Human colorectal cell line
<b>HTS</b>	High-throughput screening
<b>HTVS</b>	High-throughput virtual screening
<b>IAM</b>	Iodoacetamide
<b>IC<sub>50</sub></b>	Half maximal inhibitory concentration
<b>ICAT</b>	Isotope-coded affinity tag
<b>IPTG</b>	Isopropyl $\beta$ -D-1-thiogalactopyranoside
<b>IQAC</b>	Institut de Química Avançada de Catalunya
<b>ISQCH</b>	Instituto de Síntesis Química y Catálisis
<b>iTRAQ</b>	Isobaric tags for relative and absolute quantitation
<b>JC-1</b>	Tetraethylbenzimidazolylcarbocyanine iodide
<b>JNK</b>	c-Jun <i>N</i> -terminal kinase
<b>Km</b>	Michaelis constant

<b>LAMP-2A</b>	Lysosome-associated membrane protein 2A
<b>LC</b>	Liquid chromatography
<b>LCD</b>	Lysosomal cell death
<b>Lipidex 5000</b>	Hydroxypropyl dextran beads
<b>LMP</b>	Lysosomal membrane permeabilization
<b>LOCI</b>	Luminescent Oxygen Channelling Immunoassay
<b>LOQ</b>	Limit of Quantification
<b>MALDI</b>	Matrix-Assisted Laser Desorption/Ionization
<b>MAP1LC3</b>	Microtubule-Associated Protein 1A/1B-light chain 3
<b>MAPK14</b>	Mitogen-Activated Protein Kinase 14
<b>MCF7</b>	Michigan Cancer Foundation-7, breast cancer cell line
<b>MDCK</b>	Madin-Darby Canine Kidney epithelial cell line
<b>MDL Drug Database Report</b>	Model description language drug database report
<b>MEF</b>	Mouse Embryonic Fibroblasts
<b>MHC</b>	Major Histocompatibility Complexes
<b>MS</b>	Mass spectrometry
<b>mTOR</b>	Mammalian target of rapamycin
<b>mTORC1</b>	mTOR complex 1
<b>mTRAQ</b>	Mass differential tags for relative and absolute quantification
<b>MTT</b>	3-(4,5-dimethylthiazol-2-yl)-2,5-diphenyltetrazolium bromide
<b>MUFA</b>	Monounsaturated fatty acid
<b>MUL1</b>	Mitochondrial E3 ubiquitin protein ligase 1
<b>N.A.</b>	No active
<b>NBR1</b>	Neighbour of Brca1 gene 1
<b>NCI</b>	National Cancer Institute (USA)
<b>NCI-60</b>	60 Human cancer cell lines used by the National Cancer Institute
<b>NDP52</b>	Nuclear dot protein 52
<b>Nec-1</b>	Necrostatin-1
<b>NEM</b>	N-ethylmaleimide
<b>NMDA</b>	N-Methyl-D-Aspartate
<b>NMR</b>	Nuclear Magnetic Resonance
<b>NP-40</b>	Tergitol-type NP-40
<b>OCFA</b>	Odd-chain fatty acids
<b>OPTN</b>	Optineurin
<b>ORPL1</b>	Oxysterol-binding protein-related protein 1L

<b>PAINS</b>	Pan-Assay Interference compounds
<b>PAS</b>	Phagophore assembly site
<b>PC</b>	Phosphatidylcholine
<b>PCK</b>	Z,L-Phe-chloromethylketone
<b>PCR</b>	Polymerase chain reaction
<b>PDB</b>	Protein database
<b>PE</b>	Phosphatidylethanolamine
<b>PEG</b>	Polyethylene glycol
<b>PG</b>	Phosphatidylglycerol
<b>PI</b>	Protein inhibitors of autophagy
<b>PI3K</b>	Phosphatidylinositol 3-kinase
<b>PtdIns3P</b>	Phosphatidylinositol 3 phosphate
<b>PINK1</b>	PTEN-induced putative kinase 1
<b>PKA</b>	Protein kinase A
<b>PKC</b>	Protein kinase C
<b>PL</b>	Phospholipid
<b>PMSF</b>	Phenylmethylsulfonyl fluoride
<b>PMT</b>	Photo multiplier tube
<b>Plks</b>	Polo-like kinases
<b>POPE</b>	1-Palmitoyl-2-oleoyl- <i>sn</i> -glycero-3-phosphatidylethanolamine
<b>proLC3B-Biotin</b>	N-(His) <sub>6</sub> -proLC3B(L123C)-Biotin
<b>proLC3B</b>	N-(His) <sub>6</sub> -proLC3B(L123C)
<b>Prot</b>	Protein
<b>PS</b>	Phosphatidylserine
<b>PtdIns</b>	Phosphatidylinositol
<b>PVDF</b>	Polyvinylidene difluoride
<b>Rab7</b>	Ras related protein Rab7
<b>RILP</b>	Rab-interacting lysosomal protein
<b>RIP</b>	Kinases of the receptor interacting protein
<b>RNA</b>	Ribonucleic acid
<b>RNAi</b>	Ribonucleic acid interference
<b>RNA-seq</b>	Transcriptome sequencing
<b>ROS</b>	Reactive oxygen species
<b>S/B</b>	Signal/background
<b>S1P</b>	Sphingosine-1-phosphate
<b>Saos-2</b>	Sarcoma osteogenic 2 cell line
<b>Sav</b>	Streptavidin
<b>SCAB</b>	Servicio Central de Análisis de Bizkaia
<b>SD</b>	Standard deviation
<b>SDS-PAGE</b>	Sodium dodecyl sulphate polyacrylamide gel



	electrophoresis
<b>SEA</b>	Similarity ensemble approach
<b>shRNA</b>	Short hairpin RNA
<b>SH-SY5Y</b>	Human neuroblastoma cell line
<b>SIAH1</b>	Seven in absentia homolog 1
<b>SILAC</b>	Stable isotopic labelling with amino acids in cell culture
<b>SILAM</b>	Stable isotopic labelling of mammals
<b>Sirt1</b>	Silent mating type information regulation 2 homolog 1
<b>SL</b>	Sphingolipids
<b>SM</b>	Sphingomyelin
<b>SMURF1</b>	Ubiquitin ligase Smad ubiquitination regulatory factor-1
<b>SNARE</b>	Soluble NSF attachment proteins receptor
<b>SQSTM1</b>	Sequestosome 1 or p62
<b>SRB</b>	Sulforhodamine B
<b>T98</b>	Human glioblastoma cell line
<b>TBK1</b>	Tank-binding kinase 1
<b>TCEP</b>	Tris(2-carboxyethyl)phosphine
<b>TGF-<math>\beta</math></b>	Transforming growth factor beta
<b>TMT</b>	Tandem mass tags
<b>TNFR1</b>	Tumor necrosis factor receptor 1
<b>TNF-<math>\alpha</math></b>	Tumor necrosis factor alpha
<b>TOF</b>	Time of flight
<b>TRF</b>	Time-resolved fluorescence
<b>TR-FRET</b>	Time-resolved fluorescence energy transfer
<b>TX114</b>	Triton X-114
<b>U87</b>	Human primary glioblastoma cell line
<b>U87DND</b>	Human primary glioblastoma cell line defective in ceramide production de novo
<b>UBC13</b>	Ubiquitin-conjugating enzyme E2 13
<b>Ubl</b>	Ubiquitin-like
<b>ULK1 kinase</b>	Unc-51 like autophagy activating kinase
<b>UPLC</b>	Ultra-performance liquid chromatography
<b>UVRAG</b>	UV radiation resistance-associated gene
<b>V-ATPase</b>	Vacuolar-type H <sup>+</sup> -ATPase
<b>VEGF</b>	Vascular endothelial growth factor
<b>Vero</b>	VERda Reno (green kidney in esperanto) African green monkey kidney cell line
<b>Vps15</b>	Vacuolar protein sorting 15
<b>Vps34</b>	Vacuolar protein sorting 34

<b>Vps38</b>	Vacuolar protein sorting 38
<b>WHO</b>	World Health Organization
<b>WIPI</b>	WD-repeat protein interacting with phosphoinositides
<b>WOMBAT</b>	WOrld of Molecular BioAcTivity
<b>YFP</b>	Yellow fluorescent protein
<b>Z-IETD</b>	Z-IETD-FMK
<b>Z-LEHD</b>	Z-LEHD-FMK
<b>Z-VAD</b>	Z-VAD-FMK



# AGRAÏMENTS

Resulta curiós que la part de la tesi que em sembla més fàcil de fer i menys científica sigui probablement la que més gent llegirà. Però tinc molt clar a qui han d'anar dirigits els agraïments d'aquesta tesi.

Com no pot ser d'una altra manera, gràcies per la direcció, paciència, recomanacions, dedicació i temps invertit a la Dra. Gemma Triola. Mai havia après tantes coses en tan poc temps, gràcies per donar-me la possibilitat de realitzar la tesi al centre, ha estat una bona experiència. Gràcies també a la meva tutora, la Dra. Josefa Badia, que sempre hi ha estat quan l'he necessitat i m'ha ajudat amb una eficàcia i rapidesa sorprenents.

Voldria també fer menció a la Dra. Gemma Fabriàs, la Dra. Josefina Casas, el Dr. Antonio Delgado i el Dr. José Luís Abad que sempre m'han escoltat, aconsellat i ajudat tant en tots els seminaris que hem fet plegats com al laboratori. Començar un grup de recerca de zero no és fàcil, i menys per una doctoranda sense experiència, sense ells hagués estat impossible. Gràcies també al Dr. Jordi Bujons per la seva col·laboració en la part computacional de la tesi i al Dr. Òscar Meca per la producció de cèl·lules amb transfeccions estables.

Durant aquests gairebé cinc anys de laboratori han passat molts estudiants pel grup amb qui sempre hem treballat fort i hem tingut tant moments de desesperació com moments de no poder parar de riure. Espero seguir en contacte amb vosaltres durant molt de temps i que m'expliqueu què en feu de les vostres vides. Espero haver estat a l'altura, gràcies per tot el que va aportar a l'Ana Guillén, la Kristina Lang, la Laia Benítez, la Laura de la Hoz, la Meritxell Fernández, la Sònia Vives i en Joan Barceló. Gràcies especialment al Dr. Alegre-Requena que va realitzar tota la primera part del primer capítol. I com no pot ser d'una altra manera, deixo a la més especial pel final, gràcies Ana Bilbao per tota la feina feta pel que fa a la síntesi dels compostos del segon capítol, però també per ser més que una simple companya de grup, has estat una amiga amb qui ens hem recolzat en els moments més difícils de les dues tesis però amb qui també m'ho he passat superbé mentre treballàvem. Compta amb mi pel que vulguis.

Gràcies a la gent del RUBAM, puc dir molt clar que sense ells aquesta tesi hagués estat impossible. Durant aquests anys ha passat molta gent però m'agradaria especialment fer menció a la Mireia Casasampere, la Núria Bielsa, l'Àlex García, l'Eva Dalmau, en Pedro Rayo, la Yadira Ordóñez i la Francesca Cingolani. Tots heu estat essencials.

Començar a fer recerca en un grup sense gent és difícil, i més si no hi ha ningú que t'ho pugui ensenyar. Així que voldria agrair l'ajuda com a postdocs sense esperar res a canvi al Dr. Karel Hernández i al Dr. Roman Bonet. Van ser uns mentors essencials pel que fa a l'expressió i purificació de proteïnes.

Voldria recordar també les estones, xerrades, dinars i inclús festivals amb l'Ana Pou, l'Ana Bilbao i la Raquel Calderón. Totes ben diferents i totes tan divertides, hem tingut moments de tots colors que són impossibles d'oblidar. Espero seguir fent sopars i birretes per posar-nos al dia! Posteriorment els dinars tampoc haurien estat el mateix sense la Mercè Hereu, la Raquel Roldán, la Roser Marin, en Pol Sanllehí i en Carlos Moreno. Dinars que han desembocat en caminades, caps de setmana i sortides vàries, segur que tots els nervis pel futur s'esvairan d'aquí no gaire. Sort a tots!

També vull agrair l'amistat de la Cristina Alonso i en Víctor Carrer, "la extraña pareja" però taaan divertits! Cris, gràcies per les estones de bàsquet, les tardes de jocs i les xerrades a peu de CSIC.

Tot i que ja han aparegut entre aquests agraïments, vull donar molt fort les gràcies a la Raquel Calderón i a en Víctor Carrer. Hem viscut plegats molt més que una tesi. Crec que tinc una sort immensa d'haver pogut compartir aquests anys de doctorat amb dos dels meus millors amics de la universitat. A la Raquel per ser el meu "enxufe" amb el CSIC, per creure'm capaç de fer la tesi al laboratori del seu davant, per confiar, escoltar i fer-me riure sempre. Ens queden moltes coses per viure juntes, per sort ja fora del doctorat! I a en Víctor, que encara et visualitzo cada setmana al final de la jornada assegut al tamboret del costat del meu ordinador explicant-nos la vida. Gràcies per parlar sempre amb sinceritat amb mi, per la teva professionalitat en fer tonteries que fan que encara no pugui parar de riure i per ser font de tantes fotos que passaran a la història. Mai t'oblidaré.

Tot i que no han estat mai al laboratori, també m'agradaria agrair a l'Alba Sala i a la Mònica Solà la seva amistat i comprensió. M'imagino que no ha de ser senzill viure amb una noia que un dia tan aviat t'intenta explicar els problemes d'un experiment que no entens com es queixa durant una hora de lo difícil que és escriure una tesi. Gràcies per aguantar-me.

Als amics de la "uni" i als del "Lokal", els de tota la vida. Tots ells suports bàsics a la meua vida que mai fallen quan se'ls necessita i que segueixen proveint bones estones i records.

A la meua família, que no només m'han permès estudiar el que he volgut sinó que sempre m'han recolzat en totes les meves eleccions, inclús quan vaig dir que volia intentar fer doctorat tot i que estava segura que no trobaria lloc. Gràcies per sempre intentar que estigui bé. Al meu avi Josep, que sempre va creure cegament en mi, tot i que no va tenir mai ni idea del què feia. I a l'Eloi, que has tingut la mala sort d'enganxar-me en l'any més difícil de tots, si ja ens ha anat bé fins ara, imagina't després!

Gràcies a tots!

*A en Víctor Carrer,*

*Com tantes altres coses, el dia de  
la defensa ho farem els dos junts.*



# INDEX

<b>GENERAL INTRODUCTION.....</b>	<b>1</b>
1. Treatment strategies in cancer .....	3
2. Novel approaches to Drug Discovery.....	6
2.1. Screening methodologies.....	6
2.2. Identification of new hits.....	8
2.3. Identification of new targets.....	9
<b>CHAPTER 1 .....</b>	<b>15</b>
INTRODUCTION.....	17
OBJECTIVES .....	23
RESULTS AND DISCUSSION.....	27
1. Screening and compound selection.....	29
2. Mechanism of action of squaramide <b>34</b> .....	36
2.1. Cell cycle analysis.....	36
2.2. Apoptotic cell death study .....	38
2.3. Caspase-dependent cell death.....	42
2.4. Alternative cell death mechanism .....	43
2.4.1. Cathepsin-dependent cell death.....	43
2.4.2. Necrosis.....	44
2.4.3. Autophagy .....	44
2.5. Mitochondria and ROS .....	47
3. Summary and conclusions.....	49
<b>CHAPTER 2 .....</b>	<b>55</b>
INTRODUCTION.....	57
1. Types of autophagy.....	59
1.1. Macroautophagy.....	62
1.1.1. Autophagosome formation .....	63
2. Autophagy and diseases .....	69
2.1. Cancer.....	69



2.2.	Neurodegeneration .....	70
2.3.	Immunity and Inflammation .....	71
2.4.	Ageing and longevity .....	71
2.5.	Cell death .....	72
3.	Autophagy modulators .....	72
3.1.	Inductors .....	73
3.2.	Inhibitors .....	74
4.	Estimation of Autophagic Activity .....	76
5.	Atg4B .....	77
	OBJECTIVES .....	81
	RESULTS AND DISCUSSION .....	85
6.	TR-FRET-based assay and protein modification .....	87
6.1.	TR-FRET .....	87
6.2.	A TR-FRET based assay to find Atg4B inhibitors .....	88
7.	Atg4B expression and purification .....	90
8.	Biotinylated N-(His) <sub>6</sub> -proLC3B(L123C) expression and purification .....	93
9.	TR-FRET assay development .....	95
10.	AlphaScreen technology .....	97
10.1.	AlphaScreen optimization .....	98
11.	A Mass Spectrometry-based assay as an alternative method to determine Atg4B activity .....	107
11.1.	Assay optimization .....	107
12.	Screening .....	110
12.1.	Virtual Screening .....	110
12.2.	Biological Screening (AlphaScreen) .....	112
13.	Synthesis of focused libraries based on <b>NSC126353</b> and <b>NSC611216</b> structures 117	
14.	Evaluation of hits in the MS-based assay .....	122
15.	Biological characterisation of <b>57</b> .....	124
	CONCLUSIONS .....	129
	<b>CHAPTER 3</b> .....	<b>133</b>

INTRODUCTION.....	135
1. Lipid Posttranslational modifications.....	137
2. Membrane heterogeneity and function .....	141
3. Posttranslational modifications and autophagy.....	145
4. Lipids and autophagy .....	146
5. Mass spectrometry-based lipid analysis.....	149
OBJECTIVES .....	153
RESULTS AND DISCUSSION .....	157
6. A MS-based method to analyse PEs derived from LC3/GABARAP .....	159
7. Calibration curves of PEs detected by UPLC/TOF-MS.....	160
8. Identification and quantification of PEs from treated cell lysates .....	161
9. Identification and quantification of PEs from total lipidome.....	168
10. Lipid profiling of HeLa cells treated with heptadecanoic acid.....	170
11. Immunoprecipitation of LC3B .....	175
11.1. Optimization of the immunoprecipitation method .....	175
11.2. Alternative validation of immunoprecipitation method through KO cells .....	180
12. N-(His) <sub>6</sub> -3C-Atg4B analysis.....	182
13. N-(His) <sub>6</sub> -3C-Atg4B delipidation.....	185
14. Summary and outlook .....	186
CONCLUSIONS.....	189
<b>MATERIALS AND METHODS.....</b>	<b>193</b>
1. Reagents .....	195
2. Biological material.....	197
2.1. Eukaryotic cells .....	197
2.2. Bacterial cells .....	198
2.3. Plasmids.....	198
2.4. Oligonucleotides .....	199
2.5. Culture media .....	200
3. General procedures for cell culture .....	200
3.1. Transfection of plasmid pOPIN-GFP-LC3 and	

generation of stable HEK293 cell line .....	201
3.2. Production of retroviral particles and transduction in HEK293 cells .....	201
4. MALDI-TOF MS analysis .....	201
5. UPLC-TOF MS analysis .....	202
6. Expression and purification of the proteins .....	203
6.1. Atg4B production .....	203
6.2. N-(His) <sub>6</sub> -proLC3B(L123C)-Biotin production .....	205
6.3. N-(His) <sub>6</sub> -proLC3B(L123C) Biotin as Atg4B substrate monitored by SDS-PAGE .....	207
6.4. Detection of biotinylated protein using HRP-streptavidin .....	207
7. MTT assay .....	207
8. Other cell viability assays .....	208
8.1. SRB assay .....	208
8.2. Luminescent Cell Viability Assay .....	209
9. Cell cycle analysis .....	210
10. Evaluation of dead cells using Annexin V-FITC/PI and flux cytometry .....	210
11. Protein analysis by Western Blot .....	211
12. Analysis of mitochondrial membrane potential .....	213
13. ROS detection .....	214
14. TR-FRET measurements .....	214
15. AlphaScreen assay .....	215
16. UPLC/TOF-MS-based assays to measure Atg4B activity .....	218
17. Papain assay .....	220
18. Calibration curves of phosphatidylethanolamine samples .....	220
19. Determination of the required amount of N-(His) <sub>6</sub> -3C-Atg4B for PE cleavage .....	220
20. Analysis of proteome-bound PEs .....	221
21. Extraction and analysis of cell lipidome .....	222
22. Extraction and analysis of cell lipidome in HeLa cells treated with heptadecanoic	

acid.....	222
23. Immunoprecipitation of PEs released from LC3B-II.....	223
24. Lipid content analysis of N-(His) <sub>6</sub> -3C-Atg4B .....	226
25. Delipidation of N-(His) <sub>6</sub> -3C-Atg4B.....	226
26. Activity of delipidated N-(His) <sub>6</sub> -3C-Atg4B .....	227
<b>REFERENCES.....</b>	<b>229</b>
<b>ANNEXES .....</b>	<b>261</b>
<b>ARTICLES</b>	



# GENERAL INTRODUCTION



Europe, the US and most of the developed world are facing a rapidly ageing population. Thus, according to the World Health Organization (WHO), the number of people over 60s is estimated to grow from 10% in 2010 to more than 20% in 2050. However, increased longevity and life expectancy does not come without significant costs. Cancer, dementia and coronary diseases are one of the leading medical and societal challenges faced by our society and our current healthcare system. As a result, to understand the causes and mechanisms underlying health, healthy ageing and disease and to develop strategies aimed to prevent, detect and treat such pathological disorders is one of the main goals of many current research strategies.

## 1. Treatment strategies in cancer

Cancer is one of the leading causes of death worldwide. Current cancer research strategies address major challenges including cancer initiation and progression, mechanisms of metastasis and the development of novel therapies. Traditional approaches to treat cancers include surgery, radiotherapy and chemotherapy. Although anticancer treatments have significantly improved their efficacy, relevant toxicity and side effects are still associated to all anticancer therapies, making necessary the development of alternative strategies.<sup>1</sup>

Traditional chemotherapy kills healthy cells as well as cancer cells. Therefore, the use of chemotherapy is often limited by the small range of effective dose and toxic side effects caused to healthy cells. Since these drugs target various steps of cell proliferation, such as DNA formation and function or the mitosis spindle, the main side effects of the treatment affects tissues with high proliferative capacity (bone marrow elements, gastrointestinal tract mucosa and hair follicles).<sup>2</sup> Toxicity is acute and reversible (nausea, fatigue, pain) but there are also long-term effects which are delayed and irreversible.<sup>1</sup>

Drug resistance is also a serious concern in anticancer therapies. Despite most of cancers are initially susceptible to chemotherapy, some of them develop resistance over time by many mechanisms including drug inactivation, drug target alteration, drug efflux, DNA damage repair, cell death inhibition and epithelial-mesenchymal transition. Cell heterogeneity inherent in cancerous tumours and epigenetics can also be involved in drug resistance.<sup>3</sup> Relevant examples of these mechanisms of acquired resistance will be mentioned as follows. Hence, example of drug target alteration include the mutation of the tumour suppressor protein p53.<sup>4</sup> Changes of drug efflux can be observed in paclitaxel resistant ovarian cancer patients where there is an overexpression of the transport P-glycoprotein leading to a major paclitaxel efflux.<sup>5</sup> Signalling mechanisms, such as DNA repair pathways, can also result altered as a response against DNA-damaging agents like cisplatin.<sup>6</sup> In addition, both apoptosis and autophagy are modified in tumour cells in order to increase their survival. Examples



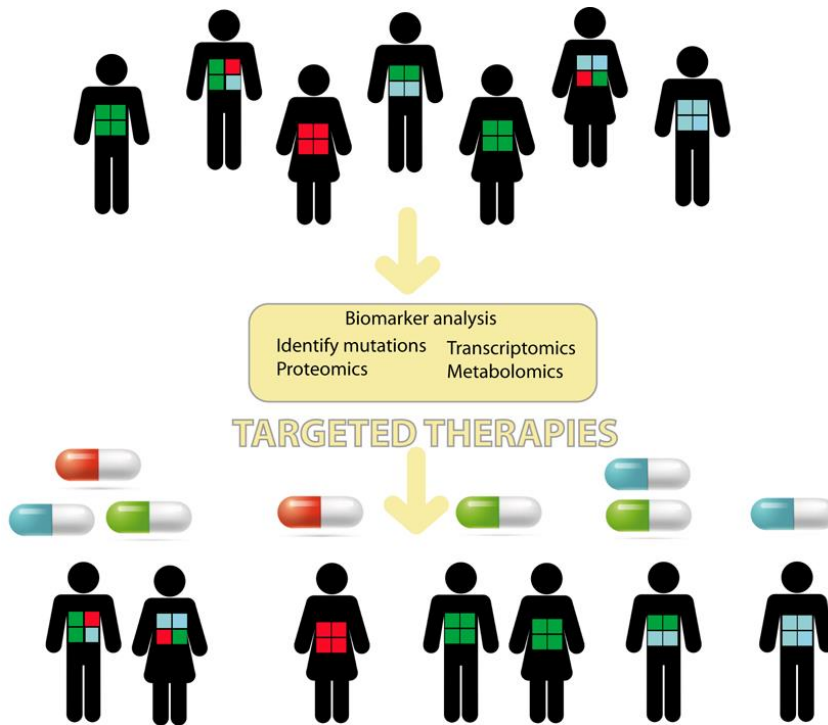
thereof are the overexpressed B-cell lymphoma 2 (Bcl-2) family proteins showing an important antiapoptotic effect<sup>3</sup> and the increased levels of autophagy detected in colon cancer cells treated with 5-fluorouracil.<sup>7</sup> The most relevant epigenetic changes include DNA methylation and histone acetylation or methylation. Hence, as resistance mechanism, oncogenes are usually overexpressed via hypomethylation whereas tumour suppressor genes are commonly hypermethylated causing a decrease in the expression of these genes. This the case of RGS10, whose expression is inactivated in ovarian cancer cells resulting in the silencing of tumour suppressor genes.<sup>8</sup> The epithelial-mesenchymal transition is the mechanism by which tumours become metastatic and it is a very complex event where several pathways are involved, including angiogenesis and induction of cell motility. For instance, the increase of integrin  $\alpha\beta6$  expression enable cells to activate TGF- $\beta$ , which is required for epithelial-mesenchymal transition and it also produces drug resistance.<sup>9</sup>

Apart from the problems associated to drug resistance, a major issue is the lack of new targets. Remarkably, the drugs currently in use target no more than a few hundred proteins. Thus, the development of novel therapeutic targets and strategies is an attractive and emerging area of research. Major advances of the last decades have enabled the identification of new druggable targets and the rapid development of the concept of personalized cancer treatment. As a result, classical chemotherapy is switching to more directed treatments due to its milder side effects and increased effectivity. Some relevant examples of targeted therapies include hormone-based treatments, monoclonal antibodies or kinases inhibitors (**Figure 1**).<sup>10</sup>

Hormone therapy disrupts the endocrine system and it can be applied to tumours that test positively for androgen, estrogen and/or progesterone receptors such as some types of breast cancers<sup>1</sup> or prostate cancers.<sup>11</sup>

Monoclonal antibodies have revolutionized the treatment of cancer. Some monoclonal antibodies act by boosting the immune response against cancer cells. As example, ipilimumab<sup>12</sup> activates the immune system by blocking the cytotoxic T-lymphocyte-associated antigen 4 (CTLA-4) and it is employed for the treatment of melanomas. The immune response against cancer cells can also be modulated via antibodies that attach to cancer cells and act as a marker for destruction. A relevant example of this class include rituximab,<sup>13</sup> designed to bound the CD20 antigen primarily found on the surface of immune B lymphocytes and employed to treat B cell lymphomas. Monoclonal antibodies can also act though the blocking of antigens present on cancer cells and required for cell growth or spread. For example, trastuzamab<sup>14</sup> binds the human epidermal growth factor 2 (HER2) protein found in large amounts on the surface of breast and stomach cancer cells, and cetuximab<sup>15</sup> target the epidermal growth factor (EGFR) found overexpressed in 75% of metastatic colorectal cancers. However, there are side effects that have to be considered in all

these strategies, such as central nervous system toxicities and cytokine-release syndrome (CRS) which is a systemic inflammatory response caused by released cytokines and cytotoxic damage that can cause a variety of symptoms that usually can be managed with standard drugs.<sup>10</sup>



**Figure 1.** More personalized diagnostics will enable tailored treatments (this image has been designed using resources from Freepik.com).

Other small-molecule drugs target drivers of common cancers such as the vascular endothelial growth factor (VEGF),<sup>16,17</sup> Bcl-2 family proteins that controls cell survival and apoptosis<sup>18</sup> or protein kinases (B-Raf,<sup>19</sup> PIK3CA,<sup>20</sup> BCR-ABL) among others. Indeed, Imatinib (Gleevec®) is considered the perfect example of how it is possible to learn how to treat cancer through the understanding of cancer biology. Thus, the fusion of the BCR-ABL gene results in a protein with abnormal and deregulated tyrosine kinase activity. Structure-based designed compounds led to the discovery of a specific inhibitor of this kinase that cause complete remission in some chronic myelogenous leukaemia (CML) patients.<sup>21</sup> Moreover, there is an increasing number of highly effective clinical trials combining targeted therapies with traditional chemo- or radiotherapy.<sup>22,23</sup> Alternatively, the combination of different targeted therapies is also under investigation. Examples thereof include the combined use of the EGFR tyrosine kinase inhibitor erlotinib and the humanized VEGF receptor monoclonal antibody bevacizumab in the treatment of advanced chemotherapy-refractory non-small cell

lung cancer.<sup>17</sup>

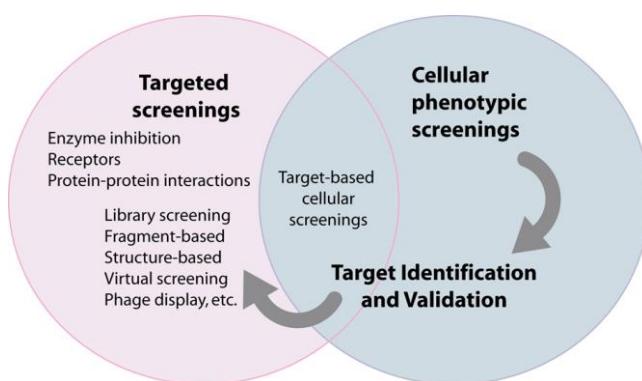
Efficient therapeutic strategies to eliminate cancer stem cells (CSCs) are also under investigation. Hence, recent studies have suggested the existence of CSCs subpopulations sharing similar characteristics as normal stem cells such as self-renewal and differentiation ability and with a key contribution in metastasis and tumour recurrence.<sup>24,25</sup>

All in all, personalized anticancer therapy alone or in combination with traditional therapies has significantly improved the disease-free survival and the overall survival for many cancer patients. This improvement has been only possible thanks to our gained knowledge about the biology of tumours. Thus, the identification of novel tumour markers and druggable targets, both enzymes or non-enzymatic proteins, has been greatly facilitated by the advances in our understanding of disease pathophysiology and the molecular mechanism regulating cellular processes. However, there are still important limitations in cancer drug discovery. Around 20% of industrial cancer drug development programs focus on just eight proteins. In addition, drug discovery, which has been mostly led by pharmaceutical industry, has now recessed due to high failure rates and early patents expiration. This decrease may be caused by lack of mechanistic understanding and a poor rigor in the target selection and validation.<sup>26</sup> Clearly, more research is required to dissect the specific cell actions that cause cancer cells to grow and new approaches are needed to identify and validate new biomarkers and targets leading to novel therapeutic strategies.

## **2. Novel approaches to Drug Discovery**

### **2.1. Screening methodologies**

The two main strategies used to identify potential drugs include target-based screenings (fragment-based ligand discovery, structure-based design, modification of natural products) and phenotypic screenings.<sup>27</sup> The main difference between these two strategies is the knowledge or unknowledge of the target. Phenotypic screenings are based on finding compounds that modulate a disease-linked phenotype, whereas target-based screenings are biochemical assays that rely upon specific hypotheses of a disease pathway, so compounds are tested against unique targets like proteins, genes or RNA (**Figure 2**).



**Figure 2.** In targeted screenings, molecules are tested against a specific target. These type of screenings are usually based on biochemical assays (but can also be performed in cells). Phenotypic screenings measure a cellular outcome. Target identification approaches may be required to elucidate the target of the identified active molecule.

Phenotypic assays have been long restricted to just evaluate the effect of compounds on cell viability. However, these assays are now resurging thanks to improved readouts, more sophisticated cell models and its potential to be applied to not fully understood diseases. More importantly, phenotypic screenings enable the identification of active compounds in physiologically relevant model systems. However, their major limitation and challenge is the downstream identification of drug's target and mechanism of action. Thus, other techniques and assays are required to validate hits but also to unravel their mode of action. This initial limitation can also be seen as an opportunity since it could lead to the identification of other active compounds, therapeutic strategies or the improvement of the assays.<sup>28</sup> Phenotypic assays combined with mass spectrometry (MS)-based proteomics are useful tools to detect active compounds and novel pathologically significant targets. These techniques enable the understanding of the mechanisms that control the cellular processes of cancer cells, which includes protein-protein interactions, but also lipid-protein and transcription factors-protein interactions modulating gene expression.<sup>29</sup>

Target-based assays have been the leading approach during the last 20 years, largely supported by the revolution in genomics, the development of protein expression techniques and the advances in combinatorial chemistry enabling the synthesis of vast compound libraries. These assays are especially useful when there is a substantial knowledge of the pathway and thus, the target is well known. The most important limitation encountered in targeted-based assays is usually derived from the use of chemical libraries (insufficient coverage of chemical space, lack of chemical diversity and drug-like properties) and the fact that in vitro activity is not always necessarily correlated with good cellular activity.<sup>28</sup>

Targeted-based assays to discover small bioactive molecules are usually simpler than phenotypic assays and require less components (effect of hits found by phenotypic assays sometimes are caused by a superposition of multiple effects). In target-based assays, less mechanisms of action are involved, and this feature facilitates the design of second-generation drugs with improved affinity. For these reasons, this type of assays is often more suitable to screen large compound libraries. Besides, phenotypic assays tend to require more economical resources due to their complexity and the subsequent research needed to identify and validate the targets. They also exhibit more safety risks since the target and mechanisms of action are usually unknown.<sup>30</sup>

Simplification and reliability have been the major improvements for targeted-based assays. Hence, current techniques require less steps and do not need radioactive readouts. Target-based assay can be biochemical but also cellular and employ a variety of techniques such as fluorescence, fluorescence polarization, fluorescence resonance energy transfer (FRET), time-resolved fluorescence, AlphaScreen™, high-content screening, fluorescent-imaging plate reader, protein fragment complementation assays, microfluidics, flux cytometry and label free technologies.<sup>31</sup> Despite their differences, both screening strategies are valuable, complementary and widely employed. Thus, whereas target-based assays can be considered a primary screen enabling the identification of specific inhibitors, phenotypic screenings will be next required as a secondary or follow-up assay to characterize their cellular effects. Moreover, phenotypic assays are good tools to reveal first-in-class drugs without considering a well-known mechanism of action, whereas targeted assays are useful to run screenings from big libraries when the target has been well characterized. Nevertheless, both assays required a good design that considers miniaturizing capacity, robustness, signal-to-noise, reproducibility, controls availability, screen locations, and screen follow-up, which has to avoid false positive and has to enable the selection of most promising hits depending on its properties and potency.<sup>32</sup>

## 2.2. Identification of new hits

Another major challenge to be met in the drug discovery process is the identification of new hits and leads compounds. Thus, hit identification can rely on traditional strategies such as random high-throughput screening (HTS) of chemical libraries, fragment-based assays (i.e. X-ray screening<sup>33</sup> or NMR screening<sup>34</sup> of molecular fragments), structure-based design, computer-aided drug design and virtual screening (the design and identification of hits based on a known target structure and the observed docking *in silico*),<sup>35</sup> the modification of known active compounds and natural products (synthesis of derivatives and focused libraries) and more modern approaches including DNA-encoded library screenings<sup>36</sup> and phage-display technologies. In addition, the past decades have seen an explosive advancement in the field of biological medicines or substances including antibodies, proteins, viral and

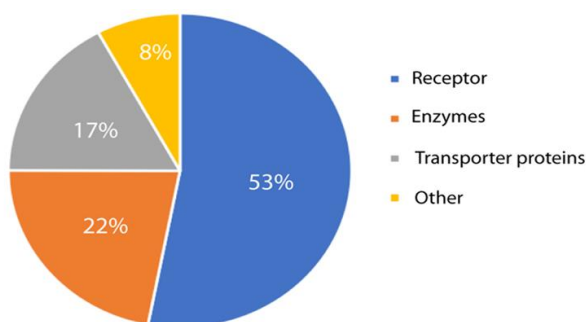
bacterial derived products or gene therapy. Nowadays, all these technologies coexist. Hence, a report has recently summarized the clinical candidates extracted from published reports between 2016 and 2017.<sup>36</sup> The analysis of these data has revealed that the most widely used lead generation approaches were based on previously known active compounds while 29% were obtained by random high throughput screenings, followed by focused screenings (8%),<sup>37</sup> structure-based drug designs (14%), fragment-based lead generation (5%) and DNA-encoded library screening (1%).

### 2.3. Identification of new targets

There are approximately 20000 human protein-coding genes, but the druggable proteome, i.e. the fraction of proteins linked to a disease that can be modulated, could be restricted to ~ 3.800 genes. The current Food and Drug Administration (FDA) approved drugs are directed to only 667 human proteins and 189 proteins belonging to pathogens (**Table 1** and **Figure 3**). On average, 18 new drugs are approved for marketing by the FDA every year, of which 4 act on novel target structures encoded by the human genome.<sup>38</sup> Hence, the identification of new targets remains a critical challenge and an emerging field of research.<sup>39</sup>

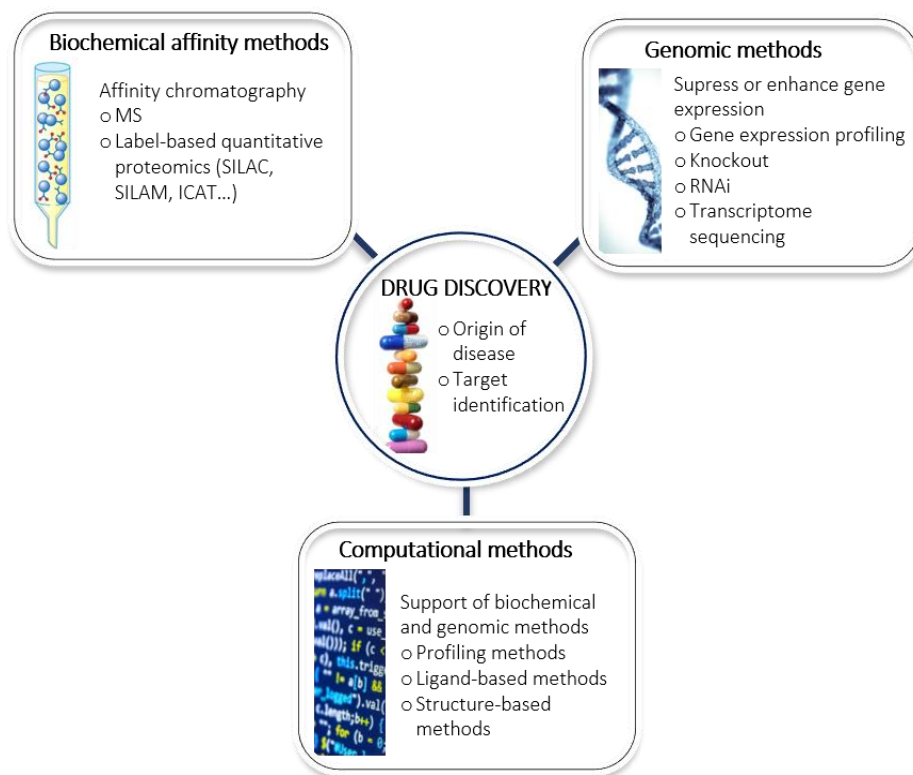
	Targets	
	Small molecule	Biologics
Human proteins	549	146
Pathogens proteins	184	7

**Table 1.** Molecular targets of FDA-approved drugs. Whereas 549 human proteins are targeted by small molecules, only 146 proteins are targets of biologic drugs. Similar ratios can be found when analysing pathogen proteins (184 vs 7).<sup>38</sup>



**Figure 3.** Classification of the currently employed drugs directed to human proteins. The vast majority (563 drugs) target receptors including G-protein-coupled receptors, receptor tyrosine kinase and nuclear receptors, 234 drugs target enzymes such as hydrolases, ligases or oxidoreductases and 181 drugs are directed to transporter proteins (voltage-gated ion channels, active transporters,<sup>40</sup> among others).

A key step in the drug discovery process is to understand the **molecular mechanism of a disease** and the potential targets for intervention. Thus, basic research aims to identify the biological origin of a disease, that together with a number of different approaches for target identification will become increasingly necessary. Three complementary methods are mostly used to discover novel pharmacological targets and drugs: direct biochemical approaches, genetic interaction and computational inference methods (**Figure 4**).<sup>41</sup>



**Figure 4.** Drug discovery relies on study of the origin of diseases and specific target identification. In basic research three types of methods are employed, biochemical affinity, genomic and computational methods.

**Biochemical affinity methods** are based in physical interactions and are useful both for target identification and drug discovery. Affinity chromatography is a biochemical method that relies on the high affinity of a protein present in a sample mixture to a molecule linked to some support.<sup>42</sup> Usually it is used as a purification technique but coupled with MS-based proteomics has led to the development of new methods to identify both protein-protein and small molecule-protein interactions. More recently, **affinity chromatography combined with label-based quantitative proteomics** is emerging as a powerful tool enabling a more in-depth and, in some cases,

quantitative analysis of the identified proteins. Typically, these methods are based on the incorporation of mass differences enabling relative quantification. Examples thereof include SILAC (stable isotopic labelling with amino acids in cell culture), SILAM (stable isotopic labelling of mammals),<sup>43</sup> ICAT (isotope-coded affinity tag), trypsin-catalysed <sup>18</sup>O labelling and iTRAQ (isobaric tags for relative and absolute quantitation). SILAC relies on the incorporation of isotope-labelled amino acids added directly to cultured cells and the subsequent expression of labelled proteins,<sup>44</sup> what limits its use in primary cells and tissues studies. ICAT uses a trifunctional probe, containing a cysteine reacting group, an isotope-coded linker and a biotin, that it is added to the proteins prior to enrichment.<sup>45,46</sup> Quantitative proteomics analyses have been also achieved performing tryptic digestion in the presence of H<sub>2</sub><sup>18</sup>O and H<sub>2</sub><sup>16</sup>O leading to the enzymatic incorporation of isotopes at the C-terminus of peptides.<sup>47</sup> Finally, iTRAQ is also employed for quantitative proteomics in which peptides are labelled with different isobaric mass tags that during fragmentation produce abundant MS/MS signature ions with relative areas that can be employed for protein quantitation.<sup>48</sup> Additional methods include mTRAQ (mass differential tags for relative and absolute quantification), TMT (tandem mass tags) and stable isotope dimethyl labelling. All of these strategies are useful since they can be applied to many substrates, although they are carried out at peptide level instead of protein level, so they might have less accuracy.<sup>41</sup>

**Genomic methods** are based on suppressing or enhancing a specific gene expression. Therefore, they can be used to both reveal new targets and to validate drug mechanisms of action. **Gene expression profiling** compare gene transcription in treated cells versus control cells. This strategy allows for the identification of genes that are overexpressed or underexpressed, thus suggesting potential key proteins for specific biological processes that are under investigation, that combined with appropriate bioinformatics tools, provide a powerful mechanism to study specific targets or pathways that are important for a biological process.

The expression of a certain protein can be also modified by knockout and RNAi, allowing to analyse the effect of a chemical compound in a protein or pathway by comparing phenotypes in treated cells with the ones observed in cells underexpressing the investigated protein. Knockout is the suppression of a specific gene expression through different mechanisms such as the introduction of a mutated gene, altered sequences of DNA or mutagenic substances, whereas RNAi is the suppression of RNA translation employing siRNA (small interfering RNA), miRNA (microRNA) or piRNA (Piwi-interacting RNA).<sup>32</sup> However, some issues have to be taken into account including the risk of genetic compensation, the appropriate selection of knocked-out organisms or cell lines and the unobserved side effects caused by the compound. As a positive remark, this strategy can be applied to human cell lines or mammalian organisms, so the assays are carried out in a more physiologically



environment.<sup>41</sup> **Transcriptome sequencing** (RNA-seq) based on the massive sequencing of a biological sample to quantify RNA, is another genomic method that could be used, for instance, to identify resistant targets of a cytotoxic compound. This strategy has been applied to the mutated polo-like kinase (Plks) 1 after treatment with bortezomib in the HCT-116 cell line.<sup>49</sup> Although the only observed phenotype is cell viability, the main advantage of this method is that there is no need of chemical modifications and it can be applied to different cell lines.

**Computational methods** include a wide range of techniques that provides analytical support to genetic and biochemical methods. There are several types of computational strategies. Profiling methods that are based on pattern recognition to compute the results from different experiments, ligand-based methods which combine phenotypic information with small molecules to predict new targets and structure-based methods that predict interactions between small molecules and/or proteins through three-dimensional protein structure. A relevant example is the NCI-60 data from the US National Cancer Institute that comprise the results of a huge chemical library on 60 different cell lines. The patterns of differential growth inhibition and protein expression produced by tested compounds among cultured cell lines was analysed and compared by the COMPARE algorithm. These results can be then employed to elucidate targets and mechanism of actions of new tested compounds.<sup>50</sup> Another example is The Connectivity Map created in 2006 by the Broad Institute. This is a public database of gene-expression profiles from cultured human cells treated with bioactive small molecules, together with a pattern-matching software to mine all these data. Signatures with high similarity might represent unrecognized connections among drugs and diseases or among different small molecules sharing common target or mechanism of action.<sup>51</sup>

Models to predict ligand-protein interactions are particularly useful to identify new targets. As an example, a Laplacian-modified naive Bayesian modelling trained with the WOMBAT database (World Of Molecular BioAcTivity) was able to predict the most likely protein targets of compounds included in the MDL Drug Database Report.<sup>52</sup> A different strategy, termed similarity ensemble approach (SEA), relates proteins based on the chemical similarity of their ligands. This technique has been employed to reveal unexpected targets of known bioactive molecules such as methadone (antagonist of the muscarinic M3 receptor), emetine (antagonist of the adrenergic receptor) and loperamide (antagonist of neurokinin NK2 receptor).<sup>53</sup> In addition, all these techniques can also provide information about mechanisms of action, toxicity, drug resistance and side effects.<sup>41</sup> These tool has led to promising results and the access to this kind of information is increasing with useful public databases. However, since these approaches rely on already performed experiments, one should have in mind that the results could be biased by the unknown details of the original experiments and new or unknown interactions could not be computationally

detected.<sup>41</sup>

Taken all together it seems clear that a combination of all described technologies will support and facilitate the progress in this research field. The integration of big data is crucial to reveal new pathways, targets and to determine the mechanisms of action of small molecules as well as to suggest new chemical structures. Chemical biology also has a key role in this area by clarifying biological pathways, identifying new targets or find new strategies against drug resistance and toxicity.

This thesis addresses three different subjects closely related. First, a phenotypic screening measuring cytotoxicity in the gastric cancer cell line HGC-27 is reported. A library of squaramides is tested identifying a compound displaying a substantial specificity for this cell line over non-tumour cells. Next, a study is performed to characterize its mechanism of action.

Since autophagy is a big concern for chemotherapy drug resistance, a targeted-based screening assay in order to find autophagy inhibitors directed to the cysteine protease Atg4B has been next optimized. The assay employs AlphaScreen technology, a sensitive method based on energy transfer between two beads bounded to a modified substrate. The HTS screening together with a counter screen based on mass spectrometry were developed and employed to identify small molecule inhibitors of the enzyme. Next, the screening of a 250-compound library obtained after a virtual screening performed on Atg4B structure in presence or absence of the substrate protein MAP1-LC3 (microtubule-associated protein 1A/1B-light chain 3) enabled the identification of some hits. Potency of the initial hits was improved by a medicinal chemistry approach and cellular studies confirmed autophagy inhibition.

Finally, a basic research study was carried out in order to gain knowledge of the molecular mechanisms that control autophagy. LC3 is a key marker of autophagy that requires C-terminal lipidation with a phosphatidylethanolamine to be active. The main goal of this section is to profile the lipid modifications present in LC3 proteins and to elucidate if structural heterogeneity (fatty acids of different length and unsaturation degree) exists and if this diversity in lipid composition may have an impact on protein function. These results could lead to the identification of new biomarkers or targets with potential therapeutic interest for autophagy modulation.



# CHAPTER 1:

BIOLOGICAL EVALUATION AND INVESTIGATION OF THE  
MECHANISM OF ACTION OF SQUARAMIDES WITH  
CYTOTOXIC EFFECTS AGAINST HGC-27 CELLS



# INTRODUCTION



Phenotypic assays in tumoral cells and screening of compound libraries result an attractive and effective strategy for the identification of novel active compounds, often called hits. In addition, after target identification and validation approaches, phenotypic assays may also contribute to the identification of new therapeutic targets and mechanisms of action. Research detailed in this chapter one is focused on the characterization of the biological activity of a compound library formed by squaric acid derivatives.

Squaric acid esters and squaramides have shown interesting physicochemical properties that allow their use in several fields. These compounds are formed by a four-membered ring aromatic system with two adjacent carbonyls and two NH groups that present potential as both hydrogen bond donors and acceptors. Each hydrogen bond seems to confer more aromaticity to the molecule.<sup>54</sup> The structure of squaramides, formed by a rigid and planar ring, is also important to explain their properties. This hydrogen bonding, aromatic switching and structural rigidity have been studied in many applications ranging from chemical synthesis to biomedicine.<sup>54</sup>

Squaramides were originally developed as non-covalent organocatalyst, since their rigid structure and the strength of their hydrogen binding transition states<sup>55</sup> provide a chiral environment for asymmetric induction (**Figure 5**).<sup>56,57</sup> The unique structural features of squaramides may also facilitate its interaction with biological targets via specific molecular recognition.<sup>54</sup> These properties have promoted a recent interest of medicinal chemists on squaramide motifs as promising candidates for drug design, as bioisosteres of ureas, guanidines or phosphates, and interesting tools as transmembrane anion transporters among other applications.

In the last years pharmaceutical companies have shown increasing interest in compounds containing the squaramide framework and some of them progressed to clinical studies. Examples thereof include BMY-25368, an H<sub>2</sub> antagonist for the treatment of ulcers developed by Bristol Myers Squibb (**Figure 5**), or perzinfotel, an NMDA antagonist for the treatment of pain reported by Wyeth.<sup>54</sup> In addition, squaramides have been proposed as isosteres of carboxylic acids<sup>58</sup> and amino acids.<sup>59</sup> An example of this application is the replacement of glutamic acid and asparagine in nephilatoxin-8 that resulted in molecules with more potent paralytic activities than the original one found in spider venom.<sup>60</sup> Squaramides have also been employed as phosphate isosteres. In 2002, Sekine *et al.* reported an oligodeoxynucleotide where the phosphate group was replaced by a squaramide. *In vitro* studies revealed similar properties preserving base pair complementarity but less stability (**Figure 5**).<sup>61</sup> More recently, squaramides were incorporated to 7-methylguanosine monophosphate to obtain cell permeable inhibitors of the initiator of the translation machinery eIF4E. Although the derivatives presented similar properties, none of the compounds showed cellular activity.<sup>62</sup> Squaramides have also served as isosteres of ureas,





conjugated to known antimalarial compounds also showed lower IC<sub>50</sub> values than the original compounds.<sup>66</sup> Actual treatments for Chagas disease are focused on acute phase, whereas there is a lack of treatments acting on the chronic phase. However, a squaramide-based compound has been recently described to be effective on the chronic phase of the disease and it is considered a candidate for preclinical investigation (**Figure 5**).<sup>67</sup> Their activity, stability, low cost and their easy preparation makes them appropriate to improve the current, inefficient and toxic treatment.

Moreover, squaramides have also showed activity as kinase inhibitor. Thus, cyclosquaramides inhibited important kinases such as ABL1, CDK4, CHK1, PKC, c-MET and FGFR among others, and also displayed cell specific antiproliferative effects when screened against the NCI-60 human tumour cell line panel.<sup>68</sup> In addition, squaramide containing an aromatic amine showed high potency inhibiting Plks, a big family of serine/threonine kinases involved in the regulation of cell cycle progression and mitosis.<sup>69</sup>

The hydrogen bonding properties of squaramides have also been exploited to develop transmembrane chloride transporters that act presumably via mobile-carrier and anion-exchange mechanisms. As an example, an environment-sensitive chloride ion receptor based on the squaramide scaffold was shown to avoid ion binding in apolar solvents and allow it in polar solvents.<sup>70</sup> This type of compounds could be employed to restore anion permeability in diseases caused by malfunctioning of ion channels, as is the case for cystic fibrosis (**Figure 5**).<sup>71</sup> Moreover, squaramide-based ion transports can also promote sodium chloride influx into the cytosol and have shown to alter apoptosis. In addition, some of these compounds could also disrupt autophagy through impairment of lysosomal activity.<sup>72</sup>

Apart from their application in medicinal chemistry, squaramides are also gaining interest for their use in chemical biology.<sup>73</sup> Hence, squaramides have been widely employed for the conjugation of proteins, glycoprotein, glycopeptides and antibodies. This strategy was followed to prepare bifunctional ligands that could recruit antibodies to tumour cells expressing  $\alpha_v\beta_3$  integrin.<sup>74</sup> In addition, the high reactivity of squaramides has been used to create haptens that can be employed to isolate monoclonal antibodies. For example, antibodies against the insecticide paraoxon were generated by using a reactive immunogen linked to BSA via a squaric acid ring.<sup>75</sup>

All in all, these previous results suggest that the unique structural features of squaramides make them an attractive scaffold that may serve as a good starting point to identify bioactive molecules. These features, together with our interest in identifying novel chemotherapeutic agents with new modes of action, prompted us to evaluate the antitumor activity of a variety of squaramides synthesised, provided and partially tested by Dr J.V. Alegre from the group of Dr R. Pérez-Herrera and Dr M. E. Marqués-López (Instituto de Síntesis Química y Catálisis Homogénea,

CSIC/Universidad de Zaragoza). Hence, we envisioned that the ability of squaramides to generate hydrogen bonds and electrostatic interactions could be an interesting property to design specific recognition systems with potential antitumor effects. Herein, a series of squaramides and squaramates has been screened against different cancer cell lines. The obtained results confirm the antitumor properties of this family of promising drug candidates.

# OBJECTIVES



The general aim of this section of the thesis is to search for new applications of squaramates and squaramides based on their interesting physicochemical properties that makes them attractive compounds able to specifically interact with biomolecules. This general aim can be split into the following specific goals:

- To identify active cytotoxic compounds with potential selectivity on tumoral cells
- To explore the mechanisms of action involved in the effect displayed by the tested squaramides

With this aim, the potential antitumor activity of a library of differently substituted squaramates and squaramides will be evaluated in different cancer cell lines.



# RESULTS AND DISCUSSION





## 1. Screening and compound selection

A battery of squaramates (**1-14**, **Chart 1**) and squaramides (**15-39**, **Chart 2** and **Chart 3**) having different substituents, stereoelectronic properties and lipophilicities was synthesised by Dr Juan Vicente Alegre-Requena, from the Asymmetric Organocatalysis group belonging to the Institute of Chemical Synthesis and Homogenous Catalysis ISQCH (CSIC-Universidad de Zaragoza). The optimized reaction conditions have been recently published.<sup>76,77</sup> The overall aim of this chapter was to study the cytotoxic effect of the squaramates and squaramides and explore if their biological activity correlates with the presence of different NH amide-type donor sites.

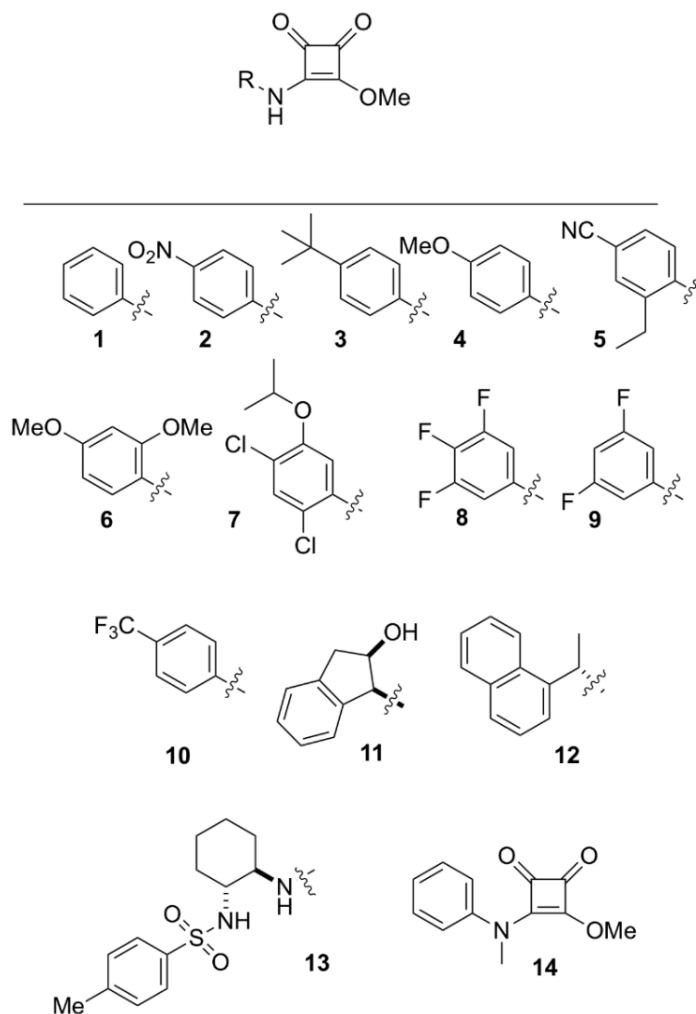


Chart 1

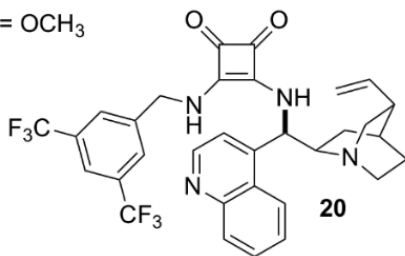
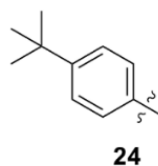
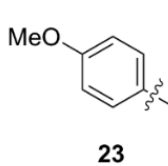
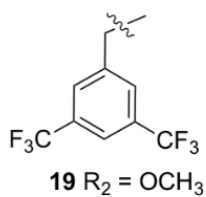
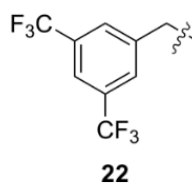
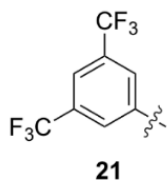
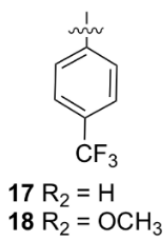
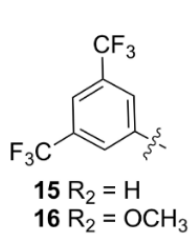
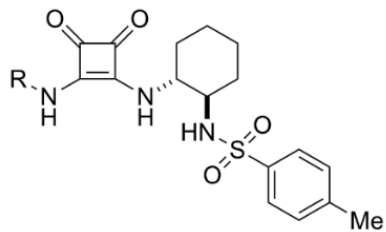
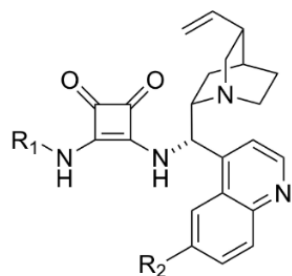


Chart 2

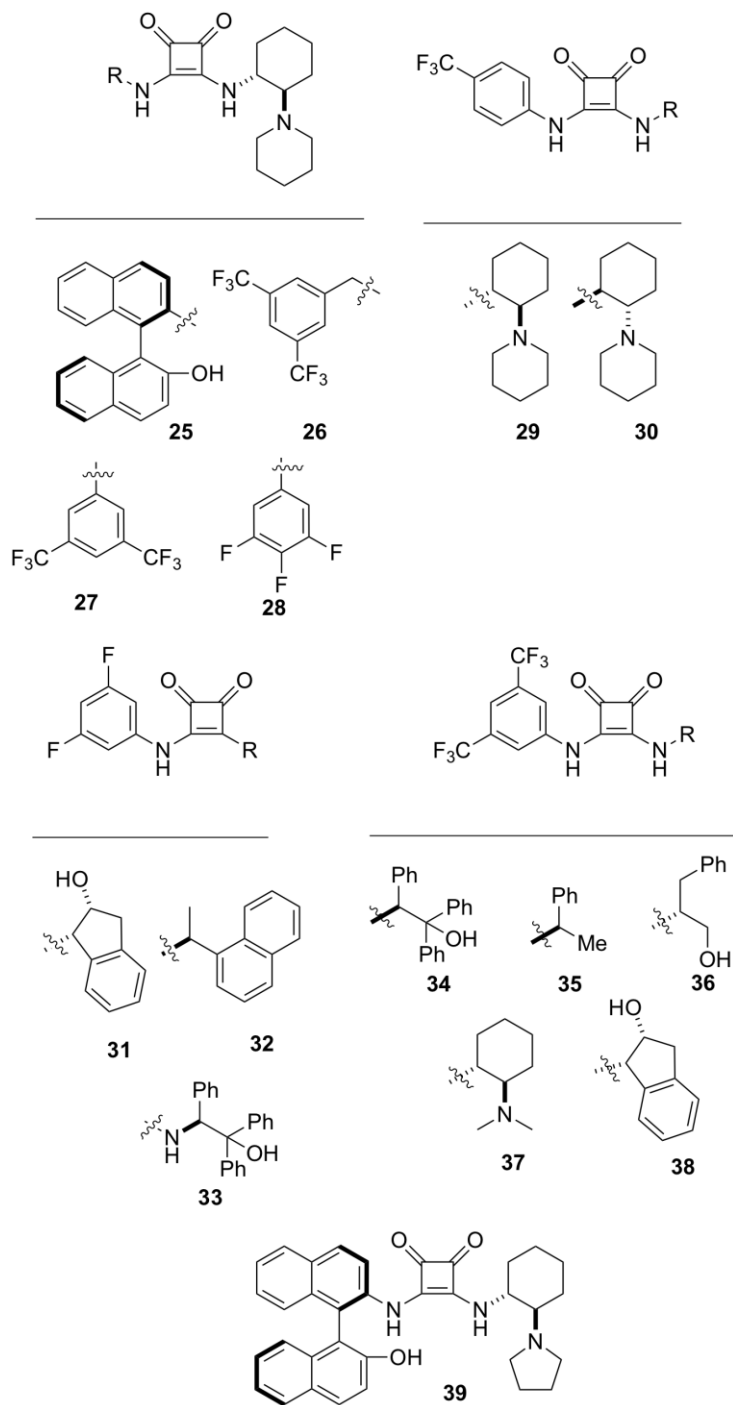


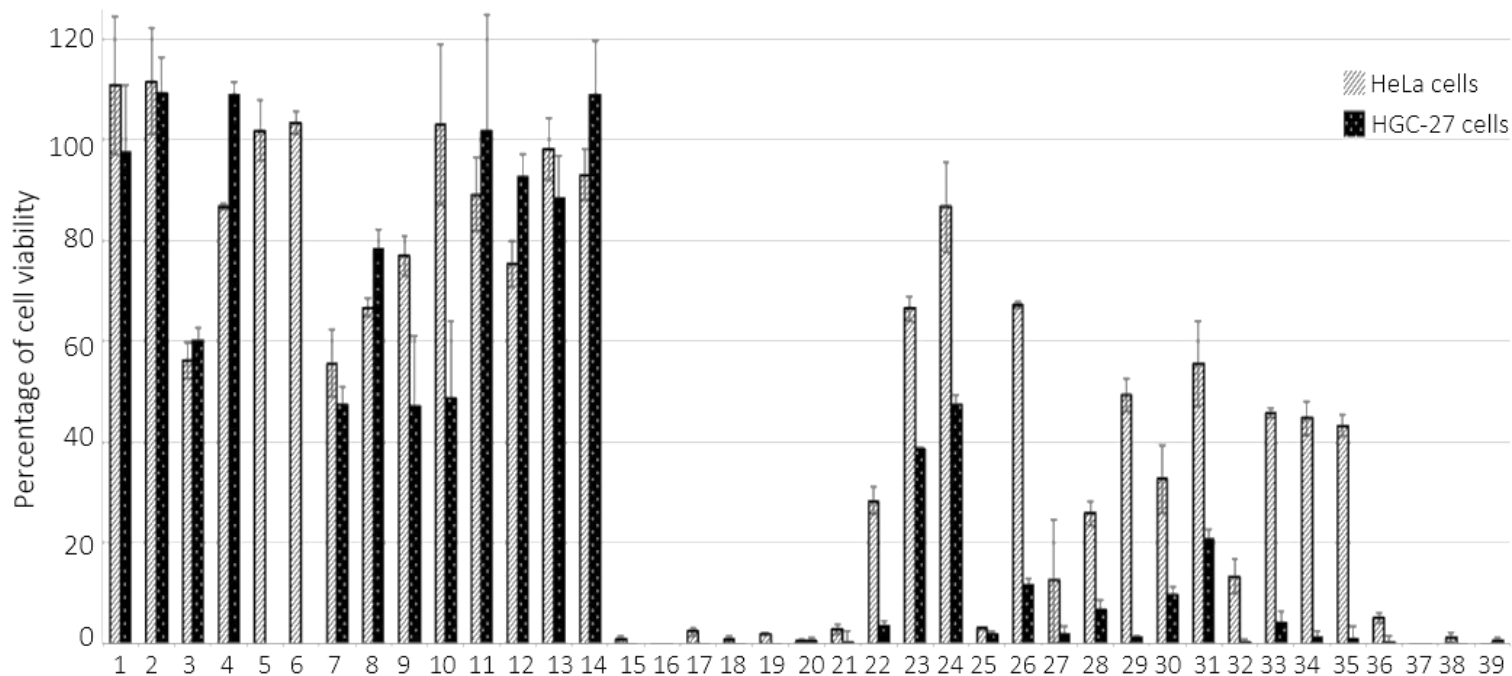
Chart 3

An initial screening was carried out by Dr Alegre-Requena based on the effect of squaramates and squaramides on cell viability on different tumour cell lines. The epithelial human cell lines HeLa, cervical carcinoma, and HGC-27, derived from the metastatic lymph node of gastric carcinoma, were employed in this initial screening. The cytotoxicity of the compounds was evaluated using an MTT assay after 24h treatment at 100  $\mu$ M. The MTT assay is a colorimetric assay that measures cellular viability. It is based on the reduction of 3-(4,5-dimethylthiazol-2-yl)-2,5-diphenyltetrazolium bromide (MTT) to formazan catalysed by mitochondrial enzymes.

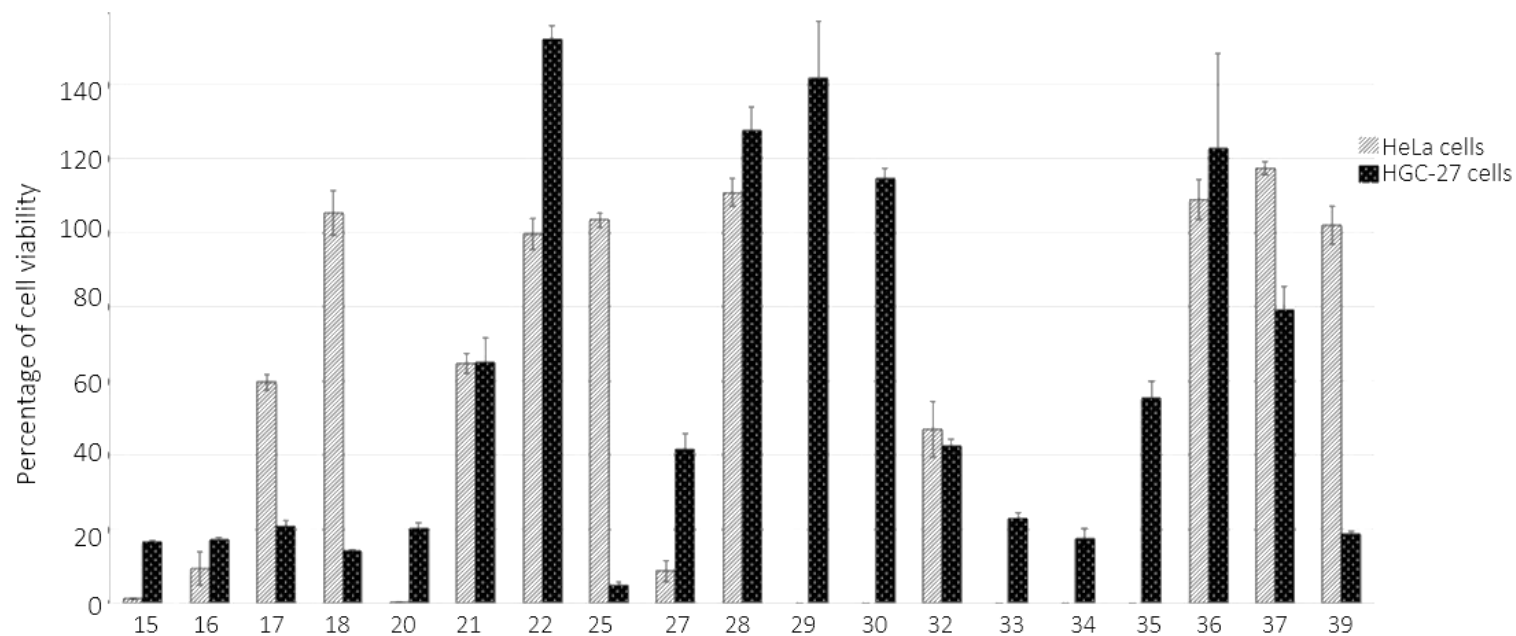
As shown in **Figure 6**, squaramates **1-14** did not show significant effect, thus suggesting that the second NH amide bond is required for the activity (**Figure 6**). On the contrary, some of the squaramides caused significant loss of cell viability. Some structural-activities relationship can be disclosed from this initial screening. Compounds **15 to 20**, which shared a cinchona-based substituent, caused a marked effect on cell viability. A significant decrease in the cell viability is also associated with the presence of a 3,5-bis(trifluoromethyl)phenyl moiety (**15, 16, 21, 27, 34-38**), irrespectively of the other substituent present at the other amide. Similar results were obtained with the 3,5-bis(trifluoromethyl)benzyl substituted squaramides **22** and **26**. Generally, HGC-27 cells resulted more sensitive to the tested squaramides than HeLa cells.

Once squaramates and less potent compounds were discarded, the most potent compounds were further investigated at a 20  $\mu$ M concentration during 24 h. Again, except for compound **27**, HGC-27 cells were in general more sensitive to all treatments than HeLa cells. This cell-type specific effect is interesting and may discard a general non-specific toxicity (**Figure 7**). The cinchona-based compounds **15-20** resulted again in very high inhibition independently of the substituents present at the other point of diversity. Compounds **25** and **39**, bearing bulky and chiral substituents at both sides, were more potent than the corresponding *p*-trifluoromethylphenyl analogues **29** and **30**. The squaramides **34-38** that are substituted with a 3,5-bis(trifluoromethyl)phenyl showed different potencies depending on its substitution pattern, being the lipophilic **33** and **34** the most potent compounds. As a result of this second screening, the squaramides **21, 22, 28-30, 32** and **35-37** were discarded due to the low potency displayed at 20  $\mu$ M and IC<sub>50</sub> values were measured for the remaining compounds.

HGC-27 and HeLa cells were treated separately with serially diluted concentrations. The corresponding IC<sub>50</sub> values were then calculated from the cell viability curves obtained with the MTT assays (**Table 2**). The increased sensitivity of the HGC-27 cells



**Figure 6.** Percentage of cell viability after 24 h treatment with a 100  $\mu$ M concentration as measured by an MTT assay. The cells were grown on a 96-well plate and treated with the squaramides or DMSO (vehicle group). After 24 h of treatment, cell viability was evaluated using an MTT assay, as described in the Material and Methods section. Cell viability is represented in relation to DMSO. Data are the average  $\pm$  SD of three experiments. Note: compounds **5** and **6** were not investigated in HGC-27 cells at 100  $\mu$ M.



**Figure 7.** Percentage of cell viability after 24 h treatment with a 20  $\mu\text{M}$  concentration as measured by an MTT assay. The cells were grown on a 96-well plate and treated with the squaramides or DMSO (vehicle group). After 24 h of treatment, cell viability was evaluated using an MTT assay, as described in the Material and Methods section. Cell viability is represented in relation to DMSO. Data are the average  $\pm$  SD of three experiments. Note: compounds **29**, **30** and **33-35** were not investigated in HeLa cells at 20  $\mu\text{M}$ .

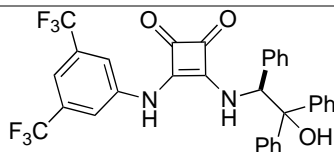
compared to HeLa cells was again proven showing IC<sub>50</sub> values at the low micromolar range. The most potent compound was **34**, a 1,1,2-triphenylethanol and trifluoromethylphenyl disubstituted squaramide that exhibited an IC<sub>50</sub> of 34.63 μM and 1.81 μM in HeLa and HGC-27 cells, respectively. A similar activity pattern could be detected for compound **33** where the 3,5-bis(trifluoromethyl)phenyl has been replaced by a 3,5-difluorophenyl group. Cisplatin and doxorubicin were added as positive controls. Since doxorubicin perturbs the mitochondrial structure and function by increasing the level of reactive oxygen species (ROS)<sup>78</sup> and the MTT assay is based on mitochondrial activity, the effect of doxorubicin on cell viability was calculated employing the sulforhodamine B (SRB) assay.

Compound	Mean IC <sub>50</sub> (95% CI) in μM	
	HeLa cells	HGC-27 cells
<b>15</b>	11.26 (10.33-12.20)	8.12 (7.14-9.24)
<b>16</b>	15.17 (13.20-17.40)	8.21 (7.68-8.78)
<b>17</b>	10.79 (9.49-12.26)	4.53 (3.83-5.36)
<b>18</b>	> 20	12.76 (11.84-13.70)
<b>20</b>	12.08 (11.37-3.93)	3.01 (2.26-5.02)
<b>25</b>	> 20	11.11 (10.51-11.74)
<b>33</b>	> 20	3.39 (2.85- 4.04)
<b>34</b>	34.63 (27.97-42.87)	1.81 (1.47-2.23)
<b>39</b>	> 20	10.79 (10.30-11.20)
<b>Cisplatin</b>	-	20.44 (19.84-22.18)
<b>Doxorubicin</b>	-	15.82 (9.52-26.20)

**Table 2.** Effect of selected squaramides on cell viability against HeLa and HGC-27 cell lines as measured by an MTT or the SRB assay (doxorubicin). Cisplatin and doxorubicin were added as a positive control. IC<sub>50</sub> values are indicated as the average of three experiments with the confidence interval at 95%.

The activity profile of the promising compound **34** was next explored employing different cell lines were. Cell viability was measured using an MTT assay, thus obtaining the corresponding IC<sub>50</sub> values. The following cell lines were investigated: the glioblastoma cell lines T98 and U87MG (the most aggressive type of primary brain tumour), and the non-cancer cells HEK293 (Human embryonic kidney cells), MDCK (Madin-Darby Canine kidney epithelial cells) and Vero cell line (African green monkey kidney cell line). Results are displayed in **Table 3** and confirmed certain specific effect on HGC-27 cells. In addition, when the treatment with **34** was extended for 48 h, these cell displayed a nanomolar IC<sub>50</sub> (660 nM) value.





Cell line	Compound 34 Mean IC <sub>50</sub> (95% CI) in μM
HeLa	34.63 (27.97-42.87)
HGC-27	1.81 (1.47-2.23)
T98	0.66* (0.57-0.76)
U87MG	7.15 (6.12-8.34)
HEK293	60.25 (41.52-87.42)
MDCK	9.03 (7.07-11.54)
Vero	70.20 (50.58-97.43)
	33.40 (27.96-39.90)

**Table 3.** Effect of squaramide **34** on cell viability in different cell lines as measured by an MTT assay. IC<sub>50</sub> values are indicated as the average of three experiments with the confidence interval at 95%. \*IC<sub>50</sub> measured after 48 h treatment.

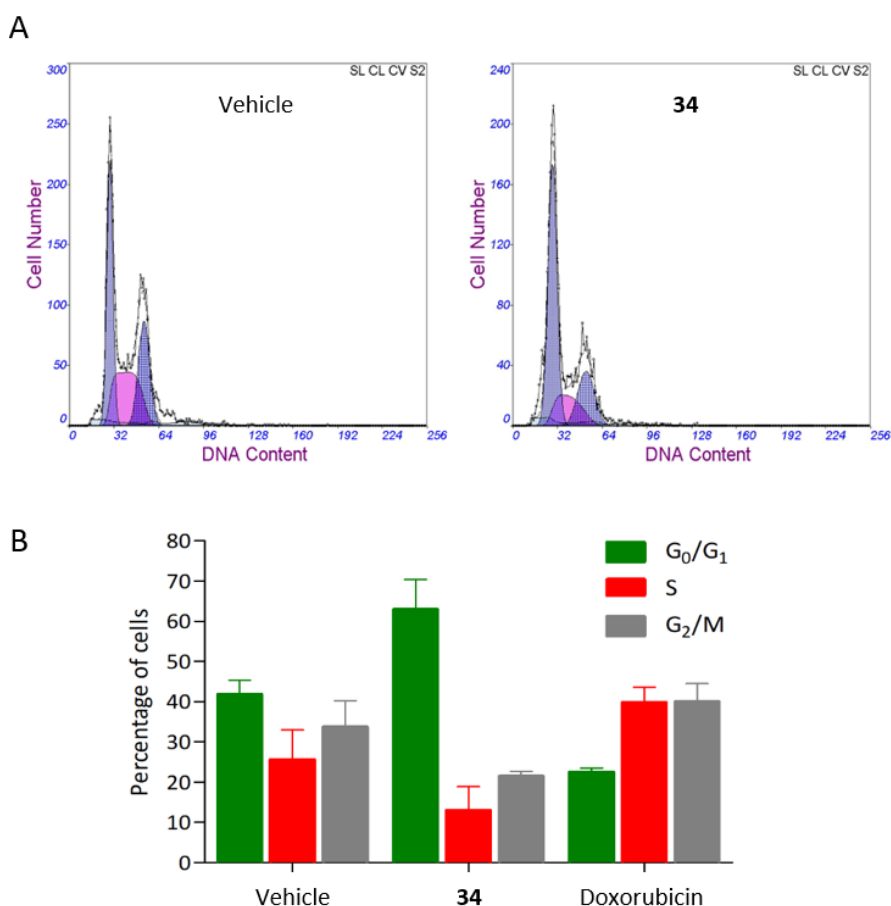
## 2. Mechanism of action of squaramide 34

Gastric cancer accounts for 8% of the total cases of cancer and 10% of total deaths, and it is the second most common cause of cancer-related death in the world.<sup>79</sup> The survival for patients with this type of cancer has improved only modestly over the last 50 years and the median overall survival for patients with advanced or metastatic gastric cancer remains less than a year.<sup>80</sup> One of the reason of this poor prognosis is the late diagnosis. Moreover, gastric cancer presents high molecular heterogeneity, what prevents the uniform application of specific targeted agents.<sup>81</sup> As a result, there is still a clear need for the development of more efficient treatments for gastric cancer.<sup>82</sup> In addition, the identification of novel targets or compounds active on gastric cancer cells is an important field of research.<sup>83</sup> With this aim, and due to the high potency displayed by **34** in the gastric cancer cells HGC-27, together with its interesting selectivity profile observed in other cell lines, we aimed to further examine the molecular mechanisms underlying **34**-mediated cell death.

### 2.1. Cell cycle analysis

The MTT assay reflects viable cells but cannot be employed as a marker of cell proliferation. A decrease in the number of viable cells can be attributable to cell-cycle arrest and/or cell death. To determine whether **34**-induced decrease in cell viability in HGC-27 cells was accompanied by alterations in cell cycle distribution, the percentage of cells in the different stages of cell cycle was analysed by flow cytometry. With this aim, cells were permeabilised after treatment and stained with a propidium iodide solution, a fluorescent dye that stains DNA stoichiometrically. Thus, the fluorescence

intensity of the stained cells correlates with the amount of DNA allowing the differentiation of cells in  $G_0/G_1$ , S phase and  $G_2/M$ . Because propidium iodide also stains double-stranded RNA, the latter is removed by the addition of RNase. The DNA content is then plotted as their frequency histograms to provide information about the percentage of cells in each phase of the cell cycle. Quantification is expressed as the percentage of cells in each phase from total counted events (10.000).<sup>84</sup>



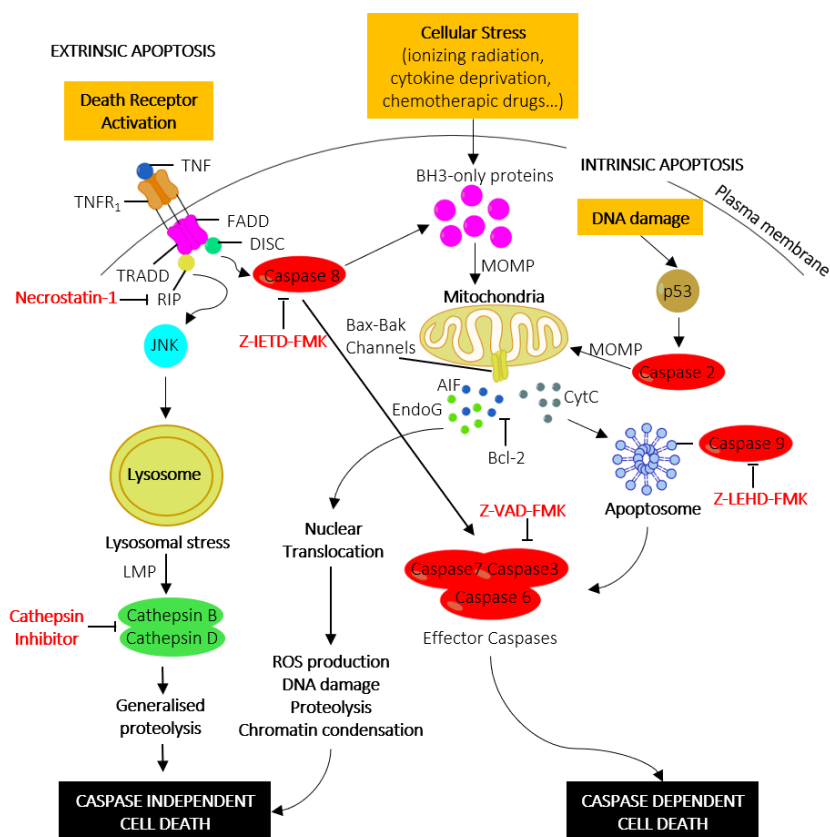
**Figure 8** Cell cycle distribution of HGC-27 cells with or without treatment of compound **34** at 5  $\mu$ M in DMSO for 24 h. Doxorubicin (500 nM) was included as a positive control. The cells were collected and processed for cell cycle analysis. **A**) Histograms of DNA content in each event after treatment with the vehicle or **34**. **B**) Quantification of the relative number of HGC-27 cells in each stage of the cell cycle (Multicycle AV software). Data are the average  $\pm$  SD of three experiments.

As shown in **Figure 8**, treatment with **34** for 24 h in HGC-27 cells induced a significant accumulation of  $G_0/G_1$  cells associated with a decrease in the S- $G_2/M$  cell population,

suggesting that a cell cycle arrest at G<sub>0</sub>/G<sub>1</sub> phase contributes to the observed effect, whereas treatment of cells with Doxorubicin, included as a positive control at 500 nM, resulted in a G<sub>2</sub>/M arrest. Hence, loss of viability observed in the MTT assay may be partially caused for the cell cycle arrest at G<sub>0</sub>/G<sub>1</sub> phase.

## 2.2. Apoptotic cell death study

Cell death can be controlled by several mechanisms or pathways (Figure 9).<sup>85</sup> Therefore, the specific cell death modality caused by **34**, which is mainly apoptosis, necrosis or autophagy, was next investigated. With this aim, the apoptotic effect of **34** on HGC-27 cells was evaluated using an Annexin V-FITC/propidium iodide staining assay and analysing the stained cells by flow cytometry.<sup>86</sup> Briefly, loss of plasma membrane integrity is indicative of cell death and this can be assessed using cell-

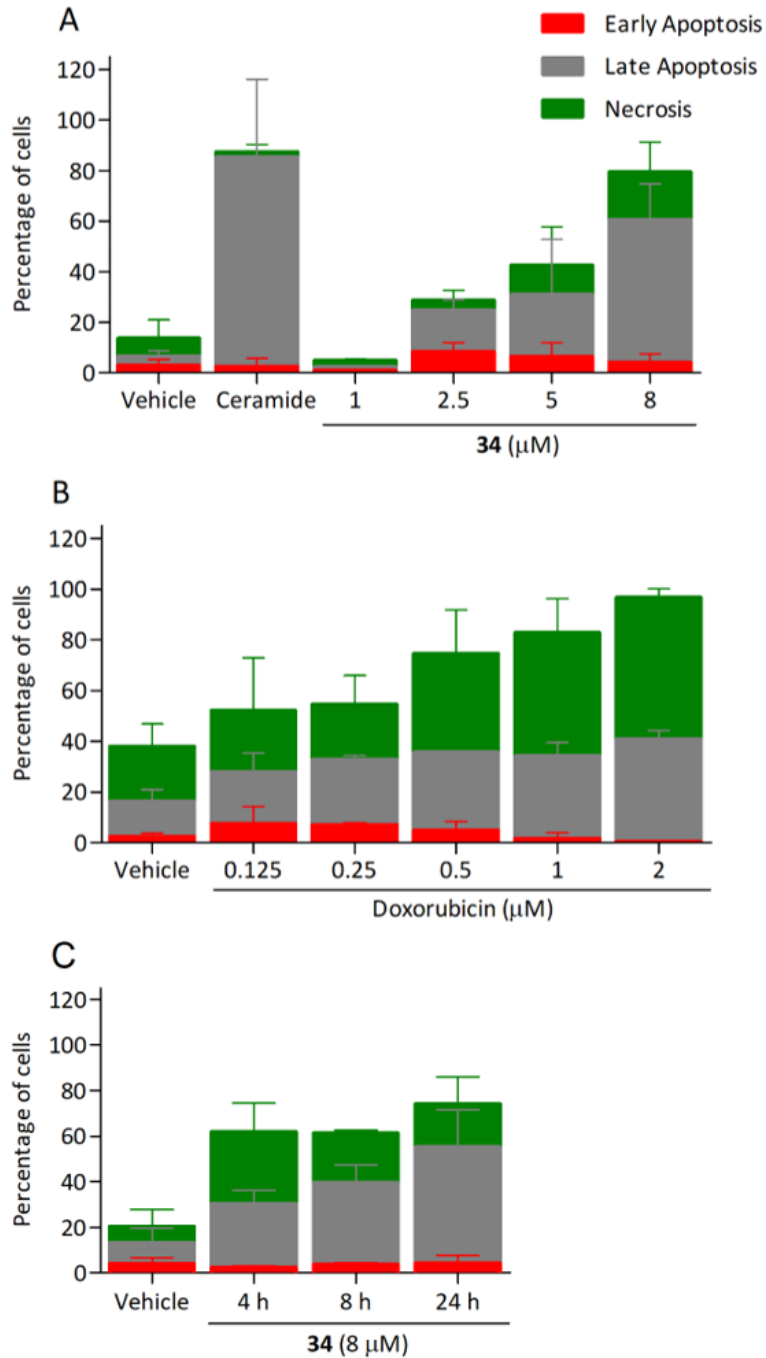


**Figure 9. Extrinsic apoptosis:** This pathway is activated after ligation with the death receptors such as TNFR1, which results in the recruitment of many proteins like FAS-associated death domain (FADD), TNFR1-associated death domain (TRADD) and caspase 8. Caspase 8 can be inhibited by the commercially available compound Z-IETD-FMK. When it is active, it activates the effector caspases or truncates BH3-only protein,

which activates the intrinsic pathway of apoptosis by translocating to mitochondria. Effector caspases are composed by Caspase 3, 6 and 7. Caspase 5 can be inhibited by the commercially available Z-VAD-FMK. **Intrinsic apoptosis:** Mitochondrial outer membrane permeabilization (MOMP) defines this pathway, it results with the release of cytochrome C (Cyt C), apoptosis inducing factor (AIF) and endonuclease G (EndoG). Cytosolic Cyt C lead the assembly of a caspase-activating complex or apoptosome. Caspase 9 involved in the activation of apoptosome can be inhibited with the commercially available Z-LEHD-FMK. MOMP can be induced by the activation of BH3-only proteins or by transcriptional upregulation after p53 activation stimulated by DNA damage. BH3-only proteins produce MOMP through oligomerization of BCL-2-associated protein (Bax) and BCL-2-antagonist or killer (Bak) in the outer mitochondrial membrane, which originates channels to release proteins from mitochondria. AIF and EndoG promote caspase-independent cell death through different processes such as ROS production, DNA damage, proteolysis and chromatin condensation. **Caspase independent cell death** can also be triggered after stimuli that promotes lysosomal membrane permeabilization (LMP) that release cathepsin to the cytosol. Cathepsin can be inhibited by the commercially available Cathepsin inhibitor III. **Necroptosis** is a caspase-independent death pathway that involves the receptor-interacting protein 1 (RIP1), which can be inhibited by the commercially available Necrostatin-1.<sup>87</sup>

impermeable dyes that are able to enter the cell once the integrity of the plasma membrane is lost, such as propidium iodide. Moreover, apoptotic cells expose phosphatidylserine (PS) before membrane rupture, whereas in necrotic cells PS exposure and membrane disruption occurs simultaneously, thus discriminating early and late apoptotic cells as well as necrotic cells. Annexin V is a member of the annexin family of intracellular proteins that binds PS in a calcium-dependent manner. Thus, the fluorescently labelled Annexin V-FITC can be used to specifically identify apoptotic and necrotic cells. To study the effect of **34** on HGC-27 cells, cells were treated with vehicle alone as a control or with **34** at four different concentrations (1, 2.5, 5 and 8  $\mu$ M). The concentrations were selected based on the results obtained in the previous MTT assays. After 24 hours, the samples were doubly stained with Annexin V-FITC and propidium iodide and the percentage of cells was analysed.

**Figure 10A** displays the obtained results. Thus, in the case of HGC-27 cells treated with 1  $\mu$ M, 2.5  $\mu$ M, 5  $\mu$ M and 8  $\mu$ M of **34**, the total percentage of early and late apoptotic cells were 2.4%, 24.7%, 31.0% and 60.1%, respectively. In contrast, only 6.7% of late apoptotic cells were detected in the control cells, which revealed that compound **34** efficiently induces apoptosis in HGC-27 cells in a dose-dependent manner.

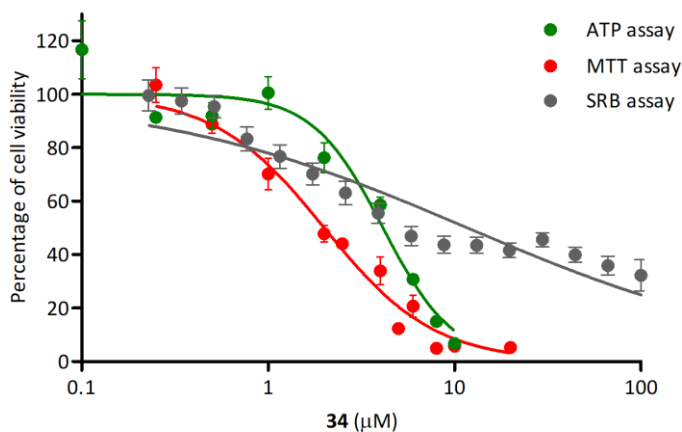


**Figure 10.** Apoptotic effect of compound **34** on HGC-27 cells. Cells were treated with vehicle group (DMSO) or **34** alone. *N*-octanoylsphingosine (C8-Ceramide, 20 μM) was employed as positive control of apoptosis induction in all assays. **A**) Apoptotic dose-dependent effect of **34** after 24 h treatment with Four different concentrations (1, 2.5, 5 and 8 μM). **B**) Apoptotic dose-dependent effect of doxorubicin as positive control for

apoptosis induction. Five different concentrations were analysed (0.125, 0.25, 0.5, 1 and 2  $\mu\text{M}$ ) after 24 h treatment. **C**) Apoptotic time-dependent effect of **34** at 8  $\mu\text{M}$  analysed at 4, 8 and 24 h. After the corresponding time of treatment, the cells were double-stained with Annexin V and propidium iodide and analysed. The percentage of apoptotic and necrotic cells upon incubation with **34** or doxorubicin were quantitated by flow cytometry as described in the experimental section (live cells (bottom left quadrant), early apoptotic cells (bottom right quadrant), late apoptotic cells (upper right quadrant) and necrotic cells (upper left quadrant)). The graph shows the quantitative analysis of necrosis and early and late apoptosis of cells treated with **34**. The data were obtained from three independent experiments.

Doxorubicin and cisplatin have been used for the treatment of gastric cancer, usually in combination with other anticancer agents. Therefore, the effect of doxorubicin in HGC-27 cells was also investigated. To this end, HGC-27 cells were treated with 0.125, 0.25, 0.5, 1 or 2  $\mu\text{M}$  of doxorubicin<sup>88</sup> causing 20.4%, 25.6%, 30.8%, 32.4% and 40.6% of late apoptosis compared to the 13.8% observed in control cells (**Figure 10B**). Moreover, when higher doses were tested early apoptosis resulted decreased in favour of necrosis. To explore whether the effect of squaramide **34** was time-dependent, cells were treated with 8  $\mu\text{M}$  concentration of **34** for 4, 8 and 24 h. Indeed, longer treatments were well correlated with increasing percentages of late apoptosis (27.9%, 35.8% and 51.1% after 4, 8 and 24 h treatment respectively (**Figure 10C**)).

To explain the high doses required to detect cell death compared to the  $\text{IC}_{50}$  values obtained in the MTT assays, the effect of these compounds on cell viability was evaluated by an alternative assay based on the quantification of cellular ATP levels, as indicator of metabolically active cells (CellTiter-Glo<sup>®</sup> Luminescent Cell Viability Assay). Indeed, although  $\text{IC}_{50}$  values resulting from these studies were in a similar range, the dose-dependent curve obtained in the ATP-based analysis was in agreement with concentrations required in cells to cause an apoptotic effect ( $\text{IC}_{50}$  MTT 1.81  $\mu\text{M}$ ,  $\text{IC}_{50}$  ATP 4.13  $\mu\text{M}$ , **Figure 11**). Alternatively, a sulforhodamine B (SRB) assay was also employed to investigate the cytotoxicity of **34**. SRB is a dye that binds proteins under mild acidic conditions, and the amount of detected dye can be correlated to the cell mass.<sup>89</sup> Hence, the SRB assay is independent of the mitochondrial function. In this case, an  $\text{IC}_{50}$  of 9.74  $\mu\text{M}$  was obtained for squaramide **34** in HGC-27 cells (vs 149  $\mu\text{M}$  and 73.85  $\mu\text{M}$  in MDCK and Vero cells respectively). In contrast to the MTT assay that requires cellular metabolic activity and therefore only stains viable cells, SRB stains viable and dead cells, thus giving generally slightly higher  $\text{IC}_{50}$  values (**Figure 11**).<sup>89</sup>



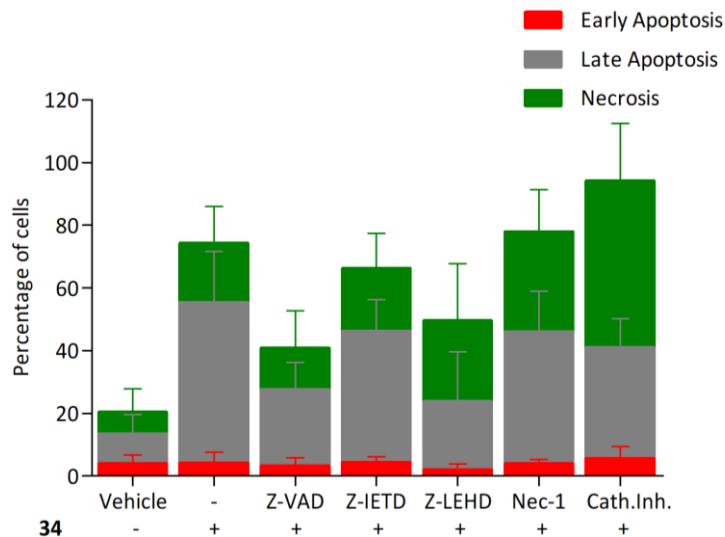
**Figure 11.** Overlapping dose-dependent curves obtained with an ATP-based assay, an MTT assay and an SRB assay show the differences in cell viability at given concentrations. The SRB assay displayed a higher  $IC_{50}$  than the one obtained with the MTT assay, thus suggesting that mitochondrial damage could be partially related with loss of viability.

### 2.3. Caspase-dependent cell death

Apoptosis can be triggered through caspase-dependent or independent mechanisms. To explore whether **34** induces cell death through a caspase-dependent mechanism, Z-VAD-FMK, a pan-caspase inhibitor was employed. Hence, pre-treatment of cells with Z-VAD-FMK (20  $\mu$ M) for 1 h partially prevented **34**-induced cell death (55.3% and 27.6% of total apoptotic cells after treatment with **34** in absence or presence of Z-VAD-FMK respectively), thus suggesting that a caspase-dependent mechanisms may be involved (**Figure 12**).

Apoptosis may be initiated by the extrinsic or the intrinsic signalling pathway. The extrinsic signalling pathways involve death receptors located at the membrane, such as FasL/FasR and TNF- $\alpha$ /TNFR1, the transmission of the signal from the cell surface to intracellular signalling pathways and the implication of caspase 8 (**Figure 9**). The intrinsic pathway is the mitochondrial pathway and may be caused by different stimuli including free radicals, toxins, or hypoxia and involves the activation of caspase 9. The extrinsic pathway and the intrinsic pathway converge on the final execution phase, mediated by the effector caspase 3.<sup>90</sup> Therefore, the implication of both pathways was next investigated by pre-treatment of the cells with a caspase 8 (Z-IETD-FMK) or a caspase 9 (Z-LEHD-FMK) inhibitor. Interestingly, the percentage of apoptotic cells decreased markedly upon treatment with the caspase 9 inhibitor Z-LEHD-FMK, compared to the results obtained with the other caspase inhibitors (46.1% and 23.7% of total apoptotic cells in samples treated with **34** in the presence of Z-IETD-FMK and Z-LEHD-FMK, respectively), thereby suggesting the implication of

the mitochondrial pathway (Figure 12). These results also correlate with the higher IC<sub>50</sub> values obtained using the SRB assay. A slighter decrease in apoptosis rate was also observed when cells were treated with caspase inhibitor Z-IETD-FMK, which could be due to the described cross reactivity for these inhibitors.<sup>91</sup>



**Figure 12.** Apoptotic effect of squaramide **34** on HGC-27 cells. Cells were treated with DMSO (vehicle group) or **34** alone or together with Z-VAD-FMK (Z-VAD, 20  $\mu$ M), Z-IETD-FMK (Z-IETD, 20  $\mu$ M), Z-LEHD-FMK (Z-LEHD, 20  $\mu$ M), Nec-1 (10  $\mu$ M) or Cathepsin inhibitor III (10  $\mu$ M). Cells were pre-treated for 1 h with Z-VAD-FMK, Z-IETD-FMK, Z-LEHD-FMK and Cathepsin inhibitor III (Cath. Inh.) and 3 h with Nec-1 before adding **34**. C8-Ceramide (20  $\mu$ M) was added as a positive control (data not shown). After 24 h of treatment, the cells were double-stained with Annexin V and propidium iodide and analysed. The percentage of apoptotic and necrotic cells upon incubation with **34** were quantitated by flow cytometry as described in the experimental section (live cells (bottom left quadrant), early apoptotic cells (bottom right quadrant), late apoptotic cells (upper right quadrant) and necrotic cells (upper left quadrant)). The graph shows the quantitative analysis of necrosis and early and late apoptosis in cells treated with **34**. The data were obtained from three independent experiments.

## 2.4. Alternative cell death mechanism

### 2.4.1. Cathepsin-dependent cell death

Cell death can also be mediated by lysosomal cathepsin proteases in the so-called lysosomal cell death (LCD). In this process there is a lysosomal membrane permeabilization (LMP), which causes a subsequent release of lysosomal proteases to the cytosol.<sup>92</sup> Extensive LMP leads to uncontrolled necrosis whereas limited LMP can activate caspase-dependent or independent pathways<sup>93</sup> resulting in a cell death that can be prevented upon cathepsin inhibition.



In order to elucidate whether part of the cell death observed in **34**-treated cells was due to a cathepsin-mediated process, cells were incubated with **34** in the presence or absence of a cathepsin inhibitor cocktail (Cathepsin inhibitor III, EMD Millipore) which primarily targets cathepsin B. The extent of cell death was then measured by an Annexin V-FITC/propidium iodide staining assay. As shown in **Figure 12**, the presence of the cathepsin inhibitor did not have any effect on the percentage of live cells but on the contrary it dramatically induced necrosis on HGC-27 cells (18.9% of necrotic cells after **34** treatment and 46.4% of necrotic cells after combined treatment with **34** and the cathepsin inhibitor). Treatment of HGC-27 cells with the Cathepsin inhibitor III alone did not have remarkable apoptotic effects (not shown). The increased toxicity observed after concomitant treatment with **34** and the Cathepsin Inhibitor cocktail suggest a yet unknown synergic effect. All in all, the obtained results discard the involvement of LCD in the molecular mechanism responsible for **34** effects.

### 2.4.2. Necrosis

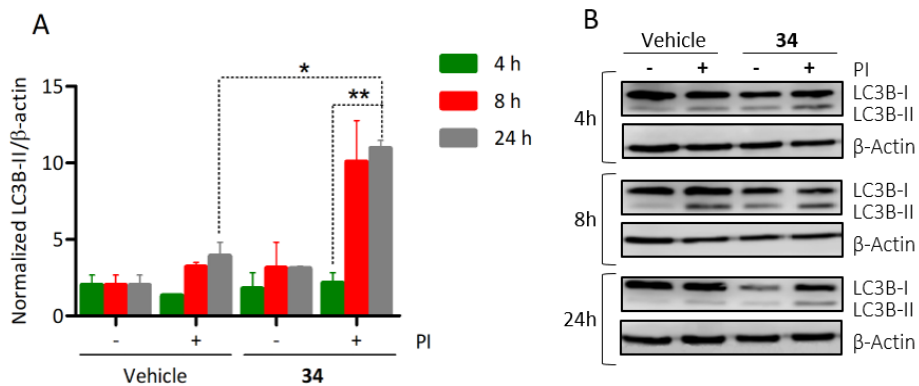
Initial cell death analysis by flow cytometry studies revealed that **34** also causes a significant increase in the number of necrotic cells (14.8%, **Figure 12**). Necrosis can be primary or secondary. Secondary necrotic cells follow apoptosis, whereas primary necrosis, also termed necroptosis, is a non-apoptotic programmed cell death that is mediated by kinases of the receptor interacting protein (RIP) family.<sup>94</sup> Hence, we then investigated if necroptosis could contribute to the caspase-independent cell death. With this aim, HGC-27 cells were pre-treated with Necrostatin-1 (Nec-1) a RIP1 inhibitor that blocks this pathway. Thus, if necroptosis was involved, a decrease in the percentage of necrotic cells should be expected. Interestingly, the necrosis induced by **34** turned out to be not Nec-1 sensitive (32.0 % of necrotic cells in the population treated with **34** in the presence of Nec-1, **Figure 12**). These results discard the involvement of necroptosis as a cell death method and suggest that the necrotic cells observed in the flow cytometry analysis were probably post-apoptotic cells.

### 2.4.3. Autophagy

Apart from apoptosis or necrosis, another mechanism of programmed cell death is associated with excessive levels of autophagy in a process known as autophagic cell death (ACD) or autosis.<sup>95</sup> Considering that an autophagic pathway could play a role in **34**-mediated effect, we determined whether this compound induced autophagy in HGC-27 cells and how this process might impact on cellular fate. Therefore, the effects of squaramide **34** on autophagy were evaluated by assessing a key marker of this process, LC3-II. During autophagosome formation, microtubule-associated protein 1 light chain 3 (LC3-I) gets lipidated at the C-terminus with a phosphatidylethanolamine (PE) unit (LC3-II) and it is subsequently associated with the autophagosome membrane. Since the amount of accumulated LC3-II correlates well with the number of autophagosomes, levels of this protein have been widely

employed to monitor autophagy. However, LC3 accumulation can occur as a result of autophagy induction or due to impairment of the lysosomal function. Moreover, certain cells present a high basal autophagic flux, and as a consequence, autophagy induction does not cause a clear LC3-II accumulation.<sup>96</sup> To discard these possibilities, LC3-II levels were also measured upon inhibition of lysosomal proteases (protease inhibitors (PI)) in order to arrest the physiological LC3-II degradation and thus, correctly quantify the so-called autophagic flux.<sup>97</sup>

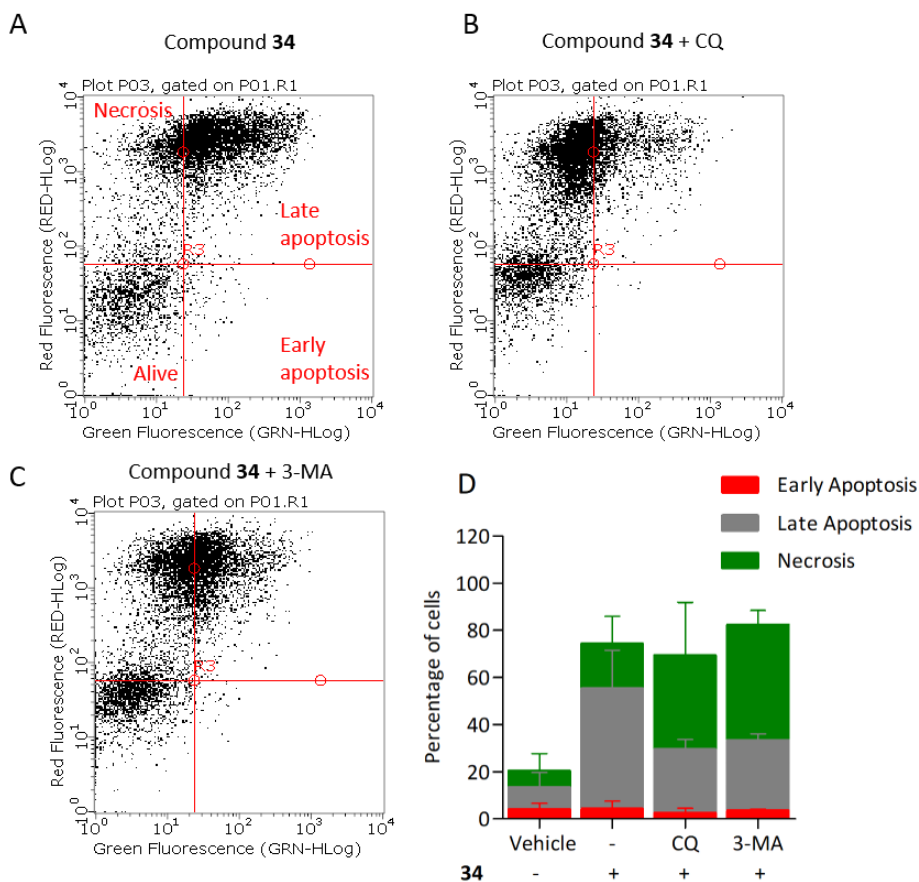
To this end, HGC-27 cells were treated with **34** for 4, 8 and 24 h, and the cell lysates were subjected to Western blotting to determine changes in expression of LC3B-II. As shown in **Figure 13**, these studies revealed a minor accumulation of LC3B-II in **34**-treated cells and a pronounced accumulation cells treated also with protease inhibitors. The increase was more considerable after 8 and 24 h of treatment, but not after short treatments. These results indicate a correct autophagic flux and an unmasked LC3B-II accumulation probably due to its rapid turnover, thereby confirming an important autophagy induction.



**Figure 13.** HGC-27 cells were exposed to 2  $\mu$ M of **34** for 4, 8 and 24 h. **A)** Bar chart shows the quantification of LC3B-II protein levels respect to the  $\beta$ -actin control. **B)** Protein levels of LC3B-II and  $\beta$ -actin were assessed by Western blotting of cell lysates as described in Materials and Methods. Representative blots of two independent experiments with similar results.

Although it has been proven that autophagy can contribute to cell death,<sup>98</sup> there is still controversial whether it is a cell death caused by autophagy or a cell death accompanied by an induction of autophagy that may exert a survival or cytoprotective effect.<sup>99,100</sup> To determine how this autophagy induction impacts on cell fate, it was next investigated whether autophagy plays a causative role in preventing **34**-induced cell death by including autophagy inhibitors in these studies. Thus, two autophagy inhibitors were used, chloroquine (CQ), a lysosomotropic agent that impairs

lysosomal function that it is involved in the last steps of autophagy, and 3-methyladenine (3-MA), a pan-inhibitor of the lipid kinase phosphatidylinositol 3-kinase (PI3K) involved in the first steps of autophagosome formation. The percentage of apoptotic/necrotic and live cells upon autophagy inhibition was then analysed.



**Figure 14.** HGC-27 cells were exposed to **34** for 24 h. Effect of autophagy inhibition on apoptosis/necrosis of treated HGC-27 cells. Cells were treated with DMSO (vehicle group), 8  $\mu$ M of **34** alone (A) or Chloroquine (CQ, 50  $\mu$ M in EtOH) (B) or 3-methyladenine (3-MA, 2 mM in DMSO) (C). The cells were pre-treated for 2 h with CQ or 3 h with 3-MA before adding **34**. After 24 h of treatment, the cells were double-stained with Annexin V and propidium iodide and analysed. The percentage of apoptotic and necrotic cells upon incubation with **34** were quantitated by flow cytometry as described in the experimental section (live cells (bottom left quadrant), early apoptotic cells (bottom right quadrant), late apoptotic cells (upper right quadrant) and necrotic cells (upper left quadrant)). The bar chart (D) shows the quantitative analysis of necrosis and early and late apoptosis in cells treated with **34**. The data were obtained from three independent experiments.

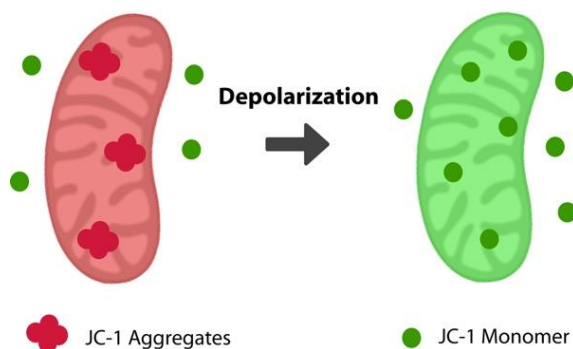
As shown in **Figure 14**, co-treatment of **34** with autophagy inhibitors such as CQ or

3-MA did not increase the number of live cells, but on the contrary significantly increased the number of necrotic cells (18.9%, 39.8%, 48.9% of necrotic cells treated with **34** alone or together with CQ or 3-MA, respectively). Taken all together, the data described above suggest that autophagy is triggered by **34** exposure in HGC-27 cells as a protective response to alleviate its cytotoxicity. Moreover, since cathepsin inhibition also causes lysosomal dysfunction, this observation correlates well with the increased cell death previously noted in cells treated with cathepsin inhibitors (74.2% and 94.1% of total apoptotic and necrotic cells in **34** in absence or presence of cathepsin inhibitors, respectively).

## 2.5. Mitochondria and ROS

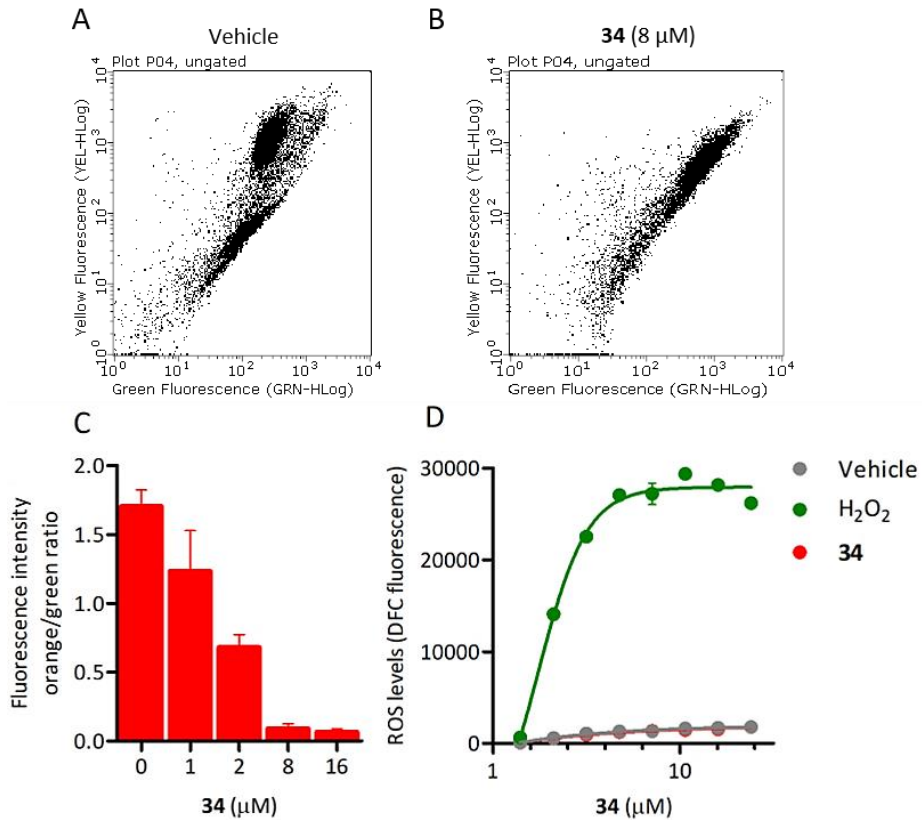
MTT assays measure the activity of succinate dehydrogenase, a mitochondrial enzyme, hence reflecting the activity status of this organelle and suggesting that differences observed in both cell viability methods employed above (MTT vs ATP-based assay and SRB assay) may be caused by mitochondrial damage. This hypothesis would also be in agreement with the increased viability upon treatment with the caspase 9 inhibitor, marker of the intrinsic mitochondrial pathway.

If the intrinsic mitochondrial pathway is activated, it results in alterations in the inner mitochondrial membrane which causes changes in transmembrane potential, loss of membrane permeability and activation of caspases. Therefore, the mitochondrial membrane potential in HGC-27 cells treated with squaramide **34** was next investigated. JC-1 (5,5',6,6'-tetrachloro-1,1',3,3'-tetraethylbenzimidazolylcarbocyanine iodide) accumulates as aggregates in the mitochondria (red/orange colour) and its colour changes from orange to green fluorescence in case of depolarization of mitochondrial membrane potential. JC-1 diffuses to the cytosol and the low concentration results in the formation of monomers (Figure 15).<sup>101</sup> Therefore, JC-1 has been widely used to detect mitochondrial depolarization during apoptosis.



**Figure 15.** JC-1 shows a concentration dependent colour shift. Thus, JC-1 concentrates into

mitochondria and forms aggregates yielding a red/orange coloured emission at  $\lambda_{em}$  of 590 nm. In case of low mitochondrial membrane potential JC-1 diffuses to the cytosol forming monomeric species that yields green fluorescence ( $\lambda_{em}$  of 530 nm).



**Figure 16** Mitochondrial membrane potential measured in HGC-27 cells after treatments with the vehicle (A) and **34** (B) for 24 h, it was evaluated by JC-1 staining and flow cytometry analysis. An increase in yellow/orange fluorescence was observed in **34**-treated cells. C) Quantification of the orange/green ratio of HGC-27 cells treated with increasing concentrations (0-16  $\mu$ M) for 24 h. Data are the average  $\pm$  SD of three experiments. D) Detection of intracellular ROS levels in HGC-27 cells exposed to increased concentrations of H<sub>2</sub>O<sub>2</sub> and **34** for 5 h.

The results showed that **34** efficiently caused mitochondrial membrane depolarization (Figure 16A-C). When  $\Delta\psi_m$  levels were assessed quantitatively by the ratio of orange/green fluorescence intensity, there was a significant reduction of  $\Delta\psi_m$  in HGC-27 cells compared to control cells after a 1  $\mu$ M, 2  $\mu$ M, 8  $\mu$ M or 16  $\mu$ M treatment for 24 h, which indicates that compound **34** induces  $\Delta\psi_m$  changes in HGC-27 cells during apoptosis. These results confirmed the implication of the intrinsic pathway in the **34**-mediated cell death.

Reactive oxygen species (ROS) are known triggers of the intrinsic apoptotic cascade.<sup>102</sup> Therefore, oxidative damage caused by the generation of ROS may be one of the underlying mechanisms of **34**-mediated cell death. Thus, to elucidate whether oxidative stress mediated by ROS generation plays a critical role in the onset of cell death caused by **34**, we determined the changes of the intracellular redox potential after treatment with **34** during 5 h by employing the fluorescent probe 2',7'-dichlorofluorescein diacetate (DCFH-DA). This probe is converted to highly fluorescent dichlorofluorescein (DCF) in the presence of intracellular ROS. As depicted in (Figure 16D), the formation highly increased after H<sub>2</sub>O<sub>2</sub> treatment, employed as a positive control, whereas no remarkable increase in ROS formation could be detected in cells treated with compound **34**, thus discarding the implication of oxidative damage in the molecular mechanism responsible for **34**-mediated cell death.

### 3. Summary and conclusions

The cellular screening of a library of squaramides and squaramates has enabled the identification of compound **34**, effectively and specifically inhibiting the cell proliferation of the gastric cell line HGC-27 in a concentration-dependent manner. The mechanism of action of this probe was next investigated. Two simultaneous pathways were affected including a G<sub>0</sub>/G<sub>1</sub> cell cycle arrest and an induction of apoptosis dependent of caspases that implicates the activation of the intrinsic pathway and the subsequent mitochondrial membrane depolarization. The implication of ROS as initiating stimuli for the activation of the intrinsic pathway has been discarded, suggesting that other stimuli or pro-apoptotic proteins may be involved. Apart from the observed caspase-dependent apoptosis, no sign of cathepsin mediated cell death and necroptosis could be detected. Although an induction of autophagy has been observed, it has been determined that it plays a protective role since there is no increase in the number of living cells when cells are simultaneously treated with autophagy inhibitors. Since the identification of compounds inducing a specific cell death subroutine are preferred to avoid side-effects and non-specific cytotoxic effects, the squaramide **34** can be considered a promising agent for the treatment of gastric carcinomas. An in-depth study to identify the molecular targets responsible for the observed effects would be of great interest and contribute to the identification of attractive targets for the treatment of gastric cancer.



# CONCLUSIONS





Based on the results obtained in this chapter, one active squaramide against gastric carcinoma was selected and studied in more detail. The following assessments could be concluded from the research done:

- The squaramide **34** was selected from a library of squaramides and squaramates due to the low IC<sub>50</sub> displayed after 24 and 48 h treatments in HGC-27 cells, cancer cells derived from the metastatic lymph node of gastric carcinoma
- Two mechanisms were observed to take place: a G<sub>0</sub>/G<sub>1</sub> cell cycle arrest and the induction of apoptosis dependent of caspases, though the activation of the intrinsic pathway together with mitochondrial membrane depolarization.
- The implication of ROS as initiating stimuli for the activation of the intrinsic pathway has been discarded, therefore, other stimuli of pro-apoptotic proteins may be involved.
- The implication of cathepsin mediated cell death and necroptosis were discarded.
- An induction of autophagy has been detected, although it has been determined that it plays a protective role since there is no increment of living cells after treatment with autophagy inhibitors.
- The squaramide **34** can be considered a promising agent for the treatment of gastric carcinomas since the identification of compounds inducing a specific cell death subroutine are preferred to avoid side-effects and non-specific cytotoxic effects.
- The identification of the cellular targets of **34** would be of great interest, enabling a more straightforward improvement of its properties and potency as well as the identification of attractive and novel targets for the treatment of gastric carcinoma



# CHAPTER 2:

DEVELOPMENT OF AN ALPHASCREEN-BASED HTS ASSAY,  
SCREENING AND BIOLOGICAL EVALUATION OF ATG4B  
INHIBITORS AS NOVEL ANTICANCER AGENTS



# INTRODUCTION



The term autophagy, referred as macroautophagy, comes from ancient Greek “phagein” meaning to eat, and “auto”, meaning self. It was first coined by Christian de Duve during his seminal work on the discovery of lysosomes in the 1950s. For this work he was awarded the Nobel Prize in Physiology or Medicine in 1974 along with George Palade and Albert Claude. Autophagy is an evolutionary conserved cellular pathway that controls protein and organelle degradation by delivering cytoplasmic components into mammalian lysosomes or plant and yeast vacuoles for their degradation. In eukaryotic cells, two pathways are mostly responsible for the degradation of cellular proteins: the ubiquitin-proteasome system, which generally degrades 80-90% of damaged proteins,<sup>103</sup> and autophagy, that degrades intracellular misfolded, long-lived or aggregated proteins and superfluous or damaged cellular organelles. The resulting metabolites can be then reused into sources of energy or building blocks for the synthesis of new macromolecules.<sup>104</sup> This recycling process allows the cell to degrade also invading microorganisms<sup>105</sup> and has several essential functions for the cell physiology.

## 1. Types of autophagy

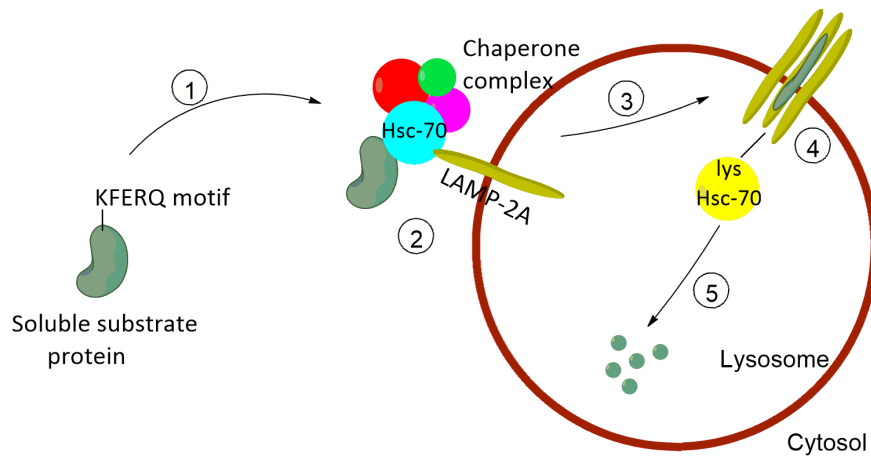
Autophagy has been classified into three main groups: the non-selective macroautophagy and microautophagy and the selective chaperone-mediated autophagy. In addition, other forms of selective autophagy have been described including mitophagy, lipophagy, pexophagy, erphagy, or ribophagy (removal of damaged mitochondria, lipid droplets, peroxisomes, endoplasmic reticulum (ER) and ribosomes, respectively).

**Microautophagy** is referred to the transfer of cytosolic components into lysosomes by direct invagination of the lysosomal membrane.<sup>106</sup> Its functions are the maintenance of organellar size, membrane homeostasis and cell survival under nitrogen deprivation. The lysosomal/vacuolar membrane is randomly invaginated and differentiated into the autophagic tube and encloses portions of cytosol. Vesicles formed at the top of the tube fuse and go to the lumen.<sup>107</sup>

**Chaperone-mediated autophagy (CMA)** (**Figure 17**) is a selective form of autophagy that modulates the turnover of a specific pool of soluble cytosolic proteins.<sup>108</sup> In this type of autophagy, the proteins are identified by a cytosolic chaperone that release them to the surface of lysosomes, then the proteins unfold and cross the lysosomal membrane.<sup>109</sup> All the proteins to be degraded contain in their amino acid sequence a pentapeptide motif (KFERQ) that is necessary for their targeting to lysosomes. Proteins with this pentapeptide KFERQ-like sequence are recognized by the Heat shock cognate 70 (Hsc70) chaperone. This protein associates with the integral lysosome-associated membrane protein 2A (LAMP-2A) that catalyses its oligomerization with chaperones, what results in unfolding and translocation of the



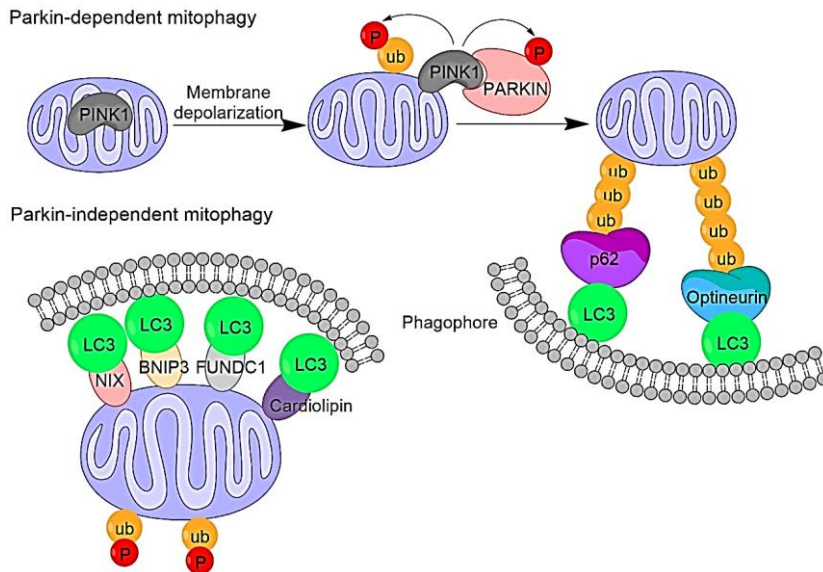
bound protein into the lysosome.<sup>105</sup>



**Figure 17.** Chaperone-mediated autophagy is a selective form of autophagy in which single soluble proteins are directed one-by-one to lysosomes for degradation. The steps are: **1)** Binding of Hsc70 to the targeting motif in the substrate protein. **2)** Delivery to LAMP-2A, the chaperone-mediated autophagy receptor at the lysosomal membrane. **3)** Unfolding of substrate protein. **4)** Translocation across the lysosomal membrane by the lysosomal resident form of Hsc70. **5)** Degradation by the lysosomal proteases.

**Mitophagy** is a selective type of autophagy directed to remove dysfunctional or superfluous mitochondria. Mitochondrial turnover is necessary for cellular homeostasis and differentiation. As a result, these organelles are replaced every 2-4 weeks. This process occurs through mitophagy that can be mediated by the ubiquitin E3 ligase Parkin that translocates into damaged mitochondria in a process that requires PINK1 ((PTEN)-induced putative kinase 1) expression (ubiquitin E3 ligase are proteins that mediate the covalent linkage between the target protein and ubiquitin moieties). Once translocated to the mitochondrial surface, Parkin ubiquitinates numerous proteins and initiates the clearance of damaged mitochondria via autophagy (**Figure 18**).<sup>110</sup> Gp78, SMURF1, SIAH1, MUL1 and ARIH1 are alternative ubiquitin E3 ligases that target mitochondrial proteins. When these proteins are located in the mitochondrial surface, ubiquitination promotes the recruitment of autophagic receptors such as optineurin (OPTN), nuclear dot protein 52 (NDP52) and p62 (also known as SQSTM1). PINK1 and Parkin are mutated in some types of Parkinson's disease, thus indicating that mitochondrial damage has a key role in this disorder.<sup>111</sup> Mitophagy can also be Parkin-independent. In that case, receptors on the outer mitochondrial membrane surface such as BNIP3, NIX, FUNDC1 or the lipid cardiolipin interact with LC3/GABARAP resulting in the recruiting of damaged mitochondria to autophagosomes (**Figure 18**).<sup>110,112,113,114</sup> More recently, it has been described that the interaction of ceramide with LC3B-II also results in selective

targeting of mitochondria to autophagosomes causing mitophagy and autophagic cell death.<sup>115</sup>



**Figure 18. Parkin-dependent mitophagy.** In case of depolarized mitochondria, Parkin is translocated to the outer membrane. This process is regulated by PINK1. Once Parkin translocates to mitochondria, it promotes selective mitophagy mediated by protein ubiquitination and recruitment of autophagy receptor proteins like p62 and optineurin, which further recruit LC3-positive autophagosomes. **Parkin-independent mitophagy.** In the absence of Parkin, different proteins such as BNIP3, NIX, FUNDC1 or the lipid cardiolipin directly interact with LC3 resulting in the recruitment of autophagosomes to the damaged mitochondria.<sup>114</sup>

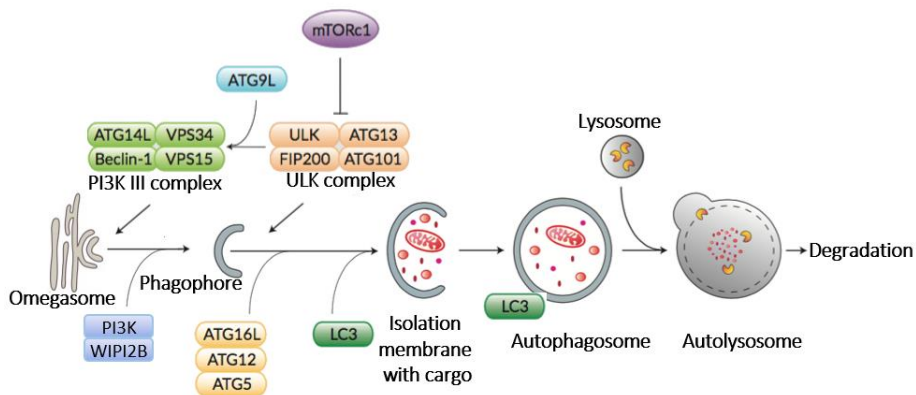
**Pexophagy** is another type of selective autophagy. It was initially observed in the yeast *Pichia pastoris* in a process involving autophagy related (Atg) proteins such as Atg24, Atg25 and Atg26 (see below).<sup>112</sup> In recent years, mammalian pexophagy has also been described.<sup>116</sup> The relation between autophagy and peroxisome turnover was established with an ATG7-knockout mice, showing that this autophagy essential gene leads also to defects in pexophagy.<sup>117</sup> In both yeast and mammal cells, pexophagy has shown to be the principal peroxisome degradation system.

Several autophagy related (ATG) genes also participate in the cytoplasm-to-vacuole targeting (Cvt) pathway, which is a non-degradative process for protein transportation observed only in yeast. Proteins are synthesized in the cytosol and packed into Cvt vesicles that fuse with vacuoles, where the proteins are processed to their active form. This pathway involves Atg proteins such as Atg11, Atg19, Atg20 and Atg21.<sup>112</sup>

**Lipophagy** is another selective degradation process of cellular organelles. During times of nutrient sufficiency, cells store lipids in the form of lipid droplets. A lipid droplet is an *organelle* composed of a neutral lipid core of triglycerides and cholesteryl esters enclosed in a phospholipid monolayer with a family of coat proteins named as perilipins. Lipophagy is an essential process observed in many different cell types, such as hepatocytes, glial cells, fibroblast and adipocytes, and based on the selective autophagy of lipid droplets. Its activation is cell-type dependent. In liver, lipophagy is activated during fasting, whereas in neurons it is used to get free fatty acids and activate pathways that ultimately stimulate feeding.<sup>118</sup> The exact mechanisms regulating lipophagy remain unknown but an enrichment of autophagosomal LC3-II has been observed in lipid droplets from fasted mice, thus indicating a role of this autophagy marker in the consumption of lipid droplets.<sup>118</sup>

### 1.1. Macroautophagy

Macroautophagy, hereafter referred to as autophagy, is a crucial process to maintain the cellular homeostasis through degradation of cytoplasmic contents, protein aggregates and organelles. This recycling mechanism begins with the formation of a double-membrane called phagophore which is then elongated around a portion of cytosol. It eventually closes engulfing the cargo to be degraded to form the autophagosome, which ultimately fuses with a lysosome to form the autolysosome (**Figure 19**). Lysosomal hydrolases in the autophagolysosome digest its cargo. Autophagy can be induced both by extracellular and intracellular signals including oxidative stress, growth factor withdrawal, hypoxia, ceramide, ER stress, pathogen infection and glucose, amino acid and serum starvation.



**Figure 19.** Schematic simplified model of autophagosome formation and degradation of cargo including the key proteins involved. Autophagy starts with the formation of an omegasome probably formed at the ER which becomes the phagophore, an isolation double-membrane. The ULK1 complex is involved in this initial steps. The phagophore then elongates engulfing the cytoplasmic cargo to be degraded. Class III PI3K, Atg9 and

lipidated LC3-II participate in the autophagosome formation. Once it is closed, the autophagosome fuses with lysosomes forming the autophagolysosome. Macromolecules and obsolete organelles are then degraded by lysosomal hydrolases. Recycling of the resulting macromolecules is carried out by permeases.<sup>119</sup>

Non-selective macroautophagy is primarily a starvation response that randomly engulf cytoplasmic cargo for degradation. However, cells can also use selective macroautophagy for specific elimination of proteins and organelles. Selective methods for organelles clearance have been described above. The selective elimination of proteins relies on autophagic receptors such as p62, NBR1, NDP52, OPTN, histone deacetylase (HDAC6) or NIX. These receptors recognize ubiquitinated proteins and deliver them directly to the core autophagic machinery. Deregulation of autophagy is implicated in the onset of various diseases including tumorigenesis, neurodegenerative disorders, cardiomyopathy, Crohn's disease, fatty liver, type II diabetes and ageing.<sup>112</sup> Therefore, new tools and modulators of autophagy are crucial for elucidating the molecular mechanisms deregulated in diseases and can potentially lead to novel therapeutic agents and strategies.

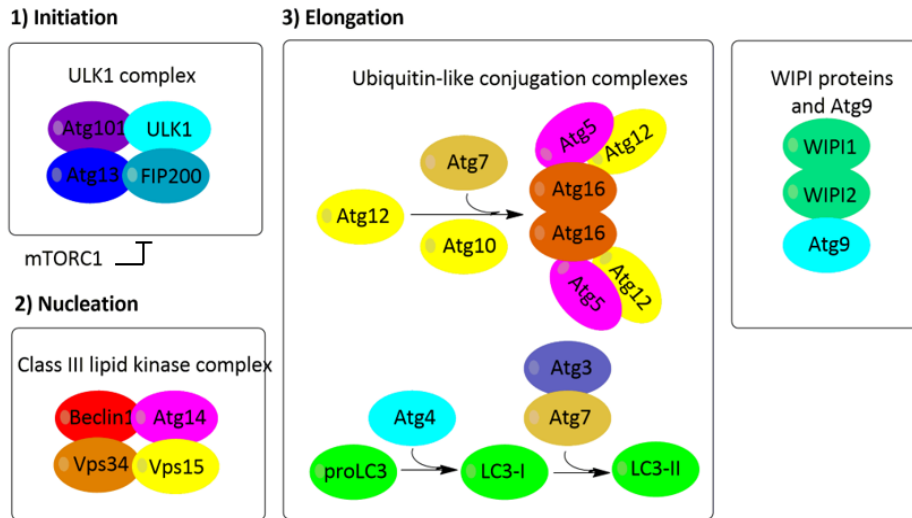
### 1.1.1. Autophagosome formation

#### *Core proteins*

The formation of the autophagosome includes different steps, i.e. initiation, phagophore nucleation, elongation and closure of the double membrane vesicle (**Figure 19**). The membrane source of the nascent phagophore membrane remains controversial and may include the endoplasmic reticulum (ER exit sites, ERES),<sup>120</sup> the Golgi complex, the ER-Golgi intermediate compartment, mitochondria, recycling endosomes, the nuclear membrane and the plasma membrane.<sup>121</sup>

In the last decade significant advances have been made in the identification of the molecular machinery regulating autophagy. Seminal key studies performed in yeast in 1993 by Yoshinori Ohsumi led to the characterization of the so-called autophagy related genes/proteins (ATG/Atg<sup>122</sup>).<sup>123</sup> This initial screen led to the identification of 15 genes involved in the regulation of autophagy, but today 41 yeast ATG genes have been described and most of them have orthologues in humans. This discovery opened the path to understanding the importance of autophagy in many physiological and pathological processes. As a result, Yoshinori Ohsumi was awarded in 2016 the Nobel Prize in Physiology or Medicine for his overall work aimed at elucidating the underlying mechanisms of autophagy. However, these proteins do not seem to be exclusively involved in autophagy and may present unravelled functions in non-autophagic processes.<sup>124</sup> In addition, other non-Atg proteins are also involved in this process. Thus, autophagy is orchestrated by a myriad of proteins, which usually form functional multiprotein complexes (**Figure 20**).<sup>125,112</sup> The role of these proteins

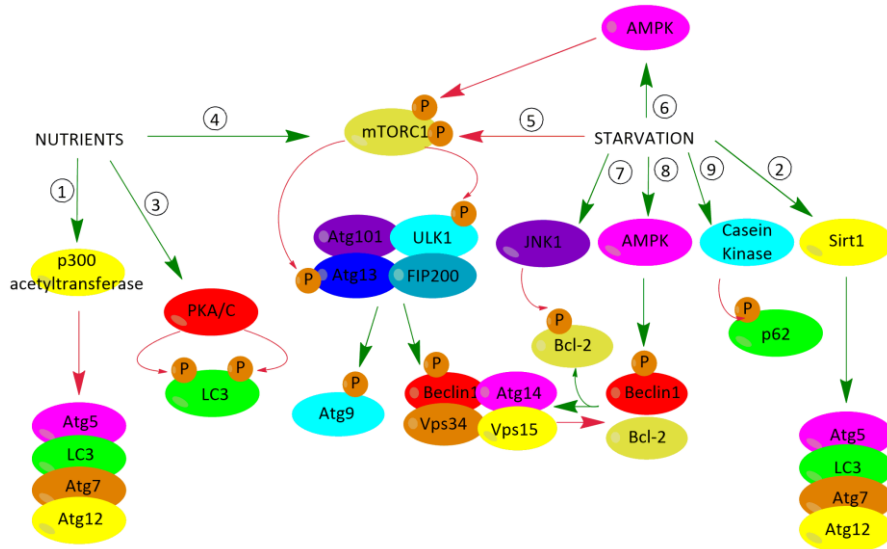
and complexes will be briefly discussed below.



**Figure 20.** Core proteins involved in autophagy. **1) Initiation.** ULK1 complex is responsible for the initiation of autophagy upon generation of the phagophore. It is negatively regulated by mTORC1. **2) Nucleation.** A class III lipid kinase complex regulates the autophagosome formation and nucleation. **3) Elongation.** Two ubiquitin-like conjugation systems mediate the elongation of the autophagosome. WIPI proteins and Atg9 are also involved in this elongation step.<sup>126</sup>

- *ULK1-Atg13-FIP200-Atg101/ULK complex, a serine-threonine kinase complex*

**Initiation** under nutrient deprivation is tightly controlled by the mammalian target of rapamycin (mTOR), the protein kinase A (PKA) and the AMP-activated protein kinase (AMPK), which converge at the ULK1 kinase complex, the mammal homologs of the yeast Atg1. The mTOR complex 1 (mTORC1) is the most studied regulator. This kinase negatively regulates autophagy by inhibiting the ULK1 complex through direct phosphorylation. In the presence of nutrients, amino acids and growth factors, mTORC1 is stimulated, whereas in case of starvation, levels of ATP decrease and mTORC1 becomes inhibited via AMPK phosphorylation (AMPK is a sensor of cellular energy levels and is activated by a high AMP/ATP ratio, (Figure 19 and Figure 21).<sup>105</sup>



**Figure 21.** Schematic representation of the proteins involved in the regulation of autophagy. Red arrows indicate inhibition, green arrows activation. Under normal conditions autophagy is downregulated: p300 acetyltransferase acetylates several proteins such as Atg5, LC3, Atg7 and Atg12 (1), whereas Sirt1 deacetylates and therefore, upregulates the same proteins in case of nutrient deprivation (2). PKA can also produce less recruitment of LC3 by the autophagosome through LC3 phosphorylation which inhibits its lipidation. Protein kinase C (PKC) can also phosphorylate LC3 but no effect in autophagy flux has been observed<sup>127</sup> (3). In the presence of nutrients, mTORC1 negatively regulates autophagy through ULK1 phosphorylation (4). In case of starvation, mTORC1 becomes phosphorylated and inactivated by AMPK (6) or other proteins such as protein kinase B, also known as Akt (5), leading to the release of ULK1/Atg1 complex, its dephosphorylation and the activation of ULK1 kinase activity. AMPK is an energy sensor that gets activated when increases the AMP/ATP ratio due to nutrient deficiency or hypoxia. The mechanism by which Atg9 travels through different cellular localizations is still unclear but it is known that the ULK1 complex directly phosphorylates Atg9, which is crucial for autophagosome formation. The ULK1 complex also recruits the class III PI3K complex to form the phagophore. Under nutrient excess conditions, Bcl-2 binds beclin 1 and inhibits autophagy, whereas during starvation AMPK phosphorylates it, which promotes the incorporation on class I PI3K complex (7). After nutrient depletion, Bcl-2 is phosphorylated in three different sites causing the dissociation from beclin 1 and thus, it induces autophagy (8). Casein kinase phosphorylates p62 increasing its affinity for ubiquitinated substrates, which potencies autophagy (9).

mTOR blockage activates the ULK1 complex formed by ULK1, Atg13, Focal adhesion kinase family Interacting Protein of 200 kDa (FIP200, partially homologous to Atg17) and Atg101. ULK1 is phosphorylated and stabilised by FIP200 and Atg101 stabilises the phosphorylation of ULK1 and Atg13. The ULK1 complex induces **vesicle nucleation**

which will be then mediated by the recruited class III PI3K complex formed by Atg14, Vps34, Vps15 and beclin 1 (**Figure 19** and **Figure 21**). Phosphorylation of beclin 1 by ULK1 facilitates the localization of the protein to the phagophore.<sup>128</sup> The PI3K complex also modulates autophagy induction through beclin 1 and by the generation of phosphatidylinositol 3 phosphate (PtdIns3P), which becomes the entrance signal for autophagosome formation. In case of nutrient deprivation, c-Jun *N*-terminal kinase (JNK1) causes the dissociation of beclin 1 and Bcl-2, allowing beclin 1 to associate with the PI3K complex. AMPK also stimulates autophagy in response to glucose starvation by phosphorylating Bcl-2 on an amino acid different to that of the inhibitory kinases, that modifications enhances beclin 1 incorporation into the PI3K complex (**Figure 21**).<sup>105</sup>

- *WIPI proteins and Atg9*

Atg9 it is the only transmembrane protein identified in the yeast autophagic protein machinery. Two orthologs can be found in mammals, mAtg9/Atg9L1 (expressed ubiquitously) and Atg9L2 (specific for the placenta and pituitary gland). If there are enough nutrients, mAtg9 is located in the trans-Golgi region and partially in the endosomes, but under starvation conditions gets located in autophagosomes by a process depending on ULK1. These dynamic cycling between multiples subcellular localizations suggest that these protein may provide donor membrane for **expansion** of the phagophore. The other member of the complex is the human WD-repeat protein interacting with phosphoinositides (WIPI) family proteins, which accumulate in the ER upon interaction with the generated PtdIns3P and become part of the initially formed phagophore. Once in the membrane, WIPI proteins promote the recruitment of the Atg16L complex required for the LC3 lipidation (**Figure 21**).

- *Class III phosphatidylinositol 3-kinase complexes*

Different lipid kinases complexes are involved in autophagy:

- The Atg14-Vps34-Vps15-beclin 1 complex already mentioned above is essential for autophagosome formation and it also enhances autophagosome maturation and endocytic traffic.
- The UV irradiation resistance associated gene (UVRAG)-beclin 1-Vps34 complex facilitates autophagosome maturation and fusion with the lysosome. The interaction of Rubicon with the complex blocks the fusion between autophagosome and lysosome.

- *Ubiquitin-like conjugation complexes*

Two ubiquitin-like conjugation systems are required for membrane **elongation and maturation**. The first one involves Atg7 and Atg10 and is responsible for the formation of the Atg5-Atg12-Atg16L complex. The second one consists of Atg4, Atg3 and Atg7. These proteins drive the lipidation of the Atg8 family members (LC3A, B and C, GABARAP, GABARAPL1, and GABARAPL2/GATE-16) (**Figure 19**). The generated LC3-II, conjugated to a phosphatidylethanolamine unit at the C-terminus, gets associated to the autophagosome membrane and it is essential for autophagosome formation.

These protein complexes are an additional key regulatory points.<sup>129</sup> LC3 lipidation can be blocked by phosphorylation by PKA and PKC<sup>127</sup> and phosphorylation of p62 by the casein kinase 2 favours its interaction with ubiquitinated proteins.<sup>130</sup> Some Atg proteins can be also regulated by acetylation. This is the case of Atg5, Atg7, LC3 and Atg12, which are acetylated by p300 acetyltransferase in nutrient rich conditions, and deacetylated by Sirt1 in nutrient deprivation (**Figure 21**).<sup>131</sup>

### ***Initiation and Nucleation***

Once the involved proteins have been described, an overview will be given of the molecular mechanisms regulating autophagosome formation and maturation.

Autophagosomes originate from a crescent-shaped structure termed the isolation membrane or phagophore (**Figure 19**). As mentioned before the formation of the phagophore starts with the activation of ULK1-Atg13-FIP200-Atg101 kinase complex, negatively regulated by the upstream nutrient and energy sensing kinases mTOR and AMPK. This is done by translocating the complex to the ER. This step is possible due to the presence of Atg9, that marks the final location in ER. The transmembrane protein Atg9 is the main connection between phagophore formation and the Golgi complex. However, its exact function has not yet been resolved and different hypothesis have been suggested. Thus, Atg9 vesicles could nucleate the domain forming the omegasome, directly fuse with the growing phagophore membrane or reside dynamically in a larger intermediate compartment called the Atg9 compartment.<sup>125</sup> Then, class III PI3K complex (consisting of Vps34, beclin 1, Atg14L and Vps15) is recruited thereby catalysing the formation of PtdIns3P and generating the omegasome, highly curve regions that are considered the origin of the phagophore. These structures stimulate the recruitment of PI3K and WIPI2B, the protein responsible of the recruitment of the complex Atg12-Atg5-Atg16L1.<sup>125</sup> The initial omegasome seem to arise from the ER, but as mentioned above, other membrane sources are considered and further elongation of the membrane is also found to rely on input from several membranes.



### ***Elongation of the phagophore and formation of autophagosome***

The expansion and elongation of the phagophore is regulated by a ubiquitin-like (Ub-like) conjugation machinery. Ubiquitination, the covalent addition of ubiquitin to a substrate protein, is regulated by ubiquitin-activating enzymes (E1), ubiquitin-conjugating enzymes (E2) and ubiquitin-ligases (E3). Since the discovery of ubiquitin in 1975,<sup>132</sup> many related proteins have been identified. All of them share a common  $\beta$ -grasp fold and their ability to covalently modify macromolecules. To date, nine Ub-like proteins have been reported including SUMO (small ubiquitin-related modified) and the 2 complexes involved in LC3/GABARAP lipidation.

The first Ub-like-conjugation system involved in autophagy comprises Atg12-Atg5 and Atg16L. Atg12-Atg5 complex is formed by a ubiquitin-like process where Atg7 (E1) activates Atg12 and Atg10 (E2) transfers it. The enzyme acting as E3 in the conjugation step of Atg12 to Atg5 remains to be identified. Atg16 interacts with Atg5, forming a multimeric complex (**Figure 19**).<sup>112</sup> The second Ub-like protein conjugation system is the modification of LC3/GABARAP (mammalian homologs of Atg8) with the phospholipid phosphatidylethanolamine (PE),<sup>133</sup> a crucial step in the formation of the autophagosome mediated by Atg7 and Atg3. To date, two subfamilies have been identified in mammals: the microtubule-associated protein 1 light chain 3 (MAP1-LC3 including LC3A, B and C) and the GABA receptor-associated protein (GABARAP, including GABARAP, GABARAPL1 and GABARAPL2, which is also known as GATE-16). LC3 is the best characterized protein. LC3 lipidation starts with the cleavage of a C-terminal peptide in proLC3 mediated by Atg4, thus generating a LC3-I protein with an exposed C-terminal Gly.<sup>112</sup> LC3-I is then activated by Atg7 (E1, shared with Atg12), transferred to Atg3 (E2) and finally conjugated with the amino group of the lipid PE to form LC3-II (**Figure 19** and **Figure 20**). The Atg12-Atg5-Atg16 complex acts as an E3 enzyme for the conjugation reaction of LC3-I, it enhances the E2 activity of Atg3 and specifies the membrane site for LC3-II production.<sup>134</sup> LC3-I is localised in the cytosol whereas LC3-II is able to interact with the phagophore membrane and localize to both sides of the phagophore. After elongation, the membrane closes with the cargo inside to form the autophagosome. Both LC3 and GABARAP subfamilies are essential for autophagy. However, they seem to have different roles. LC3 subfamily is involved in the elongation of the phagophore membrane whereas GABARAP subfamily has been suggested to act in the maturation or closure of autophagosomes.<sup>135</sup>

### ***Autophagosome-Lysosome Fusion and Degradation***

Mature autophagosomes need to move along microtubule tracks towards the perinuclear region where lysosomes localize. This transport is facilitated by the small GTPase Rab7 that interacts with the Rab-interacting lysosomal protein (RILP), the

cholesterol sensor ORPL1, with dynein and with microtubule motors through FYCO1 (FYVE and coiled-coil domain-containing 1).<sup>136</sup> The outer membrane of the autophagosome fuses then with lysosomes to form an autolysosome (**Figure 19**). The fusion is mediated by SNARE proteins, a protein complex in charge of vesicle fusion. First, the outer autophagosomal membrane fuses with the single lysosomal membrane. This process is upregulated by the UVRAG-Vps34-beclin 1 PI3K complex and downregulated by the Rubicon-UVRAG-Vps34-beclin 1 PI3K complex. Then the inner membrane is degraded by lysosomal hydrolases and the content of the autophagosome results then exposed. The autophagolysosome cargo can be then also degraded by lysosomal hydrolases, including lipases and cathepsins, which also target LC3-II on the intra-autophagosomal surface. In yeast there are certain proteins in charge of autophagic bodies degradation, like Atg15 and Atg22, though their counterparts in mammals remains to be identified.<sup>112</sup>

The degradation products, including amino acids and sugars, are transported out of the autolysosome through members of a family of lysosome efflux transporters. Following autolysosome formation, Atg4B delipidates LC3-II on the cytoplasmic surface to recycle LC3-I<sup>112</sup> and the Atg12-Atg5/Atg16 complex progressively dissociates from the membrane.

Autolysosomes disintegrate once autophagy is finished in a process called autophagic lysosome reformation (ALR) in which membrane proteins are recycled from autolysosomes through tubular structures where new lysosomes will be formed and matured.<sup>125</sup> In yeast, the process is a bit different since vacuoles play the role of lysosomes, the autophagy machinery is concentrated in the phagophore assembly site (PAS) which is a perivacuolar site that results in phagophore elongation and autophagosome formation as well.<sup>104</sup>

## 2. Autophagy and diseases

Since autophagy is essential for cellular homeostasis maintenance, its dysregulation has been related with several pathological processes including cancer, neurodegenerative disorders (Parkinson's, Alzheimer's, Huntington's and Creutzfeldt-Jakob diseases), infection, autoimmune and inflammatory diseases and ageing processes.<sup>112,137,138,139,140</sup>

### 2.1. Cancer

Cancer was one of the first diseases found to be related with autophagy alterations. First insights came from studies examining mice with allelic loss of beclin 1. This protein inhibits autophagy upon formation of a complex with the anti-apoptotic Bcl-2. These studies revealed that a monoallelic deletion of beclin 1 leads to loss of this protein and results in an increased cellular proliferation, reduced autophagy and

promoted tumorigenesis.<sup>141,142</sup> In addition, overexpression of beclin 1 results in autophagy induction and inhibition of tumorigenesis.<sup>143</sup>

Autophagy can have two functions in cancer. It can act both positively and negatively in the regulation of cancer cell survival. Thus, autophagy can be tumour suppressive through elimination of oncogenic proteins such as p62 (often upregulated in cancer cells), as well as damaged proteins and organelles. As a result, autophagy-defective cells present an accumulation of p62 protein, damaged mitochondria, an increase of reactive oxygen species (ROS) and protein aggregates. All these effects result in DNA damage, activation of oncogenic signalling pathways and inflammation, thereby creating a tumour-initiating environment. Autophagy can also be tumour promoting in established cancers by facilitating the substrates required for tumour cell survival. This process is particularly activated by starvation, growth factor deprivation or metabolic stress, especially in hypoxic regions.<sup>144</sup> The close relationship between autophagy and tumour survival has prompted the interest in combining cytotoxic treatments with autophagy inhibitors. We are at the early stages of using this information to benefit patients. Thus, current efforts in the clinic are focused on combined treatments of antitumoral agents with the known antimalaria drugs chloroquine (CQ) or hydroxychloroquine (HCQ). However, their overall lysosomal inhibition together with some toxic side-effects associated to long term treatments make preferable the identification of new therapeutic targets, preferentially acting on the initial stages of autophagosome formation.<sup>145</sup> In addition, alternative strategies for combined therapies have lagged behind due to the lack of specific inhibitors of autophagy-related targets. All in all, the future identification of new targets and active compounds should have a deep impact in this research field.

## 2.2. Neurodegeneration

Autophagy is essential for protein homeostasis and organelle turnover. This role is particularly important in non-proliferating cells such as neurons, because there is no cell division-mediated dilution of intracellular debris. Consequently, neurons strongly rely on autophagy to prevent accumulation of protein aggregates and deficiencies in this clearance is clearly correlated with the onset of neurodegenerative diseases.<sup>104</sup> Autophagy can also remove protein aggregates via autophagic receptors such as p62, NBR1, NDP53, OPTN, HDAC6 or NIX. These proteins have an interacting region for LC3 binding and a ubiquitin-associated domain that allow to deliver polyubiquitylated, misfolded, aggregated and damaged proteins directly to autophagosomes.<sup>146</sup> Some neurodegenerative disorders such as Alzheimer's disease<sup>147</sup>, amyotrophic lateral sclerosis<sup>148</sup> and Parkinson's disease<sup>149,150</sup> have been related to defects in some of these receptors or at different stages of the autophagic pathway. On the contrary, an autophagy induction seems to be involved in the production of A $\beta$ 40 and the pathogenesis of Alzheimer's disease.<sup>151</sup> More research will be required to elucidate

how autophagy modulation can contribute to the treatment of neurodegenerative disorders.

### 2.3. Immunity and Inflammation

Several studies support the claim of autophagy playing an important role in the defence against virus, bacteria and parasites<sup>137</sup> in a process also known as xenophagy. Efficient engulfment and clearance of intracellular pathogens requires cargo receptors that link molecular tags (such as polyubiquitin) or adaptor proteins (such as p62) to Atg8 orthologs present on the phagophore membrane. A relevant example is NDP52, which detects *Salmonella enterica* serovar *Typhimurium* presents in the cytosol<sup>152</sup> and recruits Tank-binding kinase 1 (TBK1), which induces antibacterial autophagy.<sup>153</sup> The recruitment of NDP52 to invading bacteria can be mediated by its interaction with ubiquitin-coated bacteria<sup>153</sup> or with *Salmonella*-containing vesicles decorated with galectin.<sup>154</sup> NDP52 seems to be also involved in the clearance of *Listeria*, *Shigella* and *Salmonella*.<sup>155</sup> In addition, *Shigella* relies on VirG, a protein required for intracellular actin-based motility that induces autophagy by binding to Atg5.<sup>156</sup> Bacteria and virus show different strategies to avoid this degradation. For example, *Shigella* inhibits host autophagy by secreting the protein IcsB, that competitively binds and blocks VirG.<sup>156</sup> The *Legionella* effector RavZ blocks host autophagy by irreversibly cleaving LC3/GABARAP yielding a protein that lacks the essential C-terminal glycine required for lipidation.<sup>157</sup> More recently, *Legionella* has been shown also to block autophagy by disrupting host sphingolipid biosynthesis<sup>158</sup> and the Herpes simplex virus type 1 (HSV-1) neurovirulence factor ICP34.5 inhibits autophagy by binding to beclin 1.<sup>159</sup>

Autophagy also plays a role in adaptive immune response including the development and homeostasis of the immune system (maintenance of normal numbers of T cells) and antigen handling and presentation. Hence, processed antigenic peptides can be loaded on Class I or II major histocompatibility complexes (MHC) and presented by T-cells or antigen-presenting cells. In general, peptides generated by the proteasome are presented on MHC I and products of lysosomal degradation are displayed on MHC II. A number of studies revealed that autophagy has a strong role in the presentation of antigens via MHC II.<sup>160</sup> However, additional studies performed in HSV-1 infected cells have indicated that distinct forms of autophagy facilitated the presentation of its antigens also on MHC class I molecules.<sup>161</sup>

### 2.4. Ageing and longevity

One of the main characteristics of ageing cells is the accumulation of damaged proteins and organelles. Consequently, autophagy turns to be a key process with potential longevity effects. In addition, reduced autophagy (for example, downregulation of Atg5, Atg7 and beclin 1<sup>162</sup>) has been associated with premature

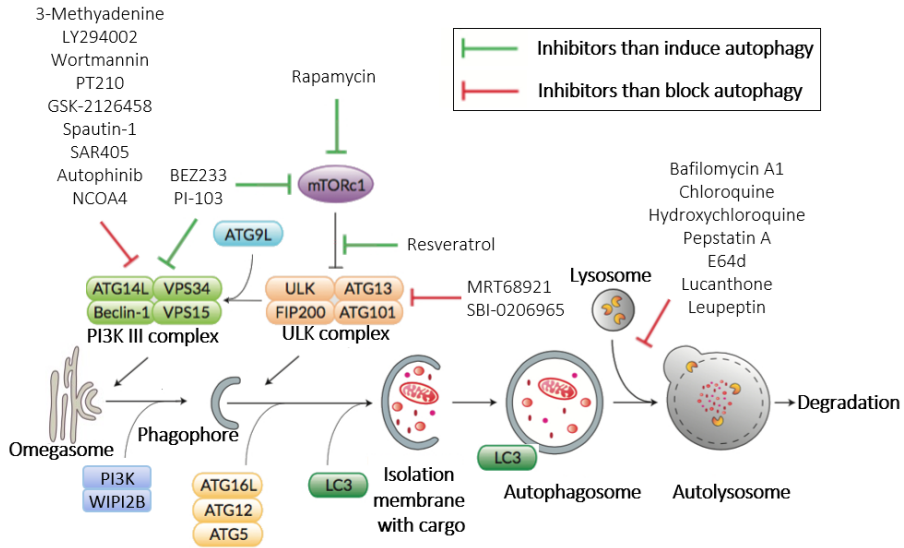
ageing, whereas increased autophagy is correlated with anti-ageing effects (caloric restriction extends lifespan and retards the appearance of age-associated diseases by stimulating autophagy<sup>163</sup> and rapamycin treatment extend the life span in mice<sup>164</sup>). Therefore, many strategies have tried to improve healthy ageing by inducing autophagy. Examples thereof include intermittent fasting and diets based on proautophagic factors like rapamycin, resveratrol<sup>165</sup> or spermidine.<sup>166</sup>

## 2.5. Cell death

Although autophagy has been well described as a survival mechanism, a role of this process in cell death induction has also been described. Thus, when apoptosis is compromised, alternative cell death pathways may take place. For example, clinical therapies involving caspase inhibition can block apoptosis causing the simultaneous and unexpected effect of promoting cell death through increased autophagy.<sup>167</sup> This autophagic cell death, is also known as autosis and seems to be independent from other cellular pathways.<sup>168</sup> Autosis has also been reported in HEK293, U87 and HeLa cells after reactive oxygen species (ROS) induction.<sup>169</sup> In some cases the same stimuli can lead to different cell death pathways suggesting that the final outcome may depend on the state of the cells.<sup>170</sup> Alternatively, autophagic cell death may be also involved in development. Thus, previous studies in *Drosophila melanogaster* have shown that autophagy is required in several processes from larval to adult state.<sup>171,172,173</sup> In mammals there is no clear evidence of autophagy having a specific role in development, although autosis has been detected in mouse embryonic fibroblasts (MEF) resistant to apoptosis (*bax*<sup>-/-</sup> and *bak*<sup>-/-</sup>)<sup>174</sup> and in rat hippocampal neural stem cells.<sup>175</sup> Autophagy can also induce cell death by sensitizing cells to apoptosis modulators<sup>176</sup> or by promoting the switch from apoptosis to necroptosis.<sup>177</sup> Further investigations are yet required to unveil the underlying mechanisms involved in pro-survival and pro-death autophagy.<sup>170</sup>

## 3. Autophagy modulators

The close relationship between autophagy alterations and physiological and pathological processes such as cancer, neurodegeneration and ageing has prompted an increasing interest to target autophagy with both activators and inhibitors.<sup>178</sup> However, one of the current limitations is the low specificity of most of the existing modulators (**Figure 22** and **Figure 19**).



**Figure 22.** Two classes of modulators have been described, one group interacting with enzymes upstream on the autophagy pathway and another group interacting downstream. Inducers: **rapamycin** and **resveratrol** are autophagy inducers acting via mTORC1 inhibition and **BEZ235** and **PI-103** are dual mTOR and PI3K inhibitors. Inhibitors: **3-methyladenine** has a dual inhibitory effect due the inhibition of Vps34 and class I PI3K. **Wortmannin**, **LY294002**, **PT210** and **GSK-2126458** inhibit all classes of PI3K, Vps34 and mTOR, but wortmannin showed persistent effects on Vps34 and only transient on mTOR. On the other hand, **PT210** has higher selectivity for Vps34 and **GSK-2126458** is currently being studied as an inhibitor but also an activator of autophagy. **Spautin-1** enhances the degradation of Vps34 complexes. **MRT68921** and **SBI-0206965** are two novel ULK1 complex inhibitors albeit with low specificity. The rest of known inhibitors are found downstream of the autophagic pathway and they mostly modify lysosomal function and its fusion with the autophagosome. **Bafilomycin A1** blocks proton transport in the lysosome and inhibit hydrolases, **chloroquine** and **hydroxychloroquine** also inhibit them by increasing the lysosomal pH. **Pepstatin A**, **E64d** and **leupeptin** inhibit several cathepsins, and as a consequence inhibit autophagosome degradation. **Lucanthone** disrupts the lysosomal membrane.

### 3.1. Inductors

Autophagy inducing agents such as rapamycin have shown promising neuroprotective effects and can improve autoimmune disorders and extend lifespan. **Rapamycin** is a macrolide used to prevent organ transplant rejection. It forms a complex with the immunophilin FK506-binding protein 12 (FKB12) that stabilizes the complex of mTOR with the protein raptor and inhibits mTOR activity.<sup>179</sup> However, mTORC1 blockage using rapamycin results in inhibition of cellular growth and proliferation.<sup>180</sup> In addition, serious toxicity effects prevent long treatments with rapamycin.

**Resveratrol** is a polyphenolic substance found in the skin of grapes. It is considered a multi-target or promiscuous molecule and around 20 proteins have already been identified as potential targets of this natural substance.<sup>181</sup> Among others, it inhibits the mTOR-ULK1 pathway by docking into the ATP-binding site of mTOR.<sup>182</sup> It has been also studied as an anticancer drug for its effects on extracellular growth factors and receptor tyrosine kinases, and it also prevents drug resistance by increasing the chemosensitivity of some cancer cells.<sup>183</sup>

The imidazoquinoline derivative **BEZ235** is a novel and oral dual inhibitor of PI3K and mTOR, which binds competitively the ATP binding cleft of both enzymes. It is currently being tested in phase I and II clinical trials for the treatment of solid tumours in breast cancer. BEZ235 induces autophagy and promotes cell death. It has been also tested in combination with autophagy inhibitors, such as chloroquine, with similar results.<sup>184,185</sup> **PI-103** also inhibits the PI3K/mTOR pathway and enhances the efficacy of chemotherapy in combined treatments. The effect has been studied in models of gliomas,<sup>186</sup> acute myeloid leukaemia (AML),<sup>187</sup> prostate and breast carcinomas.<sup>188</sup> The dual targeting of both kinases complicate the understanding of the effects caused by **BEZ235** and **PI-103**.

### 3.2. Inhibitors

Autophagy inhibitors can be mainly divided in two groups: compounds targeting the initial steps of the autophagosome formation (ULK1, Vps34, beclin 1) and compounds that inhibit the lysosomal activity and compromise the final stages of the autophagic pathway.

The class III phosphatidylinositol 3 kinase (PI3K) Vps34 is in charge of the synthesis of PtdIns3P, a lipid essential for the recruitment of WIPI2 proteins and the E3-like complex Atg12-Atg5-Atg16L1.<sup>125,189</sup> The other members of the PI3K family have different roles. Class I PI3K triggers mTOR signalling pathway and inhibits autophagy, thus having an opposite effect, whereas the role of class II PI3K in autophagy remains unclear. Most of the described class III PI3K inhibitors, **3-methyladenine** (3-MA), **wortmannin**, **LY294002**, **PT210** and **GSK-2126458**, are pan-PI3K inhibitors that act in a non-selective manner.<sup>189</sup> **3-MA** is the most widely used autophagy inhibitor. It was first isolated in 1982 from rat hepatocytes<sup>190</sup> and it inhibits both class III and class I PI3K, thus having a dual effect that may cause complicated outputs. In addition, *in vitro* assays require ~10 mM concentrations, high enough to compromise other pathways like glycogen metabolism, lysosomal acidification, endocytosis and mitochondrial permeability transition. Another problem is its low solubility. Some synthetic efforts have led to derivatives with increased solubility but the potency of the resulting analogues remain limited.<sup>191</sup> **Wortmannin** is a natural product that irreversibly blocks all PI3K isoforms with IC<sub>50</sub> values ranging from 10 to 50 nM.<sup>192</sup>

Another interesting compound is **LY294002**, a morpholino-derivative of quercetin developed by Lilly and the first synthetic inhibitor of PI3K that works on cellular assays. Although it displays low potency ( $IC_{50}$  values at  $\mu M$  range), its improved chemical stability has promoted its wide use. Both compounds also target many other kinases such as mTOR, DNA-dependent protein kinase and ataxia telangiectasia mutated protein kinase, resulting in confusing outputs.<sup>189,193</sup> In addition, neither **wortmannin** nor **LY294002** have progressed to clinical trials due to their poor pharmacokinetic properties and high toxicity although they have been widely employed as tools in basic research. **GSK-2126458** was initially developed as an inhibitor of mTOR and class I PI3K, but it also turned out to be a potent inhibitor of Vps34. This compound is thought to be able to both activate and inactivate autophagy, although more research needs to be done to confirm it.<sup>194</sup>

**Vps34** (vesicle-mediated vacuolar protein sorting) is the only class III PI3K in mammals and, as a result, it has emerged over the time as a promising target for specific autophagy inhibition. The crucial role of this lipid kinase is proven by the fact that cells lacking Vps34 cannot undergo autophagic degradation and starvation-induced autophagosome formation.<sup>195</sup> Some important advances have already been done in this direction. **Spautin-1** is an indirect inhibitor that does not affect the catalytic activity of Vps34, but it promotes the degradation of Vps34 complexes by inhibiting two ubiquitin-specific peptidases, USP10 and USP13, which deubiquitinate beclin 1.<sup>196</sup> This compound is especially interesting since it only affects cells that are carcinogenic and are under nutrient deprivation without affecting healthy cells. Preclinical studies have suggested a synergic effect in combination with imatinib for the treatment of chronic myeloid leukemia.<sup>197</sup> In 2010, the X-ray crystal structure of a Vps34 complex with different inhibitors was solved. This study showed that **PIK-93** binds a unique hydrophobic pocket not present in related kinases, providing insight into developing more potent and specific Vps34 inhibitors. Further medicinal chemistry development led to the specific inhibitor **PT210**.<sup>198</sup> Later, a potent and selective inhibitor was described, **SAR405**. However, due to the role of Vps34 in the regulation of endocytic trafficking, this compound affects both autophagy and the trafficking from late endosomes to lysosome.<sup>199</sup> This growing interest in Vps34<sup>200</sup> has led to the identification of other inhibitors such as **autophinib**,<sup>201</sup> a tetrahydropyrimidopyrimidinone derivative which is an optimized and more selective Vps34 inhibitor for the treatment of solid tumours<sup>202</sup> and **NCOA4** that has shown to modulate the selective autophagy of ferritin.<sup>203</sup>

**ULK1** has also been defined as a promising target to inhibit autophagy since it functions as the most upstream protein kinase in the autophagy machinery.<sup>204</sup> The group of K. M. Shokat reported recently the crystal structure of ULK1 and the identification of a potent inhibitor after the screening of around 700 compounds.<sup>205</sup> Other recently reported inhibitors targeting this kinase are **MRT68921**<sup>206</sup> and **SBI-**



**0206965.**<sup>207</sup> However they all exhibit low specificity by inhibiting around 50% of all the tested kinases.

Another strategy to inhibit autophagy is through blocking lysosomal degradation. Examples thereof are **pepstatin A** and **E64d** that inhibit **cathepsins** D, E and B, H, L, respectively, two drugs commonly used in basic research to suppress autophagy.<sup>189,208</sup> Similarly, leupeptin is a membrane-permeable cysteine protease inhibitor that inhibits cathepsin B, H and L, and also impairs autophagosome-lysosome fusion.<sup>209</sup> Another significant target is the **vacuolar-type H<sup>+</sup>-ATPase** that maintain the acidic environment required for the activity of the hydrolases. **Bafilomycin A1** is a known inhibitor of this proton pump.<sup>210</sup> Other inhibitors of autophagic degradation include the approved drug for psychiatric disorders **clomipramine**, which blocks the autophagosome-lysosome fusion<sup>211</sup> and the anti-schistosome agent **lucanthone** which disrupts the lysosomal membrane permeabilization.<sup>212</sup> Other well-established autophagy inhibitors are **CQ** and **HCQ**, widely employed as antimalaria agents and for the treatment of some autoimmune diseases. These two compounds act as **lysosomotropic agents**. Thus, at neutral pH they remain uncharged and diffuse across membranes, but once in the acidic environment of the lysosome they get protonate and trapped inside the organelle. This accumulation cause an increase of the lysosomal pH which leads to the inactivation of the hydrolytic enzymes.<sup>213</sup> Since these drugs are well tolerated, although present some toxicity associated to long treatments, other therapeutic indications have been also investigated.<sup>214</sup> In the last decade, many clinical trials have explored the use of CQ or HCQ alone or in combination with chemotherapeutic agents. However it is yet unclear if the final anticancer effect is caused by autophagy inhibition or lysosomal activity inhibition.<sup>189,215</sup> In addition CQ completely blocks the lysosomal function including degradation of endosomes and exerts additional effects independent of their role on autophagy.<sup>216</sup>

All in all, a myriad of autophagy inhibitors has been described. However, most of them do not target exclusively the autophagic pathway and thus, they inhibit other cell processes leading to off-target effects. Therefore, much efforts are still required to develop selective autophagy inhibitors that will strongly contribute to expand the available toolbox in autophagy research.

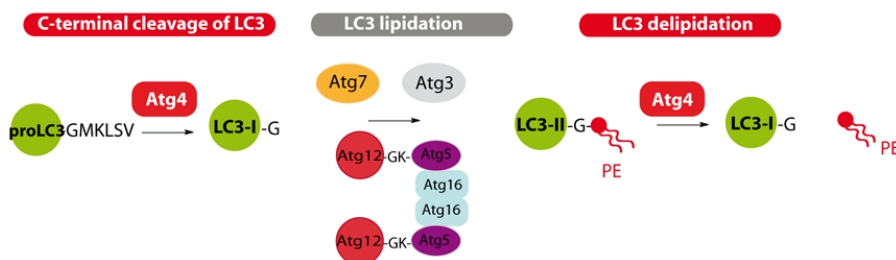
#### 4. Estimation of Autophagic Activity

Autophagy is a dynamic process and its correct quantification is not a trivial issue. The autophagosome membrane associated LC3-II has become the main biomarker of autophagy since it increases as autophagy does. To date, the main methods employed to monitor autophagy is the detection of LC3-II by immunoblotting, electron microscopy or fluorescence microscopy.<sup>217</sup> However, the accumulation of

autophagosomes and LC3-II could indicate an autophagic activation or a blockage of their lysosomal degradation. To solve this issue, scientists measure autophagic flux, which refers to the whole process including autophagosome formation, maturation, fusion with lysosome and subsequent hydrolysis.<sup>112</sup> These measurements are performed in the presence of inhibitors of the lysosomal function. Typically, an inhibitor cocktail is used containing E64d and pepstatin A, although leupeptide and bafilomycin A1 have been also employed. If accumulated LC3-II does not increase further upon lysosomal inhibition, the measurements probably reflect a blockage of lysosomal degradation instead of a real induction of autophagy.

## 5. Atg4B

The conversion of the soluble proLC3 into LC3-I and the delipidation of the membrane associated LC3-II to regenerate LC3-I requires the activity of the cysteine protease Atg4 (**Figure 23**). There is only one Atg4 protein in yeast,<sup>218</sup> but four homologs (Atg4A, Atg4B, Atg4C, Atg4D) in mammals<sup>219</sup> with different substrate specificity.<sup>220</sup> Atg4A is the one showing a broader selectivity for the GABARAP subfamily, while Atg4C and Atg4D are nearly inactive.<sup>221</sup> Atg4B is 1500-fold more catalytically efficient for LC3B than the rest of the homologues,<sup>219</sup> although it can cleave all the members of the LC3 and the GABARAP subfamily. The functional redundancy of these proteins in cells is poorly understood.



**Figure 23.** Atg4 catalyses the cleavage of the last five amino acids of proLC3 but it also catalyses the hydrolysis of the lipid bound to LC3-II.

Atg4B has been considered an attractive target for autophagy regulation. Overexpression of an inactive mutant of Atg4B inhibits autophagic degradation, probably caused by the accumulation of proLC3, and leads to a high amount of non-closed autophagic membranes.<sup>220</sup> Contrarily, its genetic silencing and chemical inhibition results in an accumulation of LC3-II, also causing notable defects in autophagy<sup>222,223</sup> and tumour growth inhibition.<sup>145,224</sup> Alternatively, studies performed in ATG4B knock-out (KO) cells led to an accumulation of proLC3. Interestingly, lipidated GABARAPs could still be detected in these cells, suggesting that this enzyme is required for LC3B lipidation whereas GABARAPL1 and GABARAPL2 could be

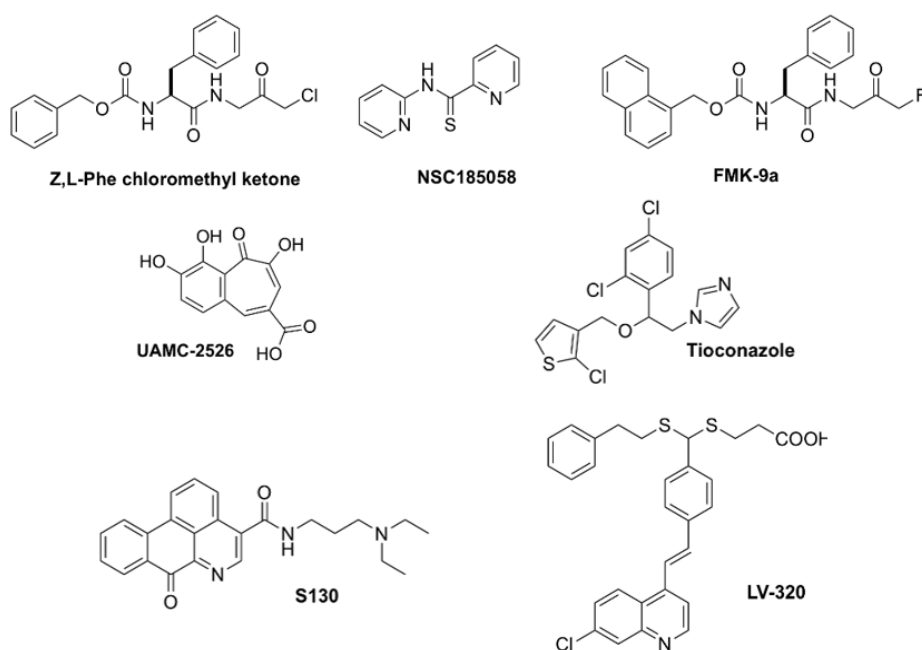
lipidated independently of ATG4B.<sup>225</sup> It has been also reported that a Atg4B KO mice showed a defective autophagy, although they were still viable and fertile, probably due to the presence of the other Atg4 homologues. Moreover, the same study suggested that homologues could have tissue-specific functions since some histopathological, neurological and balance alterations were detected.<sup>221,222</sup>

These controversial results may be due to the different models employed (genetic attenuation, chemical inhibition or KO cells causing reduction or elimination of gene function, respectively). In addition, the different outputs may be also caused by the different recognition of soluble proLC3 and membrane associated LC3-II by Atg4 isoforms. Hence, recent studies have showed that Atg4B mediates a very fast priming of LC3/GABARAP subfamilies, whereas delipidation is inherently slow and regulated by all Atg4 homologs. As a consequence, Atg4 inhibition may have a stronger effect on the delipidation step.<sup>226</sup> The different activity on proLC3 and LC3-II is also visible in the ROS-mediated inhibition of Atg4. Thus, Atg4 activity can also be regulated by reactive oxygen species (ROS). Under starvation conditions, cells form ROS (more specifically H<sub>2</sub>O<sub>2</sub>) leading to Atg4 inhibition that affects primarily the delipidation step without blocking the priming activity. The mechanism of action seems to involve the oxidation of Cys81 located four amino acids from the catalytic residue.<sup>227</sup>

Some data further support the choice of Atg4B as a target. Hence, patients treated with imatinib mesylate against chronic myeloid leukaemia presented increased autophagy with the highest transcript levels detected for Atg4B. Knockdown of Atg4B suppressed autophagy and impaired the survival of cancer stem cells sensitizing them to imatinib mesylate treatment.<sup>228</sup>

Despite the controversial results seen regarding proLC3 and LC3-II accumulation and the dual activity of Atg4B on both the priming of proLC3 and the delipidation of LC3-II, Atg4B blockage seem to be beneficial for the treatment of cancer cells. In addition, potent and specific inhibitors should strongly contribute to explore in detail the role of this enzyme as well as the other isoforms. Up to now, several attempts have been carried out in order to find Atg4B inhibitors. Certain Atg4B inhibitors have been synthesized or screened out from compound libraries and showed effectivity *in vitro* or/and *in vivo* (**Chart 4**). In 2014, **Z,L-Phe-chloromethylketone** (PCK) was identified from a fluorescence resonance energy transfer (FRET) HTS assay using a doubly fluorescent ligand YFP-LC3B-EmGFP as a substrate. The authors described an IC<sub>50</sub> of 0.63 μM, but this inhibitor also targets other cysteine proteases.<sup>224</sup> Later, **NSC185058** was identified as an allosteric Atg4B inhibitor that prevented tumour formation with no effect on mTOR and PI3K activities. However, the compound showed cytotoxic effects that would not make it suitable for clinical use.<sup>145</sup> In 2016, another halomethylketone derivative (**FMK-9a**, IC<sub>50</sub> of 80) was identified from a TR-FRET and a cellular-based luciferase release assay.<sup>229</sup> This covalent inhibitor shows poor specific

over other cysteine proteases and cellular studies showed that induces autophagy in a manner independent of Atg4B enzyme inhibition.<sup>230</sup> Later, the benzotropolone **UAMC-2526** was reported. The researchers observed a synergic effect with cisplatin in mice, but the low solubility prevented the administration of higher doses.<sup>223</sup> More recently, independent research groups have identified **S130**,<sup>219</sup> the antifungal drug **tioconazole**<sup>231</sup> and the quinoline **LV-320**<sup>232</sup> as Atg4 inhibitors displaying low micromolar IC<sub>50</sub> values. Hence, important advances have been made in this research field in the last decade. However, most of the identified compounds are known promiscuous inhibitors lacking the necessary drug-like properties for lead optimization or non-specific cysteine protease inhibitors. As a result, the identification of novel chemotypes for Atg4 inhibition still remains an urgent need.



**Chart 4.** Identified Atg4B inhibitors.

Taken all together, the main aim of this chapter is the identification of novel Atg4B inhibitors through a combination of a variety of techniques. A novel HTS screening assay has been established for the identification of Atg4B inhibitors. A structure-based virtual screening has been carried up based on two known X-ray structures of the enzyme (alone or in complex with the LC3 substrate) and a virtual library from the National Cancer Institute (NCI) open database. The potential inhibitors have been selected and tested. The potential hits identified in the established assay have been validated using alternative methods, including an alternative activity assay based on mass spectrometry (MS). Finally, biochemical and cellular studies were done *in vitro* in order to characterize the potential identified hits.



# OBJECTIVES



In this chapter, the general aim is the identification of compounds with inhibitory activity against Atg4B. Various approaches and techniques will be employed to achieve this objective. This general aim can be split into the following specific goals:

- To optimize a novel HTS assay for the identification of Atg4B inhibitors
- To validate the HTS assay by an optimized alternative MS-based method.
- To identify molecules with inhibitory activity against Atg4B. A virtual screening of a compound library obtained from the National Cancer Institute (NCI) Open Database will be performed and potential hits will be selected.
- To experimentally evaluate the activity of *hits* and synthesized derivatives activity in order to select the most potent compounds for further assays.
- To explore the biological activity of the selected compounds through biochemical and cellular studies.

The ultimate aim of this chapter is to find bioactive compounds that completely or partially inhibit autophagy acting on Atg4B. These compounds could serve as a starting point for the development of more selective and potent inhibitors and also serve as research tools to explore the role of Atg4 isoforms.





# RESULTS AND DISCUSSION



## 6. TR-FRET-based assay and protein modification

### 6.1. TR-FRET

During the past years a limited number of protocols for assaying small-molecule Atg4B inhibitors have been described. One of the major limitations is that Atg4B requires full length protein substrates since short peptides spanning the natural pro-LC3B cleavage site cannot be efficiently processed by the enzyme<sup>233,224,234</sup> or present moderate  $K_m$  values.<sup>235</sup> The existing assays include the electrophoretic separation of a cleaved LC3B-GST protein,<sup>233,234</sup> and an indirect assay based on a LC3-PLA<sub>2</sub> fusion protein.<sup>236</sup> However, the first approach is not suitable for high-throughput screening (HTS) and the second assay requires a counter screen to eliminate compounds directly inhibiting PLA<sub>2</sub>. A doubly fluorescence LC3B protein has been also employed in a fluorescence resonance energy transfer (FRET)-based assay<sup>224,237</sup> but it presented significant donor-acceptor emission overlap and fluorescence photobleaching. More recently in 2016, a TR-FRET assay was reported employing a doubly-tagged GABARAPL2/GATE-16 as substrate because LC3B could not be efficiently processed under the same conditions.<sup>238</sup> The main aim at the beginning of this project was to set up a high-throughput screenings (HTS) assay based on TR-FRET and using LC3B as a substrate.

Fluorescence-based techniques are highly used in HTS due to its simplicity and high sensitivity. Relevant examples of fluorescence-based techniques include fluorescence polarisation (FP) fluorescence or Förster resonance energy transfer (FRET), time-resolved fluorescence (TRF) among others. FRET was first described by Förster in 1959.<sup>239</sup> It is based on overlapping fluorophore pairs, in which the acceptor has an excitation spectrum matching the emission spectrum of the donor molecule. In FRET measurements, the excited state energy from a fluorophore donor molecule is non-radiatively transferred to a close acceptor molecule, that in turn emits fluorescence energy at a specific wavelength. The distance between the two fluorophores is a key point to get a good FRET signal. The working distances is characterized by the Förster's radius ( $R_0$ ), the distance between the fluorophores at which FRET efficiency is 50% (typically 3-6 nm). Thus, the working distance usually ranges from 1 to 10 nm (10-100 Å)<sup>240</sup> and it allows the study of biomolecules and intra- and intermolecular interactions. In addition, as the efficiency of the energy transferred is inversely proportional to the sixth power of the distance between both fluorophores, small changes in distance can be clearly determined.<sup>239</sup> Apart from the distance, the rate of energy transfer also depends on the quantum yield of the donor and the relative orientation of the donor and acceptor transition dipoles.<sup>241</sup>

Time-resolved fluorescence energy transfer (TR-FRET) is a variation of FRET that commonly results in superior sensitivity and assay robustness. Initially reported by Morrison *et al.*,<sup>242</sup> TR-FRET measurements combine the FRET principle with

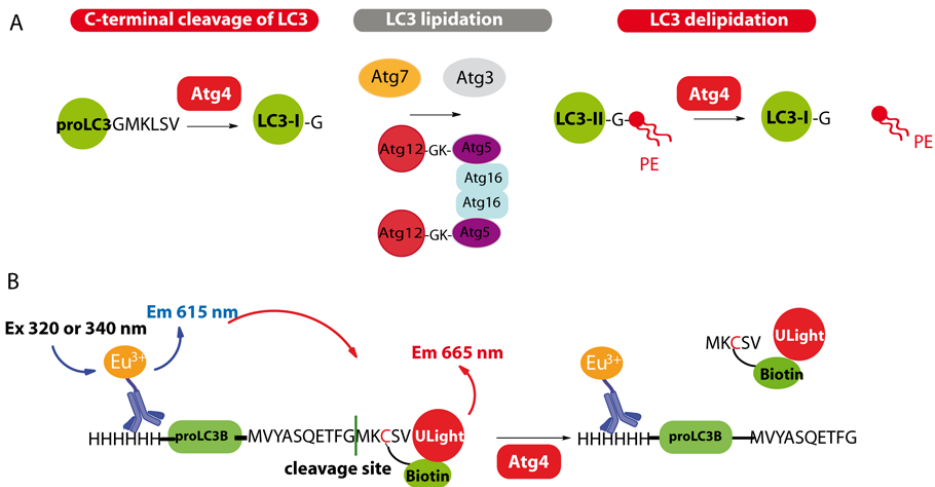
fluorescence dyes based on rare earth lanthanides such as Terbium ( $Tb^{2+}$ ) or Europium ( $Eu^{3+}$ ). These complexes or cryptates, have a macrocycle within which a  $Eu^{3+}$  or a  $Tb^{2+}$  ion is tightly embedded. These ions are only fluorescent while inserted in this cage and the complexes are extremely stable and not subject to photo-bleaching.<sup>243</sup> In addition, the large Stokes shifts (separation of excitation and emission wavelengths) and long lifetime of these fluorophores (1 to 2 milliseconds (ms)) results in a delay of 50-150 microseconds ( $\mu s$ ) between the excitation and measurement of the emission signal, which allows the background fluorescence (assay components, tested compounds) to decay.<sup>244</sup> Moreover, lanthanides have a narrow fluorescent emission peak, which is advantageous because the signal to background ratio (S/B) can be markedly increased if the right excitation and emission filters are selected.<sup>241</sup> This technique has been widely used during the last two decades in a diverse number of assays such as detection of protein and small-molecule interactions,<sup>245</sup> protein-protein interactions,<sup>246</sup> assembly of cell-surface receptors,<sup>247</sup> enzymatic assays<sup>248</sup> and biomarker detection.<sup>249</sup>

## 6.2. A TR-FRET based assay to find Atg4B inhibitors

As mentioned in the introduction, substantial progress has been recently made with the identification of more than 36 autophagy-related proteins (Atgs). These proteins are responsible for the core machinery of autophagosome formation, thereby serving as a starting point for the development of specific inhibitors. One of the best-characterized Atg proteins is the autophagy yeast marker Atg8 divided in mammals in two subfamilies MAP1LC3 (microtubule-associated proteins 1 LC3 (light chain 3) and commonly referred as LC3) A, B and C, that together with the other mammal homolog GABARAP ( $\gamma$ -aminobutyric acid receptor-associated protein, including GABARAP, GABARAPL1 and GABARAPL2), are recruited to autophagosomal membranes after conjugation with phosphatidylethanolamine. The conversion of the precursor proLC3 in the soluble LC3-I, which is then converted to the membrane associated LC3-II, and the subsequent delipidation of LC3-II to regenerate LC3-I requires the activity of the cysteine protease Atg4 (**Figure 24A**). Although there are four Atg4 homologs (Atg4A, Atg4B, Atg4C, Atg4D) in mammals,<sup>250</sup> Atg4B seems to be the principal homolog as it can cleave all members of the LC3 and the GABARAP subfamily.<sup>251</sup> Moreover, genetic deletion of Atg4B results in notable defects in autophagy<sup>252,253</sup> and inhibits tumour growth in cancer cells.<sup>254,255</sup> Thus, Atg4B can be considered as a promising target for the identification of selective autophagy modulators.

Our initial aim was to design a TR-FRET-based assay that allowed the identification of Atg4B inhibitors and could be applied to HTS assays. The most important advantage of TR-FRET assays is the reduced interference of low molecular weight compounds due to their short fluorescence life-times compared to the extended life-time of the

lanthanides. To this end, a TR-FRET assay aimed to find Atg4B inhibitors was designed employing proLC3B as a substrate and Atg4B as the enzyme. As mentioned above, Atg4B is involved in the C-terminal cleavage of proLC3B and in the delipidation of LC3-II to recycle LC3-I. The synthesis of lipid posttranslationally modified proteins is a challenge, whereas proLC3B and Atg4B have already been successfully expressed in *Escherichia coli* (*E. coli*) simplifying the protein expression and facilitating the purification of higher protein quantities.<sup>256</sup> As a result, proLC3B was chosen as a substrate of the HTS screening.



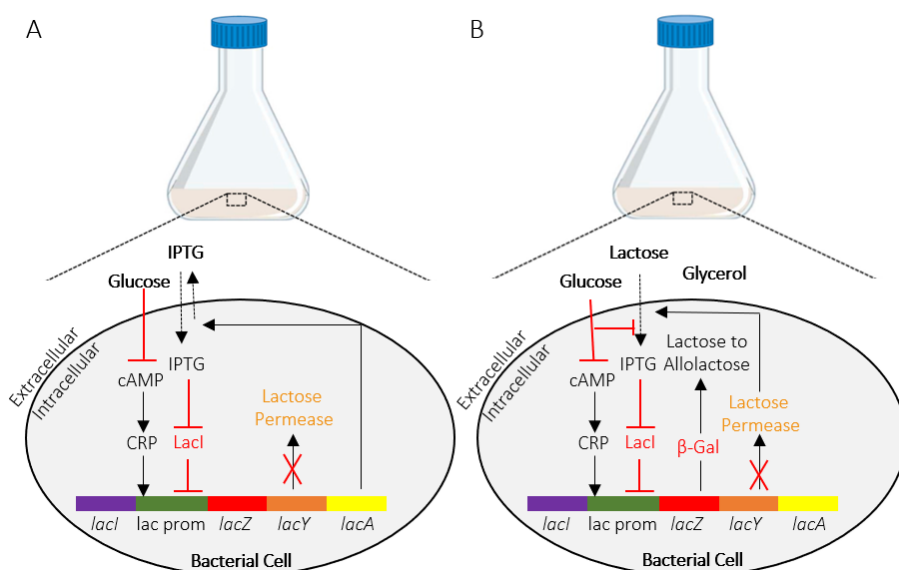
**Figure 24. A)** Atg4B is involved in the cleavage of proLC3 to generate LC3-I and also in the delipidation step to remove the phosphatidylethanolamine attached to the C-terminal glycine in LC3-II, thus regenerating LC3-I. **B)** Diagram of the designed TR-FRET based assay. A biotin moiety should be introduced on a mutated residue of N-(His)<sub>6</sub>-proLC3B located after the cleavage site. The presence of the biotin moiety will enable the binding of ULight™ streptavidin, whereas the anti-6xHis antibody conjugated to Eu<sup>3+</sup> should bind to the (His)<sub>6</sub>-tag present at the N-terminus of the protein. TR-FRET signal should decrease in case of cleavage by Atg4B on Glycine 120 due to the release of the biotinylated pentapeptide MKC(Biotin)SV.

TR-FRET assays require appropriate fluorophore pairs available from a variety of commercial sources (Trace™, CisBio; LANCE™, Perkin Elmer). The fluorophores can recognize specific tags/sequences present in the protein or can be employed to label antibodies that will recognize a specific protein. As a first approach it was decided to employ a doubly-tagged LC3 containing a (His)<sub>6</sub>-tag at the N-terminus and a biotin at the C-terminus. Hence, the (His)<sub>6</sub>-tag could be recognized by a Europium (Eu<sup>3+</sup>) labelled anti-6xHis antibody and the biotin moiety will be recognized by a streptavidin (Sav) labeled with an acceptor fluorophore (ULight™). Europium has an  $\lambda_{ex}$  of 320-340 nm and an  $\lambda_{em}$  of 615 nm whereas the ULight™ fluorophore has an  $\lambda_{ex}$  of 615 nm and

an  $\lambda_{em}$  of 665 nm. Thus, upon excitation at 320-340 nm, energy can be transferred from the donor  $\text{Eu}^{3+}$  chelate to the acceptor fluorophore resulting in the emission of light at 665 nm. If protein substrate is cleaved by Atg4B, the C-terminal biotinylated peptide will be released thereby increasing the distance and causing a decrease in the FRET signal (**Figure 24B**).

## 7. Atg4B expression and purification

Atg4B was expressed in bacteria fused to a  $(\text{His})_6$ -tag at the N-terminus, enabling purification with agarose derivatized with nickel<sup>2+</sup>-nitriloacetic ( $\text{Ni}^{2+}$ -NTA) groups. The plasmid encoding the Atg4B protein prepared in a pOPIN vector was a kind gift of Yaowen Wu, MPI Dortmund.



**Figure 25.** Schematic representation of protein expression mediated by IPTG induction (**A**) or employing the autoinduction method (**B**).  $\beta$ -Gal:  $\beta$ -galactosidase, cAMP: cyclic adenosine monophosphate, CRP: C-reactive protein.

(From <https://www.sciencedirect.com/science/article/pii/S1046592819300257>)<sup>257</sup>

Traditionally, bacterial expression in *E. coli* has relied on the use of promoters that drive overexpression of proteins through induction using relatively inexpensive chemicals. *E. coli*, among other enteric bacteria, requires the *lac* operon for the metabolization and transport of lactose.<sup>258</sup> Regulation of these genes expression rely on lactose availability, which makes the *lac* operon a useful tool for the controlled expression of proteins in transformed *E. coli*. In absence of lactose, the *lac* repressor binds the operator sequence blocking the access of the T7 RNA polymerase to the promoter site and thus, preventing transcription of the gene of interest.<sup>259,260</sup> In the

presence of lactose, the *lac* repressor protein binds to lactose preventing its binding to the operator in an allosteric manner. Then, T7 RNA polymerase can bind to the T7 promoter, trigger transcription of the *lac* operon and induce protein expression. Isopropyl  $\beta$ -D-1-thiogalactopyranoside (IPTG) is a molecular mimic of allolactose that acts in a similar way but it cannot be metabolized by the cells. Thus, IPTG concentration remains constant and the expression of *lac*-controlled genes would not be inhibited during the experiment (**Figure 25A**).

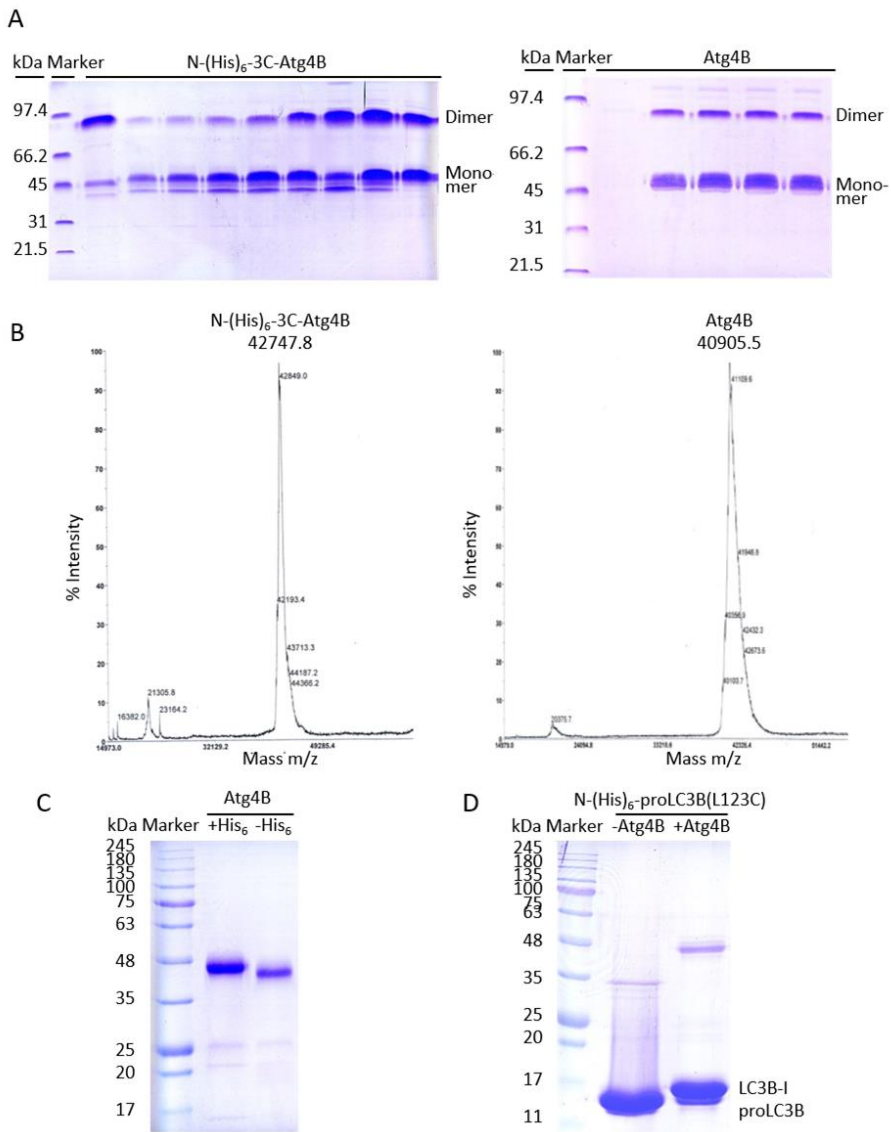
More recently, Studier described a method for protein expression based on autoinduction.<sup>261</sup> This method relies on the ability of certain media to induce protein expression when cells reach saturation. It occurs under control of natural cellular networks that sense the energy levels and nutritional status of the cells.<sup>262</sup> Autoinduction can be regulated by adjusting the glucose/lactose/glycerol levels in media. Glucose is preferentially metabolized during growth. When glucose is depleted, lactose is then uptaken inducing protein expression, usually in mid to late log phase. Higher yields are usually obtained containing less protein aggregates and without the need of monitoring the cell growth (**Figure 25B**).<sup>261</sup>

In a first attempt, the N-(His)<sub>6</sub>-Atg4B expression was explored using the traditional IPTG-mediated induction. However, since this approach failed due to protein aggregation, the desired protein was finally obtained applying the autoinduction method, obtaining 8.4 mg of protein per litre of medium. Identity and purity of the enzyme was assessed by sodium dodecyl sulphate-polyacrylamide gel electrophoresis (SDS-PAGE) followed by Coomassie staining of the gel and matrix-assisted laser desorption/ionization-time-of-flight (MALDI-TOF-MS) (**Figure 26A** and **B**, right). As observed, in absence of reducing agents a dimer is formed due to the presence interchain disulphide bonds. Dimer formation can be prevented by the addition of reducing reagents such as tris(2-carboxyethyl)phosphine (TCEP) or dithiothreitol (DTT).

The N-terminal (His)<sub>6</sub>-tag of Atg4B was then cleaved to prevent the binding of the Eu<sup>3+</sup>-labelled anti-6xHis antibody. The Atg4B protein is cloned into a pOPIN vector containing a PreScission protease cleavage sequence.<sup>263</sup> The cleavable tag has the following sequence MAHHHHHSSGLEVLFG-*cleavage site*-GP and it is recognized by the human rhinovirus 3C protease (HRV 3C). Thus, Atg4B was incubated with a GST-tagged 3C protease overnight at 4 °C. The 3C protease was then removed from the reaction mixture employing a GST-Trap4B Column and the released (His)<sub>6</sub>-tag was eliminated by size exclusion chromatography. Identity and purity of the cleaved enzyme was assessed by SDS-PAGE followed by Coomassie staining of the gel and MALDI-TOF mass analysis (**Figure 26A** and **B**, left). The difference in molecular weight of the protein was analysed by MALDI-TOF and SDS-PAGE (**Figure 26B** and **C**). The activity of the expressed N-(His)<sub>6</sub>-Atg4B was also confirmed by SDS-PAGE upon



incubation with the substrate proLC3B and the subsequent detection of the cleaved LC3B-I (Figure 26D).

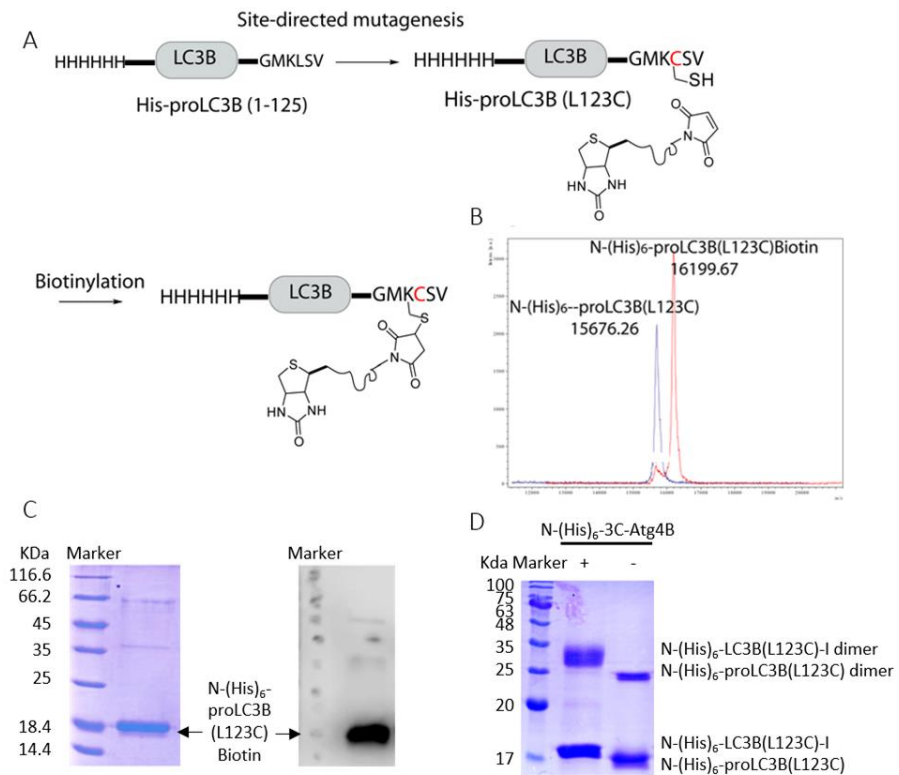


**Figure 26.** Characterization of the purified N-(His)<sub>6</sub>-3C-Atg4B and Atg4B. **A**) Collected aliquots after purification through Ni<sup>2+</sup>-NTA agarose and size exclusion chromatography of N-(His)<sub>6</sub>-3C-Atg4B (left) and Atg4B after (His)<sub>6</sub>-tag cleavage (right), respectively. In absence of reducing agents in the buffer, part of the protein formed a dimer, that runs at the doubled molecular weight. **B** and **C**) Removal of (His)<sub>6</sub>-tag was checked by MALDI-TOF analysis (**B**) and SDS-PAGE followed by Coomassie staining (**C**) Calculated molecular mass for the cleaved sequence (calcd. mass for C<sub>88</sub>H<sub>126</sub>N<sub>30</sub>O<sub>23</sub>S<sub>1</sub> [M+H]<sup>+</sup>: 2004.22) closely

matches the observed mass difference ( $m/z$  1882.). **D**) Enzyme activity was confirmed by incubation with its substrate, N-(His)<sub>6</sub>-proLC3B(L123C), for 2 h at 37 °C. As shown, all proLC3B was transformed to LC3B-I, thereby indicating the activity of the purified enzyme.

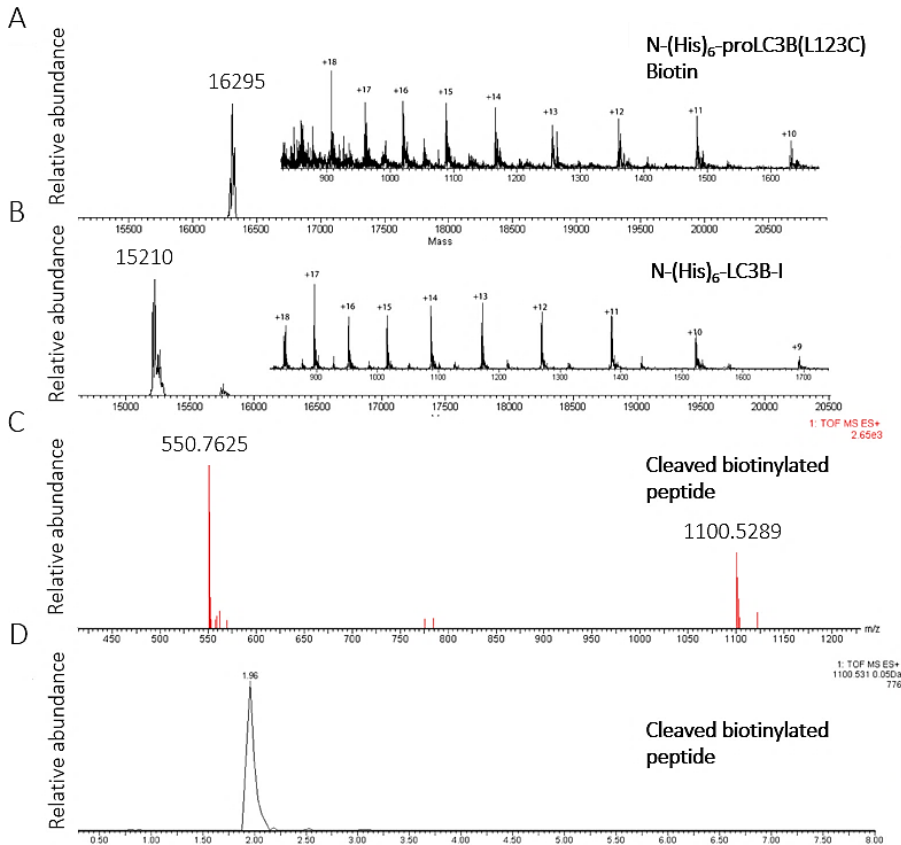
## 8. Biotinylated N-(His)<sub>6</sub>-proLC3B(L123C) expression and purification

The plasmid encoding proLC3B, fused to a (His)<sub>6</sub>-tag at the N-terminus and cloned into a pOPIN-vector, was a kind gift of Yaowen Wu, MPI Dortmund. The strategy for large-scale production and purification of the resulting N-(His)<sub>6</sub>-proLC3B(L123C)-Biotin (referred thereafter to as proLC3B-Biotin) is illustrated in **Figure 27A** and involves the expression and site-specific modification of the His<sub>6</sub>-tagged protein.



**Figure 27.** **A**) L123C mutation was introduced in proLC3B by site-directed mutagenesis. The resulting protein was treated with a maleimide-containing Biotin to generate a doubly labelled proLC3B with a (His)<sub>6</sub>-tag at the N-terminus and a biotin at the C-terminus (N-(His)<sub>6</sub>-proLC3B(L123C)-Biotin). **B**) Purity and identity of the modified protein was confirmed by MALDI-TOF analysis. **C**) SDS-PAGE gel stained with Coomassie Blue reveals the migration of biotinylated N-(His)<sub>6</sub>-proLC3B(L123C), designated proLC3B-Biotin. Immunoblot of SDS-PAGE gel transferred to PDFV and detected using Sav-horseradish

peroxidase antibody to stain the biotinylated protein. **D)** SDS-PAGE gel stained with Coomassie Blue reveals the capacity of Atg4B to cleave the modified proLC3B. A dimer of proLC3B can be detected due to the presence of the introduced cysteine and the lack of the reducing agent in the buffer solution.



**Figure 28.** Cleavage studies of Biotinylated LC3 by Atg4B. (His)<sub>6</sub>-Atg4B was shown to cleave the N-(His)<sub>6</sub>-LC3B-L123C-Biotin (EZ-Link™ BMCC-Biotin) and release the expected C-terminal peptide with an observed molecular mass of 1100.5289 Da that matches its calculated monoisotopic mass (C), with the simultaneous conversion of proLC3 (calcd. mass for C<sub>728</sub>H<sub>1149</sub>N<sub>205</sub>O<sub>206</sub>S<sub>7</sub> [M+H]<sup>+</sup>: 16294) to LC3-I (calcd. mass for C<sub>680</sub>H<sub>1070</sub>N<sub>194</sub>O<sub>195</sub>S<sub>4</sub> [M+H]<sup>+</sup>: 15209, B). Spectrum of N-(His)<sub>6</sub>-LC3B-L123C (A) and LC3-I (B). The insert shows the original mass spectra before deconvolution. Extracted-ion chromatogram of mono-charged peptide *m/z*: 1100.5310 (D) and MS spectra of the peak (C).

The proLC3B sequence lacks cysteine residues. Thus, a cysteine could be introduced after the cleavage site by site-directed mutagenesis. Thus, using the appropriate nucleotides leucine 123 was successfully converted to cysteine as confirmed by sequence analysis. The resulting mutated protein was then expressed in *E. coli* by IPTG induction. The resulting recombinant protein was purified by nickel (Ni<sup>2+</sup>-NTA)

affinity chromatography followed by size exclusion chromatography, yielding an average yield of 12.8 mg of protein per litre of bacteria culture. The absence of other cysteine residues enabled the subsequent site-specific biotinylation of the mutated protein by treatment with a maleimide-containing biotin (EZ-Link™ BMCC-Biotin) bound to each other via an aliphatic linker. Identity and purity of the modified protein were assessed by SDS-PAGE followed by Coomassie staining and Western-Blot of the gel and MALDI-TOF-MS (Figure 27B and C). The role as an Atg4B substrate was also confirmed by SDS-PAGE followed by Coomassie staining (Figure 27D) and MS-based analysis (Figure 28).

## 9. TR-FRET assay development

Typically, HTS assays have been developed to measure product formation or substrate depletion. Depending on the reaction type and the substrate employed this can turn into increasing or decreasing signal assays. An example of an TR-FRET assay based on increasing signal are the ones established with kinases and employing biotinylated substrates and a  $\text{Eu}^{3+}$ -labelled antibodies recognizing the phosphate group.<sup>264</sup> In the other hand, an example of a signal decreasing assay is the screening of inhibitors against the ubiquitin conjugating enzyme E2 UBC13. In that case ubiquitin and the E1 enzyme were labelled and their complex generated a TR-FRET signal whereas in case of E2 inhibition the signal decayed.<sup>245</sup> Assays relying on increasing or decreasing signals have different requirements.<sup>265</sup>

The designed assay was a substrate depletion assay. A decreasing signal was expected due to the increased distance between the two tags upon cleavage mediated by Atg4B. In this type of assays initial conditions are critical for the development of a sensitive assay. If the amount of labelled substrate is too large compared to the  $\text{Eu}^{3+}$ -labelled antibody concentration, small changes may remain undetected. Recommended concentrations of the reagents are 2 nM of antibody and 5-50 nM of streptavidin. Thus, the assay was carried out employing two concentrations of the antibody (2 and 5 nM) and the labelled streptavidin in a 1:4 ratio (Sav:protein). Streptavidin has four binding sites for biotin and the Sav:protein ratio should be kept constant not only to capture all biotin-peptide molecules but also to generate a constant background signal. Different ratios of non-biotinylated and biotinylated protein were employed with an overall concentration of 100 nM with the aim of determining which protein concentrations would yield a high TR-FRET signal and a significant net signal reduction. Reagents were added and followed by 1 h incubation at room temperature in the dark. TR-FRET measurements were made using the following settings:  $\lambda_{\text{ex}}$  of 340 nm,  $\lambda_{\text{em}}$  of 620m,  $\lambda_{\text{em}}$  of 665 nm and a delay time of 100  $\mu\text{sec}$ . As it can be seen in **Table 4**, although a consistent increase in light emission at 665 nm can be observed with increasing concentrations of biotinylated protein, the transfer of energy was low in all the cases and the S/B ratio (light emission observed

at 665 nm in absence of biotinylated protein compared to the one obtained in the presence of the highest concentration of biotinylated proLC3B) was just 2.0.

Biotin:non-biotin proLC3B (total conc. 100 nM)	620	665	665/620 ratio
0:1	4563.86	163.33	0.035
0.25:1	4575.64	255.77	0.047
0.66:1	4813.44	300.08	0.068
1:0	4363.22	395.35	0.094

**Table 4.** Average of the signals obtained with 100 nM proLC3B containing increasing ratios of biotinylated protein. This table shows the results from samples treated with 2 nM of Eu<sup>3+</sup>-labelled antibody, although similar results were obtained using a 5 nM concentration.

The absence of TR-FRET signal can be caused by different reasons. The solubility of the protein is a key point since an aggregated protein can significantly alter the binding with the reagents and the distance between the two protein terminuses. For this reason, a detergent was included (0.1% Triton X-100) and the reducing agent TCEP was also added to the buffer, but not significant changes could be observed. Moreover, low binding plates were employed to avoid non-specific binding of the protein to the plate. Concentration of the protein is also a point of interest, a titration from 0 to 100 nM of the protein is recommended for the optimization, however, similar results were obtained in all the cases. An appropriate plate reader is also an important issue. TR-FRET measurements were performed with a Spectramax M5 device. According to the supplier, this plate reader employs monochromators and it can be used for TR-FRET measurements. However, according the supplier of the LANCE™-based reagents, filter-based fluorometers are preferred to obtain a good sensitivity. One of the main reasons for this choice is that filter-based devices ensure a transmission efficiency of light more than 90%, whereas monochromators need a complicated series of narrow light apertures, gratings and mirrors to select a wavelength, what can cause problems at the low fluorophore concentration employed in TR-FRET. In addition, TR-FRET assays may have low energy transfer. In order to enable full optimisation of the assay, it may be preferable to use a short and intense excitation pulse with a very sharp tailing edge, such the one provided by a laser, which results in an enhanced signal to background ratio for optimum Z', whereas the Spectramax employs a Xenon flash lamp as a light source, in which the interfering tail generally lasts 50 microsec. Finally, the distance between the two tags should range between 1 and 10 nm. Recently a TR-FRET assay employing as a substrate a GABARAPL2/GATE16 protein bearing a (His)<sub>6</sub>-tag at the N-terminus and a GST tag at the C-terminus has been established and employed to identify Atg4B inhibitors.<sup>238</sup> Differences here can be attributed to the use of GABARAPL2/GATE-16 as a substrate and to the larger size of the GST tag that may facilitate the transfer of the

energy. However, other factors cannot be discarded such as low solubility and stability of the protein in the buffer. Due to the limitations observed in the TR-FRET assay, an AlphaScreen-based assay was next investigated.

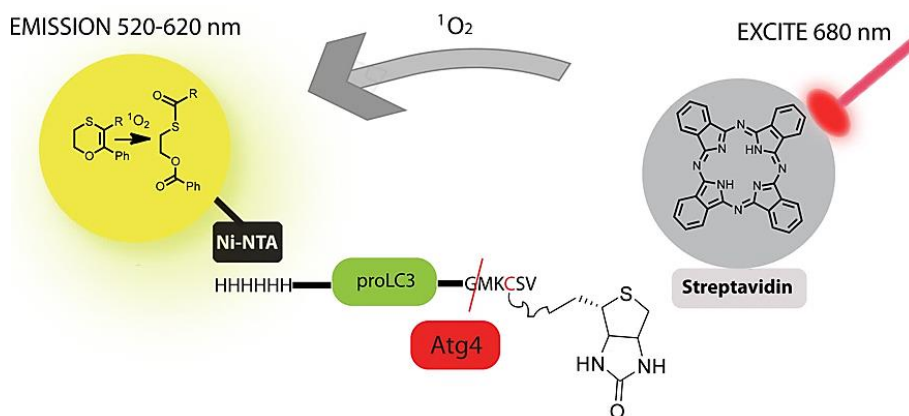
## 10. AlphaScreen technology

The lack of detectable FRET signal prompted us to investigate alternative assay conditions. AlphaScreen (Amplified Luminescent Proximity Homogeneous Assay Screen) is a versatile assay technology based on bead proximity and developed from a methodology known as LOCI (Luminescent Oxygen Channelling Immunoassay).<sup>266</sup> Briefly, donor beads contain a phthalocyanine photosensitizer that excites ambient oxygen into a singlet state after high energy irradiation (at  $\lambda_{\text{ex}}$  of 680 nm). The generated singlet oxygen species can travel over a constrained distance (approximately 200 nm). If acceptor beads are within this distance then get excited leading to a cascade of chemical reactions in the acceptor beads that result in the generation of a chemiluminescent signal at  $\lambda_{\text{em}}$  of 520-620 nm (**Figure 29**).<sup>267</sup>

There are some common features shared by TR-FRET and AlphaScreen methods. For example, both are based on proximity between donor and acceptor molecules or beads, do not require wash steps and can be miniaturized to very small volumes, making them suitable for the development of HTS assays. However, they also present some significant differences. The maximum allowed distance for the energy to transfer from the donor to the acceptor molecules in TR-FRET is 10 nm, whereas in AlphaScreen the distance gets extended to 200 nm.<sup>268</sup> Thus, AlphaScreen technology can be applied to a wider range of substrates. Moreover, AlphaScreen results more sensitive than TR-FRET. Thus, each donor bead can release up to 60.000 singlet oxygen molecules per second resulting in a very high signal amplification that enables to detect molecular interactions at a femtomolar scale and assay miniaturization up to 5  $\mu\text{L}$  final volume. In addition, apart from the high signal it also presents a very low background due to the time-resolved detection (20  $\mu\text{s}$ ) and the fact that the  $\lambda_{\text{em}}$  of the acceptor bead is higher than  $\lambda_{\text{ex}}$  of the donor bead.<sup>267</sup> These rare properties prevent the interference of assay components and low molecular weight compounds. Moreover, the required beads concentrations are very low, which avoids non-specific proximity interactions between donor and acceptor beads. The principal disadvantages of AlphaScreen are the costly reagents and the need of a specific microplate reader having an intense light source, preferably a laser exciting samples exactly at 680 nm (Xenon Flash based systems and luminometers will not work) together with an emission filter discriminating between different wavelengths and a Photo Multiplier Tube (PMT) detector. Based on all these features, it was decided to explore AlphaScreen as a suitable technology to set up an HTS assay aimed to identify Atg4B inhibitors. Furthermore, the commercially available AlphaScreen reagents (modified beads) allowed the use of the same doubly tagged protein already

developed for the TR-FRET-based assay.<sup>267,268</sup>

The conceptual design of this new assay is very similar to the previously developed TR-FRET-based assay (**Figure 29**). Appropriate donor and acceptor beads were next chosen. Donor beads coated with streptavidin should bind biotin with high affinity, whereas acceptor beads coated with nickel strongly bind to the (His)<sub>6</sub>-tag located at the *N*-terminus of the protein. Thus, the intact substrate would yield a high signal and the cleavage of the protein by Atg4B would result in an increase of the distance between donor and acceptor bead and a subsequent loss of signal that could be prevented in the presence of compounds inhibiting Atg4B.



**Figure 29.** Mechanism of AlphaScreen-based assay. Cys123 of proLC3B, located after the cleavage site at the *C*-terminus, is biotinylated, and thus recognized by donor beads coated with streptavidin. Donor beads contain phthalocyanine, which transforms the ambient oxygen (O<sub>2</sub>) to oxygen singlet (<sup>1</sup>O<sub>2</sub>) when it is excited at 680 nm. Oxygen singlet species travel to the acceptor beads if the distance is less than 200 nm. Acceptor beads are coated with nickel<sup>2+</sup>-NTA, which chelates the histidines of the (His)<sub>6</sub>-tag of proLC3B-Biotin, located at the *N*-terminus of the protein. Donor beads contains thioxene, anthracene and rubrene, oxygen singlet species excites thioxene and, after a reaction cascade, rubrene emits chemiluminescence at λ<sub>em</sub> of 520-620 nm.

## 10.1. AlphaScreen optimization

### *Buffer selection and substrate concentration*

As it occurs in other systems based on saturable detection fluorescence-based assays, in AlphaScreen the signal obtained is concentration-dependent up to a point where the signal starts to drop, known as the Hook point. Above this point, donor and acceptor beads are saturated and their association is inhibited causing a progressive signal decrease. Hence, to set up a screening assay directed to find inhibitors, it is

necessary to choose a protein concentration below this Hook point. In addition, assay conditions (buffer components, pH, ionic strength, etc) should ensure integrity, stability and activity of the proteins. Thus, to start with, different assay components and optimal substrate concentrations were investigated. With this aim, as shown in **Table 5** different buffers were essayed. The use of 25 mM Hepes buffer resulted in protein aggregation and high signal due to non-specific interactions (entry 1). The combined addition of 0.5% Triton™ X-100 and 0.1% Bovine serum albumin (BSA) to 25 mM Hepes (pH 7.4) resulted necessary to avoid protein aggregation and protein binding to the

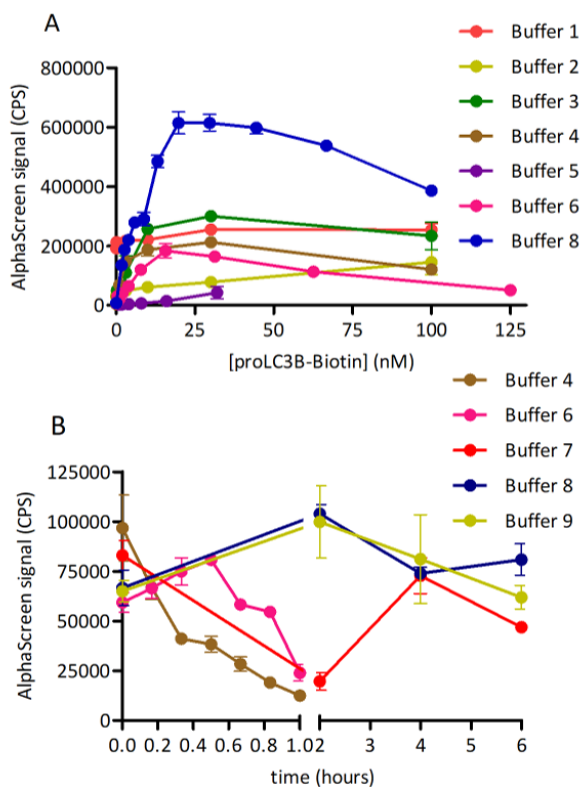
	Buffer	Result
1	25 mM Hepes pH 7.4	Saturated AlphaScreen signal due to aggregates.
2	25 mM Hepes pH 7.4, 0.5 % Triton™ X-100	Low AlphaScreen signal due to protein binding to the plate.
3	25 mM Hepes pH 7.4, 0.1 % BSA	Confusing AlphaScreen signal and high SD, probably due to aggregates.
4	25 mM Hepes pH 8, 0.5 % Triton™ X-100, 0.1 % BSA, 1 mM TCEP	Although Hook effect was observed with low SD, the protein was not stable in the buffer.
5	50 mM Tris pH 8, 150 mM NaCl, 0.5 % Triton™ X-100, 0.1 % BSA, 1 mM TCEP	Low AlphaScreen signal due to the interaction of Tris with the beads.
6	25 mM Hepes pH 8, 150 mM NaCl, 0.5 % Triton™ X-100, 0.1 % BSA, 1 mM TCEP	Although Hook effect was observed with low SD, the protein was not stable over time.
7	25 mM Hepes pH 8, 150 mM NaCl, 1 % Triton™ X-100, 0.1 % BSA, 1 mM TCEP	High SD due to high viscosity.
8	25 mM Hepes pH 8, 150 mM NaCl, 0.5 % Triton™ X-100, 0.1 % BSA, 1 mM TCEP, 1 % glycerol	Hook Effect was observed with low SD and the AlphaScreen signal remained stable for 6 h.
9	25 mM Hepes pH 8, 150 mM NaCl, 0.5 % Triton™ X-100, 0.1 % BSA, 1 mM TCEP, 2 % glycerol	AlphaScreen signal was stable for 4 h but it showed high SD due to the high viscosity.

**Table 5.** Summary of all the tested buffers and the results observed. SD: standard deviation.

plate. With these components in the solution, it was possible to obtain a curve displaying a Hook Effect, as shown in **Figure 30A** for *buffer 4*. Similar conditions employing a Tris buffered solution (entry 5) resulted in a complete loss of signal. In addition, to ensure proper activity of Atg4B, the pH was adjusted to 8 and tris-2-carboxyethyl-phosphine (TCEP) was included as reducing agent to maintain the catalytic cysteine in a reduced form. However, these assay components did not provide good conditions for signal stability over time (**Figure 30B**). For this reason, the



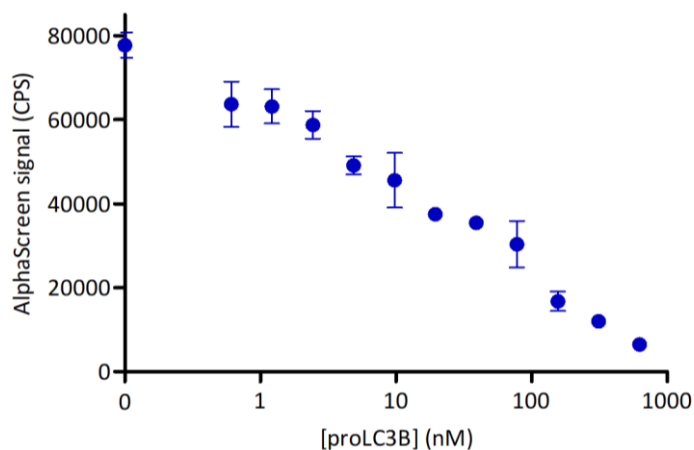
ionic strength was increased (150 mM NaCl, entries 6-9) and glycerol was also added (entries 8-9), ensuring a stable signal during at least 6 h (a ~ 40% reduction was observed after 24 h) (**Figure 30B**). Larger amounts of detergent (entry 7) or glycerol (entry 9) were discarded due to high signal variability. Therefore, the strongest and more stable signal was obtained with the buffer solution 8 containing 25 mM Hepes pH 8, 150 mM NaCl, 0.5 % Triton X-100, 0.1 % BSA, 1 mM TCEP and 1% glycerol, a final bead concentration of 20  $\mu\text{g}/\text{mL}$  and a protein concentration of 8.75 nM (**Figure 30**).



**Figure 30.** **A)** Hook Effect and linearity could be observed increasing concentrations of proLC3B-Biotin when the protein was solubilized in Buffer 3, 4 and 8. **B)** ProLC3B-Biotin incubated in Buffer 4 and 6 at room temperature from 0 to 60 min did not showed stability of the signal over time. Buffer 7 and 9, containing 1% of Triton X-100 and 2% glycerol, respectively, showed high signal variability due to viscosity. Buffer 8 containing 0.5% Triton X-100 and 1% glycerol displayed stable signal for at least 6 h.

Next, signal linearity was investigated employing a competitive assay with increasing concentrations of non-biotinylated proLC3B. As predicted, the loss of signal was observed as non-biotinylated protein concentration increased in a linear manner (**Figure 31**). Hence, the presence of 50% (~8 nM) of non-biotinylated protein resulted

in a ~40% decrease of signal and the presence of 90% (~90 nM) reduced the signal in a ~60%. Small changes can be due to small variability in protein concentration. Therefore, it was concluded that 8.75 nM was the appropriated concentration of proLC3B-Biotin for the assay given that it was possible to detect the signal decrease caused by the protein cleavage catalysed by Atg4B.



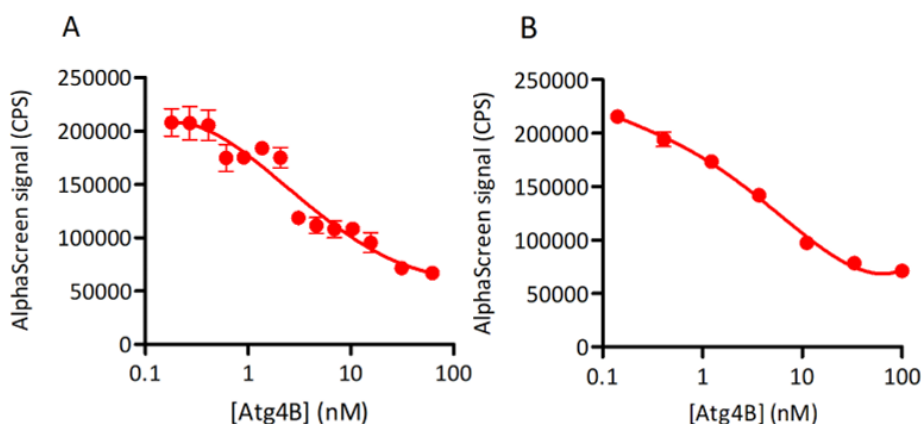
**Figure 31.** Competitive assay with increasing concentrations of non-biotinylated proLC3B mixed with 8.75 nM of proLC3B-Biotin. As observed, the signal decreased in a dose-dependent manner, which confirms that changes in the concentration of non-cleaved substrate would be detected in further assays.

### **Enzyme concentration**

The determination of an optimal enzyme (Atg4B) concentration is also a key point. Enzyme concentration should allow the detection of changes in AlphaScreen signal at a rate which is linear with time. To find an appropriate enzyme concentration, proLC3B-Biotin was titrated against increasing concentrations of Atg4B (30 min incubation at 37 °C). Despite getting a linear dose-dependent reduction of the signal, high enzyme concentrations were required to achieve complete cleavage of the substrate as shown in **Figure 32A**, (almost equimolar amount in relationship to substrate concentration), which makes the assay unreliable.

Reaction rates strongly depends on substrate concentration. Hence, if substrate concentrations far below the  $K_m$  are employed, small changes in substrate concentration can affect the enzymatic rate. As the measured  $K_m$  value for a fusion LC3B-GST protein ranges from 1 to 12  $\mu\text{M}$ ,<sup>233,224</sup> we next explored Atg4B activity employing substrate concentrations close to the  $K_m$  (**Figure 32B**) Indeed, a substantial increase in Atg4B activity could be detected using proLC3B-Biotin concentrations of 1 and 10  $\mu\text{M}$  that resulted more appropriate for the detection of inhibitors. However, despite achieving a linear dose-dependent reduction of the signal, the signal to

background S/B ratio obtained at the highest concentration did not rise over 2.9, suggesting the existence of non-specific interactions.

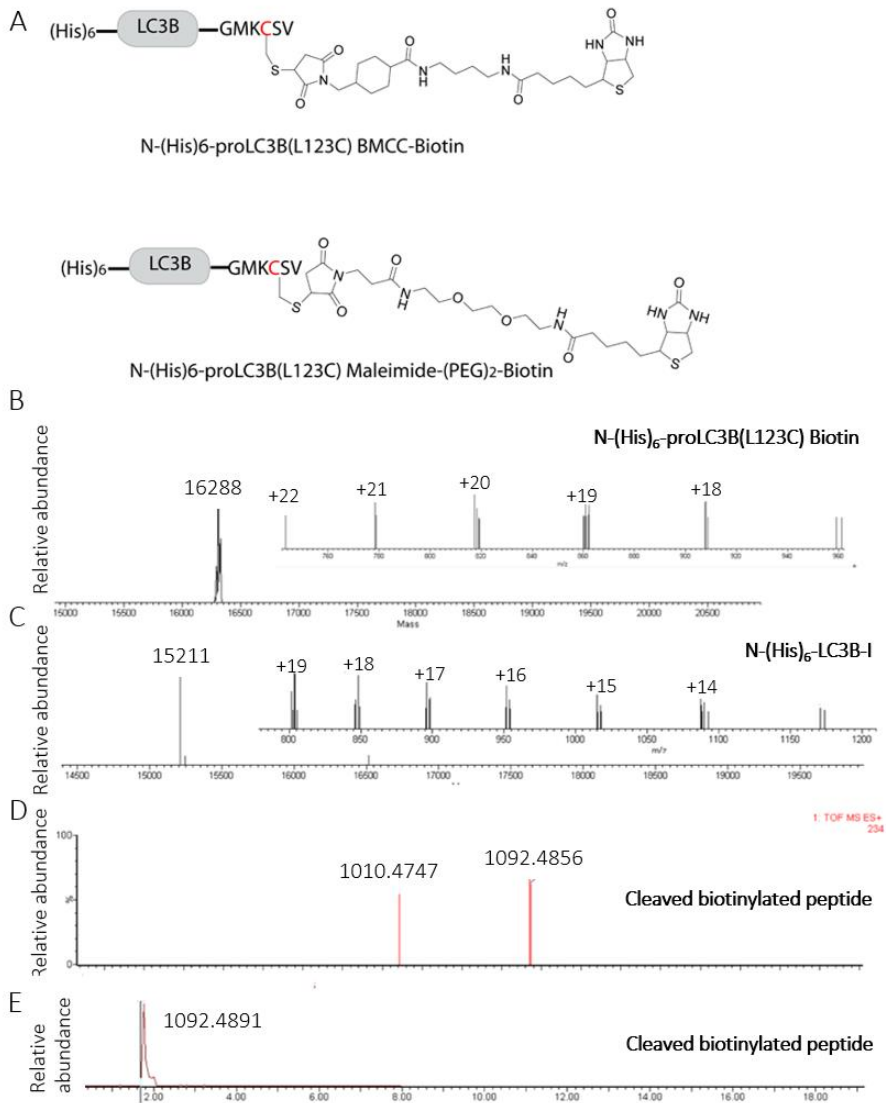


**Figure 32.** A) Atg4B titration in buffer 8 employing a concentration of 8.75 nM proLC3B-Biotin. B) Atg4B titration in buffer 8 employing a concentration of 1  $\mu$ M proLC3B-Biotin.

#### ***Reduction of the high background***

High background signal is usually caused by non-specific interactions between assay components. Blocking agents, BSA or detergents are commonly employed to minimize such interactions. However, the inclusion of 0.1-0.5% of BSA, 0.1% Casein, and detergents such as 0.5%-1% Triton™ X-100, 0.1%, 0.5% and 1% Tween-20, 0.05% and 0.1% CHAPS to the assay buffer could not preclude the existence of non-specific interactions. Other agents were investigated such as 2% glycerol or 1 mM EDTA but any of these agents decreased the high background signal.

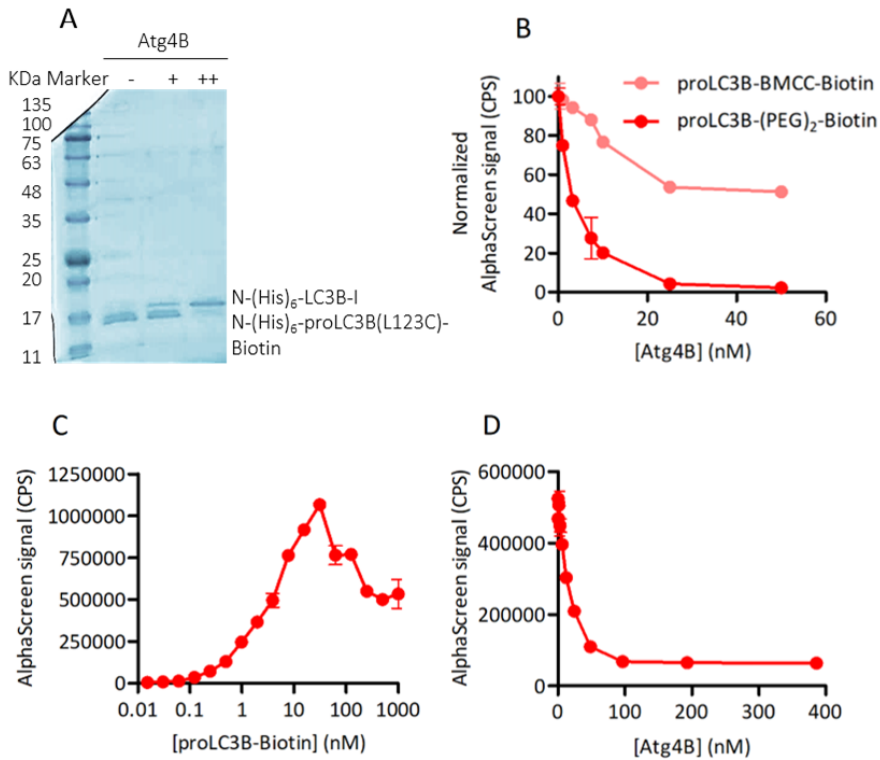
Next, it was explored whether the high background was caused by non-specific interactions of the cleaved biotinylated peptide with the generated LC3-I. To explore this possibility, an additional biotinylated protein was prepared using a maleimide-containing biotin linked to each other via a polyethylene glycol (PEG) linker instead of an aliphatic linker (**Figure 33A**). The presence of the PEG should increase the aqueous solubility of the released peptide, thereby preventing non-specific interactions with the protein surface. Identity of the modified protein was again confirmed by MS analysis (**Figure 33B-E**). The role of this new modified protein as substrate of the enzyme Atg4B was also confirmed by SDS-PAGE followed by Coomassie staining (**Figure 34A**).



**Figure 33.** **A**) Structures of the two biotinylated proteins prepared. **B**) Cleavage studies of Biotinylated LC3 by Atg4B. (His)<sub>6</sub>-Atg4B was shown to cleave the N-(His)<sub>6</sub>-LC3B-L123C-Biotin (EZ-Link™Maleimide-PEG<sub>2</sub>-Biotin) and release the expected C-terminal peptide with an observed molecular mass of 1092.4856 Da that matches its calculated monoisotopic mass **(D)**, with the simultaneous conversion of proLC3 (calcd. mass for C<sub>725</sub>H<sub>1145</sub>N<sub>205</sub>O<sub>208</sub>S<sub>7</sub> [M+H]<sup>+</sup>: 16286) to LC3-I (calcd. mass for C<sub>680</sub>H<sub>1070</sub>N<sub>194</sub>O<sub>195</sub>S<sub>4</sub> [M+H]<sup>+</sup>: 15209, **B**). Spectrum of N-(His)<sub>6</sub>-LC3B-L123C **(B)** and LC3-I **(C)**. The insert shows the original mass spectra before deconvolution. Extracted-ion chromatogram of mono-charged peptide *m/z*: 1092.4891 **(E)** and MS spectra of the peak **(D)**.

A preliminary assay was done in order to compare the signal displayed by proLC3B

biotinylated with biotin or PEG-Biotin employing 1  $\mu\text{M}$  of the protein and increasing concentrations of Atg4B. Gratifyingly, after titration with increasing concentrations of Atg4B, the S/B ratio at the highest tested concentrations was higher, ranging from 23 at 25 nM to 40 at 50 nM of Atg4B (**Figure 34B**). However, determining of new conditions was required and, after establishing the concentration causing a Hook point (31.25 nM, **Figure 34C**), Atg4B activity was again investigated using a substrate concentration of 10  $\mu\text{M}$  and including a dilution step before analysis.



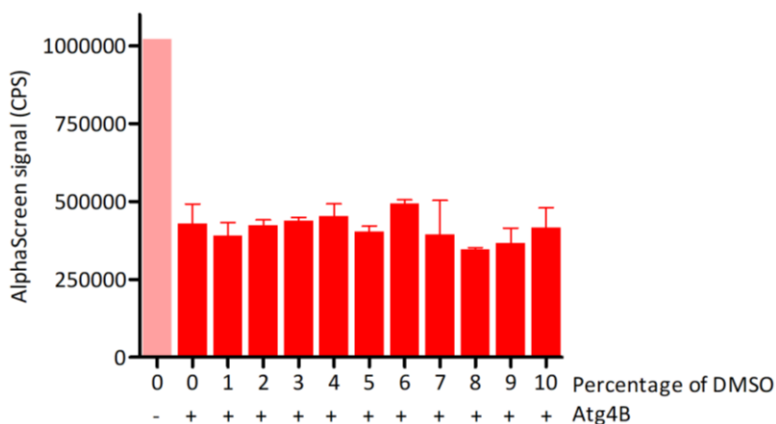
**Figure 34.** **A)** ProLC3B-Biotin with a PEG linker was treated with Atg4B at 37 °C for 2h, then the cleavage was analysed by SDS-PAGE stained with Coomassie. As depicted, the substrate was partially cleaved when the relation between proLC3B-Biotin and Atg4B was 4:0.1 w/w (+) whereas the cleavage was complete when the ratio was 4:1 w/w (++) and all the substrate became N-(His)<sub>6</sub>-LC3B-I. **B)** Normalised AlphaScreen signal by highest AlphaScreen values displayed by proLC3B-Biotin (1  $\mu\text{M}$ ) biotinylated with EZ-Link™ BMCC-Biotin and EZ-Link™ Maleimide-PEG<sub>2</sub>-Biotin after treatment with increasing concentrations of Atg4B (0-50 nM) for 30 min at 37 °C. **C)** ProLC3B-Biotin biotinylated with EZ-Link™ Maleimide-PEG<sub>2</sub>-Biotin was titrated in buffer 8 in order to select the optimal proLC3B-Biotin concentration for the readout, 31.25 nM was the maximum concentration before the Hook point. **D)** 10  $\mu\text{M}$  of proLC3B-Biotin were treated with Atg4B (0-386 nM) for 30 min at 37 °C. Aliquots of the mixtures were diluted to a final concentration of

proLC3B-Biotin of 2.5 nM and measured. 25 nM was the selected working concentration for Atg4B.

In assays measuring product formation, ~10% conversion is generally preferred. However, substrate depletion measurements are based on signal changes from a high baseline value. In this case, to obtain a sufficient assay window, the substrate turnover may need to be close to 50% or higher.<sup>269,265</sup> When working at substrate concentration close to the  $K_m$ , this high conversion has only a slight effect on the obtained  $IC_{50}$  values. As a result, a 10  $\mu M$  concentration of the substrate and a 25 nM concentration of Atg4B was chosen providing a S/B ratio close to ~3 (Figure 34D).

### DMSO tolerance

Compound libraries are generally stored in in dimethyl sulfoxide (DMSO) solutions. Thus, it was next necessary to evaluate the DMSO tolerance of the assay. To this end, the effect of DMSO on enzyme activity and assay performance was determined by incubating the assay mixture with increasing concentrations of DMSO. No significant differences were observed in any case, indicating that the assay can tolerate up to 10% of DMSO (Figure 35).

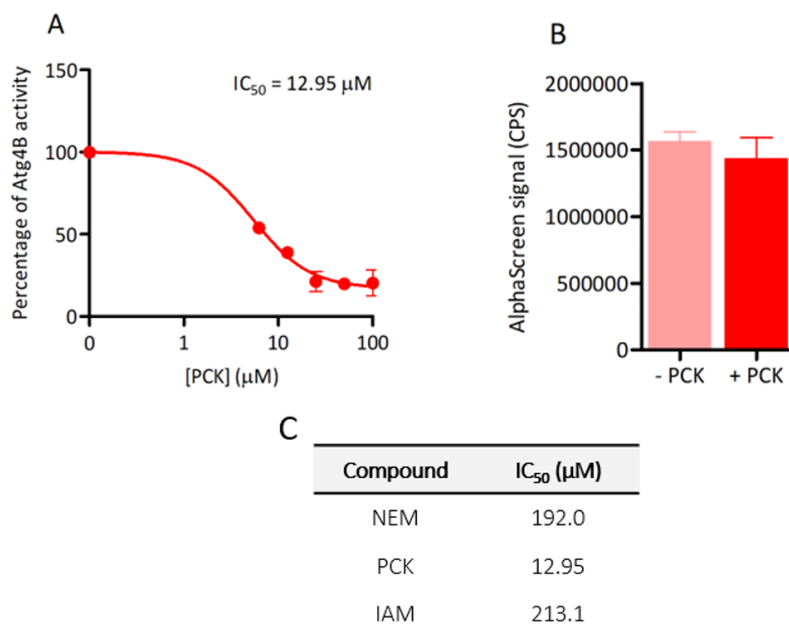


**Figure 35.** Determination of DMSO tolerance. DMSO content up to 10% was added to the mixture of proLC3B-Biotin and Atg4B and, after incubation of 30 min at 37 °C, AlphaScreen signal was determined. An untreated control without Atg4B was added.

### Positive controls of inhibition

To investigate the ability of the assay to detect inhibitors, three known Atg4B inhibitors were purchased and analysed: Z,L-Phe-chloromethylketone (PCK), N-ethylmaleimide (NEM) and iodoacetamide (IAM).<sup>224,270,271</sup> All of them are known cysteine alkylating agents which irreversibly inactivate reduced Atg4B. Concentration-response curves in triplicate were generated from fresh drug stocks resulting in positive inhibition curves (Figure 36A and C), which confirms the suitability of the

assay for the detection of Atg4B inhibitors. Since PCK was the most potent inhibitor, this compound was selected as a positive control to be used in further assays. To discard that PCK was non-specifically interfering with the AlphaScreen signal, this compound was evaluated in a counter screen assay using a (His)<sub>6</sub>-biotinylated peptide as a substrate (**Figure 36B**). Differences in IC<sub>50</sub> values can be caused by different assay conditions. Hence, whereas the initial IC<sub>50</sub> value reported for PCK was 0.63 μM,<sup>224</sup> a recent work could not detect inhibition with PCK using an SDS-PAGE assay.<sup>234</sup>



**Figure 36.** Concentration-response curve and IC<sub>50</sub> values of NEM, PCK and IAM were calculated from the results obtained in AlphaScreen based assay through preincubation with Atg4B during 1 h. **A)** PCK, concentrations ranging from 0 to 100 μM were employed to determine the IC<sub>50</sub> value. **B)** AlphaScreen signal displayed employing the biotinylated control peptide (His)<sub>6</sub>-Biotin as a substrate in presence and absence of PCK, to confirm that the compound did not interfere with the AlphaScreen signal. **C)** Table showing IC<sub>50</sub> values obtained for NEM (concentrations ranging from 0 to 5 mM), PCK (concentrations ranging from 0 to 100 μM) and IAM (concentrations ranging from 0 to 500 μM).

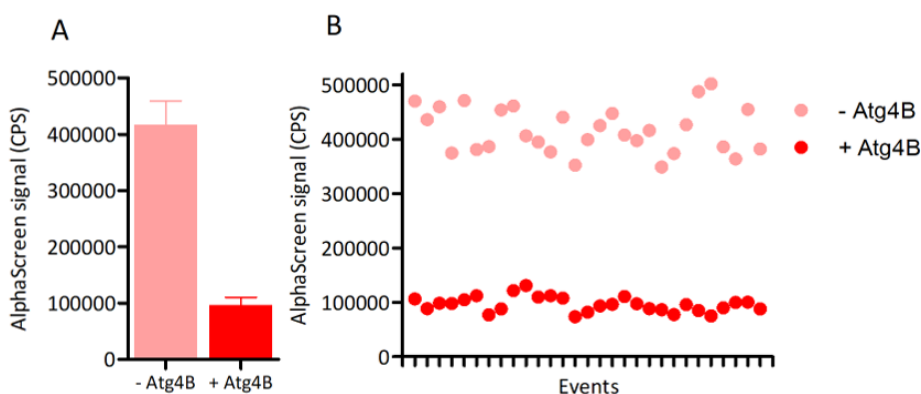
### Z-Factor

The Z-factor, commonly written as Z', is a simple statistical parameter that is commonly used to assess the overall quality of an HTS assay. It is unitless and considers the factors affecting either the dynamic range or the variation in measured signals of both a group of positive controls and a group of negative controls. It was proposed by Zhang and Oldenburg in 1999 and it can be estimated with the following

formulae, where SD is the standard deviation, pos refers to positive and neg to negative controls.<sup>272</sup>

$$Z' - \text{factor} = 1 - \frac{3\text{SD of pos controls} + 3\text{SD of neg controls}}{|\text{mean of pos controls} - \text{mean of neg controls}|}$$

Generally, a Z-factor value close to 1 is an ideal assay for HTS, values between 0.5 and 1 are considered good quality, values <0.5 are considered to have a moderate to good quality and < 0 indicated that the assay cannot be used in HTS. Thus, to determine the Z-factor of the established assay, thirty positive controls and thirty negative controls were measured and the corresponding Z-factor was calculated and established in 0.52, indicating that the assay can be employed for HTS (**Figure 37**). One should have in mind that although a higher Z-factor value would be preferred, signal decreasing assays present always some limitations since the assay window is restricted by the amount of enzyme that can be employed without losing sensitivity. In addition, manual pipetting of small quantities may suffer from higher variability affecting the final Z-factor. These variations should be minimized in future studies using automatic liquid handling devices.



**Figure 37.** Z-Factor of the assay. Thirty aliquots of 10  $\mu\text{M}$  of proLC3B-Biotin were prepared and incubated for 30 min at 37  $^{\circ}\text{C}$  in the presence or absence of 25 nM of Atg4B. Then the AlphaScreen signal was measured and the corresponding Z-factor was calculated.

## 11. A Mass Spectrometry-based assay as an alternative method to determine Atg4B activity

### 11.1. Assay optimization

The hit validation process involves the confirmation of activity of the identified using orthogonal assays, i.e. an assay that test the activity against the target protein using a different output than the primary assay. With this aim, an assay based on mass spectrometry detection of the released peptide was next developed. Thus, N-(His)<sub>6</sub>-

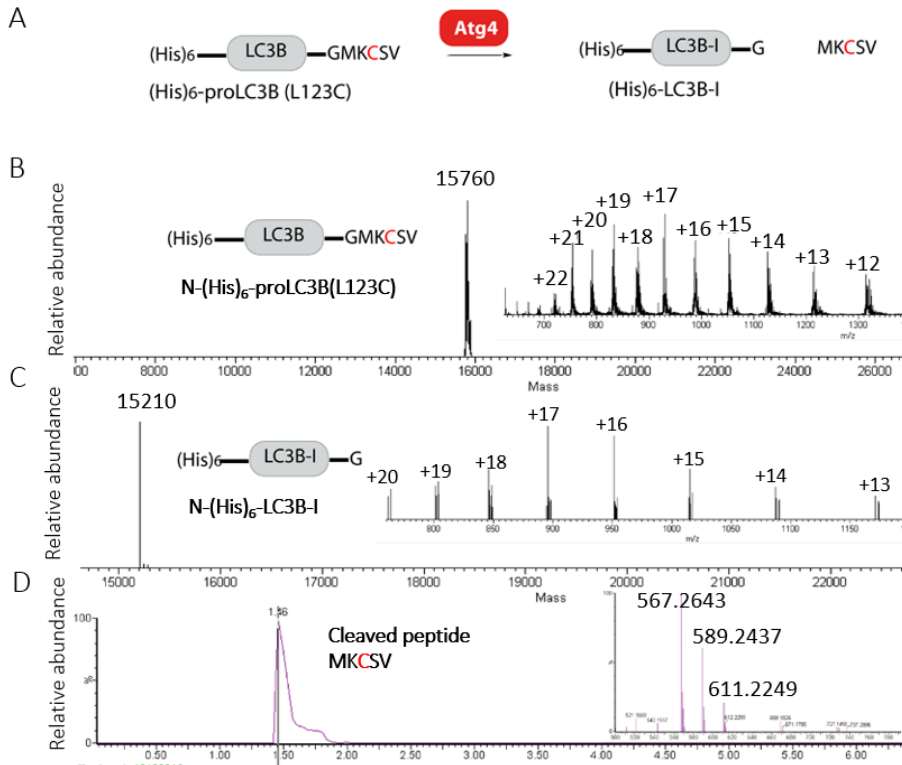


3C-Atg4B should cleave the N-(His)<sub>6</sub>-proLC3B(L123C) (molecular mass [M+H]<sup>+</sup> of 15761.1445) and convert it to N-(His)<sub>6</sub>-LC3-I(L123C) (molecular mass [M+H]<sup>+</sup> of 15211.8975), together with the release of the corresponding C-terminal peptide MKCSV (molecular mass [M+H]<sup>+</sup> of 567.2635) and the analysis of the samples by ultra-performance liquid chromatography (UPLC)-TOF should enable to monitor the extent of the formation of the cleaved peptide. The non-biotinylated protein was employed in this case as a substrate to discard any effect of the biotin on the final readout and to avoid the use of the biotinylated protein, that requires additional steps for its preparation and purification.

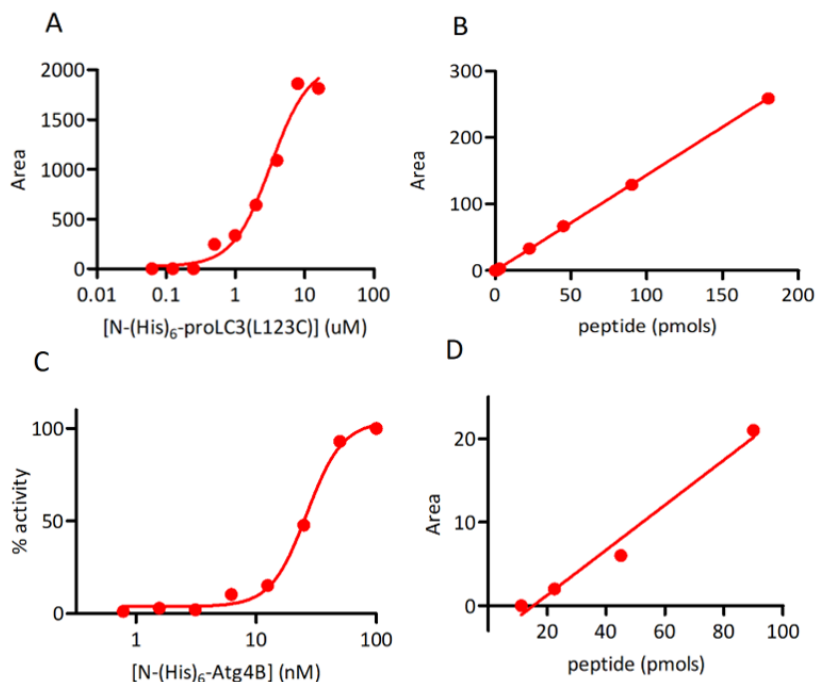
A buffer similar to the one used in the AlphaScreen assay was employed in the MS-based assay but displaying some differences. Thus, BSA was discarded since the assay was carried out in glass vials therefore preventing the non-specific interaction of protein to the plastic surface. Glycerol was removed to reduce the viscosity of the sample and the non-ionic detergent Triton X-100 was eliminated due to incompatibility with MS-based analysis. The resulting assay buffer was 25 mM Hepes pH 8, 150 mM NaCl and 1 mM TCEP, and the proteins turn out to be stable in this buffer during the assay time frame (30 min incubation).

First, the limit of detection of the uncleaved protein was investigated by injecting serially diluted samples of the target protein (**Figure 38A** and **Figure 39A**). Next, a calibration curve for the cleaved peptide was established by injecting serially diluted samples of N-(His)<sub>6</sub>-proLC3B(L123C) (18 μM) fully cleaved by incubation with 100 nM of Atg4B at 37 °C for 2 h. Complete reaction was confirmed by disappearance of N-(His)<sub>6</sub>-proLC3B(L123C) and formation of N-(His)<sub>6</sub>-LC3B-I (**Figure 38** and **Figure 39B**). Linearity of the signal-concentration relationship was confirmed in all the range of concentrations investigated.

Then, varying concentrations of N-(His)<sub>6</sub>-Atg4B (0-100 nM) were titrated to a fixed protein substrate concentration (18 μM) and the mixture was incubated at 37 °C during 30 min. The amount of formed peptide was quantified and changes in peak areas were used to calculate the rate of the cleavage by comparison with the calibration curve (**Figure 39C** and **D**). Based on these results, a 10 nM concentration of N-(His)<sub>6</sub>-Atg4B was chosen to ensure that the enzyme was working at the initial rate, thereby showing a linear response.



**Figure 38.** N-(His)<sub>6</sub>-3C-Atg4B was shown to cleave the N-(His)<sub>6</sub>-proLC3B(L123C) and release the expected C-terminal peptide with an observed molecular mass of 567.2643 Da that matches its calculated monoisotopic mass, with the simultaneous conversion of the N-(His)<sub>6</sub>-proLC3B(L123C) (calcd. mass for C<sub>702</sub>H<sub>1110</sub>O<sub>201</sub>N<sub>200</sub>S<sub>6</sub> [M+H]<sup>+</sup>: 15760) to N-(His)<sub>6</sub>-LC3B-I (calcd. mass for C<sub>680</sub>H<sub>1070</sub>N<sub>194</sub>O<sub>195</sub>S<sub>4</sub> [M+H]<sup>+</sup>: 15209). Mass of N-(His)<sub>6</sub>-proLC3B(L123C) (**A**) and N-(His)<sub>6</sub>-LC3B-I (**B**). The insert shows the original mass spectra before deconvolution. **C**) Extracted-ion chromatogram of mono-charged peptide m/z: 567.2643. The insert shows the MS spectra of the peak.



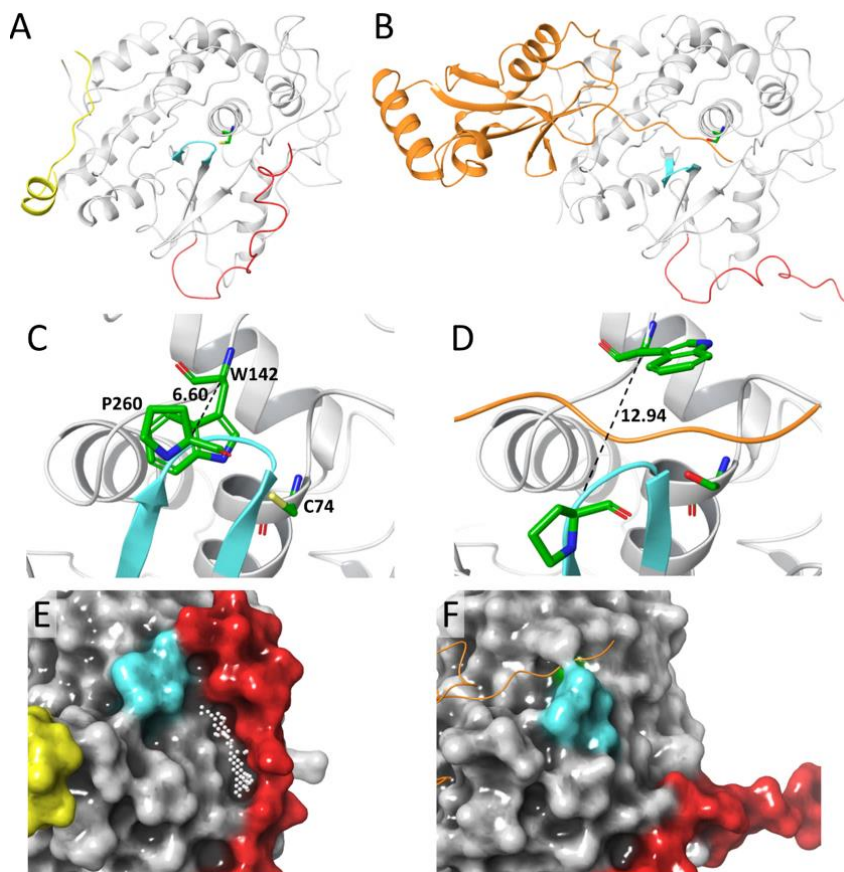
**Figure 39.** **A)** A titration of the untreated protein N-(His)<sub>6</sub>-LC3B(L123C) was analyzed by UPLC-TOF. The protein could be well detected until 0.5 μM (retention time: 2.4 min). **B)** Released peptide. Linearity and robustness of the signal (peak areas) was assessed employing aliquots of serially diluted samples from fully cleaved protein and using extracted ion chromatograms with a mass tolerance window of 5 ppm. The limit of quantification (LOQ) was on the order of 1.4 nmol and the response was linear from 2.81 up to 180 pmol, the coefficient of correlation resulted 0.9999. **C)** Varying concentrations of N-(His)<sub>6</sub>-3C-Atg4B (0-100 nM) were titrated to a fixed protein substrate concentration (18 μM) and the mixture was incubated at 37 °C during 30 min. Then, aliquots of 130 μl were analysed at UPLC/TOF-MS. **D)** Biotinylated peptide. Linearity and robustness of the signal (peak areas) was assessed employing aliquots of serially diluted samples and using extracted ion chromatograms with a mass tolerance window of 5 ppm. The limit of quantification (LOQ) was on the order of 1.4 nmol and the response was linear from 2.81 up to 90 pmol ( $r : 0.9780$ ).

## 12. Screening

### 12.1. Virtual Screening

There are a few crystal structures reported for human Atg4B in the literature<sup>273,274,275</sup> which show the existence of two structurally different forms of the enzyme: an apo form in absence of substrate, where a regulatory loop (residues 258-263) together with tryptophan 142 (W142) masks the entrance to the active site, and another one with the LC3 substrate bound to the enzyme, where the regulatory loop is displaced

from its original location. PDB structure 2CY7<sup>275</sup> is representative of the closed Atg4B (Figure 40A and C), and structure 2ZZP,<sup>274</sup> corresponding to the complex of the inactive Atg4B C74S mutant with a bound LC3 substrate, is representative of the open form (Figure 40B and D).



**Figure 40.** Crystal structure of (A) free Atg4B (PDB 2CY7) and (B) the LC3-Atg4B C74S complex (PDB 2ZZP), showing the regulatory loop (258-263) in cyan, the LC3 substrate in orange including the key residues P119 and G120, the W142 and the catalytic cysteine (C74, A) in yellow. Detailed view of the active centre of (C) free Atg4B, showing the distance between the C $\alpha$ -atoms of residues W142 and P260, and (D) the same for the LC3-Atg4B C74S complex. Surface representation of Atg4B in 2CY7 (E) and 2ZZP (F) showing the region close to residues D278 and H280, where a potential ligand binding site present only in the closed form is highlighted with white spheres. Surface colouring is the same as in panels A-B.

Briefly, interaction of regulatory loop with W142 keeps closed the entrance of the binding site. Upon LC3 binding to Atg4B, the interaction of phenylalanine (P119) with W142 moves the regulatory loop creating a small cavity at the entrance of the active

site, in which only a small glycine (G) can be adjusted. The interaction of the C-terminal region is not enough to open the cavity, requiring the interaction with the full LC3 protein. These results explain the low affinity observed for peptide substrates resembling the C-terminal tail of LC3.

A virtual screening was performed by Dr. Jordi Bujons (Institute of Advanced Chemistry of Catalonia) employing the National Cancer Institute (NCI) Open Database as source of potential ligands (265242 compounds) and both Atg4B structures. After an initial filtering to remove compounds with undesired properties and a structure expansion step to generate different tautomers, protomers, and ring conformers of each compound, a total of 395712 structures resulted which were submitted to high-throughput Virtual Screening (HTVS). Two potential binding sites were explored, the active site and an alternative potential binding site close to residues D278 and H280, at the interface between the detachable *N*-terminal tail and the core of the closed form of the protein. This alternative binding site has also been proposed as target to identify compounds which could lock Atg4B in its closed-inactive form.<sup>224</sup> This site is depicted in **Figure 40E** and the results of MD studies show that, although with small changes in shape, it perdures during the whole simulation. On the contrary, binding of LC3 induces a change in the conformation of the *N*-terminal tail that removes this site (**Figure 40F**) and it is not restored during the simulation. Thus, the Atg4B structure from 2ZZP\_full was chosen to identify ligands that could bind into the active site while that from 2CY7\_full would allow to identify ligands that could target the second alternative site. A virtual screening workflow<sup>276</sup> that uses the docking software Glide<sup>277,278,279,280</sup> and the software Vina<sup>281,282</sup> to perform the flexible docking of the ligand structures at different levels of accuracy was employed. At the end, four potential list of ligands were obtained: Glide VS2CY7, Glide VS 2ZZP, Vina 2CY7, Vina 2 ZZP.

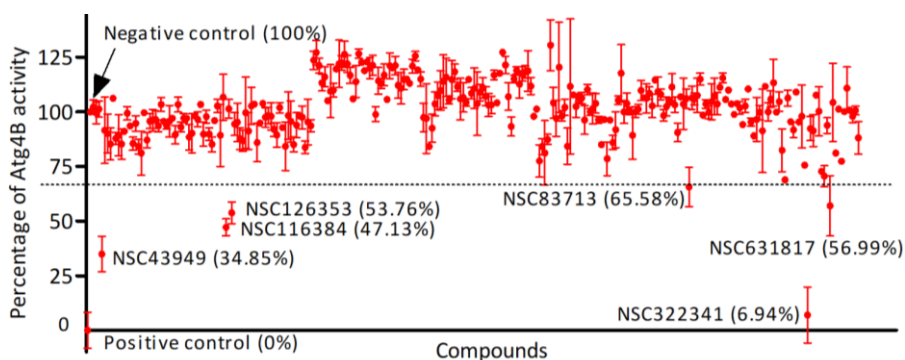
## 12.2. Biological Screening (AlphaScreen)

The top scored compounds from virtual screening at the two Atg4B sites were visually inspected to discard potential pan assay interference compounds (PAINS), intrinsically promiscuous compounds sharing common structural motifs that tend to interact non-specifically with proteins giving false positive results.<sup>283</sup> Mechanism of these non-specific interactions are various and include reactivity with protein nucleophiles such as thiols and amines, metal chelation that can interfere with proteins or assay reagents, redox activity, physicochemical interferences (micelle formation, protein aggregates) or having photochromic properties that might interfere with common assays readouts such as absorption and fluorescence. In addition, frequent hitters in AlphaScreen assays due to their interference with the measured signal or because can prevent the binding of the (His)<sub>6</sub>-tag to the nickel chelate (Ni<sup>2+</sup>-NTA) beads, were also identified and discarded.<sup>284</sup>

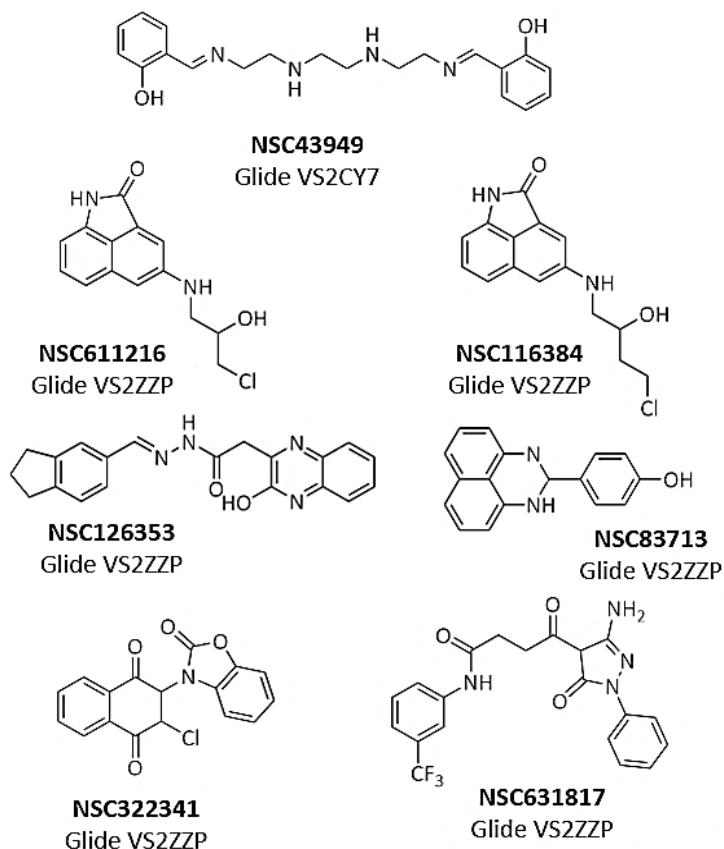
Once promiscuous and non-specific compounds were discarded and availability was checked, 250 compounds were selected as potential binders against the Atg4B active site or against the second alternative site (**Table 6** and **Annexes**). These compounds were obtained from the NCI for biological testing (40 compounds/month). All compounds were initially checked at a single concentration of 200  $\mu$ M in DMSO. Atg4B was first pre-treated with the buffer containing TCEP for 1 h on ice and the compounds were next added and incubated for 1 additional hour at room temperature, then the substrate proLC3B-Biotin was added to the mixture and incubated at 37 °C during 30 min.

Method	Selected	Atg4B activity (%)		
		<85-65	<65-40	<40
Glide VS 2CY7	81	3		1
Glide VS 2ZZP	75	7	2	1
Vina VS 2CY7	41	5		
Vina VS 2ZZP	53	7	1	1

**Table 6.** Number of compounds selected from the HTVS employing the Glide and Vina software and identified active compounds depending on the displayed activity in the AlphaScreen assay (<85-60% enzyme activity, <60-40 or <40%).



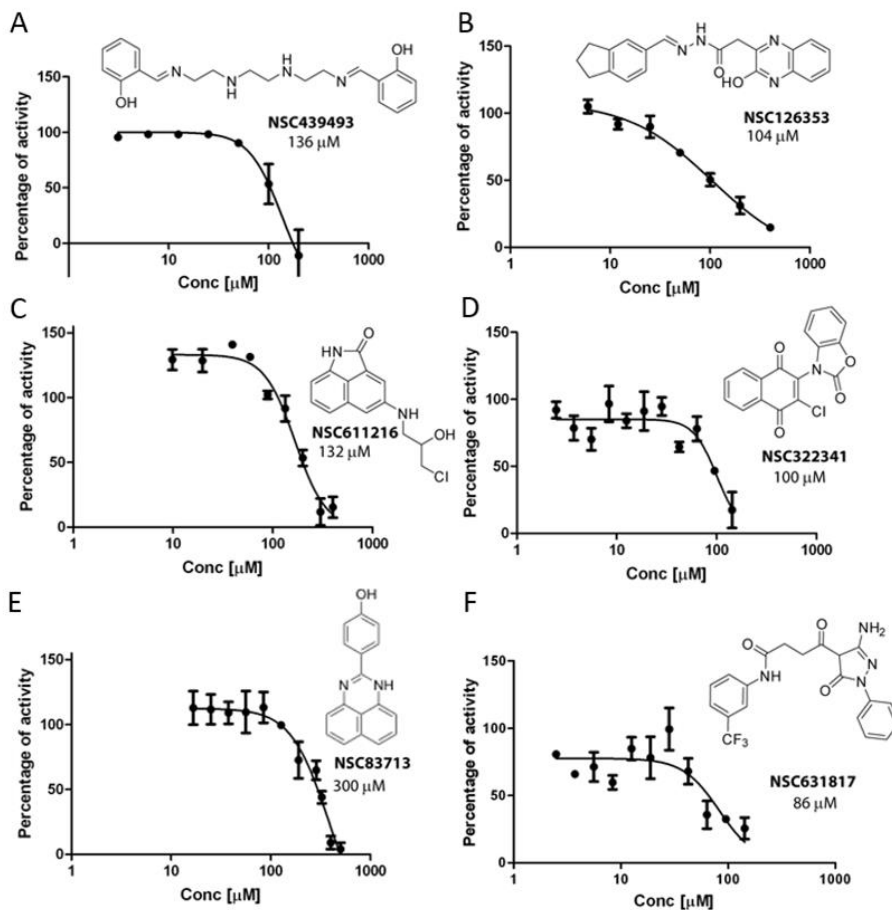
**Figure 41.** Compound library was screened using the established AlphaScreen-based assay. 250 compounds were preincubated on ice for 1 h with Atg4B and then the mixture was added to proLC3B and was incubated for 30 min at 37 °C. A sample without Atg4B was employed as positive control and a sample with Atg4B but without compounds was employed as negative. Six compounds showed <65% of activity (**NSC43949**, **NSC126353** and **NSC116384**, **NSC83713**, **NSC322341** and **NSC631817**) and were selected for further analysis.



**Chart 5.** Compounds showing a decrease in Atg4B activity around 40% or more,  $IC_{50}$  were calculated for these compounds

Five active-site directed compounds (**NSC83713**, **NSC126353**, **NSC116384**, **NSC322341** and **NSC631817**) showed around 65% or better inhibition in a preliminary single concentration assay (200  $\mu$ M), while only one (**NSC43949**) of the hits against the second binding site showed >40% inhibition (**Figure 41** and **Chart 5**). In general, the Glide software show a slight better success rate that the Vina software.

Half-maximal inhibitory concentrations ( $IC_{50}$ ) were then determined for these initial hits in concentration response studies. The compounds showed promising dose-dependent inhibition of Atg4B with  $IC_{50}$  values ranging from 86 to 300  $\mu$ M. The inhibitory profiles of these five compounds with an unambiguous, dose-dependent effect are shown in **Figure 42**. As initial screenings were performed at a concentration of 200  $\mu$ M employing compound stock solutions of 10 mM (2.86% of DMSO), no solvent effects were considered. Similarly, dose-dependent studies were later performed with 10 mM or 100 mM stock solution and as a result the total amount of DMSO never exceeded 5%.

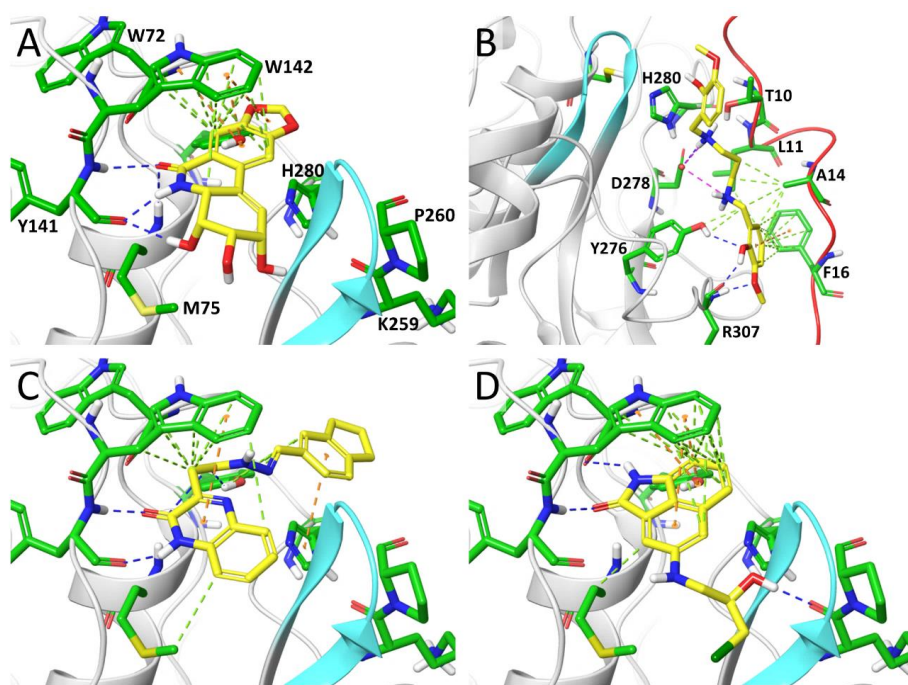


**Figure 42.** Atg4B concentration-response curves of hit molecules **NSC439493** (A), **NSC126353** (B), **NSC611216** (C), **NSC322341** (D) **NSC83713** (E) and **NSC631817** (F). Values shown are means of 3 experiments performed in duplicate.

Purity and identity of the active library samples were checked by MS and Nuclear Magnetic Resonance (RMN). These validation assays temporarily discarded **NSC43949**, **NSC322341** and **NSC631817** that did not fulfil the analysis requirements (purity was acceptable, but the determined mass was not the expected according to their molecular formula) and corrected the structure of **NSC83713** and **NSC116384** provided by the NCI. **NSC83713** corresponded to an unsaturated analogue whereas **NSC116384** turn out to correspond to the halohydrin **NSC611216** also present in the list of potential inhibitors, even with a better docking score, but that could not be initially obtained from the NCI due to lack of availability. In addition, all active hits, except for **NSC322341**, **NSC631817** and the commercially available **NSC126353**, were resynthesized by Ana Bilbao and Dr. Julia Comas to confirm the identity of the library samples and their inhibitory activity.



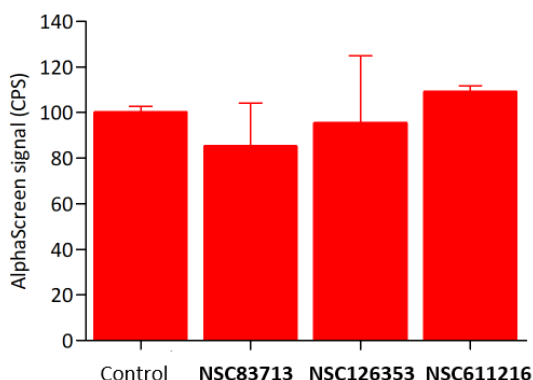
The results of this virtual screening showed that many of the potential and identified best hits at the AtgB4 active site were mainly stabilized by hydrophobic contacts and  $\pi$ -stacking interactions with residue W142 (**Figure 43**). This residue has been shown to be crucial for the processing activity of Atg4B since it acts as a clamp to keep residues P119 and G120 of the natural LC3 substrate in place, previous to the cleavage of the contiguous peptide scissile-bond.<sup>274</sup> On the other hand, common features of the best hits from screening at the second site were the presence of at least one cationic group (i.e. protonated amine), that could establish electrostatic interactions with residue D278 of Atg4B, and an extended structure that allowed them to occupy the relatively narrow groove at the interface between the *N*-terminal tail and the Atg4B core, making hydrophobic contacts with residues like L11, A14 and F16.



**Figure 43.** Docked poses for the best hits from HTVS against (A) the active site of Atg4B (**NSC349155**) and (B) the second alternative site (**NSC86286**). These compounds could not be tested biologically because they were not available from the NCI. Docked poses for the two best Atg4B inhibitors determined by biological testing, (C) **NSC126353** and (D) **NSC611216**. Ligands are shown with yellow C-atoms and protein residues with green C-atoms. The regulatory loop is highlighted in cyan and the *N*-terminal tail in red. Interactions are depicted with dashed lines: Hydrogen bonds in blue, salt bridges in magenta, hydrophobic in green and  $\pi$ -stacking in orange.

To identify compounds that interfere with the AlphaScreen signal (oxygen quenchers, colour quenchers, biotin mimetics, and nickel chelate competitors), the most active compounds were also evaluated in counter screen employing a (His)<sub>6</sub>-tagged

biotinylated peptide as substrate to discard false positives or target-independent hits. As shown in **Figure 44** none of the hits selected interfered with the assay.



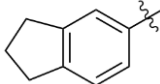
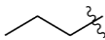
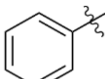
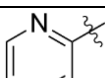
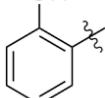
**Figure 44.** AlphaScreen signal displayed using a biotinylated control peptide His<sub>6</sub>-Biotin as a substrate in presence and absence of compounds to confirm that compounds did not interfere with the measured signal.

### 13. Synthesis of focused libraries based on NSC126353 and NSC611216 structures

Focused libraries based on the more potent scaffolds were next designed and synthesized. Quinoxaline derivatives as **NSC126353** are privileged scaffolds with a wide array of biological activities.<sup>285,286</sup> In addition, the naphtostyryl scaffold of **NSC611216** has attracted increasing attention in the last years. Thus, the 5,6-disubstituted benzo[*cd*]indol-2(1*H*)-one core has been shown to be effective thymidylate synthase inhibitors<sup>287</sup> and 5-sulfonamide derivatives of benzo[*cd*]indol-2(1*H*)-ones have been described as BET bromodomain inhibitors<sup>288</sup> and phosphodiesterase 2A inhibitors.<sup>289</sup> However, amino- benzo[*cd*]indol-2(1*H*)-ones derivatives represents a novel class of inhibitors with no biological activity associated. Hence, a series of **NSC126353** were designed and synthesized by Dr Júlia Comas and **NSC611216** derivatives were prepared by Ana Bilbao during her PhD thesis with the final aim to explore the chemical space for affinity improvement (**Table 7**, **Table 8** and **Table 9**).

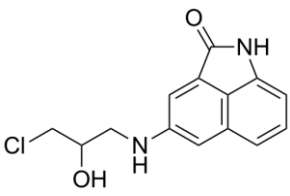
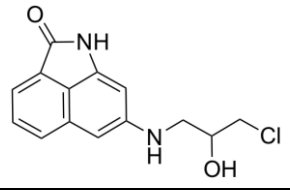
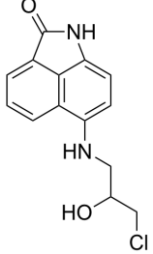
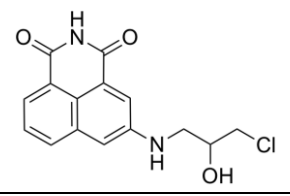
Activities of the **NSC126353** analogues were then investigated using the established assays. Unfortunately, none of the synthesized compounds lead to inhibitors showing higher potency. Only Compound **14** (**Table 7**) bearing a dichlorohydroxyquinoxaline scaffold and a hydroxybenzene moiety showed moderate response. However, with a 3-fold decrease in activity compared to **NSC126353**, it was less potent than the parent

compound thereby suggesting that the presence of the indane ring is important for compound activity.

Compound	R <sup>1</sup>	R <sup>2</sup>	R <sup>3</sup>	Act. (%)	IC <sub>50</sub> (μM)
NSC126353		-	-	55	104 (87 to 125)
40		H	H	76	-
41	-	CN	H	N.A.	-
42		Cl	Cl	N.A.	-
43		H	H	74	-
44		H	H	71	-
45		CN	H	78	-
46		Cl	Cl	70	-
47		H	H	93	-
48		Cl	Cl	64	-
49	OH	H	H	61	-
50		Cl	Cl	51	315 (292 to 337)

**Table 7.** Residual activities (Act. %) of Atg4B compared to control with no inhibitor present and IC<sub>50</sub> values of the most active compounds. Residual activities are mean values of three independent experiments performed in duplicate. Assay conditions as in **Figure 42**. IC<sub>50</sub> values were calculated from AlphaScreen assay and validated with the MS-based assay (95% confidence intervals). N.A.: not active.

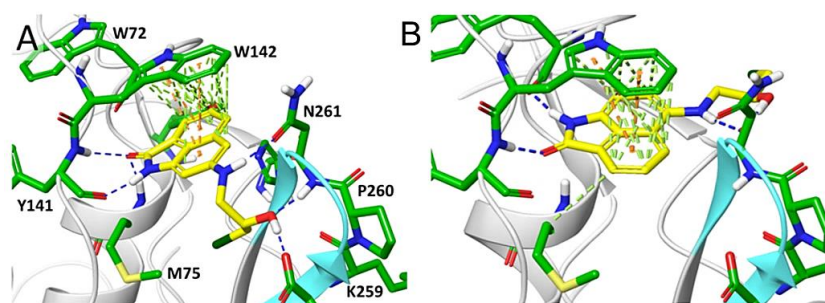
We then focused on **NSC611216** structure. Initially, **NSC61116** was resynthesized, obtaining at the same time its regioisomer **51**. Separately, the other regioisomer **52** with the scaffold of 6-amino-benzo[*cd*]indol-2(1*H*)-one was also prepared (**Table 8**).

Compound	IC <sub>50</sub> (μM)
<b>NSC611216</b> 	132 (99 to 163)
<b>51</b> 	69 (55 to 84)
<b>52</b> 	>300
<b>53</b> 	N. A.

**Table 8.** Activities of compounds **NSC611216**, **51**, **52** and **53**. IC<sub>50</sub> values were calculated employing the established AlphaScreen assay and validated with the MS-based assay; IC<sub>50</sub> (95% confidence intervals). Data from at least three independent experiments performed in duplicate. N. A.: not active.

The activity of the synthesized analogues was then evaluated. The resynthesized **NSC611216** displayed a similar potency than the parent compound (126 μM vs 132 μM), whereas the 7-substituted analog (**51**) showed a potency enhancement of about two-fold (69 μM). However, the 6-substituted analog (**52**) exhibited a significant decrease in potency. Observed activities are compatible with the binding modes of both compounds. Thus, despite having the acyclic substituent at a different position of the main core, the results from Induced Fit Docking suggest that **51** could adopt a

disposition at the Atg4B active site inverted 180 degrees relative to that of **NSC611216**, that allows it to keep the main interactions of the benzo[*cd*]indol-2(1*H*)-one core with residue W142, as well as the hydrogen bonds established by the endocyclic amide group. The decreased potency of compound **52** seems to correlate with a binding mode where the exocyclic chain is placed at the other end of the active site cavity, more exposed to the bulk solvent (**Figure 45**).

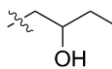
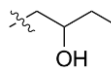
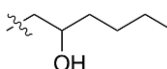
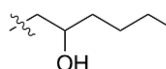
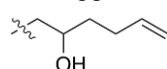
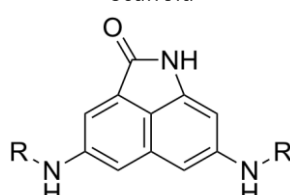
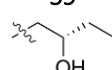
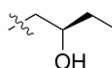
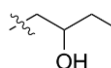


**Figure 45.** Best poses from Induced Fit Docking of (A) (*S*)-**51**, (B) (*R*)-**52**. Ligands are shown with yellow C-atoms and protein residues with green C-atoms. The regulatory loop is highlighted in cyan. Interactions are depicted with dashed lines: Hydrogen bonds in blue, hydrophobic in green and  $\pi$ -stacking in orange. Similar binding modes were observed for the alternative enantiomers.

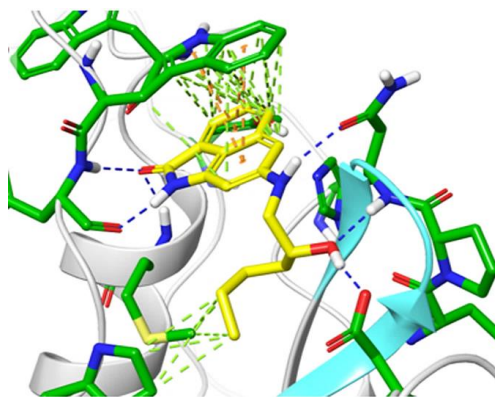
The benzo[*cd*]indol-2(1*H*)-one core was then replaced by a 1,8-naphthalimide scaffold. This class of compounds has gained attention as anticancer and antiviral agents. Amonafide, with activity as DNA intercalating agent and topoisomerase II inhibitor,<sup>290</sup> has entered into phase II clinical trials for prostate cancer, and sulfonated derivatives of 1,8-naphthalimides can block viral expression in HIV-infected human peripheral blood mononuclear cells by inhibiting reverse transcriptase.<sup>291</sup> However, the resulting analogue **53** did not show activity as Atg4B inhibitor. Thus, **NSC611216** and compound **51** were selected for further structural modification.

The 4-amino and 7-aminobenzo[*cd*]indol-2-[1*H*]-one core was kept and modifications on the alkyl group were investigated. Replacement of the chlorine by a methyl group improved the inhibition and the effect was more pronounced in **55** than in **54** which exhibited a more than two-fold increase in potency relative to **51** (**Table 9**). To explore the structure-activity relationship (SAR), the disubstituted 4,7-diaminobenzo[*cd*]indol-2(1*H*)-one lactam (**61**) was also prepared but it displayed an intermediated potency, with an  $IC_{50}$  of 68  $\mu$ M. Extension of the alkyl chain gave different results depending on the regioisomers. Thus, whereas the 7-aminobenzo[*cd*]indol-2-[1*H*]-one derivative (**57**) showed an improved  $IC_{50}$  of 12  $\mu$ M, the activity of the 4-aminobenzo[*cd*]indol-2-[1*H*]-one derivative (**56**) dropped significantly (**Table 9**). The activity of compound **57** could be rationalized on the basis of its binding to Atg4B

which is similar to that of analogue **51** (Figure 46). However, the longer hydrophobic chain of **57** allows it to establish new hydrophobic interactions with residues M75, P145 and A263, which could explain the improved activity observed.

Scaffold			Scaffold		
Compound	R	IC <sub>50</sub> (μM)	Compound	R	IC <sub>50</sub> (μM)
<b>54</b>		111 (76 to 161)	<b>55</b>		29 (15 to 56)
<b>56</b>		235 (195 to 284)	<b>57</b>		12 (6 to 18)
<b>58</b>		N. A.	Scaffold 		
<b>59</b>		113 (92 to 138)			
<b>60</b>		119 (98 to 145)	<b>61</b>		68 (47 to 88)

**Table 9.** Activities of compounds **54-61**. IC<sub>50</sub> values were calculated employing the established AlphaScreen assay and validated with the MS-based assay; IC<sub>50</sub> (μM, 95% confidence intervals). Data from at least three independent experiments performed in duplicate. N. A.: not active.



**Figure 46.** Best poses from Induced Fit Docking of **(R)-57**. Ligands are shown with yellow C-atoms and protein residues with green C-atoms. The regulatory loop is highlighted in cyan. Interactions are depicted with dashed lines: Hydrogen bonds in blue, hydrophobic in green and  $\pi$ -stacking in orange. Similar binding modes were observed for the alternative enantiomer.

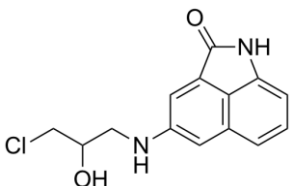
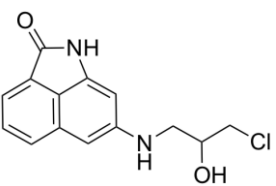
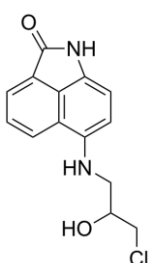
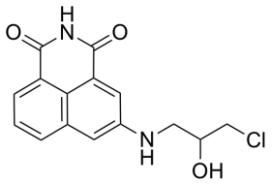
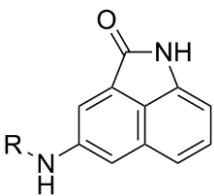
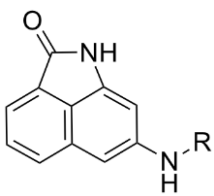
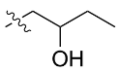
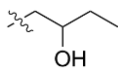
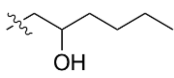
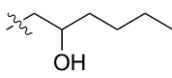
#### 14. Evaluation of hits in the MS-based assay

Inhibitory activity for hits found using the AlphaScreen-based assay was next determined by the developed MS-based assay. All compounds were found to inhibit the activity of Atg4B with lower but similar  $IC_{50}$  values when employing the MS-based assay (**Table 10** and **Table 11**). Moreover, since the AlphaScreen assay is performed in the presence of 0.5% Triton X-100 and the LC-MS assay is done in the absence of detergents, the comparable  $IC_{50}$  values obtained suggest that the inhibition is likely to proceed via specific binding rather than mediated by the formation of aggregates,<sup>292</sup> although this could explain the lower  $IC_{50}$  found in some cases. Alternatively, The MS-based assay employs higher substrate and lower enzyme concentrations, what can also contribute to explain the better  $IC_{50}$  values obtained.

Compound	$IC_{50}$
NSC83713	150 $\mu$ M
NSC126353	79 $\mu$ M
NSC611216	97 $\mu$ M

**Table 10.** Activities of compounds **NSC83713**, **NSC126353** and **NSC611216**.  $IC_{50}$  ( $\mu$ M) values were calculated using the MS-based assay. Data from at least three independent experiments performed in duplicate. Next,  $IC_{50}$  for the synthesised analogues from **NSC611216** were also determined (**Table 11**).  $IC_{50}$  values were similar or lower than the ones obtained with the AlphaScreen assay. Unfortunately, in some cases activities could not be determined due to solubility problems. The lack of detergents in the employed buffer may difficult the solubilization of some compounds. It is planned to explore a MS-

based assay using detergents, but this will require an optimization protocol that was beyond this PhD thesis.

Compound	IC <sub>50</sub> (μM)	Compound	IC <sub>50</sub> (μM)		
NSC611216		51			
	97		68		
52		53			
	238		>200		
Scaffold		Scaffold			
					
Compound	R	IC <sub>50</sub> (μM)	Compound	R	IC <sub>50</sub> (μM)
54		34.45	55		13.89
56		166.7	57		N.D.

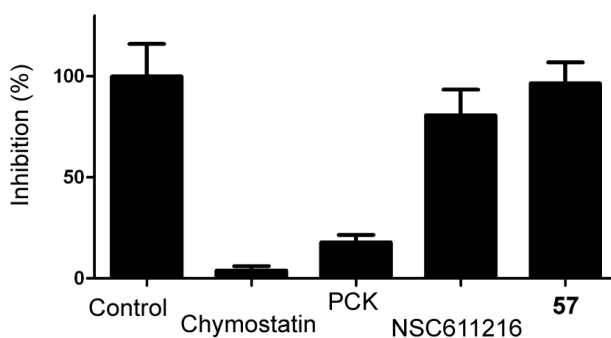


Compound	R	IC <sub>50</sub> (μM)	Compound	R	IC <sub>50</sub> (μM)
58		193	Scaffold  61	N.D.	
59		43.65			
60		55.79			

**Table 11.** Activities of **NSC611216** derivatives. IC<sub>50</sub> (μM) values were calculated with the MS-based assay. Data from at least three independent experiments performed in duplicate. N.D. not determined due to solubility issues.

## 15. Biological characterisation of 57

Atg4B shows the highest structural similarity to papain and its homologous proteases.<sup>275</sup> Thus to evaluate the selectivity over other cysteine proteases, in collaboration with Joan Barceló, it was investigated whether **NSC611216** and compound **57** could also inhibit papain activity. Neither **NSC611216** nor **57** inhibited the activity of this cysteine protease thus suggesting certain selectivity for Atg4B, whereas chymostatin completely block the activity and substantial inhibition was observed with PCK (**Figure 47**).



**Figure 47.** Atg4B was treated by the vehicle (control, DMSO), 10 μM of Chymostatin as positive control, 50 μM of PCK as negative control, 100 μM of **NSC611216** or 100 μM of **57**.

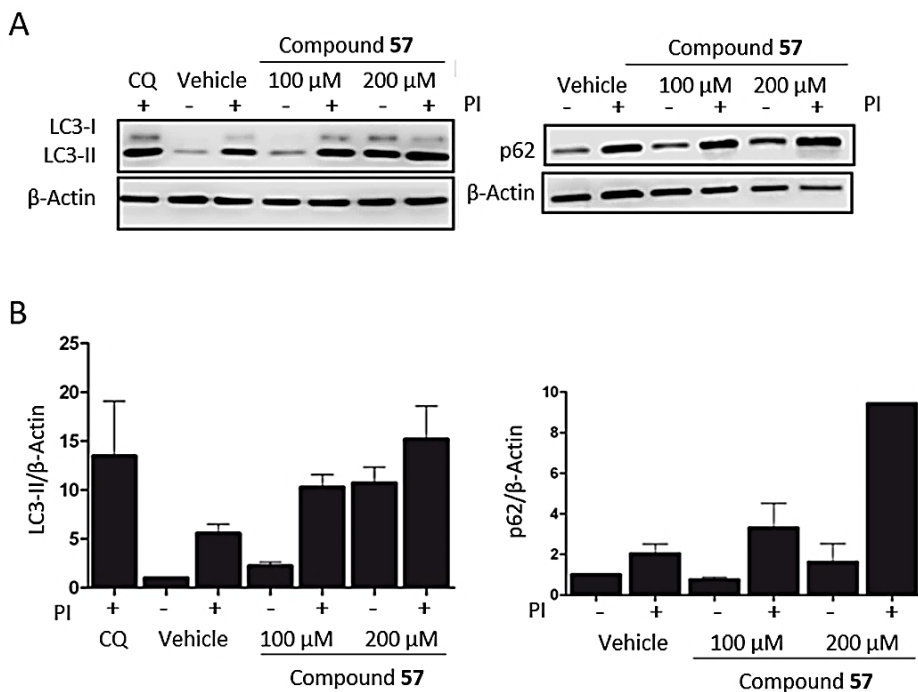
Based on the structure-activity relationship (SAR) investigation, compounds **54**, **55**, **56** and **57** were chosen for further in-depth characterization. Thus, we next studied if the treatment of cells with these compounds resulted in changes in cell viability. For that

purpose, two cell lines were selected: HT-29, human epithelial cells from colorectal adenocarcinoma, and HEK293, human epithelial cells from embryonic kidney, overexpressing green fluorescent protein (GFP) conjugated to LC3B. Cells were treated with compounds for 24 h and cell viability was evaluated employing the MTT and SRB assays. As shown in **Table 12**, although HEK293 cells overexpressing GFP-LC3B were not cancerous, they resulted more sensitive to the treatments. IC<sub>50</sub> values determined in MTT and SRB assays resulted similar for derivatives **56** and **57**, however **54** and **55** displayed lower toxicity. Compound **57** was selected for further investigation in HT-29 cells due to its higher potency unveiled in SRB assay.

	HEK293 (GFP-LC3B)		HT-29	
	MTT	SRB	MTT	SRB
<b>54</b>	82.27 (53.34-126.90)	116.11 (102.40-131.50)	No active	No active
<b>55</b>	No active	102.90 (95.83-110.60)	No active	No active
<b>56</b>	46.87 (37.99-57.82)	49.06 (44.21-54.44)	96.13 (82.21-112.40)	164.70 (144.90-187.30)
<b>57</b>	72.65 (65.17-81.00)	57.00 (53.38-60.87)	123.00 (73.90-204.70)	116.60 (108.00-126.10)

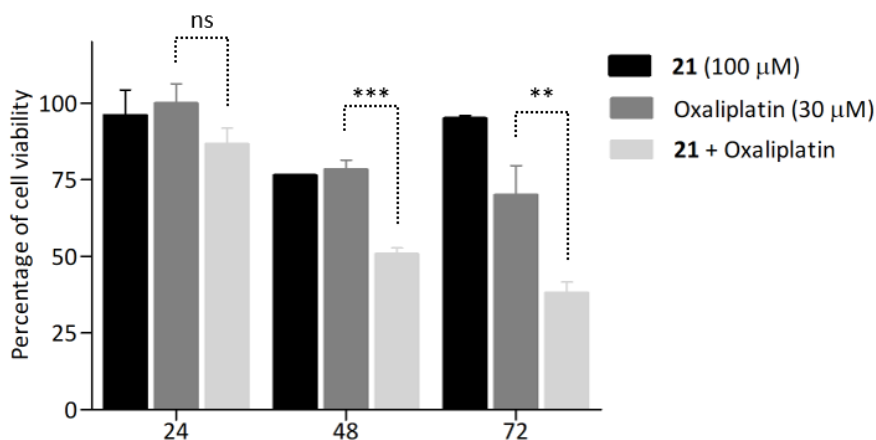
**Table 12** Cell viability in HEK293 cells overexpressing GFP-LC3B and HT-29 cells after treatment with compounds **54**, **55**, **56** and **57** during 24 h. IC<sub>50</sub> were determined by the MTT and the SRB assays.

Changes in autophagic flux due to **57** treatment were next evaluated in the colorectal adenocarcinoma cell line HT-29. To do this, autophagy was induced by amino acid deprivation (Earle's Balanced Salt Solution, EBSS) and the levels of the autophagy markers LC3-II and p62 were examined by immunoblotting. Typically, the chemical and genetic inhibition of Atg4B leads to accumulation of LC3-II and increased levels of the cargo adaptor of proteins p62 due to its decreased clearance.<sup>232</sup> Moreover, as differences in the protein levels can be caused by both modulation in autophagy or changes in lysosomal degradation of the proteins, these studies were performed in the presence lysosomal inhibitors to estimate the overall autophagic flux.<sup>217</sup> As depicted in **Figure 48**, **57** resulted in an increase of LC3-II in starved HT-29 cells comparable to Chloroquine (CQ). Autophagy flux analysis indicated that **57** enhanced the LC3-II accumulation induced by protease inhibitors (**Figure 48**). In addition, treatment with **57** decreased the autophagy-induced degradation of p62. The observed changes support an impairment of autophagy and suggest an inhibition of autophagic flux.



**Figure 48** **A)** Analysis of autophagy inhibition in nutrient deprived HT-29 cells, treated with **57** (or vehicle) and subjected to western blotting to assess LC3-II and p62 expression in presence (+) or absence of protease inhibitors (PI).  $\beta$ -Actin served as a loading control. Representative blots from three independent experiments are shown. **B)** Bar graph shows LC3-II and p62 expression normalized to  $\beta$ -actin loading control (fold change); mean  $\pm$  SEM; n=3.

Oxaliplatin is a drug commonly used for the treatment of colorectal cancer. Its mechanism of action is mediated by the formation of inter-strand and intra-strand crosslinks with DNA, thereby inhibiting DNA replication and resulting in apoptosis. It has been reported that compounds which inhibit autophagy can sensitize cancer cells to oxaliplatin, and beclin1 knockdown enhances oxaliplatin sensitivity in colon cancer cells under normoxic and hypoxic conditions.<sup>293</sup> Hence, we next investigated the antitumor activity of **57** against HT-29 cells in the presence and absence of oxaliplatin. Cell viability inhibition by oxaliplatin was first investigated by an MTT assay at 24, 48 and 72 h with resulting  $IC_{50}$  of 240.30, 90.00 and 44.81  $\mu$ M, respectively. A concentration of 30  $\mu$ M of oxaliplatin was then chosen to evaluate if conjugated treatment with **21** at 100  $\mu$ M ( $IC_{35}$ ) enhanced the toxic effect on HT-29 cells. As shown in **Figure 49**, cell viability inhibition by oxaliplatin was markedly enhanced in the presence of a non-toxic concentration of **57**, thus indicating that autophagy inhibition may result in an additive or synergic anticancer effect.



**Figure 49.** HT29 cells were treated during 24, 48 or 72 h with 100  $\mu\text{M}$  of **57**, 30  $\mu\text{M}$  of oxaliplatin or a mixture of **57** and oxaliplatin at the same concentrations. Data are the average  $\pm$  SD of three experiments. Statistics were carried out employing GraphPad were ns: no significant, \*\*:  $P \leq 0.01$  and \*\*\*:  $P \leq 0.001$ .

In summary, in the course of this thesis a novel AlphaScreen-based assay for measuring the catalytic activity of the cysteine protease Atg4B has been established. This assay combined with a structure-based high-throughput virtual screening of a library of about 265242 compounds yielded a series of novel autophagy inhibitors. Medicinal chemistry optimization of the initial hit **NSC611216** provided insight into the structural requirements for the inhibition of Atg4B. The most potent compound **57** shows a 10-fold improvement relative to the parent hit and in vitro activities in the range or better than inhibitors previously identified.

The identified inhibitor also demonstrated a good cytotoxicity profile while maintaining autophagy inhibition, as measured by LC3-II and p62 protein levels. Moreover, the synergistic effect of **57** combined with oxaliplatin resulted in an enhanced cell death in the human colorectal adenocarcinoma cell line HT-29. All in all, the developed AlphaScreen and MS-based assays can be key tools enabling the high-throughput identification of novel Atg4B inhibitors. Moreover, the aminobenzo[*cd*]indol-2-[1*H*]-one scaffold represents a novel chemotype for the further development of small molecule inhibitors of Atg4B. These results will contribute to expand the toolbox used to study autophagy in mammal cells and to unravel the role of Atg4B in cancer treatment.

Some limitations of the current work should be also mentioned. The identification of potent and selective Atg4B inhibitors is an emerging field of research, as proven by the publication of six articles focused on this topic just in the last two years.<sup>294,231,219,230,232,238</sup> Although different chemotypes and structures have been reported, all of them display similar potencies (low micromolar) and the identification

of potent (nanomolar) compounds still remain an unsolved problem. Unfortunately, compounds displaying nanomolar potencies could not be detected during the course of this work. However, it is expected that additional medicinal chemistry approaches could further improve the potency of the inhibitors identified. Moreover, the use of the established assay with alternative libraries can also be a source of novel inhibitors. An additional unsolved problem that has not been covered in this work is the identification of Atg4B inhibitors displaying selectivity in front of the other Atg4 isoforms (A, C and D). Indeed, selective inhibitors would be invaluable tools to explore the different selectivity and substrate specificity of these proteins, and as a result the activity of the identified structure in front of the other Atg4 isoforms should be addressed in the near future.

# CONCLUSIONS



Based on the results obtained in this chapter, a novel HTS assay to find Atg4B inhibitors has been developed allowing the identification and characterization of a novel scaffold for further biological studies. In summary, the following assessments can be concluded from the research done:

- A novel HTS assay based on AlphaScreen technology has been established to measure the activity of the cysteine protease Atg4B. The novel HTS assay required the previous expression and modification of LC3B and Atg4B, that could be obtained in good yields. Assay conditions were optimized such as the buffer composition, the type of biotin employed, the substrate and enzyme concentrations, the stability of the signal and the proteins in the buffer and DMSO tolerance. This described optimization provided a sensitive HTS assay with a resulting Z'-factor of 0.5.
- An alternative MS-based assay was optimized in order to validate *hits* found in AlphaScreen and discard false positives. Assay conditions were also optimized (buffer composition, substrate and enzyme concentrations, limit of detection of the method), providing a robust alternative assay for measuring Atg4B activity.
- The developed HTS assay could be employed to evaluate 250 compounds selected from the NCI Open Database were selected after a HTVS approach. Four compounds (**NSC83713**, **NSC126353**, **NSC611216** and **NSC43949**) showed  $\geq 50\%$  inhibition in a preliminary single concentration assay.
- After resynthesizing or purchasing the four compounds, **NSC43949** was discarded since it did not fulfil the analysis requirements.  $IC_{50}$  values of the rest of compounds ranged from 104 to 300  $\mu M$ .
- **NSC83713**, **NSC126353** and **NSC611216** were confirmed as *hits* with similar  $IC_{50}$  using the established MS-based assay.
- The characterization of the activity of the synthesized series of **NSC126353** and **NSC611216** derivatives allowed the discovering of the compounds **54**, **55**, **56** and **57** for further in-depth investigation. The aminobenzo[*cd*]indol-2-[1H]-one scaffold represents a novel chemotype for the development of small molecule inhibitors of Atg4B
- Compound **57** was selected for additional characterization based on its high potency, a 10-fold improved activity and a good cytotoxicity profile on cell lines. Moreover, inhibition of the autophagic flux was maintained, as measured by LC3-II and p62 protein levels. Finally, the synergistic effect of **57**



combined with oxaliplatin resulted in an enhanced cell death in the human colorectal adenocarcinoma cell line HT-29.

- The established HTS assays are useful tools to evaluate potential Atg4B inhibitors. The assay is sensitive and can be miniaturized with the appropriate equipment. The reported HTVS combined with the HTS assay has shown effective to identify novel chemotypes inhibiting Atg4B activity.

# CHAPTER 3:

STUDY OF THE LIPID DIVERSITY OF THE AUTOPHAGY  
BIOMARKER LC3



# INTRODUCTION



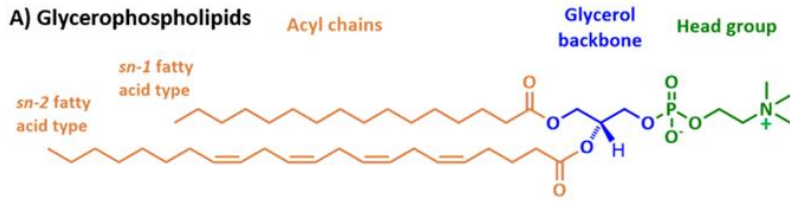
Biological membranes are composed of a variety of lipid species, being glycerophospholipids (GPLs), sphingolipids and cholesterol the major lipid components (**Figure 50**). Glycerophospholipids are composed by a polar head group, a glycerol moiety and two fatty acids esterified to the *sn-1* and *sn-2* positions. Generally, most of these species contain a saturated acyl chain at the *sn-1* position and an unsaturated chain at the *sn-2* position. Some lipid species, as plasminogens, present ether-bonded fatty acids instead. The phosphate group at the *sn-3* position can be in turn coupled with different head groups to produce various species such as phosphatidylcholine (PC), phosphatidylethanolamine (PE), phosphatidylserine (PS), phosphatidylinositol (PtdIns), phosphatidylglycerol (PG), and cardiolipin (CL).<sup>295</sup>

Sphingolipids (SL) are derived from the long chain aminodiol sphingosine. Relevant examples of this lipid class include ceramide (Cer), sphingosine-1-phosphate (S1P) and sphingomyelin (SM). Whereas Cer has apoptotic properties, S1P is involved in cell growth and proliferation. SM is one of the major components of plasma membrane and it is essential for the formation of membrane microdomains or rafts, which function as hubs to get more efficient signal transduction pathways.<sup>296,297</sup> Finally, cholesterol represents 10-20% of total lipids present in the plasma membrane, one of the highest concentration in mammalian cells,<sup>298</sup> though it is also found in organelles membranes. It displays a sterol-based structure of four fused hydrocarbon rings and modulates the physical properties of the membrane.<sup>299</sup>

Membrane lipids cover a wide variety of cellular functions: serve as energy storage, establish the barrier between different compartments and organelles, modulate the membrane curvature, fluidity and polarity, facilitate the transport of molecules or mediate the microdomains formation. In addition, lipids can also act as signalling molecules (ceramide, eicosanoids),<sup>296</sup> mediate temporary association of proteins to membranes or they covalently modify proteins to modulate their localization and function. Examples of lipid posttranslational modifications include the attachment of glycosylphosphatidylinositol (GPI) anchors, the *S*-prenylation and *S*-acylation of cysteines, the *N*-myristoylation of glycines, the cholesterylation of members of Hedgehog family and the *C*-terminal phosphatidylethanolamination (PE) in Atg8, GABARAP and LC3 (**Figure 51**).

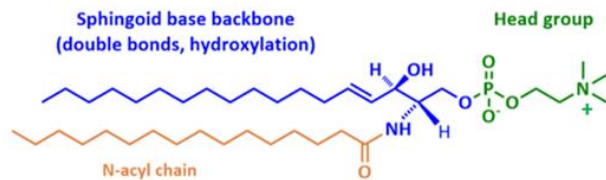
## 1. Lipid Posttranslational modifications

**Prenylation** is a post-translational covalent modification in which cysteine residues close to the *C*-terminal regions of some eukaryotic proteins are modified with a 15-carbon (farnesyl) or a 20-carbon (geranylgeranyl) isoprenoid lipid via thioether linkage. This attachment provides the proteins with a hydrophobic domain that is able



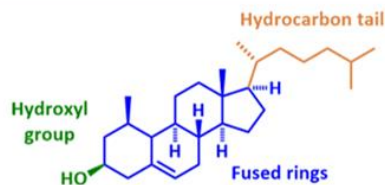
GPL examples	Head group substituent
Phosphatidic acid	-
Phosphatidylcholine	Choline
Phosphatidylethanolamine	Ethanolamine
Phosphatidylserine	Serine
Phosphatidylinositol	Inositol
Cardiolipin	Phosphatidylglycerol

**B) Sphingolipids**

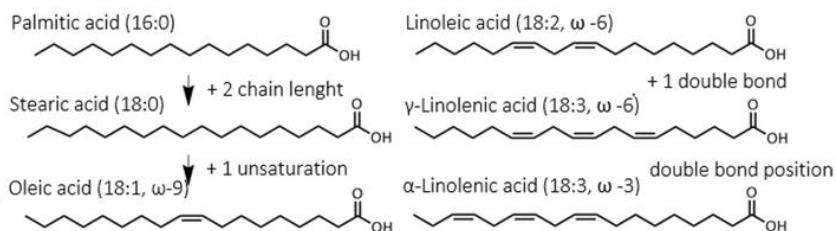


Shingolipid examples	Head group substituent
Ceramide	Hydroxyl
Sphingomyelin	Phosphocoline
Ceramide Phosphoethanolamine	Phosphoethanolamine
Glucosylceramide	Glucose

**C) Cholesterol**

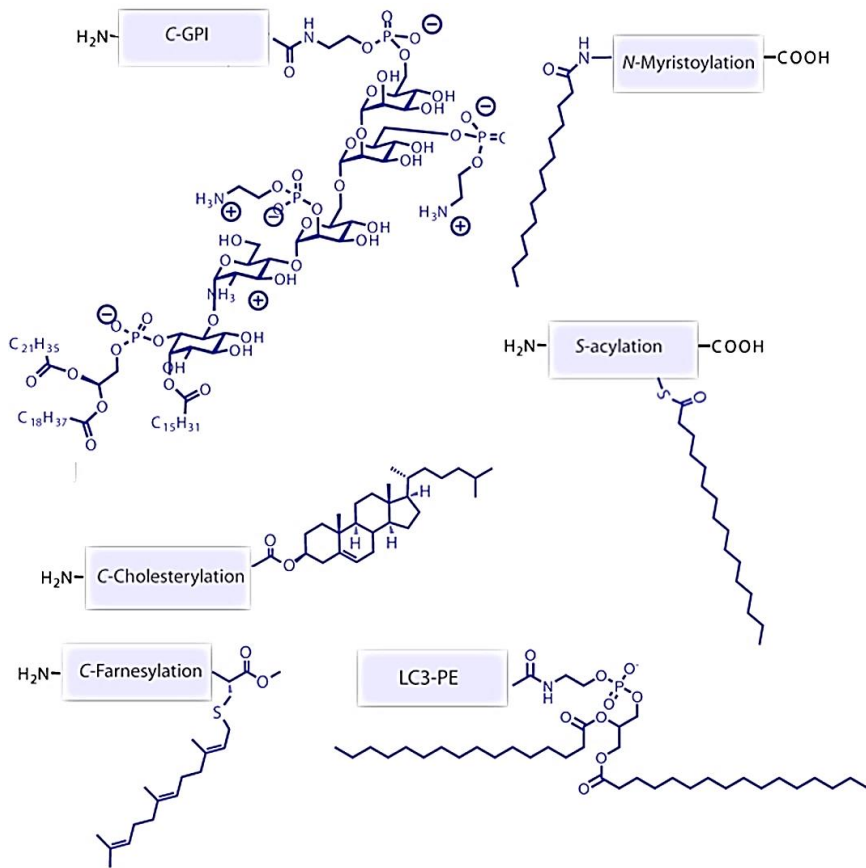


**D) Fatty acids diversity**



**Figure 50.** Chemical diversity of membrane lipids in mammals. **A)** GPLs present a glycerol backbone with two fatty acids at the *sn*-1 and *sn*-2 positions, the head group is a phosphate group and an ester bond between the backbone and acyl chain on *sn*-1/2

confers them diversity. The name of GPL is determined by the head groups as shown in the inserted table. **B)** Sphingolipids consist of a sphingoid base, an *N*-acyl chain and a head group. The sphingolipid name is determined by the combination of head group and *N*-acyl chain, as shown in the inserted table and also depends on the hydroxylation and unsaturation degree of the sphingoid backbone. **C)** Cholesterol is the major mammalian sterol. **D)** Fatty acid diversity is based on the differences in chain length, unsaturation degree and the position of double bonds.



**Figure 51.** Posttranslational modifications of proteins. The glycosylphosphatidylinositol (GPI) anchor is a posttranslational modification which is positioned at the C-terminus of many eukaryotic proteins and localize them in the outer leaflet of the cell membrane. Myristoylation corresponds to the irreversible covalent linkage of the 14-carbon saturated fatty acid, myristic acid, to the *N*-terminal glycine of many eukaryotic and viral proteins. Cholesterylation is the attachment of sterols to proteins. This modification has been a characteristic of the family of hedgehog proteins (Hh). Farnesylation is a type of prenylation, by which an isoprenyl group is added to a cysteine residue. Protein S-acylation involves the posttranslational addition of a lipid (typically, but not exclusively, palmitate) via a labile thioester bond to intracellular cysteine residues. The reversible conjugation to autophagy proteins of a phosphatidylethanolamine represents a unique



posttranslational modification.

to interact with membranes.<sup>300</sup> This modification controls signalling activities of several proteins, such as prenylated small GTPases like Ras, Rac1 and Rab, and the phosphatase of regenerating liver family of PTPs.<sup>301</sup>

Protein ***N*-myristoylation** is a specific irreversible lipidation of the  $\alpha$ -amino group on an *N*-terminal glycine residue catalysed by *N*-myristoyl transferase. Typically, myristoylation is cotranslational on new synthesized polypeptides after the cleavage of an initiator methionine, but it can also occur posttranslational after the cleavage of an *N*-terminal glycine. Myristoylated proteins are involved in several cellular signalling pathways, protein-protein interactions and are essential for cell survival and regulation of both innate and adaptive immune responses.<sup>302</sup> *N*-myristoylation can be found in Src family kinases, non-receptor tyrosine kinases which are mediators of cellular signal transduction and cellular proliferation. All these proteins need to be myristoylated at the *N*-terminus in order to anchor the protein to a membrane, although in most of the cases one lipid modification is not sufficient to ensure stable membrane association, and as a result, it is usually combined with palmitoylation.<sup>303</sup>

***S*-acylation** is the enzymatic reversible addition of long-chain lipids, typically palmitate, onto intracellular cysteine residues of soluble and transmembrane proteins through a labile thioester linkage. This modification increases protein hydrophobicity and can modulate its structure, assembly, maturation, trafficking and function. A wide range of proteins, most of them with key roles in cellular processes, are *S*-acylated, including membrane receptors, ion channels and transporters, enzyme and kinases, signalling adapters, chaperones and structural proteins.<sup>304</sup> Thus, **palmitoylation** of Wnt proteins is necessary for their secretion and function in controlling embryogenesis and adult tissue homeostasis.<sup>305</sup> Ras proteins are monomeric GTPases that are involved in early steps in signal cascades that regulate many processes such as survival, growth and differentiation. All Ras proteins are farnesylated on their C-terminal extreme cysteine residue, which enables weak membrane binding.<sup>306</sup> Stable membrane binding in plasma membrane, ER or Golgi complex is facilitated by additional single or double palmitoylation.

**Cholesterylation** is the attachment of sterol to proteins. As far as it is known, this posttranslational modification is only characteristic of Hedgehog (Hh) family of proteins, with a crucial role in embryonic development, tissue repair and regeneration. Both cholesterylation and palmitoylation are widely conserved in all the Hh homologues. The cholesterol moiety in Hh is involved in membrane association, binding to specific receptors, secretion, transport and association to some transport molecules.<sup>307</sup>

Another unique lipid modification is **the reversible conjugation of the yeast autophagy marker Atg8 to PE**. This lipidation occurs at the C-terminus on the Gly120 residue and it is crucial to facilitate association with the phagophore membrane and the subsequent membrane elongation to form the autophagosome. On the other hand, membrane associated Atg8 recruits other motor proteins enabling hemifusion and fusion processes.<sup>308</sup> In higher eukaryotes, Atg8 has evolved into two subfamily of proteins LC3 and GABARAP consisting of LC3A, LC3B, LC3C and GABARAP, GABARAPL1 and GABARAPL2/GATE-16.

## 2. Membrane heterogeneity and function

Biological cell membranes are formed by mixtures of proteins and different lipids, with GPLs, cholesterol, sphingolipids being the major components. A typical cell can contain more than 1000 different lipids, generated by multiple combinations of acyl chain and head groups, what results in a complex, diverse, dynamic and heterogeneous membrane composition. The requirements of the membrane as a barrier do not justify this enormous degree of structural diversity. Indeed, lipids have several additional functions: membrane structure maintenance, energy and heat sources, signalling molecules, protein recruitment platforms and substrates for posttranslational protein-lipid modification. Therefore, lipid diversity results essential in order not only to provide membranes with different properties but also to modulate protein function and cellular processes.

Two types of diversity have been defined: chemical diversity that refers to the variety of different chemical structures detected in cellular lipids, and compositional diversity, which is the ratio between different species that can be found in tissues or cells, organelles, membrane leaflets or membrane subdomains. Whereas chemical diversity affects the properties of lipids, compositional diversity influences membrane behaviour through lipid-lipid and lipid-protein interactions.

Fatty acids from GPLs and sphingolipids may vary in chain length, unsaturation degree, double bond position and hydroxylation degree. Thus, **chemical diversity** of GPLs relies on the nature of the attached fatty acids, their localisation at *sn-1* or *sn-2* position (saturated or monounsaturated can be usually found at *sn-1* whereas the fatty acid at the *sn-2* position tends to be monounsaturated or polyunsaturated) and the head group present at the *sn-3* position. Sphingolipid chemical diversity arises from the type of the sphingoid base, the head group and the *N*-acyl chain. Head groups are basic for protein-lipid interaction and their diversity is especially important in order to interact with specific proteins. Sterols and oxysterols and their derivative bile acids also have different structures and functions (**Figure 50**).<sup>309</sup>

Many different enzymes are involved in the biosynthesis and homeostasis of cellular

lipids. Hence, the diversity of fatty acid is given by different processes such as elongation, desaturation, partial  $\beta$ -oxidation and hydroxylation (**Figure 50**). Ceramides, which can result in complex sphingolipids, are synthesized by ceramide synthases that transfer acyl chains to sphingoid bases with different substrate preferences. In addition, mammals cannot synthesize some polyunsaturated fatty acids and they need to be acquired by diet. Therefore, nutrition can also modify lipid composition.

Chemical diversity not only relies on biosynthesis. PC and PE are synthesized from diacylglycerol through the CDP-choline and CDP-ethanolamine pathways. After biosynthesis the acyl chains are remodeled by acyltransferases and phospholipases, thereby generating a large variety of lipid species including short, long and/or unsaturated fatty acids (i.e. 16:0/18:2-PE, 18:0/20:4 PE, 18:1/18:1 PE).<sup>310</sup> GPLs containing saturated and unsaturated fatty acid are required to strike a balance between impermeable and flexible membranes. Unsaturated fatty acids make more flexible membranes and are required for shaping, fission and division activities, whereas saturated fatty acids diminish membrane permeability, forming a cellular barrier and preventing ions and molecules to freely cross the membrane.

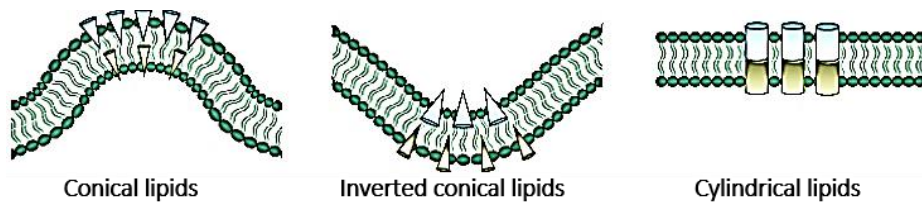
**Compositional diversity** can be found at cell types, organelles, and inner/outer plasma membrane leaflets. PC is the major cellular phospholipid comprising 40-50%, PE can be found in a 15-25% whereas PS is less abundant (5-10%). Moreover, the different subcellular organelles have distinct phospholipid composition. As example, ER contains more unsaturated GPLs while plasma membrane include large amounts of cholesterol and sphingolipids.<sup>311</sup>

Apart from the unequal distribution among organelles, there is also an uneven distribution among different leaflets (charge and type of lipids). This latter is remarkably visible at the plasma membrane with a different composition at the outer leaflet (phosphatidylcholines (PC) and sphingolipids).<sup>298</sup> PE is particularly enriched in inner membranes of the mitochondria (35-40%) where CL (cardiolipin) is also exclusively found. Similarly, PS is only found in the cytoplasmic leaflet of plasma membrane,<sup>309</sup> and lysobisphosphatidic acid is only detected in late endosomes.<sup>312</sup> This distribution suggest the implication of specialized proteins to generate, sense and maintain this specific composition.<sup>313</sup> Moreover, proteins such as flippases, floppases and scramblases are also required to establish and maintain the transbilayer asymmetry of lipids.<sup>295</sup> Another key point is the compartmentalization of lipid synthesis not only at organelle level but also at suborganelle scale. For example, some lipids are enriched in the membrane contact sites between ER and mitochondria, such as the discovered novel subdomain in ER in which phosphatidylinositol (PtdIns) is synthesized.<sup>314</sup> Cells invest substantial energy on keeping this diverse and **asymmetric distribution** of lipids, mainly by the action of actively demanding ATPases,<sup>295</sup> thus

indicating the importance of lipid composition on cellular function.

As the membrane composition is tightly regulated, alterations in membrane homeostasis have been **associated with many diseases**. In recent years, advances in lipid analysis techniques have allowed to gain knowledge about this field and its related diseases, although many processes are not clear yet. Genetic diseases related to lipids are the result of mutations in enzyme belonging to specialized pathways. Examples thereof are the Sjögren-Larsson syndrome related to sphingolipid degradation<sup>315</sup> or the hereditary sensory and autonomic neuropathy where serine palmitoyltransferase 1 and 2, the first step in ceramide biosynthesis, are mutated.<sup>316</sup> Lipid alterations have also been observed in non-heritable diseases. Thus, type 2 diabetes, cancer, Alzheimer and cystic fibrosis present increased ceramide levels.<sup>317</sup> Changes in PC acyl chains are also observed in many cancers, although the mechanisms underlying these changes remain yet unclear.<sup>309</sup> It is easier to explain altered phenotypes when the function of the lipid is directly related with its physical properties. Hence, reduced levels of dipalmitoyl-PC (DPPC) results in a partial neonatal lethality and lung injury due to the role of this lipid in facilitating breathing through reduction of the surface tension of the lung epithelium.<sup>318</sup> However, other phenotypes are not so easy to unravel. Hence, the mechanism responsible of brain malfunctions in humans and mice with abnormal acyl chains in PtdIns remains elusive.<sup>319</sup> An additional complication in the lipidomic field is the fact that a disrupted metabolic pathway can lead to the disappearance or accumulation of a substrate but also of unexpected products, thereby complicating its analysis.<sup>309</sup>

Lipid composition has also a key role in the regulation of **membrane curvature (Figure 53)**. Hence, cylindrical lipids (PC, PS) tend to form flat monolayers, lipids with small polar headgroups (PE, diacylglycerol (DAG) or CL) have a conical shape and present a negative curvature, whereas lipids with a larger headgroup (lysophosphatidylcholine (lysoPC), PtdIns) present an inverted conical shape that favours the bending of the membrane into a positive curvature.<sup>320</sup> Thus, the size of the head group and the hydrophobic tail affects the curvature of the membrane. For example, the negative curvature caused by PE disrupts the bilayer and promotes membrane fusion.<sup>321</sup> Chain length and unsaturation degree also play a role. Long and saturated fatty acids make membranes thicker and less fluid since their tails are tight and have stronger lipid-lipid interactions, whereas unsaturated lipids makes the membrane more fluid. Polyunsaturated fatty acids are another example of curvature alteration since they decrease the rigidity of the membrane. One example is the docosahexaenoic acid (22:6,  $\omega$ -3, DHA) present in GPLs, which promote highly curved membranes and endocytosis.<sup>322</sup> In addition, the propensity of the membrane to undergo fission and shaping activities increase with the level of phospholipids polyunsaturation (18:1-18:0 < 20:4:18:0, 22:6-18:0) being  $\omega$ -3 fatty acids better for vesiculation than then  $\omega$ -6 counterparts.<sup>323</sup>

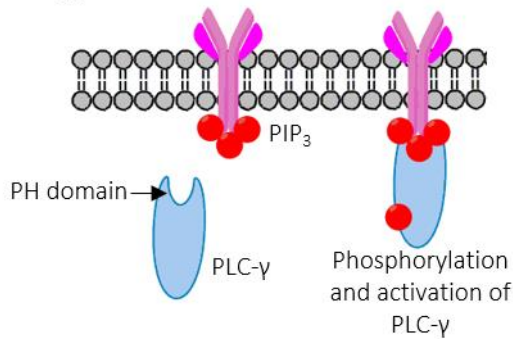


**Figure 52.** Lipids like PE, DAG and CL have a smaller head group than the acyl chain and, thus, present a conical shape that confers negative curvature to the membrane, whereas inverted conical lipids like PtdIns have a larger head group than the acyl chain, which confers positive curvature of the membrane. Finally, PC and PS are cylindrical lipids, which form a flat layer.<sup>320</sup>

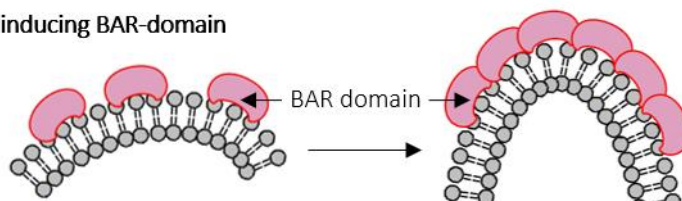
Lipid can also modulate cellular function through interaction with other lipids. Thus, **lipid-lipid interactions** are important to stabilize nanodomains that form lipid rafts (cholesterol and sphingolipids interact through hydrogen-bonds).<sup>324</sup> Lipids can also interact across bilayers. Hence, PS aggregated in the cytosolic leaflet of plasma membrane promotes clustering of GPI anchors in the other leaflet through interaction of cholesterol and PS with one or more long saturated acyl chain, thereby contributing to nanodomain formation.<sup>325</sup>

Lipid can also function through their interaction with proteins. There are several types of **protein-lipid interactions**.<sup>309</sup> Examples thereof are the specific protein localization through interaction of protein domains with lipids, proteins that extract lipids from membrane *via* lipid-binding pockets, lipid transfer proteins that regulate lipid localization and downstream functions, among others. One example is the Pleckstrin homology (PH) domain, a ~100 amino acid sequence that binds to phosphatidylinositol phosphate lipids (PIP) and by doing so directs proteins to membranes enriched with this type of lipids (**Figure 54**). Other lipids, such as DAG and PS (involved in intracellular trafficking)<sup>326</sup> can also recruit proteins to cellular membranes.<sup>309</sup> BAR-domain-containing proteins binds membranes with a certain **curvature** (**Figure 53**), which is in turn modulated by lipid composition.<sup>327</sup> Another important membrane property are the packing defects, which is the exposure degree of membrane hydrophobic regions to the aqueous environment. Small head groups and unsaturated fatty acids promote packing defects, whereas polyunsaturated fatty acids not.<sup>328</sup> Related to this behaviour, some proteins can sense lipid composition and curved membranes or vesicles (i.e. select ER-vesicles and allow them to enter to Golgi).<sup>329</sup> Lipid composition of membranes also affects localization and conformation of transmembrane proteins and ion channels.

### Pleckstrin homology domain



### Curvature inducing BAR-domain



**Figure 53.** Examples of protein-lipid interactions. **Pleckstrin homology domain** is a sequence of approximately 100 amino acids included in a range of proteins involved in cell signalling or with structural roles which binds regions enriched with PIP. PH domain can recruit proteins to different membranes, such as phospholipase C- $\gamma$  (PLC- $\gamma$ ) that is recruited via this domain to specific membrane where it will be activated by phosphorylation.<sup>330</sup> **BAR-domains** are highly conserved dimerization domains present in many proteins involved in membrane dynamics that can sense, induce and stabilize lipid membrane curvature.<sup>331</sup>

## 3. Posttranslational modifications and autophagy

As explained in more detail in the previous chapters, Atg proteins are crucial to control autophagy through regulation of phagophores formation, autophagosome elongation and closure and fusion with autolysosomes. Their function is tightly modulated by posttranslational modifications like phosphorylation, glycosylation, ubiquitination, methylation, acetylation, lipidation, and proteolysis. These modifications can be reversible or irreversible depending on their nature.<sup>332</sup> Some relevant examples will be mentioned as follows. **Phosphorylation** is a common posttranslational modification that regulates the activity of many proteins involved in autophagy such as the ULK1 complex, AMPK, mTORC1 and AKT. For example, autophosphorylation of ULK1 complex at different amino acid sites is essential for the regulation of the initial stages of the phagophore formation.<sup>333</sup> Atg5, a protein of the Atg12-Atg5 conjugation system, which acts as E3-like ubiquitin ligase to convert LC3-I into LC3-II, can be phosphorylated at the Thr75 by MAPK14 to inhibit starvation-induced autophagy.<sup>334</sup> Atg9A is a transmembrane protein required for the early

stages of autophagy. Its **glycosylation** facilitates the coordination of membrane transport from donor sources to the autophagosome formation site.<sup>335</sup> Ubiquitination also plays multiple roles in the regulation of autophagy. Hence, **ubiquitination** of beclin 1<sup>336</sup> and ULK1<sup>337</sup> has a key role in autophagy induction. Another posttranslational modification is the **acetylation** of Atg5, Atg7, Atg8 and Atg12 by EP300 which decreases autophagy,<sup>131</sup> in contrast to the deacetylation of the same proteins catalysed by SIRT1 (sirtuin-1) which induces autophagy.<sup>338</sup>

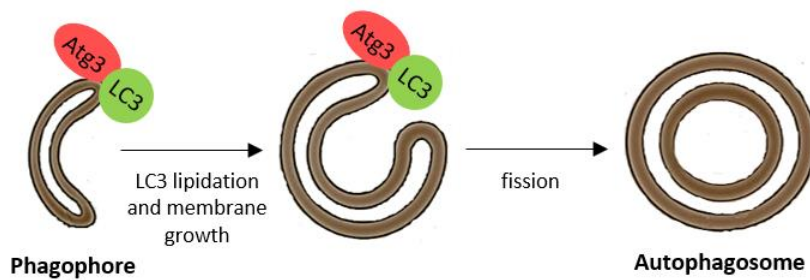
**Lipidation** of LC3/GABARAP family members is essential for their association with phagophore membranes and regulates its role in membrane elongation, fusion and cargo recognition. The C-terminal conjugation of a phosphatidylethanolamine moiety drives the growth of autophagosomal membranes by facilitating membrane-tethering and hemifusion.<sup>339</sup> However, how this process is performed is yet not clear. In addition, a peptide corresponding to N-terminal helix of LC3 and GABARAPL2/GATE16 can also interact with membranes and promote membrane fusion, thereby complicating the overall analysis.<sup>340</sup> Apart from the covalent lipidation with PE, other membrane lipids, such as of C18-ceramide and cardiolipin (CL), have been proposed to **transiently interact** with LC3/GABARAP proteins. Thus, generation of C18-ceramide mediates autophagic cell death by mitophagy through selective targeting of ceramide localized in mitochondria by LC3-II containing autophagolysosomes.<sup>115</sup> Cardiolipin is a unique lipid formed by two phosphatidic acid moieties that are bridged by a glycerol enriched with linoleoyl (18:2) acyl chains.<sup>341</sup> This lipid is located exclusively at the inner membrane of mitochondria facing the mitochondrial matrix and it is only released in case of apoptosis or mitophagy. The interaction between CL and LC3 has been involved in mitophagy induction.<sup>342</sup> The binding of LC3 with CL was also proven by direct liposome-binding studies, computational modelling and site-directed mutagenesis. Moreover, treatment with a mitophagy inhibitor causes an altered distribution of CL in primary rat cortical neurons.<sup>343,344</sup> In addition, knockdown of Tafazzin, a phospholipid transacylase that catalyses the remodelling of cardiolipin, caused only defective mitophagosome biogenesis, suggesting that CL interaction with LC3 is only essential in mitophagy.<sup>345</sup>

#### 4. Lipids and autophagy

Autophagosomes seem to be generated from multiple membrane sources. Hence, PtdIns3P-dependent formation of the omegasome starts at the endoplasmic reticulum (ER)<sup>346,347</sup> and LC3 lipidation seems to take place in ER-Golgi intermediate compartment (ERGIC)-enriched membranes, but membrane lipids can also come from the outer membrane of the mitochondria,<sup>348</sup> Golgi<sup>349</sup> or early endosomes.<sup>350</sup> In addition, phagophore expansion can be mediated by clathrin-coated vesicles derived from the plasma membrane<sup>351</sup> or Atg9-positive vesicles that cycle between distinct cytoplasmic compartments.<sup>352</sup> Even though the process of the autophagosome

biogenesis remains unclear, increasing evidences indicate that **strongly curved membranes** may be the precursors of autophagosome. Thus, the components of the lipidation machinery have been shown to work optimally in small vesicles resembling highly curved membranes, probably resembling the strongly deformed rim of the growing autophagosome.<sup>353</sup> Moreover, intact membrane curvatures can promote protein lipidation,<sup>354</sup> that does not occur in flat surfaces, presumably avoiding the accumulation of LC3-II in other membranes.<sup>355</sup> In addition, the conjugation and deconjugation reactions also show a significant curvature preference. As example, the E2-like enzyme Atg3, in charge of LC3-I lipidation, possess a sequence of 20 amino acids at the *N*-terminus forming a membrane curvature-sensing amphipathic helix which interacts more strongly with negatively-charged vesicles and cone-shaped anionic phospholipids and facilitates LC3/GABARAP lipidation with PE (**Figure 54**).<sup>332,356</sup> In agreement with these results, it has been observed that length reduction of this  $\alpha$ -helix reduces LC3-I lipidation whereas its enlargement causes a loss of specificity for highly curved membranes and then Atg3-mediated lipidation of LC3-I occurs in all cellular membranes.<sup>356</sup> The legionella effector RavZ, which cleaves Atg8 family proteins just one amino acid over from the Atg4 cleavage site, also show strong preference for highly curved membranes. RavZ membrane binding relies on a PtdIns3P-binding (PH) domain and a catalytic domain helix with preference for high-curvature membranes.<sup>357</sup> Moreover, LC3 insertion into the membrane has also curvature-inducing properties and can change the membrane spontaneous curvature as shown by recent studies performed in liposomes.<sup>308</sup> Not only membrane curvature but also membrane composition has a role in this process. Thus, LC3/GABARAP lipidation also relies on PE concentration. At physiological membrane concentrations of DOPE (30 mol%), lipidation becomes membrane curvature dependent, being more efficient in liposomes of smaller diameter, and therefore highly curved. Moreover, in liposomes prepared by replacing the cone-shaped unsaturated DOPE with cylindrical and fully saturated DPPE and DSPE, lipidation is only possible after sonication which produced small liposomes near their curvature limit.<sup>356</sup> Other conic-shaped lipids with intrinsic negative curvature, such as DAG and CL have also shown to induce their lipidation.<sup>353,358</sup> After elongation, closure of the autophagosome would minimize membrane curvature and prevent LC3-II accumulation. All these data may explain the regulation of autophagosome size by lipidated proteins observed in yeast.<sup>359</sup> However, how membrane curvature or the proportion of conical lipids in the membrane might influence the lipidation of Atg8 family proteins is not fully understood.





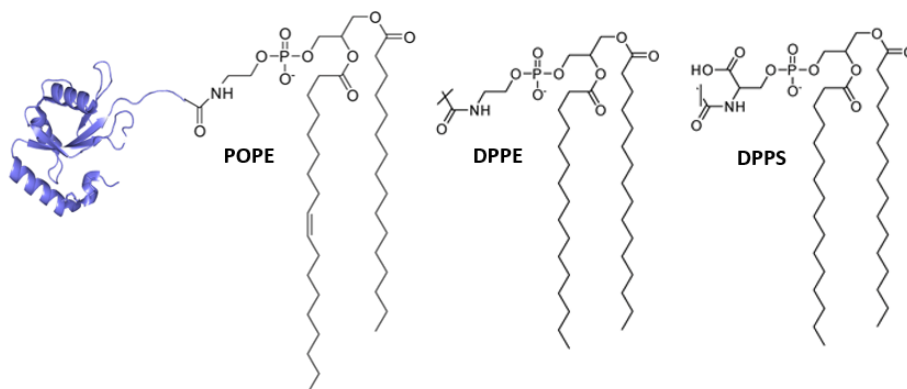
**Figure 54.** The *N*-terminal 20 amino acids of human Atg3 form a membrane curvature-sensing amphipathic helix which promotes the lipidation of the LC3 protein family. The phagophore exhibits an extreme local curvature that distinguishes it from most other intracellular membranes and temporally from the later stages of autophagosome maturation.

Lipidation of LC3/GABARAP is crucial for their attachment to a growing phagophore membrane and it is a critical event in autophagosome elongation and maturation. It has been reported that specific members of LC3/GABARAP family act at different stages of autophagosome formation. GABARAP promote higher liposome aggregation *in vitro* than LC3, which sustains its role in membrane tethering and fusion processes and the implication of LC3-II in autophagosome elongation mediated by hemifusion.<sup>135</sup> This different function could be related with an  $\alpha$ -helix present at the *N*-terminus.<sup>135</sup> Different possible explanations have arisen in the last years for this different function. All Atg8 orthologs share a *C*-terminal ubiquitin-like structure and differ at the *N*-terminal helix, basic in LC3, neutral in GABARAPL2 and acidic in GABARAP. Therefore, it has been hypothesized that the divergent *N*-terminal  $\alpha$ -helices might be important for specific functions via protein-protein, protein-lipid interactions or through post-translational modifications.<sup>360</sup> Differences have been also observed in the processing by the cysteine protease Atg4 homologs. Hence, whereas Atg4A is specific for GABARAP and GABARAPL2, Atg4B process all the members of LC3 subfamily albeit with different affinities.

The identification and detailed characterization of the lipid bound to Atg8 was described in seminal studies done by the group of Yoshinori Ohsumi in 2000, who identified that Atg8 is covalently bound to phosphatidylethanolamine through an amide bond with the *C*-terminal glycine (**Figure 55**).<sup>361</sup> Indeed, he was awarded the 2016 Medicine Nobel prize for this work together with all his studies directed to characterize the molecular mechanism controlling autophagy. There is some controversy regarding the nature of the lipid attached to Atg8 family members. Hence, although in cells LC3 proteins have been only shown to lipidate on PE head groups, *in vitro* studies have proven that PS could be also used as a substrate.<sup>362</sup> The

discrepancy between in vitro and in vivo reactions suggest that there may be unknown selective factors regulating LC3 lipidation. Regarding the delipidation step, whereas an in vitro prepared GABARAP1-PE could be cleaved by Atg4B, the equivalent GABARAP1-PS was not substrate of Atg4B but could be completely cleaved by RavZ.<sup>226</sup> Contrarily, Atg4 proteins could cleave LC3 proteins bearing various C-terminal modifications (ethanolamine, ethanolamine phosphate, glycerophosphoethanolamine, DPPE, diacetyl-PE or esterified with hexadecanol), whereas RavZ required a PE moiety esterified to long fatty acids.<sup>363</sup>

Regarding the fatty acid composition, the preliminary studies performed by Ohsumi based on isolation of a N-(His)<sub>6</sub>-tagged LC3 and the release of attached fatty acids after alkaline hydrolysis, suggested the presence of palmitic, stearic, palmitoleic and oleic acids. However, a detailed analysis of fatty acid composition has not been performed. Thus, if the enzymes in charge of lipidation and delipidation show in some cases broad substrate preference, **which is the rationale behind the choice of PE** (vs PS or PC) as a substrate? And have **phospholipids with different fatty acid composition** a role in the regulation of LC3/GABARAP activity?



**Figure 55.** Members of the LC3/GABARAP subfamilies are C-terminally modified by attachment with a phosphatidylethanolamine unit. Conjugation to PS has been suggested and studied in vitro but it could not be detected in cellular experiments. Fatty acid composition of the bound glycerophospholipids (POPE (palmitoyl, oleoyl), DPPE, (dipalmitoyl), DOPE (dioleoyl), etc.) remains elusive.

## 5. Mass spectrometry-based lipid analysis

Compared to the great advances seen in proteomic field in the last decades, lipid research has clearly lagged behind. Their amphipathic nature, structural diversity and the fact that lipids often work in heterogeneous ensembles with proteins and other cellular components has complicated this field of research. In recent years, the study of lipids has gained importance due to their multiple roles in cell biology, physiology and pathology. Moreover, thanks to the progress in mass spectrometry (MS) and

computational methods, great advances have been achieved in the lipidomic field that have pushed forwards this area of research.<sup>364</sup> Considerable efforts are being spent to develop methods aimed to detect, identify, quantify and discover lipid species and its related genes and proteins.<sup>365</sup> Demands from proteomics, lipidomics and metabolomics have also strongly contributed to these advancements resulting in equipment with more efficient fragmentation, increased sensitivity and higher mass accuracy. Available techniques include matrix-assisted desorption/ionization (MALDI), atmospheric pressure chemical ionization (APCI) and electrospray ionization (ESI) methods in conjunction with automated liquid chromatography (LC). In addition, high-resolution MS coupled to liquid chromatography (LC) have shown the ability to resolve, profile and accurately identify multiple lipid species. The advances of the last decade now allow the detection of small quantities of lipids in complex mixtures like cell extracts.<sup>364</sup> However, all these methods share a common limitation since they cannot determine the exact structure of the molecule, i.e. distinguish chiral centres, position of functional groups and double bond location. More exhaustive structural investigation can be done employing tandem mass spectrometry (MS/MS), which provides important information including carbon-chain length and degree of unsaturation of fatty-acid components. Moreover, there are MS/MS databases which can be used for fragment identification by comparison between the experimental and theoretical results.<sup>366</sup>

Lipidomic analysis have also been facilitated by consortiums such as Lipid Maps (lipidmaps.org) that has greatly simplified the analysis by providing protocols and improving the availability of internal standards and by providing a website containing resources such experimental data or MS prediction tools for glycerolipids and glycerophospholipids.<sup>367</sup> Other helpful online resources are *The European Lipidomics Initiative* (lipidomics.net) who has developed the Lipidomics Expertise Platform (a wikipedia-based data and knowledge resources on lipids), the *Lipid Library* (lipidlibrary.co.uk; the), the *Lipid Bank* (lipidbank.jp) and *Cyberlipids* (cyberlipid.org).<sup>364</sup> Despite the advances in lipid analyses by MS, there are still some issues that needs further research. Usually analyses are carried out with the total cell lipidome instead of the specific origins of interest, therefore there is a need to improve the biochemical isolation of certain regions/organelles for subsequent MS techniques.<sup>364</sup>

Having in mind all the reported information, the idea behind the project developed in this chapter arises from two simple concepts:

- The structural diversity of the cellular lipidome, containing thousands of individual lipid species, can be translated to lipid-modified proteins.
- Heterogenous protein acylation may play an additional role in the regulation of cellular processes.

With this aim, a detailed MS-based lipidomic analysis of these class of lipid-modified

proteins is planned to clarify the potential role of PE as modulators of protein function and localization, which could eventually result in the identification of new targets and the development of novel therapeutic strategies.



# OBJECTIVES



The general purpose of this section of the thesis is to advance in the knowledge of the molecular mechanisms involved in the regulation of autophagy, with a focus on the lipid modifications present in the autophagic biomarkers LC3/GABARAP. This characterization could further contribute to the identification of disease biomarkers and novel targets. Thus, the general aim of this chapter is to study lipid diversity present in LC3/GABARAP and can be split into the following specific goals:

- To optimize and validate a novel method for the extraction of lipids conjugated to LC3/GABARAP from cell lysates through Atg4B treatment of the proteome. Lipids obtained will be analysed and quantified using UPLC/TOF-MS analysis.
- To explore the diversity of PEs conjugated to LC3/GABARAP from a variety of cell lines and to compare this composition with the lipid profile obtained from the cellular lipidome.
- To optimize and validate a method for the extraction of lipids conjugated to an immunoprecipitated LC3-II.





# RESULTS AND DISCUSSION

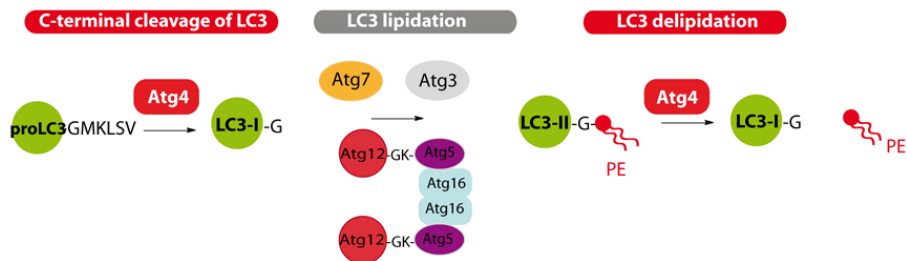


## 6. A MS-based method to analyse PEs derived from LC3/GABARAP

A key step in the drug discovery process is to understand the molecular mechanism of a disease. Thus, basic research aimed to identify the physiological and pathological role of LC3-II lipidation in autophagy regulation and the enzymes or proteins involved in their synthesis and degradation would be of great value. In addition, these studies could lead to the identification of new targets for therapeutic intervention, which remains a critical challenge and an emerging field of research.

The principal aim of this chapter was to perform a detailed molecular characterization of the GPLs bound to LC3-II in order to unveil a potential role of lipid modification in autophagy regulation. For that purpose, an MS-based method employing ultra-performance liquid chromatography/tandem time of flight-mass spectrometry (UPLC/TOF-MS) was applied, since it allows the simultaneous and accurate identification and quantification of multiple lipid species. The designed approach relies on the recent advances observed in the lipidomic field and the great experience gathered by the IQAC Lipidomics Core facility in this area of research.

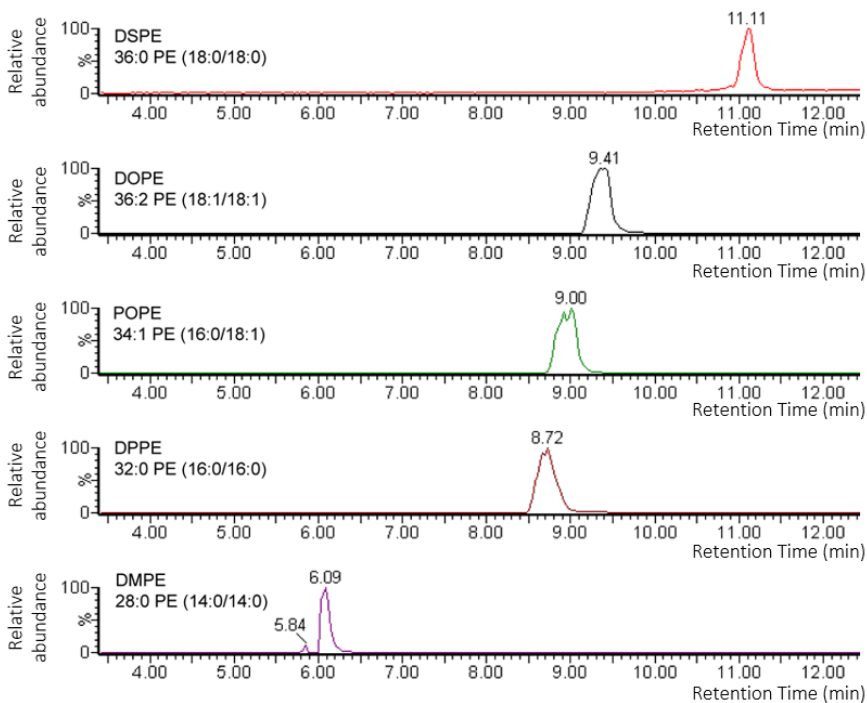
Seminal work by Sakakibara *et al.* described the previous identification of a phosphatidylethanolamine (PE) moiety bound to LC3. In addition, saturated C16:0 and C18:0 and unsaturated C16:1 and C18:1 fatty acids were detected upon mild alkaline treatment of an isolated His-tagged LC3 protein and subsequent analysis of the released fatty acids by GC-MS.<sup>368</sup> However, this strategy presents some important limitations. First, fatty acid analysis of GC-MS requires previous conversion to esters. As a result, GC-MS analysis of lipids has been mainly overtaken by MS systems employing electrospray ionization (ESI) usually combined with a previous separation by liquid chromatography (LC). Indeed, the combination of LC with high resolution MS (HRMS), providing mass accuracy at a level of 0.001-0.002 m/z, enhances the ability to resolve, profile and accurately identify multiple lipids. Secondly and more important, the method previously employed relies on alkaline treatment of GPLs and subsequent fatty acid release. As a result, it cannot be applied to analyse the nature of the GPLs bound to the protein. To overcome this limitation, an enzymatic release of the attached lipid was considered. As mentioned above, Atg4B is involved in two steps of this process (**Figure 56**). It first cleaves the last five amino acids from proLC3 to generate the cytosolic LC3-I and it also recycles LC3-II cleaving the C-terminally attached lipid.<sup>369</sup>



**Figure 56.** Atg4 has a dual role in autophagy, it cleaves the last five amino acids of proLC3 and it also hydrolyses the PE conjugated to LC3-II.

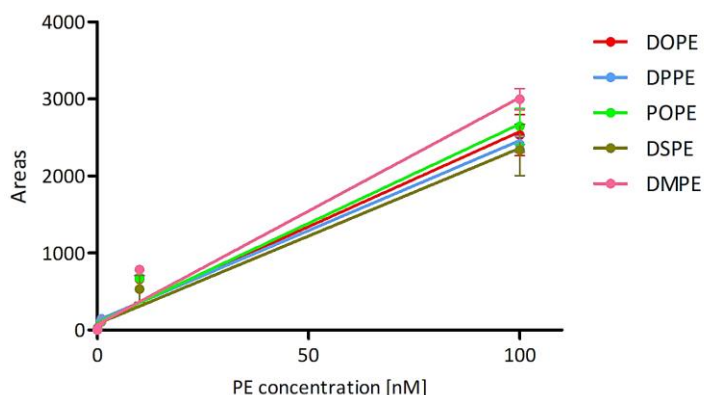
## 7. Calibration curves of PEs detected by UPLC/TOF-MS

As a first step, linearity and robustness of the MS-based detection of PEs was explored. Hence, serial dilutions of five commercially available PEs were analysed: 1,2-Dimyristoyl-*sn*-glycero-3-phosphoethanolamine (DMPE), 1,2-Dipalmitoyl-*sn*-glycero-3-phosphoethanolamine (DPPE), 1,2-Dioleoyl-*sn*-glycero-3-phosphoethanolamine (DOPE), 1,2-Distearoyl-*sn*-glycero-3-phosphoethanolamine (DSPE) and 1-palmitoyl-2-oleoyl-*sn*-glycero-3-phosphatidylethanolamine (POPE) (Figure 57 and Figure 58). The



**Figure 57.** Extracted ion chromatograms (EICs) from negative mode analysis of commercially available PE species. From the top down: DSPE (EIC  $m/z$  746.570), DOPE (EIC  $m/z$  742.539), POPE (EIC  $m/z$  716.523), DPPE (EIC  $m/z$  690.507) and DMPE ( $m/z$  634.445).

detection of glycerophospholipids was performed with a methodology already optimized at the IQAC Lipidomics Core facility. Basically, negative-ion ESI enables the analysis of PE, whereas positive ion mode permits the analysis of PS and PC that usually become ionized as  $\text{NH}_4^+$  adducts. As shown in **Figure 58**, unambiguous identification was performed by accurate mass and elemental composition analysis with a mass window of 5 mDa. All compounds showed a good linear response up to 100 nM and a limit of detection 0.01 nM, which proves UPLC/TOF-MS to be enough sensitive for further cell endogenous PEs quantification. The established retention times were employed for future comparison with cellular samples (**Figure 58**). This method should allow the characterization of the lipid diversity of LC3/GABARAP.

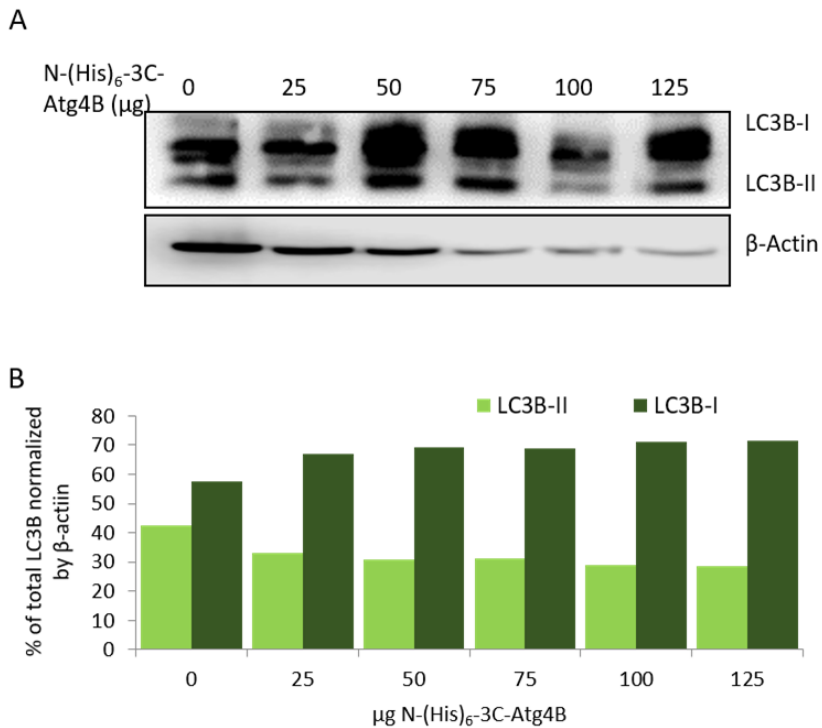


**Figure 58.** Calibration curves of DOPE, DPPE, POPE, DSPE and DMPE. All compounds were diluted from a stock solution of 100  $\mu\text{M}$  to 1  $\mu\text{M}$ . Samples were 10-fold serially diluted up to 0.001 nM and compounds were analysed using a UPLC/TOF/MS (6 points were measured). DPPE and DSPE showed slightly smaller areas, which correlates with their decreased solubility. Correlation coefficients were determined as 0.952, 0.953, 0.967, 0.953 and 0.983 for DOPE, DPPE, POPE, DSPE and DMPE respectively.

## 8. Identification and quantification of PEs from treated cell lysates

The lipid composition of autophagy related proteins was analysed in lysates derived from three cell lines: HEK293 (human epithelial cells from embryonic kidney), HeLa (human epithelial cells from cervix adenocarcinoma) and SH-SY5Y (human epithelial cells from bone marrow neuroblastoma). As initial approach, the required amount of N-(His)<sub>6</sub>-3C-Atg4B was determined through treatment of the obtained suspended proteome with different quantities of enzyme (25-125  $\mu\text{g}$ ) during 2 h at 37 °C. Protein levels were detected by western blotting using antibodies anti-LC3B (**Figure 59**). The resulting LC3B-I and II were quantified by densitometric analysis of protein signal normalized to actin levels. A dose dependent decrease on LC3B-II/LC3B-I ratio could be observed with increasing concentrations of proteins, ranging from 1/1.5 to 1/3.

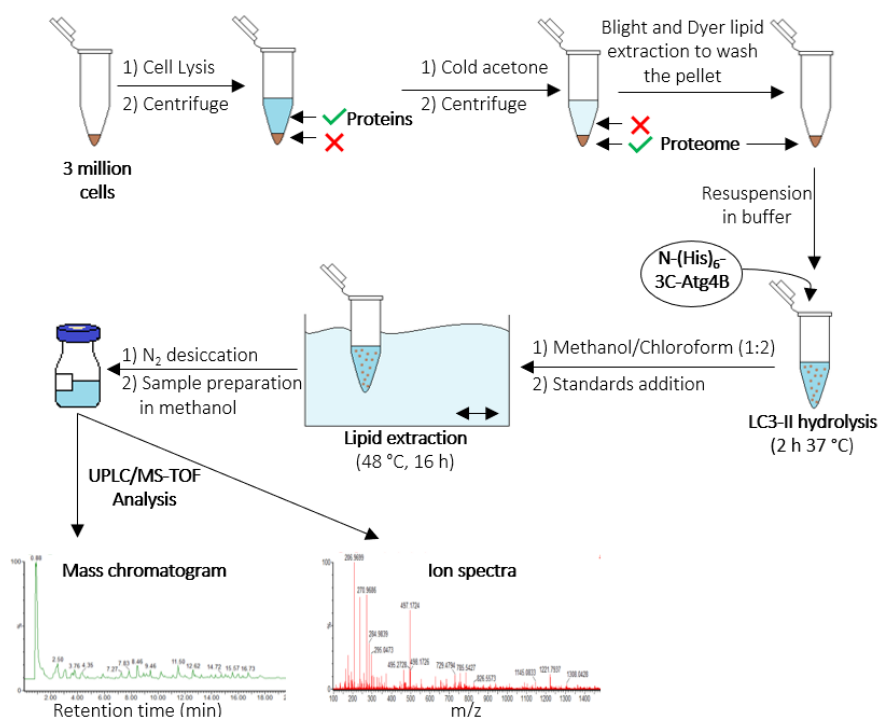
However, a complete delipidation of LC3B-II could not be detected. Different reasons are considered for these results. On one side, the slow kinetics of Atg4B-mediated delipidation has been recently reported.<sup>226</sup> On the other side, one cannot discard that the acetone-mediated protein precipitation, although carried out at below zero temperatures, causes partial denaturation thereby preventing Atg4 recognition of their substrates. A 25 µg amount of Atg4B was chosen for further optimisation.



**Figure 59.** Proteome was treated with different amounts of N-(His)<sub>6</sub>-3C-Atg4B. An untreated sample was employed as a control. **(A)** The amount of LC3B-I and LC3B-II was determined by western blotting and normalized to  $\beta$ -actin control. **(B)** Quantitative analysis of western blots from **A** as bar graphs. Data from **A** were quantified by densitometry and are depicted as percentage of total LC3B.

Next, the PEs bound to the proteome were investigated. Atg4B presents a broad specificity for all mammalian Atg8 homologues (LC3 and GABARAP subfamily members).<sup>370,275</sup> As a result, the previously expressed N-(His)<sub>6</sub>-3C-Atg4B was employed to release PEs from LC3/GABARAP present in cell lysates. Briefly, the general method designed to identify and quantify PEs included the precipitation of the proteome by adding cold acetone and the subsequent removal of non-covalently bound lipids (membrane lipids) by the Bligh and Dyer lipid extraction protocol.<sup>371</sup> As mentioned above, protein precipitation and lipid removal with organic solvents can

cause protein denaturation. However, membrane lipid extraction is strictly required otherwise the released PEs would be diluted and thus non-detectable. Moreover, many protein spontaneous refold into their native functional structure if resuspend in the appropriate buffer. Thus, this first approach was initially explored assuming that if GPLs could be detected at the end of the protocol, proteins should have been correctly refolded (**Figure 61**). Hence, the resulting pellets were then resuspended in the corresponding buffer containing TCEP to enhance Atg4B activity and finally, PEs were released from LC3-II by treatment with N-(His)<sub>6</sub>-3C-Atg4B. Negative control was treated only with buffer. Subsequently, an internal standard was spiked into each sample. Structurally related isotope-labelled standards were employed such as 1-palmitoyl-*d*31-2-oleoyl-*sn*-glycero-3-phosphoethanolamine (16:0-*d*31-18:1 PE) and other deuterated GPLs (16:0-*d*31-18:1 PS, 16:0-*d*31-18:1 PC and lysophospholipids such as C17:1 LysoPE) and enabled appropriate quantification of GPLs. Lipids were extracted, dried, resuspended in methanol and analysed by high resolution mass spectrometry (HRMS) using the UPLC/TOF-MS.

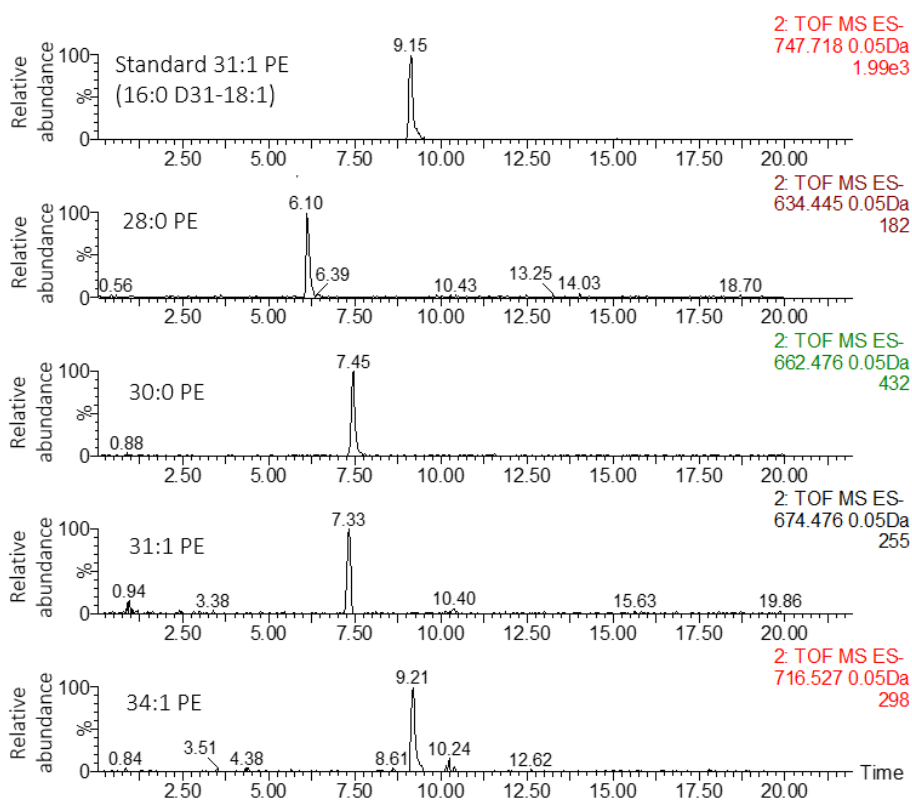


**Figure 60.** Procedure for the extraction of lipids bound to Atg8 homologues. 3 million cells were lysed through ice-sonication cycles and the suspended proteins were precipitated by cold acetone for 30 min at 0 °C. Then, the mixture was centrifuged, and the supernatant discarded. The pellet containing the precipitated proteome was washed with mixtures of organic solvents following Blight and Dyer lipid extraction protocol. Next, the proteome was resuspended in the reaction buffer and the enzyme N-(His)<sub>6</sub>-3C-Atg4B was added



followed by an incubation of 2 h at 37 °C to facilitate the hydrolysis of the lipids from the Atg8 homologues. The hydrolysed lipids were extracted by incubation of the mixture with organic solvents for 16 h at 48 °C followed by N<sub>2</sub>-mediated desiccation. Lipids were resuspended in methanol and analysed by UPLC/TOF-MS.

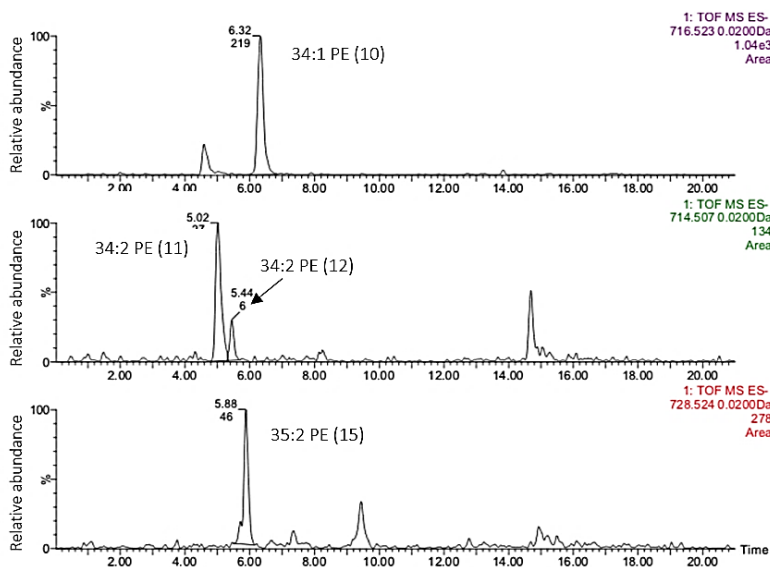
Interestingly, MS-based analysis provided a vast profile of PEs species (**Figure 61**). Appropriate quantification was done by comparison with the spiked internal standard. Detection and quantification of PEs species was performed employing the extracted ion chromatograms (EICs) from negative mode analysis ([M-H]<sup>-</sup>). PEs species annotation reflect the structural information derived from the analysis (number of C-atoms: number of double bonds followed by lipid class abbreviation, not counting carbons of the glycerol backbone or head groups).



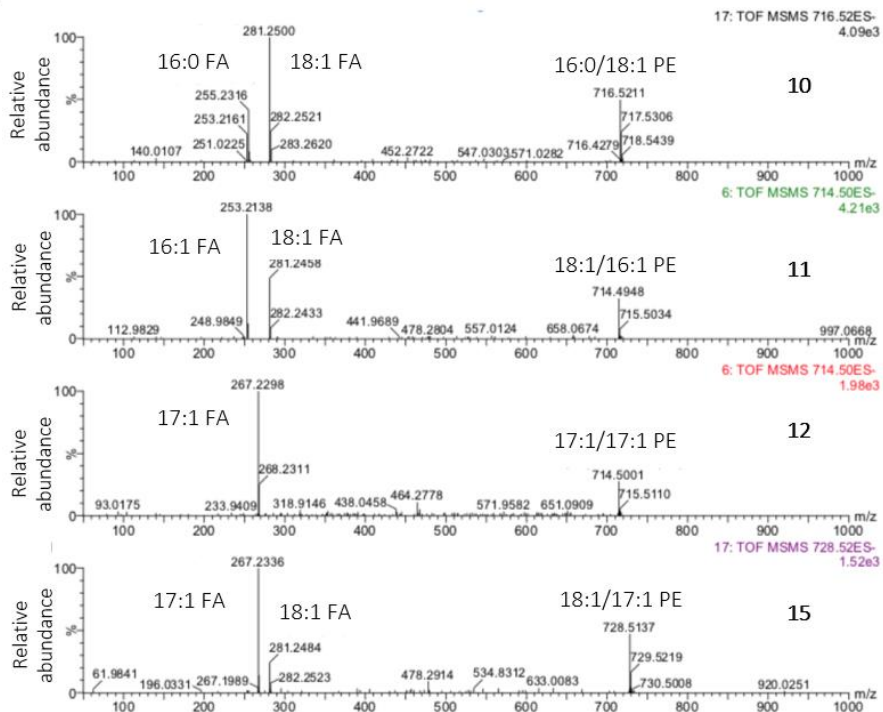
**Figure 61.** Extracted ion chromatograms (EICs) from negative mode analysis of a cellular lysate treated with N-(His)6-3C-Atg4B. Some detected PEs species are shown. From top down EIC m/z 747.718 corresponding to the spiked internal standard (16:0 d31-18:1 PE), EIC m/z 634.445 corresponding to 28:0 PE, EIC m/z 662.476 corresponding to 30:0 PE, EIC m/z 674.476 corresponding to 31.1 PE and EIC m/z 716.527 corresponding to 34:1 PE.

The identity of 28:0 PE as DMPE, 32:0 PE as DPPE, 34:1 PE as POPE and 36:2-PE as

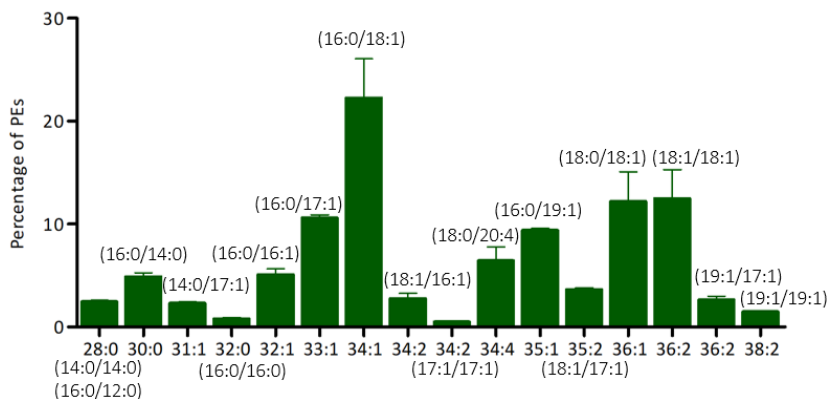
DOPE could be confirmed by comparison of their retention times with the ones obtained with commercially available samples (6.03, 8.83, 9.24, 9.65, respectively). More exhaustive structural investigations were done employing tandem mass spectrometry (MS/MS), which provides important information including carbon-chain length, and degree of unsaturation of fatty-acid components. The MS/MS analyses were performed by Dr. Beatriz Abad in collaboration with Dr. Felix Goñi and Dra. Alicia Alonso (Biofisika, CSIC-UPV/EHU) in SCAB (Servicio Central de Análisis de Bizkaia, Facultad de Ciencia y Tecnología, Universidad del País Vasco) and enabled the identification of the fatty acids bound to the glycerol backbone. As example, MS/MS analysis of species **10** (34:1 PE), **11** and **12** (34:2 PE) and **15** (35:2 PE) are depicted in **Figure 62** and **Figure 63**. Thus, **10** (34:1 PE) was formed by a palmitic (16:0) and oleic acid (18:1). The two species **11** and **12**, with the same global compositions 34:2 PE presented different acyl chains. Hence, whereas **11** contained a hexadecenoic (16:1) and an octadecenoic acid (18:1), **12** was formed by two residues of 17:1. The specie **15** (35:2 PE) also presented the odd-chain fatty acid 17:1 combined with octadecenoic acid 18:1. Similar analysis were performed in all the cases enabling the identification of all PE species detected.



**Figure 62.** Extracted ion chromatograms (EICs) from negative mode analysis of the following deprotonated molecular ions  $[M-H]^-$ : 34:1 PE (**10**), 34:2 PE (**11**) and (**12**) and 35:2 PE (**15**).



**Figure 63.** MS/MS spectra of compounds **10**, **11**, **12** and **15** revealed the corresponding fatty acid composition.



**Figure 64.** Relative quantification of PEs from HeLa cells. The lipids were obtained through precipitation of the proteome, treatment with N-(His)6-3C-Atg4B and extraction by organic solvents. Identity (in parenthesis) of PEs was confirmed by MS/MS from samples analysed at SCAB, UPV/EHU.

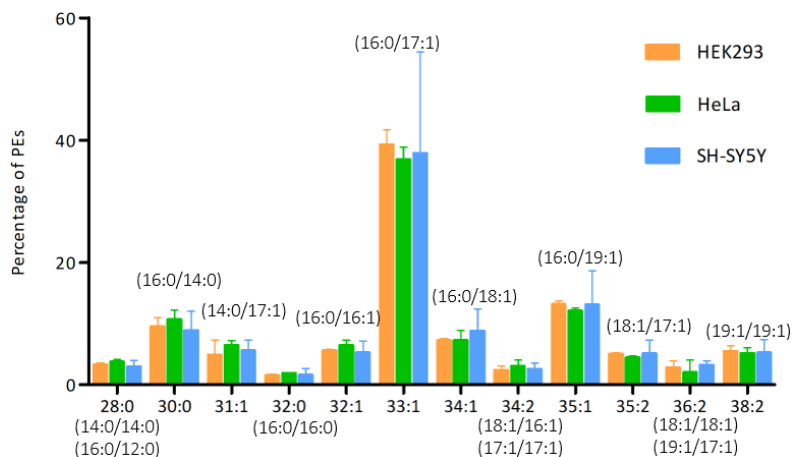
As depicted in **Figure 64**, the most abundant PLs identified were asymmetric PLs containing a saturated fatty acid and an unsaturated one. These species include: 32:2

(16:0/16:1), 33:1 (16:0/17:1), 34:1 (16:0/18:1) and 35:1 (16:0/19:1) all of them bearing a saturated palmitic and a monounsaturated fatty acid such as hexadecenoic (16:1), heptadecenoic acid (17:1), octadecenoic (18:1) and nonadecanoic acid (19:1), respectively. Similarly, 36:1 and 34:4 species contain a saturated stearic acid and a monounsaturated octadecenoic acid or a polyunsaturated acid, probably arachidonic acid. Other interesting observations could be also summarized. Hence, some PEs species contain two saturated fatty acids such as the symmetrical 28:0 (14:0/14:0) and 32:0 (16:0/16:0) esterified with two moieties of myristic or palmitic acid respectively, or the asymmetrical 28:0 (16:0/12:0), and 30:0 (16:0/14:0) containing a palmitic acid combined with either a residue of lauric or myristic acid. In addition, other species contain two monounsaturated fatty acids such as 34:2 (18:1/16:1 and 17:1/17:1), 35:2 (18:1/17:1) and 36:2 (18:1/18:1 and 19:1/17:1). Double bond positions are difficult to distinguish by MS. As a result, unsaturated species cannot be unambiguously identified and whereas 16:1 species likely correspond to  $\omega$ -7 palmitoleic acid, 18:1 could correspond to  $\omega$ -7 vaccenic acid, *cis*  $\omega$ -9 oleic acid or *trans*  $\omega$ -9 elaidic acid. In addition, the existence of methyl-branched fatty acids can also not be discarded. Interestingly, some traces of PS (16:0/18:0, 18:0/18:1 and 18:1/18:1) could also be identified in this case (data not shown).

Unexpectedly, some abundant PEs are formed by rare odd-chain fatty acids (OCFA), usually less abundant in biological samples. Initial literature reports have attributed the origin of C15:0 and C17:0 and C19:0 fatty acids to the diet, specifically from ruminant foods such as meats or dairy products and they seem to be synthesized by the rumen bacterial flora.<sup>372,373</sup> However, there are also some evidences that ruminant can synthesize *de novo* OCFA using propionyl-CoA instead of acetyl-CoA.<sup>374</sup> More recently, it has been hypothesized that this *de novo* biosynthesis can also occurs in humans,<sup>375</sup> as C15:0 and C17:0 fatty acids can be detected in healthy volunteers, and their levels increases after propionate supplementation. Moreover, vegans, vegetarians and omnivores contain comparable concentrations of OCFA, suggesting that there must be other sources than ruminant foods.<sup>376</sup> An endogenous biosynthesis of OCFA is also supported by the fact that patients with propionic acidaemia, a rare genetic disorders characterized by a deficiency of propionyl-CoA carboxylase, present an increased intracellular concentration of propionyl-CoA and abnormally high levels of 15:0 and 17:0 fatty acids.<sup>377,378</sup> In agreement with these results, an exhaustive lipidomic analysis revealed a remarkable diversity of lipids in human plasma, including the presence of C15:0, C17:0 (margaric acid) and C17:1 free fatty acids in 0.3, 0.5 and 0.46 % respectively compared to the 29% of palmitic acid and the 36% of oleic acid detected.<sup>379</sup> Low levels of C19:0 and C23:0 could also be identified by the authors<sup>380</sup> whereas references to unsaturated OCFA apart from 17:1 could not be found in the literature.

Thus, OCFA have been detected in humans but in general in low amounts. However,

in the studies performed during this thesis, all cell lines (HEK293, HEK293 and SH-SY5Y) exhibit similar proportion of PEs. Slight changes can be observed in some species from one measurement to another, but the overall composition remains quite constant (**Figure 65**).

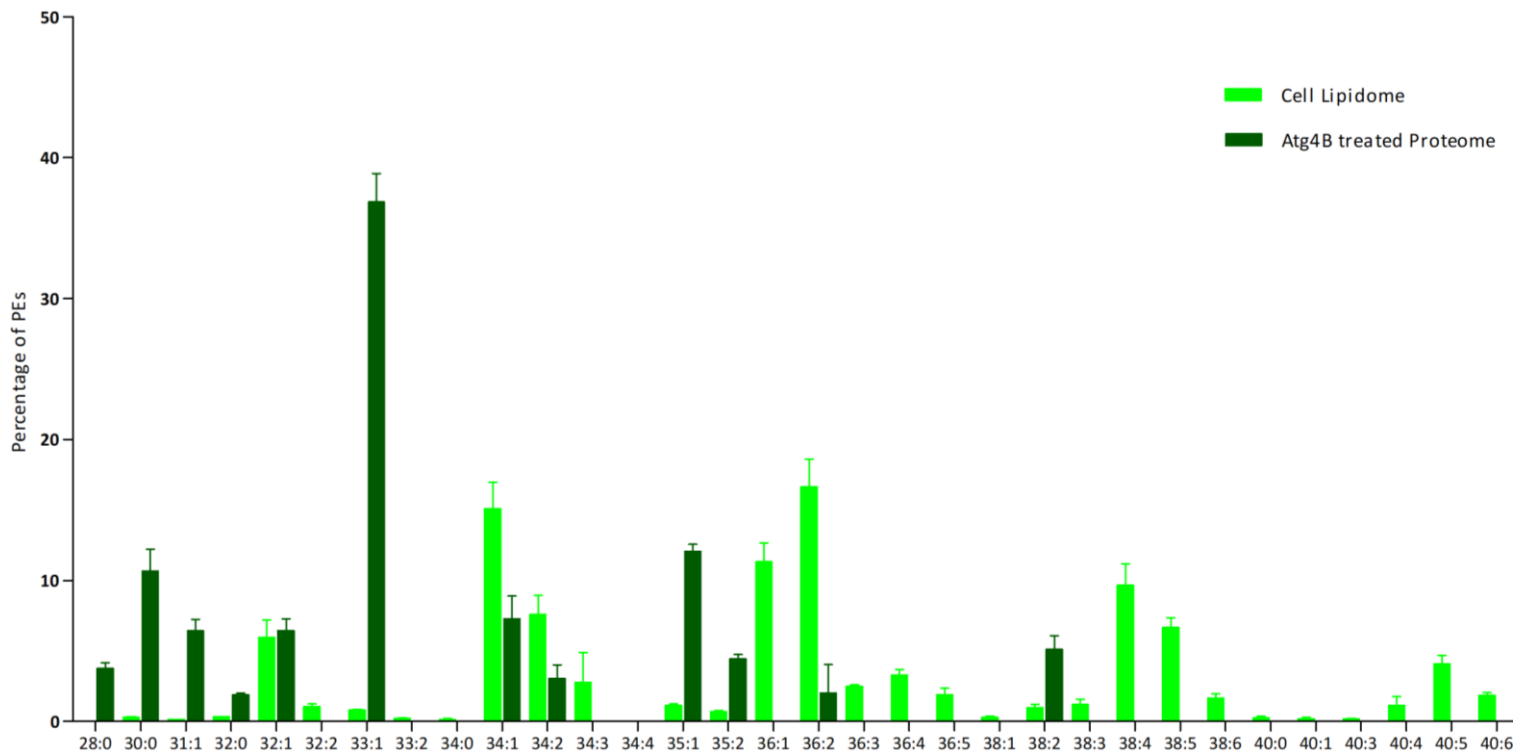


**Figure 65.** Relative quantification of PEs from HeLa, HEK293 and SH-SY5Y cells. Analysis were performed at IQAC. Numbers shown represent the mean of at least three experiments (include SEM).

## 9. Identification and quantification of PEs from total lipidome

We next investigated the cellular lipidome of each cell line in order to compare the PEs content with the ones previously found bound to LC3/GABARAP-II. Hence, lipid analysis of cellular membranes was done by incubating cell lysates derived from 1 million of HeLa cells with a mixture of organic solvents consisting in chloroform, methanol and water (5:5:1) overnight at 48 °C. A mixture of lipids (such as 16:0-*d*31-18:1 PE and other deuterated GPLs) was added to each sample as internal standards. Lipids were then dried, resuspended in methanol and analysed by HRMS.

Results showed significant differences among the two lipid profiles (**Figure 66**). Thus, the cellular lipidome and the lipids obtained after treatment of the proteome with N-(His)<sub>6</sub>-3C-Atg4B shared common species such as 34:1, 34:2 and 36:2. However, whereas the cellular lipidome was enriched with very long chain and polyunsaturated fatty acids such as 36:3, 36:4, 36:5, 38:4, 38:5, 40:5 or 40:6 among others, the PEs released by N-(His)<sub>6</sub>-3C-Atg4B presented a higher proportion of shorter chain fatty acids (28:0, 30:0, 31:1, 32:0 and more importantly 33:1 and 35:1).



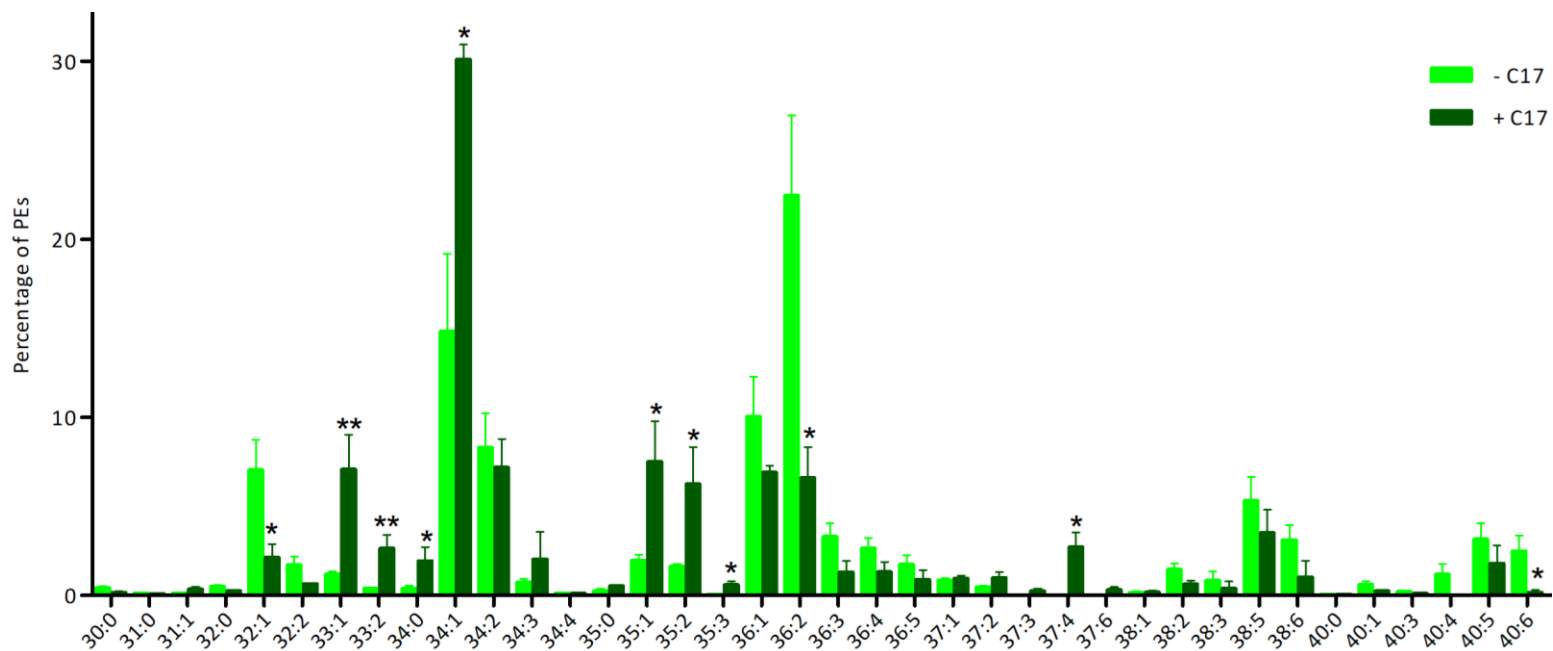
**Figure 66.** Quantification of PEs species detected in the cellular lipidome (HeLa cells, light green) and after treatment of precipitated proteome with N-(His)<sub>6</sub>-3C-Atg4B during 2 h at 37 °C (dark green). Internal standards were added for proper quantification. Results are expressed as percentages of total PEs. Numbers shown represent the mean of at least three experiments ± SEM.

Hence, monounsaturated OCFA, mainly 17:1 and 19:1, can be found in major proportion in N-(His)<sub>6</sub>-3C-Atg4B treated samples than in the total lipidome. Interestingly, the cellular lipidome also presented some PEs formed by OCFA but in a remarkable lower abundance. Examples thereof in HeLa cells are 33:1 (16:0/17:1) 0.79% vs 36.84%, 35:1 (16:0/19:1) 1.12% vs 12.05%, 35:2 (18:1/19:1) 0.70% vs 4.46%, 38:2 (19:1/19:1) 0.98% vs 5.12% of relative percentages in lipidome and N-(His)<sub>6</sub>-3C-Atg4B treated proteome, respectively. It is expected that the previously identified species (MS/MS) would also correspond to the same PEs here. However additional MS/MS analysis would be required to characterize the additional PEs detected here. For clarity, PEs species annotation is restricted to the number of C-atoms: number of double bonds). Similar studies were also performed in HEK293 and SH-SY5Y obtaining similar results, as shown in **Figure 1** and **Figure 2** from the **Annexes**.

## 10. Lipid profiling of HeLa cells treated with heptadecanoic acid

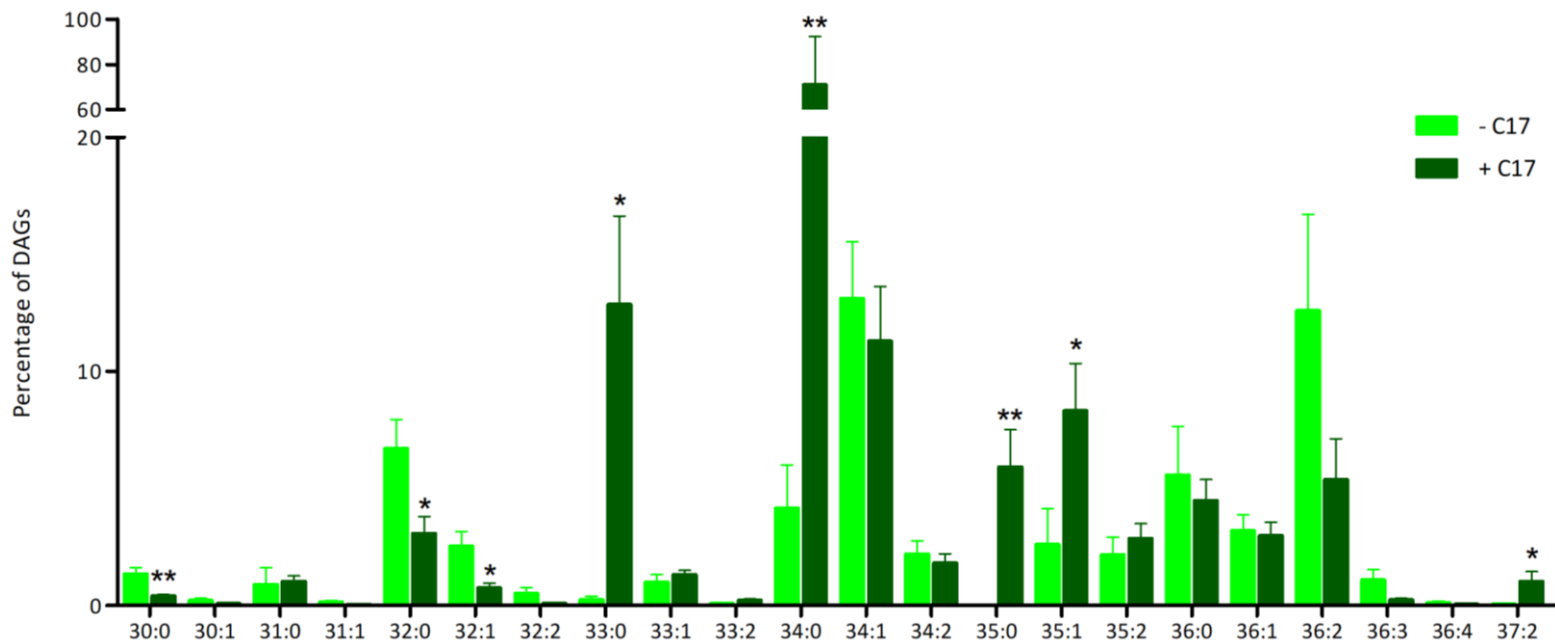
As mentioned above, 15:0, 17:0 and 19:0 fatty acids have been long considered biomarkers for dairy fat intake and more recently their endogenous biosynthesis from propionate has also been investigated. The levels of unsaturated OCFA are less studied and apart from 17:1, no references from the literature can be found for other species and the general role of OCFA remains also under study. It has been described that the risk of type 2 diabetes is inversely correlated with plasma concentrations of OCFA<sup>381</sup> and tissue levels of OCFA are lower in Alzheimer's disease patients,<sup>382</sup> thereby implicating OCFA in the regulation of physiological and pathological processes. However, very much efforts are yet needed to clarify the biological relevance of these fatty acids.

The substantial enrichment observed in OCFA in the extracted lipidome samples resulted unexpected. Hence, this modification was next studied in more detail. As a first approach, HeLa cells were treated with exogenous heptadecanoic acid (17:0) for 24 h in order to find out if the lipidome composition could be modified with dietary intake of fatty acids. To this end, HeLa cells were treated with heptadecanoic acid or vehicle (in the control samples), and then the total lipidome was extracted and analysed by HRMS. To investigate a potential enrichment of OCFA in the treated samples, PEs species formed by all potential combinations of heptadecanoic acid were searched, including fatty acids derived from the elongation and desaturation of C17:0. As shown in **Figure 67**, PEs potentially containing 17:0 resulted significantly enriched, 33:2 (16:1/17:1), 35:0 (18:0/17:0 or 16:0/19:0), 35:2 (18:1/17:1 or 16:1/19:1), 35:3 (18:1/17:2 or 16:1/19:2). The presence of species containing two double bonds (33:2, 35:2) suggest that heptadecanoic acid may be desaturated by the cells. Further MS/MS analysis would be required to determine the exact identity of the fatty acids.



**Figure 67.** Quantification of PEs species found in the cellular lipidome (HeLa cells) after treatment with heptadecanoic acid (C17). Internal standard was added for proper quantification. Results are expressed as percentages of total PEs quantified in each sample. Numbers shown represent the mean of at least three experiments. Statistical significance was determined by two tailed unpaired t-test (\*p < 0.05, \*\*: P < 0.01, \*\*\*: P < 0.001).

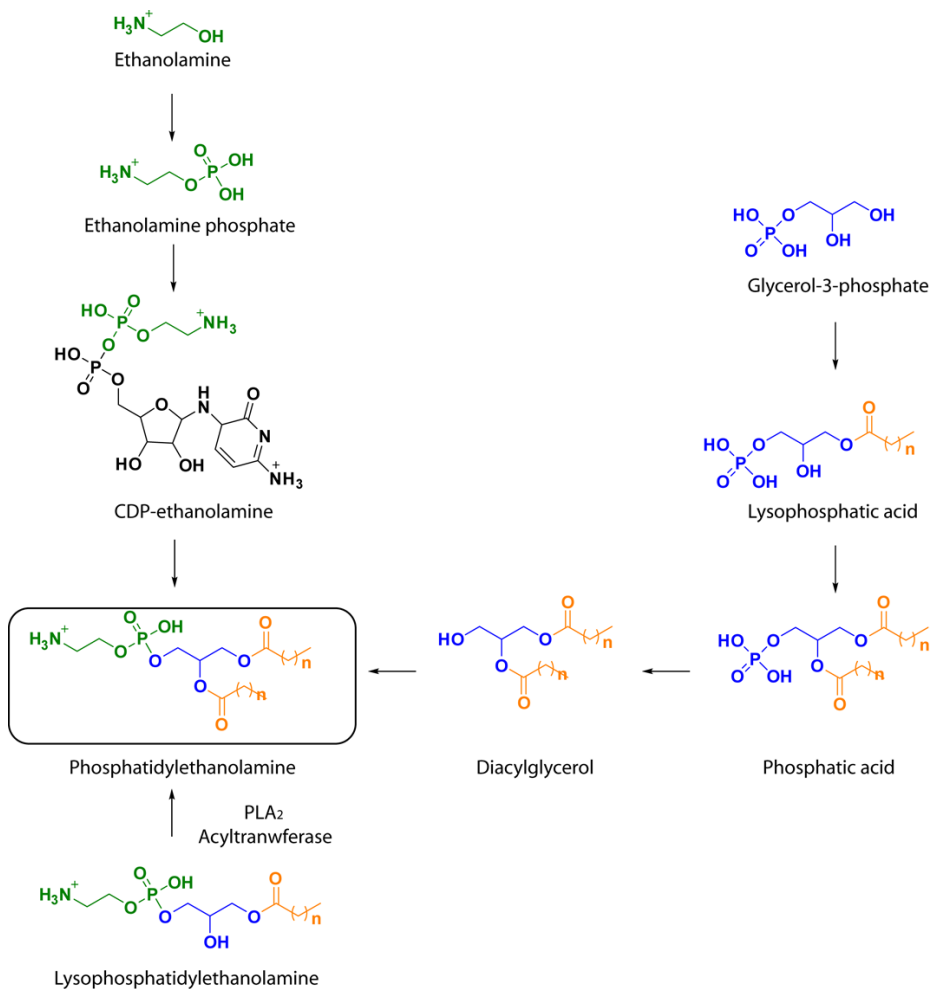




**Figure 68.** Profile of DAGs species determined by HRMS of the lipidome extracted from HeLa cells after treatment with heptadecanoic acid (C17). Internal standard was added for the quantification. Results are expressed as percentages of total DAGs quantified in each sample. Numbers shown represent the mean of at least three experiments. Statistical significance was determined by two tailed unpaired t-test (\* $p \leq 0.05$ , \*\* $p \leq 0.01$ , \*\*\* $p \leq 0.001$ ).

De novo formation of PE in eukaryotes may occur via several pathways: the CDP-ethanolamine branch of the Kennedy pathway,<sup>383</sup> decarboxylation of phosphatidylserine (PS)<sup>384</sup> and base-exchange of PS.<sup>385</sup> In addition, PE can be generated by acylation of lyso-phospholipids taken up by cells from the environment (Figure 69).<sup>386</sup>

The Kennedy pathway plays a key role in the generation of PE and is indispensable for mammalian development (Figure 69). First, the phosphorylation of ethanolamine is catalysed by two specific kinases and then the reaction with cytidine triphosphate (CTP) forms cytidine diphosphoethanolamine. In a final step, the membrane bound CDP-ethanolamine:diacylglycerol ethanolaminephosphotransferase catalyse the reaction with diacylglycerol (DAG) to form PE.

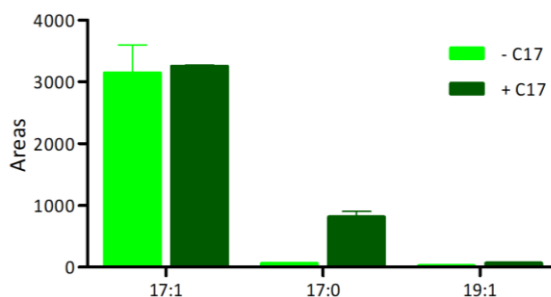


**Figure 69.** Typical phosphatidylethanolamine biosynthesis pathways in eukaryotes. Synthesis starts with the formation of ethanolaminephosphate that reacts with cytidine triphosphate (CTP) to form CDP ethanolamine. Next, the attachment of a DAG yields PE

(DAG is obtained by acylation of glycerol-3-phosphate to lysophosphatidic acid and phosphatidic acid). Alternatively, PEs can also be obtained by acylation of lysoPE.

Since diacylglycerols (DAG) are the main precursor of PEs, DAGs species were also characterized and quantified. Thus, lipidomic analysis of DAGs in HeLa cells treated with heptadecanoic were compared to the ones detected in untreated samples. As expected, a significant enrichment in DAGs derived from C17:0 fatty acids could be observed such as 33:0 DAG (16:0, 17:0), 35:0 (17:0, 18:0) 35:1 (17:0,18:1) and most importantly 34:0 (17:0, 17:0). Potential lipid molecular species are described in brackets, although further structural elucidation would require MS/MS techniques (Figure 68).

All in all, 17:0 fatty acids are clearly incorporated into DAG species as detected by HRMS-based profiling. The incorporation of C17 is significant in DAGs species containing saturated fatty acids. PEs species also show a significant enrichment in C17 containing species although in this case the enrichment is more important in unsaturated PEs without being able to confirm if they are derived from C17:1 fatty acid or upon attachment of C17:0 to species already containing unsaturated fatty acids. Interestingly, the important increase observed in 34:0 DAG (14-fold) is reduced when translated to PEs species (8-fold). A possible synthesis upon remodelling of already existing lysophosphatidylethanolamine (lysoPE) formed from 17:0 could also be in charge of the enrichment observed in PEs species. Indeed, a significant increase in the levels of 17:0 lysoPE could be observed in treated cells. Unfortunately, changes in the levels of C17:1-lysoPE could not be explored because this specie is exactly the one added as internal standard for quantification of the other lysoPEs. No traces of 15:0 lysoPE or changes in 19:0 lysoPE levels were observed (Figure 70). Lipidomic profiling of PEs species derived from LC3/GABARAP isolated from cells treated with C17:0 should be next investigated to explore if the enrichment of PEs containing 17:0 fatty acid can be also translated to the lipid modifications present in these proteins.



**Figure 70.** Specific LysoPE species determined by HRMS analysis (in areas) of the lipidome extracted from HeLa cells after treatment with heptadecanoic acid (C17). Results are expressed as integrated areas of the chromatogram of each sample. Numbers shown represent the mean of at least three experiments  $\pm$  SEM.

## 11. Immunoprecipitation of LC3B

Atg4B is involved in the cleavage of the C-terminal amino acid of Atg8 family proteins to reveal a C-terminal glycine and it is also involved in its delipidation.<sup>251</sup> Atg8 homologs in mammals include two subfamily of proteins LC3 and GABARAP, consisting of LC3A, LC3B, LC3C and GABARAP, GABARAPL1 and GABARAPL2/GATE-16. It has been suggested that these proteins may have different roles in the autophagic machinery.<sup>135</sup> In addition, they may present different affinities to the enzymes involved in their synthesis and delipidation.<sup>226</sup> Thus, as a next experiment it was planned to profile the PEs derived exclusively from LC3B-II.

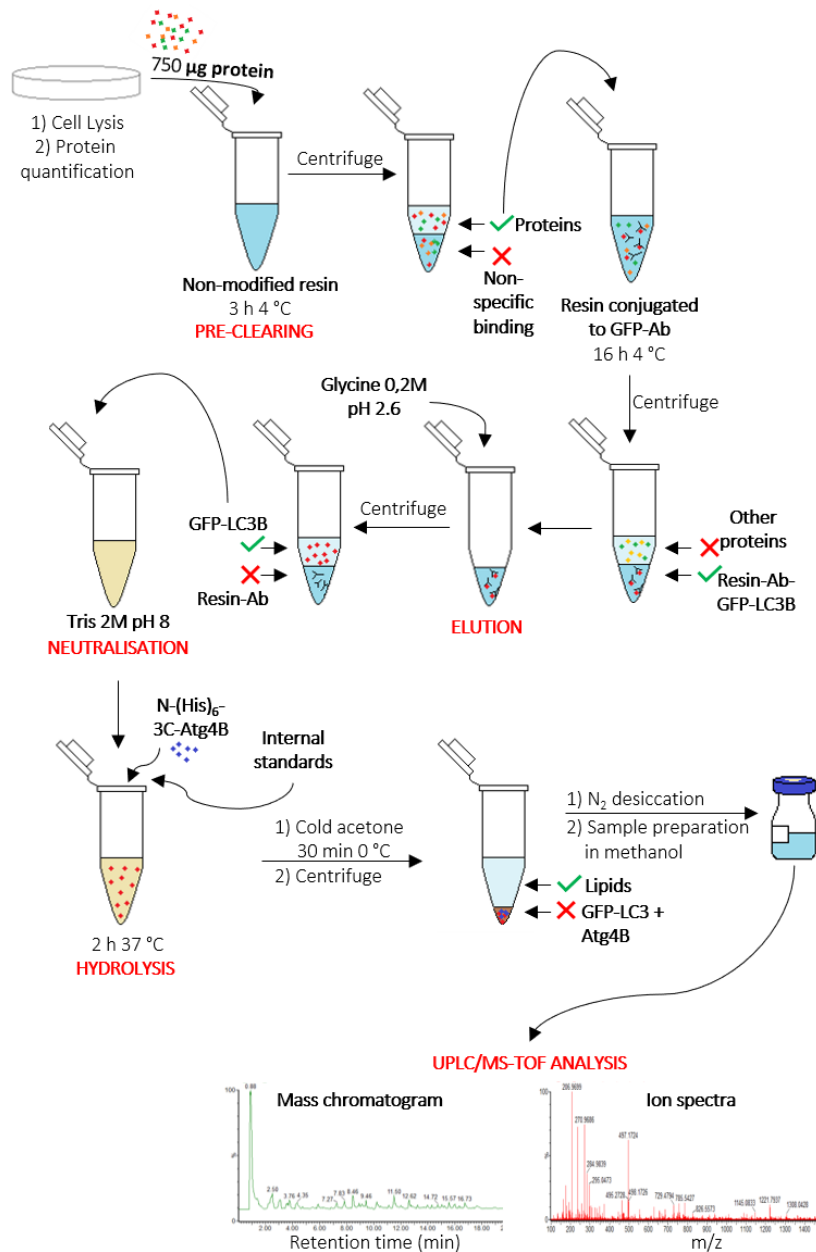
### 11.1. Optimization of the immunoprecipitation method

Detection of endogenous proteins remains challenging. Thus, since high amounts of PEs are required to be detected by HRMS, HEK293 cells overexpressing GFP-LC3B were initially chosen to carry out the optimization. The selected method was the immunoprecipitation (IP) of the GFP-fusion protein employing an anti-GFP antibody immobilized to a sepharose resin (no cross-reactivity for GABARAP proteins has been described for LC3B antibodies).

To avoid proteome precipitation, cell lysates were directly loaded onto the resin. A preclearing step was added to the general protocol due to the high affinity of protein A to other cellular proteins. Preclearing consisted in incubating the cell lysates with unmodified resin to remove proteins that non-specifically bind to the resin. Atg4B requires full length protein substrates since short peptides spanning the natural pro-LC3B cleavage site cannot be efficiently processed by the enzyme.<sup>233,224</sup> Therefore non-denaturing conditions were required to facilitate Atg4B-based recognition of the substrates. As a result, three lysis buffers with increasing denaturing capacity were investigated:

- Non-denaturing lysis buffer 1: 50 mM Tris, pH 7.5, 150 mM NaCl, 10% glycerol, 1% NP-40 and 1 mM PMSF.
- Non denaturing lysis buffer 2: 50 mM Tris, pH 8, 150 mM NaCl, 10% glycerol, 0.1% Triton X-100 and 1 mM PMSF.
- Mild-denaturing lysis buffer 3: 50 mM Tris, pH 8, 150 mM NaCl, 1% NP-40, 0.25% sodium deoxycholate and 1 mM PMSF.

Cells were collected and lysed in each buffer, then protein was quantified by the BCA method, and 750 µg of protein were added to the non-modified resin (pre-clearing



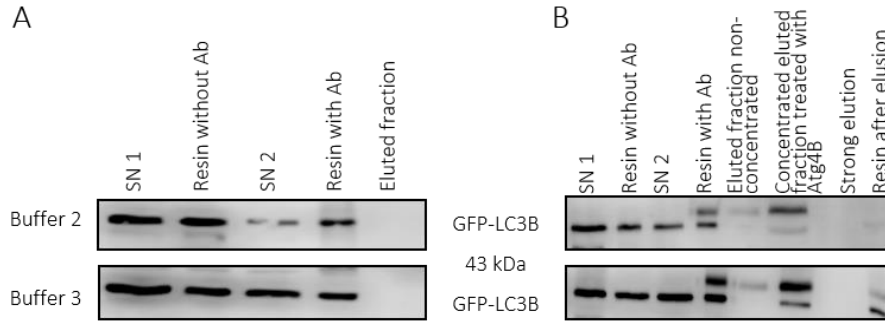
**Figure 71.** Procedure for the extraction of lipids bound to GFP-LC3B. 8 million cells were lysed and the protein was quantified. Then, 750  $\mu\text{g}$  of protein were applied to non-modified resin for 3h at 4 °C for the pre-clearing step. After centrifugation, the supernatant was transferred to resin conjugated to anti-GFP antibody and the mixture was incubated for 16 h at 4 °C. After centrifugation, GFP-LC3B was eluted from the resin employing an acid buffer (0.2 M glycine pH 2.6). The pH of the solution was neutralized by the addition of the same volume of a basic buffer (2 M Tris pH 8). Next, the enzyme N-(His)<sub>6</sub>-3C-Atg4B and the internal standards were added followed by an incubation of 2 h at

37 °C to facilitate the hydrolysis of the lipids from the GFP-LC3B-II. The hydrolysed lipids were extracted by incubation of the mixture with cold acetone, which lead to protein precipitation. After centrifugation, the supernatant was desiccated under a N<sub>2</sub> stream. Lipids were resuspended in methanol and analysed by UPLC/TOF-MS.

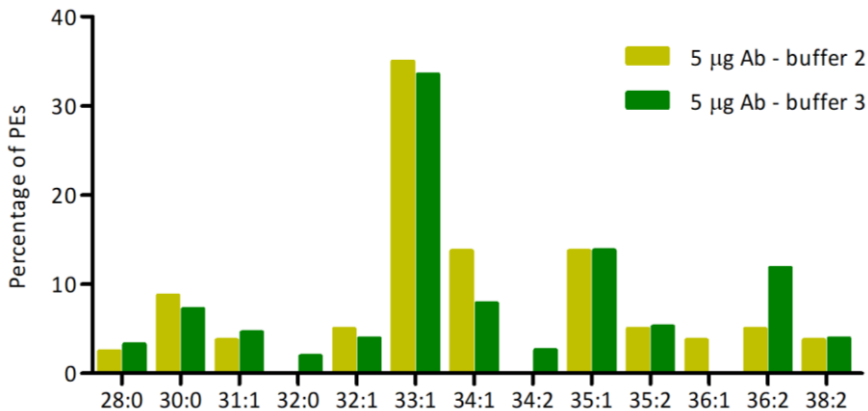
step) (**Figure 71**). After 3 h incubation at 4 °C, the resin was centrifuged and the supernatant (SN) was collected (a sample of SN and resin were collected for immunoblotting control of the process, most of GFP-LC3B should be on the SN). The supernatant was then loaded to the resin conjugated to anti-GFP antibody and it was incubated overnight at 4 °C. After this time, a sample of the SN and the resin were collected for immunoblotting control, GFP-LC3B should be now on the resin conjugated to the antibody. Western blot analysis of LC3 proteins present in cell lysates confirmed lysis using buffer 2 and 3. However, no proteins could be observed using buffer 1, thus suggesting that cell lysis was not taking place under these conditions. Hence, buffer 1 was discarded. Remarkably, although immunoblot analysis was performed using previously reported conditions (12% and 10% SDS PAGE), no separation between both GFP-LC3-I and GFP-LC3-II forms could be observed (**Figure 72**).

Protein affinity isolation relies on the specific immobilized of the protein on a solid support. After washing away non-bound component, the captured protein can be released and recovered (i.e. eluted) using buffer conditions that disrupt de affinity interaction. The ideal elution system should release the antigen without irreversibly denaturing or inactivating it. However, all elution buffers cause some loss of protein function. The most widely used elution buffer is 0.2 M glycine pH 2.5-3.0, as it is able to dissociate the antigen-antibody interaction without permanently affecting protein structure. To avoid permanent damages, eluted fractions should be immediately neutralized by addition of alkaline buffer. Hence, 2 M Tris pH 8 was chosen as a neutralizing buffer. A sample of the eluted fraction was collected for immunoblotting. Unfortunately, GFP-LC3B could not be detected initially in the Western Blot (**Figure 72A**), probably due to sample dilution (total volume 300 µl). Therefore, the eluted samples were concentrated using Amicon® centrifugal filters. Additional stronger denaturing elution was carried out using 0.2% SDS and 0.1% Tween 20 in order to confirm the absence of GFP-LC3B in the resin after the first elution with 0.2 M glycine. As observed in **Figure 72B**, GFP-LC3B was detected in the eluted concentrated fraction and almost no protein remained in the resin afterwards fraction.

The equilibrated eluted fractions were then treated with 25 µg of N-(His)<sub>6</sub>-3C-Atg4B at 37 °C during 2 h in a total volume of 305 µl. PEs were extracted after protein precipitation with cold acetone and the organic fraction was directly analysed. PEs species detected are depicted in **Figure 73**.



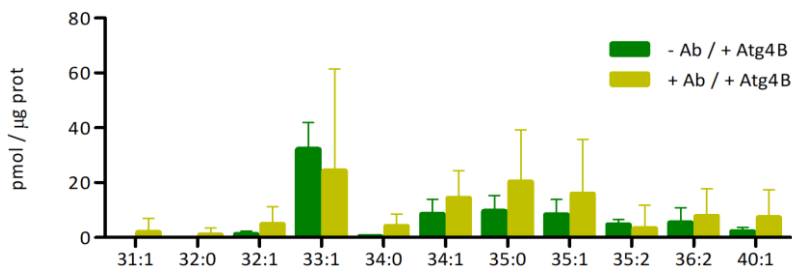
**Figure 72.** Optimization of the GFP-LC3B immunoprecipitation procedure. Samples from each step were retained for analysed. **A)** Cells were lysed employing buffers 2 and 3 followed by centrifugation. The SN (SN 1) fraction (750  $\mu$ g of protein) was precleared with resin, the resulting supernatant was incubated overnight with beads conjugated to anti-GFP antibody. After this time, proteins were eluted by treatment with 0.2 M glycine pH 2.5. The eluted fraction was immediately equilibrated with 2 M Tris pH8. Protein could not be detected by Western Blot probably due to the sample dilution. **B)** Eluted fraction was concentrated with Amicon® filters. A stronger elution was done to confirm that all protein was eluted in the first elution, samples of each step were collected for immunoblotting. An additional unidentified band was observed in this case.



**Figure 73.** PEs obtained after IP using an anti-GFP antibody and lysis buffer 2 or 3, followed by N-(His)<sub>6</sub>-3C-Atg4B treatment (25  $\mu$ g of enzyme) at 37 °C for 2 h. PEs were analysed using a UPLC/TOF-MS. Results are expressed as percentages of total PEs quantified in each sample.

Similar results (Annexes) were obtained when IP was carried out in HEK293 cells stably transfected through lipofection (pOPIN-GFP-LC3B) and viral production (pBABEpuro-GFP-LC3B) by Dr Oscar Meca and with MCF7 cells overexpressing GFP-LC3B (a kind gift of Dr. Yaowen Wu, MPI Dortmund). Remarkably, the profiling of PEs

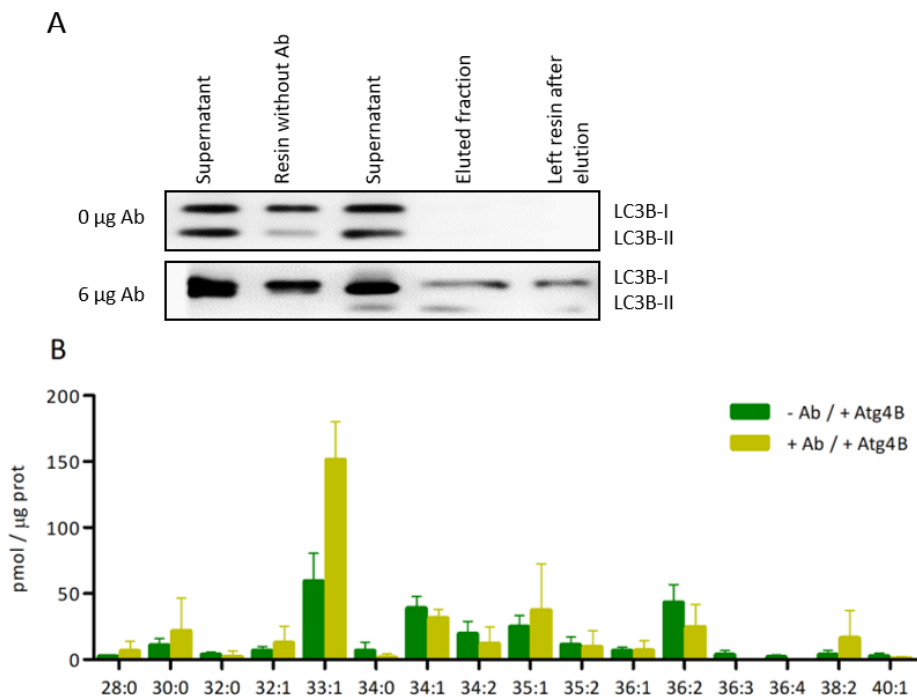
species detected in the negative control (non-modified resin treated with enzyme) was quite similar to the one obtained with beads conjugated to anti-GFP antibody (Figure 74). These results suggested some non-specific binding of proteins to the agarose.



**Figure 74.** PEs from MCF7 cells overexpressing GFP-LC3B. PEs were obtained after IP using anti-GFP antibody followed by N-(His)<sub>6</sub>-3C-Atg4B treatment and lipid extraction with cold acetone (light green). Negative controls are samples obtained from non-modified beads treated by N-(His)<sub>6</sub>-3C-Atg4B (dark green). Numbers shown represent the mean of at least three experiments ± SEM.

Non-specific binding of proteins to beads may be an issue in IP experiments. Since too much antibody can lead to non-specific binding, lower concentration of anti-GFP antibody were explored, however with similar results (see Materials and Methods). Next, as overexpressed proteins show a tendency to non-specifically bind to beads, IP of native LC3 was explored. To this end, HeLa cells were lysed in buffer 3 (50 mM Tris, pH 8, 150 mM NaCl, 1% NP-40, 0.25% sodium deoxycholate and 1 mM PMSF) and 750 µg of protein were precleared with non-modified resin. Again, samples from each step were retained for immunoblot analysis. The resulting SN was then added to the beads treated with 6 µg of LC3B antibody and incubated overnight at 4 °C. The elution and equilibration steps were again done with 0.2 M glycine pH 2.5 and 2 M Tris pH 8 respectively. Finally, purified LC3B was treated by N-(His)<sub>6</sub>-3C-Atg4B for 2 h at 37 °C and PEs were extracted by protein precipitation with cold acetone. As observed in Figure 75A, although the elution employing 0.2 M glycine pH 2.5 could not totally detach the immobilized LC3B, the protein was also detected in the equilibrated eluted fractions, which confirmed the isolation of endogenous LC3B from HeLa (a dilution effect is responsible for the decreased amount of proteins observed in the eluted fraction of Figure 75A). Disappointingly, lipidomic analysis of PEs species observed in samples derived from modified and non-modified resin were again quite similar (Figure 75B).





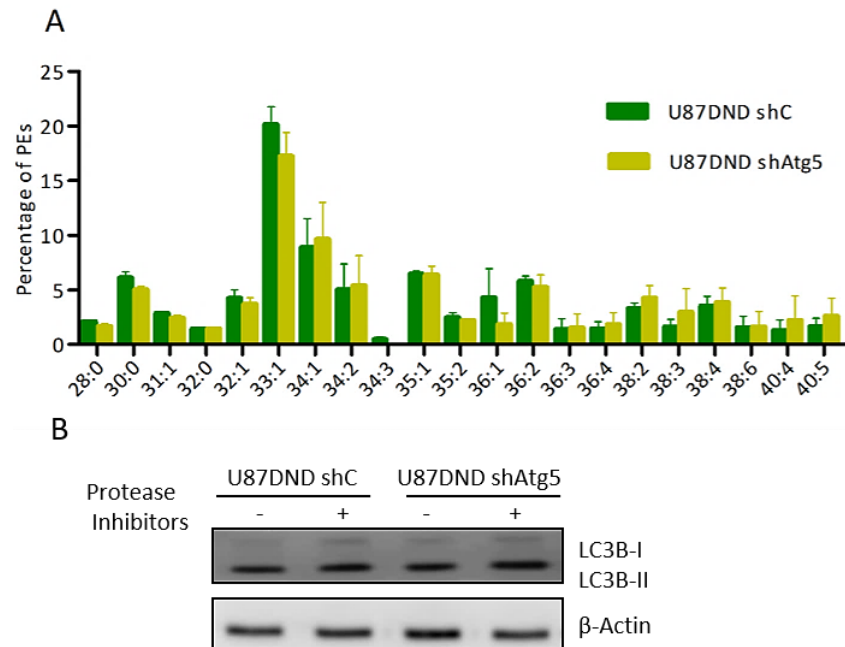
**Figure 75.** Cells were lysed employing buffer 3, 750 µg of protein were precleared with non-modified beads, the supernatant was added to resin treated with 6 µg of anti-LC3B antibody and, after incubation, it was eluted with a solution of 0.2 M glycine pH 2.5. The eluted fraction was immediately equilibrated with 2 M Tris pH8 and treated with 25 µg of N-(His)<sub>6</sub>-3C-Atg4B for 2 h at 37 °C. PEs were finally extracted by precipitation of the proteins with cold acetone, dried and resuspended in methanol for UPLC/TOF-MS analysis. A) Immunoblot analysis of IP protocol using anti-LC3B antibody. B) Released PEs were analysed by UPLC/TOF-MS. Non-modified resin treated with Atg4B served as negative control. Numbers shown represent the mean of at least three experiments ± SEM.

## 11.2. Alternative validation of immunoprecipitation method through KO cells

The results obtained in the affinity purification studies suggested a non-specific binding of proteins to the resin or some unresolved problem that deserved an in-depth characterization. With this aim, we decided to apply the general protocol developed to cells lacking LC3-II. Hence, the appearance of PEs species in such cells would be a hint of an unresolved problem in the designed experimental protocol.

Atg5 is an E3 ubiquitin ligase essential for autophagy and necessary for LC3-II generation.<sup>387,388</sup> Thus, as a first approach, human primary glioblastoma cell line U87DND shAtg5, kindly provided by Research Unit on Bioactive Molecules and

originally generated by Prof. G. Velasco (Universidad Complutense, Madrid), were chosen. These cells present a decreased ability to undergo autophagy and were generated upon stably silencing of Atg5 gene using transduction-ready viral particles containing shRNA target specific constructs.<sup>389</sup> U87DND-shC cells (infected with viral particles containing non-targeted control shRNA constructs) were employed as a control. However, lipid analysis of the PEs bound to the proteome of these cells provided results similar to the ones previously obtained with no substantial differences detectable between the amounts of PEs in shAtg5 cells and control cells (Figure 76A).

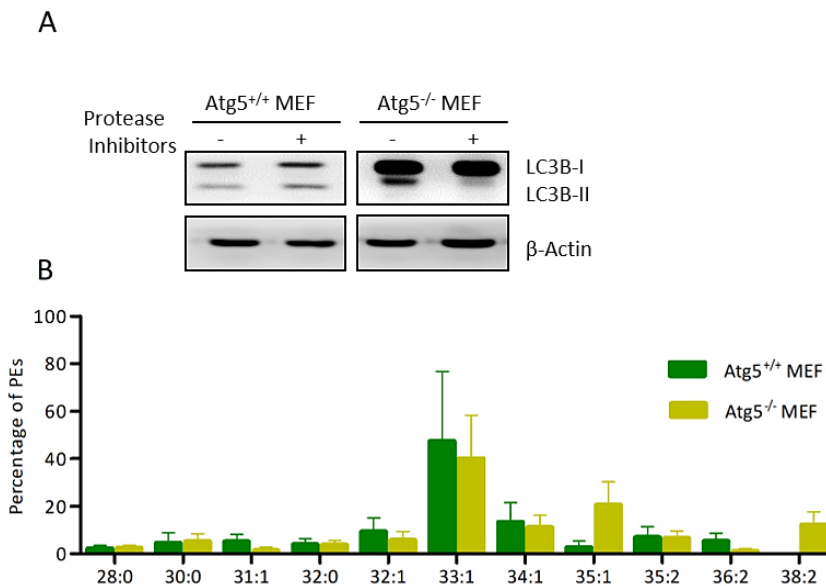


**Figure 76. A)** Quantified PEs detected in U87DND shC and U87DND shAtg5 cells after PEs extraction through N-(His)<sub>6</sub>-3C-Atg4B treatment of the precipitated proteome. Lipid extracts were analysed by UPLC/TOF-MS. Untreated samples were employed as controls. Results are expressed as percentages of total PEs quantified in each sample, but similar amounts (pmols) were detected in both cases. **B)** Western Blot of U87DND shC and shAtg5 cell lysates employing anti LC3B antibody (β-actin was used as loading control).

Although initial studies reported in the literature indicated an inhibition of autophagy, as determined by decreased LC3B-II lipidation and a reduction in Atg5 mRNA levels determined by real-time quantitative PCR, in our hands both cell types presented similar levels of LC3B-II (Figure 76B). Loss of silencing in stable transfected cells can occur after some passages due to the higher viability of non-transfected cells, thus they could eventually become non-transfected over time. Therefore, the same studies were repeated employing oncogene-transformed embryonic fibroblasts

derived from Atg5<sup>+/+</sup> and Atg5<sup>-/-</sup> (autophagy deficient) mice kindly provided by J.M. Lizcano (Facultat de Medicina, Universitat Autònoma de Barcelona) and originally generated by Dr. Mizushima (Tokyo Medical University, Tokyo, Japan).

Cells were lysed and LC3 lipidation was visualized by immunoblotting. As previously observed for these cells, the amount of LC3-II was greatly reduced or absent in Atg5<sup>-/-</sup> MEFs (**Figure 77A**). Nevertheless, the quantification of PEs extracted after precipitation of the proteome and treatment with N-(His)<sub>6</sub>-3C-Atg4B resulted in similar levels of PEs both in wild type and Atg5<sup>-/-</sup> MEFs (**Figure 77B**), whereas PEs could not be detected in cells not treated with the enzyme.



**Figure 77.** **A)** Western Blot analysis of lysates derived from Atg5<sup>+/+</sup> and Atg5<sup>-/-</sup> MEF cells employing anti-LC3B antibody. β-actin was used as loading control. **B)** Quantified PEs detected in Atg5<sup>+/+</sup> and Atg5<sup>-/-</sup> MEF cells after PEs extraction through N-(His)<sub>6</sub>-3C-Atg4B treatment of the precipitated proteome. Lipid extracts were analysed by UPLC/TOF-MS. Untreated samples were employed as controls. Internal standard was added for the quantification. Results are expressed as percentages of total PEs quantified in each sample.

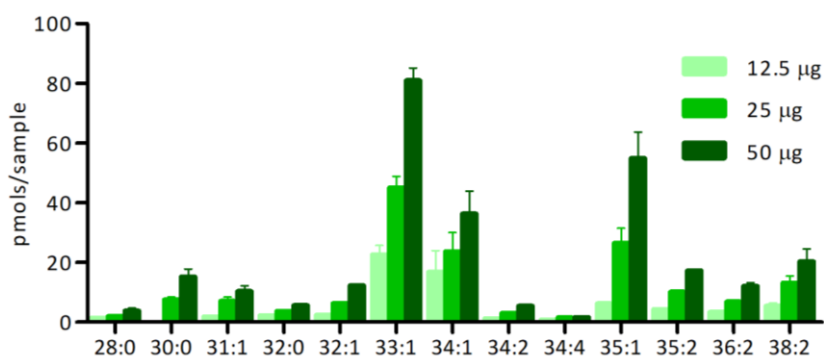
## 12. N-(His)<sub>6</sub>-3C-Atg4B analysis

As explained in Chapter 3 of this thesis and detailed in Materials and Methods, N-(His)<sub>6</sub>-3C-Atg4B production involved several purification steps. Thus, after E. coli lysis, 1% Triton X-100 was added to the lysate in order to solubilize lipids and membranes adhered to the protein of interest and facilitate the solubilization of the protein and thus its column-based purification. Next, N-(His)<sub>6</sub>-3C-Atg4B was purified using metal

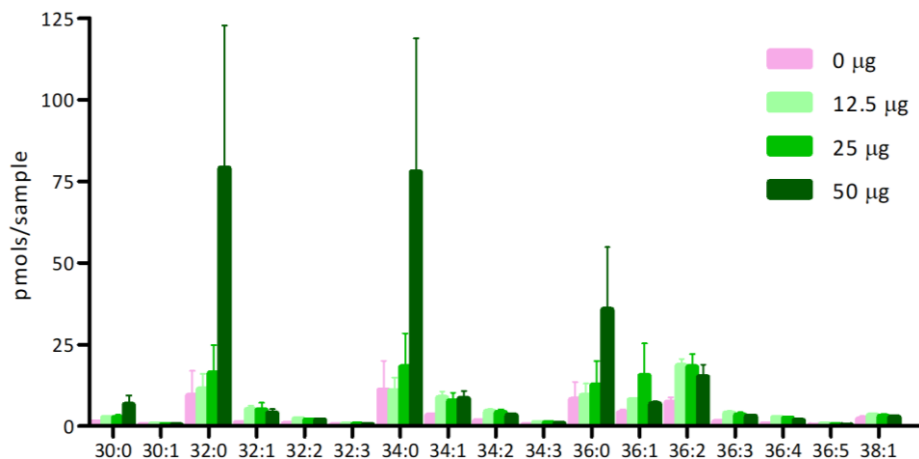
affinity chromatography ( $\text{Ni}^{2+}$ -nitriloacetic acid). In addition, protein was concentrated using Amicon centrifugal filter units with a molecular weight cut-off (MWCO) 10 KDa. Briefly, solutes above the MWCO are retained in the cell, while water and solutes below this molecular weight pass into the filtrate, thereby facilitating concentration and removal of low molecular weight contaminants. Hence, a potential lipid contamination of the protein was not initially considered as an option. However, the previous results obtained with immunoprecipitated proteins as well as with knockout cells suggested that the primary source of the PEs species detected may not be the lipids specifically bound to LC3/GABARAP proteins. As a first hint, the purified N-(His)<sub>6</sub>-3C-Atg4B was investigated to elucidate whether the enzyme could be the source of the PEs detected in all the performed analyses.<sup>390</sup>

Therefore, lipid extractions of the protein alone were next performed by treatment with organic solvents at 48 °C overnight and the resulting released lipids were analysed by UPLC/TOF-MS. Unfortunately, as shown in **Figure 78**, the same PEs previously detected were also visualized here. Moreover, the quantity of PEs detected turned out to be dependent on N-(His)<sub>6</sub>-3C-Atg4B amount, which strongly suggest a lipid contamination of the enzyme. Interestingly, no traces of phosphatidylserine or phosphatidylcholine species could be detected in any sample (not shown).

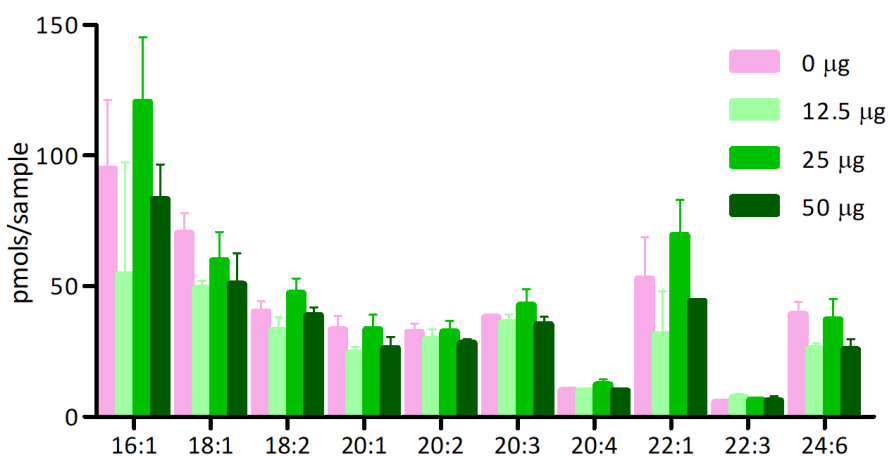
In general, phospholipids and cholesterol are the major hydrophobic constituents of biological mixtures. Thus, to explore whether the observed lipid contamination was caused by the intrinsic activity of the enzyme or was just non-specific, cellular abundant lipids, such as diacylglycerols (DAGs) or cholesterol esters (CEs), were also quantified.



**Figure 78.** PEs obtained from lipid extraction of different quantities of N-(His)<sub>6</sub>-3C-Atg4B (0, 12.5, 25 and 50 µg) with chloroform, methanol and water (5:5:1) after overnight shaking at 48 °C. The extract was dried and resuspended in methanol for MS analysis. Internal standard was added for the quantification. Numbers shown represent the mean of at least three experiments ± SEM (data from 0 µg samples is not shown since any lipid was detected in any of the triplicates).



**Figure 79.** DAGs obtained from lipid extraction of different quantities of N-(His)6-3C-Atg4B (0, 12.5, 25 and 50 µg) with chloroform, methanol and water (5:5:1) incubated overnight at 48 °C. The extract was dried and resuspended in methanol for MS analysis. Results are expressed as percentages of total DAGs quantified in each sample. Numbers shown represent the mean of at least three experiments ± SEM.



**Figure 80.** CEs (cholesterylester esters) obtained from lipid extraction of different quantities of N-(His)6-3C-Atg4B (0, 12.5, 25 and 50 µg) with chloroform, methanol and water (5:5:1) incubated overnight at 48 °C in agitation. The extract was dried and resuspended in methanol for MS analysis. Results are expressed as percentages of total CEs quantified in each sample. Numbers shown represent the mean of at least three experiments ± SEM.

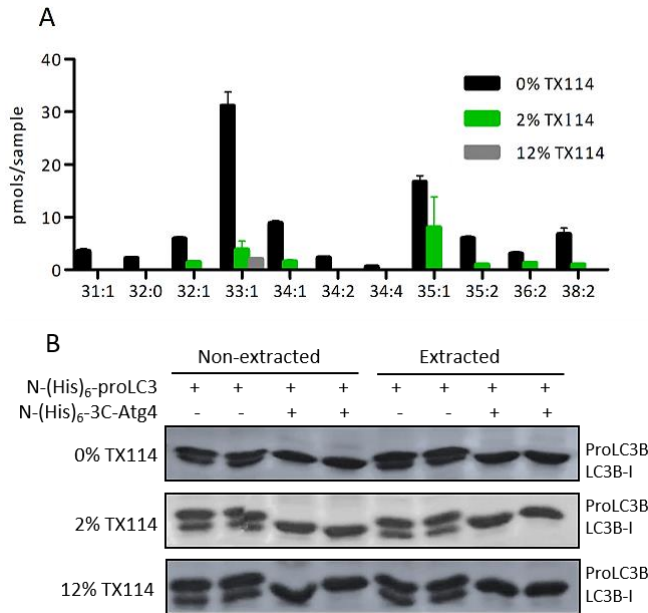
In agreement with the lack of PC detected, one of the most abundant GPLs, low levels of DAGs and CEs were identified, and similar results were obtained in control samples and samples containing different amounts of proteins (except some DAG species that are strongly enriched at the highest protein concentration) (Figure 79 and Figure 80).

Altogether, these results suggest that the low level of DAGs and CEs observed could be an artefact or derived from residual contamination of the column, whereas the dose-dependent amount of PEs seem to be strongly related to the enzymatic activity of Atg4B.

### 13. N-(His)<sub>6</sub>-3C-Atg4B delipidation

A source of lipid contamination can be endogenous lipids generated during *E. coli* growth that bound tightly to expressed proteins. Previous examples have employed different delipidation methods to remove these hydrophobic materials. Thus, common method of delipidation rely on protein precipitation using different organic solvents (cold acetone, acetone/methanol, chloroform/methanol). However, native conformation cannot be ensured and at least partial denaturation should be considered. Adipocyte fatty acid-binding protein was obtained in pure form after removal of bound lipids by mixing with hydrophobically functionalised hydroxypropyl dextran beads (Lipidex 5000).<sup>391</sup> Different concentrations of the non-ionic detergent Triton X-114 have been also employed to delipidate protein samples through a protocol termed cloud-point extraction (CPE).<sup>392,393</sup> Triton X-114 (TX114) is a non-ionic detergent that above the cloud point (22 °C), a temperature near or above the critical micellar concentration at which a detergent separates into detergent and aqueous phases, sequesters hydrophobic and hydrophilic solutes into each corresponding phase, thereby facilitating the separation of proteins from lipid contaminants. Moreover, TX114 tolerates a variety of conditions such as different pH.<sup>393</sup> Hence, the TX114-based extraction was explored to delipidate N-(His)<sub>6</sub>-3C-Atg4B.

To this end, samples were incubated with 12% and 2% of TX114 in 50 mM Tris pH 8, 35 mM NaCl and 5 mM TCEP buffer for 10 min at 37 °C. After centrifugation and detergent phase removal, protein samples followed usual lipid extraction with organic solvents at 48 °C overnight and HRMS-based analysis. As shown in **Figure 81A**, PEs were found in control sample and in 2% TX114 treated sample at lower abundancies and were not detected in the samples extracted with 12% TX114, which suggests that this approach can successfully eliminate de observed lipid contamination. Activity of the delipidated enzyme was additionally checked by incubating proLC3B with N-(His)<sub>6</sub>-proLC3B for 2 h at 37 °C followed by SDS-PAGE and Coomassie staining of the gel. The enzyme showed activity under the usual assay conditions (**Figure 81B**). Thus, delipidated N-(His)<sub>6</sub>-Atg4B still retains activity and can be therefore employed to cleave the lipid residues bound to proteins.



**Figure 81.** **A)** PEs obtained from N-(His)<sub>6</sub>-3C-Atg4B after delipidation with increasing quantities of TX114 (0, 2 and 12%). Lipid extractions were done with chloroform, methanol and water (5:5:1) incubated overnight at 48 °C. The extract was dried and resuspended in methanol for MS analysis. Numbers shown represent the mean of at least three experiments  $\pm$  SEM. **B)** Equal amounts of N-(His)<sub>6</sub>-proLC3B were treated with or without N-(His)<sub>6</sub>-3C-Atg4B for 2h at 37 °C after lipid extraction with 0, 2 or 12% TX114 (controls included non-extracted samples and non-treated samples with N-(His)<sub>6</sub>-3C-Atg4B). The conversion from proLC3B to LC3B-I could be observed by SDS PAGE in all samples containing the enzyme, which confirms the maintaining of its catalytic activity.

## 14. Summary and outlook

Lipid contamination of Atg4B seems to be responsible of the detected PEs species. However, it could be proven that appropriate enzyme delipidation can be performed by washing the protein with Triton X-114, as the amount of the identified lipids is greatly reduced while the protein retains enzymatic activity. Nevertheless, other limitations should be also considered. The similar amounts of PEs species detected in samples treated in presence and absence of N-(His)<sub>6</sub>-3C-Atg4B suggest that no hydrolysis took place in the cell lysates. Several reasons can be given for this situation. If the amount of released PEs is low, experiments could be performed using a higher number of cells. In addition, induction of autophagy combined with lysosomal inhibitors could be considered to increase the overall levels of LC3-II in cells. Alternatively, a recent study has shown that Atg4B is order of magnitude faster at processing a soluble unprimed protein than a lipidated one. As a result, delipidation of membrane bound is intrinsically slow and may require longer reaction times.

Another aspect to have in mind is that substrate proteins denaturated during lipid extraction may not be properly refolded. Hence, as activity of the expressed N-(His)<sub>6</sub>-3C-Atg4B could be confirmed using cell lysates as a source, the lack of activity observed here may be caused by denaturation of LC3/GABARAP.

Similar results were obtained in IP studies, where no significant differences in the amount of PEs could be observed in samples and negative controls. In this case, there was no protein precipitation or lipid extraction potentially causing protein denaturation. One possible explanation here is that the amount of released PEs was low and got unmasked by the contamination. Another possibility would be the degradation of LC3-II during overnight incubation with the beads. However, cells were treated with a protease inhibitor cocktail and lysosomal inhibitors to prevent general protein degradation and degradation by lysosomal enzymes of LC3-II.

The bacterial contamination also helps to understand the high content in OCFA observed in some cases. Hence, even chain fatty acids (carbon chain length of 2-26) represent the majority of the fatty acid plasma concentration in humans. However, low concentrations of OCFA (usually <1%) are also detected in plasma, mainly C15:0, C17:0, C17:1.<sup>394,395,396</sup> The origin of these fatty acids is not clear. It could be endogenously generated and they have also been considered a biomarker of dairy fat intake since they are produced in relatively high levels by rumen microbial fermentation and de-novo lipogenesis. These lipids are mainly present in bacterial membrane (may correspond up to 40% of fatty acids depending on the bacterial species) and are then transferred into the host.<sup>397</sup> Thus, the bacterial origin of the detected PEs would explain the high levels of species containing OCFA. However, as it seems that the detected PEs are not just a non-specific lipid contamination but probably caused by the intrinsic activity of the enzyme, these results would suggest a diverse composition of PEs in bacterial LC3/GABARAP. Additional studies will be required to confirm these data.

As an alternative approach to overcome all the mentioned limitations, one may consider establishing an approach based on enzymatic release of lipids using the RavZ effector protein from *Legionella pneumophila* (**Figure 82**) Ravz is a protease employed by *Legionella* to hijack and block host autophagy. It cleaves the amide bond between the PE-conjugated terminal glycine and the phenylalanine preceding it, thereby rendering LC3/GABARAP resistant to PE re-conjugation.<sup>357</sup>



**Figure 82.** RavZ is an enzyme from *Legionella pneumophila* that cleaves the terminal glycine from phenylalanine, which produces a LC3/GABARAP that cannot be re-conjugated



to PE.

The resulting Gly-PE could be clearly differentiated from membrane phospholipids, allowing the use of cell lysates as a source without the need of lipid extraction and thus avoiding the risk of protein denaturation. However, since current used standards (isotopically labelled GPLs) are structurally different from the products that would be obtained with RavZ, new internal deuterated standards would be required. As isotopically labelled lipids are expensive, one could consider to synthesize a labelled Gly-PE starting from commercially available Gly-*d*5. A second argument in favour of this approach is that RavZ exhibits a nearly specific preference for lipidated substrates and can cleave them rapid and efficiently.<sup>226,398</sup> However, one could argue against this approach that RavZ activity is likely limited to membrane bound proteins and the protein exhibits certain preference for long fatty acid chains. Thus, the catalytic efficiency of RavZ for LC3-PE (16:0) is 12 times higher than that for LC3-PE (6:0), what could have an impact on the planned study.<sup>363</sup>

All in all, the preliminary results included in this chapter suggest that LC3 may be modified with structurally different PEs. All the pitfalls encountered during this project will serve as a strong basis for the development of alternative approaches aimed to characterize the lipid diversity in autophagy related proteins.

# CONCLUSIONS



Several approaches have been explored with the aim of analysing the lipids bound to the autophagy proteins LC3/GABARAP. The following assessments could be concluded from the work included in this chapter:

- Several studies were performed with cell lysates and immunoprecipitated proteins leading in some cases to confusing results. Although LC3 could be successfully isolated, similar lipids content could be observed in samples and negative controls
- A detailed optimization has been carried out leading to the identification of Atg4B as a source of lipid contamination.
- Mainly PE species were detected bound to the expressed Atg4B, whereas no traces of PE and PS were observed. Low levels of DAG and cholesterol esters were identified in both control samples without the enzyme and Atg4B. These results suggest that the observed PE profile may be originated by the intrinsic activity of Atg4B and indicate a heterogenous lipid content of bacterial LC3/GABARAP.
- The enzyme could be delipidated N-(His)<sub>6</sub>-3C-Atg4B by treatment with 12% TX114. The purified protein has shown to be active, thus it can be used in further assays.
- Future studies will explore the use of the delipidated enzyme or the legionella effector RavZ for the release of lipids bound to LC3/GABARAP.



# MATERIALS AND METHODS



## 1. Reagents

Minimum Essential Medium Eagle (MEM), Dulbecco's Modified Eagle Medium (DMEM) High Glucose with L-glutamine and sodium bicarbonate, Earl's balanced salt solution (EBSS), Eagle's minimum essential medium (EMEM), F12 medium, fetal bovine serum (FBS), non-essential amino acids, antibiotics (penicillin/streptomycin), the cell culture flasks of 175 cm<sup>2</sup>, 75 cm<sup>2</sup> and 25 cm<sup>2</sup> (Corning® cell culture flasks, angled neck, cap (plug seal), ethylenediaminetetraacetic acid (EDTA), trypsin in EDTA (1:250) 10x, trichloroacetic acid (TCA), sulforhodamine B (SRB), acetic acid, doxorubicin, bovine serum albumin (BSA), *N*-octanoylsphingoin (C8-Cer), Necrostatin-1, 3-[4,5-dimethylthiazol-2-yl]-2,5-diphenyltetrazolium bromide (MTT), Tween-20®, chloroquine diphosphate, 3-Methyladenine, Pepstatin A, Triton X-100, 2',7'-dichlorofluorescein diacetate, KCl, MgCl<sub>2</sub>, MgSO<sub>4</sub>, KHPO<sub>4</sub>, glucose,  $\alpha$ -lactose-monohydrate, ampicillin for bacteria culture, Triton X-100, dithiothreitol (DTT), Hepes, glycerol, NSC126353, heptadecanoic acid, sodium deoxycholate, NP-40 Tergitol® solution, Triton X-114 (TX114) and Coomassie Brilliant Blue G-250, papain and chymostatin were purchased from Sigma.

Annexin V-FITC Early Apoptosis Detection Kit and CellSimple™ propidium iodide/RNase Staining Kit were obtained from Cell Signalling. Sterile 96-well microplates, PS, F-bottom (167008) were from Nunc and non-sterile non-binding 96-well plates (141804) from Daslab. CellTiter-Glo® Reagent was from Promega.

LANCET™-labelled Eu-W1024 anti-6xHis antibody and ULight-labeled streptavidin (Sav), ½ AreaPlate-96 and AlphaScreen® Histidine Detection Kit (Nickel Chelate) were purchased from Perkin Elmer. Dimethyl Sulfoxide (DMSO) was from Merck, Guava® Mitopotential Kit, Amicon® Ultra-0.5 mL Centrifugal Filters Ultracel MWCO 3K were purchased from Merck Millipore.

Phosphate Buffered Saline (PBS) 10X pH 7.2 was from Gibco. Laemmli buffer and 30% acrylamide/Bis Solution 37.5:1 were from BioRad. Tris-Cl, Polyvinylidene difluoride (PVDF) membranes, protease inhibitors cocktail and DNAase were purchased from Roche.

Tryptone and European Bacteriological Agar were from Pronadisa (Madrid, Spain) and yeast extract from Oxoid. Sodium chloride was from Carlo Erba.

The sterile 96-well microplates, the sterile 96-well opaque microplates and the 6-well plates, SDS were from Fluka. The microBCA protein assay kit, isopropyl- $\beta$ -D-1-thiogalactoside (IPTG) and Pierce® High Sensitivity streptavidin-HRP were obtained from Thermo Scientific.

Enhanced Chemiluminescence (ECL) Prime Western blotting detection reagent, PD-10



desalting columns, EZ-Link™ BMCC-Biotin, EZ-Link™ Maleimide-PEG<sub>2</sub>-Biotin, PlusOne Glycine were purchased from GE Healthcare.

Protease inhibitor cocktail contained 2 µg/mL aprotinin, 5 µg/mL leupeptin, and 1 mM phenylmethylsulphonyl fluoride purchased separately from Enso Life Sciences. Z-VAD-FMK and E-64-D were also from Enzo Life Science. Z-IEDT-FMK and Z-LEHD-FMK were ordered from Alfa Aesar. Cathepsin Inhibitor III was from CalBioChem.

Sodium dodecyl sulfate (SDS) was from Fluka and Recombinant Protein A Sepharose FF Resin from Generon. Oxaliplatin was ordered from Adipogen. Organic solvents and imidazole were from Panreac.

Glass vials were from Waters and inserts with polymer feet for mass spectrometry analysis were purchased from Agilent.

The Antibodies employed include microtubule-associated protein 1-light chain 3 (LC3) II (rabbit) (Abcam (ab48394)); p62 (rabbit) (Bionova (PM045)); β-actin (mouse) (Sigma (A2228)) and GFP (rabbit) (CliniSciences (TP401)). Anti-rabbit and anti-mouse HRP-conjugated secondary antibodies were from GE Healthcare (anti-mouse, reference RPN4201V; anti-rabbit, reference NA934V). HRP-streptavidin was purchased from Thermo Fischer (21130).

Absorbance measurements and TR-FRET measurements were performed in a Spectramax M5, Molecular Devices. AlphaScreen assays were analysed on an Enspire™ Alpha 2390 Multilabel Reader (Perkin Elmer). The flow cytometer employed for cell cycle and death studies was the Guava EasyCyte™ (Merk Millipore, Billerica, MA). LI-COR-C-Digit® blot scanner was employed for Western Blot analysis and quantification. The sonifier probe employed in the preparation and solubilization of cell lysates was the Branson Ultrasonics Sonifier™ SFX150 Cell Disruptor.

Mutations were introduced using the QuikChange II Site-directed Mutagenesis Kit (Agilent) and PCR was conducted in a MJ Mini Personal Thermal Cycler from Bio-Rad. DNA production was carried out by a QIAGEN Plasmid Mini Kit. The expected mutations in the gene sequence were confirmed by DNA sequencing, performed at the Centre de Recerca Agrigenòmica (CRAG) Sequencing Service (Cerdanyola, Spain).

All the columns used for protein purification were purchased from GE Healthcare. N-(His)<sub>6</sub>-LC3B(L123C) was purified with a HisTrap™ Excel 5 mL column and N-(His)<sub>6</sub>-Atg4B with a HisTrap™ HP 5 mL column. The cleaved His6-tag was removed from Atg4B by GSTrap 4B 1 mL column. Size exclusion chromatography purifications were performed using a HiLoad 16/600 Superdex 200 PG. Protein purification was performed with an ÄKTA Purifier (GE Healthcare). If necessary, proteins were

concentrated with Amicon® Ultra-4 Centrifugal Filters MWCO 3 kDa or 10 kDa (Merck Millipore). Protein quantification was performed using a NanoDrop ND-8000 spectrophotometer assuming extinction coefficients of 5960 and 65890, and molecular weights of 15891.31 and 44294.39 Da for N-(His)<sub>6</sub>-LC3B(L123C) and N-(His)<sub>6</sub>-Atg4B, respectively, and employing the Micro BCA™ Protein Assay Kit (Thermo Scientific). Bacteria was lysed by passing them through a CF Cell Disruptor from Constant Systems LTD. The molecular mass of proteins and peptides were calculated using the ExPasy Bioinformatic Portal ([https://web.expasy.org/compute\\_pi/](https://web.expasy.org/compute_pi/)).

## 2. Biological material

### 2.1. Eukaryotic cells

Cells employed in this work, their provenance and their most relevant characteristics are shown in **Table 14** and **Table 14**.

Cell line	Description	Provenance
HGC-27	Human cells from gastric carcinoma, epithelial, adherent.	Kind gift from the Research Unit of Bioactive Molecules (RUBAM) – IQAC/CSIC
Vero	African green monkey cells from kidney, fibroblast-like, epithelial, adherent.	Eucellbank (University of Barcelona, UB)
T98	Human cells from glioblastoma multiforme, fibroblast, adherent.	Kind gift from the Research Unit of Bioactive Molecules (RUBAM) – IQAC/CSIC
U87MG	Human cells from glioblastoma, epithelial, adherent.	Kind gift from the Research Unit of Bioactive Molecules (RUBAM) – IQAC/CSIC
MDCK	Madin-Darby Canine Kidney Epithelial cells, adherent.	Eucellbank (University of Barcelona, UB)
HeLa	Human cells from cervix adenocarcinoma, epithelial, adherent.	Kind gift from Nucleic Acid Chemistry group – IQAC/CSIC
HEK293	Human cells from embryonic kidney, epithelial, adherent.	Kind gift from Nucleic Acid Chemistry group – IQAC/CSIC
HEK293 overexpressing GFP-LC3B	Human cells from embryonic kidney, epithelial, adherent. Stable cell lines expressing GFP-LC3.	Stably transfected by Dr. Oscar Meca

**Table 13.** Cell lines employed in this thesis.

Cell line	Description	Provenance
MCF7 overexpressing GFP-LC3B	Human cells from breast adenocarcinoma, epithelial, adherent. Stable cell line expressing GFP-LC3.	Kind gift of Dr. Yaowen Wu, MPI Dortmund
SH-SY5Y	Human cells from bone marrow neuroblastoma, epithelial, mixed adherent and suspension.	Eucellbank (University of Barcelona, UB)
MEF wild type (WT)/Atg5-Knockout (KO)	Fibroblasts from mouse embryo, adherent, Atg5 Knockout.	Kind gift from Dr. JM Lizcano Protein Kinases in Cancer Research group – Institute of Neurosciences/UAB
U87 DND shAtg5	Human cells from glioblastoma, epithelial, adherent, Atg5 silenced and control cells.	Kind gift from Dr. Guillermo Velasco (Universidad Complutense de Madrid)
U87 DND shC		
HT-29	Human colorectal adenocarcinoma	Eucellbank (University of Barcelona, UB)

**Table 14.** Cell lines employed in this thesis.

## 2.2. Bacterial cells

*E. coli* strains employed in this work, their provenance and their most relevant characteristics are shown in **Table 15**. *E. coli* NovaBlue was used for mutagenesis and DNA purification, while *E. coli* BL21 was employed for protein production.

<i>E. coli</i> strain	Genotype	Provenance
NovaBlue	<i>endA1 hsdR17 (rk<sub>12</sub><sup>-</sup> mk<sub>12</sub><sup>+</sup>) supE44 thi-1 recA1 gyrA96 relA1 lac F'[proA<sup>+</sup>B<sup>+</sup> lac1<sup>q</sup>ZΔM15::Tn10] (Tet<sup>R</sup>)</i>	Merck Millipore
BL21(DE3)	<i>F<sup>-</sup> ompT hsdS<sub>B</sub> (r<sub>B</sub><sup>-</sup>, m<sub>B</sub><sup>-</sup>) gal dcm (DE3)</i>	New England Biolabs

**Table 15.** *E. coli* strands employed in this thesis.

## 2.3. Plasmids

Plasmids employed in this thesis, their provenance and their most relevant characteristics are shown in **Table 16**.

Plasmid	Description	Provenance
pOPIN-N(His) <sub>6</sub> -3C-Atg4B	pOPIN vector, high copy number type with T7 promotor and elements of the repressor lac. His <sub>6</sub> -tag at the <i>N</i> -terminus. Ampicillin resistance. Origin of replication pUC. Termination of transcription by T7 terminator.	Kind gift from Dr. Y-W. Wu (Max Planck Institute, Dortmund)
pOPIN-N(His) <sub>6</sub> -LC3B	pOPIN vector, high copy number type with T7 promotor and elements of the repressor lac. His <sub>6</sub> -tag at the <i>N</i> -terminus. Ampicillin resistance. Origin of replication pUC. Termination of transcription by T7 terminator.	Kind gift from Dr. Y-W. Wu (Max Planck Institute, Dortmund)
pOPIN-N(His) <sub>6</sub> -LC3B(L123C)	pOPIN vector, high copy number type with T7 promotor and elements of the repressor lac. His <sub>6</sub> -tag at the <i>N</i> -terminus. Ampicillin resistance. Origin of replication pUC. Termination of transcription by T7 terminator.	Obtained from pOPIN-N(His) <sub>6</sub> -LC3B by mutagenesis
pOPINn-eGFP-LC3B	pOPIN vector, high copy number type with T7 promotor and elements of the repressor lac. His <sub>6</sub> -tag at the <i>N</i> -terminus. Ampicillin resistance. Origin of replication pUC. Termination of transcription by T7 terminator.	Kind gift from Dr. Y-W. Wu (Max Planck Institute, Dortmund)
pBABEpuro GFP-LC3	pBABE lentiviral vector, high copy type with CMV promoter. GFP conjugated to LC3B ( <i>R. norvegicus</i> ) at the <i>N</i> -terminus. Ampicillin and puromycin resistance. Origin of replication pBR322. Termination of transcription by LTR region.	Addgene

**Table 16.** Plasmids employed in this thesis.

## 2.4. Oligonucleotides

Oligonucleotides employed for point mutation of pOPIN-N(His)<sub>6</sub>-LC3B(L123C) are described in the **Table 17**. All oligonucleotides were purchased from Sigma (purified using standard desalting).

Primer	Sequence
Forward	5'- GACGTTCCGGGATGAAATGCTCAGTGTAAGAATTC-3'
Reverse	5'- CTGAGAATTCTTACACTGAGCATTTTCATCCCGAACG-3'

**Table 17.** Primers employed in this thesis for point mutation.

## 2.5. Culture media

### *Eukaryotic cell culture media*

- *Complete MEM*. Minimum essential medium (MEM) supplemented with 10% fetal bovine serum and 1% non-essential amino acids. Cells lines cultured with this medium were: HGC-27, MCF7, HT-29 and Vero.
- *Complete DMEM*. Dulbecco's modified Eagle's medium (DMEM) supplemented with 10% fetal bovine serum. Cell lines cultured with this medium were: T98, U87DND, HEK293 and the stable transfected lines, HeLa, MDCK and MEF WT/*Atg5*-KO.
- *Complete EMEM*. Eagle's minimum essential medium (EMEM) and F12 medium supplemented with 10% fetal bovine serum. The cell line cultured with this medium was SH-SY5Y.
- *EBSS medium*. Earl's balanced salt solution (EBSS). This medium was employed in starvation treatments to induce autophagy.

All mediums, except EBSS, were supplemented with 100 ng/mL each of penicillin and streptomycin.

### *Bacterial cell media*

- *LB Medium (Lysogeny Bertani)*. Tryptone (10 g/L), yeast extract (5 g/L), NaCl (10 g/l). In case of employing this medium in solid form, bacterial agar (15 g/L) was added to the mixture.
- *TB Medium (Terrific Broth)*.  $\text{KHPO}_4$  (1 M),  $\text{MgSO}_4$  (2 mM), glucose (1 %),  $\alpha$ -lactose-monohydrate (0.01%).

100  $\mu\text{g mL}^{-1}$  of ampicillin was added to all media.

## 3. General procedures for cell culture

The human gastric cancer cell line HGC-27, MCF7 cells overexpressing GFP-LC3, HT-29 and also Vero cells were maintained in a humidified chamber at 37 °C with 5% CO<sub>2</sub> in minimum essential medium supplemented with 10% fetal bovine serum, 1% non-essential amino acids and 100 ng/mL each of penicillin and streptomycin. Glioblastoma cells T98 and U87 MG as well as HEK293, HeLa, MDCK and MEF WT/*Atg5*-KO cells were maintained at 37 °C with 5% CO<sub>2</sub> in Dulbecco's modified Eagle's medium supplemented with 10% fetal bovine serum and 100 ng/mL each of penicillin and streptomycin. Human neuroblastoma cell line SH-SY5Y, was cultured at 37 °C with 5% CO<sub>2</sub> in 1:1 Eagle's minimum essential medium and F12 medium

supplemented with 10% fetal bovine serum and 100 ng/mL each of penicillin and streptomycin. Cells were routinely grown at 80% maximum confluence.

### **3.1. Transfection of plasmid pOPIN-GFP-LC3 and generation of stable HEK293 cell line**

HEK293 cells (ATCC) were seeded in culture dishes (Corning) at a density of  $1.5 \times 10^4$  cells  $\text{cm}^{-2}$  and allowed to attach o/n. Transfection of pOPIN-GFP-LC3B was performed using lipotransfectin as vehicle (Nitorlab) according to manufacturer's instructions. Stability of GFP expression was monitored weekly (5 weeks) by flow cytometry (Gallios instrument, Beckman Coulter) and once the GFP expression was stable (<1% positive cells), positive cells were sorted using a FACSAria Fusion cells sorter (B&D). Analysis of data was done using BD FACSDIVA 8.0.1 software.

### **3.2. Production of retroviral particles and transduction in HEK293 cells**

pBABE-puro was a gift from Hartmut Land & Jay Morgenstern & Bob Weinberg (Addgene plasmid #1764).<sup>399</sup> pBABEpuro-mCherry-eGFP-LC3B and pBABEpuro-GFP-LC3 were a gift from Jayanta Debnath (Addgene plasmid #22418 & 22405, respectively).<sup>400,401</sup> Retroviruses were generated adapting the protocol described by Weinberg's lab (Addgene). Briefly, the retrovirus packaging cell line Phoenix (ATCC) was co-transfected for 12 h with these DNAs and pVSV-G (Clontech) using lipotransfectin as vehicle. Supernatants were collected during the following 48 h and filtered through 0.45  $\mu\text{m}$  cellulose acetate filters (Millipore). HEK293 cells were infected using supernatants (MOI=10) supplemented with 8  $\mu\text{g}/\text{mL}$  hexadimethrine bromide (polybrene, Sigma-Aldrich) at 37 °C o/n. Transduced cells were allowed to recover in fresh medium for 24-48 h and then selected for 7 days in medium supplemented with 1  $\mu\text{g}/\text{mL}$  puromycin (Sigma-Aldrich) or 4 days and then GFP positive cells were sorted using a FACSAria Fusion cells sorter (B&D). Analysis of data was done using BD FACSDIVA 8.0.1 software.

## **4. MALDI-TOF MS analysis**

MALDI-TOF mass spectra were acquired using a MALDI-TOF/TOF 4700 Proteomics Analyzer (Applied Biosystems).

Matrixes employed for the sample preparation were:

- DHB matrix: 2,5-Dihydroxybenzoic acid (20 mg/mL) in ACN/H<sub>2</sub>O with 0.1% TFA (30:70 [v/v])
- SA matrix: Sinapinic acid (10 mg/mL) in ACN/ H<sub>2</sub>O with 0.1% TFA (50:50 [v/v])

## 5. UPLC-TOF MS analysis

The liquid chromatography-mass spectrometer consisted of a Waters Acquity UPLC system connected to a Waters LCT Premier orthogonal accelerated time of flight mass spectrometer (Waters, Millford, MA, USA), operated in negative or positive electrospray ionisation mode and controlled with Waters Micromass MassLynx v.4.1 software. Full scan spectra from 50 to 1500 Da were acquired and individual spectra were summed to produce data points each 0.2 s. Mass accuracy and reproducibility were maintained by using an independent reference spray by the Lock Spray interference.

The analytical columns employed were an Acquity UPLC BEH300 C18 column (particle size 1.7  $\mu\text{m}$ ; 2.1 mm x 100 mm; Waters, Ireland) for peptide detection and an Acquity UPLC BEH C8 (particle size 1.7  $\mu\text{m}$ ; 2.1 mm x 100 mm; Waters, Ireland) for lipid detection.

Data was analysed by Micromass MassLynx v.4.1 software and mass spectra of protein samples were analysed applying the MagTran software 1.03 (Amgen Inc.), which implements de Zscore algorithm.<sup>402</sup>

LC-MS/MS analysis performed at the Universidad del País Vasco. Ultrahigh Pressure Liquid Chromatography was ACQUITY UPLC from Waters coupled to a mass detector quadrupole time-of-flight (Q-ToF, SYNAPT G2 HDMS, Waters). Water, methanol, acetonitrile, 2-propanol and formic acid were Optima® quality purchased at Fisher Scientific. Hydrated leucin acetate enkephalin (95% purity), sodium hydroxide solution (0.1 M) and ammonium acetate (99.99% purity) were from Sigma Aldrich. The analytical column was Acquity UHPLC CSH C18 2.1x 100 mm, 1.7  $\mu\text{m}$  (Waters). Employed softwares were MassLynx V4.1 (Waters) for data acquisition and treatment, and Simlipid software (Premier Biosoft) for the structural identification of lipids. It was operated in negative electrospray ionisation mode. Full scan spectra from 50 to 1200 Da for the quantification and from 50 to 1000 Da for the identification were acquired and individual spectra were summed to produce data points each 0.3 s and 0.1 s, respectively. Mass accuracy and reproducibility were maintained by using an independent reference spray by the Lock Spray interference. The two mobile phases were phase A: Acetonitrile/H<sub>2</sub>O (40:60, v/v) and 10 mM ammonium formate + 0.1% formic acid; phase B: Acetonitrile/Isopropanol (10:90, v/v) and 10 mM ammonium formate+ 0.1% formic acid. The gradient was: 0-2 min from 40 to 43% of B, 2.1 min 54% of B, 12.1 min 70% of B, 18 min 100% of B, 19 min isocratic 100% of B. The flow rate was 0.5 mL/min. The column was held at 65 °C.

#### ***Acquity UPLC BEH300 C18 column***

10  $\mu$ l were injected and eluted at a flow rate of 0.3 mL/min. The mobile phase employed consisted of a 20 mM formic acid solution in acetonitrile (solution A) and a 20 mM formic acid solution in water (solution B). Gradient elution started at 10% solution A, was increased to 100% solution A over 5 min, held for 1.5 min, and then returned to 10% solution A over 1.5 min. The acquisition range of the TOF detector was  $m/z$  50 to 1.500, the capillary voltage was set to 3.0 kV, the desolvation temperature was 350°C, and the desolvation gas flow rate was 600 L/h. Individual chromatographic peaks of the peptides were isolated from full-scan MS spectra by selecting the theoretical exact mass using the Micromass MassLynx software. Positive identification of the species was based on accurate mass measurement with an error <5 ppm.

#### ***Acquity UPLC BEH C8 column***

10  $\mu$ l were injected at 30 °C and eluted at a flow rate of 0.3 mL/min. The 2 mobile phases were 1 mM ammonium formate in methanol (phase A) and 2 mM ammonium formate in H<sub>2</sub>O (phase B), both phases with 0.05 mM formic acid. A linear gradient was programmed – 0.0 min: 80% B; 3 min: 90% B; 6 min: 90% B; 15 min: 99% B; 18 min: 99% B; 20 min: 80% B. The flow rate was 0.3 mL/min. The column was held at 30 °C. The acquisition range of the TOF detector was  $m/z$  50 to 1.500, the capillary voltage was set to 3.0 kV, the desolvation temperature was 350°C, and the desolvation gas flow rate was 600 L/h. The linear dynamic range was determined by injecting standard mixtures. Positive identification of compounds was based on the accurate mass measurement with an error < 5 ppm and its LC retention time, compared to that of a reference compounds ( $\pm$  2%).

## **6. Expression and purification of the proteins**

### **6.1. Atg4B production**

#### ***Expression and purification of N-(His)<sub>6</sub>-3C-Atg4***

The pOPIN-N-(His)<sub>6</sub>-3C-Atg4B plasmid was transformed into *E. coli* BL21 (DE3) cells, transformed cells were selected by plating on nutrient agar containing ampicillin (100  $\mu$ g mL<sup>-1</sup>) and overnight incubation at 37 °C. A single colony was then inoculated into 60 mL of autoinduction media (Terrific Broth (TB) media: 1 M KHPO<sub>4</sub>, 2 mM MgSO<sub>4</sub>, 1 % glucose) containing 100  $\mu$ g mL<sup>-1</sup> of ampicillin, and the culture was grown overnight at 37 °C and 200 rpm. This pre-culture was used to seed 7.5 L of fresh TB medium (containing 100  $\mu$ g mL<sup>-1</sup> of ampicillin and 0.01 %  $\alpha$ -lactose-monohydrate), and the culture was incubated at 37 °C and 190 rpm until the optical density (OD<sub>600</sub>) reached 0.6-0.8, followed by overnight incubation at 30 °C and 190 rpm. The cells were then harvested by centrifugation (6000 rpm, 20 min, 4 °C).



The bacterial pellet was resuspended in lysis buffer (50 mM KHPO<sub>4</sub>, pH 8, 0.3 M NaCl, 20 mM imidazole) containing 1X protease inhibitors cocktail. Cells were lysed by passing them through a CF Cell Disruptor. Triton X-100 (1% final concentration) and DNase (10 µg/mL) were added into the cell lysate and the lysate was centrifuged at 13000, 4 °C for 20 min. The protein was initially purified by Ni-NTA-affinity purification. To this end, the supernatant was filtered through a 0.4 µm paper (Whatman) and loaded onto a HisTrap<sup>TM</sup> HP 5 mL column equilibrated with lysis buffer by Äkta. The column was washed with 100% lysis buffer, and then the protein was eluted with a step gradient of 7-16 % elution buffer (50 mM KHPO<sub>4</sub>, pH 8, 0.3 M NaCl, 0.5 M imidazole) followed by a linear gradient of 16-100 % of elution buffer until absorbance reached baseline. The fractions were analysed by SDS-PAGE and collected. N-(His)<sub>6</sub>-3C-Atg4B was then concentrated to a final volume of 3 mL employing an Amicon® centrifugal filter (Amicon MWCO 10 KDa).

The protein was further purified by size exclusion chromatography using a HiLoad 16/600 Superdex 200 PG column connected to an Äkta and equilibrated with Gel Filtration Buffer (25 mM Hepes pH 7.5, 40 mM NaCl, 1mM DTT). The pooled fractions were quantified (4.1 mg/mL) employing a NanoDrop ND-8000 spectrophotometer in conjunction with the Scope's method<sup>403</sup> and the BCA assay, aliquoted, shock frozen and stored at -80 °C.

#### ***His<sub>6</sub>-tag cleavage and purification of the resulting Atg4B***

To release the N-(His)<sub>6</sub>-3C-Atg4B protein from the affinity tag, the fusion protein was cleaved by overnight incubation at 4 °C with a human rhinovirus 3C protease (HRV 3C) bearing a N-terminal GST (a kind gift of Dr. Roman Bonet). Briefly, 10 mg of protein were treated overnight at 4 °C without shaking with 100 U of HRV 3C (1 U = 1 mg). HRV 3C was then removed using a GSTrap 4B 1 mL column (GE Healthcare) on Äkta. The protein was further purified by size exclusion chromatography using a HiLoad 16/600 Superdex 200 PG column coupled to Äkta and equilibrated with Gel Filtration Buffer (25mM Hepes pH 7.5, 40mM NaCl, 1mM DTT). The pooled fractions were quantified (4.1 mg/mL) by NanoDrop ND-8000 spectrophotometer and the BCA assay. After aliquoting, the protein was shock frozen and stored at -80 °C. Identity and purity of cleaved protein was verified by SDS-PAGE and MALDI/TOF using sinapinic acid as matrix.

## 6.2. N-(His)<sub>6</sub>-proLC3B(L123C)-Biotin production

### *Site-directed mutagenesis*

L123C Mutation was introduced in proLC3B by site-directed mutagenesis using the following primers:

Forward: 5'-GACGTTCCGGGATGAAATGCTCAGTGTAAGAATTC-3'

Reverse: 5'-CTGAGAATTCTTACTACTGAGCATTTTCATCCCGAACG-3'

For individual mutagenesis, PCR was carried out in 50  $\mu$ L reaction mixture containing the following components: 35.5  $\mu$ L ddH<sub>2</sub>O, 5  $\mu$ L plasmid template (25 ng of total plasmid templates per reaction, 5  $\mu$ L reaction buffer 10X (Agilent), 1.25  $\mu$ L dNTP mix provided by the kit, 1.25  $\mu$ L of each mutagenic primer (125 ng of each primer at 10 mM in ddH<sub>2</sub>O per reaction, Sigma Aldrich), and 1  $\mu$ L PfuUltra HF DNA Polymerase (2.5 U/ $\mu$ L; Agilent). PCR conditions were: 30 s at 95 °C to denature the template, followed by 16 cycles of 30 s at 95 °C, 1 min at 55 °C, and 1 min/kb at 68°C. PCR products were treated at 37°C during 1 h with 1  $\mu$ L DpnI (10 U/ $\mu$ L; Agilent) to digest methylated parental DNA, leaving the non-methylated amplified DNA containing the desired mutations. DNA amplification of the plasmid (2  $\mu$ L) was then carried out by transformation in chemically competent *E. coli* NovaBlue (Merck Millipore). 50  $\mu$ L of competent cells were gently added and mixed with 1  $\mu$ L DNA and kept 5 min on ice. Tubes were transferred to a 42 °C water bath and incubated for 30 s, followed by 2 min on ice. Subsequently, 0.5 mL of LB media was added to each tube and, following a 10 min incubation at 37 °C, all the content was transferred onto LB-Ampicillin plates and grown overnight at 37 °C. One colony was grown in LB-Ampicillin media by overnight incubation and shaking at 200 rpm and 37 °C. The plasmid DNA was isolated with a QIAGEN Plasmid Mini Kit and the expected mutation was confirmed by DNA sequencing.

### *Expression and purification of N-(His)<sub>6</sub>-proLC3B(L123C)*

pOPIN-N-(His)<sub>6</sub>-proLC3B was transformed into *E. coli* BL21 (DE3) competent cells (Biolabs) and transformed cells were selected by plating on nutrient agar containing ampicillin (100  $\mu$ g mL<sup>-1</sup>) and overnight incubation at 37 °C. A single colony was then inoculated into 60 mL of LB medium containing ampicillin (100  $\mu$ g mL<sup>-1</sup>) and the culture was grown overnight at 37°C at 200 rpm. This pre-culture was used to seed 3.6 L of fresh LB medium (containing 100  $\mu$ g mL<sup>-1</sup> ampicillin), and the culture was incubated at 37 °C until the optical density at 600 nm (OD<sub>600</sub>) reached 0.6-0.8. After cooling down, protein expression was induced with IPTG, final concentration 1 mM, overnight at 25 °C at 200 rpm. The cells were harvested by centrifugation (6000 rpm, 20 min, 4 °C).

The bacterial pellet was resuspended in breaking buffer (25 mM NaH<sub>2</sub>PO<sub>4</sub>, pH 7.5, 0.5 M NaCl, 1 mM PMSF and 1X protease inhibitors cocktail) and cells were then lysed using a CF Cell Disruptor (Constant Systems Ltd.). Triton X-100 (1% final concentration) and DNase (10 µg/mL) were added into the cell lysate and the lysate was centrifuged at 13,000 rpm, 4 °C for 20 min. The supernatant was filtered through a 0.4 µm filter (Whatman) and loaded onto a HisTrap™ excel 5 mL column coupled to Äkta and equilibrated with buffer A (50 mM NaH<sub>2</sub>PO<sub>4</sub>, pH 7.5, 0.5 M NaCl, 0.02 M imidazole). The column was washed with buffer A, and then the protein was eluted using a 3 mL/min flux with a step gradient of 8% and then 16% of buffer B (50 mM NaH<sub>2</sub>PO<sub>4</sub>, pH 7.5, 0.5 M NaCl, 0.5 M imidazole) of 5 column volumes each one, followed by a linear gradient 16-100% of buffer B until absorbance reached baseline (5 column volumes). The fractions were analysed by SDS-PAGE and collected fractions were then concentrated to 3 mL by size exclusion filtration (Amicon MWCO 3 kDa), the buffer was then exchanged to phosphate-buffered saline (PBS, pH 7.2, 70013 from Gibco®) containing 5 mM DTT.

The protein was further purified by size exclusion chromatography using a HiLoad 16/600 Superdex 200 PG column equilibrated with PBS containing 5 mM DTT at 2 mL/mL flow. The pooled fractions were quantified (23.2 mg/mL) using a NanoDrop spectrophotometer in conjunction with the Scope's method<sup>403</sup> and the bicinchoninic acid assay (BCA), aliquoted, shock frozen and stored at -80 °C.

### ***Biotinylation***

N-(His)<sub>6</sub>-LC3B(L123C) (2.5 mL, 10.5 mg/mL) were mixed with 10 eq of tris(2-carboxyethyl) phosphine (TCEP, Sigma) dissolved in DMSO (stock solution 25 mg/mL) and the resulting mixture was then shaken 1 h at room temperature. TCEP was then removed employing a PD-10 desalting column (GE Healthcare) and the protein was concentrated to a final volume < 2 mL. 10 eq of EZ-Link™ BMCC-Biotin dissolved in DMSO (stock solution 4.2 mg/mL) or 10 eq of EZ-Link™ Maleimide-PEG<sub>2</sub>-Biotin dissolved in ddH<sub>2</sub>O (stock solution 10.52 mg/mL) were then added and the reaction mixture was incubated for 2.5 h at room temperature on a rotary shaker. PBS was added up to a final volume of 2.5 mL and the reaction mixture was desalted employing a PD-10 desalting column. Finally, the total protein amount was quantified using the BCA assay yielding 5 mg of biotinylated protein. Identity and purity of the biotinylated protein was confirmed by MALDI-TOF using sinapinic acid as matrix, SDS-PAGE and Western Blot analysis using a streptavidin-HRP conjugate.

### 6.3. N-(His)<sub>6</sub>-proLC3B(L123C) Biotin as Atg4B substrate monitored by SDS-PAGE

In order to confirm ability of the enzyme to cleave the biotinylated substrate, both purified proteins were mixed (4:1 w/w of N-(His)<sub>6</sub>-proLC3B(L123C) and Atg4B) and incubated for 2 h at 37 °C. After that, samples were diluted in Laemmli Buffer and boiled for 5 min. 1 µg of protein of each sample was loaded onto a 15% polyacrylamide gel separated by electrophoresis at 160 V/1.5 h. The gel was then stained by Coomassie.

### 6.4. Detection of biotinylated protein using HRP-streptavidin

100 ng of N-(His)<sub>6</sub>-LC3(L123C) Biotin were diluted in Laemmli Buffer and boiled for 5 min. Samples were loaded onto a 15% polyacrylamide gel, separated by electrophoresis at 160 V/1 h and transferred onto a PVDF membrane (100 V/1 h). Unspecific binding sites were then blocked with 5% milk in TBST (50 mM Tris HCl pH 7.6, 150 mM NaCl and 0.1 % Tween 20) for 2 h at room temperature. After washing with TBST, membranes were probed with 1:20000 diluted HRP-streptavidin (initial concentration 1 mg/mL) in 3% in TBST for 1 h at room temperature. Excess of HRP-streptavidin was eliminated by washing with TBST and protein detection was carried out by ECL a, densitometry analysis of the bands was assessed using a LI-COR C-DiGit® Blot Scanner.

## 7. MTT assay

### *General Procedure*

To determine cell viability, the colorimetric MTT metabolic activity assay was employed. Cells were seeded at a density of  $0.1 \times 10^6$  cells/mL, 0.1 mL/well (96-well plates) and cultured at 37 °C and 5% CO<sub>2</sub>. Twenty-four hours after seeding cells were exposed to varying concentrations of the investigated compounds and viability was determined after 24 h, 48 h or later. The control culture was prepared by adding culture medium (cell viability control) or DMSO (vehicle control) in the absence of treatment. After treatment, MTT solution (10 µl at 5 mg/mL in PBS) was added to each well and the cells were incubated for another 3 h. The solution was removed from the precipitate and the resultant formazan crystals were dissolved in DMSO (100 µl), the absorbance intensity was then measured using a microplate reader (Molecular Devices, SpectramaxM5) at 570 nm. All experiments were performed in triplicate, and the relative cell viability (%) is expressed as a percentage of cell viability relative to the cells treated with the DMSO (0.1%, vehicle group).

### *Screening of squaramates and squaramides at 100 µM and 20 µM*

Compounds were employed at single concentrations in triplicate (100 µM or 20 µM), the rest of the protocol was followed as detailed in the general procedure. A first

screening was done by treating HGC-27 and HeLa cells at 100  $\mu\text{M}$  for 24 h. The second screening was also carried out on HGC-27 and HeLa cells for 24 h but the compounds were applied at a 20  $\mu\text{M}$  concentration.

### ***IC<sub>50</sub> determination of selected squaramides***

Dose-dependent toxicity was explored by the selected squaramides (**15-18**, **20**, **25**, **33**, **34** and **39**) identified from the initial MTT assay. Cisplatin toxicity was also explored using an MTT assay. In all cases HGC-27 and HeLa cells were employed. Moreover, the activity of compound **34** was also studied in other cell lines (T98, U87, HEK293, MDCK and Vero) during 24 h and after 48 h treatment in HGC-27 cells. All compounds were dissolved and diluted in DMSO (stock concentration of 10 mM). Blank controls were cells treated with the vehicle (DMSO) at 0.1%.

### ***Compounds identified with the AlphaScreen-based assay***

Cell viability was studied for the selected compounds (**54**, **55**, **56** and **57**) identified after AlphaScreen-based HTS. Cell viability was determined using an MTT assay at 24 h in HT-29 and HEK293 overexpressing GFP-LC3B cells. All compounds were dissolved and diluted in DMSO (stock concentration of 10 mM). Controls were cells treated with the vehicle (DMSO) at 0.1%.

### ***Study of the synergic effect of compound 57 with Oxaliplatin***

Cell viability inhibition by oxaliplatin was first investigated using an MTT assay. IC<sub>50</sub> values were obtained after treating HT-29 cells during 24, 48 and 72 h with serially diluted samples of oxaliplatin. Oxaliplatin was dissolved in DMSO (stock solution 50 mM). Blank controls were cells treated with the vehicle (DMSO) at 0.1%. Next, cells were treated with a mix of oxaliplatin (33  $\mu\text{M}$ ) and compound **57** (100  $\mu\text{M}$ ) diluted in DMSO for 24, 48 and 72 h. The controls included cells treated individually by either oxaliplatin at 33  $\mu\text{M}$  or compound **57** at 100  $\mu\text{M}$ .

## **8. Other cell viability assays**

### **8.1. SRB assay**

#### ***General Procedure***

Cells were seeded in 96-well plates at a density of  $1 \times 10^5$  cells/mL (0.1 mL/well), cultured at 37 °C and 5% CO<sub>2</sub>, and then subjected to various treatments for 24, 48 or 72 h. The control culture was prepared by adding DMSO (vehicle control) in the absence of treatment. Once the treatment was finished, cells were fixed with 50  $\mu\text{L}$  of ice-cold trichloroacetic acid (TCA) 50% w/v and 200  $\mu\text{L}$  of ice-cold PBS for 1 h at 4 °C. The solution was then removed, and the plate was washed with Milli-Q water four times. After that, 100  $\mu\text{L}$ /well of SRB solution (0.4% sulforhodamine B w/v in 0.1% acetic acid) was added and the samples were incubated for another 30 min at room

temperature. To remove unbound dye, plates were washed five times with 1% v/v acetic acid. SRB was solubilized by adding 200  $\mu$ L of a 10 mM Tris solution (pH 10.5) to each well and shaking for 5 min on a shaker platform. The absorbance intensity was measured using a microplate reader (Molecular Devices, SpectramaxM5) at 564 nm. All experiments were performed in triplicate, and the relative cell viability (%) is expressed as a percentage of cell viability relative to the cells treated with DMSO (0.1%, vehicle group).

#### ***IC<sub>50</sub> determination of the selected squaramides***

Cell viability was determined for squaramide **34** in HGC-27, MDCK and Vero cells at 24 h using an SRB assay. Compound **34** was dissolved in DMSO (stock solution 10 mM) and control cells were treated with 0.1% DMSO. Cell viability was also determined in HGC-27 cells after doxorubicin treatment for 24 h. Doxorubicin was dissolved in DMSO (stock solution 172 mM) and control cells were treated with 0.1% DMSO.

#### ***IC<sub>50</sub> determination of selected compounds in AlphaScreen-based assay***

Cell viability was studied for the selected compounds (**54**, **55**, **56** and **57**) employing an SRB assay after 24 h treatment. In all cases HT-29 and HEK293 overexpressing GFP-LC3B cells were employed. All compounds were dissolved in DMSO (stock solution 10 mM) and controls cells were treated with 0.1% DMSO.

## **8.2. Luminescent Cell Viability Assay**

Cells were seeded in 96-opaque well plates at a density of  $1 \times 10^5$  cells/mL (0.1 mL/well), cultured at 37 °C and 5% CO<sub>2</sub> for 24 h, and then subjected to **34** treatment for 24 h. The control culture was prepared by adding DMSO (vehicle control) in the absence of treatment. Control wells containing medium without cells were also prepared to obtain a value for the background fluorescence. Once the treatment was finished, the plate and its contents were equilibrated at room temperature for approximately 30 min and 100  $\mu$ L of CellTiter-Glo<sup>®</sup> Reagent were added and mixed by an orbital shaker for 2 min in order to induce cell lysis. The luminescent signal was then stabilized through incubating the plate at room temperature for 10 min. The luminescence was then recorded using a microplate reader (Molecular Devices, SpectramaxM5). All experiments were performed in triplicate, and the relative cell viability (%) is expressed as a percentage of cell viability relative to the cells treated with DMSO (0.1%, vehicle group)

## 9. Cell cycle analysis

Cells were seeded at  $1.5 \times 10^5$  cells/mL into 6-well plates (1 mL/well). Cells were allowed to adhere for 24 h, and then they were treated with vehicle (0.1% ethanol), **34** (5  $\mu$ M) or doxorubicin (500 nM). After exposure for 24 h, cell media were discarded, and cells were washed with 400  $\mu$ l PBS-EDTA 1% BSA and harvested with 400  $\mu$ l trypsin-EDTA 1% BSA (37 °C/2 min). Cells were pulled down by centrifugation at 1.300 rpm/3 min; cell pellet was washed once with 400  $\mu$ l PBS-EDTA 1% BSA and again centrifuged at the same speed/time. Cells were fixed with a -20 °C overnight incubation with a 70% ethanol (9.5 mL) in 1X PBS solution (0.5 mL). Fixed cells were pulled down, washed once with PBS-EDTA 1% BSA and stained at 37 °C for 2 h with propidium iodide solution (0.1 mg/mL in PBS) and RNase, DNase-free (10  $\mu$ g/mL). Stained cells were analysed by using a Guava EasyCyte™ flow cytometer (Merck Millipore, Billerica, MA). Data analysis was performed using the Multicycle AV program (Phoenix Flow Systems, San Diego, CA). Cell cycle assays on cells treated with **34** were carried out by Dr Juan Vicente Alegre whereas assays on cells treated with doxorubicin were done by Mireia Quintana.

## 10. Evaluation of dead cells using Annexin V-FITC/PI and flux cytometry

### *General procedure*

HGC-27 cells were plated in 6-well plates ( $1 \times 10^5$  cells/mL per well) and were treated with compound **34**; 0.1% DMSO was used as a vehicle control. Controls consisted in N-octanoylsphingoine (C8Cer) at 20  $\mu$ M as positive control of late apoptosis induction and the vehicle as negative control. After induction for 24 h, cells were collected (Trypsin and PBS with 5% BSA) and the cells were washed with PBS containing 5% BSA. The percentages of living, apoptotic and necrotic cells were estimated by staining with Annexin-V-FITC and PI (Annexin-V- FITC Apoptosis Detection Kit, Cell signalling). Almost 10.000 events were collected for each sample and analysed by flow cytometry. In brief, cells were incubated with 96  $\mu$ l of binding buffer, 1  $\mu$ l of Annexin V-FITC and 12.5  $\mu$ l of PI solution at room temperature for 10 min in the dark. After a final addition of 150  $\mu$ L of PBS, HGC-27 cells were immediately analysed on a Guava easyCyte™ Single Sample Flow Cytometer. Samples were excited by the light wavelength of 488 nm with barrier filters of 525 nm and 575 nm for FITC fluorescence and PI detection, respectively. Data were analysed by InCyte Software and plotted for Annexin V-FITC and PI in a two-way dot plot. Live, early apoptotic, late apoptotic and necrotic cells are designed as Annexin-/PI-, Annexin +/PI-, and Annexin+/PI+, respectively. Results are shown as a percentage of cells.

### ***Apoptosis assays with squaramide 34***

Cells were treated with compound **34** at 1, 2.5, 5 and 8  $\mu\text{M}$  (stock solutions in DMSO) for 24 h on HGC-27 cells. Doxorubicin effect on the same cells was also evaluated at concentrations of 0.125, 0.25, 0.5, 1 and 2  $\mu\text{M}$  for 24 h. The effect carried out by **34** squaramide over time was also investigated by treatment with a 8  $\mu\text{M}$  solution of the compound in HGC-27 cells during 4, 8 and 24 h. All assays were performed in triplicate as described in the *General Procedure*.

### ***Apoptosis and necroptosis assays with inhibitors***

In order to study the cell death mechanism, some pathways were inhibited before **34** treatment. After the appropriated incubation time, treatment with **34** and analysis by flow cytometry were done in triplicate as described in the *General Procedure*. Inhibitors employed are described in the following **Table 18**:

<b>Inhibitor</b>	<b>Pathway inhibited</b>	<b>Final concentration</b>	<b>Use</b>
Z-VAD-FMK	pancaspase inhibitor, caspase-dependent apoptosis	20 $\mu\text{M}$ in DMSO	1 h before treatment
Z-IETD-FMK	caspase-8 inhibitor, extrinsic caspase-dependent apoptosis	20 $\mu\text{M}$ in DMSO	1 h before treatment
Z-LEHD-FMK	caspase-9 inhibitor, intrinsic caspase-dependent apoptosis	20 $\mu\text{M}$ in DMSO	1 h before treatment
Cathepsin Inhibitor III	cathepsin B, cathepsin-L, cathepsin-S, and papain inhibitor, lysosomal cell death	10 $\mu\text{M}$ in DMSO	1 h before treatment
Necrostatin-1	RIP1 inhibitor, necroptosis	10 $\mu\text{M}$ in DMSO	3 h before treatment

**Table 18.** Inhibitors of specific cell death pathways employed in HGC-27 cells to discern the cell death mechanism followed after treatment with **34**.

## **11. Protein analysis by Western Blot**

### ***General procedure***

The 15% polyacrylamide gel loaded with the proteins was separated by electrophoresis at 140 V/60 min and transferred onto a polyvinylidene fluoride (PVDF) membrane (100 V/1 h). PVDF membranes were then cut to separate LC3B and  $\beta$ -actin bands. Unspecific binding sites were then blocked with 5% milk in TBS with 0.1% Tween 20 (TBST) in case of LC3B and p62 membranes and with 3% BSA in TBST in case



of anti- $\beta$ -actin antibody. Anti-LC3B antibody was diluted 1:1000 in 5% milk in TBST, anti-p62 antibody was diluted 1:1000 in milk in TBST and anti- $\beta$ -actin antibody was diluted 1:2000 in 3% BSA in TBST. Membranes were incubated overnight at 4 °C under gentle agitation. After washing with TBST, membranes were probed with the correspondent secondary antibody for 1 h at 25 °C (LC3B: 1:1000 dilution in 3% BSA in TBST; p62: 1:1000 dilution in 3% BSA in TBST; Actin: 1:10000 dilution in 5% milk in TBST). Antibody excess was eliminated by washing with TBST and protein detection was carried out using ECL and membrane scanning with LI-COR C-DiGit® blot scanner. Band intensities were quantified using the LI-COR Image Studio Lite software. All experiments were performed in triplicate and band intensities are expressed as a relation of the samples to the control protein.

### ***Study of the time dependence effect of 34 in HGC-27 cells***

$1 \times 10^5$  HGC-27 cells were plated in 6-well plates and were allowed to adhere for 24 h. In the samples containing protease inhibitors, cells were treated with 1  $\mu$ L of pepstatin A at a concentration of 1 mg/mL in 9:1 of methanol and acetic acid 1%, and 1  $\mu$ L of E-64-D at a concentration of 10 mg/mL in ethanol. After 2 h incubation, cells were treated with **34** (2  $\mu$ M) or DMSO (0.1%) for 4, 8 and 24 h, collected with trypsin, and then the pellets were washed twice with cold PBS. Cell lysis was performed with 30  $\mu$ L of lysis buffer (50mM Tris-Cl (pH 7.5), 150 mM NaCl, 0.5% Triton X-100, 2  $\mu$ g/mL aprotinin, 5  $\mu$ g/mL leupeptin and 1 mM PMSF) by five cycles of bath sonication (20 s)/rest on ice (20 s). Then samples were kept on ice for 30 min and centrifuged for 3 min at 10,000 rpm. Supernatants were collected, and protein determination was performed using the Micro BCA™ protein assay kit. Supernatants were combined with Laemmli sample buffer and boiled for 5 min. Equal amounts of proteins (20  $\mu$ g) were loaded onto a 15% polyacrylamide gel and the *General Procedure* for protein analysis by Western Blot technique was applied.

### ***Assay to determine the autophagy induced by 34 on HGC-27 cells***

The same procedure described in the previous section was performed in the presence of autophagy inhibitors (inhibitors employed are described in **Table 19**):

Inhibitor	Pathway inhibited	Final concentration	Use
Chloroquine (CQ)	Inhibitor of autophagosome fusion with lysosomes	20 $\mu$ M in ethanol	2 h before treatment
3-methyladenine (3-MA)	PI3K inhibitor	2 mM in DMSO	2 h before treatment

**Table 19.** Autophagy inhibitors employed.

### ***Study of the changes in autophagic flux by 57 on HT-29 cells***

For protein analysis,  $1 \times 10^5$  cells were plated in 6-well plates and were allowed to adhere for 24 h. In the samples containing protease inhibitors, cells were treated with 5  $\mu$ l of pepstatin A at a concentration of 1 mg/mL in 9:1 of methanol and acetic acid 1%, and 5  $\mu$ l of E-64-D at a concentration of 2 mg/mL in ethanol. After 2 h incubation, cells were treated with compound **57** at 100 and 200  $\mu$ M or DMSO (0.1%) for 24 h. In case of autophagy induction, test compounds were diluted in Earle's Balanced Salt Solution (EBSS) and cells were incubated for 3 h with this mixture. Cells were directly lysed in Laemmli sample buffer and boiled for 5 min. Samples were loaded onto a 15% polyacrylamide gel and the *General Procedure* for Western Blot technique was followed.

### ***Analysis of LC3B-II by immunoblotting in U87DND shAtg5 and MEF Atg5-KO and the corresponding control cells***

For protein analysis,  $1 \times 10^5$  cells were plated in 6-well plates and were allowed to adhere for 24 h. In the samples containing protease inhibitors, cells were treated with 1  $\mu$ L of pepstatin A at a concentration of 1 mg/mL in 9:1 of methanol and acetic acid 1%, and 1  $\mu$ L of E-64-D at a concentration of 10 mg/mL in ethanol. After 2 h incubation, cells were collected with trypsin and then the pellets were washed twice with cold PBS. Cell lysis was performed with 30  $\mu$ l of lysis buffer (50mM Tris-Cl (pH 7.5), 150 mM NaCl, 0.5% Triton X-100, 2  $\mu$ g/mL aprotinin, 5  $\mu$ g/mL leupeptin and 1 mM PMSF) by five cycles of bath sonication (20 s)/rest on ice (20 s). Then samples were kept on ice for 30 min and centrifuged for 3 min at 10,000 rpm. Supernatants were collected and protein determination was performed using the Micro BCA™ protein assay kit. Supernatants were combined with Laemmli sample buffer and boiled for 5 min and analysed by Western Blot as described in the *General Procedure* for Western Blot with LC3 and  $\beta$ -actin antibody as primaries antibodies.

## **12. Analysis of mitochondrial membrane potential**

HGC-27 cells were seeded at a density of 100.000 cells/mL (1 mL/well) in 6-well plates, cultured at 37 °C and 5% CO<sub>2</sub>, and allowed to adhere for 24 h. Cells were treated with **34** at various concentrations (1  $\mu$ M, 2  $\mu$ M, 8  $\mu$ M and 16  $\mu$ M in DMSO) or DMSO (0.1%) as negative control (vehicle group). After 24 h incubation, cells were collected (Trypsin with 5% BSA) and washed with PBS containing 5% BSA. Cell pellet was then resuspended in 200  $\mu$ L medium and seeded into a 96-well plate (1 sample / well). 4  $\mu$ L of a previously prepared 50X solution of JC-1 and 7-AAD (7-aminoactinomycin) were added to each well and cells were incubated for 30 min at 37 °C and 5% CO<sub>2</sub>. Finally, cells were collected in Eppendorf tubes and analysed on a Guava easyCyte™ Single Sample Flow Cytometer. Data were analyzed by InCyte Software and plotted for orange (JC-1 aggregates) and green fluorescence (JC-1 monomers).

### 13. ROS detection

Oxidative metabolism was examined in triplicate samples by using 2',7'-dichlorofluorescein diacetate, a non-fluorescent membrane-permeable compound which can be oxidised to 2',7'-dichlorofluorescein in case cell has high levels of reactive oxygen species. HGC-27 cells were seeded at a density of  $0.1 \times 10^6$  cells/mL, 0.1 mL/well (96-well plates), cultured at 37 °C and 5% CO<sub>2</sub> and allowed to adhere for 24 h. 2',7'-dichlorofluorescein diacetate (25 μM) in DMSO was then added and incubated for 1 h. Compound **34** was then added at various concentrations (24 to 1.40 μM). DMSO and H<sub>2</sub>O<sub>2</sub> were added too as a negative and positive control, respectively. After 5 h incubation, fluorescence was measured using a microplate reader (SpectramaxM5, Molecular Devices) at an excitation wavelength of 485 nm and emission wavelength of 538 nm.

### 14. TR-FRET measurements

**Assay 1.** A titration of biotinylated N-(His)<sub>6</sub>-proLC3B(L123C) was done (100-0 nM) in buffer consisting of 50 mM Tris-Cl pH 8, 35 mM NaCl and 5 mM TCEP. Next, 10 μl, 5 μl of 2 or 5 nM Eu-Ab and 5 μl of *ULight-Sav* at a 1:4 ratio compared to the protein were added diluted in buffer. The mixture was then incubated for 1 h at room temperature in the dark. After that, fluorescence was measured at  $\lambda_{\text{ex}}$  of 340 nm and  $\lambda_{\text{em}}$  of 665 nm with a time delay of 100 μs. As a control, a non-biotinylated N-(His)<sub>6</sub>-proLC3B(L123C) protein as included at the same concentration. All samples were measured in triplicate.

**Assay 2.** Biotinylated and non-biotinylated N-(His)<sub>6</sub>-proLC3B(L123C) were mixed at different ratios (0-10-40-100% biotinylated protein) to a final concentration of 100 nM in a buffer consisting of 50 mM Tris-Cl pH 8, 35 mM NaCl, 0.1% Triton X-100 and 5 mM TCEP. Next, 10 μl, 5 μl of 2 or 5 nM Eu-Ab and 5 μl of *ULight-Sav* at a 1:4 ratio compared to the protein were added in the same buffer. The mixture was then incubated for 1 h at room temperature in the dark. After that, the fluorescence was measured at  $\lambda_{\text{ex}}$  of 340 nm and  $\lambda_{\text{em}}$  of 665 nm with a time delay of 100 μs. As a control, a non-biotinylated N-(His)<sub>6</sub>-proLC3B(L123C) at 100 nM (0% biotinylation) was included in the assay. All samples were measured in triplicate.

## 15. AlphaScreen assay

### *General Procedure*

Screening based on AlphaScreen technology was conducted in a volume of 70  $\mu\text{L}$ . Atg4B was previously incubated in the assay buffer (Hepes 25 mM, 150 mM NaCl, 0.5% Triton X-100, 0.1% BSA, 1 mM TCEP and 1% glycerol at pH 8) for 1 h at 0 °C and 1 additional hour at room temperature in the presence of 1  $\mu\text{L}$  of the compounds dissolved in DMSO to a final concentration of 200  $\mu\text{M}$ . For the screen, a mixture of N-(His)<sub>6</sub>-LC3B(L123C) Biotin (10  $\mu\text{M}$ ) and Atg4B (25 nM) in assay buffer, containing either the compounds or vehicle, was added to a 96-well plate. The resulting mixture was incubated for 30 min. An aliquot of the reaction mixture was diluted to a final concentration of 2.5 nM N-(His)<sub>6</sub>-LC3B(L123C) Biotin in a final volume of 40  $\mu\text{L}$ , which were added to ½ AreaPlate 96-well plates. Then, nickel chelate acceptor beads (5  $\mu\text{L}$ ) were added to a final concentration of 20  $\mu\text{g}/\text{mL}$  and the resulting mixture was incubated 1h in the dark at room temperature followed by the addition of streptavidin donor beads (5  $\mu\text{L}$ , final concentration 20  $\mu\text{g}/\text{mL}$ ). The mixture was incubated for 1 h and the plates were read on an EnSpire™ Alpha 2390 Multilabel Reader (Perkin Elmer). AlphaScreen assays were carried out in white, non-binding 96-well plates (141804, Daslab) and measured in ½ AreaPlate 96 (white) from Perkin Elmer in an EnSpire™ Alpha 2390 Multilabel Reader (Perkin Elmer). AlphaScreen® Histidine (Nickel Chelate) Detection 500 assay points Kit, which includes streptavidin coated Donor Beads and Nickel chelate Acceptor Beads, as well as the Biotin-(His)<sub>6</sub> linker peptide employed for the counter screen assay, were purchased from PerkinElmer.

### *Optimization assays*

- ***Buffer optimization and determination of appropriate N-(His)<sub>6</sub>-LC3B(L123C) Biotin concentration***

Titration of the protein (0-100 nM) in a variety of buffers was carried out to determine both the additives of the buffer giving a better AlphaScreen signal and also the N-(His)<sub>6</sub>-LC3B(L123C) Biotin concentration before hook effect. N-(His)<sub>6</sub>-LC3B(L123C) Biotin was diluted in the buffers to a final volume of 40  $\mu\text{L}$ , then beads were added as described in the *General Procedure*. All samples were prepared in triplicate. A blank sample without the protein was prepared as control.

Studied buffers are described in the following **Table 20**. Buffer 8 was the selected buffer for further assays.

Buffer	Composition
1	25 mM Hepes pH 7.4
2	25 mM Hepes pH 7.4, 0.5 % Triton X-100
3	25 mM Hepes pH 7.4, 0.1 % BSA
4	25 mM Hepes pH 8, 0.5 % Triton X-100, 0.1 % BSA, 1 mM TCEP
5	50 mM Tris pH 8, 150 mM NaCl, 0.5 % Triton X-100, 0.1 % BSA, 1 mM TCEP
6	25 mM Hepes pH 8, 150 mM NaCl, 0.5 % Triton X-100, 0.1 % BSA, 1 mM TCEP
7	25 mM Hepes pH 8, 150 mM NaCl, 1 % Triton X-100, 0.1 % BSA, 1 mM TCEP
8	25 mM Hepes pH 8, 150 mM NaCl, 0.5 % Triton X-100, 0.1 % BSA, 1 mM TCEP, 1 % Glycerol
9	25 mM Hepes pH 8, 150 mM NaCl, 0.5 % Triton X-100, 0.1 % BSA, 1 mM TCEP, 2 % Glycerol

**Table 20.** Buffers employed in AlphaScreen-based assay optimisation.

- ***Stability evaluation***

Aliquots of N-(His)<sub>6</sub>-LC3B(L123C)Biotin at 8.75 nM each at a final volume of 40 µl were incubated at room temperature for different times (from 0 to 6 h). At each time-point, beads were added to each sample following the *General Procedure* and, after incubations in dark, AlphaScreen signal was determined. All samples were prepared in triplicate. A blank sample without the protein was included as a control.

- ***Competitive assay***

N-(His)<sub>6</sub>-LC3B(L123C)Biotin and the same protein without biotin were mixed at different proportions in order to obtain 1 µM of N-(His)<sub>6</sub>-LC3B(L123C) with different biotinylation degree (0 – 100% biotinylation). Then, 40 µl of each sample were added to ½ AreaPlate96 and the beads were added as stated above. All samples were prepared in triplicate. A blank sample without proteins was included as a control.

- ***Atg4B concentration***

A titration of Atg4B (0 – 100 nM) was employed to treat 8.75 nM of N-(His)<sub>6</sub>-LC3B(L123C) Biotin for 30 min at 37 °C in a final volume of 40 µl. Then the described *General Procedure* was followed in order to determine the required Atg4B concentration. All samples were prepared in triplicate. A sample without proteins and a sample with N-(His)<sub>6</sub>-LC3B(L123C) Biotin alone were included as controls.

- ***Counter screen using a Biotin-(His)<sub>6</sub>-peptide***

Each primary hit compound or Atg4B was incubated with a Biotin-(His)<sub>6</sub>-peptide at a final concentration of 10 nM (stock solution 0.1 µM) diluted in assay buffer for 1 h at room temperature and then 30 min at 37 °C. Donor beads and acceptor beads (final concentration of 20 µg/mL) were then added and incubated for 1 h as described in the *General Procedure*.

- **Comparative assay employing N-(His)<sub>6</sub>-proLC3B(L123C)Biotin biotinylated with either EZ-Link™ BMCC-Biotin or EZ-Link™ Maleimide-PEG<sub>2</sub>-Biotin**

1 μM of the corresponding proLC3B-Biotin was treated with increasing concentrations of Atg4B (0-50 nM) for 30 min at 37 °C in buffer 8. An aliquot was then diluted to 12.5 nM of proLC3B-Biotin and beads were added as described in the *General Procedure*. A blank control without enzyme was added in each sequence in order to normalize AlphaScreen values.

- **Determination of the appropriate concentration of N-(His)<sub>6</sub>-LC3B(L123C) modified with EZ-Link™ Maleimide-PEG<sub>2</sub>-Biotin**

Titration of the protein (0-1000 nM) was carried out in a final volume of 40 μl. Beads were then added and signal was measured as described in the *General Procedure*.

- **Atg4B concentration**

The enzyme (0 -386 nM) was incubated on ice for 1 h and mixed with 1 or 10 μM of N-(His)<sub>6</sub>-LC3B(L123C) Biotin to a final volume of 70 μl in a 96-well plate. After incubation for 30 min at 37 °C, aliquots of the reaction mixtures were diluted to a final concentration of 2.5 nM (N-(His)<sub>6</sub>-LC3B(L123C) Biotin) in a final volume of 40 μL. Then beads were added and the signal was measured as described in the *General Procedure*.

- **DMSO tolerance**

The effect of DMSO on assay signal was determined by incubating the assay reaction (10 μM of N-(His)<sub>6</sub>-LC3B(L123C) Biotin with 25 nM of Atg4B) in different wells at various DMSO concentrations (0 – 10% of DMSO) and read at the same time as described in the *General Procedure*. All samples were added in triplicate. A blank sample without protein and a reaction sample without DMSO were employed as controls.

- **Z-Factor**

Z' factor, an index for assay quality control, and S/B ratios were determined through performing the assay reaction in presence and absence of Atg4B, that served as positive and negative controls. Thirty aliquots of each were prepared as described in the *General Procedure*. Then the Z-factor was calculated employing the following equation:

$$Z' - \text{factor} = 1 - \frac{3\text{SD of pos controls} + 3\text{SD of neg controls}}{|\text{mean of pos controls} - \text{mean of neg controls}|}$$

### ***Screening***

Screening of 250 compounds obtained from the NCI Open Database was followed as detailed in the *General Procedure*. Identification and obtained docking value are shown in **Table 1** from **Annexes**. Percentage of Atg4B activity was calculated from AlphaScreen signals obtained in control samples. N-(His)<sub>6</sub>-LC3B(L123C) Biotin corresponded to 0% of activity and the reaction sample without inhibitors corresponded to 100% of the enzyme activity. Z,L-Phenylchloromethylcetone was included as a positive control of inhibition. All samples were prepared in duplicate.

### ***IC<sub>50</sub> determination***

For dose-response curves, compounds were tested at decreasing concentrations starting from 400  $\mu$ M to 0  $\mu$ M. Inhibitors were all added, as described in the *General Procedure*, dissolved in 2  $\mu$ l of DMSO at the desired concentration. All samples were prepared in triplicate. Percentage of Atg4B activity was calculated from AlphaScreen signals obtained in control samples. N-(His)<sub>6</sub>-LC3B(L123C) Biotin corresponded to 0% of activity control and the reaction sample without inhibitors corresponded to 100% of the enzyme activity. Data analysis for the screen and IC<sub>50</sub> measurements was performed using GraphPad Prism 5.0 Software (GraphPad, Inc. San Diego, CA).

## **16. UPLC/TOF-MS-based assays to measure Atg4B activity**

### ***General Procedure***

The assay was carried out in glass vials in a total volume of 130  $\mu$ l containing a final concentration of 18  $\mu$ M N-(His)<sub>6</sub>-LC3B(L123C) and 10 nM Atg4B. Atg4B was initially treated with assay buffer (25 mM Hepes pH 8, 150 mM NaCl and 1 mM TCEP) on ice for 1 h, and then 60  $\mu$ l were dispensed into the vials. Next, solutions of compounds to be tested as inhibitors were prepared in assay buffer (stock solutions in DMSO), 10  $\mu$ l were added to each vial and the mixture was incubated at room temperature for 1 h. N-(His)<sub>6</sub>-LC3B(L123C) was diluted in assay buffer and 60  $\mu$ l were then added to each vial. A blank sample with untreated N-(His)<sub>6</sub>-LC3B(L123C) was also included. The samples were then incubated at 37 °C during 30 min. 10  $\mu$ l were injected to the UPLC-TOF for MS-based analysis.

Appropriate quantification was performed with an 8-point calibration curve, prepared by serially diluting a fully cleaved sample of 18  $\mu$ M N-(His)<sub>6</sub>-LC3B(L123C) treated with 10 nM Atg4B for 2 h at 37 °C. Individual chromatographic peaks of the peptides were isolated from full-scan MS spectra by selecting the theoretical exact mass using the Micromass MassLynx software. Positive identification of the species was based on accurate mass measurement with an error <5 ppm. The data presented are the results of 3 independent experiments and determinations.

### ***Expected and found peaks***

Cleaved peptide: HR-MS (TOF):  $m/z$ : calcd. for  $C_{22}H_{42}N_6O_7S_2$   $[M+H]^+ = 567.2635$ , found  $[M+H]^+ = 567.2698$  (RT: 1.5)

N-(His)<sub>6</sub>-proLC3B(L123C): HR-MS (TOF):  $m/z$ : calcd. for  $C_{702}H_{1110}N_{200}O_{201}S_6$   $[M+H]^+ = 15761.1445$ , found  $[M+H]^+ = 15760$  (RT: 2.4)

N-(His)<sub>6</sub>-LC3B-I: HR-MS (TOF):  $m/z$ : calcd. for  $C_{680}H_{1070}N_{194}O_{195}S_4$   $[M+H]^+ = 15211.8975$ , found  $[M+H]^+ = 15210$  (RT: 2.4)

Biotinylated cleaved Peptide: HR-MS (TOF):  $m/z$ : calcd. for  $C_{45}H_{77}N_{11}O_{14}S_3$   $[M+H]^+ = 1092.4891$ , found  $[M+H]^+ = 1092.4874$  (RT: 1.77)

N-(His)<sub>6</sub>-proLC3B(L123C) Biotin: HR-MS (TOF):  $m/z$ : calcd. for  $C_{725}H_{1145}N_{205}O_{208}S_7$   $[M+H]^+ = 16286.3701$ , found  $[M+H]^+ = 16286$  (RT: 2.4)

### ***Optimization assays***

- ***N-(His)<sub>6</sub>-LC3B(L123C) concentration***

Titration of the protein (0-63  $\mu$ M) in the assay buffer was done to a final volume of 130  $\mu$ l. A blank sample without N-(His)<sub>6</sub>-proLC3B(L123C) was also included. 10  $\mu$ l were injected to the UPLC/TOF for MS-based analysis as described in the *General Procedure*. Data was analysed using MicroMass MassLynx v4.1 and MagTran software 1.03.

- ***Atg4B concentration***

Varying concentrations of N-(His)<sub>6</sub>-3C-Atg4B (0-100 nM) were titrated to a fixed protein substrate concentration (18  $\mu$ M) and the mixture was incubated at 37 °C during 30 min. Then, serial dilutions were done in the assay buffer and aliquots of 130  $\mu$ l were analysed at UPLC/TOF-MS as described in the *General Procedure*. One sample without proteins and one with the untreated sample were included as controls. The amount of formed peptide was quantified and changes in peak areas were used to calculate the rate of the cleavage by comparison with the calibration curve.

- ***Calibration curve of the non-biotinylated and biotinylated MKCSV peptide***

18  $\mu$ M of N-(His)<sub>6</sub>-proLC3B(L123C) (biotinylated or not) were treated with 100 nM (excess of enzyme) of N-(His)<sub>6</sub>-3C-Atg4B in a final volume of 300  $\mu$ l at 37 °C during 2 h. Then, serial dilutions were done in the assay buffer and aliquots of 10  $\mu$ l were analysed at UPLC/TOF/MS as described in the *General Procedure*. One sample without any protein and one with the untreated sample were included as controls.



### ***IC<sub>50</sub> determination***

For dose-response curves, compounds were tested at decreasing concentrations starting from 500  $\mu$ M to 0  $\mu$ M. Inhibitors were all added, as described in the *General Procedure*, dissolved in 10  $\mu$ l in DMSO at the desired concentration. All samples were prepared in triplicate. Percentage of Atg4B activity was calculated from extrapolated pmols obtained in control samples, N-(His)<sub>6</sub>-proLC3B(L123C) corresponded to 0% of activity control the protein treated with an excess of N-(His)<sub>6</sub>-3C-Atg4B (100 nM) for 2 h at 37 °C without inhibitors corresponded to 100% of the enzyme activity control. Data analysis for the screen and IC<sub>50</sub> measurements was performed using Prism software (GraphPad Software, Inc. San Diego, CA).

## **17. Papain assay**

Papain activity was determined in 96-well plates by modification of the reported procedure.<sup>404</sup> The reaction mixture contained 250  $\mu$ l of 0.1 M phosphate buffer (pH 6.5) with 0.3 M KCl, 0.1 mM EDTA and 3 mM DTT; 30  $\mu$ l of substrate solution (L-pyroglutamyl-L-phenylalanyl-L-leucine-p-nitroanilide; 2.2 mM in DMSO, 0.22 mM final concentration); 20  $\mu$ l of enzyme solution (30  $\mu$ g/mL in reaction buffer); and 3  $\mu$ l of inhibitor solution or vehicle (DMSO). Chymostatin at 10  $\mu$ M was used as positive control of inhibition of papain activity and 50  $\mu$ M of Z,L-PCK was employed as negative control. The reaction was stopped by addition of 20  $\mu$ l of 1 N HCl, and the OD was measured at 410 nm on a microplate reader (SpectramaxM5, Molecular Devices).

## **18. Calibration curves of phosphatidylethanolamine samples**

Phosphatidylethanolamine samples (PEs) were dissolved in methanol at a concentration of 1  $\mu$ M upon sonication. Samples were 10-fold serially diluted. 10  $\mu$ l were injected and analysed using an UPLC/TOF-MS and an *Acquity UPLC BEH C8 column*. Blank controls containing only methanol were added in measurement.

## **19. Determination of the required amount of N-(His)<sub>6</sub>-3C-Atg4B for PE cleavage**

Aliquots of three million cells each were collected and centrifuged, the pellets were then resuspended in PBS and lysed using a sonifier probe through five cycles of sonication (10 s) and ice (10 s). Tubes were then centrifuged for 3 min at 3.000 rpm and pellet was discarded. The proteome was immediately precipitated by adding 1 mL of cold acetone and 30 min incubation on ice. Then, the tubes were centrifuged at 13.000 rpm during 10 min at 4 °C and the supernatant was discarded. Then, the pellet containing the washed proteome was dissolved in 0.5 mL buffer (50 mM Tris pH 8, 35mM NaCl, 5mM TCEP). 25  $\mu$ g to 125  $\mu$ g of N-(His)<sub>6</sub>-3C-Atg4B were added to each sample and the mixture was incubated 2 h at 37 °C. An untreated samples was used

as control. After that, protein was quantified by Micro BCA™ protein assay kit and samples were mixed with 4X Laemmli buffer and boiled at 96 °C for 5 min. Equal amounts of proteins (20 µg) were loaded onto a 15% polyacrylamide gel and the *General Procedure* of protein analysis using western blot was applied to determine the levels of actin, LC3-I and LC3-II.

## 20. Analysis of proteome-bound PEs

Cells were seeded in a 175 cm<sup>2</sup> cell culture flask (20 mL/flask) and were allowed to adhere for 24 h and grow to a confluency of 80 % at 37 °C in 5% CO<sub>2</sub>. Cells were then washed with PBS and treated with 6 mL of Trypsin-EDTA 1X in PBS for 5 min. Next, 10 mL of culture media were added, and cells were counted using a Neubauer chamber. 3 million cells/sample were collected and centrifuged at 3000 rpm for 3 min. After discarding the supernatant, the pellet was washed with 10 mL of PBS and centrifuged again. Samples were then stored at -80 °C until the assay day.

Pellets were then resuspended in PBS and cells were lysed using a sonifier probe through five cycles of sonication (10 s) and ice (10 s). Tubes were then centrifuged for 3 min at 3000 rpm and pellet was discarded. The proteome was immediately precipitated using 1 mL of cold acetone addition followed by 30 min incubation on ice. Then, tubes were centrifuged at 13.000 rpm during 10 min at 4 °C and the supernatant was discarded. Lipid extraction of the samples was carried out by adding 1 mL of a mixture of chloroform and methanol (2:1), vortexing during 1 min, incubation during 10 min at room temperature and centrifugation at 10.000 rpm and room temperature for 2 min. The supernatant was discarded and this procedure was repeated three times. The resulting pellet was then washed two more times with chloroform, methanol and water (1:1:0.3) and one more time with methanol. Then, pellet containing proteome was dissolved in 0.1 mL buffer (50mM Tris pH 8, 35mM NaCl, 5mM TCEP) using the sonifier probe and 25 µg of N-(His)<sub>6</sub>-3C-Atg4B were added to hydrolyse the lipids bounded to LC3/GABARAP and the mixture was incubated for 2 h at 37 °C. Untreated samples were added as negative controls. After that, 250 µl of methanol were added to each sample and the mixture was transferred to a glass vial. 500 µl of chloroform and 10 µl of the internal standards (20 µM, 200 pmol/sample) were then added, and the mixture was sonicated until dispersion. Samples were incubated in a bath at 48 °C overnight and the following day were dried under a N<sub>2</sub> stream and stored at -18 °C.

On the same day of the analysis, pellets were resuspended in 150 µl of methanol and centrifuged at 10.000 rpm during 3 min. 130 µl were then transferred to glass vials for UPLC/TOF-MS analysis.

### ***PEs analysis at Universidad del País Vasco***

Relative quantification of PEs was carried out in a UPLC/ESI/MS and identification of fatty acids composition of the detected species was done in a UHPLC/ESI/MS/MS. Samples were prepared as mentioned in the previous section and reconstituted in 100  $\mu$ l of methanol and 7.5  $\mu$ l were injected in UPLC-Q-TOF.

### ***PE Analysis at IQAC-CSIC***

The procedure for lipid extraction detailed in *PEs analysis extraction from LC3/GABARAP* was followed with HeLa, HEK293, SH-SY5Y, U87DND shC and U87DND shAtg5, MEF WT and MEF *Atg5*-KO cells. The method employed for UPLC/TOF-MS analysis is described in the *Acquity UPLC BEH C8 column* section. Blank controls with only methanol were added in each assay.

## **21. Extraction and analysis of cell lipidome**

Cells were seeded at 175 cm<sup>2</sup> cell culture flask (20 mL/flask) and were allowed to adhere for 24 h and grow to a confluency of 80% at 37 °C in 5% CO<sub>2</sub>. Cells were then washed with PBS and treated with 6 mL of Trypsin-EDTA 1X in PBS for 5 min. Next, 10 mL of culture media were added and cells were counted using a Neubauer chamber. 3 million cells/sample were collected in a tube and were centrifuged at 3.000 rpm for 3 min. After discarding the supernatant, pellet was washed with 10 mL of PBS and recentrifuged. Samples were then stored at -80 °C until the assay day.

Next, 100  $\mu$ l of <sup>18</sup>O<sub>2</sub>H<sub>2</sub>O and 250  $\mu$ l of methanol were added to each sample and the mixture was transferred to a glass vial 500  $\mu$ l of chloroform and 10  $\mu$ l of the internal standards (20  $\mu$ M, 200 pmol/sample) were then added, and the mixture was sonicated until dispersion. Samples were incubated in a bath at 48 °C overnight and the following day were dried under a N<sub>2</sub> stream and stored at -18 °C.

On the same day of the analysis, pellets were resuspended in 500  $\mu$ l of methanol and transferred to Eppendorf tubes where they were dried by under a N<sub>2</sub> stream. Next, samples were resuspended again in 150  $\mu$ l of methanol and centrifuged at 1.0000 rpm during 3 min. 130  $\mu$ l were transferred to UPLC/TOF-MS glass vials for analysis following the method described at *Acquity UPLC BEH C8 column* section. Blank controls with only methanol were added in each assay.

## **22. Extraction and analysis of cell lipidome in HeLa cells treated with heptadecanoic acid**

For the preparation of heptadecanoic acid solution, a 10X solution of heptadecanoic acid (5 mM) was first prepared by dissolving the acid in 40  $\mu$ l of ethanol. 300  $\mu$ l of NaOH 0.1 M were then added and the mixture was heated on termoblock at 60 °C for

10 min. Next, it was sonicated and cell culture media containing 5% of BSA but not FBS were added to the mixture to a final volume of 5 mL. Finally, the solution was filtered in sterile conditions and it was stored at 4 °C. The same procedure was followed without the addition of heptadecanoic acid in order to prepare the blank control, which was composed by the vehicles.

Cells were seeded at a concentration of  $3 \times 10^5$  cells/mL into 6 well plates (1 mL/well) and were allowed to adhere for 24 h. Medium was replaced with fresh medium without FBS containing heptadecanoic acid at 1X (0.5 mM) or just the vehicles in blank control. Cells were then incubated for 16 h at 37 °C in 5% of CO<sub>2</sub>. Next, cells were counted using a Neubauer chamber, collected in Eppendorf of 3 million cells/sample and the lipidome extraction procedure was followed as described in *Extraction of lipidome*.

On the same day of the analysis, pellets were resuspended in 500 µL of methanol and transferred to Eppendorf tubes where they were dried under a N<sub>2</sub> stream. Next, samples were resuspended again in 150 µL of methanol and centrifuged at 10.000 rpm during 3 min. 130 µL were transferred to UPLC/TOF-MS glass vials for analysis following the method described at *Acquity UPLC BEH C8 column* section. Blank controls with only methanol were added in each measurement.

## 23. Immunoprecipitation of PEs released from LC3B-II

### *General Procedure*

Cells were seeded at a concentration of  $5.5 \times 10^5$  cells/mL into 10 cm treated-surface culture dishes (8 mL/well) and were allowed to adhere for 24 h. Cells were treated with protease inhibitors (1 µL of pepstatin A at a concentration of 1 mg/mL in 9:1 of methanol and acetic acid 1%, and 1 µL of E-64-D at a concentration of 10 mg/mL in ethanol). After 2 h incubation, the cells were then washed with cold PBS and collected by a pre-cooled scraper in mild-denaturing lysis buffer (50 mM Tris pH 8, 150 mM NaCl, 1% NP-40, 0.25% sodium deoxycholate, 1 mM PMSF) containing protease inhibitor cocktail (2 µg/mL aprotinin, 5 µg/mL leupeptin, and 1 mM phenylmethylsulphonyl fluoride). The samples were left on ice for 30 min and then centrifuged at 12.000 rpm for 10 min, the pellet was discarded and the total protein content of the supernatant was quantified using the BCA assay. Next, a preclearing was performed. To this end, 30 µL of resin with Protein A were placed in an Eppendorf tube and were centrifuged at 1.500 rpm for 3 min, the supernatant was discarded and the resin was washed three times with lysis buffer. After that, 750 µg of protein was loaded to the resin and incubated at 4 °C for 3 h in rotation. The mixture was then centrifuged at 1500 rpm for 3 min and the supernatant was then transferred to 50 µL of resin previously washed and treated overnight with 2 µL anti-GFP or 6 µL anti-LC3B antibody at 4 °C with end-over-end rotation. Samples in the treated resin were

incubated overnight at 4 °C with end-over-end rotation. After 16 h, the resin was washed with lysis buffer for three times and then eluted three times with elution buffer (0.2 M glycine pH 2.6). 50 µl were added to the resin, incubated at room temperature for 10 min with end-over-end and centrifuged for 3 min at 1.500 rpm, the supernatant was collected and neutralized by adding 1:1 v/v of neutralizing buffer (2 M Tris pH 8).

Samples were then treated with 25 µg of N-(His)<sub>6</sub>-3C-Atg4B for 2 h at 37 °C and internal standards were added. After that, proteins were precipitated by adding 500 µl of cold acetone and the supernatant was dried up under a N<sub>2</sub> stream until the analysis.

Immunoprecipitation was confirmed by Western Blot by employing anti-GFP antibody in case of GFP immunoprecipitation of HEK293 and MCF-7 cells overexpressing GFP-LC3B, or anti-LC3B antibody in case immunoprecipitation of LC3B in HeLa cells.

For the analysis by UPLC/TOF-MS, samples were reconstituted in 45 µl methanol and placed in vials with inserts containing polymer feet. The analysis was conducted following the method previously described. Blank controls containing only methanol were added in each measurement.

### ***Optimization***

**Assay 1.** After collecting and lysing HEK293 cells overexpressing GFP-LC3B in PBS, the proteome was immediately precipitated by 1 mL of cold acetone and 30 min incubation on ice. Then, tubes were centrifuged at 13.000 rpm during 10 min at 4 °C and the supernatant was discarded.

Lipid extraction of the samples was carried out by addition of 1 mL of a mixture of chloroform and methanol (2:1), vortex during 1 min, incubation during 10 min at room temperature and centrifugation at 10000 rpm and room temperature for 2 min, supernatant was discarded. This was repeated three times and pellet was then washed two more time with chloroform, methanol and water (1:1:0.3) and one more time with methanol.

Then pellet, containing the proteome was resuspended in 0.5 mL buffer (50 mM Tris pH 8, 35 mM NaCl, 5mM TCEP) using the sonifier probe and protein amount was quantified by the BCA assay. Protein (750 µg) should have been loaded to the resin modified with the anti-GFP antibody, however, the pellet could not be resuspended.

**Assay 2.** HEK293 cells overexpressing GFP-LC3B were collected and lysed using a cell scrappers and three different buffers: Non-denaturing lysis buffer 1 (50 mM Tris, pH 7.5, 150 mM NaCl, 10% glycerol, 1% NP-40 and 1 mM PMSF), non denaturing lysis buffer 2 (50 mM Tris, pH 8, 150 mM NaCl, 10% glycerol, 0.1% Triton X-100 and 1 mM

PMSF) and mild-denaturing lysis buffer 3 (50 mM Tris, pH 8, 150 mM NaCl, 1% NP-40, 0.25% sodium deoxycholate and 1 mM PMSF). Protein was then quantified using the BCA assay and 750 µg of proteins were loaded to 25 µl of non-modified resin. The procedure followed as in the explained *General Procedure* for immunoprecipitation was carried out employing 3 µl of anti-GFP antibody. GFP-LC3B equilibration of the eluted fraction was initially carried out with the same three lysis buffers. A sample of 15 µl was collected in each step: supernatant and resin after centrifugation of preclearing step, supernatant and resin after centrifugation of the sample loaded in the resin with antibody and the eluted fraction. Then, 5 µl of Laemmli buffer were added to each sample and all the tubes were boiled for 5 min and analysed by Western Blot as described in the *General Procedure* for Western Blot with GFP antibody as primary antibody.

**Assay 3.** The procedure was followed as detailed in **Assay 2**, although equilibration of the eluted fraction of GFP-LC3B from the resin with antibody, was carried out using (x mL) of 2 M Tris pH 8.

**Assay 4.** The same procedure as detailed in **Assay 2**, although the eluted fraction was concentrated using any Amicon® Ultra - 0.5 mL centrifugal filter Ultracel – MWCO 3K. Moreover, after elution, the resin was again washed with buffer 3 containing 0.2% SDS and 0.1% Tween-20. Samples of each step were collected and analysed by Western Blot with anti-GFP antibody: supernatant and resin after centrifugation of preclearing step, supernatant and resin after centrifugation of the sample loaded in the resin with antibody, non-concentrated eluted fraction and concentrated eluted fraction with 0.2 M pH 2.6 glycine, eluted fraction after the second elution and remaining resin.

**Assay 5.** Immunoprecipitation was performed as described in *General Procedure* although the resin was treated with 5 µg of anti-GFP antibody. The amount of PEs obtained were checked by UPLC/TOF-MS analysis. For the analysis by UPLC/TOF-MS, samples were reconstituted in 45 µl methanol and placed in vials with inserts. The analysis was conducted following the method described at *Acquity UPLC BEH C8 column* section. Blank controls with only methanol were added in each assay.

#### ***PEs analysis of HEK293 and MCF7 cells overexpressing GFP-LC3***

The *General Procedure* was followed employing two stably transfected cell lines: HEK293 expressing pOPIN-eGFP-LC3B or pBABE-GFP-LC3B (by Dr. Oscar Meca). Transfection employing the first plasmid was carried out by cationic lipid transfection whereas transfection employing the second plasmid was a virus-mediated transfection. In both cases selection of transfected cells for stable transfection was done by flow cytometry. Control samples employed for the PEs analysis were: resin modified with anti-GFP antibody treated and untreated with N-(His)<sub>6</sub>-3C-Atg4B. The *General Procedure* was also followed for the analysis of MCF7 cells overexpressing

GFP-LC3B. Control samples employed for the analysis were resin with and without anti-GFP antibody untreated and treated with N-(His)<sub>6</sub>-3C-Atg4B. Identification and quantification of the bound PEs was performed following the method described at *Acquity UPLC BEH C8 column* section. Blank controls with only methanol were added.

## 24. Lipid content analysis of N-(His)<sub>6</sub>-3C-Atg4B

N-(His)<sub>6</sub>-3C-Atg4B was prepared at four different protein amounts in triplicate samples (0, 12.5, 25 and 50 µg) in mild denaturing lysis buffer (50 mM Tris, pH 8, 150 mM NaCl, 1% NP-40, 0.25% sodium deoxycholate and 1 mM PMSF). Then, 10 µl of the internal standards (20 µM, 200 pmol/sample), 100 µL of <sup>d<sub>4</sub></sup>H<sub>2</sub>O and 250 µl of methanol were added and the mixture was then transferred to glass vials and 500 µl of chloroform were added. Next, it was incubated at 48 °C in agitation overnight and it was dried under a stream of N<sub>2</sub>. Samples were reconstituted in 100 µl of methanol and analysed by UPLC/TOF-MS as described in the *Acquity UPLC BEH C8 column* section. Blank controls with only methanol were added in each assay.

## 25. Delipidation of N-(His)<sub>6</sub>-3C-Atg4B

For the preparation of 12% Triton X-114 (TX114) assay buffer, 3 mL of TX114 were added to a prepared buffer (50 mM Tris pH8, 35 mM NaCl and 5 mM TCEP) in a 50 mL centrifuge tube. The mixture was vortexed, shaken and placed on ice until it clarified. Then, it was shaken and incubated on ice again until clarification. The mixture was next incubated at 37 °C without agitation for some hours until detergent phase was formed below with a volume approximately of 24 mL. Aqueous phase (above) was discarded and buffer was added to 50 mL. Vortex, shaking and incubation on ice until clarification was repeated 4-6 times. Finally, aqueous phase was discarded and the rest was kept in the dark at 4 °C.

For the preparation of 2% TX114 buffer, 42 mL of buffer without TX114 and 8 mL of buffer containing 12% TX114 were mixed at room temperature. The solution was clarified on ice and stored at 4 °C in the dark.

For the delipidation procedure, 25 µg/sample of N-(His)<sub>6</sub>-3C-Atg4B were prepared, 200 µl of buffer were added to each sample (0% TX114 as control, 2% TX114 buffer and 12% TX114 buffer) and the solutions were vortexed and incubated at 37 °C for 10 min. After that, it was centrifuged at 4.000 rpm for 4 min at 37 °C. Aqueous phase (above) was transferred to another tube and incubated on ice.

Phospholipid extraction of the aqueous phase was followed by the addition of 10 µl of the internal standards (20 µM, 200 pmol/sample), 100 µL of <sup>d<sub>4</sub></sup>H<sub>2</sub>O and 250 µl of methanol, then it was transferred to glass vials and 500 µl of chloroform were added. Next, it was incubated at 48 °C in agitation overnight and it was dried by N<sub>2</sub>. Samples

were reconstituted in 100  $\mu$ l of methanol and analysed by UPLC/TOF/MS as described in the *Acquity UPLC BEH C8 column method*. Blank controls with methanol were added in each assay.

## **26. Activity of delipidated N-(His)<sub>6</sub>-3C-Atg4B**

Activity of the delipidated enzyme was checked by SDS-PAGE. Delipidated protein was quantified by the BCA assay and 23  $\mu$ g (18  $\mu$ l) of N-(His)<sub>6</sub>-3C-Atg4B was used to treat 23  $\mu$ g of N-(His)<sub>6</sub>-proLC3B(L123C) (12  $\mu$ l) at 37 °C for 2 h. Next, 10  $\mu$ l of Laemmli buffer were added to each sample and it was then boiled for 10 min. 10  $\mu$ l/well of each sample were added to SDS-PAGE 15 % polyacrylamide SDS-PAGE. Electrophoresis was performed followed by gel staining with Coomassie.





# REFERENCES



1. Cleeland, C. S. *et al.* Reducing the toxicity of cancer therapy: Recognizing needs, taking action. *Nat. Rev. Clin. Oncol.* **9**, 471–478 (2012).
2. Remesh, A. Toxicities of anticancer drugs and its management. *Int. J. Basic Clin. Pharmacol.* **1**, 2 (2012).
3. Housman, G. *et al.* Drug resistance in cancer: An overview. *Cancers (Basel)*. **6**, 1769–1792 (2014).
4. Rivlin, N., Brosh, R., Oren, M. & Rotter, V. Mutations in the p53 tumor suppressor gene: Important milestones at the various steps of tumorigenesis. *Genes and Cancer* **2**, 466–474 (2011).
5. Chen, F. Q. *et al.* Reversal of paclitaxel resistance in human ovarian cancer cells with redox-responsive micelles consisting of  $\alpha$ -Tocopheryl succinate-based polyphosphoester copolymers. *Acta Pharmacol. Sin.* **38**, 859–873 (2017).
6. Bonanno, L., Favaretto, A. & Rosell, R. Platinum drugs and DNA repair mechanisms in lung cancer. *Anticancer Res.* **34**, 493–501 (2014).
7. Sasaki, K. *et al.* Chloroquine potentiates the anti-cancer effect of 5-fluorouracil on colon cancer cells. *BMC Cancer* **10**, (2010).
8. Cacan, E., Ali, M. W., Boyd, N. H., Hooks, S. B. & Greer, S. F. Inhibition of HDAC1 and DNMT1 modulate RGS10 expression and decrease ovarian cancer chemoresistance. *PLoS One* **9**, e87455 (2014).
9. Bates, R. C. & Mercurio, A. The epithelial-mesenchymal transition (EMT) and colorectal cancer progression. *Cancer Biol. Ther.* **4**, 371–376 (2005).
10. Kroschinsky, F. *et al.* New drugs, new toxicities: Severe side effects of modern targeted and immunotherapy of cancer and their management. *Crit. Care* **21**, 1–11 (2017).
11. Wilson, E. M. Androgen receptor molecular biology and potential targets in prostate cancer. *Ther. Adv. Urol.* **2**, 105–117 (2010).
12. Hodi, F. S. *et al.* Improved Survival with Ipilimumab in Patients with Metastatic Melanoma. *New Engl. J.* **363**, 711–723 (2010).
13. Weiner, G. J. Rituximab: Mechanism of action. *Semin. Hematol.* **47**, 115–123 (2010).
14. Hudis, C. A. Trastuzumab — Mechanism of Action and Use in Clinical Practice. *N. Engl. J. Med.* **357**, 39–51 (2007).
15. Jonker, D. J. *et al.* Cetuximab for the Treatment of Colorectal Cancer. *N. Engl.*

*J. Med.* **357**, 2040–2048 (2007).

16. Rosen, L. S. VEGF-Targeted Therapy: Therapeutic Potential and Recent Advances. *Oncol. Clin. Pharmacol.* **10**, 382–391 (2005).
17. Cascone, T., Gridelli, C. & Ciardiello, F. Combined targeted therapies in non-small cell lung cancer: A winner strategy? *Curr. Opin. Oncol.* **19**, 98–102 (2007).
18. Thomas, S. *et al.* Targeting the Bcl-2 family for cancer therapy. *Expert Opin. Ther. Targets* **17**, 61–75 (2013).
19. Dienstmann, R. & Tabernero, J. BRAF as a target for cancer therapy. *Anticancer. Agents Med. Chem.* **11**, 285–295 (2011).
20. Gustin, J. P., Cosgrove, D. P. & Park, B. H. The PIK3CA Gene as a Mutated Target for Cancer Therapy. *Curr Cancer Drug Targets* **8**, 733–740 (2008).
21. Zoubir, M., Tursz, T., Menard, C., Zitvogel, L. & Chaput, N. Imatinib mesylate (Gleevec): targeted therapy against cancer with immune properties. *Endocr Metab Immune Disord Drug Targets* **10**, 1–7 (2010).
22. Johnson, D. H. *et al.* Targeted therapies in combination with chemotherapy in non-small cell lung cancer. *Clin. Cancer Res.* **12**, 4451–4457 (2006).
23. Flaherty, K. T. Chemotherapy and targeted therapy combinations in advanced melanoma. *Clin. Cancer Res.* **12**, 2366–2371 (2006).
24. Navin, N. *et al.* Inferring tumor progression from genomic heterogeneity. *Genome Res.* **20**, 68–80 (2010).
25. Battle, E. & Clevers, H. Cancer stem cells revisited. *Nat. Med.* **23**, 1124–1134 (2017).
26. Editorial. Stay on target. *Nat. Chem. Biol.* **9**, 193 (2013).
27. Swinney, D. C. & Anthony, J. How were new medicines discovered? *Nat. Rev. Drug Discov.* **10**, 507–519 (2011).
28. Wagner, B. K. The resurgence of phenotypic screening in drug discovery and development. *Expert Opin. Drug Discov.* **11**, 121–125 (2016).
29. Huang, R. *et al.* Mass spectrometry-assisted gel-based proteomics in cancer biomarker discovery: Approaches and application. *Theranostics* **7**, 3559–3572 (2017).
30. Moffat, J. G., Vincent, F., Lee, J. A., Eder, J. & Prunotto, M. Industry Perspective. *Nat. Rev. Drug Discov.* **16**, 531–543 (2017).
31. Janzen, W. P. Screening technologies for small molecule discovery: The state

- of the art. *Chem. Biol.* **21**, 1162–1170 (2014).
32. Eggert, U. S. The why and how of phenotypic small-molecule screens. *Nat. Chem. Biol.* **9**, 206–209 (2013).
  33. Blundell, T. L. & Patel, S. High-throughput X-ray crystallography for drug discovery. *Curr. Opin. Pharmacol.* **4**, 490–496 (2004).
  34. Campos-Olivas, R. NMR Screening and Hit Validation in Fragment Based Drug Discovery. *Curr. Top. Med. Chem.* **11**, 43–67 (2011).
  35. Anderson, A. C. The Process of Structure-Based Drug Design. *Chem. Biol.* **10**, 787–797 (2003).
  36. Brown, D. G. & Boström, J. Where do recent small molecule clinical development candidates come from? *J. Med. Chem.* **61**, 9442–9468 (2018).
  37. Valler MJ & D, G. Diversity screening versus focussed screening in drug discovery. *Drug Discov. Today* **5**, 286–293 (2000).
  38. Santos, R. *et al.* A comprehensive map of molecular drug targets. *Nat. Rev. Drug Discov.* **16**, 19–34 (2016).
  39. Uhlén, M. *et al.* Tissue-based map of the human proteome. *Science* **347**, 1260419 (2015).
  40. Rask-Andersen, M., Almén, M. S. & Schiöth, H. B. Trends in the exploitation of novel drug targets. *Nat. Rev. Drug Discov.* **10**, 579–590 (2011).
  41. Schenone, M., Dančik, V., Wagner, B. K. & Clemons, P. A. Target identification and mechanism of action in chemical biology and drug discovery. *Nat. Chem. Biol.* **9**, 232–240 (2013).
  42. Ito, T. *et al.* Identification of a Primary Target of Thalidomide Teratogenicity. *Science* **327**, 1345–1350 (2010).
  43. Rauniyar, N., McClatchy, D. B. & Yates, J. R. Stable isotope labeling of mammals (SILAM) for in vivo quantitative proteomic analysis. *Methods* **61**, 260–268 (2013).
  44. Macleod, A. K. *et al.* A Targeted in Vivo SILAC Approach for Quantification of Drug Metabolism Enzymes: Regulation by the Constitutive Androstane Receptor. *J. Pharmacol. Exp. Ther.* **13**, 866–874 (2014).
  45. Gygi, S. P. *et al.* Quantitative analysis of complex protein mixtures using isotope-coded affinity tags. *Nat. Biotechnol.* **17**, 994–999 (1999).
  46. Oda, Y. *et al.* Quantitative Chemical Proteomics for Identifying Candidate Drug Targets. *Anal. Chem.* **75**, 2159–2165 (2003).

47. Morrison, E. *et al.* Quantitative analysis of the human T cell palmitome. *Sci. Rep.* **5**, 1–7 (2015).
48. Ross, P. L. *et al.* Multiplexed Protein Quantitation in *Saccharomyces cerevisiae* Using Amine-Reactive Isobaric Tagging Reagents. *Mol. Cell. Proteomics* **3**, 1154–1169 (2004).
49. Wacker, S. A., Houghtaling, Benjamin R., Elemento, O. & Kapoor, T. M. Using transcriptome sequencing to identify mechanisms of drug action and resistance. *Nat. Chem. Biol.* **8**, 235–237 (2012).
50. Paull, K. D. *et al.* Display and analysis of patterns of differential activity of drugs against human tumor cell lines: development of mean graph and COMPARE algorithm. *J. Natl. Cancer Inst.* **81**, 1088–1092 (1989).
51. Lamb, J. *et al.* The connectivity map: Using gene-expression signatures to connect small molecules, genes, and disease. *Science* **313**, 1929–1935 (2006).
52. Nidhi, Glick, M., Davies, J. W. & Jenkins, J. L. Prediction of biological targets for compounds using multiple-category bayesian models trained on chemogenomics databases. *J. Chem. Inf. Model.* **46**, 1124–1133 (2006).
53. Keiser, M. J. *et al.* Relating protein pharmacology by ligand chemistry. *Nat. Biotechnol.* **25**, 197–206 (2007).
54. Storer, R. I., Aciroa, C. & Jones, L. H. Squaramides: physical properties, synthesis and applications. *Chem. Soc. Rev.* **40**, 2330–2346 (2011).
55. Jiang, H., Rcio, M., Paixã, W., Monge, D. & Anker Jørgensen, K. Acyl Phosphonates: Good Hydrogen Bond Acceptors and Ester/Amide Equivalents in Asymmetric Organocatalysis. *J. Am. Chem. Soc.* **132**, 2775–2783 (2012).
56. Zhou, H. B. *et al.* Design, synthesis and structure of new chiral squaric acid monoaminoalcohols and diaminoalcohols and their use as catalysts in asymmetric reduction of ketones and diketones. *Tetrahedron* **57**, 9325–9333 (2001).
57. Malerich, J. P., Hagihara, K. & Rawal, V. H. Chiral squaramide derivatives are excellent hydrogen bond donor catalysts. *J. Am. Chem. Soc.* **130**, 14416–14417 (2008).
58. Soll, R. M. *et al.* 3-hydroxy-3-cyclobutene-1,2-dione: Application of novel carboxylic acid bioisostere to an in-vivo active non-tetrazole angiotensin-II antagonist. *Bioorg. Med. Chem. Lett.* **3**, 757–760 (1993).
59. Shinada, T. *et al.* Efficient synthesis of a novel 4-hydroxy-2,3-dioxocyclobut-1-enyl group containing amino acids. *Org. Lett.* **1**, 1663–1666 (1999).
60. Shinada, T. *et al.* Synthesis and paralytic activities of squaryl amino acid-containing polyamine toxins. *Amino Acids* **24**, 293–301 (2003).

61. Sato, K., Seio, K. & Sekine, M. Squaryl group as a new mimic of phosphate group in modified oligodeoxynucleotides: Synthesis and properties of new oligodeoxynucleotide analogues containing an internucleotidic squaryldiamide linkage. *J. Am. Chem. Soc.* **124**, 12715–12724 (2002).
62. Soukarieh, F. *et al.* Design of nucleotide-mimetic and non-nucleotide inhibitors of the translation initiation factor eIF4E: Synthesis, structural and functional characterisation. *Eur. J. Med. Chem.* **124**, 200–217 (2016).
63. Butera, J. A. *et al.* Design and SAR of Novel Potassium Channel Openers Targeted for Urge Urinary Incontinence. 1. N-Cyanoguanidine Bioisosteres Possessing in Vivo Bladder Selectivity. *J. Med. Chem.* **43**, 1187–1202 (2000).
64. Lee, C. W., Cao, H., Ichiyama, K. & Rana, T. M. Design and synthesis of a novel peptidomimetic inhibitor of HIV-1 Tat-TAR interactions: Squaryldiamide as a new potential bioisostere of unsubstituted guanidine. *Bioorg. Med. Chem. Lett.* **15**, 4243–4246 (2005).
65. Glória, P. M. C. *et al.* Aza vinyl sulfones: Synthesis and evaluation as antiplasmodial agents. *Bioorg. Med. Chem. Lett.* **19**, 7635–7642 (2011).
66. Ribeiro, C. J. A. *et al.* Squaric acid/4-aminoquinoline conjugates: Novel potent antiplasmodial agents. *Eur. J. Med. Chem.* **69**, 365–372 (2013).
67. Olmo, F. *et al.* Synthesis and biological evaluation of N, N'-squaramides with high in vivo efficacy and low toxicity: Toward a low-cost drug against Chagas disease. *J. Med. Chem.* **57**, 987–999 (2014).
68. Villalonga, P. *et al.* Cyclosquaramides as Kinase Inhibitors with Anticancer Activity. *ChemMedChem* **7**, 1472–1480 (2012).
69. Zhang, Q. *et al.* Hit to Lead optimization of a novel class of squarate-containing polo-like kinases inhibitors. *Bioorg. Med. Chem. Lett.* **22**, 7615–7622 (2012).
70. Ramalingam, V., Domaradzki, M. E., Jang, S. & Muthyala, R. S. Carbonyl Groups as Molecular Valves to Regulate Chloride Binding to Squaramides. *Org. Lett.* **10**, 3315–3318 (2008).
71. Busschaert, N. *et al.* Squaramides as potent transmembrane anion transporters. *Angew. Chemie - Int. Ed.* **51**, 4426–4430 (2012).
72. Busschaert, N. *et al.* A synthetic ion transporter that disrupts autophagy and induces apoptosis by perturbing cellular chloride concentrations. *Nat. Chem.* **9**, 667–675 (2017).
73. Wurm, F. R. & Klok, H. A. Be squared: Expanding the horizon of squaric acid-mediated conjugations. *Chem. Soc. Rev.* **42**, 8220–8236 (2013).
74. Owen, R. M. *et al.* Bifunctional ligands that target cells displaying the



- $\alpha\beta 3$ integrin. *ChemBioChem* **8**, 68–82 (2007).
75. Xu, Y., Yamamoto, N., Ruiz, D. I., Kubitz, D. S. & Janda, K. D. Squaric monoamide monoester as a new class of reactive immunization hapten for catalytic antibodies. *Bioorg. Med. Chem. Lett.* **15**, 4304–4307 (2005).
  76. Alegre-Requena, J. V., Marqués-López, E. & Herrera, R. P. One-pot synthesis of unsymmetrical squaramides. *RSC Adv.* **5**, 33450–33462 (2015).
  77. Marqués-Lopez, E., Alegre-Requena, J. V. & Herrera, R. P. One-pot synthesis of squaramides. EP14382260 (2014).
  78. Armstrong, J. & Dass, C. R. Doxorubicin Action on Mitochondria: Relevance to Osteosarcoma Therapy? *Curr. Drug Targets* **19**, 432–438 (2018).
  79. Sitarz, R. *et al.* Gastric cancer : epidemiology , prevention , classification , and treatment. *Cancer Manag. Res.* **10**, 239–248 (2018).
  80. Carcas, L. P. Gastric cancer review. *J. Carcinog.* **13**, (2014).
  81. Cervantes, A., Roda, D., Tarazona, N., Roselló, S. & Pérez-Fidalgo, J. A. Current questions for the treatment of advanced gastric cancer. *Cancer Treat. Rev.* **39**, 60–67 (2013).
  82. Jemal, A. *et al.* Global Cancer Statistics. *A Cancer J. Clin.* **61**, 69–90 (2011).
  83. Maugeri-Saccà, M. *et al.* FOLFIRI as a second-line therapy in patients with docetaxel-pretreated gastric cancer: A historical cohort. *J. Exp. Clin. Cancer Res.* **32**, 1–7 (2013).
  84. Pozarowski, P. & Darzynkiewicz, Z. Analysis of Cell Cycle by Flow Cytometry. in *Methods in Molecular Biology* **281**, 301–311 (1996).
  85. Kepp, O., Galluzzi, L., Lipinski, M., Yuan, J. & Kroemer, G. Cell death assays for drug discovery. *Nat. Rev. Drug Discov.* **10**, 221–237 (2011).
  86. Liu, G. *et al.* Discovery of Potent, Selective, Orally Bioavailable Stearoyl-CoA Desaturase 1 Inhibitors. *J. Med. Chem.* **50**, 3086–3100 (2007).
  87. Mariño, G., Niso-Santano, M., Baehrecke, E. H. & Kroemer, G. Self-consumption: The interplay of autophagy and apoptosis. *Nat. Rev. Mol. Cell Biol.* **15**, 81–94 (2014).
  88. Yu, H. G. *et al.* Phosphoinositide 3-kinase/Akt pathway plays an important role in chemoresistance of gastric cancer cells against etoposide and doxorubicin induced cell death. *Int. J. Cancer* **122**, 433–443 (2008).
  89. Vichai, V. & Kirtikara, K. Sulforhodamine B colorimetric assay for cytotoxicity screening. *Nat. Protoc.* **1**, 1112–1116 (2006).

90. Elmore, S. Apoptosis: A Review of Programmed Cell Death. *Toxicol. Pathol.* **35**, 495–516 (2007).
91. Berger, A. B., Sexton, K. B. & Bogyo, M. Commonly used caspase inhibitors designed based on substrate specificity profiles lack selectivity. *Cell Res.* **16**, 961–963 (2006).
92. Aits, S. & Jaattela, M. Lysosomal cell death at a glance. *J. Cell Sci.* **126**, 1905–1912 (2013).
93. Kirkegaard, T. & Jäättelä, M. Lysosomal involvement in cell death and cancer. *Biochim. Biophys. Acta - Mol. Cell Res.* **1793**, 746–754 (2009).
94. Sawai, H. & Domae, N. Discrimination between primary necrosis and apoptosis by necrostatin-1 in Annexin V-positive/propidium iodide-negative cells. *Biochem. Biophys. Res. Commun.* **411**, 569–573 (2011).
95. Triola, G. Chemical tools for modulating autophagy. *Tetrahedron* **71**, 387–406 (2015).
96. Castino, R., Fiorentino, I., Cagnin, M., Giovia, A. & Isidoro, C. Chelation of lysosomal iron protects dopaminergic SH-SY5Y neuroblastoma cells from hydrogen peroxide toxicity by precluding autophagy and Akt dephosphorylation. *Toxicol. Sci.* **123**, 523–541 (2011).
97. Loos, B., Du Toit, A. & Hofmeyr, J. H. S. Defining and measuring autophagosome flux - Concept and reality. *Autophagy* **10**, 2087–2096 (2014).
98. Elgendy, M., Sheridan, C., Brumatti, G. & Martin, S. J. Oncogenic Ras-Induced Expression of Noxa and Beclin-1 Promotes Autophagic Cell Death and Limits Clonogenic Survival. *Mol. Cell* **42**, 23–35 (2011).
99. Katayama, M., Kawaguchi, T., Berger, M. S. & Pieper, R. O. DNA damaging agent-induced autophagy produces a cytoprotective adenosine triphosphate surge in malignant glioma cells. *Cell Death Differ.* **14**, 548–558 (2007).
100. Kroemer, G. & Levine, B. Autophagic cell death: The story of a misnomer. *Nat. Rev. Mol. Cell Biol.* **9**, 1004–1010 (2008).
101. Ly, J. D., Grubb, D. R. & Lawen, A. The mitochondrial membrane potential ( $\Delta\psi_m$ ) in apoptosis ; an update. *Apoptosis* **8**, 115–128 (2003).
102. Tsujimoto, Y. & Shimizu, S. Role of the mitochondrial membrane permeability transition in cell death. *Apoptosis* **12**, 835–840 (2006).
103. Rock, K. L. *et al.* Inhibitors of the proteasome block the degradation of most cell proteins and the generation of peptides presented on MHC class I molecules. *Cell* **78**, 761–771 (1994).
104. Yang, Z. & Klionsky, D. J. Eaten alive: A history of macroautophagy. *Nat. Cell*

- Biol.* **12**, 814–822 (2010).
105. Boya, P., Reggiori, F. & Codogno, P. Emerging regulation and functions of autophagy. *Nat. Cell Biol.* **15**, 713–720 (2013).
  106. Royal Society of Chemistry. Microautophagy definition. ID: GO:0016237 Available at: <https://www.rsc.org/publishing/journals/prospect/ontology.asp?id=GO:0016237&MSID=COMB00114G>.
  107. Li, W. W., Li, J. & Bao, J. K. Microautophagy: Lesser-known self-eating. *Cell. Mol. Life Sci.* **69**, 1125–1136 (2012).
  108. Bejarano, E. & Cuervo, A. M. Chaperone-Mediated Autophagy. *Proc. Am. Thorac. Soc.* **7**, 29–39 (2010).
  109. Kaushik, S. & Cuervo, A. M. Chaperone-mediated autophagy: A unique way to enter the lysosome world. *Trends Cell Biol.* **22**, 407–417 (2012).
  110. Jin, S. M. & Youle, R. J. PINK1- and Parkin-mediated mitophagy at a glance. *J. Cell Sci.* **125**, 795–799 (2012).
  111. Pickrell, A. M. & Youle, R. J. The roles of PINK1, Parkin, and mitochondrial fidelity in parkinson’s disease. *Neuron* **85**, 257–273 (2015).
  112. Tanida, I. Autophagosome Formation and Molecular Mechanism of Autophagy. *Antioxid. Redox Signal.* **14**, 2201–2214 (2011).
  113. Palikaras, K., Lionaki, E. & Tavernarakis, N. Mechanisms of mitophagy in cellular homeostasis, physiology and pathology. *Nat. Cell Biol.* **20**, 1013–1022 (2018).
  114. Ni, H. M., Williams, J. A. & Ding, W. X. Mitochondrial dynamics and mitochondrial quality control. *Redox Biol.* **4**, 6–13 (2015).
  115. Sentelle, R. D. *et al.* Ceramide targets autophagosomes to mitochondria and induces lethal mitophagy. *Nat. Chem. Biol.* **8**, 831–838 (2012).
  116. Iwata, J. I. *et al.* Excess peroxisomes are degraded by autophagic machinery in mammals. *J. Biol. Chem.* **281**, 4035–4041 (2006).
  117. Till, A., Lakhani, R., Burnett, S. F. & Subramani, S. Pexophagy: The selective degradation of peroxisomes. *Int. J. Cell Biol.* **2012**, (2012).
  118. Ward, C. *et al.* Autophagy, lipophagy and lysosomal lipid storage disorders. *Biochim. Biophys. Acta - Mol. Cell Biol. Lipids* **1861**, 269–284 (2016).
  119. Invivogen. Autophagy mechanism and inhibitors. <https://www.invivogen.com/autophagy-inhibitors>

120. Graef, M., Friedman, J. R., Graham, C., Babu, M. & Nunnari, J. ER exit sites are physical and functional core autophagosome biogenesis components. *Mol. Biol. Cell* **24**, 2918–2931 (2013).
121. Tooze, S. A. & Yoshimori, T. The origin of the autophagosomal membrane. *Nat. Cell Biol.* **12**, 831–835 (2010).
122. Klionsky, D. J. *et al.* A unified nomenclature for yeast autophagy-related genes. *Dev. Cell* **5**, 539–545 (2003).
123. Tsukada, M. & Ohsumi, Y. Isolation and characterization of autophagy-defective mutants of *Saccharomyces cerevisiae*. *FEBS Lett.* **333**, 169–174 (1993).
124. Subramani, S. & Malhotra, V. Non-autophagic roles of autophagy-related proteins. *EMBO Rep.* **14**, 143–151 (2013).
125. Yu, L., Chen, Y. & Tooze, S. A. Autophagy pathway: Cellular and molecular mechanisms. *Autophagy* **14**, 207–215 (2018).
126. Cui, J., Chew, S. J. L., Shi, Y., Gong, Z. & Shen, H. M. CRISPR system for genome engineering: The application for autophagy study. *BMB Rep.* **50**, 247–256 (2017).
127. Cherra, S. J. *et al.* Regulation of the autophagy protein LC3 by phosphorylation. *J. Cell Biol.* **190**, 533–539 (2010).
128. Wesselborg, S. & Stork, B. Autophagy signal transduction by ATG proteins: From hierarchies to networks. *Cell. Mol. Life Sci.* **72**, 4721–4757 (2015).
129. McEwan, D. G. & Dikic, I. The Three Musketeers of Autophagy: Phosphorylation, ubiquitylation and acetylation. *Trends Cell Biol.* **21**, 195–201 (2011).
130. Matsumoto, G., Wada, K., Okuno, M., Kurosawa, M. & Nukina, N. Serine 403 phosphorylation of p62/SQSTM1 regulates selective autophagic clearance of ubiquitinated proteins. *Mol. Cell* **44**, 279–289 (2011).
131. Lee, I. H. & Finkel, T. Regulation of autophagy by the p300 acetyltransferase. *J. Biol. Chem.* **284**, 6322–6328 (2009).
132. Goldstein, G. *et al.* Isolation of a polypeptide that has lymphocyte-differentiating properties and is probably represented universally in living cells. *Proc. Natl. Acad. Sci. U. S. A.* **72**, 11–5 (1975).
133. Pyo, J. O., Nah, J. & Jung, Y. K. Molecules and their functions in autophagy. *Exp. Mol. Med.* **44**, 73–80 (2012).
134. Nakatogawa, H. Two ubiquitin-like conjugation systems that mediate membrane formation during autophagy. *Essays Biochem.* **55**, 39–50 (2013).

135. Weidberg, H. *et al.* LC3 and GATE-16/GABARAP subfamilies are both essential yet act differently in autophagosome biogenesis. *EMBO J.* **29**, 1792–1802 (2010).
136. Pankiv, S. *et al.* FYCO1 is a Rab7 effector that binds to LC3 and PI3P to mediate microtubule plus end - Directed vesicle transport. *J. Cell Biol.* **188**, 253–269 (2010).
137. Levine, B., Mizushima, N. & Virgin, H. W. Autophagy in immunity and inflammation. *Nature* **469**, 323–335 (2011).
138. Nixon, R. A. The role of autophagy in neurodegenerative disease. *Nat. Med.* **19**, 983–997 (2013).
139. White, E. Deconvoluting the context-dependent role for autophagy in cancer. *Nat. Rev. Cancer* **12**, 401–410 (2012).
140. Rubinsztein, D. C., Mariño, G. & Kroemer, G. Autophagy and aging. *Cell* **146**, 682–695 (2011).
141. Qu, X. *et al.* Promotion of tumorigenesis by heterozygous disruption of the beclin 1 autophagy gene. *J. Clin. Invest.* **112**, 1809–1820 (2003).
142. Yue, Z., Jin, S., Yang, C., Levine, A. J. & Heintz, N. Beclin 1, an autophagy gene essential for early embryonic development, is a haploinsufficient tumor suppressor. *Proc. Natl. Acad. Sci.* **100**, 15077–15082 (2003).
143. Liang, X. H. *et al.* Induction of autophagy and inhibition of tumorigenesis by beclin 1. *Nature* **402**, 672–676 (1999).
144. Degenhardt, K. *et al.* Autophagy promotes tumor cell survival and restricts necrosis, inflammation, and tumorigenesis. *Cancer Cell* **10**, 51–64 (2006).
145. Akin, D. *et al.* A novel ATG4B antagonist inhibits autophagy and has a negative impact on osteosarcoma tumors. *Autophagy* **10**, 2021–2035 (2014).
146. Pankiv, S. *et al.* p62/SQSTM1 binds directly to Atg8/LC3 to facilitate degradation of ubiquitinated protein aggregates by autophagy\*[S]. *J. Biol. Chem.* **282**, 24131–24145 (2007).
147. Uddin, M. S. *et al.* Autophagy and Alzheimer’s disease: From molecular mechanisms to therapeutic implications. *Front. Aging Neurosci.* **10**, 1–18 (2018).
148. Nguyen, D. K. H., Thombre, R. & Wang, J. Autophagy as a common pathway in amyotrophic lateral sclerosis. *Neurosci. Lett.* **697**, 34–48 (2019).
149. Karabiyik, C., Lee, M. J. & Rubinsztein, D. C. Autophagy impairment in Parkinson’s disease. *Essays Biochem.* **61**, 711–720 (2017).

150. Wang, B., Abraham, N., Gao, G. & Yang, Q. Dysregulation of autophagy and mitochondrial function in Parkinson's disease. *Transl. Neurodegener.* **5**, 1–9 (2016).
151. Cho, S. J. *et al.* SUMO1 promotes A $\beta$  production via the modulation of autophagy. *Autophagy* **11**, 100–112 (2015).
152. Verlhac, P., Viret, C. & Faure, M. Handcuffs for bacteria - NDP52 orchestrates xenophagy of intracellular Salmonella. *Microb. Cell* **2**, 214–215 (2015).
153. Thurston, T. L. M. The tbk1 adaptor and autophagy receptor ndp52 restricts the proliferation of ubiquitin-coated bacteria. *Nat. Immunol.* **10**, 1215–1222 (2009).
154. Thurston, T. L. M., Wandel, M. P., Von Muhlinen, N., Foeglein, Á. & Randow, F. Galectin 8 targets damaged vesicles for autophagy to defend cells against bacterial invasion. *Nature* **482**, 414–418 (2012).
155. Mostowy, S. *et al.* p62 and NDP52 proteins target intracytosolic Shigella and Listeria to different autophagy pathways. *J. Biol. Chem.* **286**, 26987–26995 (2011).
156. Ogawa, M. *et al.* Escape of intracellular Shigella from autophagy. *Science* **307**, 727–731 (2005).
157. Ichimura, Y. *et al.* A ubiquitin-like system mediates protein lipidation. *Nature* **408**, 488–492 (2000).
158. Rolando, M. *et al.* Legionella pneumophila S1P-lyase targets host sphingolipid metabolism and restrains autophagy. *Proc. Natl. Acad. Sci.* **113**, 1901–1906 (2016).
159. Orvedahl, A. *et al.* HSV-1 ICP34.5 Confers Neurovirulence by Targeting the Beclin 1 Autophagy Protein. *Cell Host Microbe* **1**, 23–35 (2007).
160. Paludan, C. *et al.* Endogenous MHC class II processing of a viral nuclear antigen after autophagy. *Science* **307**, 593–596 (2005).
161. English, L. *et al.* Autophagy enhances the presentation of endogenous viral antigens on MHC class I molecules during HSV-1 infection. *Nat. Immunol.* **10**, 480–487 (2009).
162. Lipinski, M. M. *et al.* Genome-wide analysis reveals mechanisms modulating autophagy in normal brain aging and in Alzheimer's disease. *Proc. Natl. Acad. Sci.* **107**, 14164–14169 (2010).
163. Cavallini, G., Donati, A., Gori, Z. & Bergamini, E. Towards an Understanding of the Anti-Aging Mechanism of Caloric Restriction. *Curr. Aging Sci.* **1**, 4–9 (2008).

164. Harrison, D. E. *et al.* Rapamycin fed late in life extends lifespan in genetically heterogeneous mice. *Nature* **460**, 392–395 (2009).
165. Morselli, E. *et al.* Caloric restriction and resveratrol promote longevity through the Sirtuin-1-dependent induction of autophagy. *Cell Death Dis.* **1**, e10-10 (2010).
166. Eisenberg, T. *et al.* Induction of autophagy by spermidine promotes longevity. *Nat. Cell Biol.* **11**, 1305–1314 (2009).
167. Yu, L. Regulation of an ATG7-beclin 1 Program of Autophagic Cell Death by Caspase-8. *Science* **304**, 1500–1502 (2004).
168. Liu, Y. *et al.* Autosis is a Na<sup>+</sup>,K<sup>+</sup>-ATPase-regulated form of cell death triggered by autophagy-inducing peptides, starvation, and hypoxia-ischemia. *Proc. Natl. Acad. Sci.* **110**, 20364–20371 (2013).
169. Chen, Y., McMillan-Ward, E., Kong, J., Israels, S. J. & Gibson, S. B. Oxidative stress induces autophagic cell death independent of apoptosis in transformed and cancer cells. *Cell Death Differ.* **15**, 171–182 (2008).
170. Doherty, J. & Baehrecke, E. H. Life, death and autophagy. *Nat. Cell Biol.* **20**, 1110–1117 (2018).
171. Martin, D. N. Caspases function in autophagic programmed cell death in *Drosophila*. *Development* **131**, 275–284 (2003).
172. Berry, D. L. & Baehrecke, E. H. Growth Arrest and Autophagy Are Required for Salivary Gland Cell Degradation in *Drosophila*. *Cell* **131**, 1137–1148 (2007).
173. Nezis, I. P. *et al.* Autophagic degradation of dBruce controls DNA fragmentation in nurse cells during late *Drosophila melanogaster* oogenesis. *J. Cell Biol.* **190**, 523–531 (2010).
174. Shimizu, S. *et al.* Role of Bcl-2 family proteins in a non-apoptotic programmed cell death dependent on autophagy genes. *Nat. Cell Biol.* **6**, 1221–1228 (2004).
175. Yu, S.-W. *et al.* Autophagic Death of Adult Hippocampal Neural Stem Cells Following Insulin Withdrawal. *Stem Cells* **26**, 2602–2610 (2008).
176. Thorburn, J. *et al.* Autophagy controls the kinetics and extent of mitochondrial apoptosis by regulating PUMA levels. *Cell Rep.* **7**, 45–52 (2014).
177. Goodall, M. L. *et al.* The Autophagy Machinery Controls Cell Death Switching between Apoptosis and Necroptosis. *Dev. Cell* **37**, 337–349 (2016).
178. Galluzzi, L., Bravo-San Pedro, J. M., Levine, B., Green, D. R. & Kroemer, G. Pharmacological modulation of autophagy: Therapeutic potential and persisting obstacles. *Nat. Rev. Drug Discov.* **16**, 487–511 (2017).

179. Sarkar, S., Ravikumar, B., Floto, R. A. & Rubinsztein, D. C. Rapamycin and mTOR-independent autophagy inducers ameliorate toxicity of polyglutamine-expanded huntingtin and related proteinopathies. *Cell Death Differ.* **16**, 46–56 (2009).
180. Laplante, M. & Sabatini, D. M. MTOR signaling in growth control and disease. *Cell* **149**, 274–293 (2012).
181. Britton, R. G., Kover, C. & Brown, K. Direct molecular targets of resveratrol: identifying key interactions to unlock complex mechanisms. *Ann. N. Y. Acad. Sci.* **1348**, 124–133 (2015).
182. Park, D. *et al.* Resveratrol induces autophagy by directly inhibiting mTOR through ATP competition. *Sci. Rep.* **6**, 1–11 (2016).
183. Buhrmann, C. *et al.* Resveratrol induces chemosensitization to 5-fluorouracil through up-regulation of intercellular junctions, Epithelial-to-mesenchymal transition and apoptosis in colorectal cancer. *Biochem. Pharmacol.* **98**, 51–58 (2015).
184. Oh, I. *et al.* Blockage of Autophagy Rescues the Dual PI3K/mTOR Inhibitor BEZ235-induced Growth Inhibition of Colorectal Cancer Cells. *Dev. Reprod.* **20**, 1–10 (2016).
185. Li, H., Jin, X., Zhang, Z., Xing, Y. & Kong, X. Inhibition of autophagy enhances apoptosis induced by the PI3K/AKT/mTor inhibitor NVP-BEZ235 in renal cell carcinoma cells. *Cell Biochem. Funct.* **31**, 427–433 (2013).
186. Fan, Q. W. *et al.* Akt and autophagy cooperate to promote survival of drug-resistant glioma. *Sci. Signal.* **3**, (2010).
187. Park, S. *et al.* PI-103, a dual inhibitor of Class IA phosphatidylinositide 3-kinase and mTOR, has antileukemic activity in AML. *Leukemia* **22**, 1698–1706 (2008).
188. Raynaud, F. I. *et al.* Pharmacologic characterization of a potent inhibitor of class I phosphatidylinositide 3-kinases. *Cancer Res.* **67**, 5840–5850 (2007).
189. Pasquier, B. Autophagy inhibitors. *Cell. Mol. Life Sci.* **73**, 985–1001 (2016).
190. Seglen, P. O. & Gordon, P. B. 3-Methyladenine: Specific inhibitor of autophagic/lysosomal protein degradation in isolated rat hepatocytes. *Proc. Natl. Acad. Sci.* **79**, 1889–1892 (1982).
191. Wu, Y. *et al.* Synthesis and screening of 3-MA derivatives for autophagy inhibitors. *Autophagy* **9**, 595–603 (2013).
192. Powis, G. *et al.* Wortmannin, a Potent and Selective Inhibitor of Phosphatidylinositol-3-Kinase566. *Cancer Res.* **54**, 2419–2423 (1994).
193. Knight, Z. A. & Shokat, K. M. Chemically targeting the PI3K family: Figure 1.



*Biochem. Soc. Trans.* **35**, 245–249 (2007).

194. Knight, S. D. *et al.* Discovery of GSK2126458, a highly potent inhibitor of PI3K and the mammalian target of rapamycin. *ACS Med. Chem. Lett.* **1**, 39–43 (2010).
195. Jaber, N. *et al.* Class III PI3K Vps34 plays an essential role in autophagy and in heart and liver function. *Proc. Natl. Acad. Sci.* **109**, 2003–2008 (2012).
196. Liu, J. *et al.* Beclin1 Controls the Levels of p53 by Regulating the Deubiquitination Activity of USP10 and USP13. *Cell* **147**, 223–234 (2011).
197. Shao, S. *et al.* Spautin-1, a novel autophagy inhibitor, enhances imatinib-induced apoptosis in chronic myeloid leukemia. *Int. J. Oncol.* **44**, 1661–1668 (2014).
198. Miller, S. *et al.* Shaping development of autophagy inhibitors with the structure of the lipid kinase Vps34. *Science* **327**, 1638–1642 (2010).
199. Ronan, B. *et al.* A highly potent and selective Vps34 inhibitor alters vesicle trafficking and autophagy. *Nat. Chem. Biol.* **10**, 1013–1019 (2014).
200. Fassy, F. *et al.* *In Vitro Characterization of VPS34 Lipid Kinase Inhibition by Small Molecules.* *Methods Enzymol.* **587**, (Elsevier Inc., 2017).
201. Robke, L. *et al.* Phenotypic Identification of a Novel Autophagy Inhibitor Chemotype Targeting Lipid Kinase VPS34. *Angew. Chemie - Int. Ed.* **56**, 8153–8157 (2017).
202. Pasquier, B. *et al.* Discovery of (2 S)-8-[(3 R)-3-Methylmorpholin-4-yl]-1-(3-methyl-2-oxobutyl)-2-(trifluoromethyl)-3,4-dihydro-2 H -pyrimido[1,2-a ]pyrimidin-6-one: A novel potent and selective inhibitor of Vps34 for the treatment of solid tumors. *J. Med. Chem.* **58**, 376–400 (2015).
203. Dowdle, W. E. *et al.* Selective VPS34 inhibitor blocks autophagy and uncovers a role for NCOA4 in ferritin degradation and iron homeostasis in vivo. *Nat. Cell Biol.* **16**, 1069–79 (2014).
204. Russell, R. C. *et al.* ULK1 induces autophagy by phosphorylating Beclin-1 and activating VPS34 lipid kinase. *Nat. Cell Biol.* **15**, 741–750 (2013).
205. Lazarus, M. B., Novotny, C. J. & Shokat, K. M. Structure of the human autophagy initiating kinase ULK1 in complex with potent inhibitors. *ACS Chem. Biol.* **10**, 257–261 (2015).
206. Petherick, K. J. *et al.* Pharmacological inhibition of ULK1 kinase blocks mammalian target of rapamycin (mTOR)-dependent autophagy. *J. Biol. Chem.* **290**, 11376–11383 (2015).
207. Egan, D. F. *et al.* Small Molecule Inhibition of the Autophagy Kinase ULK1 and

- Identification of ULK1 Substrates. *Mol. Cell* **59**, 285–297 (2015).
208. Jung, M., Lee, J., Seo, H. Y., Lim, J. S. & Kim, E. K. Cathepsin inhibition-induced lysosomal dysfunction enhances pancreatic beta-cell apoptosis in high glucose. *PLoS One* **10**, 1–18 (2015).
209. Berg, O. T., Monica, F., Eivind, S. P., Trond, B. & P.O., S. Isolation and Characterization of Rat Liver Amphisomes. *J. Biol. Chem.* **273**, 21883–21892 (1998).
210. Yamamoto, A. *et al.* Bafilomycin A<sub>i</sub> Prevents Maturation of Autophagic Vacuoles by Inhibiting Fusion between Autophagosomes and Lysosomes in Rat Hepatoma Cell Line H-4-II-E Cells. *Cell Struct. Funct.* **23**, 33–42 (1998).
211. Rossi, M. *et al.* Desmethylclomipramine induces the accumulation of autophagy markers by blocking autophagic flux. *J. Cell Sci.* **122**, 3330–3339 (2009).
212. Carew, J. S. *et al.* Lucanthone is a novel inhibitor of autophagy that induces cathepsin D-mediated apoptosis. *J. Biol. Chem.* **286**, 6602–6613 (2011).
213. Homewood, C., Warhurst, D., Peters, W. & Baggaley, V. Lysosomes, pH and the Anti-malarial Action of Chloroquine. *Nature* **235**, 50–52 (1972).
214. Levy, G. D. *et al.* Incidence of hydroxychloroquine retinopathy in 1,207 patients in a large multicenter outpatients practice. *Arthritis Rheum.* **40**, 1482–1486 (1997).
215. Harhaji-Trajkovic, L. *et al.* Chloroquine-mediated lysosomal dysfunction enhances the anticancer effect of nutrient deprivation. *Pharm. Res.* **29**, 2249–2263 (2012).
216. Maes, H. *et al.* Tumor vessel normalization by chloroquine independent of autophagy. *Cancer Cell* **26**, 190–206 (2014).
217. Klionsky, D. J. *et al.* Guidelines for the use and interpretation of assays for monitoring autophagy (3rd edition). *Autophagy* **12**, 1–222 (2016).
218. Kirisako, T. *et al.* The reversible modification regulates the membrane-binding state of Apg8/Aut7 essential for autophagy and the cytoplasm to vacuole targeting pathway. *J. Cell Biol.* **151**, 263–275 (2000).
219. Fu, Y. *et al.* Discovery of a small molecule targeting autophagy via ATG4B inhibition and cell death of colorectal cancer cells in vitro and in vivo. *Autophagy* **20**, 1–17 (2018).
220. Fujita, N. *et al.* An Atg4B Mutant Hampers the Lipidation of LC3 Paralogues and Causes Defects in Autophagosome Closure. *Mol. Biololgy Cell* **19**, 4651–4659 (2008).

221. Read, R., Savelieva, K., Baker, K., Hansen, G. & Vogel, P. Histopathological and neurological features of Atg4b knockout mice. *Vet. Pathol.* **48**, 486–494 (2011).
222. Mariño, G. *et al.* Autophagy is essential for mouse sense of balance. *J. Clin. Invest.* **120**, 2331–2344 (2010).
223. Kurdi, A. *et al.* ATG4B inhibitors with a benzotropolone core structure block autophagy and augment efficiency of chemotherapy in mice. *Biochem. Pharmacol.* **138**, 150–162 (2017).
224. Nguyen, T. G. *et al.* Development of Fluorescent Substrates and Assays for the Key Autophagy-Related Cysteine Protease Enzyme, ATG4B. *Assay Drug Dev. Technol.* **12**, 176–189 (2014).
225. Agrotis, A., Pengo, N., Burden, J. J. & Ketteler, R. Redundancy of human ATG4 protease isoforms in autophagy and LC3/GABARAP processing revealed in cells. *Autophagy* **15**, 976–997 (2019).
226. Kauffman, K. J. *et al.* Delipidation of mammalian Atg8-family proteins by each of the four ATG4 proteases. *Autophagy* **14**, 992–1010 (2018).
227. Scherz-Shouval, R. *et al.* Reactive oxygen species are essential for autophagy and specifically regulate the activity of Atg4. *EMBO J.* **26**, 1749–1760 (2007).
228. Rothe, K. *et al.* The core autophagy protein ATG4B is a potential biomarker and therapeutic target in CML stem / progenitor cells. *Blood* **123**, 3622–3634 (2014).
229. Qiu, Z. *et al.* Discovery of Fluoromethylketone-Based Peptidomimetics as Covalent ATG4B (Autophagin-1) Inhibitors. *ACS Med. Chem. Lett.* **7**, 802–806 (2016).
230. Chu, J. *et al.* ATG4B inhibitor FMK-9a induces autophagy independent on its enzyme inhibition. *Arch. Biochem. Biophys.* **644**, 29–36 (2018).
231. Liu, P. F. *et al.* Drug repurposing screening identifies tioconazole as an ATG4 inhibitor that suppresses autophagy and sensitizes cancer cells to chemotherapy. *Theranostics* **8**, 830–845 (2018).
232. Bosc, D. *et al.* A new quinoline-based chemical probe inhibits the autophagy-related cysteine protease ATG4B. *Sci. Rep.* **8**, 1–17 (2018).
233. Li, M. *et al.* Kinetics comparisons of mammalian Atg4 homologues indicate selective preferences toward diverse Atg8 substrates. *J. Biol. Chem.* **286**, 7327–7338 (2011).
234. Cleenewerck, M. *et al.* Inhibitor screening and enzymatic activity determination for autophagy target Atg4B using a gel electrophoresis-based assay. *Eur. J. Med. Chem.* **123**, 631–638 (2016).

235. Vezenkov, L. *et al.* Development of fluorescent peptide substrates and assays for the key autophagy-initiating cysteine protease enzyme, ATG4B. *Bioorganic Med. Chem.* **23**, 3237–3247 (2015).
236. Shu, C. W. *et al.* High-throughput fluorescence assay for small-molecule inhibitors of Autophagins/Atg4. *J. Biomol. Screen.* **16**, 174–182 (2011).
237. Li, M., Chen, X., Ye, Q. Z., Vogt, A. & Yin, X. M. A high-throughput FRET-based assay for determination of Atg4 activity. *Autophagy* **8**, 401–412 (2012).
238. Xu, D. *et al.* Identification of new ATG4B inhibitors based on a novel high-throughput screening platform. *SLAS Discov.* **22**, 338–347 (2017).
239. Förster, T. & Förster, T. Transfer Mechanisms of Electronic Excitation Energy. *Radiat. Res. Suppl.* **2**, 326 (1960).
240. Cardullo, R. A. Theoretical principles and practical considerations for fluorescence resonance energy transfer microscopy. *Methods Cell Biol.* **114**, 441–456 (2013).
241. Chen-Ting Ma & Sergienko, E. A. Time-Resolved Fluorescence Assays. *Methods Mol. Biol.* **1439**, 131–142 (2016).
242. Morrison, L. E. Time-resolved detection of energy transfer: Theory and application to immunoassays. *Anal. Biochem.* **174**, 101–120 (1988).
243. Degorce, F. *et al.* HTRF: A Technology Tailored for Drug Discovery –A Review of Theoretical Aspects and Recent Applications. *Curr. Chem. Genomics* **3**, 22–32 (2009).
244. Bazin, H., Trinquet, E. & Mathis, G. Time resolved amplification of cryptate emission: A versatile technology to trace biomolecular interactions. *Rev. Mol. Biotechnol.* **82**, 233–250 (2002).
245. Madiraju, C. *et al.* TR-FRET-based high-throughput screening assay for identification of UBC13 inhibitors. *J. Biomol. Screen.* **17**, 163–176 (2012).
246. Carlson, C. B., Horton, R. A. & Vogel, K. W. A Toolbox Approach to High-Throughput TR-FRET-Based SUMOylation and DeSUMOylation Assays. *Assay Drug Dev. Technol.* **7**, 348–355 (2009).
247. Fernández-Dueñas, V. *et al.* Fluorescence resonance energy transfer-based technologies in the study of protein-protein interactions at the cell surface. *Methods* **57**, 467–472 (2012).
248. Zhang, W. G., Shor, B. & Yu, K. Identification and characterization of a constitutively T-loop phosphorylated and active recombinant S6K1: Expression, purification, and enzymatic studies in a high capacity non-radioactive TR-FRET Lance assay. *Protein Expr. Purif.* **46**, 414–420 (2006).

249. Nguyen, H. P. *et al.* Cerebellar Soluble Mutant Ataxin-3 Level Decreases during Disease Progression in Spinocerebellar Ataxia Type 3 Mice. *PLoS One* **8**, (2013).
250. Mariño, G. *et al.* Human autophagins, a family of cysteine proteinases potentially implicated in cell degradation by autophagy. *J. Biol. Chem.* **278**, 3671–3678 (2003).
251. Tanida, I. *et al.* HsAtg4B/HsApg4B/autophagin-1 cleaves the carboxyl termini of three human Atg8 homologues and delipidates microtubule-associated protein light chain 3- and GABAA receptor-associated protein-phospholipid conjugates. *J. Biol. Chem.* **279**, 36268–36276 (2004).
252. Nakatogawa, H., Ishii, J., Asai, E. & Ohsumi, Y. Atg4 recycles inappropriately lipidated Atg8 to promote autophagosome biogenesis. *Autophagy* **8**, 177–186 (2012).
253. Yu, Z. Q. *et al.* Dual roles of Atg8 - PE deconjugation by Atg4 in autophagy. *Autophagy* **8**, 883–892 (2012).
254. Bortnik, S. *et al.* Identification of breast cancer cell subtypes sensitive to ATG4B inhibition. *Oncotarget* **7**, (2016).
255. Liu, P. F. *et al.* ATG4B promotes colorectal cancer growth independent of autophagy flux. *Autophagy* **10**, 1454–1465 (2014).
256. Yang, A., Li, Y., Pantoom, S., Triola, G. & Wu, Y.-W. Semisynthetic Lipidated LC3 Protein Mediates Membrane Fusion. *ChemBioChem* **14**, 1296–1300 (2013).
257. Crowley, E. L. & Rafferty, S. P. Review of lactose-driven auto-induction expression of isotope-labelled proteins. *Protein Expr. Purif.* **157**, 70–85 (2019).
258. Davanloo, P., Rosenberg, A. H., Dunn, J. J. & Studier, F. W. Cloning and expression of the gene for bacteriophage T7 RNA polymerase. *Proc. Natl. Acad. Sci.* **81**, 2035–2039 (1984).
259. Studier, F. W. & Moffatt, B. A. Use of bacteriophage T7 RNA polymerase to direct selective high-level expression of cloned genes. *J. Mol. Biol.* **189**, 113–130 (1986).
260. William Studier, F., Rosenberg, A. H., Dunn, J. J. & Dubendorff, J. W. Use of T7 RNA polymerase to direct expression of cloned genes. *Methods Enzymol.* **185**, 60–89 (1990).
261. Studier, F. W. Protein production by auto-induction in high density shaking cultures. *Protein Expr. Purif.* **41**, 207–234 (2005).
262. Fox, B. G. & Blommel, P. G. Autoinduction of protein expression. in *Curr Protoc Protein Sci.* Chapter 5 Unit 5 23 (2009).

263. Berrow, N. S. *et al.* A versatile ligation-independent cloning method suitable for high-throughput expression screening applications. *Nucleic Acids Res.* **35**, e45 (2007).
264. Plante, H., Evans, K., Beaudet, L. & Dahan, S. Phosphatase Assays Using the LANCE Ultra Technology ([https://www.perkinelmer.com/lab-solutions/resources/docs/PST\\_LANCE\\_Phosphatase\\_Assays.pdf](https://www.perkinelmer.com/lab-solutions/resources/docs/PST_LANCE_Phosphatase_Assays.pdf)). *Perkin Elmer Inc*
265. Acker, M. G. & Auld, D. S. Considerations for the design and reporting of enzyme assays in high-throughput screening applications. *Perspect. Sci.* **1**, 56–73 (2014).
266. Ullman, E. F. *et al.* Luminescent oxygen channeling immunoassay: measurement of particle binding kinetics by chemiluminescence. *Proc. Natl. Acad. Sci. U. S. A.* **91**, 5426–5430 (1994).
267. Eglén, R. M. *et al.* The Use of AlphaScreen Technology in HTS: Current Status. *Curr. Chem. Genomics* **1**, 2–10 (2008).
268. PerkinElmer. AlphaLISA and AlphaScreen No-wash Assays. <http://www.perkinelmer.com/es/lab-products-and-services/application-support-knowledgebase/alphalisa-alphascreen-no-wash-assays/alphalisa-alphascreen-no-washassays-main.html>
269. Wu, G., Yuan, Y. & Hodge, C. N. Determining appropriate substrate conversion for enzymatic assays in high-throughput screening. *J. Biomol. Screen.* **8**, 694–700 (2003).
270. Perez-Perez, M. E., Zaffagnini, M., Marchand, C. H., Crespo, J. L. & Lemaire, S. D. The yeast autophagy protease Atg4 is regulated by thioredoxin. *Autophagy* **10**, 1953–1964 (2014).
271. Maruyama, T. & Noda, N. N. Autophagy-regulating protease Atg4: Structure, function, regulation and inhibition. *J. Antibiot. (Tokyo)*. **71**, 72–78 (2018).
272. Zhang, J. H., Chung, T. D. Y. & Oldenburg, K. R. A simple statistical parameter for use in evaluation and validation of high throughput screening assays. *J. Biomol. Screen.* **4**, 67–73 (1999).
273. Ueno, T. *et al.* The Crystal Structure of Human Atg4b, a Processing and Deconjugating Enzyme for Autophagosome-forming Modifiers. *J. Mol. Biol.* **355**, 612–618 (2005).
274. Satoo, K. *et al.* The structure of Atg4B-LC3 complex reveals the mechanism of LC3 processing and delipidation during autophagy. *EMBO J.* **28**, 1341–1350 (2009).
275. Inagaki, F. *et al.* Structural Basis for the Specificity and Catalysis of Human Atg4B Responsible for Mammalian Autophagy. *J. Biol. Chem.* **280**, 40058–

- 40065 (2005).
276. Schrödinger LLC: New York, N. Schrödinger: Release 2016-4: Virtual Screening Workflow. (2016).
277. Friesner, R. A. *et al.* Glide: A New Approach for Rapid, Accurate Docking and Scoring. 1. Method and Assessment of Docking Accuracy. *J. Med. Chem.* **47**, 1739–1749 (2004).
278. Banks, J. L. *et al.* Glide: A New Approach for Rapid, Accurate Docking and Scoring. 2. Enrichment Factors in Database Screening. *J. Med. Chem.* **47**, 1750–1759 (2004).
279. Schrödinger, LLC: New York, N. Schrödinger: Release 2016-4: Glide. (2016).
280. Repasky, M. P. *et al.* Extra Precision Glide: Docking and Scoring Incorporating a Model of Hydrophobic Enclosure for Protein–Ligand Complexes. *J. Med. Chem.* **49**, 6177–6196 (2006).
281. Trott, O. & Olson, A. J. AutoDock Vina: Improving the Speed and Accuracy of Docking with a New Scoring Function, Efficient Optimization, and Multithreading. *J. Comput. Chem.* **31**, 455–461 (2009).
282. Seeliger, D. & de Groot, B. L. Ligand docking and binding site analysis with PyMOL and Autodock/Vina. *J. Comput. Aided. Mol. Des.* **24**, 417–22 (2010).
283. Baell, J. B. & Holloway, G. A. New substructure filters for removal of pan assay interference compounds (PAINS) from screening libraries and for their exclusion in bioassays. *J. Med. Chem.* **53**, 2719–2740 (2010).
284. Schorpp, K. *et al.* Identification of small-molecule frequent hitters from alphascreen high-throughput screens. *J. Biomol. Screen.* **19**, 715–726 (2014).
285. Badran, M. M., Moneer, A. A., Refaat, H. M. & El-malah, A. A. Synthesis and Antimicrobial Activity of Novel Quinoxaline Derivatives. *J. Chinese Chem. Soc.* **54**, 469–478 (2007).
286. Tariq, S., Somakala, K. & Amir, M. Quinoxaline: An insight into the recent pharmacological advances. *Eur. J. Med. Chem.* **143**, 542–557 (2018).
287. Varney, M. D. *et al.* Crystal-structure-based design and synthesis of benz[cd]indole-containing inhibitors of thymidylate synthase. *J. Med. Chem.* **35**, 663–676 (1992).
288. Xue, X. *et al.* Discovery of Benzo[cd]indol-2(1H)-ones as Potent and Specific BET Bromodomain Inhibitors: Structure-Based Virtual Screening, Optimization, and Biological Evaluation. *J. Med. Chem.* **59**, 1565–1579 (2016).
289. Luo, H.-B. *et al.* Discovery of Novel Phosphodiesterase-2A Inhibitors by Structure-Based Virtual Screening, Structural Optimization, and Bioassay. *J.*

*Chem. Inf. Model.* **57**, 355–364 (2017).

290. Hsiang, Y., Jiang, J. & Liu, L. Topoisomerase II-mediated DNA cleavage by amonafide and its structural analogs. *Mol. Pharmacol.* **36**, 371–376 (1989).
291. Chiang, L.-C. *et al.* Derivatives of 4-amino-3,6-disulfonato-1, 8-naphthalimide inhibit reverse transcriptase and suppress human and feline immunodeficiency virus expression in cultured cells. *J. Cell. Biochem.* **51**, 446–457 (2014).
292. Aldrich, C. *et al.* The Ecstasy and Agony of Assay Interference Compounds. *J. Chem. Inf. Model.* **3**, 143–147 (2017).
293. Selvakumaran, M., Amaravadi, R. K., Vasilevskaya, I. A. & O’Dwyer, P. J. Autophagy inhibition sensitizes colon cancer cells to antiangiogenic and cytotoxic therapy. *Clin. Cancer Res.* **19**, 2995–3007 (2013).
294. Tanc, M. *et al.* Synthesis and evaluation of novel benzotropolones as Atg4B inhibiting autophagy blockers. *Bioorg. Chem.* **87**, 163–168 (2019).
295. Hishikawa, D., Hashidate, T., Shimizu, T. & Shindou, H. Diversity and function of membrane glycerophospholipids generated by the remodeling pathway in mammalian cells. *J. Lipid Res.* **55**, 799–807 (2014).
296. Epan, R. M. Introduction to membrane lipids. in *Methods in membrane lipids* 1–7 (2015).
297. Bartke, N. & Hannun, Y. A. Bioactive sphingolipids: metabolism and function. *J. Lipid Res.* **50**, S91–S96 (2009).
298. Vance, J. E. Phospholipid Synthesis and Transport in Mammalian Cells. *Traffic* **16**, 1–18 (2015).
299. Julie Grouleff, Irudayam, S. J., Skeby, K. K. & Schiøtt, B. The influence of cholesterol on membrane protein structure, function, and dynamics studied by molecular dynamics simulations. *Biochim. Biophys. Acta - Mol. Cell Biol. Lipids* **1848**, 1783–1795 (2015).
300. Magee, T. & Seabra, M. C. Fatty acylation and prenylation of proteins: What’s hot in fat. *Curr. Opin. Cell Biol.* **17**, 190–196 (2005).
301. Pechlivanis, M. & Kuhlmann, J. Hydrophobic modifications of Ras proteins by isoprenoid groups and fatty acids-More than just membrane anchoring. *Biochim. Biophys. Acta - Proteins Proteomics* **1764**, 1914–1931 (2006).
302. Udenwobele, D. I. *et al.* Myristoylation: An important protein modification in the immune response. *Front. Immunol.* **8**, 1–16 (2017).
303. Patwardhan, P. & Resh, M. D. Myristoylation and Membrane Binding Regulate c-Src Stability and Kinase Activity. *Mol. Cell. Biol.* **30**, 4094–4107 (2010).



304. Chamberlain, L. H. & Shipston, M. J. The Physiology of Protein S-acylation. *Physiol. Rev.* **95**, 341–376 (2015).
305. Janda, C. Y. & Garcia, K. C. Wnt acylation and its functional implication in Wnt signalling regulation. *Biochem. Soc. Trans.* **43**, 211–216 (2015).
306. Laude, A. J. & Prior, I. A. Palmitoylation and localisation of RAS isoforms are modulated by the hypervariable linker domain. *J. Cell Sci.* **121**, 421–427 (2008).
307. Ciepla, P., Magee, A. I. & Tate, E. W. Cholesterylation: a tail of hedgehog: Figure 1. *Biochem. Soc. Trans.* **43**, 262–267 (2015).
308. Thukral, L. *et al.* The Molecular Mechanism Underlying Recruitment and Insertion of Lipid-Anchored LC3 Protein into Membranes. *Biophys. J.* **109**, 2067–2078 (2015).
309. Harayama, T. & Riezman, H. Understanding the diversity of membrane lipid composition. *Nat. Rev. Mol. Cell Biol.* **19**, 281–296 (2018).
310. Yamashita, A., Sugiura, T. & Waku, K. Acyltransferases and transacylases involved in fatty acid remodeling of phospholipids and metabolism of bioactive lipids in mammalian cells. *J. Biochem.* **122**, 1–16 (1997).
311. Meer, G. van, Voelker, D. R. & Feigenson, G. W. Membrane lipids: where they are and how they behave. *Nat. Rev. Mol. Cell Biol.* **9**, 112–124 (2008).
312. Paradies, G., Paradies, V., De Benedictis, V., Ruggiero, F. M. & Petrosillo, G. Functional role of cardiolipin in mitochondrial bioenergetics. *Biochim. Biophys. Acta - Bioenerg.* **1837**, 408–417 (2014).
313. Kamal, M. M., Mills, D., Grzybek, M. & Howard, J. Measurement of the membrane curvature preference of phospholipids reveals only weak coupling between lipid shape and leaflet curvature. *Proc. Natl. Acad. Sci.* **106**, 22245–22250 (2009).
314. Kim, Y. J., Guzman-Hernandez, M. L. & Balla, T. A highly dynamic ER-derived phosphatidylinositol-synthesizing organelle supplies phosphoinositides to cellular membranes. *Dev. Cell* **21**, 813–824 (2011).
315. Malheiro, A. R., da Silva, T. F. & Brites, P. Plasmalogens and fatty alcohols in rhizomelic chondrodysplasia punctata and Sjögren-Larsson syndrome. *J. Inherit. Metab. Dis.* **38**, 111–121 (2014).
316. Gable, K. *et al.* A disease-causing mutation in the active site of serine palmitoyltransferase causes catalytic promiscuity. *J. Biol. Chem.* **285**, 22846–22852 (2010).
317. Grösch, S., Schiffmann, S. & Geisslinger, G. Chain length-specific properties of ceramides. *Prog. Lipid Res.* **51**, 50–62 (2012).

318. Harayama, T. *et al.* Lysophospholipid acyltransferases mediate phosphatidylcholine diversification to achieve the physical properties required in vivo. *Cell Metab.* **20**, 295–305 (2014).
319. Johansen, A. *et al.* Mutations in MBOAT7, Encoding Lysophosphatidylinositol Acyltransferase I, Lead to Intellectual Disability Accompanied by Epilepsy and Autistic Features. *Am. J. Hum. Genet.* **99**, 912–916 (2016).
320. McMahon, H. T. & Boucrot, E. Membrane curvature at a glance. *J. Cell Sci.* **128**, 1065–1070 (2015).
321. Zick, M., Stroupe, C., Orr, A., Douville, D. & Wickner, W. T. Membranes linked by trans-SNARE complexes require lipids prone to non-bilayer structure for progression to fusion. *Elife* **3**, 1–13 (2014).
322. Rawicz, W., Olbrich, K. C., McIntosh, T., Needham, D. & Evans, E. Effect of Chain Length and Unsaturation on Elasticity of Lipid Bilayers. *Biophys. J.* **79**, 328–339 (2000).
323. Manni, M. M. *et al.* Acyl chain asymmetry and polyunsaturation of brain phospholipids facilitate membrane vesiculation without leakage. *Elife* **7**, 1–23 (2018).
324. Sezgin, E., Levental, I., Mayor, S. & Eggeling, C. The mystery of membrane organization: Composition, regulation and roles of lipid rafts. *Nat. Rev. Mol. Cell Biol.* **18**, 361–374 (2017).
325. Anilkumar, A. A. *et al.* Transbilayer Lipid Interactions Mediate Nanoclustering of Lipid-Anchored Proteins Article Transbilayer Lipid Interactions Mediate Nanoclustering of Lipid-Anchored Proteins. *Cell* **161**, 581–594 (2015).
326. Lee, S. *et al.* Impaired retrograde membrane traffic through endosomes in a mutant CHO cell defective in phosphatidylserine synthesis. *Genes Cells* **17**, 728–736 (2012).
327. Daumke, O., Roux, A. & Haucke, V. Review BAR Domain Scaffolds in Dynamin-Mediated Membrane Fission. *Cell* **156**, 882–892 (2014).
328. Antonny, B. Mechanisms of Membrane Curvature Sensing. *Annu. Rev. Biochem.* **80**, 101–123 (2011).
329. Magdeleine, M., Gautier, R., Gounon, P., Vanni, S. & Antonny, B. A filter at the entrance of the Golgi that selects vesicles according to size and bulk lipid composition. *Elife* **5**, 1–22 (2016).
330. Falasca, M. *et al.* Activation of phospholipase C $\gamma$  by PI 3-kinase-induced PH domain-mediated membrane targeting. *EMBO J.* **17**, 414–422 (1998).
331. Stanishneva-Konovalova, T. B., Derkacheva, N. I., Polevova, S. V. & Sokolova, O. S. The Role of BAR Domain Proteins in the Regulation of Membrane

- Dynamics. *Acta Naturae* **8**, 60–69 (2016).
332. Xie, Y. *et al.* Posttranslational modification of autophagy-related proteins in macroautophagy. *Autophagy* **11**, 28–45 (2014).
333. Bach, M., Larance, M., James, D. E. & Ramm, G. The serine / threonine kinase ULK1 is a target of multiple phosphorylation events. **291**, 283–291 (2011).
334. Keil, E. *et al.* Phosphorylation of Atg5 by the Gadd45 b – MEKK4-p38 pathway inhibits autophagy. *Cell Death Differ.* **20**, 321–332 (2013).
335. Young, A. R. J. *et al.* Starvation and ULK1-dependent cycling of mammalian Atg9 between the TGN and endosomes. *J. Cell Sci.* **119**, 3888–3900 (2006).
336. Shi, C. & Kehrl, J. H. TRAF6 and A20 Regulate Lysine 63–Linked Ubiquitination of Beclin-1 to Control TLR4-Induced Autophagy. *Sci. Signal.* **3**, 1–10 (2010).
337. Nazio, F. *et al.* mTOR inhibits autophagy by controlling ULK1 ubiquitylation , self-association and function through AMBRA1 and TRAF6. *Nat. Cell Biol.* **15**, 406–416 (2013).
338. Lee, I. H. *et al.* A role for the NAD-dependent deacetylase Sirt1 in the regulation of autophagy. *Proc. Natl. Acad. Sci.* **105**, 3374–3379 (2008).
339. Nakatogawa, H., Ichimura, Y. & Ohsumi, Y. Atg8, a Ubiquitin-like Protein Required for Autophagosome Formation, Mediates Membrane Tethering and Hemifusion. *Cell* **130**, 165–178 (2007).
340. Weidberg, H. *et al.* LC3 and GATE-16 N Termini Mediate Membrane Fusion Processes Required for Autophagosome Biogenesis. *Dev. Cell* **20**, 444–454 (2011).
341. Vinay A. Patil & Greenberg, M. L. Cardiolipin-Mediated Cellular Signaling. in *Lipid-mediated Protein Signaling* 195–213 (2013).
342. Antón, Z., Landajuela, A., Hervás, J. H., Montes, L. R. & Hernández-, S. Human Atg8-cardiolipin interactions in mitophagy : Specific properties of LC3 , GABARAPL2 and GABARAP. *Autophagy* **2**, 2386–2403 (2016).
343. Chu, C. T., Bayir, H. & Kagan, V. E. LC3 binds externalized cardiolipin on injured mitochondria to signal mitophagy in neurons. *Autophagy* **10**, 376–378 (2014).
344. Chu, C. T. *et al.* Cardiolipin externalization to the outer mitochondrial membrane acts as an elimination signal for mitophagy in neuronal cells. *Nat. Cell Biol.* **15**, 1197–1205 (2013).
345. Hsu, P. *et al.* Cardiolipin Remodeling by TAZ / Tafazzin Is Selectively Required for the Initiation of Mitophagy. *Autophagy* **11**, 643–652 (2015).
346. Ge, L., Melville, D., Zhang, M. & Schekman, R. The ER–Golgi intermediate

compartment is a key membrane source for the LC3 lipidation step of autophagosome biogenesis. *Elife* **2**, 1–23 (2013).

347. Axe, E. L. *et al.* Autophagosome formation from membrane compartments enriched in phosphatidylinositol 3-phosphate and dynamically connected to the endoplasmic reticulum. *J. Cell Biol.* **182**, 685–701 (2008).
348. Hailey, D. W. *et al.* Mitochondria Supply Membranes for Autophagosome Biogenesis during Starvation. *Cell* **141**, 656–667 (2010).
349. Yen, W. L. *et al.* The conserved oligomeric Golgi complex is involved in double-membrane vesicle formation during autophagy. *J. Cell Biol.* **188**, 101–114 (2010).
350. Longatti, A. *et al.* TBC1D14 regulates autophagosome formation via Rab11- and ULK1-positive recycling endosomes. *J. Cell Biol.* **197**, 659–675 (2012).
351. Ravikumar, B., Moreau, K., Jahreiss, L., Puri, C. & Rubinsztein, D. C. Plasma membrane contributes to the formation of pre-autophagosomal structures. *Nat. Cell Biol.* **12**, 747–757 (2010).
352. Yamamoto, H. *et al.* Atg9 vesicles are an important membrane source during early steps of autophagosome formation. *J. Cell Biol.* **198**, 219–233 (2012).
353. Landajuela, A. *et al.* Lipid Geometry and Bilayer Curvature Modulate LC3 / GABARAP-Mediated Model Autophagosomal Elongation. *Biophys. J.* **110**, 411–422 (2016).
354. Knorr, R. L. *et al.* Membrane morphology is actively transformed by covalent binding of the protein Atg8 to PE-lipids. *PLoS One* **9**, 1–14 (2014).
355. Dancourt, J. & Melia, T. J. Lipidation of the autophagy proteins LC3 and GABARAP is a membrane-curvature dependent process. *Autophagy* **10**, 1470–1471 (2014).
356. Nath, S. *et al.* Lipidation of the LC3 / GABARAP family of autophagy proteins relies on a membrane-curvature-sensing domain in Atg3. *Nat. Cell Biol.* **16**, 415–424 (2014).
357. Horenkamp, F. A. *et al.* The Legionella Anti-autophagy Effector RavZ Targets the Autophagosome via PI3P- and Curvature-Sensing Motifs. *Dev. Cell* **34**, 569–576 (2015).
358. Hervás, J. H., Landajuela, A., Antón, Z., Shnyrova, A. V & Goñi, F. M. Human ATG3 binding to lipid bilayers : role of lipid geometry , and electric charge. *Sci. Rep.* **7**, 1–15 (2017).
359. Knorr, R. L., Dimova, R. & Lipowsky, R. Curvature of double-membrane organelles generated by changes in membrane size and composition. *PLoS One* **7**, (2012).

360. Lee, Y. K. & Lee, J. A. Role of the mammalian ATG8/LC3 family in autophagy: Differential and compensatory roles in the spatiotemporal regulation of autophagy. *BMB Rep.* **49**, 424–430 (2016).
361. Ichimura, Y. *et al.* A ubiquitin-like system mediates protein lipidation. *Nature* **408**, 488–492 (2000).
362. Sou, Y., Tanida, I., Komatsu, M., Ueno, T. & Kominami, E. Phosphatidylserine in Addition to Phosphatidylethanolamine Is an in Vitro Target of the Mammalian Atg8 Modifiers , LC3 , GABARAP , and GATE-16 \*. *J. Cell Biol.* **281**, 3017–3024 (2006).
363. Yang, A., Pantoom, S. & Wu, Y.-W. Elucidation of the anti-autophagy mechanism of the Legionella effector RavZ using semisynthetic LC3 proteins. *Elife* **6**, 1–23 (2017).
364. Muro, E., Atilla-Gokcumen, G. E. & Eggert, U. S. Lipids in cell biology: how can we understand them better? *Mol. Biol. Cell* **25**, 1819–1823 (2014).
365. Smith, W. L. The eicosanoids and their biochemical mechanisms of action. *Biochem. J.* **259**, 315–324 (1989).
366. Fahy, E., Cotter, D., Sud, M. & Subramaniam, S. Lipid classification, structures and tools. *Biochim. Biophys. Acta* **1811**, 637–647 (2011).
367. Hancock, J. F., Magee, A. I., Childs, J. E. & Marshall, C. J. All ras proteins are polyisoprenylated but only some are palmitoylated. *Cell* **57**, 1167–1177 (1989).
368. Sakakibara, K. *et al.* Phospholipid methylation controls Atg32-mediated mitophagy and Atg8 recycling. *EMBO J.* **34**, 2703–2719 (2015).
369. Tanida, I., Ueno, T. & Kominami, E. LC3 conjugation system in mammalian autophagy. *Int. J. Biochem. Cell Biol.* **36**, 2503–2518 (2004).
370. Hemelaar, J., Lelyveld, V. S., Kessler, B. M. & Ploegh, H. L. A Single Protease, Apg4B, Is Specific for the Autophagy-related Ubiquitin-like Proteins GATE-16, MAP1-LC3, GABARAP, and Apg8L. *J. Biol. Chem.* **278**, 51841–51850 (2003).
371. Blich, E. G. & Dyer, W. J. A Rapid Method of Total Lipid Extraction and Purification. *Can. J. Biochem. Physiol.* **37**, 911–917 (1959).
372. Smedman, A. E. M., Gustafsson, I. B., Berglund, L. G. T. & Vessby, B. O. H. Pentadecanoic acid in serum as a marker for intake of milk fat: Relations between intake of milk fat and metabolic risk factors. *Am. J. Clin. Nutr.* **69**, 22–29 (1999).
373. Brevik, A., Veierød, M. B., Drevon, C. A. & Andersen, L. F. Evaluation of the odd fatty acids 15:0 and 17:0 in serum and adipose tissue as markers of intake of milk and dairy fat. *Eur. J. Clin. Nutr.* **59**, 1417–1422 (2005).

374. Massart-Leën, A. M., Roets, E., Peeters, G. & Verbeke, R. Propionate for Fatty Acid Synthesis by the Mammary Gland of the Lactating Goat. *J. Dairy Sci.* **66**, 1445–1454 (1983).
375. Weitkunat, K. *et al.* Odd-chain fatty acids as a biomarker for dietary fiber intake: A novel pathway for endogenous production from propionate. *Am. J. Clin. Nutr.* **105**, 1544–1551 (2017).
376. Kornsteiner, M., Singer, I. & Elmadfa, I. Very low n-3 long-chain polyunsaturated fatty acid status in Austrian vegetarians and vegans. *Ann. Nutr. Metab.* **52**, 37–47 (2008).
377. Pfeuffer, M. & Jaudszus, A. Pentadecanoic and Heptadecanoic Acids: Multifaceted Odd-Chain Fatty Acids. *Adv. Nutr. An Int. Rev. J.* **7**, 730–734 (2016).
378. Sperl, W. *et al.* Odd-numbered long-chain fatty acids in propionic acidaemia. *Eur. J. Pediatr.* **159**, 54–58 (2000).
379. Quehenberger, O. *et al.* Lipidomics reveals a remarkable diversity of lipids in human plasma. *J. Lipid Res.* **51**, 3299–305 (2010).
380. De Oliveira Otto, M. C. *et al.* Genome-wide association meta-analysis of circulating odd-numbered chain saturated fatty acids: Results from the CHARGE Consortium. *PLoS One* **13**, 1–12 (2018).
381. Meikle, P. J. *et al.* Plasma Lipid Profiling Shows Similar Associations with Prediabetes and Type 2 Diabetes. *PLoS One* **8**, (2013).
382. Fonteh, A. N., Cipolla, M., Chiang, J., Arakaki, X. & Harrington, M. G. Human cerebrospinal fluid fatty acid levels differ between supernatant fluid and brain-derived nanoparticle fractions, and are altered in Alzheimer’s disease. *PLoS One* **9**, 1–14 (2014).
383. Kennedy, E. P. & Weiss, S. B. The function of cytidine coenzymes in the biosynthesis of phospholipides. *J Biol Chem* **222**, 193–214 (1956).
384. Vance, J. E. Phosphatidylserine and phosphatidylethanolamine in mammalian cells: two metabolically related aminophospholipids. *J. Lipid Res.* **49**, 1377–1387 (2008).
385. Sundler, R., Akesson, B. & Nilsson, A. Quantitative role of base exchange in phosphatidylethanolamine synthesis in isolated rat hepatocytes. *FEBS Lett.* **43**, 303–307 (1974).
386. Stein, Y. & Stein, O. Metabolism of labeled lysolecithin, lysophosphatidyl ethanolamine and lecithin in the rat. *Biochim. Biophys. Acta - Mol. Cell Biol. Lipids* **116**, 95–107 (1966).
387. Hwang, S. H., Han, B. I. & Lee, M. Knockout of ATG5 leads to malignant cell

- transformation and resistance to Src family kinase inhibitor PP2. *J. Cell. Physiol.* **233**, 506–515 (2018).
388. Sharifi, M. N. *et al.* Autophagy Promotes Focal Adhesion Disassembly and Cell Motility of Metastatic Tumor Cells through the Direct Interaction of Paxillin with LC3. *Cell Rep.* **15**, 1660–1672 (2016).
389. Hernández-Tiedra, S. *et al.* Dihydroceramide accumulation mediates cytotoxic autophagy of cancer cells via autolysosome destabilization. *Autophagy* **12**, 2213–2229 (2016).
390. Kuma, A. *et al.* The role of autophagy during the early neonatal starvation period. *Nature* **432**, 1032–1036 (2019).
391. Wang, Q. *et al.* Protocols and pitfalls in obtaining fatty acid-binding proteins for biophysical studies of ligand-protein and protein-protein interactions. *Biochem. Biophys. Reports* **10**, 318–324 (2017).
392. Shevchenko, G., Sjödin, M. O. D., Malmström, D., Wetterhall, M. & Bergquist, J. Cloud-point extraction and delipidation of porcine brain proteins in combination with bottom-up mass spectrometry approaches for proteome analysis. *J. Proteome Res.* **9**, 3903–3911 (2010).
393. Taguchi, Y. & Schätzl, H. M. Small-scale Triton X-114 Extraction of Hydrophobic Proteins. *Bio-protocol* **4**, (2014).
394. Çoker, M., de Klerk, J. B. C., Poll-The, B. T., Huijmans, J. G. M. & Duran, M. Plasma total odd-chain fatty acids in the monitoring of disorders of propionate, methylmalonate and biotin metabolism. *J. Inherit. Metab. Dis.* **19**, 743–751 (1996).
395. Phillips, G. B. & Dodge, J. T. Composition of phospholipids and of phospholipid fatty acids of human plasma. *J. Lipid Res.* **8**, 667–75 (1967).
396. P.J., N. *et al.* Specific plasma lipid classes and phospholipid fatty acids indicative of dairy food consumption associate with insulin sensitivity. *Am. J. Clin. Nutr.* **99**, 46–53 (2014).
397. Vlaeminck, B., Fievez, V., Cabrita, A. R. J., Fonseca, A. J. M. & Dewhurst, R. J. Factors affecting odd- and branched-chain fatty acids in milk: A review. *Anim. Feed Sci. Technol.* **131**, 389–417 (2006).
398. Choy, A. *et al.* The Legionella effector RavZ inhibits host autophagy through irreversible Atg8 deconjugation. *Science* **338**, 1072–1076 (2012).
399. Morgenstern, J. P. & Land, H. Advances mammalian gene transfer: high titre retroviral vectors with multiple drug selection markers and a complementary helper-free packaging cell line. *Nucleic Acids Res.* **18**, 3587–3596 (1990).
400. N'Diaye, E. N. *et al.* PLIC proteins or ubiquilins regulate autophagy-dependent

cell survival during nutrient starvation. *EMBO Rep.* **10**, 173–179 (2009).

401. C, C. F., Lock, R., Gao, S., Salas, E. & Debnath, L. Induction of autophagy during extracellular matrix detachment promotes cell survival. *Mol. Biol. Cell* **19**, 797–806 (2008).
402. Zhang, Z. & Marshall, A. G. A universal algorithm for fast and automated charge state deconvolution of electrospray mass-to-charge ratio spectra. *J. Am. Soc. Mass Spectrom.* **9**, 225–233 (1998).
403. SCOPES, R. K. Measurement of Protein by Spectrophotometry at 205 nm. *Anal. Biochem.* **59**, 277–252 (1974).
404. Filippova, Iy., Lysogorskaya, E., Oksenoit, E., Rudenskaya, G. & Stepanov, V. L-*Pyroglutamyl-L-phenylalanyl-L-leucine-p-nitroanilide*--a chromogenic substrate for thiol proteinase assay. *Anal. Biochem.* **143**, 293–297 (1984).





# ANNEXES



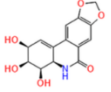
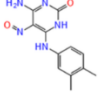
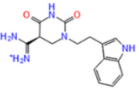
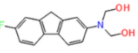
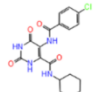
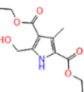
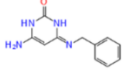
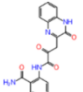
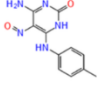
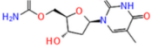
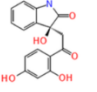
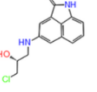
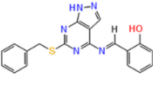
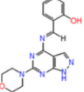
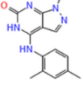
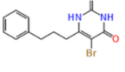
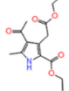
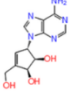
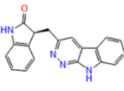
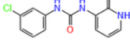
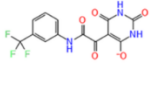
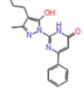
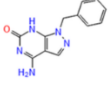
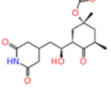
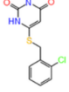
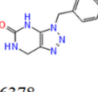
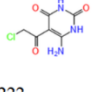
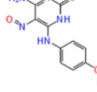
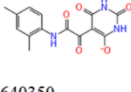
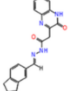
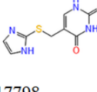
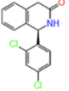
**Table 1.** Screened compounds from the NCI Open Database

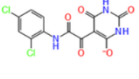
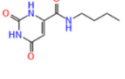
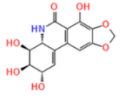
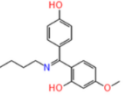
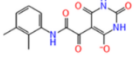
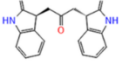
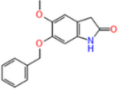
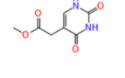
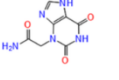
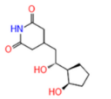
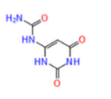
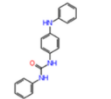
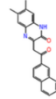
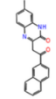
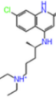
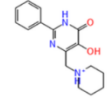
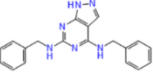
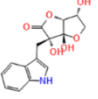
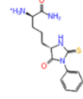
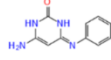
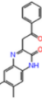
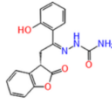
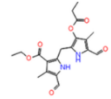
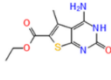
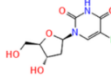
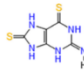
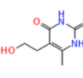
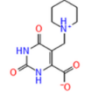
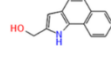
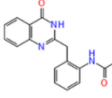
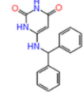
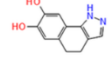
<b>NCI Compounds</b>	<b>Docking value</b>	<b>NCI Compounds</b>	<b>Docking value</b>	<b>NCI Compounds</b>	<b>Docking value</b>
<b>10768</b>	-10,994	<b>86286</b>	-10,467	<b>337734</b>	-7,685
<b>11614</b>	-9,228	<b>87042</b>	-8,900	<b>339180</b>	-7,105
<b>11966</b>	-7,648	<b>88860</b>	-9,108	<b>343971</b>	-7,111
<b>12155</b>	-7,254	<b>91309</b>	-8,345	<b>349155</b>	-11,651
<b>12270</b>	-7,289	<b>91408</b>	-10,521	<b>352709</b>	-9,219
<b>13004</b>	-7,509	<b>92542</b>	-7,579	<b>354315</b>	-10,000
<b>13449</b>	-8,687	<b>94498</b>	-7,901	<b>356826</b>	-8,800
<b>13718</b>	-7,124	<b>95027</b>	-8,054	<b>364277</b>	-8,700
<b>16737</b>	-7,731	<b>101685</b>	-9,494	<b>364435</b>	-7,335
<b>19142</b>	-10,306	<b>109325</b>	-7,884	<b>373049</b>	-9,404
<b>19148</b>	-9,491	<b>109327</b>	-7,986	<b>373058</b>	-9,522
<b>22907</b>	-7,286	<b>111285</b>	-9,307	<b>373058</b>	-9,522
<b>25353</b>	-8,800	<b>115535</b>	-7,770	<b>374818</b>	-9,100
<b>26692</b>	-9,204	<b>116384</b>	-10,155	<b>377095</b>	-8,446
<b>27640</b>	-9,335	<b>117829</b>	-7,882	<b>378143</b>	-9,300
<b>28570</b>	-7,637	<b>118071</b>	-8,725	<b>400842</b>	-9,600
<b>28570</b>	-7,637	<b>118950</b>	-9,568	<b>401011</b>	-7,237
<b>29189</b>	-9,310	<b>119608</b>	-8,094	<b>401299</b>	-9,300
<b>31075</b>	-9,300	<b>122883</b>	-8,600	<b>401397</b>	-7,445
<b>31166</b>	-9,200	<b>123301</b>	-9,597	<b>406291</b>	-9,499
<b>32743</b>	-9,904	<b>123301</b>	-9,597	<b>407632</b>	-9,400
<b>33565</b>	-9,093	<b>123355</b>	-8,600	<b>601826</b>	-7,136
<b>34318</b>	-7,288	<b>123403</b>	-7,528	<b>602693</b>	-8,900
<b>35843</b>	-9,500	<b>126353</b>	-9,847	<b>602695</b>	-9,683
<b>35847</b>	-8,700	<b>130898</b>	-7,675	<b>605767</b>	-7,879
<b>38094</b>	-9,365	<b>130898</b>	-7,675	<b>607743</b>	-9,302
<b>38094</b>	-9,365	<b>131354</b>	-9,100	<b>608628</b>	-9,230
<b>38280</b>	-9,000	<b>131684</b>	-8,375	<b>610501</b>	-9,157
<b>39225</b>	-8,891	<b>132830</b>	-7,538	<b>610936</b>	-9,417
<b>39265</b>	-9,760	<b>133357</b>	-9,000	<b>610936</b>	-9,417
<b>41527</b>	-8,601	<b>141058</b>	-11,099	<b>612216</b>	-9,221
<b>43949</b>	-9,406	<b>142537</b>	-8,900	<b>613315</b>	-7,500
<b>45723</b>	-9,901	<b>143347</b>	-7,782	<b>617744</b>	-9,490

NCI Compounds	Docking value	NCI Compounds	Docking value	NCI Compounds	Docking value
45818	-9,259	147893	-7,492	617794	-8,600
48443	-7,805	149051	-9,204	617798	-9,831
48454	-7,135	149898	-9,625	618679	-8,600
48687	-8,134	151802	-9,500	621178	-10,499
48870	-8,259	152439	-8,584	621453	-9,683
50469	-9,500	153540	-7,716	622937	-9,942
51187	-8,800	157286	-10,244	624948	-11,073
51646	-7,951	162039	-7,355	625255	-7,255
51654	-7,819	164414	-9,553	625381	-8,661
51661	-7,759	171131	-8,800	636783	-9,200
52389	-9,302	173352	-9,623	637876	-9,612
52444	-9,233	186031	-10,096	640349	-9,675
52643	-7,116	186258	-9,647	640350	-9,853
53312	-7,188	201602	-8,700	645017	-8,647
55143	-7,416	211381	-10,244	646366	-9,782
55982	-10,558	211608	-9,409	646375	-10,077
57148	-9,600	211608	-9,409	646380	-10,579
57153	-8,800	212407	-10,789	648585	-9,397
58479	-9,400	212407	-10,789	648585	-9,397
58480	-9,500	212412	-9,249	652564	-8,163
62494	-11,556	241470	-10,200	656991	-11,170
62495	-9,864	241572	-9,000	658245	-7,315
63271	-8,900	250293	-8,058	658620	-9,354
63688	-8,800	251209	-9,248	664569	-7,323
63688	-8,800	261042	-7,664	664724	-9,971
63696	-9,400	261042	-7,664	667758	-7,573
65372	-9,400	279836	-9,857	669720	-8,731
66761	-9,100	281913	-7,303	677285	-10,009
66785	-7,834	282125	-7,728	680919	-8,926
67734	-9,300	282456	-7,942	681167	-8,600
67737	-8,800	290111	-9,100	681168	-8,600
70393	-7,607	293888	-8,707	681604	-9,000
71204	-9,700	296330	-8,600	704320	-9,200
73607	-8,700	299187	-8,640	708458	-7,135

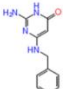
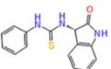
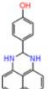
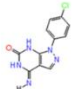
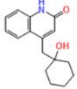
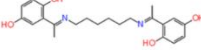
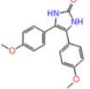
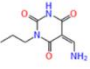
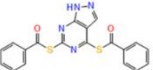
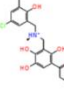
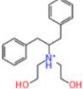
<b>NCI Compounds</b>	<b>Docking value</b>	<b>NCI Compounds</b>	<b>Docking value</b>	<b>NCI Compounds</b>	<b>Docking value</b>
<b>73849</b>	-9,200	<b>310191</b>	-9,791	<b>717956</b>	-9,500
<b>74105</b>	-7,131	<b>316458</b>	-10,178	<b>722944</b>	-9,189
<b>75329</b>	-9,400	<b>320866</b>	-9,100	<b>723574</b>	-9,363
<b>79222</b>	-9,867	<b>322921</b>	-8,700	<b>723574</b>	-9,363
<b>80117</b>	-9,100	<b>326057</b>	-7,228	<b>724949</b>	-10,389
<b>80362</b>	-8,800	<b>327396</b>	-8,032	<b>725602</b>	-7,251
<b>80965</b>	-7,438	<b>328107</b>	-7,730	<b>725687</b>	-8,800
<b>81537</b>	-8,436	<b>329254</b>	-10,084	<b>725687</b>	-10,353
<b>83458</b>	-9,500	<b>330687</b>	-9,200	<b>728031</b>	-9,000
<b>83713</b>	-9,229	<b>336378</b>	-9,880		
<b>84389</b>	-7,245	<b>337734</b>	-7,685		

**Table 2.** Structures of the compounds from the NCI Open Database selected by HTVS against the active site of Atg4B (**Glide VS 2 ZPP**). Compounds are depicted as the stereoisomer/tautomer/protomer state selected by the docking procedure.

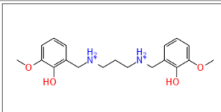
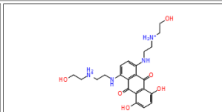
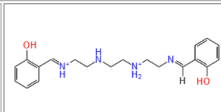
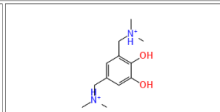
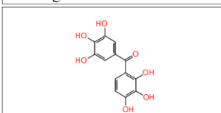
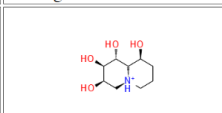
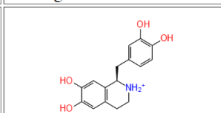
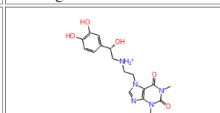
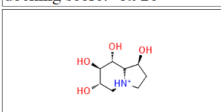
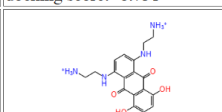
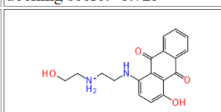
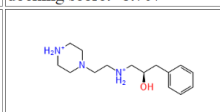
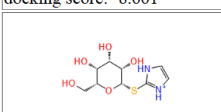
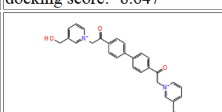
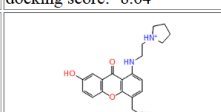
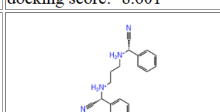
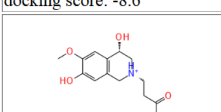
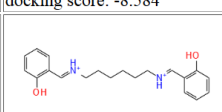
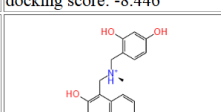
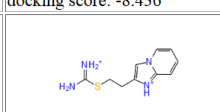
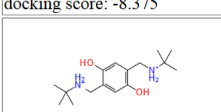
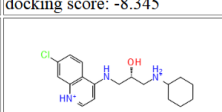
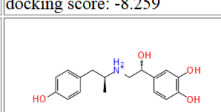
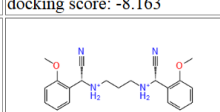
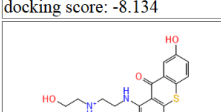
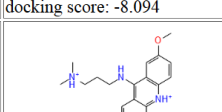
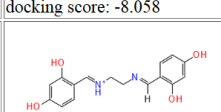
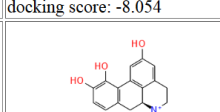
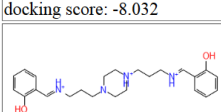
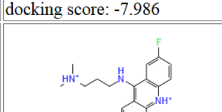
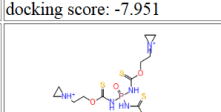
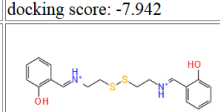
 NSC: 349155 docking score: -11.651	 NSC: 62494 docking score: -11.556	 NSC: 656991 docking score: -11.17	 NSC: 141058 docking score: -11.099
 NSC: 624948 docking score: -11.073	 NSC: 10768 docking score: -10.994	 NSC: 212407 docking score: -10.789	 NSC: 646380 docking score: -10.579
 NSC: 55982 docking score: -10.558	 NSC: 91408 docking score: -10.521	 NSC: 621178 docking score: -10.499	 NSC: 611216 docking score: -10.496
 NSC: 724949 docking score: -10.389	 NSC: 725687 docking score: -10.353	 NSC: 19142 docking score: -10.306	 NSC: 211381 docking score: -10.244
 NSC: 157286 docking score: -10.244	 NSC: 316458 docking score: -10.178	 NSC: 186031 docking score: -10.096	 NSC: 329254 docking score: -10.084
 NSC: 646375 docking score: -10.077	 NSC: 664724 docking score: -9.971	 NSC: 622937 docking score: -9.942	 NSC: 32743 docking score: -9.904
 NSC: 45723 docking score: -9.901	 NSC: 336378 docking score: -9.88	 NSC: 79222 docking score: -9.867	 NSC: 62495 docking score: -9.864
 NSC: 640350 docking score: -9.853	 NSC: 126353 docking score: -9.847	 NSC: 617798 docking score: -9.831	 NSC: 310191 docking score: -9.791

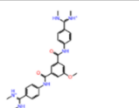
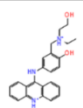
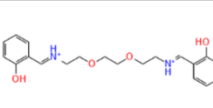
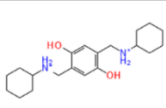
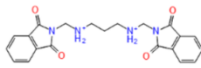
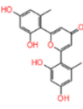
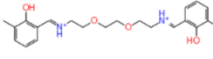
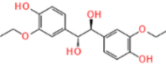
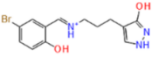
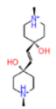
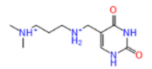
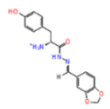
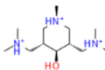
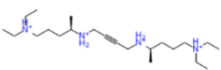
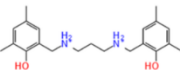
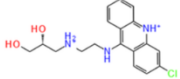
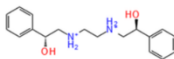
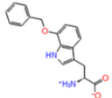
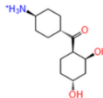
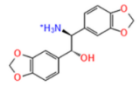
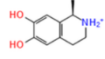
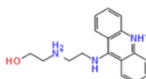
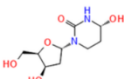
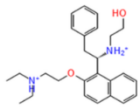
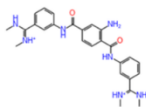
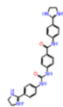
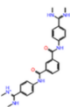
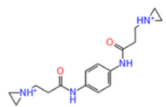
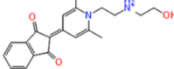
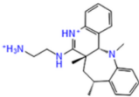
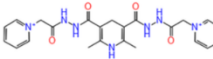
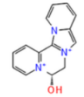
 NSC: 646366 docking score: -9.782	 NSC: 39265 docking score: -9.76	 NSC: 266535 docking score: -9.726	 NSC: 602695 docking score: -9.683
 NSC: 640349 docking score: -9.675	 NSC: 186258 docking score: -9.647	 NSC: 149898 docking score: -9.625	 NSC: 173352 docking score: -9.623
 NSC: 637876 docking score: -9.612	 NSC: 123301 docking score: -9.597	 NSC: 118950 docking score: -9.568	 NSC: 164414 docking score: -9.553
 NSC: 373050 docking score: -9.526	 NSC: 373058 docking score: -9.522	 NSC: 406291 docking score: -9.499	 NSC: 101685 docking score: -9.494
 NSC: 19148 docking score: -9.491	 NSC: 617744 docking score: -9.49	 NSC: 610936 docking score: -9.417	 NSC: 211608 docking score: -9.409
 NSC: 373049 docking score: -9.404	 NSC: 648585 docking score: -9.397	 NSC: 38094 docking score: -9.365	 NSC: 723574 docking score: -9.363
 NSC: 27640 docking score: -9.335	 NSC: 29189 docking score: -9.31	 NSC: 111285 docking score: -9.307	 NSC: 52389 docking score: -9.302
 NSC: 607743 docking score: -9.302	 NSC: 401299 docking score: -9.3	 NSC: 212412 docking score: -9.249	 NSC: 251209 docking score: -9.248

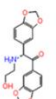
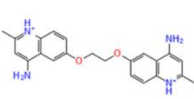
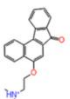
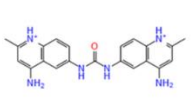
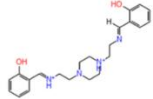
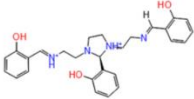
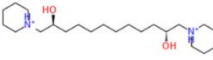
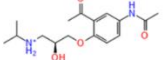
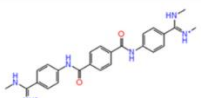
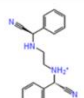
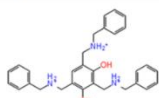
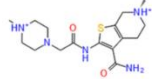
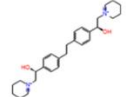
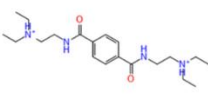
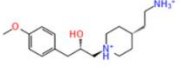
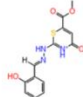
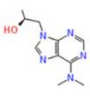


 <p>NSC: 52444 docking score: -9.233</p>	 <p>NSC: 608628 docking score: -9.23</p>	 <p>NSC: 83713 docking score: -9.229</p>	 <p>NSC: 11614 docking score: -9.228</p>
 <p>NSC: 612216 docking score: -9.221</p>	 <p>NSC: 352709 docking score: -9.219</p>	 <p>NSC: 26692 docking score: -9.204</p>	 <p>NSC: 149051 docking score: -9.204</p>
 <p>NSC: 722944 docking score: -9.189</p>	 <p>NSC: 88860 docking score: -9.108</p>	 <p>NSC: 33565 docking score: -9.093</p>	

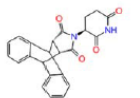
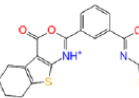
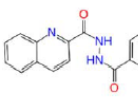
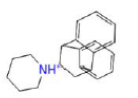
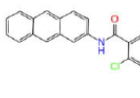
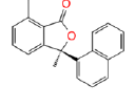
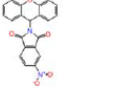
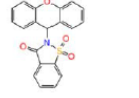
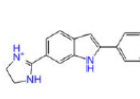
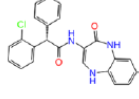
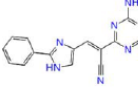
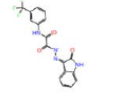
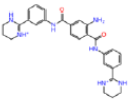
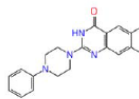
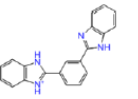
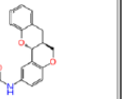
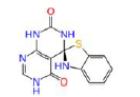
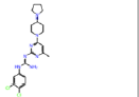
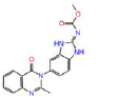
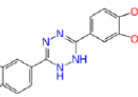
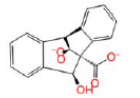
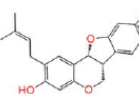
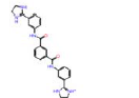
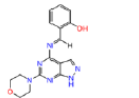
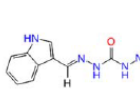
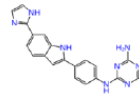
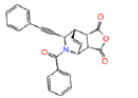
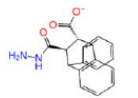
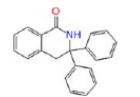
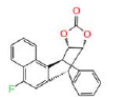
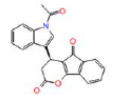
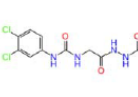
**Table 3.** Structures of the compounds from the NCI Open Database selected by HTVS against the second alternative site of Atg4B (**Glide VS 2CY7**). Compounds are depicted as the stereoisomer/tautomer/protomer state selected by the docking procedure.

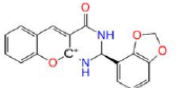
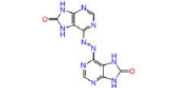
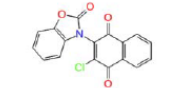
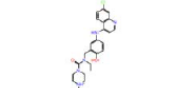
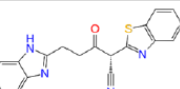
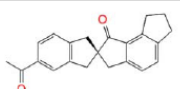
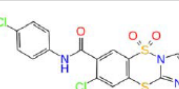
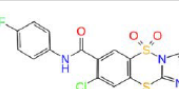
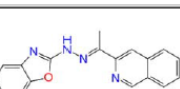
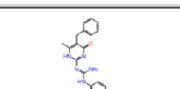
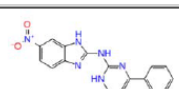
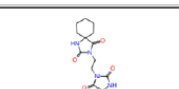
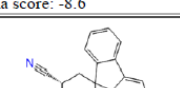
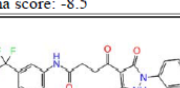
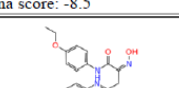
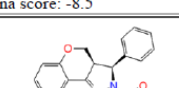
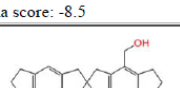
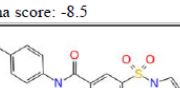
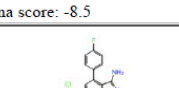
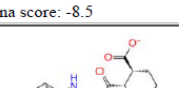
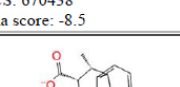
 NSC: 86286 docking score: -10.467	 NSC: 279836 docking score: -9.857	 NSC: 43949 docking score: -9.406	 NSC: 39225 docking score: -8.981
 NSC: 680919 docking score: -8.926	 NSC: 669720 docking score: -8.731	 NSC: 118071 docking score: -8.725	 NSC: 293888 docking score: -8.707
 NSC: 625381 docking score: -8.661	 NSC: 645017 docking score: -8.647	 NSC: 299187 docking score: -8.64	 NSC: 41527 docking score: -8.601
 NSC: 617794 docking score: -8.6	 NSC: 152439 docking score: -8.584	 NSC: 377095 docking score: -8.446	 NSC: 81537 docking score: -8.436
 NSC: 131684 docking score: -8.375	 NSC: 91309 docking score: -8.345	 NSC: 48870 docking score: -8.259	 NSC: 652564 docking score: -8.163
 NSC: 48687 docking score: -8.134	 NSC: 119608 docking score: -8.094	 NSC: 250293 docking score: -8.058	 NSC: 95027 docking score: -8.054
 NSC: 327396 docking score: -8.032	 NSC: 109327 docking score: -7.986	 NSC: 51646 docking score: -7.951	 NSC: 282456 docking score: -7.942
 NSC: 94498 docking score: -7.901	 NSC: 109325 docking score: -7.884	 NSC: 117829 docking score: -7.882	 NSC: 605767 docking score: -7.879

 NSC: 66785 docking score: -7.834	 NSC: 12270 docking score: -7.829	 NSC: 51654 docking score: -7.819	 NSC: 48443 docking score: -7.805
 NSC: 143347 docking score: -7.782	 NSC: 115535 docking score: -7.777	 NSC: 51661 docking score: -7.759	 NSC: 16737 docking score: -7.731
 NSC: 328107 docking score: -7.73	 NSC: 282125 docking score: -7.728	 NSC: 153540 docking score: -7.716	 NSC: 337734 docking score: -7.685
 NSC: 130898 docking score: -7.675	 NSC: 261042 docking score: -7.664	 NSC: 11966 docking score: -7.648	 NSC: 28570 docking score: -7.637
 NSC: 70393 docking score: -7.607	 NSC: 92542 docking score: -7.579	 NSC: 667758 docking score: -7.573	 NSC: 132830 docking score: -7.538
 NSC: 123403 docking score: -7.528	 NSC: 13004 docking score: -7.509	 NSC: 613315 docking score: -7.5	 NSC: 401397 docking score: -7.445
 NSC: 80965 docking score: -7.438	 NSC: 63688 docking score: -7.437	 NSC: 55143 docking score: -7.416	 NSC: 162039 docking score: -7.355
 NSC: 364435 docking score: -7.335	 NSC: 664569 docking score: -7.323	 NSC: 658245 docking score: -7.315	 NSC: 281913 docking score: -7.303

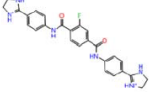
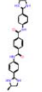
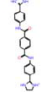
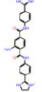
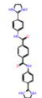
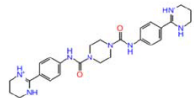
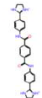
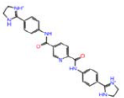
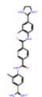
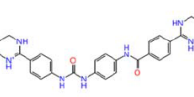
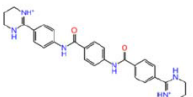
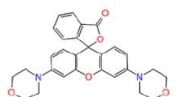
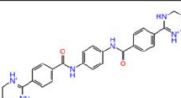
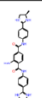
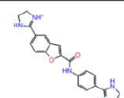
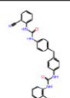
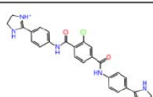
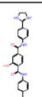
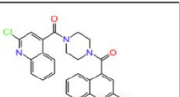
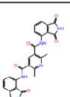
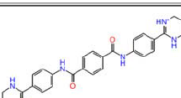
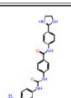
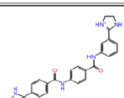
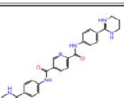
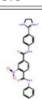
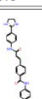
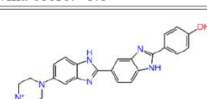
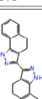
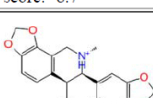
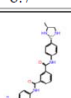
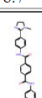
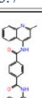
 NSC: 34318 docking score: -7.288	 NSC: 22907 docking score: -7.286	 NSC: 625255 docking score: -7.255	 NSC: 12155 docking score: -7.254
 NSC: 725602 docking score: -7.251	 NSC: 84389 docking score: -7.245	 NSC: 401011 docking score: -7.237	 NSC: 326057 docking score: -7.228
 NSC: 53312 docking score: -7.188	 NSC: 601826 docking score: -7.136	 NSC: 48454 docking score: -7.135	 NSC: 708458 docking score: -7.135
 NSC: 74105 docking score: -7.131	 NSC: 13718 docking score: -7.124	 NSC: 52643 docking score: -7.116	 NSC: 343971 docking score: -7.111
 NSC: 339180 docking score: -7.105			

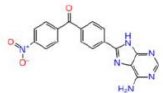
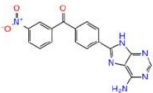
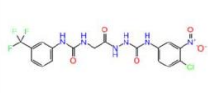
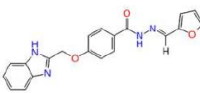
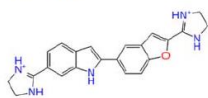
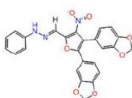
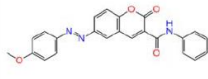
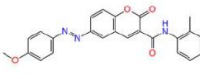
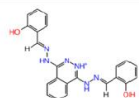
**Table 4.** Structures of the compounds from the NCI Open Database selected by HTVS against the second alternative site of Atg4B (**Vina VS 2ZZP**). Compounds are depicted as the stereoisomer/tautomer/protomer state selected by the docking procedure.

 NCS: 241470 vina score: -10.2	 NCS: 354315 vina score: -10.0	 NCS: 400842 vina score: -9.6	 NCS: 151802 vina score: -9.5
 NCS: 717956 vina score: -9.5	 NCS: 407632 vina score: -9.4	 NCS: 31075 vina score: -9.3	 NCS: 31166 vina score: -9.2
 NCS: 330687 vina score: -9.2	 NCS: 636783 vina score: -9.2	 NCS: 704320 vina score: -9.2	 NCS: 320866 vina score: -9.1
 NCS: 80117 vina score: -9.1	 NCS: 131354 vina score: -9.0	 NCS: 133357 vina score: -9.0	 NCS: 681604 vina score: -9.0
 NCS: 728031 vina score: -9.0	 NCS: 142537 vina score: -8.9	 NCS: 602693 vina score: -8.9	 NCS: 171131 vina score: -8.8
 NCS: 25353 vina score: -8.8	 NCS: 356826 vina score: -8.8	 NCS: 51187 vina score: -8.8	 NCS: 725687 vina score: -8.8
 NCS: 201602 vina score: -8.7	 NCS: 364277 vina score: -8.7	 NCS: 73607 vina score: -8.7	 NCS: 122883 vina score: -8.6
 NCS: 123355 vina score: -8.6	 NCS: 168901 vina score: -8.6	 NCS: 208736 vina score: -8.6	 NCS: 217041 vina score: -8.6

 NCS: 263638 vina score: -8.6	 NCS: 296330 vina score: -8.6	 NCS: 322341 vina score: -8.6	 NCS: 357891 vina score: -8.6
 NCS: 618679 vina score: -8.6	 NCS: 677009 vina score: -8.6	 NCS: 681167 vina score: -8.6	 NCS: 681168 vina score: -8.6
 NCS: 693638 vina score: -8.6	 NCS: 141099 vina score: -8.5	 NCS: 157308 vina score: -8.5	 NCS: 264074 vina score: -8.5
 NCS: 60502 vina score: -8.5	 NCS: 631817 vina score: -8.5	 NCS: 646377 vina score: -8.5	 NCS: 652810 vina score: -8.5
 NCS: 670438 vina score: -8.5	 NCS: 681166 vina score: -8.5	 NCS: 734133 vina score: -8.5	 NCS: 95666 vina score: -8.5
 NCS: 22090 vina score: -8.5			

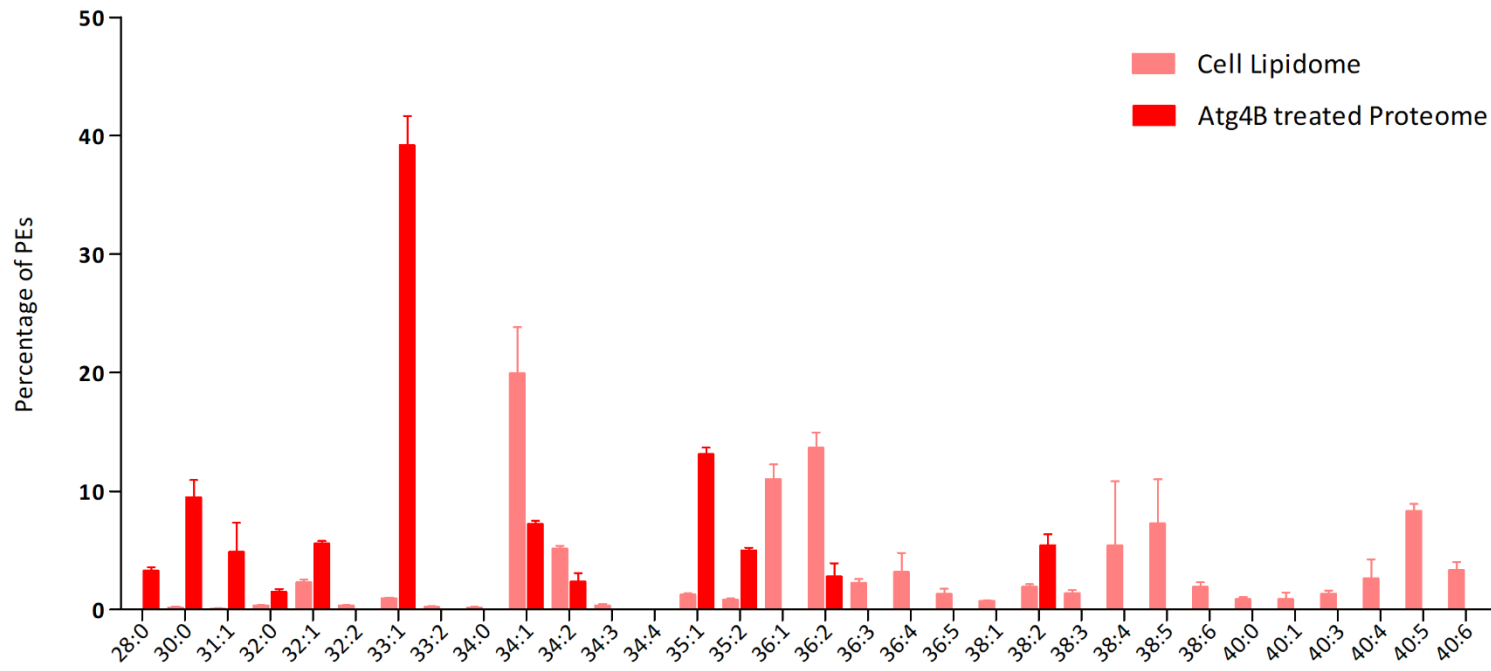
**Table 5.** Structures of the compounds from the NCI Open Database selected by HTVS against the second alternative site of Atg4B (**Vina VS 2CY7**). Compounds are depicted as the stereoisomer/tautomer/protomer state selected by the docking procedure.

 NCS: 71204 vina score: -9.7	 NCS: 57148 vina score: -9.6	 NCS: 35843 vina score: -9.5	 NCS: 50469 vina score: -9.5
 NCS: 58480 vina score: -9.5	 NCS: 83458 vina score: -9.5	 NCS: 58479 vina score: -9.4	 NCS: 63696 vina score: -9.4
 NCS: 65372 vina score: -9.4	 NCS: 75329 vina score: -9.4	 NCS: 67734 vina score: -9.3	 NCS: 378143 vina score: -9.3
 NCS: 73849 vina score: -9.2	 NCS: 66761 vina score: -9.1	 NCS: 290111 vina score: -9.1	 NCS: 374818 vina score: -9.1
 NCS: 241572 vina score: -9.0	 NCS: 63271 vina score: -8.9	 NCS: 87042 vina score: -8.9	 NCS: 658260 vina score: -8.9
 NCS: 57153 vina score: -8.8	 NCS: 63688 vina score: -8.8	 NCS: 67737 vina score: -8.8	 NCS: 80362 vina score: -8.8
 NCS: 35847 vina score: -8.7	 NCS: 65375 vina score: -8.7	 NCS: 322921 vina score: -8.7	 NCS: 371869 vina score: -8.7
 NCS: 406034 vina score: -8.7	 NCS: 57149 vina score: -8.6	 NCS: 66757 vina score: -8.6	 NCS: 110318 vina score: -8.6

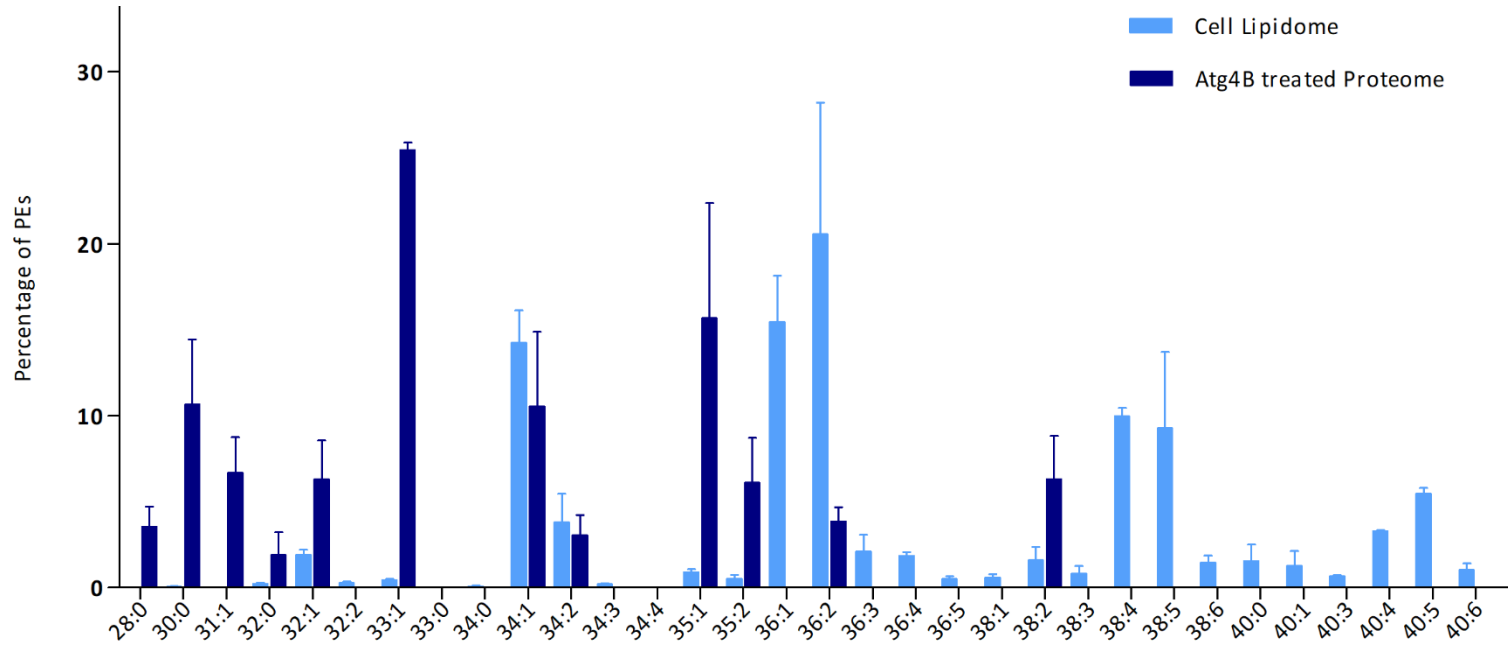
 <p>NCS: 210294 vina score: -8.6</p>	 <p>NCS: 210305 vina score: -8.6</p>	 <p>NCS: 217031 vina score: -8.6</p>	 <p>NCS: 348965 vina score: -8.6</p>
 <p>NCS: 369716 vina score: -8.6</p>	 <p>NCS: 647257 vina score: -8.6</p>	 <p>NCS: 662450 vina score: -8.6</p>	 <p>NCS: 662451 vina score: -8.6</p>
 <p>NCS: 103647 vina score: -8.5</p>			



**Figure 1.** Obtained PEs from two different procedures in HEK293. PEs found from total lipidome extraction are represented in light red. PEs found after precipitation of the proteome followed by N-(His)<sub>6</sub>-3C-Atg4B treatment are represented in dark red.



**Figure 2.** Obtained PEs from two different procedures in SH-SY5Y. PEs found from total lipidome extraction are represented in light blue. PEs found after precipitation of the proteome followed by N-(His)<sub>6</sub>-3C-Atg4B treatment are represented in dark blue.



**Figure 3.** PEs from Hek293 cells overexpressing GFP-LC3B stably transfected by cationic lipid transfection (pOPIN-GFP-LC3B) or viral transfection (pBABE-GFP-LC3B). PEs were obtained through immunoprecipitation of GFP-LC3B employing GFP antibody followed by N-(His)<sub>6</sub>-3C-Atg4B treatment and lipid extraction with cold acetone. Negative controls with untreated samples by N-(His)<sub>6</sub>-3C-Atg4B were included. Internal standard was added for the quantification. Results are expressed as percentages of total PEs quantified in each sample.

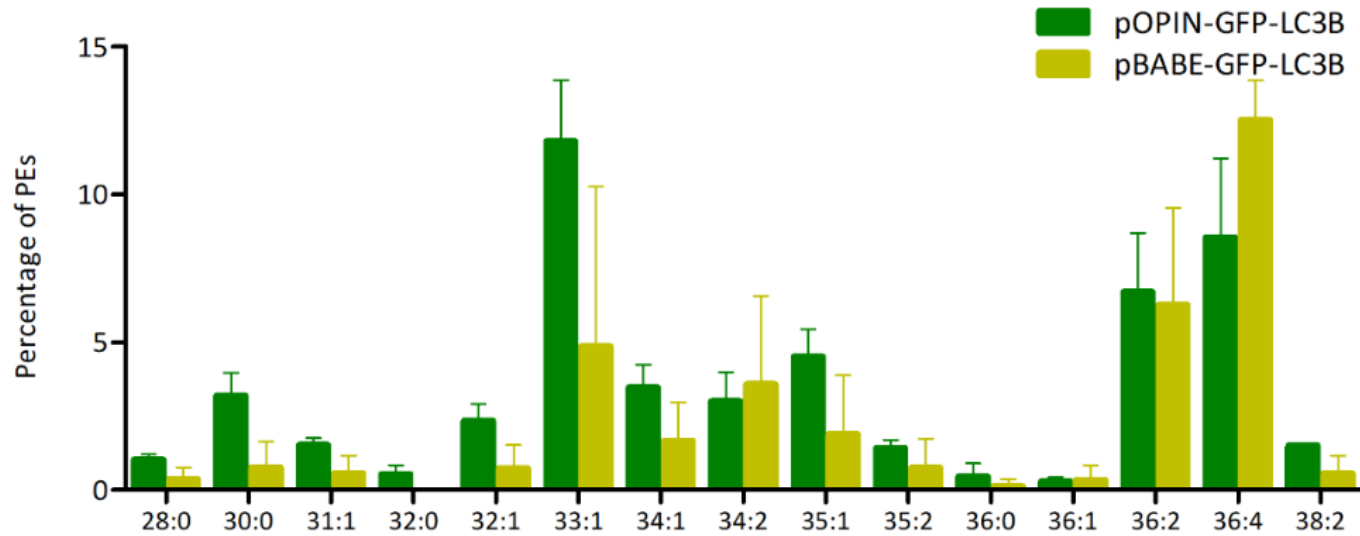


Table 6. Quantified PEs from HeLa cells. The lipids were obtained through precipitation of the proteome, treatment with N-(His)<sub>6</sub>-3C-Atg4B and extraction by organic solvents.

Class	Lipid	Calc. Mass. [M+H] <sup>-</sup>	Found Mass. [M+H] <sup>-</sup>	RT (min)	Area			Conc. (pmol/sample)			HeLa (n=3)		
					HeLa_1	HeLa_2	HeLa_3	HeLa_1	HeLa_2	HeLa_3	Mean	SD	%CV
PE	Std	747.7176	747.7162	6.13	131	193	182	200.0	200.0	200.0	200.0	0.0	0.0
PE	28:0	634.4448	634.4440	3.68	17	29	26	26.0	30.1	28.6	28.2	2.1	7.0
PE	30:0	662.4766	662.4760	4.73	38	60	43	58.0	62.2	47.3	55.8	7.7	14.0
PE	31:1	674.4766	674.4758	4.47	19	25	22	29.0	25.9	24.2	26.4	2.4	9.0
PE	32:0	690.5074	690.5064	6.14	6	7	10	9.2	7.3	11.0	9.1	1.9	20.0
PE	32:1	688.4920	688.4922	4.90	46	53	45	70.2	54.9	49.5	58.2	10.8	19.0
PE	32:2	686.4760	nd	nd	nd	nd	nd	nd	nd	nd	nd	nd	nd
PE	33:1	702.5079	702.5089	5.78	83	117	105	126.7	121.2	115.4	121.1	8.0	7.0
PE	34:0	718.5387	718.5280	6.26	nd	nd	nd	nd	nd	nd	nd	nd	nd
PE	34:1	716.5230	716.5222	6.32	222	220	178	338.9	228.0	195.6	254.2	75.2	30.0
PE	34:2	714.5074	714.5063	5.02	28	27	22	42.7	28.0	24.2	31.6	9.8	31.0
PE	34:2	714.5074	714.5090	5.44	5	5	4	7.6	5.2	4.4	5.7	1.7	29.0
PE	34:3	712.4918	nd	nd	nd	nd	nd	nd	nd	nd	nd	nd	nd
PE	34:4	710.4761	nd	nd	nd	nd	nd	nd	nd	nd	nd	nd	nd
PE	35:2	728.5236	728.5239	5.88	29	41	34	44.3	42.5	37.4	41.4	3.6	9.0
PE	35:1	730.5392	730.5368	7.52	73	102	95	111.5	105.7	104.4	107.2	3.8	4.0
PE	36:0	746.5700	nd	nd	nd	nd	nd	nd	nd	nd	nd	nd	nd
PE	36:1	744.5543	744.5518	8.29	133	118	84	203.1	122.3	92.3	139.2	57.3	41.0
PE	36:2	742.5387	742.5381	6.50	135	114	94	206.1	118.1	103.3	142.5	55.6	39.0
PE	36:2	742.5387	742.5373	7.08	25	27	22	38.2	28.0	24.2	30.1	7.2	24.0
PE	36:3	740.5230	nd	nd	nd	nd	nd	nd	nd	nd	nd	nd	nd
PE	36:4	738.5074	nd	nd	nd	nd	nd	nd	nd	nd	nd	nd	nd
PE	36:5	736.4918	nd	nd	nd	nd	nd	nd	nd	nd	nd	nd	nd
PE	36:6	734.4761	nd	nd	nd	nd	nd	nd	nd	nd	nd	nd	nd
PE	38:0	774.6013	nd	nd	nd	nd	nd	nd	nd	nd	nd	nd	nd
PE	38:1	772.5956	nd	nd	nd	nd	nd	nd	nd	nd	nd	nd	nd
PE	38:2	770.5700	770.5683	9.19	11	17	15	16.8	17.6	16.5	17.0	0.6	3.0

Class	Lipid	Calc. Mass. [M+H]-	Found Mass. [M+H]-	RT (min)	Area			Conc. (pmol/sample)			HeLa (n=3)		
					HeLa_1	HeLa_2	HeLa_3	HeLa_1	HeLa_2	HeLa_3	Mean	SD	%CV
PE	38:3	768.5543	nd	nd	nd	nd	nd	nd	nd	nd	nd	nd	nd
PE	38:4	766.5390	766.5392	6.46	68	62	48	103.8	64.2	52.7	73.6	26.8	36.0
PE	38:5	764.5230	nd	nd	nd	nd	nd	nd	nd	nd	nd	nd	nd
PE	38:6	762.5070	nd	nd	nd	nd	nd	nd	nd	nd	nd	nd	nd
PE	38:7	760.4918	nd	nd	nd	nd	nd	nd	nd	nd	nd	nd	nd
PE	40:0	802.6320	nd	nd	nd	nd	nd	nd	nd	nd	nd	nd	nd
PE	40:1	800.6169	nd	nd	nd	nd	nd	nd	nd	nd	nd	nd	nd
PE	40:2	798.6013	nd	nd	nd	nd	nd	nd	nd	nd	nd	nd	nd
PE	40:3	796.5856	nd	nd	nd	nd	nd	nd	nd	nd	nd	nd	nd
PE	40:4	794.5700	nd	nd	nd	nd	nd	nd	nd	nd	nd	nd	nd
PE	40:5	792.5543	nd	nd	nd	nd	nd	nd	nd	nd	nd	nd	nd
PE	40:6	790.5387	nd	nd	nd	nd	nd	nd	nd	nd	nd	nd	nd
PE	40:7	788.5230	nd	nd	nd	nd	nd	nd	nd	nd	nd	nd	nd

Table 7. Quantified PEs from HeLa cells. The lipids were obtained through precipitation of the proteome, treatment with N-(His)<sub>6</sub>-3C-Atg4B and extraction by organic solvents.

- Atg4														
Class	Lipid	Calc. Mass. [M+H]-	Found Mass. [M+H]-	RT (min)	Area			Conc. (pmol/sample)			HeLa (n=3)			
					HeLa_1	HeLa_2	HeLa_3	HeLa_1	HeLa_2	HeLa_3	Mean	SD	%CV	
PE	Std	747.7176	747.7201	9.18	275	285	205	200.0	200.0	200.0	200.0	0.0	0.0	
PE	28:0	634.4448	nd	nd	nd	nd	nd	nd	nd	nd	nd	nd	nd	
PE	30:0	662.4761	nd	nd	nd	nd	nd	nd	nd	nd	nd	nd	nd	
PE	31:0	676.4918	nd	nd	nd	nd	nd	nd	nd	nd	nd	nd	nd	
PE	31:1	674.4761	nd	nd	nd	nd	nd	nd	nd	nd	nd	nd	nd	
PE	32:0	690.5074	nd	nd	nd	nd	nd	nd	nd	nd	nd	nd	nd	

- Atg4													
Class	Lipid	Calc. Mass. [M+H]-	Found Mass. [M+H]-	RT (min)	Area			Conc. (pmol/sample)			HeLa (n=3)		
					HeLa_1	HeLa_2	HeLa_3	HeLa_1	HeLa_2	HeLa_3	Mean	SD	%CV
PE	32:1	688.4920	nd	nd	nd	nd	nd	nd	nd	nd	nd	nd	nd
PE	32:2	686.4760	nd	nd	nd	nd	nd	nd	nd	nd	nd	nd	nd
PE	32:3	684.4604	nd	nd	nd	nd	nd	nd	nd	nd	nd	nd	nd
PE	33:0	704.5230	nd	nd	nd	nd	nd	nd	nd	nd	nd	nd	nd
PE	33:1	702.5074	nd	nd	nd	nd	nd	nd	nd	nd	nd	nd	nd
PE	33:2	700.4918	nd	nd	nd	nd	nd	nd	nd	nd	nd	nd	nd
PE	33:3	698.4761	nd	nd	nd	nd	nd	nd	nd	nd	nd	nd	nd
PE	34:0	718.5387	nd	nd	nd	nd	nd	nd	nd	nd	nd	nd	nd
PE	34:1	716.5230	716.5266	9.33	15	7	7	10.9	4.9	6.8	7.6	2.5	33.1
PE	34:2	714.5074	714.5011	8.39	4	nd	nd	2.9	nd	nd	2.9	0.0	0.0
PE	34:3	712.4918	nd	nd	nd	nd	nd	nd	nd	nd	nd	nd	nd
PE	34:4	710.4761	nd	nd	nd	nd	nd	nd	nd	nd	nd	nd	nd
PE	35:0	732.5542	nd	nd	nd	nd	nd	nd	nd	nd	nd	nd	nd
PE	35:1	730.5387	nd	nd	nd	nd	nd	nd	nd	nd	nd	nd	nd
PE	35:2	728.5230	nd	nd	nd	nd	nd	nd	nd	nd	nd	nd	nd
PE	36:0	746.5700	nd	nd	nd	nd	nd	nd	nd	nd	nd	nd	nd
PE	36:1	744.5543	744.5506	10.62	20	7	nd	14.5	4.9	nd	9.7	4.8	49.5
PE	36:2	742.5387	742.5393	9.68	22	13	8	16.0	9.1	7.8	11.0	3.6	32.7
PE	36:3	740.5230	nd	nd	nd	nd	nd	nd	nd	nd	nd	nd	nd
PE	36:4	738.5074	nd	nd	nd	nd	nd	nd	nd	nd	nd	nd	nd
PE	36:5	736.4918	nd	nd	nd	nd	nd	nd	nd	nd	nd	nd	nd
PE	36:6	734.4761	nd	nd	nd	nd	nd	nd	nd	nd	nd	nd	nd
PE	38:0	774.6013	nd	nd	nd	nd	nd	nd	nd	nd	nd	nd	nd
PE	38:1	772.5856	nd	nd	nd	nd	nd	nd	nd	nd	nd	nd	nd
PE	38:2	770.5700	nd	nd	nd	nd	nd	nd	nd	nd	nd	nd	nd
PE	38:3	768.5543	nd	nd	nd	nd	nd	nd	nd	nd	nd	nd	nd
PE	38:4	766.5390	766.5369	9.80	19	nd	4	13.8	nd	3.9	8.9	5.0	56.0
PE	38:5	764.5230	nd	nd	nd	nd	nd	nd	nd	nd	nd	nd	nd

- Atg4													
Class	Lipid	Calc. Mass. [M+H]-	Found Mass. [M+H]-	RT (min)	Area			Conc. (pmol/sample)			HeLa (n=3)		
					HeLa_1	HeLa_2	HeLa_3	HeLa_1	HeLa_2	HeLa_3	Mean	SD	%CV
PE	38:6	762.5070	nd	nd	nd	nd	nd	nd	nd	nd	nd	nd	nd
PE	38:7	760.4918	nd	nd	nd	nd	nd	nd	nd	nd	nd	nd	nd
PE	40:0	800.6169	nd	nd	nd	nd	nd	nd	nd	nd	nd	nd	nd
PE	40:1	798.6013	nd	nd	nd	nd	nd	nd	nd	nd	nd	nd	nd
PE	40:2	796.5856	nd	nd	nd	nd	nd	nd	nd	nd	nd	nd	nd
PE	40:3	794.5700	nd	nd	nd	nd	nd	nd	nd	nd	nd	nd	nd
PE	40:4	792.5543	nd	nd	nd	nd	nd	nd	nd	nd	nd	nd	nd
PE	40:5	790.5387	790.5430	9.62	6	nd	1	4.4	nd	1.0	2.7	1.7	63.5
PE	40:6	788.5230	nd	nd	nd	nd	nd	nd	nd	nd	nd	nd	nd
PE	40:8	786.5074	nd	nd	nd	nd	nd	nd	nd	nd	nd	nd	nd
PE	44:2	852.6483	nd	nd	nd	nd	nd	nd	nd	nd	nd	nd	nd
PE	44:12	834.5074	nd	nd	nd	nd	nd	nd	nd	nd	nd	nd	nd
+ Atg4													
Class	Lipid	Calc. Mass. [M+H]-	Found Mass. [M+H]-	RT (min)	Area			Conc. (pmol/sample)			HeLa (n=3)		
					HeLa_1	HeLa_2	HeLa_3	HeLa_1	HeLa_2	HeLa_3	Mean	SD	%CV
PE	Std	747.7176	747.7122	9.21	258	266	234	200.0	200.0	200.0	200.0	0.0	0.0
PE	28:0	634.4448	634.4415	6.10	13	19	16	10.1	14.3	13.7	12.7	1.9	14.6
PE	30:0	662.4761	662.4739	7.45	33	55	48	25.6	41.4	41.0	36.0	7.4	20.4
PE	31:0	676.4918	nd	nd	nd	nd	nd	nd	nd	nd	nd	nd	nd
PE	31:1	674.4761	674.4722	7.36	21	32	29	16.3	24.1	24.8	21.7	3.9	17.7
PE	32:0	690.5074	690.5115	8.86	7	9	8	5.4	6.8	6.8	6.3	0.6	10.2
PE	32:1	688.4920	688.4959	7.89	21	31	30	16.3	23.3	25.6	21.7	4.0	18.3
PE	32:2	686.4760	nd	nd	nd	nd	nd	nd	nd	nd	nd	nd	nd
PE	32:3	684.4604	nd	nd	nd	nd	nd	nd	nd	nd	nd	nd	nd
PE	33:0	704.5230	nd	nd	nd	nd	nd	nd	nd	nd	nd	nd	nd
PE	33:1	702.5074	702.5049	8.74	148	183	141	114.7	137.6	120.5	124.3	9.7	7.8
PE	33:2	700.4918	nd	nd	nd	nd	nd	nd	nd	nd	nd	nd	nd
PE	33:3	698.4761	nd	nd	nd	nd	nd	nd	nd	nd	nd	nd	nd
PE	34:0	718.5387	nd	nd	nd	nd	nd	nd	nd	nd	nd	nd	nd
PE	34:1	716.5230	716.5241	9.30	32	44	45	24.8	33.1	38.5	32.1	5.6	17.5

+ Atg4													
Class	Lipid	Calc. Mass. [M+H]-	Found Mass. [M+H]-	RT (min)	Area			Conc. (pmol/sample)			HeLa (n=3)		
					HeLa_1	HeLa_2	HeLa_3	HeLa_1	HeLa_2	HeLa_3	Mean	SD	%CV
PE	34:2	714.5074	714.5046	8.21	9	15	18	7.0	11.3	15.4	11.2	3.4	30.6
PE	34:3	712.4918	nd	nd	nd	nd	nd	nd	nd	nd	nd	nd	nd
PE	34:4	710.4761	nd	nd	nd	nd	nd	nd	nd	nd	nd	nd	nd
PE	35:0	732.5542	nd	nd	nd	nd	nd	nd	nd	nd	nd	nd	nd
PE	35:1	730.5387	730.5347	10.02	48	57	49	37.2	42.9	41.9	40.6	2.5	6.1
PE	35:2	728.5230	728.5247	9.05	17	22	18	13.2	16.5	15.4	15.0	1.4	9.3
PE	36:0	746.5700	nd	nd	nd	nd	nd	nd	nd	nd	nd	nd	nd
PE	36:1	744.5543	744.5553	10.62	nd	4	11	nd	3.0	9.4	6.2	3.2	51.5
PE	36:2	742.5387	742.5350	9.55	16	18	32	12.4	13.5	27.4	17.8	6.8	38.3
PE	36:3	740.5230	nd	nd	nd	nd	nd	nd	nd	nd	nd	nd	nd
PE	36:4	738.5074	nd	nd	nd	nd	nd	nd	nd	nd	nd	nd	nd
PE	36:5	736.4918	nd	nd	nd	nd	nd	nd	nd	nd	nd	nd	nd
PE	36:6	734.4761	nd	nd	nd	nd	nd	nd	nd	nd	nd	nd	nd
PE	38:0	774.6013	nd	nd	nd	nd	nd	nd	nd	nd	nd	nd	nd
PE	38:1	772.5856	nd	nd	nd	nd	nd	nd	nd	nd	nd	nd	nd
PE	38:2	770.5700	770.5732	11.21	14	26	25	10.9	19.5	21.4	17.3	4.6	26.6
PE	38:3	768.5543	nd	nd	nd	nd	nd	nd	nd	nd	nd	nd	nd
PE	38:4	766.5390	766.5417	9.80	nd	nd	11	nd	nd	9.4	9.4	0.0	0.0
PE	38:5	764.5230	nd	nd	nd	nd	nd	nd	nd	nd	nd	nd	nd
PE	38:6	762.5070	nd	nd	nd	nd	nd	nd	nd	nd	nd	nd	nd
PE	38:7	760.4918	nd	nd	nd	nd	nd	nd	nd	nd	nd	nd	nd
PE	40:0	800.6169	nd	nd	nd	nd	nd	nd	nd	nd	nd	nd	nd
PE	40:1	798.6013	nd	nd	nd	nd	nd	nd	nd	nd	nd	nd	nd
PE	40:2	796.5856	nd	nd	nd	nd	nd	nd	nd	nd	nd	nd	nd
PE	40:3	794.5700	nd	nd	nd	nd	nd	nd	nd	nd	nd	nd	nd
PE	40:4	792.5543	nd	nd	nd	nd	nd	nd	nd	nd	nd	nd	nd
PE	40:5	790.5387	nd	nd	nd	nd	nd	nd	nd	nd	nd	nd	nd
PE	40:6	788.5230	nd	nd	nd	nd	nd	nd	nd	nd	nd	nd	nd



+ Atg4													
Class	Lipid	Calc. Mass. [M+H]-	Found Mass. [M+H]-	RT (min)	Area			Conc. (pmol/sample)			HeLa (n=3)		
					HeLa_1	HeLa_2	HeLa_3	HeLa_1	HeLa_2	HeLa_3	Mean	SD	%CV
PE	40:8	786.5074	nd	nd	nd	nd	nd	nd	nd	nd	nd	nd	nd
PE	44:2	852.6483	nd	nd	nd	nd	nd	nd	nd	nd	nd	nd	nd
PE	44:12	834.5074	nd	nd	nd	nd	nd	nd	nd	nd	nd	nd	nd

Table 8. Quantified PEs from HEK293 cells. The lipids were obtained through precipitation of the proteome. treatment with N-(His)<sub>6</sub>-3C-Atg4B and extraction by organic solvents.

- Atg4													
Class	Lipid	Calc. Mass. [M+H]-	Found Mass. [M+H]-	RT (min)	Area			Conc. (pmol/sample)			HEK293 (n=3)		
					HEK_1	HEK_2	HEK_3	HEK_1	HEK_2	HEK_3	Mean	SD	%CV
PE	Std	747.7176	747.7169	9.15	229	231	205	200.0	200.0	200.0	200.0	0.0	0.0
PE	28:0	634.4448	nd	nd	nd	nd	nd	nd	nd	nd	nd	nd	nd
PE	30:0	662.4761	nd	nd	nd	nd	nd	nd	nd	nd	nd	nd	nd
PE	31:0	676.4918	nd	nd	nd	nd	nd	nd	nd	nd	nd	nd	nd
PE	31:1	674.4761	nd	nd	nd	nd	nd	nd	nd	nd	nd	nd	nd
PE	32:0	690.5074	nd	nd	nd	nd	nd	nd	nd	nd	nd	nd	nd
PE	32:1	688.4920	nd	nd	nd	nd	nd	nd	nd	nd	nd	nd	nd
PE	32:2	686.4760	nd	nd	nd	nd	nd	nd	nd	nd	nd	nd	nd
PE	32:3	684.4604	nd	nd	nd	nd	nd	nd	nd	nd	nd	nd	nd
PE	33:0	704.5230	nd	nd	nd	nd	nd	nd	nd	nd	nd	nd	nd
PE	33:1	702.5074	nd	nd	nd	nd	nd	nd	nd	nd	nd	nd	nd
PE	33:2	700.4918	nd	nd	nd	nd	nd	nd	nd	nd	nd	nd	nd
PE	33:3	698.4761	nd	nd	nd	nd	nd	nd	nd	nd	nd	nd	nd
PE	34:0	718.5387	nd	nd	nd	nd	nd	nd	nd	nd	nd	nd	nd
PE	34:1	716.5230	716.5204	9.24	11	6	6	9.6	5.2	5.9	6.9	1.9	28.2
PE	34:2	714.5074	714.5052	8.36	4	nd	nd	3.5	nd	nd	3.5	0.0	0.0
PE	34:3	712.4918	nd	nd	nd	nd	nd	nd	nd	nd	nd	nd	nd
PE	34:4	710.4761	nd	nd	nd	nd	nd	nd	nd	nd	nd	nd	nd
PE	35:0	732.5542	nd	nd	nd	nd	nd	nd	nd	nd	nd	nd	nd

- Atg4													
Class	Lipid	Calc. Mass. [M+H]-	Found Mass. [M+H]-	RT (min)	Area			Conc. (pmol/sample)			HEK293 (n=3)		
					HEK_1	HEK_2	HEK_3	HEK_1	HEK_2	HEK_3	Mean	SD	%CV
PE	35:1	730.5387	nd	nd	nd	nd	nd	nd	nd	nd	nd	nd	nd
PE	35:2	728.5230	nd	nd	nd	nd	nd	nd	nd	nd	nd	nd	nd
PE	36:0	746.5700	nd	nd	nd	nd	nd	nd	nd	nd	nd	nd	nd
PE	36:1	744.5543	744.5554	10.59	13	4	5	11.4	3.5	4.9	6.6	3.4	52.3
PE	36:2	742.5387	742.5374	9.65	18	4	6	15.7	3.5	5.9	8.3	5.3	63.6
PE	36:3	740.5230	nd	nd	nd	nd	nd	nd	nd	nd	nd	nd	nd
PE	36:4	738.5074	nd	nd	nd	nd	nd	nd	nd	nd	nd	nd	nd
PE	36:5	736.4918	nd	nd	nd	nd	nd	nd	nd	nd	nd	nd	nd
PE	36:6	734.4761	nd	nd	nd	nd	nd	nd	nd	nd	nd	nd	nd
PE	38:0	774.6013	nd	nd	nd	nd	nd	nd	nd	nd	nd	nd	nd
PE	38:1	772.5856	nd	nd	nd	nd	nd	nd	nd	nd	nd	nd	nd
PE	38:2	770.5700	nd	nd	nd	nd	nd	nd	nd	nd	nd	nd	nd
PE	38:3	768.5543	nd	nd	nd	nd	nd	nd	nd	nd	nd	nd	nd
PE	38:4	766.5390	766.5397	9.77	23	7	7	20.1	6.1	6.8	11.0	6.4	58.6
PE	38:5	764.5230	764.5242	8.93	10	nd	nd	8.7	nd	nd	8.7	0.0	0.0
PE	38:6	762.5070	nd	nd	nd	nd	nd	nd	nd	nd	nd	nd	nd
PE	38:7	760.4918	nd	nd	nd	nd	nd	nd	nd	nd	nd	nd	nd
PE	40:0	800.6169	nd	nd	nd	nd	nd	nd	nd	nd	nd	nd	nd
PE	40:1	798.6013	nd	nd	nd	nd	nd	nd	nd	nd	nd	nd	nd
PE	40:2	796.5856	nd	nd	nd	nd	nd	nd	nd	nd	nd	nd	nd
PE	40:3	794.5700	nd	nd	nd	nd	nd	nd	nd	nd	nd	nd	nd
PE	40:4	792.5543	nd	nd	nd	nd	nd	nd	nd	nd	nd	nd	nd
PE	40:5	790.5387	790.5410	9.62		2			1.7		1.7	0.0	0.0
PE	40:6	788.5230	nd	nd	nd	nd	nd	nd	nd	nd	nd	nd	nd
PE	40:8	786.5074	nd	nd	nd	nd	nd	nd	nd	nd	nd	nd	nd
PE	44:2	852.6483	nd	nd	nd	nd	nd	nd	nd	nd	nd	nd	nd
PE	44:12	834.5074	nd	nd	nd	nd	nd	nd	nd	nd	nd	nd	nd

+ Atg4													
Class	Lipid	Calc. Mass. [M+H]-	Found Mass. [M+H]-	RT (min)	Area			Conc. (pmol/sample)			HEK293 (n=3)		
					HEK_1	HEK_2	HEK_3	HEK_1	HEK_2	HEK_3	Mean	SD	%CV
PE	Std	747.7176	747.7172	9.21	206	225	230	200.0	200.0	200.0	200.0	0.0	0.0
PE	28:0	634.4448	634.4413	6.12	9	13	13	8.7	11.6	11.3	10.5	1.3	12.1
PE	30:0	662.4761	662.4775	7.45	23	34	44	22.3	30.2	38.3	30.3	6.5	21.5
PE	31:0	676.4918	nd	nd	nd	nd	nd	nd	nd	nd	nd	nd	nd
PE	31:1	674.4761	nd	nd	nd	24	29	nd	21.3	25.2	23.3	1.9	8.3
PE	32:0	690.5074	690.5065	8.83	4	7	5	3.9	6.2	4.3	4.8	1.0	21.0
PE	32:1	688.4920	688.4902	7.89	17	21	21	16.5	18.7	18.3	17.8	0.9	5.3
PE	32:2	686.4760	nd	nd	nd	nd	nd	nd	nd	nd	nd	nd	nd
PE	32:3	684.4604	nd	nd	nd	nd	nd	nd	nd	nd	nd	nd	nd
PE	33:0	704.5230	nd	nd	nd	nd	nd	nd	nd	nd	nd	nd	nd
PE	33:1	702.5074	702.5060	8.74	113	147	155	109.7	130.7	134.8	125.1	11.0	8.8
PE	33:2	700.4918	700.4919	7.74	3	nd	5	2.9	nd	4.3	3.6	0.7	19.8
PE	33:3	698.4761	nd	nd	nd	nd	nd	nd	nd	nd	nd	nd	nd
PE	34:0	718.5387	nd	nd	nd	nd	nd	nd	nd	nd	nd	nd	nd
PE	34:1	716.5230	716.5261	9.21	32	32	35	31.1	28.4	30.4	30.0	1.1	3.7
PE	34:2	714.5074	714.5070	8.24	7	9	13	6.8	8.0	11.3	8.7	1.9	21.9
PE	34:3	712.4918	nd	nd	nd	nd	nd	nd	nd	nd	nd	nd	nd
PE	34:4	710.4761	nd	nd	nd	nd	nd	nd	nd	nd	nd	nd	nd
PE	35:0	732.5542	nd	nd	nd	nd	nd	nd	nd	nd	nd	nd	nd
PE	35:1	730.5387	730.5388	9.99	40	50	49	38.8	44.4	42.6	42.0	2.3	5.6
PE	35:2	728.5230	728.5208	9.05	15	19	19	14.6	16.9	16.5	16.0	1.0	6.4
PE	36:0	746.5700	nd	nd	nd	nd	nd	nd	nd	nd	nd	nd	nd
PE	36:1	744.5543	744.5504	10.59	9	9	5	8.7	8.0	4.3	7.0	1.9	27.3
PE	36:2	742.5387	742.5354	9.55	18	19	20	17.5	16.9	17.4	17.3	0.3	1.5
PE	36:3	740.5230	nd	nd	nd	nd	nd	nd	nd	nd	nd	nd	nd
PE	36:4	738.5074	nd	nd	nd	nd	nd	nd	nd	nd	nd	nd	nd
PE	36:5	736.4918	nd	nd	nd	nd	nd	nd	nd	nd	nd	nd	nd
PE	36:6	734.4761	nd	nd	nd	nd	nd	nd	nd	nd	nd	nd	nd
PE	38:0	774.6013	nd	nd	nd	nd	nd	nd	nd	nd	nd	nd	nd
PE	38:1	772.5856	nd	nd	nd	nd	nd	nd	nd	nd	nd	nd	nd

+ Atg4													
Class	Lipid	Calc. Mass. [M+H]-	Found Mass. [M+H]-	RT (min)	Area			Conc. (pmol/sample)			HEK293 (n=3)		
					HEK_1	HEK_2	HEK_3	HEK_1	HEK_2	HEK_3	Mean	SD	%CV
PE	38:2	770.5700	770.5692	11.12	13	19	26	12.6	16.9	22.6	17.4	4.1	23.6
PE	38:3	768.5543	nd	nd	nd	nd	nd	nd	nd	nd	nd	nd	nd
PE	38:4	766.5390	766.5375	9.80	2	nd	8	1.9	nd	7.0	4.4	2.5	56.4
PE	38:5	764.5230	764.5275	9.80	10	nd	nd	9.7	nd	nd	9.7	0.0	0.0
PE	38:6	762.5070	nd	nd	nd	nd	nd	nd	nd	nd	nd	nd	nd
PE	38:7	760.4918	nd	nd	nd	nd	nd	nd	nd	nd	nd	nd	nd
PE	40:0	800.6169	nd	nd	nd	nd	nd	nd	nd	nd	nd	nd	nd
PE	40:1	798.6013	nd	nd	nd	nd	nd	nd	nd	nd	nd	nd	nd
PE	40:2	796.5856	nd	nd	nd	nd	nd	nd	nd	nd	nd	nd	nd
PE	40:3	794.5700	nd	nd	nd	nd	nd	nd	nd	nd	nd	nd	nd
PE	40:4	792.5543	nd	nd	nd	nd	nd	nd	nd	nd	nd	nd	nd
PE	40:5	790.5387	nd	nd	nd	nd	nd	nd	nd	nd	nd	nd	nd
PE	40:6	788.5230	nd	nd	nd	nd	nd	nd	nd	nd	nd	nd	nd
PE	40:8	786.5074	nd	nd	nd	nd	nd	nd	nd	nd	nd	nd	nd
PE	44:2	852.6483	nd	nd	nd	nd	nd	nd	nd	nd	nd	nd	nd
PE	44:12	834.5074	nd	nd	nd	nd	nd	nd	nd	nd	nd	nd	nd

Table 9. Quantified PEs from SH-SY5Y cells. The lipids were obtained through precipitation of the proteome. treatment with N-(His)<sub>6</sub>-3C-Atg4B and extraction by organic solvents.

- Atg4													
Class	Lipid	Calc. Mass. [M+H]-	Found Mass. [M+H]-	RT (min)	Area			Conc. (pmol/sample)			SH-SY5Y (n=3)		
					SH-SY5Y_1	SH-SY5Y_2	SH-SY5Y_3	SH-SY5Y_1	SH-SY5Y_2	SH-SY5Y_3	Mean	SD	%CV
PE	Std	747.7176	747.7141	9.18	230	236	219	200.0	200.0	200.0	200.0	0.0	0.0
PE	28:0	634.4448	nd	nd	nd	nd	nd	nd	nd	nd	nd	nd	nd
PE	30:0	662.4761	nd	nd	nd	nd	nd	nd	nd	nd	nd	nd	nd
PE	31:0	676.4918	nd	nd	nd	nd	nd	nd	nd	nd	nd	nd	nd
PE	31:1	674.4761	nd	nd	nd	nd	nd	nd	nd	nd	nd	nd	nd
PE	32:0	690.5074	nd	nd	nd	nd	nd	nd	nd	nd	nd	nd	nd

- Atg4													
Class	Lipid	Calc. Mass. [M+H]-	Found Mass. [M+H]-	RT (min)	Area			Conc. (pmol/sample)			SH-SY5Y (n=3)		
					SH-SY5Y_1	SH-SY5Y_2	SH-SY5Y_3	SH-SY5Y_1	SH-SY5Y_2	SH-SY5Y_3	Mean	SD	%CV
PE	32:1	688.4920	nd	nd	nd	nd	nd	nd	nd	nd	nd	nd	nd
PE	32:2	686.4760	nd	nd	nd	nd	nd	nd	nd	nd	nd	nd	nd
PE	32:3	684.4604	nd	nd	nd	nd	nd	nd	nd	nd	nd	nd	nd
PE	33:0	704.5230	nd	nd	nd	nd	nd	nd	nd	nd	nd	nd	nd
PE	33:1	702.5074	nd	nd	nd	nd	nd	nd	nd	nd	nd	nd	nd
PE	33:2	700.4918	nd	nd	nd	nd	nd	nd	nd	nd	nd	nd	nd
PE	33:3	698.4761	nd	nd	nd	nd	nd	nd	nd	nd	nd	nd	nd
PE	34:0	718.5387	nd	nd	nd	nd	nd	nd	nd	nd	nd	nd	nd
PE	34:1	716.5230	nd	nd	nd	nd	nd	nd	nd	nd	nd	nd	nd
PE	34:2	714.5074	nd	nd	nd	nd	nd	nd	nd	nd	nd	nd	nd
PE	34:3	712.4918	nd	nd	nd	nd	nd	nd	nd	nd	nd	nd	nd
PE	34:4	710.4761	nd	nd	nd	nd	nd	nd	nd	nd	nd	nd	nd
PE	35:0	732.5542	nd	nd	nd	nd	nd	nd	nd	nd	nd	nd	nd
PE	35:1	730.5387	nd	nd	nd	nd	nd	nd	nd	nd	nd	nd	nd
PE	35:2	728.5230	nd	nd	nd	nd	nd	nd	nd	nd	nd	nd	nd
PE	36:0	746.5700	nd	nd	nd	nd	nd	nd	nd	nd	nd	nd	nd
PE	36:1	744.5543	744.5491	10.56	5	nd	nd	4.3	nd	nd	4.3	0.0	0.0
PE	36:2	742.5387	742.5323	9.68	6	nd	nd	5.2	nd	nd	5.2	0.0	0.0
PE	36:3	740.5230	nd	nd	nd	nd	nd	nd	nd	nd	nd	nd	nd
PE	36:4	738.5074	nd	nd	nd	nd	nd	nd	nd	nd	nd	nd	nd
PE	36:5	736.4918	nd	nd	nd	nd	nd	nd	nd	nd	nd	nd	nd
PE	36:6	734.4761	nd	nd	nd	nd	nd	nd	nd	nd	nd	nd	nd
PE	38:0	774.6013	nd	nd	nd	nd	nd	nd	nd	nd	nd	nd	nd
PE	38:1	772.5856	nd	nd	nd	nd	nd	nd	nd	nd	nd	nd	nd
PE	38:2	770.5700	nd	nd	nd	nd	nd	nd	nd	nd	nd	nd	nd
PE	38:3	768.5543	nd	nd	nd	nd	nd	nd	nd	nd	nd	nd	nd
PE	38:4	766.5390	nd	nd	nd	nd	nd	nd	nd	nd	nd	nd	nd
PE	38:5	764.5230	nd	nd	nd	nd	nd	nd	nd	nd	nd	nd	nd
PE	38:6	762.5070	nd	nd	nd	nd	nd	nd	nd	nd	nd	nd	nd
PE	38:7	760.4918	nd	nd	nd	nd	nd	nd	nd	nd	nd	nd	nd

- Atg4													
Class	Lipid	Calc. Mass. [M+H]-	Found Mass. [M+H]-	RT (min)	Area			Conc. (pmol/sample)			SH-SY5Y (n=3)		
					SH-SY5Y_1	SH-SY5Y_2	SH-SY5Y_3	SH-SY5Y_1	SH-SY5Y_2	SH-SY5Y_3	Mean	SD	%CV
PE	40:0	800.6169	nd	nd	nd	nd	nd	nd	nd	nd	nd	nd	nd
PE	40:1	798.6013	nd	nd	nd	nd	nd	nd	nd	nd	nd	nd	nd
PE	40:2	796.5856	nd	nd	nd	nd	nd	nd	nd	nd	nd	nd	nd
PE	40:3	794.5700	nd	nd	nd	nd	nd	nd	nd	nd	nd	nd	nd
PE	40:4	792.5543	nd	nd	nd	nd	nd	nd	nd	nd	nd	nd	nd
PE	40:5	790.5387	nd	nd	nd	nd	nd	nd	nd	nd	nd	nd	nd
PE	40:6	788.5230	nd	nd	nd	nd	nd	nd	nd	nd	nd	nd	nd
PE	40:8	786.5074	nd	nd	nd	nd	nd	nd	nd	nd	nd	nd	nd
PE	44:2	852.6483	nd	nd	nd	nd	nd	nd	nd	nd	nd	nd	nd
PE	44:12	834.5074	nd	nd	nd	nd	nd	nd	nd	nd	nd	nd	nd
+ Atg4													
Class	Lipid	Calc. Mass. [M+H]-	Found Mass. [M+H]-	RT (min)	Area			Conc. (pmol/sample)			SH-SY5Y (n=3)		
					SH-SY5Y_1	SH-SY5Y_2	SH-SY5Y_3	SH-SY5Y_1	SH-SY5Y_2	SH-SY5Y_3	Mean	SD	%CV
PE	Std	747.7176	747.7124	242.00	84	254	218	200.0	200.0	200.0	200.0	0.0	0.0
PE	28:0	634.4448	634.4474	6.10	12	14	13	28.6	11.0	11.9	17.2	8.1	47.0
PE	30:0	662.4761	662.4764	7.48	37	39	39	88.1	30.7	35.8	51.5	25.9	50.3
PE	31:0	676.4918	nd	nd	nd	nd	nd	nd	nd	nd	nd	nd	nd
PE	31:1	674.4761	674.4767	7.30	22	26	26	52.4	20.5	23.9	32.2	14.3	44.4
PE	32:0	690.5074	690.5079	8.83	9	8		21.4	6.3		13.9	7.6	54.6
PE	32:1	688.4920	688.4940	7.89	22	26	20	52.4	20.5	18.3	30.4	15.6	51.2
PE	32:2	686.4760	nd	nd	nd	nd	nd	nd	nd	nd	nd	nd	nd
PE	32:3	684.4604	nd	nd	nd	nd	nd	nd	nd	nd	nd	nd	nd
PE	33:0	704.5230	nd	nd	nd	nd	nd	nd	nd	nd	nd	nd	nd
PE	33:1	702.5074	702.5051	8.71	173	159	132	411.9	125.2	121.1	219.4	136.1	62.0
PE	33:2	700.4918	nd	nd	nd	nd	nd	nd	nd	nd	nd	nd	nd
PE	33:3	698.4761	nd	nd	nd	nd	nd	nd	nd	nd	nd	nd	nd
PE	34:0	718.5387	nd	nd	nd	nd	nd	nd	nd	nd	nd	nd	nd
PE	34:1	716.5230	716.5211	9.24	39	38	33	92.9	29.9	30.3	51.0	29.6	58.0
PE	34:2	714.5074	714.5057	8.21	11	11	10	26.2	8.7	9.2	14.7	8.1	55.5
PE	34:3	712.4918	nd	nd	nd	nd	nd	nd	nd	nd	nd	nd	nd

+ Atg4													
Class	Lipid	Calc. Mass. [M+H]-	Found Mass. [M+H]-	RT (min)	Area			Conc. (pmol/sample)			SH-SY5Y (n=3)		
					SH-SY5Y_1	SH-SY5Y_2	SH-SY5Y_3	SH-SY5Y_1	SH-SY5Y_2	SH-SY5Y_3	Mean	SD	%CV
PE	34:4	710.4761	nd	nd	nd	nd	nd	nd	nd	nd	nd	nd	nd
PE	35:0	732.5542	nd	nd	nd	nd	nd	nd	nd	nd	nd	nd	nd
PE	35:1	730.5387	730.5353	10.02	59	58	45	140.5	45.7	41.3	75.8	45.8	60.4
PE	35:2	728.5230	728.5195	9.08	23	22	18	54.8	17.3	16.5	29.5	17.8	60.4
PE	36:0	746.5700	nd	nd	nd	nd	nd	nd	nd	nd	nd	nd	nd
PE	36:1	744.5543	744.5541	10.56	3	nd	nd	7.1	nd	nd	7.1	0.0	0.0
PE	36:2	742.5387	742.5389	9.52	13	15	20	31.0	11.8	18.3	20.4	7.9	39.0
PE	36:3	740.5230	nd	nd	nd	nd	nd	nd	nd	nd	nd	nd	nd
PE	36:4	738.5074	nd	nd	nd	nd	nd	nd	nd	nd	nd	nd	nd
PE	36:5	736.4918	nd	nd	nd	nd	nd	nd	nd	nd	nd	nd	nd
PE	36:6	734.4761	nd	nd	nd	nd	nd	nd	nd	nd	nd	nd	nd
PE	38:0	774.6013	nd	nd	nd	nd	nd	nd	nd	nd	nd	nd	nd
PE	38:1	772.5856	nd	nd	nd	nd	nd	nd	nd	nd	nd	nd	nd
PE	38:2	770.5700	770.5712	11.12	23	21	22	54.8	16.5	20.2	30.5	17.2	56.5
PE	38:3	768.5543	nd	nd	nd	nd	nd	nd	nd	nd	nd	nd	nd
PE	38:4	766.5390	766.5397	9.77		3			2.4		2.4	0.0	0.0
PE	38:5	764.5230	nd	nd	nd	nd	nd	nd	nd	nd	nd	nd	nd
PE	38:6	762.5070	nd	nd	nd	nd	nd	nd	nd	nd	nd	nd	nd
PE	38:7	760.4918	nd	nd	nd	nd	nd	nd	nd	nd	nd	nd	nd
PE	40:0	800.6169	nd	nd	nd	nd	nd	nd	nd	nd	nd	nd	nd
PE	40:1	798.6013	nd	nd	nd	nd	nd	nd	nd	nd	nd	nd	nd
PE	40:2	796.5856	796.5856	10.75	nd	nd	4	nd	nd	3.7	3.7	0.0	0.0
PE	40:3	794.5700	nd	nd	nd	nd	nd	nd	nd	nd	nd	nd	nd
PE	40:4	792.5543	nd	nd	nd	nd	nd	nd	nd	nd	nd	nd	nd
PE	40:5	790.5387	nd	nd	nd	nd	nd	nd	nd	nd	nd	nd	nd
PE	40:6	788.5230	nd	nd	nd	nd	nd	nd	nd	nd	nd	nd	nd
PE	40:8	786.5074	nd	nd	nd	nd	nd	nd	nd	nd	nd	nd	nd
PE	44:2	852.6483	nd	nd	nd	nd	nd	nd	nd	nd	nd	nd	nd
PE	44:12	834.5074	nd	nd	nd	nd	nd	nd	nd	nd	nd	nd	nd

Table 10. Quantified PEs from the total lipidome of HeLa cells. The lipids were obtained through incubation of the cells with a mixture of organic solvents at 48 °C for 16h.

Class	Lipid	Calc. Mass. [M+H] <sup>-</sup>	Found Mass. [M+H] <sup>-</sup>	RT (min)	Area			Conc. (pmol/sample)			HeLa (n=3)		
					HeLa_1	HeLa_2	HeLa_3	HeLa_1	HeLa_2	HeLa_3	Mean	SD	%CV
PE	Std	747.7176	747.7186	9.21	63	45	78	200.0	200.0	200.0	200.0	0.0	0.0
PE	28:0	634.4448	364.4437	6.20	7	5	6	22.2	22.2	15.4	19.9	3.2	16.2
PE	30:0	662.4761	662.4756	7.52	55	65	66	174.6	288.9	169.2	210.9	55.2	26.2
PE	31:0	676.4918	676.4889	6.73	10	8	8	31.7	35.6	20.5	29.3	6.4	21.8
PE	31:1	674.4761	674.4785	7.20	31	25	35	98.4	111.1	89.7	99.8	8.8	8.8
PE	32:0	690.5074	690.5082	8.93	63	58	96	200.0	257.8	246.2	234.6	25.0	10.6
PE	32:1	688.4920	688.4954	7.97	1903	760	1332	6041.3	3377.8	3415.4	4278.1	1246.8	29.1
PE	32:2	686.4760	686.4781	6.95	320	144	221	1015.9	640.0	566.7	740.8	196.8	26.6
PE	32:3	684.4604	nd	nd	nd	nd	nd	nd	nd	nd	nd	nd	nd
PE	33:0	704.5230	nd	nd	nd	nd	nd	nd	nd	nd	nd	nd	nd
PE	33:1	702.5074	702.5035	8.61	211	118	202	669.8	524.4	517.9	570.7	70.1	12.3
PE	33:2	700.4918	700.4911	7.61	56	42	56	177.8	186.7	143.6	169.3	18.6	11.0
PE	33:3	698.4761	nd	nd	nd	nd	nd	nd	nd	nd	nd	nd	nd
PE	34:0	718.5387	nd	nd	nd	34	56	nd	151.1	143.6	147.4	3.8	2.6
PE	34:1	716.5230	716.5248	9.34	4247	2119	3701	13482.5	9417.8	9489.7	10796.7	1899.4	17.6
PE	34:2	714.5074	714.5116	8.37	2289	1128	1555	7266.7	5013.3	3987.2	5422.4	1369.7	25.3
PE	34:3	712.4918	712.4901	7.34	1578	112	171	5009.5	497.8	438.5	1981.9	2141.0	108.0
PE	34:4	710.4761	nd	nd	nd	nd	nd	nd	nd	nd	nd	nd	nd
PE	35:0	732.5542	nd	nd	nd	nd	nd	nd	nd	nd	nd	nd	nd
PE	35:1	730.5387	730.5365	10.00	263	211	246	834.9	937.8	630.8	801.2	127.6	15.9
PE	35:2	728.5230	728.5217	9.02	175	120	163	555.6	533.3	417.9	502.3	60.3	12.0
PE	36:0	746.5700	nd	nd	nd	nd	nd	nd	nd	nd	nd	nd	nd
PE	36:1	744.5543	744.5610	10.65	2882	2022	2412	9149.2	8986.7	6184.6	8106.8	1360.8	16.8
PE	36:2	742.5387	742.5435	9.71	4448	2782	3605	14120.6	12364.4	9243.6	11909.6	2016.9	16.9
PE	36:3	740.5230	740.5242	8.84	603	392	653	1914.3	1742.2	1674.4	1777.0	101.0	5.7
PE	36:4	738.5074	738.5095	8.52	584	640	908	1854.0	2844.4	2328.2	2342.2	404.5	17.3
PE	36:5	736.4918	736.4915	7.58	245	432	530	777.8	1920.0	1359.0	1352.3	466.3	34.5



Class	Lipid	Calc. Mass. [M+H] <sup>-</sup>	Found Mass. [M+H] <sup>-</sup>	RT (min)	Area			Conc. (pmol/sample)			HeLa (n=3)		
					HeLa_1	HeLa_2	HeLa_3	HeLa_1	HeLa_2	HeLa_3	Mean	SD	%CV
PE	36:6	734.4761	734.4765	6.55	nd	106	108	nd	471.1	276.9	374.0	97.1	26.0
PE	38:0	774.6013	nd	nd	nd	nd	nd	nd	nd	nd	nd	nd	nd
PE	38:1	772.5856	772.5889	11.84	89	50	46	282.5	222.2	117.9	207.6	68.0	32.8
PE	38:2	770.5700	770.5715	10.90	320	146	173	1015.9	648.9	443.6	702.8	236.7	33.7
PE	38:3	768.5543	768.5511	10.59	202	312	214	641.3	1386.7	548.7	858.9	375.1	43.7
PE	38:4	766.5390	766.5441	9.84	1749	2046	2380	5552.4	9093.3	6102.6	6916.1	1555.8	22.5
PE	38:5	764.5230	764.5271	8.99	1193	1215	1999	3787.3	5400.0	5125.6	4771.0	704.5	14.8
PE	38:6	762.5070	762.5068	8.24	473	284	310	1501.6	1262.2	794.9	1186.2	293.5	24.7
PE	38:7	760.4918	nd	nd	nd	nd	nd	nd	nd	nd	nd	nd	nd
PE	40:0	800.6169	800.6131	13.00	106	29	44	336.5	128.9	112.8	192.7	101.9	52.9
PE	40:1	798.6013	798.6088	12.04	nd	55	64	nd	244.4	164.1	204.3	40.2	19.7
PE	40:2	796.5856	nd	nd	nd	nd	nd	nd	nd	nd	nd	nd	nd
PE	40:3	794.5700	794.5697	10.72	42	34	45	133.3	151.1	115.4	133.3	14.6	10.9
PE	40:4	792.5543	792.5558	9.97	nd	339	363	nd	1506.7	930.8	1218.7	287.9	23.6
PE	40:5	790.5387	790.5383	9.68	841	845	922	2669.8	3755.6	2364.1	2929.8	597.1	20.4
PE	40:6	788.5230	788.5209	8.61	489	307	421	1552.4	1364.4	1079.5	1332.1	194.4	14.6
PE	40:8	786.5074	nd	nd	nd	nd	nd	nd	nd	nd	nd	nd	nd
PE	44:2	852.6483	nd	nd	nd	nd	nd	nd	nd	nd	nd	nd	nd
PE	44:12	834.5074	nd	nd	nd	nd	nd	nd	nd	nd	nd	nd	nd

Table 11. Quantified PEs from the total lipidome of HEK293 cells. The lipids were obtained through incubation of the cells with a mixture of organic solvents at 48 °C for 16h.

Class	Lipid	Calc. Mass. [M+H] <sup>-</sup>	Found Mass. [M+H] <sup>-</sup>	RT (min)	Area			Conc. (pmol/sample)			HEK293 (n=3)		
					HEK_1	HEK_2	HEK_3	HEK_1	HEK_2	HEK_3	Mean	SD	%CV
PE	Std	747.7176	747.7195	9.20	87	108	107	200.0	200.0	200.0	200.0	0.0	0.0
PE	28:0	634.4448	634.4417	6.23	5	4		11.5	7.4		9.5	2.0	21.6
PE	30:0	662.4761	662.4777	6.17	25	59	44	57.5	109.3	82.2	83.0	21.1	25.5

Class	Lipid	Calc. Mass. [M+H] <sup>-</sup>	Found Mass. [M+H] <sup>-</sup>	RT (min)	Area			Conc. (pmol/sample)			HEK293 (n=3)		
					HEK_1	HEK_2	HEK_3	HEK_1	HEK_2	HEK_3	Mean	SD	%CV
PE	31:0	676.4918	676.4883	6.80	10	10	11	23.0	18.5	20.6	20.7	1.8	8.8
PE	31:1	674.4761	674.4815	7.27	20	nd	28	46.0	nd	52.3	49.2	3.2	6.5
PE	32:0	690.5074	690.5048	8.93	70	85	64	160.9	157.4	119.6	146.0	18.7	12.8
PE	32:1	688.4920	688.4922	7.92	465	406	490	1069.0	751.9	915.9	912.2	129.5	14.2
PE	32:2	686.4760	686.4763	7.03	70	85	70	160.9	157.4	130.8	149.7	13.4	9.0
PE	32:3	684.4604	nd	nd	nd	nd	nd	nd	nd	nd	nd	nd	nd
PE	33:0	704.5230	nd	nd	nd	nd	nd	nd	nd	nd	nd	nd	nd
PE	33:1	702.5074	702.5034	8.74	176	216	175	404.6	400.0	327.1	377.2	35.5	9.4
PE	33:2	700.4918	700.4959	7.80	31	70	41	71.3	129.6	76.6	92.5	26.3	28.5
PE	33:3	698.4761	nd	nd	nd	nd	nd	nd	nd	nd	nd	nd	nd
PE	34:0	718.5387	718.5316	8.92	45	39	44	103.4	72.2	82.2	86.0	13.0	15.1
PE	34:1	716.5230	716.5269	9.34	4259	2606	4843	9790.8	4825.9	9052.3	7889.7	2187.3	27.7
PE	34:2	714.5074	714.5099	8.39	969	1062	1020	2227.6	1966.7	1906.5	2033.6	139.3	6.9
PE	34:3	712.4918	712.4920	7.57	52	128	34	119.5	237.0	63.6	140.0	72.3	51.6
PE	34:4	710.4761	nd	nd	nd	nd	nd	nd	nd	nd	nd	nd	nd
PE	35:0	732.5542	nd	nd	nd	nd	nd	nd	nd	nd	nd	nd	nd
PE	35:1	730.5387	730.5361	10.02	250	259	254	574.7	479.6	474.8	509.7	46.0	9.0
PE	35:2	728.5230	728.5247	9.15	139	220	148	319.5	407.4	276.6	334.5	54.4	16.3
PE	36:0	746.5700	nd	nd	nd	nd	nd	nd	nd	nd	nd	nd	nd
PE	36:1	744.5543	744.5598	10.62	2153	1820	2548	4949.4	3370.4	4762.6	4360.8	704.5	16.2
PE	36:2	742.5387	742.5438	9.60	2722	2429	2937	6257.5	4498.1	5489.7	5415.1	720.2	13.3
PE	36:3	740.5230	740.5208	8.74	377	605	363	866.7	1120.4	678.5	888.5	181.1	20.4
PE	36:4	738.5074	738.5077	8.39	849	12	981	1951.7	22.0	1833.6	1269.1	883.2	69.6
PE	36:5	736.4918	736.4922	7.58	168	466	173	386.2	863.0	323.4	524.2	240.9	46.0
PE	36:6	734.4761	nd	nd	nd	nd	nd	nd	nd	nd	nd	nd	nd
PE	38:0	774.6013	nd	nd	nd	nd	nd	nd	nd	nd	nd	nd	nd
PE	38:1	772.5856	772.5855	11.90	136	148	162	312.6	274.1	302.8	296.5	16.4	5.5
PE	38:2	770.5700	770.5698	10.87	383	323	435	880.5	598.1	813.1	763.9	120.4	15.8
PE	38:3	768.5543	768.5522	10.27	217	404	230	498.9	748.1	429.9	559.0	136.7	24.5
PE	38:4	766.5390	766.5386	9.93	nd	nd	3445	nd	nd	6439.3	6439.3	0.0	0.0

Class	Lipid	Calc. Mass. [M+H]-	Found Mass. [M+H]-	RT (min)	Area			Conc. (pmol/sample)			HEK293 (n=3)		
					HEK_1	HEK_2	HEK_3	HEK_1	HEK_2	HEK_3	Mean	SD	%CV
PE	38:5	764.5230	761.5272	8.99	2088	nd	2071	4800.0	nd	3871.0	4335.5	464.5	10.7
PE	38:6	762.5070	762.5087	8.29	275	321	565	632.2	594.4	1056.1	760.9	209.3	27.5
PE	38:7	760.4918	nd	nd	nd	nd	nd	nd	nd	nd	nd	nd	nd
PE	40:0	800.6169	800.6183	12.97	131	266	136	301.1	492.6	254.2	349.3	103.1	29.5
PE	40:1	798.6013	798.6026	12.03	nd	405	166	nd	750.0	310.3	530.1	219.9	41.5
PE	40:2	796.5856	796.5808	11.43	nd	160	nd	nd	296.3	nd	296.3	0.0	0.0
PE	40:3	794.5700	794.5721	10.75	195	397	229	448.3	735.2	428.0	537.2	140.3	26.1
PE	40:4	792.5543	792.5585	9.99	nd	1209	466	nd	2238.9	871.0	1555.0	683.9	44.0
PE	40:5	790.5387	790.5427	9.65	1643	1643	1637	3777.0	3042.6	3059.8	3293.1	342.2	10.4
PE	40:6	788.5230	788.5212	8.58	523	986	517	1202.3	1825.9	966.4	1331.5	362.6	27.2
PE	40:8	786.5074	nd	nd	nd	nd	nd	nd	nd	nd	nd	nd	nd
PE	44:2	852.6483	nd	nd	nd	nd	nd	nd	nd	nd	nd	nd	nd
PE	44:12	834.5074	nd	nd	nd	nd	nd	nd	nd	nd	nd	nd	nd

Table 12. Quantified PEs from the total lipidome of SH-SY5Y cells. The lipids were obtained through incubation of the cells with a mixture of organic solvents at 48 °C for 16h.

Class	Lipid	Calc. Mass. [M+H]-	Found Mass. [M+H]-	RT (min)	Area			Conc. (pmol/sample)			SH-SY5Y (n=3)		
					SH-SY5Y_1	SH-SY5Y_2	SH-SY5Y_3	SH-SY5Y_1	SH-SY5Y_2	SH-SY5Y_3	Mean	SD	%CV
PE	Std	747.7176	747.7203	9.18	84	94	107	200.0	200.0	200.0	200.0	0.0	0.0
PE	28:0	634.4448	nd	nd	nd	nd	nd	nd	nd	nd	nd	nd	nd
PE	30:0	662.4761	662.4737	7.52	nd	14	nd	nd	29.8	nd	29.8	0.0	0.0
PE	31:0	676.4918	nd	nd	nd	nd	nd	nd	nd	nd	nd	nd	nd
PE	31:1	674.4761	nd	nd	nd	nd	nd	nd	nd	nd	nd	nd	nd
PE	32:0	690.5074	690.5099	8.93	11	37	14	26.2	78.7	26.2	43.7	24.8	56.7
PE	32:1	688.4920	688.4906	7.89	149	244	177	354.8	519.1	330.8	401.6	83.7	20.8
PE	32:2	686.4760	686.4719	7.05	20	41	23	47.6	87.2	43.0	59.3	19.9	33.5
PE	32:3	684.4604	nd	nd	nd	nd	nd	nd	nd	nd	nd	nd	nd

Class	Lipid	Calc. Mass. [M+H]-	Found Mass. [M+H]-	RT (min)	Area			Conc. (pmol/sample)			SH-SY5Y (n=3)		
					SH- SY5Y_1	SH- SY5Y_2	SH- SY5Y_3	SH- SY5Y_1	SH- SY5Y_2	SH- SY5Y_3	Mean	SD	%CV
PE	33:0	704.5230	nd	nd	nd	nd	nd	nd	nd	nd	nd	nd	nd
PE	33:1	702.5074	702.5038	8.68	37	55	43	88.1	117.0	80.4	95.2	15.8	16.6
PE	33:2	700.4918	nd	nd	nd	nd	nd	nd	nd	nd	nd	nd	nd
PE	33:3	698.4761	nd	nd	nd	nd	nd	nd	nd	nd	nd	nd	nd
PE	34:0	718.5387	718.5414	8.99	nd	nd	20	nd	nd	37.4	37.4	0.0	0.0
PE	34:1	716.5230	716.5270	9.31	1202	1755	1268	2861.9	3734.0	2370.1	2988.7	564.0	18.9
PE	34:2	714.5074	714.5078	8.43	203	702	222	483.3	1493.6	415.0	797.3	493.2	61.9
PE	34:3	712.4918	712.4879	7.36	13	30	15	31.0	63.8	28.0	40.9	16.2	39.6
PE	34:4	710.4761	nd	nd	nd	nd	nd	nd	nd	nd	nd	nd	nd
PE	35:0	732.5542	nd	nd	nd	nd	nd	nd	nd	nd	nd	nd	nd
PE	35:1	730.5387	730.5360	9.97	66	122	82	157.1	259.6	153.3	190.0	49.2	25.9
PE	35:2	728.5230	718.5235	9.02	29	94	33	69.0	200.0	61.7	110.2	63.5	57.6
PE	36:0	746.5700	nd	nd	nd	nd	nd	nd	nd	nd	nd	nd	nd
PE	36:1	744.5543	744.5580	10.65	1247	2036	1297	2969.0	4331.9	2424.3	3241.8	802.3	24.7
PE	36:2	742.5387	742.5387	9.71	1302	3525	1257	3100.0	7500.0	2349.5	4316.5	2271.8	52.6
PE	36:3	740.5230	740.5255	8.77	102	398	125	242.9	846.8	233.6	441.1	286.9	65.0
PE	36:4	738.5074	738.5099	8.46	146	226	179	347.6	480.9	334.6	387.7	66.1	17.0
PE	36:5	736.4918	736.4922	7.58	30	82	36	71.4	174.5	67.3	104.4	49.6	47.5
PE	36:6	734.4761	nd	nd	nd	nd	nd	nd	nd	nd	nd	nd	nd
PE	38:0	774.6013	nd	nd	nd	nd	nd	nd	nd	nd	nd	nd	nd
PE	38:1	772.5856	772.5826	11.85	37	97	41	88.1	206.4	76.6	123.7	58.6	47.4
PE	38:2	770.5700	770.5675	10.88	75	312	88	178.6	663.8	164.5	335.6	232.1	69.2
PE	38:3	768.5543	768.5472	10.28	27	166	52	64.3	353.2	97.2	171.6	129.1	75.3
PE	38:4	766.5390	766.5474	9.84	938	1010	1017	2233.3	2148.9	1900.9	2094.4	141.1	6.7
PE	38:5	764.5230	764.5284	8.87	251	707	1999	597.6	1504.3	3736.4	1946.1	1319.0	67.8
PE	38:6	762.5070	762.5073	8.24	97	223	112	231.0	474.5	209.3	304.9	120.2	39.4
PE	38:7	760.4918	nd	nd	nd	nd	nd	nd	nd	nd	nd	nd	nd
PE	40:0	800.6169	800.6165	13.07	60	344	51	142.9	731.9	95.3	323.4	289.5	89.5
PE	40:1	798.6013	798.6000	12.06	40	292	48	95.2	621.3	89.7	268.7	249.3	92.8
PE	40:2	796.5856	nd	nd	nd	nd	nd	nd	nd	nd	nd	nd	nd

Class	Lipid	Calc. Mass. [M+H]-	Found Mass. [M+H]-	RT (min)	Area			Conc. (pmol/sample)			SH-SY5Y (n=3)		
					SH-SY5Y_1	SH-SY5Y_2	SH-SY5Y_3	SH-SY5Y_1	SH-SY5Y_2	SH-SY5Y_3	Mean	SD	%CV
PE	40:3	794.5700	794.5686	10.78	69	59	73	164.3	125.5	136.4	142.1	16.3	11.5
PE	40:4	792.5543	792.5585	9.97	301	318	359	716.7	676.6	671.0	688.1	20.3	3.0
PE	40:5	790.5387	790.5416	9.65	520	562	538	1238.1	1195.7	1005.6	1146.5	101.1	8.8
PE	40:6	788.5230	788.5226	8.68	62	177	68	147.6	376.6	127.1	217.1	113.1	52.1
PE	40:8	786.5074	nd	nd	nd	nd	nd	nd	nd	nd	nd	nd	nd
PE	44:2	852.6483	nd	nd	nd	nd	nd	nd	nd	nd	nd	nd	nd
PE	44:12	834.5074	nd	nd	nd	nd	nd	nd	nd	nd	nd	nd	nd

Table 13. Quantified PEs from the total lipidome of HeLa cells after treatment with heptadecanoic acid. The lipids were obtained through incubation of the cells with a mixture of organic solvents at 48 °C for 16h.

- C17																			
Class	Lipid	Calc. Mass. [M+H]-	Found Mass. [M+H]-	RT (min)	Area						Conc. (pmol/sample)						HeLa (n=6)		
					1	2	3	4	5	6	1	2	3	4	5	6	Mean	SD	%CV
PE	Std	747.7176	747.7119	8.93	174	160	126	75	244	242	200.0	200.0	200.0	200.0	200.0	200.0	200.0	0.0	0.0
PE	28:0	634.4448	nd	nd	nd	nd	nd	nd	nd	6	nd	nd	nd	nd	5.0	5.0	0.0	0.0	
PE	30:0	662.4761	662.4737	7.21	nd	20	22	25	47	59	nd	25.0	34.9	66.7	38.5	48.8	42.8	14.2	33.1
PE	31:0	676.4918	676.4933	7.90	nd	7	11	6	14	18	nd	8.8	17.5	16.0	11.5	14.9	13.7	3.2	23.1
PE	31:1	674.4761	674.4803	6.89	nd	10	nd	8	18	19	nd	12.5	nd	21.3	14.8	15.7	16.1	3.3	20.2
PE	32:0	690.5074	690.5103	8.62	9	27	36	18	57	61	10.3	33.8	57.1	48.0	46.7	50.4	41.1	15.4	37.5
PE	32:1	688.4920	688.4916	7.80	35	288	338	355	888	1129	40.2	360.0	536.5	946.7	727.9	933.1	590.7	322.0	54.5
PE	32:2	686.4760	686.4772	6.70	nd	59	79	95	233	271	nd	73.8	125.4	253.3	191.0	224.0	173.5	65.6	37.8
PE	32:3	684.4604	nd	nd	nd	nd	nd	nd	nd	nd	nd	nd	nd	nd	nd	nd	nd	nd	nd
PE	33:0	704.5230	nd	nd	nd	nd	nd	nd	nd	nd	nd	nd	nd	nd	nd	nd	nd	nd	nd
PE	33:1	702.5074	702.5052	8.43	71	70	85	52	86	109	81.6	87.5	134.9	138.7	70.5	90.1	100.5	26.4	26.2
PE	33:2	700.4918	700.4933	7.46	19	19	21	18	33	47	21.8	23.8	33.3	48.0	27.0	38.8	32.1	9.1	28.4

- C17																			
Class	Lipid	Calc. Mass. [M+H]-	Found Mass. [M+H]-	RT (min)	Area						Conc. (pmol/sample)						HeLa (n=6)		
					1	2	3	4	5	6	1	2	3	4	5	6	Mean	SD	%CV
PE	33:3	698.4761	nd	nd	nd	nd	nd	nd	nd	nd	nd	nd	nd	nd	nd	nd	nd	nd	nd
PE	34:0	718.5387	718.5388	9.94	78	nd	18	8	347	24	89.7	nd	28.6	21.3	284.4	19.8	88.8	101.2	114.0
PE	34:1	716.5230	716.5237	9.15	311	530	629	747	2698	3065	357.5	662.5	998.4	1992.0	2211.5	2533.1	1459.2	823.0	56.4
PE	34:2	714.5074	714.5097	8.09	108	398	471	502	881	909	124.1	497.5	747.6	1338.7	722.1	751.2	696.9	361.9	51.9
PE	34:4	710.4761	710.4799	6.74	nd	13	12	nd	12	20	nd	16.3	19.0	nd	9.8	16.5	15.4	3.4	22.1
PE	35:0	732.5543	732.5598	11.19	29	26	37	nd	nd	nd	33.3	32.5	58.7	nd	nd	nd	41.5	12.2	29.3
PE	35:1	730.5387	730.5396	9.72	241	93	108	74	129	148	277.0	116.3	171.4	197.3	105.7	122.3	165.0	59.6	36.1
PE	35:2	728.5230	728.5223	8.78	152	77	92	59	142	159	174.7	96.3	146.0	157.3	116.4	131.4	137.0	25.9	18.9
PE	35:3	726.5074	726.5036	7.80	nd	7	9	nd	nd	nd	nd	8.8	14.3	nd	nd	nd	11.5	2.8	24.0
PE	35:4	724.4918	nd	nd	nd	nd	nd	nd	nd	nd	nd	nd	nd	nd	nd	nd	nd	nd	nd
PE	35:5	722.4761	nd	nd	nd	nd	nd	nd	nd	nd	nd	nd	nd	nd	nd	nd	nd	nd	nd
PE	35:6	720.4604	nd	nd	nd	nd	nd	nd	nd	nd	nd	nd	nd	nd	nd	nd	nd	nd	nd
PE	36:0	746.5700	nd	nd	nd	nd	nd	nd	nd	nd	nd	nd	nd	nd	nd	nd	nd	nd	nd
PE	36:1	744.5543	744.5541	10.41	155	372	437	449	1531	1521	178.2	465.0	693.7	1197.3	1254.9	1257.0	841.0	423.0	50.3
PE	36:2	742.5387	742.5359	9.53	125	648	760	806	3038	3344	143.7	810.0	1206.3	2149.3	2490.2	2763.6	1593.9	944.1	59.2
PE	36:3	740.5230	740.5224	8.56	nd	238	287	133	312	364	nd	297.5	455.6	354.7	255.7	300.8	332.9	68.9	20.7
PE	36:4	738.5074	738.5090	8.15	40	205	250	109	187	233	46.0	256.3	396.8	290.7	153.3	192.6	222.6	110.3	49.6
PE	36:5	736.4918	736.4911	7.30	28	157	213	49	97	118	32.2	196.3	338.1	130.7	79.5	97.5	145.7	99.5	68.3
PE	36:6	734.4761	nd	nd	nd	nd	nd	nd	nd	nd	nd	nd	nd	nd	nd	nd	nd	nd	nd
PE	37:0	760.5856	nd	nd	nd	nd	nd	nd	nd	nd	nd	nd	nd	nd	nd	nd	nd	nd	nd
PE	37:1	758.5700	758.5739	10.97	90	43	56	17	83	82	103.4	53.8	88.9	45.3	68.0	67.8	71.2	19.8	27.8

- C17																			
Class	Lipid	Calc. Mass. [M+H]-	Found Mass. [M+H]-	RT (min)	Area						Conc. (pmol/sample)						HeLa (n=6)		
					1	2	3	4	5	6	1	2	3	4	5	6	Mean	SD	%CV
PE	37:2	756.5543	756.5510	10.09	18	26	35	21	44	46	20.7	32.5	55.6	56.0	36.1	38.0	39.8	12.6	31.6
PE	37:3	754.5387	nd	nd	nd	nd	nd	nd	nd	nd	nd	nd	nd	nd	nd	nd	nd	nd	nd
PE	37:4	752.5230	752.5236	8.84	211	nd	nd	nd	nd	nd	242.5	nd	nd	nd	nd	242.5	0.0	0.0	
PE	37:5	750.5074	nd	nd	nd	nd	nd	nd	nd	nd	nd	nd	nd	nd	nd	nd	nd	nd	nd
PE	37:6	748.4918	748.4912	7.02	41	nd	nd	nd	nd	nd	47.1	nd	nd	nd	nd	47.1	0.0	0.0	
PE	37:7	746.4761	nd	nd	nd	nd	nd	nd	nd	nd	nd	nd	nd	nd	nd	nd	nd	nd	nd
PE	38:0	774.6013	nd	nd	nd	nd	nd	nd	nd	nd	nd	nd	nd	nd	nd	nd	nd	nd	nd
PE	38:1	772.5856	772.5896	8.37	41	nd	11	5	nd	9	47.1	nd	17.5	13.3	nd	7.4	21.3	15.3	71.7
PE	38:2	770.5700	770.5714	10.60	nd	68	94	58	221	200	nd	85.0	149.2	154.7	181.1	165.3	147.1	32.9	22.4
PE	38:3	768.5543	768.5491	9.97	21	141	140	nd	nd	nd	24.1	176.3	222.2	nd	nd	nd	140.9	84.6	60.1
PE	38:4	766.5390	nd	nd	nd	nd	nd	nd	nd	nd	nd	nd	nd	nd	nd	nd	nd	nd	nd
PE	38:5	764.5230	764.5248	8.74	nd	417	535	182	472	530	nd	521.3	849.2	485.3	386.9	438.0	536.1	162.9	30.4
PE	38:6	762.5070	762.5029	7.96	nd	255	333	94	262	307	nd	318.8	528.6	250.7	214.8	253.7	313.3	112.7	36.0
PE	38:7	760.4918	nd	nd	nd	nd	nd	nd	nd	nd	nd	nd	nd	nd	nd	nd	nd	nd	nd
PE	40:0	800.6169	800.6174	9.78	13	6	7	nd	nd	nd	14.9	7.5	11.1	nd	nd	nd	11.2	3.0	27.2
PE	40:1	798.6013	798.6032	11.82	nd	21	26	25	94	117	nd	26.3	41.3	66.7	77.0	96.7	61.6	25.1	40.8
PE	40:2	796.5856	nd	nd	nd	nd	nd	nd	nd	nd	nd	nd	nd	nd	nd	nd	nd	nd	nd
PE	40:3	794.5700	794.5684	10.44	nd	15	20	nd	34	35	nd	18.8	31.7	nd	27.9	28.9	26.8	4.9	18.2
PE	40:4	792.5543	792.5552	9.69	nd	152	186	41	nd	nd	nd	190.0	295.2	109.3	nd	nd	198.2	76.1	38.4
PE	40:5	790.5387	790.5413	9.37	nd	293	344	80	268	302	nd	366.3	546.0	213.3	219.7	249.6	319.0	126.2	39.6
PE	40:6	788.5230	788.5175	8.40	nd	265	309	75	122	159	nd	331.3	490.5	200.0	100.0	131.4	250.6	143.9	57.4
PE	40:8	786.5074	nd	nd	nd	nd	nd	nd	nd	nd	nd	nd	nd	nd	nd	nd	nd	nd	nd
PE	44:2	852.6483	nd	nd	nd	nd	nd	nd	nd	nd	nd	nd	nd	nd	nd	nd	nd	nd	nd

PE	44:1 2	834.5074	nd	nd	nd	nd	nd	nd	nd	nd	nd	nd	nd	nd	nd	nd	nd	nd	nd	
- C17																				
Class	Lipid	Calc. Mass. [M+H]-	Found Mass. [M+H]-	RT (min)	Area						Conc. (pmol/sample)						HeLa (n=6)			
					1	2	3	4	5	6	1	2	3	4	5	6	Mean	SD	%CV	
DAG	Std	619.6037	619.5982	11.21	7430	12931	10809	19229	18594	17949	166.0	166.0	166.0	166.0	166.0	166.0	166.0	166.0	0.0	0.0
DAG	30:0	558.5098	558.5086	8.67	283	608	571	521	488	450	6.3	7.8	8.8	4.5	4.4	4.2	6.0	1.8	30.0	
DAG	30:1	556.4942	556.4876	7.91	93	222	229	nd	nd	nd	2.1	2.8	3.5	nd	nd	nd	2.8	0.6	20.9	
DAG	30:2	554.4786	nd	nd	nd	nd	nd	nd	nd	nd	nd	nd	nd	nd	nd	nd	nd	nd	nd	
DAG	30:3	552.4630	nd	nd	nd	nd	nd	nd	nd	nd	nd	nd	nd	nd	nd	nd	nd	nd	nd	
DAG	30:4	550.4474	nd	nd	nd	nd	nd	nd	nd	nd	nd	nd	nd	nd	nd	nd	nd	nd	nd	
DAG	31:0	572.5274	572.5271	9.36	1275	167	147	1407	1353	1269	28.5	2.1	2.3	12.1	12.1	11.7	11.5	8.8	76.5	
DAG	31:1	570.5098	570.5046	8.44	112	121	100	nd	nd	nd	2.5	1.6	1.5	nd	nd	nd	1.9	0.5	24.2	
DAG	32:0	586.5411	586.5440	10.08	3047	1944	2047	3024	2798	2520	68.1	25.0	31.4	26.1	25.0	23.3	33.1	15.8	47.8	
DAG	32:1	584.5255	584.5186	9.14	289	1346	1437	1092	1006	869	6.5	17.3	22.1	9.4	9.0	8.0	12.0	5.6	46.9	
DAG	32:2	582.5099	582.5112	8.10	65	192	213	nd	230	176	1.5	2.5	3.3	nd	2.1	1.6	2.2	0.7	30.0	
DAG	32:3	580.4943	nd	nd	nd	nd	nd	nd	nd	nd	nd	nd	nd	nd	nd	nd	nd	nd	nd	
DAG	32:4	578.4787	nd	nd	nd	nd	nd	nd	nd	nd	nd	nd	nd	nd	nd	nd	nd	nd	nd	
DAG	32:5	576.4631	nd	nd	nd	nd	nd	nd	nd	nd	nd	nd	nd	nd	nd	nd	nd	nd	nd	
DAG	33:0	600.5567	600.5592	10.70	13164	262	280	13023	18636	14822	294.1	3.4	4.3	112.4	166.4	137.1	119.6	99.8	83.5	
DAG	33:1	598.5411	594.5410	9.79	619	460	529	2653	2695	2658	13.8	5.9	8.1	22.9	24.1	24.6	16.6	7.7	46.3	
DAG	33:2	596.5254	596.5237	9.01	69	50	57	566	531	558	1.5	0.6	0.9	4.9	4.7	5.2	3.0	2.0	66.5	
DAG	34:0	614.5724	614.5691	11.33	52722	846	821	nd	44986	nd	1177.9	10.9	12.6	nd	401.6	nd	400.7	476.1	118.8	
DAG	34:1	612.5568	612.5568	10.39	3906	4118	4652	20566	28492	27683	87.3	52.9	71.4	177.5	254.4	256.0	149.9	84.1	56.1	
DAG	34:2	610.5412	610.5390	9.51	487	911	936	4342	4281	4252	10.9	11.7	14.4	37.5	38.2	39.3	25.3	13.1	51.6	
DAG	34:3	608.5256	nd	nd	nd	nd	nd	73	67	nd	nd	nd	nd	0.6	0.6	nd	0.6	0.0	2.6	
DAG	34:4	606.5100	nd	nd	nd	nd	nd	nd	nd	nd	nd	nd	nd	nd	nd	nd	nd	nd	nd	
DAG	34:5	604.4944	nd	nd	nd	nd	nd	nd	nd	nd	nd	nd	nd	nd	nd	nd	nd	nd	nd	



<b>DAG</b>	34:6	602.4788	nd	nd	nd	nd	nd	nd	nd	nd	nd	nd	nd	nd	nd	nd	nd	nd	nd
<b>DAG</b>	35:0	628.5880	628.5881	11.89	5155	nd	nd	7536	8042	7427	115.2	nd	nd	65.1	71.8	68.7	80.2	20.3	25.4
<b>- C17</b>																			
Class	Lipid	Calc. Mass. [M+H]-	Found Mass. [M+H]-	RT (min)	Area						Conc. (pmol/sample)						HeLa (n=6)		
					1	2	3	4	5	6	1	2	3	4	5	6	Mean	SD	%CV
<b>DAG</b>	35:1	626.5723	626.5743	11.02	2894	426	561	2144 7	2089 7	1706 9	64.7	5.5	8.6	185.1	186.6	157.9	101.4	78.1	77.1
<b>DAG</b>	35:2	624.5567	624.5573	11.21	185	1987	1973	7006	6512	6721	4.1	25.5	30.3	60.5	58.1	62.2	40.1	21.7	54.1
<b>DAG</b>	36:0	642.6040	642.6038	12.49	2083	254	136	7741	9153	8405	46.5	3.3	2.1	66.8	81.7	77.7	46.4	32.8	70.8
<b>DAG</b>	36:1	640.5881	640.5854	11.58	945	909	1082	6912	6889	6367	21.1	11.7	16.6	59.7	61.5	58.9	38.2	22.0	57.4
<b>DAG</b>	36:2	638.5725	638.5800	10.73	567	2013	2298	1525 5	1495 1	1398 7	12.7	25.8	35.3	131.7	133.5	129.4	78.1	53.9	69.0
<b>DAG</b>	36:3	636.5569	636.5582	9.86	116	416	449	510	483	nd	2.6	5.3	6.9	4.4	4.3	nd	4.7	1.4	29.9
<b>DAG</b>	36:4	634.5413	634.5405	8.98	58	65	167	123	65	nd	1.3	0.8	2.6	1.1	0.6	nd	1.3	0.7	54.5
<b>DAG</b>	36:5	632.5257	nd	nd	nd	nd	nd	nd	nd	nd	nd	nd	nd	nd	nd	nd	nd	nd	nd
<b>DAG</b>	36:6	630.5101	nd	nd	nd	nd	nd	nd	nd	nd	nd	nd	nd	nd	nd	nd	nd	nd	nd
<b>DAG</b>	37:0	657.6271	nd	nd	nd	nd	nd	nd	nd	nd	nd	nd	nd	0.0	0.0	0.0	nd	nd	nd
<b>DAG</b>	37:1	654.6036	nd	nd	nd	nd	nd	nd	nd	nd	nd	nd	nd	0.0	0.0	0.0	nd	nd	nd
<b>DAG</b>	37:2	652.5880	652.5921	11.42	40	nd	99	3043	3064	3285	0.9	nd	1.5	26.3	27.4	30.4	17.3	13.2	76.4
<b>DAG</b>	37:3	650.5723	650.5723	10.64	192	nd	nd	nd	nd	nd	4.3	nd	nd	nd	nd	nd	4.3	0.0	0.0
<b>DAG</b>	37:4	648.5567	648.5542	10.17	435	nd	nd	nd	nd	nd	9.7	nd	nd	nd	nd	nd	9.7	0.0	0.0
<b>DAG</b>	37:5	646.5411	646.5421	9.32	96	nd	nd	nd	nd	nd	2.1	nd	nd	nd	nd	nd	2.1	0.0	0.0
<b>DAG</b>	38:0	670.6350	670.6307	13.53	176	76	38	nd	nd	nd	3.9	1.0	0.6	nd	nd	nd	1.8	1.5	81.7
<b>DAG</b>	38:1	668.6194	668.6177	7.79	403	267	202	nd	nd	nd	9.0	3.4	3.1	nd	nd	nd	5.2	2.7	52.3
<b>DAG</b>	38:2	666.6038	666.6094	11.99	60	386	422	nd	nd	nd	1.3	5.0	6.5	nd	nd	nd	4.3	2.2	50.6
<b>DAG</b>	38:3	664.5882	664.5936	11.24	nd	279	470	nd	nd	nd	nd	3.6	7.2	nd	nd	nd	5.4	1.8	33.7
<b>DAG</b>	38:4	662.5726	662.5677	10.80	82	349	559	nd	nd	nd	1.8	4.5	8.6	nd	nd	nd	5.0	2.8	55.9

+ C17																			
Classes	Lipid	Calc. Mass. [M+H]-	Found Mass. [M+H]-	RT (min)	Area						Conc. (pmol/sample)						HeLa (n=6)		
					1	2	3	4	5	6	1	2	3	4	5	6	Mean	SD	%CV
PE	Std	747.7176	747.7150	8.93	117	173	174	171	172	171	200.0	200.0	200.0	200.0	200.0	200.0	200.0	0.0	0.0
PE	28:0	634.4448	nd	nd	nd	nd	nd	nd	nd	nd	nd	nd	nd	nd	nd	nd	nd	nd	nd
PE	30:0	662.4761	662.4766	7.20	24	nd	nd	21	23	21	41.0	0.0	nd	24.6	26.7	24.6	23.4	13.2	56.5
PE	31:0	676.4918	nd	nd	nd	nd	nd	20	19	19	nd	nd	nd	23.4	22.1	22.2	22.6	0.6	2.6
PE	31:1	674.4761	674.4783	6.95	12	nd	nd	55	61	68	20.5	nd	nd	64.3	70.9	79.5	58.8	22.8	38.7
PE	32:0	690.5074	690.5022	8.61	35	10	9	23	23	26	59.8	11.6	10.3	26.9	26.7	30.4	27.6	16.3	59.2
PE	32:1	688.4920	688.4908	7.74	367	48	42	191	198	224	627.4	55.5	48.3	223.4	230.2	262.0	241.1	192.2	79.7
PE	32:2	686.4760	686.4722	6.65	nd	5	3	59	64	67	nd	5.8	3.4	69.0	74.4	78.4	46.2	34.1	73.8
PE	32:3	684.4604	nd	nd	nd	nd	nd	nd	nd	nd	nd	nd	nd	nd	nd	nd	nd	nd	nd
PE	33:0	704.5230	nd	nd	nd	nd	nd	nd	nd	nd	nd	nd	nd	nd	nd	nd	nd	nd	nd
PE	33:1	702.5074	702.5063	8.37	89	78	74	851	794	976	152.1	90.2	85.1	995.3	923.3	1141	564.6	460.5	81.6
PE	33:2	700.4918	700.4948	7.33	24	24	22	310	328	355	41.0	27.7	25.3	362.6	381.4	415.2	208.9	178.3	85.3
PE	33:3	698.4761	nd	nd	nd	nd	nd	nd	nd	nd	nd	nd	nd	nd	nd	nd	nd	nd	nd
PE	34:0	718.5387	718.5372	9.93	21	89	85	338	113	113	35.9	102.9	97.7	395.3	131.4	132.2	149.2	114.6	76.8
PE	34:1	716.5230	716.5197	9.09	620	378	358	2819	2879	3078	1059	437.0	411.5	3297	3347	3600	2025	1408	69.5
PE	34:2	714.5074	714.5087	8.11	739	109	107	577	786	936	1263	126.0	123.0	674.9	914.0	3600	1116	1182	105.9
PE	34:3	712.4918	712.4976	7.17	56	6	5	29	30	36	95.7	6.9	5.7	33.9	34.9	1094	212.0	395.9	186.8
PE	34:4	710.4761	710.4778	6.73	17	nd	nd	nd	nd	nd	29.1	nd	nd	nd	nd	42.1	35.6	6.5	18.3
PE	35:0	732.5543	732.5555	9.35	nd	9	29	51	53	48	nd	10.4	33.3	59.6	61.6	56.1	44.2	19.7	44.6

Classes	Lipid	Calc. Mass. [M+H] <sup>-</sup>	Found Mass. [M+H] <sup>-</sup>	RT (min)	+ C17													HeLa (n=6)		
					Area						Conc. (pmol/sample)						Mean	SD	%CV	
					1	2	3	4	5	6	1	2	3	4	5	6				
PE	35:1	730.5387	730.5349	9.68	115	292	270	1080	1247	1329	196.6	337.6	310.3	1263	1450	1554	852.0	578.4	67.9	
PE	35:2	728.5230	728.5240	8.77	93	184	173	978	996	1184	159.0	212.7	198.9	1143	1158	1384	709.6	525.5	74.1	
PE	35:3	726.5074	728.5244	8.78	nd	26	27	95	97	102	nd	30.1	31.0	111.1	112.8	119.3	80.9	41.2	50.9	
PE	35:4	724.4918	nd	nd	nd	nd	nd	nd	nd	nd	nd	nd	nd	nd	nd	nd	nd	nd	nd	
PE	35:5	722.4761	nd	nd	nd	nd	nd	nd	nd	nd	nd	nd	nd	nd	nd	nd	nd	nd	nd	
PE	35:6	720.4604	nd	nd	nd	nd	nd	nd	nd	nd	nd	nd	nd	nd	nd	nd	nd	nd	nd	
PE	36:0	746.5700	nd	nd	nd	nd	nd	nd	nd	nd	nd	nd	nd	nd	nd	nd	nd	nd	nd	
PE	36:1	744.5543	744.5525	10.40	469	161	160	573	684	746	801.7	186.1	183.9	670.2	795.3	872.5	585.0	289.0	49.4	
PE	36:2	742.5387	742.5338	9.49	735	138	120	781	772	964	1256.4	159.5	137.9	913.5	897.7	1127.5	748.7	441.7	59.0	
PE	36:3	740.5230	740.5222	8.52	296	26	27	91	83	95	506.0	30.1	31.0	106.4	96.5	111.1	146.9	164.1	111.7	
PE	36:4	738.5074	738.5065	8.11	274	46	53	83	87	98	468.4	53.2	60.9	97.1	101.2	114.6	149.2	144.4	96.8	
PE	36:5	736.4918	736.4904	7.33	235	27	27	43	nd	77	401.7	31.2	31.0	50.3	nd	90.1	120.9	142.1	117.5	
PE	36:6	734.4761	nd	nd	nd	nd	nd	nd	nd	nd	nd	nd	nd	nd	nd	nd	nd	nd	nd	
PE	37:0	760.5856	nd	nd	nd	nd	nd	nd	nd	nd	nd	nd	nd	nd	nd	nd	nd	nd	nd	
PE	37:1	758.5700	758.5705	11.07	63	131	32	100	104	103	107.7	151.4	36.8	117.0	120.9	120.5	109.0	35.0	32.1	
PE	37:2	756.5543	756.5543	10.00	39	19	20	148	161	173	66.7	22.0	23.0	173.1	187.2	202.3	112.4	77.1	68.6	
PE	37:3	754.5387	754.5400	9.35	nd	39	37	nd	70	nd	nd	45.1	42.5	nd	81.4	nd	56.3	17.7	31.5	
PE	37:4	752.5230	752.5263	8.88	nd	243	222	nd	408	456	nd	280.9	255.2	nd	474.4	533.3	386.0	120.1	31.1	

+ C17																				
Class	Lipid	Calc. Mass. [M+H]-	Found Mass. [M+H]-	RT (min)	Area						Conc. (pmol/sample)						HeLa (n=6)			
					1	2	3	4	5	6	1	2	3	4	5	6	Mean	SD	%CV	
PE	37:5	750.5074	nd	nd	nd	nd	nd	nd	nd	nd	nd	nd	nd	nd	nd	nd	nd	nd	nd	
PE	37:6	748.4918	748.4950	6.99	nd	41	32	nd	nd	81	nd	47.4	36.8	nd	nd	94.7	59.6	25.2	42.2	
PE	37:7	746.4761	nd	nd	nd	nd	nd	nd	nd	nd	nd	nd	nd	nd	nd	nd	nd	nd	nd	
PE	38:0	774.6013	nd	nd	nd	nd	nd	nd	nd	nd	nd	nd	nd	nd	nd	nd	nd	nd	nd	
PE	38:1	772.5856	772.5881	8.41	nd	54	49	nd	nd	nd	nd	62.4	56.3	nd	nd	nd	59.4	3.1	5.1	
PE	38:2	770.5700	770.5669	10.62	101	15	14	63	60	68	172.6	17.3	16.1	73.7	69.8	79.5	71.5	52.1	72.9	
PE	38:3	768.5543	768.5513	10.00	157	nd	nd	nd	nd	nd	268.4	nd	nd	nd	nd	nd	268.4	0.0	0.0	
PE	38:4	766.5390	nd	nd	nd	nd	nd	nd	nd	nd	nd	nd	nd	nd	nd	nd	nd	nd	nd	
PE	38:5	764.5230	764.5247	8.74	586	nd	544	214	199	243	1001	nd	625.3	250.3	231.4	284.2	478.6	298.7	62.4	
PE	38:6	762.5070	762.5043	7.93	376	50	nd	nd	nd	nd	642.7	57.8	nd	nd	nd	nd	350.3	292.5	83.5	
PE	38:7	760.4918	nd	nd	nd	nd	nd	nd	nd	nd	nd	nd	nd	nd	nd	nd	nd	nd	nd	
PE	40:0	800.6169	800.6176	9.79	nd	15	14	nd	nd	nd	nd	17.3	16.1	nd	nd	nd	16.7	0.6	3.7	
PE	40:1	798.6013	798.6074	11.72	27	nd	5	37	29	34	46.2	nd	5.7	43.3	33.7	39.8	33.7	14.6	43.3	
PE	40:2	796.5856	nd	nd	nd	nd	nd	nd	nd	nd	nd	nd	nd	nd	nd	nd	nd	nd	nd	
PE	40:3	794.5700	794.5653	10.47	23	nd	nd	nd	nd	28	39.3	nd	nd	nd	nd	32.7	36.0	3.3	9.1	
PE	40:4	792.5543	792.5543	9.68	200	nd	nd	5	nd	nd	341.9	nd	nd	5.8	nd	nd	173.9	168.0	96.6	
PE	40:5	790.5387	790.5403	9.37	331	484	84	nd	nd	nd	565.8	559.5	96.6	nd	nd	nd	407.3	219.7	54.0	
PE	40:6	788.5230	788.5207	8.40	333	80	nd	nd	nd	nd	569.2	92.5	nd	nd	nd	nd	330.9	238.4	72.0	
PE	40:8	786.5074	nd	nd	nd	nd	nd	nd	nd	nd	nd	nd	nd	nd	nd	nd	nd	nd	nd	
PE	44:2	852.6483	nd	nd	nd	nd	nd	nd	nd	nd	nd	nd	nd	nd	nd	nd	nd	nd	nd	
PE	44:12	834.5074	nd	nd	nd	nd	nd	nd	nd	nd	nd	nd	nd	nd	nd	nd	nd	nd	nd	
DAG	Standard	619.6037	619.6060	11.27	10633	7376	6829	12525	32255	31458	166.0	166.0	166.0	166.0	166.0	166.0	166.0	166.0	0.0	0.0
DAG	30:0	558.5098	558.5098	8.69	620	276	249	1232	1315	981	9.7	6.2	6.1	16.3	6.8	5.2	8.4	3.8	45.7	

+ C17																			
Class	Lipid	Calc. Mass. [M+H]-	Found Mass. [M+H]-	RT (min)	Area						Conc. (pmol/sample)						HeLa (n=6)		
					1	2	3	4	5	6	1	2	3	4	5	6	Mean	SD	%CV
DAG	30:1	556.4942	556.4916	7.72	222	77	73	nd	nd	nd	3.5	1.7	1.8	nd	nd	nd	2.3	0.8	34.7
DAG	30:2	554.4786	nd	nd	nd	nd	nd	nd	nd	nd	nd	nd	nd	nd	nd	nd	nd	nd	nd
DAG	30:3	552.4630	nd	nd	nd	nd	nd	nd	nd	nd	nd	nd	nd	nd	nd	nd	nd	nd	nd
DAG	30:4	550.4474	nd	nd	nd	nd	nd	nd	nd	nd	nd	nd	nd	nd	nd	nd	nd	nd	nd
DAG	31:0	572.5274	572.5251	9.29	160	1069	1038	nd	225	nd	2.5	24.1	25.2	nd	1.2	nd	13.2	11.4	86.3
DAG	31:1	570.5098	570.5036	8.35	107	112	nd	nd	nd	nd	1.7	2.5	nd	nd	nd	nd	2.1	0.4	20.3
DAG	32:0	586.5411	586.5406	10.08	2226	3530	3001	2727	1267 7	5474	34.8	79.4	72.9	36.1	65.2	28.9	52.9	20.2	38.2
DAG	32:1	584.5255	584.5264	9.13	1578	284	273	2399	1946	1595	24.6	6.4	6.6	31.8	10.0	8.4	14.6	9.9	67.5
DAG	32:2	582.5099	582.5101	8.13	208	33	29	820	nd	365	3.2	0.7	0.7	10.9	nd	1.9	3.5	3.8	108. 7
DAG	32:3	580.4943	nd	nd	nd	nd	nd	nd	nd	nd	nd	nd	nd	nd	nd	nd	nd	nd	nd
DAG	32:4	578.4787	nd	nd	nd	nd	nd	nd	nd	nd	nd	nd	nd	nd	nd	nd	nd	nd	nd
DAG	32:5	576.4631	nd	nd	nd	nd	nd	nd	nd	nd	nd	nd	nd	nd	nd	nd	nd	nd	nd
DAG	33:0	600.5567	600.5529	10.61	319	1552 4	1336 7	nd	nd	nd	5.0	349.4	324.9	nd	nd	nd	226.4	156. 9	69.3
DAG	33:1	598.5411	598.5404	9.79	539	716	709	626	nd	334	8.4	16.1	17.2	8.3	nd	1.8	10.4	5.7	55.0
DAG	33:2	596.5254	596.5239	8.88	48	82	80	nd	nd	nd	0.7	1.8	1.9	nd	nd	nd	1.5	0.5	35.8
DAG	34:0	614.5724	614.5739	11.36	960	5736 0	5473 0	nd	1154 1	9187	15.0	1290. 9	1330. 4	nd	59.4	48.5	548.8	622. 3	113. 4
DAG	34:1	612.5568	612.5549	10.42	4709	4615	3980	1178 5	1298 4	1193 1	73.5	103.9	96.7	156. 2	66.8	63.0	93.3	31.9	34.1
DAG	34:2	610.5412	610.5446	9.61	967	548	511	2337	1505	1519	15.1	12.3	12.4	31.0	7.7	8.0	14.4	7.8	54.3
DAG	34:3	608.5256	608.5254	8.63	nd	nd	nd	237	nd	nd	nd	nd	nd	3.1	nd	nd	3.1	0.0	0.0
DAG	34:4	606.5100	nd	nd	nd	nd	nd	nd	nd	nd	nd	nd	nd	nd	nd	nd	nd	nd	nd
DAG	34:5	604.4944	nd	nd	nd	nd	nd	nd	nd	nd	nd	nd	nd	nd	nd	nd	nd	nd	nd
DAG	34:6	602.4788	nd	nd	nd	nd	nd	nd	nd	nd	nd	nd	nd	nd	nd	nd	nd	nd	nd
DAG	35:0	628.5880	628.5905	11.11	209	6815	5829	nd	nd	nd	3.3	153.4	141.7	nd	nd	nd	99.4	68.2	68.6

+ C17																			
Class	Lipid	Calc. Mass. [M+H]-	Found Mass. [M+H]-	RT (min)	Area						Conc. (pmol/sample)						HeLa (n=6)		
					1	2	3	4	5	6	1	2	3	4	5	6	Mean	SD	%CV
DAG	35:1	626.5723	626.5699	11.02	560	3976	3315	621	1239	1136	8.7	89.5	80.6	8.2	6.4	6.0	33.2	36.7	110.5
DAG	35:2	624.5567	624.5601	11.27	1863	756	725	1139	541	786	29.1	17.0	17.6	15.1	2.8	4.1	14.3	8.9	62.1
DAG	36:0	642.6040	642.6016	12.43	191	3960	2614	3708	16733	4650	3.0	89.1	63.5	49.1	86.1	24.5	52.6	31.2	59.3
DAG	36:1	640.5881	640.5896	11.67	1012	1402	1108	3085	3238	2728	15.8	31.6	26.9	40.9	16.7	14.4	24.4	9.7	39.8
DAG	36:2	638.5725	638.5719	10.76	2244	624	595	13012	16126	15474	35.0	14.0	14.5	172.5	83.0	81.7	66.8	55.0	82.4
DAG	36:3	636.5569	636.5588	9.92	424	114	121	1559	623	526	6.6	2.6	2.9	20.7	3.2	2.8	6.5	6.5	100.6
DAG	36:4	634.5413	634.5444	9.07	55	59	59	nd	nd	nd	0.9	1.3	1.4	nd	nd	nd	1.2	0.3	20.7
DAG	36:5	632.5257	nd	nd	nd	nd	nd	nd	nd	nd	nd	nd	nd	nd	nd	nd	nd	nd	nd
DAG	36:6	630.5101	nd	nd	nd	nd	nd	nd	nd	nd	nd	nd	nd	nd	nd	nd	nd	nd	nd
DAG	37:0	657.6271	nd	nd	nd	nd	nd	nd	nd	nd	nd	nd	nd	nd	nd	nd	nd	nd	nd
DAG	37:1	654.6036	nd	nd	nd	nd	nd	nd	nd	nd	nd	nd	nd	nd	nd	nd	nd	nd	nd
DAG	37:2	652.5880	652.5913	11.33	103	41	43	nd	nd	nd	1.6	0.9	1.0	nd	nd	nd	1.2	0.3	25.0
DAG	37:3	650.5723	nd	nd	nd	nd	nd	nd	nd	nd	nd	nd	nd	nd	nd	nd	nd	nd	nd
DAG	37:4	648.5567	648.5556	10.15	nd	510	495	nd	nd	nd	nd	11.5	12.0	nd	nd	nd	11.8	0.3	2.4
DAG	37:5	646.5411	646.5425	9.39	nd	102	100	nd	nd	nd	nd	2.3	2.4	nd	nd	nd	2.4	0.1	2.9
DAG	38:0	670.6350	670.6321	13.46	nd	456	329	nd	nd	nd	nd	10.3	8.0	nd	nd	nd	9.1	1.1	12.4
DAG	38:1	668.6194	668.6178	7.76	nd	nd	324	nd	nd	nd	nd	nd	7.9	nd	nd	nd	7.9	0.0	0.0
DAG	38:2	666.6038	666.6084	11.95	414	nd	nd	nd	nd	nd	6.5	nd	nd	nd	nd	nd	6.5	0.0	0.0
DAG	38:3	664.5882	664.6884	11.20	282	nd	nd	282	nd	nd	4.4	nd	nd	3.7	nd	nd	4.1	0.3	8.2
DAG	38:4	662.5726	662.5723	10.76	493	112	114	93	nd	nd	7.7	2.5	2.8	1.2	nd	nd	3.6	2.5	69.2

Table 14. Quantified PEs from the immunoprecipitation of HEK293 cells overexpressing pOPIN-GFP-LC3B employing anti-GFP antibody followed by treatment with N-(His)<sub>6</sub>-3C-Atg4B. Three different amounts of anti-LC3B antibody were tested (2, 3 and 5 µg).

Buffer 3 - Atg4B													
Class	Lipid	Calc. Mass. [M+H] <sup>-</sup>	Found Mass. [M+H] <sup>-</sup>	RT (min)	Area			Conc. (pmol/sample)			HEK293 pOPIN-GFP-LC3B (n=3)		
					2 µg Ab	3 µg Ab	5 µg Ab	2 µg Ab	3 µg Ab	5 µg Ab	Mean	SD	%CV
PE	Std	747.7176	747.7154	9.10	191	201	72	200.0	200.0	200.0	200.0	0.0	0.0
PE	28:0	634.4448	634.4478	6.10	7	6	2	7.3	6.0	5.6	6.3	0.8	12.1
PE	30:0	662.4761	662.4730	7.49	24	24	7	25.1	23.9	19.4	22.8	2.4	10.7
PE	31:0	676.4918	nd	nd	nd	nd	nd	nd	nd	nd	nd	nd	nd
PE	31:1	674.4761	674.4745	7.30	12	14	3	12.6	13.9	8.3	11.6	2.4	20.5
PE	32:0	690.5074	690.5073	8.83	6	6		6.3	6.0		6.1	0.2	2.6
PE	32:1	688.4920	688.4966	7.90	15	4	4	15.7	4.0	11.1	10.3	4.8	47.0
PE	32:2	686.4760	nd	nd	nd	nd	nd	nd	nd	nd	nd	nd	nd
PE	32:3	684.4604	684.4579	7.27	5	6	nd	5.2	6.0	nd	5.6	0.4	6.6
PE	33:0	704.5230	nd	nd	nd	nd	nd	nd	nd	nd	nd	nd	nd
PE	33:1	702.5074	702.5036	8.74	79	95	28	82.7	94.5	77.8	85.0	7.0	8.3
PE	33:2	700.4918	nd	nd	nd	nd	nd	nd	nd	nd	nd	nd	nd
PE	33:3	698.4761	nd	nd	nd	nd	nd	nd	nd	nd	nd	nd	nd
PE	34:0	718.5387	nd	nd	nd	nd	nd	nd	nd	nd	nd	nd	nd
PE	34:1	716.5230	716.5240	9.17	20	24	11	20.9	23.9	30.6	25.1	4.0	16.0
PE	34:2	714.5074	714.5081	8.20	6	7	nd	6.3	7.0	nd	6.6	0.3	5.2
PE	34:3	712.4918	nd	nd	nd	nd	nd	nd	nd	nd	nd	nd	nd
PE	34:4	710.4761	nd	nd	nd	nd	nd	nd	nd	nd	nd	nd	nd
PE	35:0	732.5543	nd	nd	nd	nd	nd	nd	nd	nd	nd	nd	nd
PE	35:1	730.5387	730.5447	10.02	32	39	11	33.5	38.8	30.6	34.3	3.4	10.0
PE	35:2	728.5230	728.5220	9.05	13	12	4	13.6	11.9	11.1	12.2	1.0	8.5
PE	35:3	726.5074	nd	nd	nd	nd	nd	nd	nd	nd	nd	nd	nd
PE	35:4	724.4918	nd	nd	nd	nd	nd	nd	nd	nd	nd	nd	nd
PE	35:5	722.4761	nd	nd	nd	nd	nd	nd	nd	nd	nd	nd	nd
PE	35:6	720.4604	nd	nd	nd	nd	nd	nd	nd	nd	nd	nd	nd
PE	36:0	746.5700	nd	nd	nd	nd	nd	nd	nd	nd	nd	nd	nd

Buffer 3 - Atg4B													
Class	Lipid	Calc. Mass. [M+H]-	Found Mass. [M+H]-	RT (min)	Area			Conc. (pmol/sample)			HEK293 pOPIN-GFP-LC3B (n=3)		
					2 µg Ab	3 µg Ab	5 µg Ab	2 µg Ab	3 µg Ab	5 µg Ab	Mean	SD	%CV
PE	36:1	744.5543	744.5518	10.58	4	4	3	4.2	4.0	8.3	5.5	2.0	36.4
PE	36:2	742.5387	742.5344	9.93	32	40	4	33.5	39.8	11.1	28.1	12.3	43.8
PE	36:3	740.5230	nd	nd	nd	nd	nd	nd	nd	nd	nd	nd	nd
PE	36:4	738.5074	nd	nd	nd	nd	nd	nd	nd	nd	nd	nd	nd
PE	36:5	736.4918	nd	nd	nd	nd	nd	nd	nd	nd	nd	nd	nd
PE	36:6	734.4761	nd	nd	nd	nd	nd	nd	nd	nd	nd	nd	nd
PE	38:0	774.6013	nd	nd	nd	nd	nd	nd	nd	nd	nd	nd	nd
PE	38:1	772.5856	nd	nd	nd	nd	nd	nd	nd	nd	nd	nd	nd
PE	38:2	770.5700	770.5685	11.09	11	11	3	11.5	10.9	8.3	10.3	1.4	13.5
PE	38:3	768.5543	nd	nd	nd	nd	nd	nd	nd	nd	nd	nd	nd
PE	38:4	766.5390	766.5372	9.80	3	3	nd	3.1	3.0	nd	3.1	0.1	2.6
PE	38:5	764.5230	nd	nd	nd	nd	nd	nd	nd	nd	nd	nd	nd
PE	38:6	762.5070	nd	nd	nd	nd	nd	nd	nd	nd	nd	nd	nd
PE	38:7	760.4918	nd	nd	nd	nd	nd	nd	nd	nd	nd	nd	nd
PE	40:0	800.6169	nd	nd	nd	nd	nd	nd	nd	nd	nd	nd	nd
PE	40:1	798.6013	nd	nd	nd	nd	nd	nd	nd	nd	nd	nd	nd
PE	40:2	796.5856	nd	nd	nd	nd	nd	nd	nd	nd	nd	nd	nd
PE	40:3	794.5700	nd	nd	nd	nd	nd	nd	nd	nd	nd	nd	nd
PE	40:4	792.5543	nd	nd	nd	nd	nd	nd	nd	nd	nd	nd	nd
PE	40:5	790.5387	nd	nd	nd	nd	nd	nd	nd	nd	nd	nd	nd
PE	40:6	788.5230	nd	nd	nd	nd	nd	nd	nd	nd	nd	nd	nd
PE	40:8	786.5074	nd	nd	nd	nd	nd	nd	nd	nd	nd	nd	nd
PE	44:2	852.6483	nd	nd	nd	nd	nd	nd	nd	nd	nd	nd	nd
PE	44:12	834.5074	nd	nd	nd	nd	nd	nd	nd	nd	nd	nd	nd



Buffer 3 + Atg4B													
Class	Lipid	Calc. Mass. [M+H]-	Found Mass. [M+H]-	RT (min)	Area			Conc. (pmol/sample)			HEK293 pOPIN-GFP-LC3B (n=3)		
					2 µg Ab	3 µg Ab	5 µg Ab	2 µg Ab	3 µg Ab	5 µg Ab	Mean	SD	%CV
PE	Std	747.7176	747.7154	9.10	239	246	90	200.0	200.0	200.0	200.0	0.0	0.0
PE	28:0	634.4448	634.4402	6.10	10	17	5	8.4	13.8	11.1	11.1	2.2	20.1
PE	30:0	662.4761	662.4770	7.45	31	45	11	25.9	36.6	24.4	29.0	5.4	18.6
PE	31:0	676.4918	nd	nd	nd	nd	nd	nd	nd	nd	nd	nd	nd
PE	31:1	674.4761	674.4797	7.36	18	29	7	15.1	23.6	15.6	18.1	3.9	21.6
PE	32:0	690.5074	690.5037	8.83	5	9	3	4.2	7.3	6.7	6.1	1.3	22.3
PE	32:1	688.4920	688.4927	7.89	18	25	6	15.1	20.3	13.3	16.2	3.0	18.3
PE	32:2	686.4760	nd	nd	nd	nd	nd	nd	nd	nd	nd	nd	nd
PE	32:3	684.4604	nd	nd	nd	nd	nd	nd	nd	nd	nd	nd	nd
PE	33:0	704.5230	nd	nd	nd	nd	nd	nd	nd	nd	nd	nd	nd
PE	33:1	702.5074	702.5076	8.74	131	193	51	109.6	156.9	113.3	126.6	21.5	17.0
PE	33:2	700.4918	nd	nd	nd	nd	nd	nd	nd	nd	nd	nd	nd
PE	33:3	698.4761	nd	nd	nd	nd	nd	nd	nd	nd	nd	nd	nd
PE	34:0	718.5387	nd	nd	nd	nd	nd	nd	nd	nd	nd	nd	nd
PE	34:1	716.5230	716.5230	9.18	29	44	12	24.3	35.8	26.7	28.9	5.0	17.1
PE	34:2	714.5074	714.5078	8.27	8	13	4	6.7	10.6	8.9	8.7	1.6	18.2
PE	34:3	712.4918	nd	nd	nd	nd	nd	nd	nd	nd	nd	nd	nd
PE	34:4	710.4761	nd	nd	nd	nd	nd	nd	nd	nd	nd	nd	nd
PE	35:0	732.5543	nd	nd	nd	nd	nd	nd	nd	nd	nd	nd	nd
PE	35:1	730.5387	730.5419	10.02	50	86	21	41.8	69.9	46.7	52.8	12.3	23.2
PE	35:2	728.5230	728.5239	9.05	13	24	8	10.9	19.5	17.8	16.1	3.7	23.2
PE	35:3	726.5074	nd	nd	nd	nd	nd	nd	nd	nd	nd	nd	nd
PE	35:4	724.4918	nd	nd	nd	nd	nd	nd	nd	nd	nd	nd	nd
PE	35:5	722.4761	nd	nd	nd	nd	nd	nd	nd	nd	nd	nd	nd
PE	35:6	720.4604	nd	nd	nd	nd	nd	nd	nd	nd	nd	nd	nd
PE	36:0	746.5700	nd	nd	nd	nd	nd	nd	nd	nd	nd	nd	nd
PE	36:1	744.5543	nd	nd	nd	nd	nd	nd	nd	nd	nd	nd	nd

Buffer 3 + Atg4B													
Class	Lipid	Calc. Mass. [M+H]-	Found Mass. [M+H]-	RT (min)	Area			Conc. (pmol/sample)			HEK293 pOPIN-GFP-LC3B (n=3)		
					2 µg Ab	3 µg Ab	5 µg Ab	2 µg Ab	3 µg Ab	5 µg Ab	Mean	SD	%CV
PE	36:2	742.5387	742.5389	9.93	43	70	18	36.0	56.9	40.0	44.3	9.1	20.5
PE	36:3	740.5230	nd	nd	nd	nd	nd	nd	nd	nd	nd	nd	nd
PE	36:4	738.5074	nd	nd	nd	nd	nd	nd	nd	nd	nd	nd	nd
PE	36:5	736.4918	nd	nd	nd	nd	nd	nd	nd	nd	nd	nd	nd
PE	36:6	734.4761	nd	nd	nd	nd	nd	nd	nd	nd	nd	nd	nd
PE	38:0	774.6013	nd	nd	nd	nd	nd	nd	nd	nd	nd	nd	nd
PE	38:1	772.5856	nd	nd	nd	nd	nd	nd	nd	nd	nd	nd	nd
PE	38:2	770.5700	770.5665	11.12	11	25	6	9.2	20.3	13.3	14.3	4.6	32.1
PE	38:3	768.5543	nd	nd	nd	nd	nd	nd	nd	nd	nd	nd	nd
PE	38:4	766.5390	766.5471	9.80	2	9	nd	1.7	7.3	nd	4.5	2.8	62.8
PE	38:5	764.5230	nd	nd	nd	nd	nd	nd	nd	nd	nd	nd	nd
PE	38:6	762.5070	nd	nd	nd	nd	nd	nd	nd	nd	nd	nd	nd
PE	38:7	760.4918	nd	nd	nd	nd	nd	nd	nd	nd	nd	nd	nd
PE	40:0	800.6169	nd	nd	nd	nd	nd	nd	nd	nd	nd	nd	nd
PE	40:1	798.6013	nd	nd	nd	nd	nd	nd	nd	nd	nd	nd	nd
PE	40:2	796.5856	nd	nd	nd	nd	nd	nd	nd	nd	nd	nd	nd
PE	40:3	794.5700	nd	nd	nd	nd	nd	nd	nd	nd	nd	nd	nd
PE	40:4	792.5543	nd	nd	nd	nd	nd	nd	nd	nd	nd	nd	nd
PE	40:5	790.5387	nd	nd	nd	nd	nd	nd	nd	nd	nd	nd	nd
PE	40:6	788.5230	nd	nd	nd	nd	nd	nd	nd	nd	nd	nd	nd
PE	40:8	786.5074	nd	nd	nd	nd	nd	nd	nd	nd	nd	nd	nd
PE	44:2	852.6483	nd	nd	nd	nd	nd	nd	nd	nd	nd	nd	nd
PE	44:12	834.5074	nd	nd	nd	nd	nd	nd	nd	nd	nd	nd	nd

Table 15. Quantified PEs from the immunoprecipitation of HEK293 cells overexpressing pOPIN-GFP-LC3B employing anti-GFP antibody followed by treatment with N-(His)<sub>6</sub>-3C-Atg4B.

Class	Lipid	Calc. Mass. [M+H]-	Found Mass. [M+H]-	RT (min)	Area - Atg4B			Conc. (pmol/sample) - Atg4B			Area + Atg4B			Conc. (pmol/sample) + Atg4B			HEK293 pOPIN-GFP-LC3B -Atg4 (n=3)			HEK293 pOPIN-GFP-LC3B +Atg4 (n=3)		
					1	2	3	1	2	3	1	2	3	1	2	3	Mean	SD	%CV	Mean	SD	%CV
PE	Std	747.7176	747.7167	9.30	53	165	23	200.0	200.0	200.0	114	177	246	200.0	200.0	200.0	200.0	40.5	20.3	200.0	0.0	0.0
PE	28:0	634.4448	634.4438	6.33	nd	nd	nd	nd	nd	nd	4	9	7	7.0	10.2	5.7	nd	nd	nd	7.6	1.9	24.6
PE	30:0	662.4761	662.4766	7.67	nd	nd	nd	nd	nd	nd	9	31	25	15.8	35.0	20.3	nd	nd	nd	23.7	8.2	34.6
PE	31:0	676.4918	nd	nd	nd	nd	nd	nd	nd	nd	nd	nd	nd	nd	nd	nd	nd	nd	nd	nd	nd	nd
PE	31:1	674.4761	674.4820	7.51	nd	nd	nd	nd	nd	nd	5	13	13	8.8	14.7	10.6	nd	nd	nd	11.3	2.5	21.8
PE	32:0	690.5074	690.5040	9.02	nd	nd	nd	nd	nd	nd	nd	7	5	nd	7.9	4.1	nd	nd	nd	6.0	1.9	32.1
PE	32:1	688.4920	688.4886	8.08	nd	nd	nd	nd	nd	nd	8	23	15	14.0	26.0	12.2	nd	nd	nd	17.4	6.1	35.1
PE	32:2	686.4760	nd	nd	nd	nd	nd	nd	nd	nd	nd	nd	nd	nd	nd	nd	nd	nd	nd	nd	nd	nd
PE	32:3	684.4604	nd	nd	nd	nd	nd	nd	nd	nd	nd	nd	nd	nd	nd	nd	nd	nd	nd	nd	nd	nd
PE	33:0	704.5230	nd	nd	nd	nd	nd	nd	nd	nd	nd	nd	nd	nd	nd	nd	nd	nd	nd	nd	nd	nd
PE	33:1	702.5074	702.5059	8.93	nd	nd	nd	nd	nd	nd	40	105	92	70.2	118.6	74.8	nd	nd	nd	87.9	21.8	24.9
PE	33:2	700.4918	nd	nd	nd	nd	nd	nd	nd	nd	nd	nd	nd	nd	nd	nd	nd	nd	nd	nd	nd	nd
PE	33:3	698.4761	nd	nd	nd	nd	nd	nd	nd	nd	nd	nd	nd	nd	nd	nd	nd	nd	nd	nd	nd	nd
PE	34:0	718.5387	nd	nd	nd	nd	nd	nd	nd	nd	nd	nd	nd	nd	nd	nd	nd	nd	nd	nd	nd	nd
PE	34:1	716.5230	716.5215	9.39	nd	nd	nd	nd	nd	nd	11	33	26	19.3	37.3	21.1	nd	nd	nd	25.9	8.1	31.2
PE	34:2	714.5074	714.5016	8.52	nd	nd	nd	nd	nd	nd	5	30	30	8.8	33.9	24.4	nd	nd	nd	22.4	10.4	46.3
PE	34:3	712.4918	nd	nd	nd	nd	nd	nd	nd	nd	nd	nd	nd	nd	nd	nd	nd	nd	nd	nd	nd	nd
PE	34:4	710.4761	nd	nd	nd	nd	nd	nd	nd	nd	nd	nd	nd	nd	nd	nd	nd	nd	nd	nd	nd	nd
PE	35:0	732.5543	nd	nd	nd	nd	nd	nd	nd	nd	nd	nd	nd	nd	nd	nd	nd	nd	nd	nd	nd	nd
PE	35:1	730.5387	730.5395	10.18	nd	nd	nd	nd	nd	nd	13	41	39	22.8	46.3	31.7	nd	nd	nd	33.6	9.7	28.8
PE	35:2	728.5230	728.5189	9.24	nd	nd	nd	nd	nd	nd	5	13	10	8.8	14.7	8.1	nd	nd	nd	10.5	3.0	28.0
PE	36:0	746.5700	746.5663	7.32	nd	nd	nd	nd	nd	nd	9	nd	nd	10.2	nd	nd	nd	nd	nd	10.2	0.0	0.0
PE	36:1	744.5543	744.5495	10.71	nd	nd	nd	nd	nd	nd	3	4	nd	3.4	3.3	nd	nd	nd	nd	3.3	0.1	2.1
PE	36:2	742.5387	742.5394	9.68	nd	nd	nd	nd	nd	nd	13	65	66	22.8	73.4	53.7	nd	nd	nd	50.0	20.8	41.7
PE	36:3	740.5230	740.5204	8.92	nd	nd	nd	nd	nd	nd	nd	9	nd	nd	7.3	nd	nd	nd	nd	7.3	0.0	0.0
PE	36:4	738.5074	738.5026	8.58	nd	nd	nd	nd	nd	nd	74	54	nd	83.6	43.9	nd	nd	nd	nd	63.8	19.9	31.1
PE	36:5	736.4918	nd	nd	nd	nd	nd	nd	nd	nd	nd	nd	nd	nd	nd	nd	nd	nd	nd	nd	nd	nd

Class	Lipid	Calc. Mass. [M+H] <sup>-</sup>	Found Mass. [M+H] <sup>-</sup>	RT (min)	Area - Atg4B			Conc. (pmol/sample) - Atg4B			Area + Atg4B			Conc. (pmol/sample) + Atg4B			HEK293 pOPIN- GFP-LC3B -Atg4 (n=3)			HEK293 pOPIN- GFP-LC3B +Atg4 (n=3)		
					1	2	3	1	2	3	1	2	3	1	2	3	Mean	SD	%CV	Mean	SD	%CV
PE	36:6	734.4761	nd	nd	nd	nd	nd	nd	nd	nd	nd	nd	nd	nd	nd	nd	nd	nd	nd	nd	nd	nd
PE	38:0	774.6013	nd	nd	nd	nd	nd	nd	nd	nd	nd	nd	nd	nd	nd	nd	nd	nd	nd	nd	nd	nd
PE	38:1	772.5856	nd	nd	nd	nd	nd	nd	nd	nd	nd	nd	nd	nd	nd	nd	nd	nd	nd	nd	nd	nd
PE	38:2	770.5700	770.5718	11.24	nd	nd	nd	nd	nd	nd	6	11	13	10.5	12.4	10.6	nd	nd	nd	11.2	0.9	7.9
PE	38:3	768.5543	nd	nd	nd	nd	nd	nd	nd	nd	nd	nd	nd	nd	nd	nd	nd	nd	nd	nd	nd	nd
PE	38:4	766.5390	766.5417	9.99	nd	nd	nd	nd	nd	nd	nd	234	167	nd	264.4	135.8	nd	nd	nd	200.1	64.3	32.1
PE	38:5	764.5230	764.5204	8.98	nd	nd	nd	nd	nd	nd	nd	60	42	nd	67.8	34.1	nd	nd	nd	51.0	16.8	33.0
PE	38:6	762.5070	762.5071	8.36	nd	nd	nd	nd	nd	nd	nd	222	108	nd	250.8	87.8	nd	nd	nd	169.3	81.5	48.1
PE	38:7	760.4918	nd	nd	nd	nd	nd	nd	nd	nd	nd	nd	nd	nd	nd	nd	nd	nd	nd	nd	nd	nd
PE	40:0	800.6169	nd	nd	nd	nd	nd	nd	nd	nd	nd	nd	nd	nd	nd	nd	nd	nd	nd	nd	nd	nd
PE	40:1	798.6013	nd	nd	nd	nd	nd	nd	nd	nd	nd	nd	nd	nd	nd	nd	nd	nd	nd	nd	nd	nd
PE	40:2	796.5856	nd	nd	nd	nd	nd	nd	nd	nd	nd	nd	nd	nd	nd	nd	nd	nd	nd	nd	nd	nd
PE	40:3	794.5700	nd	nd	nd	nd	nd	nd	nd	nd	nd	nd	nd	nd	nd	nd	nd	nd	nd	nd	nd	nd
PE	40:4	792.5543	792.5530	10.09	nd	nd	nd	nd	nd	nd	nd	19	23	nd	21.5	18.7	nd	nd	nd	20.1	1.4	6.9
PE	40:5	790.5387	790.5390	9.80	nd	nd	nd	nd	nd	nd	nd	146	102	nd	165.0	82.9	nd	nd	nd	123.9	41.0	33.1
PE	40:6	788.5230	788.5212	8.83	nd	nd	nd	nd	nd	nd	nd	24	15	nd	27.1	12.2	nd	nd	nd	19.7	7.5	38.0
PE	40:8	786.5074	nd	nd	nd	nd	nd	nd	nd	nd	nd	nd	nd	nd	nd	nd	nd	nd	nd	nd	nd	nd
PE	44:2	852.6483	nd	nd	nd	nd	nd	nd	nd	nd	nd	nd	nd	nd	nd	nd	nd	nd	nd	nd	nd	nd
PE	44:12	834.5074	nd	nd	nd	nd	nd	nd	nd	nd	nd	nd	nd	nd	nd	nd	nd	nd	nd	nd	nd	nd

Table 16. Quantified PEs from the immunoprecipitation of HEK293 cells overexpressing pBABEpuro-GFP-LC3B employing anti-GFP antibody followed by treatment with N-(His)<sub>6</sub>-3C-Atg4B.

Class	Lipid	Calc. Mass. [M+H] <sup>-</sup>	Found Mass. [M+H] <sup>-</sup>	RT (min)	Area - Atg4B			Conc. (pmol/sample) - Atg4B			Area + Atg4B			Conc. (pmol/sample) + Atg4B			HEK293 pBABEpuro-GFP-LC3B -Atg4 (n=3)			HEK293 pBABEpuro-GFP-LC3B +Atg4 (n=3)		
					1	2	3	1	2	3	1	2	3	1	2	3	Mean	SD	%CV	Mean	SD	%CV
PE	Std	747.7176	747.7132	9.31	122	98	78	200.0	200.0	200.0	147	111	171	200.0	200.0	200.0	200.0	25.0	12.5	200.0	0.0	0.0
PE	28:0	634.4448	634.4471	6.27	nd	nd	nd	nd	nd	nd	3	6	nd	4.1	10.8	nd	nd	nd	nd	7.4	3.4	45.2
PE	30:0	662.4761	662.4734	7.58	nd	nd	nd	nd	nd	nd	6	13	nd	8.2	23.4	nd	nd	nd	nd	15.8	7.6	48.3
PE	31:0	676.4918	nd	nd	nd	nd	nd	nd	nd	nd	nd	nd	nd	nd	nd	nd	nd	nd	nd	nd	nd	nd
PE	31:1	674.4761	674.4774	7.49	nd	nd	nd	nd	nd	nd	5	9	nd	6.8	16.2	nd	nd	nd	nd	11.5	4.7	40.9
PE	32:0	690.5074	nd	nd	nd	nd	nd	nd	nd	nd	nd	nd	nd	nd	nd	nd	nd	nd	nd	nd	nd	nd
PE	32:1	688.4920	688.4917	8.08	nd	nd	nd	nd	nd	nd	6	12	nd	8.2	21.6	nd	nd	nd	nd	14.9	6.7	45.2
PE	32:2	686.4760	nd	nd	nd	nd	nd	nd	nd	nd	nd	nd	nd	nd	nd	nd	nd	nd	nd	nd	nd	nd
PE	32:3	684.4604	nd	nd	nd	nd	nd	nd	nd	nd	nd	nd	nd	nd	nd	nd	nd	nd	nd	nd	nd	nd
PE	33:0	704.5230	nd	nd	nd	nd	nd	nd	nd	nd	nd	nd	nd	nd	nd	nd	nd	nd	nd	nd	nd	nd
PE	33:1	702.5074	702.5056	8.90	nd	nd	nd	nd	nd	nd	39	81	nd	53.1	145.9	nd	nd	nd	nd	99.5	46.4	46.7
PE	33:2	700.4918	nd	nd	nd	nd	nd	nd	nd	nd	nd	nd	nd	nd	nd	nd	nd	nd	nd	nd	nd	nd
PE	33:3	698.4761	nd	nd	nd	nd	nd	nd	nd	nd	nd	nd	nd	nd	nd	nd	nd	nd	nd	nd	nd	nd
PE	34:0	718.5387	nd	nd	nd	nd	nd	nd	nd	nd	nd	nd	nd	nd	nd	nd	nd	nd	nd	nd	nd	nd
PE	34:1	716.5230	716.5205	9.31	nd	nd	nd	nd	nd	nd	9	24	11	12.2	43.2	12.9	nd	nd	nd	22.8	14.5	63.5
PE	34:2	714.5074	714.5089	8.46	nd	nd	nd	nd	nd	nd	5	49	44	6.8	88.3	51.5	nd	nd	nd	48.9	33.3	68.2
PE	34:3	712.4918	nd	nd	nd	nd	nd	nd	nd	nd	nd	nd	nd	nd	nd	nd	nd	nd	nd	nd	nd	nd
PE	34:4	710.4761	nd	nd	nd	nd	nd	nd	nd	nd	nd	nd	nd	nd	nd	nd	nd	nd	nd	nd	nd	nd
PE	35:0	732.5543	nd	nd	nd	nd	nd	nd	nd	nd	nd	nd	nd	nd	nd	nd	nd	nd	nd	nd	nd	nd
PE	35:1	730.5387	730.5368	10.18	nd	nd	nd	nd	nd	nd	17	30	nd	23.1	54.1	nd	nd	nd	nd	38.6	15.5	40.1
PE	35:2	728.5230	728.5191	9.21	nd	nd	nd	nd	nd	nd	4	14	nd	5.4	25.2	nd	nd	nd	nd	15.3	9.9	64.5
PE	36:0	746.5700	746.5759	7.30	nd	nd	nd	nd	nd	nd	4	nd	nd	5.4	nd	9.4	nd	nd	nd	7.4	2.0	26.5
PE	36:1	744.5543	744.5579	10.74	nd	8	nd	nd	16.3	nd	nd	nd	8	nd	nd	53.8	16.3	0.0	0.0	53.8	0.0	0.0
PE	36:2	742.5387	742.5400	9.87	4	nd	nd	6.6	nd	nd	7	65	46	9.5	117.1	nd	6.6	0.0	0.0	63.3	53.8	85.0
PE	36:3	740.5230	nd	nd	nd	nd	nd	nd	nd	nd	nd	nd	nd	nd	nd	nd	nd	nd	nd	nd	nd	nd

Class	Lipid	Calc. Mass. [M+H]-	Found Mass. [M+H]-	RT (min)	Area - Atg4B			Conc. (pmol/sample) - Atg4B			Area + Atg4B			Conc. (pmol/sample) + Atg4B			HEK293 pBABEpuro-GFP-LC3B -Atg4 (n=3)			HEK293 pBABEpuro-GFP-LC3B +Atg4 (n=3)		
					1	2	3	1	2	3	1	2	3	1	2	3	Mean	SD	%CV	Mean	SD	%CV
PE	36:4	738.5074	738.5104	8.55	nd	nd	nd	nd	nd	nd	nd	102	135	nd	183.8	157.9	nd	nd	nd	170.8	12.9	7.6
PE	36:5	736.4918	736.4979	7.67	nd	nd	nd	nd	nd	nd	nd	6	nd	nd	10.8	nd	nd	nd	nd	10.8	0.0	0.0
PE	36:6	734.4761	nd	nd	nd	nd	nd	nd	nd	nd	nd	nd	nd	nd	nd	nd	nd	nd	nd	nd	nd	nd
PE	38:0	774.6013	nd	nd	nd	nd	nd	nd	nd	nd	nd	nd	nd	nd	nd	nd	nd	nd	nd	nd	nd	nd
PE	38:1	772.5856	nd	nd	nd	nd	nd	nd	nd	nd	nd	nd	nd	nd	nd	nd	nd	nd	nd	nd	nd	nd
PE	38:2	770.5700	770.5710	11.22	nd	nd	nd	nd	nd	nd	5	9	nd	6.8	16.2		nd	nd	nd	11.5	4.7	40.9
PE	38:3	768.5543	nd	nd	nd	nd	nd	nd	nd	nd	nd	nd	nd	nd	nd	nd	nd	nd	nd	nd	nd	nd
PE	38:4	766.5390	766.5372	9.93	4	nd	nd	6.6	nd	nd	nd	205	314	nd	369.4	367.3	6.6	0.0	0.0	368.3	1.1	0.3
PE	38:5	764.5230	764.5190	8.98	nd	nd	nd	nd	nd	nd	nd	72	123	nd	129.7	143.9	nd	nd	nd	136.8	7.1	5.2
PE	38:6	762.5070	762.5129	8.30	nd	nd	nd	nd	nd	nd	nd	173	353	nd	311.7	412.9	nd	nd	nd	362.3	50.6	14.0
PE	38:7	760.4918	nd	nd	nd	nd	nd	nd	nd	nd	nd	nd	nd	nd	nd	nd	nd	nd	nd	nd	nd	nd
PE	40:0	800.6169	nd	nd	nd	nd	nd	nd	nd	nd	nd	nd	nd	nd	nd	nd	nd	nd	nd	nd	nd	nd
PE	40:1	798.6013	nd	nd	nd	nd	nd	nd	nd	nd	nd	nd	nd	nd	nd	nd	nd	nd	nd	nd	nd	nd
PE	40:2	796.5856	nd	nd	nd	nd	nd	nd	nd	nd	nd	nd	nd	nd	nd	nd	nd	nd	nd	nd	nd	nd
PE	40:3	794.5700	794.5745	10.81	nd	nd	nd	nd	nd	nd	nd	7	nd	nd	12.6	nd	nd	nd	nd	12.6	0.0	0.0
PE	40:4	792.5543	792.5572	10.02	nd	nd	nd	nd	nd	nd	nd	34	36	nd	61.3	42.1	nd	nd	nd	51.7	9.6	18.5
PE	40:5	790.5387	790.5354	9.71	nd	nd	nd	nd	nd	nd	nd	145	213	nd	261.3	249.1	nd	nd	nd	255.2	6.1	2.4
PE	40:6	788.5230	788.5219	8.77	nd	nd	nd	nd	nd	nd	nd	26	40	nd	46.8	46.8	nd	nd	nd	46.8	0.0	0.1
PE	40:8	786.5074	nd	nd	nd	nd	nd	nd	nd	nd	nd	nd	nd	nd	nd	nd	nd	nd	nd	nd	nd	nd
PE	44:2	852.6483	nd	nd	nd	nd	nd	nd	nd	nd	nd	nd	nd	nd	nd	nd	nd	nd	nd	nd	nd	nd
PE	44:12	834.5074	nd	nd	nd	nd	nd	nd	nd	nd	nd	nd	nd	nd	nd	nd	nd	nd	nd	nd	nd	nd

Table 17. Quantified PEs from the immunoprecipitation of MCF7 cells overexpressing pOPIN-GFP-LC3B employing anti-GFP antibody followed by treatment with N-(His)<sub>6</sub>-3C-Atg4B.

Class	Lipid	Calc. Mass. [M+H] <sup>-</sup>	Found Mass. [M+H] <sup>-</sup>	RT (min)	- Antibody																	
					Area - Atg4B			Conc. (pmol/sample) - Atg4B			Area + Atg4B			Conc. (pmol/sample) + Atg4B			MCF7 pOPIN-GFP-LC3B -Atg4 (n=3)			MCF7 pOPIN-GFP-LC3B +Atg4 (n=3)		
					1	2	3	1	2	3	1	2	3	1	2	3	Mean	SD	%CV	Mean	SD	%CV
PE	Std	747.7176	749.7324	9.15	420	473	515	200.0	200.0	200.0	193	392	427	200.0	200.0	200.0	200.0	0.0	0.0	200.0	0.0	0.0
PE	28:0	634.4448	nd	nd	nd	nd	nd	nd	nd	nd	nd	nd	nd	nd	nd	nd	nd	nd	nd	nd	nd	nd
PE	30:0	662.4761	nd	nd	nd	nd	nd	nd	nd	nd	nd	nd	nd	nd	nd	nd	nd	nd	nd	nd	nd	nd
PE	31:0	676.4918	nd	nd	nd	nd	nd	nd	nd	nd	nd	nd	nd	nd	nd	nd	nd	nd	nd	nd	nd	nd
PE	31:1	674.4761	nd	nd	nd	nd	nd	nd	nd	nd	nd	nd	nd	nd	nd	nd	nd	nd	nd	nd	nd	nd
PE	32:0	690.5074	nd	nd	nd	nd	nd	nd	nd	nd	nd	nd	nd	nd	nd	nd	nd	nd	nd	nd	nd	nd
PE	32:1	688.4920	nd	nd	nd	nd	nd	nd	nd	nd	nd	nd	nd	nd	nd	nd	nd	nd	nd	nd	nd	nd
PE	32:2	686.4760	nd	nd	nd	nd	nd	nd	nd	nd	nd	nd	nd	nd	nd	nd	nd	nd	nd	nd	nd	nd
PE	32:3	684.4604	nd	nd	nd	nd	nd	nd	nd	nd	nd	nd	nd	nd	nd	nd	nd	nd	nd	nd	nd	nd
PE	33:0	704.5230	704.5294	8.82	nd	nd	nd	nd	nd	nd	32	50	112	33.2	25.5	52.5	nd	nd	nd	37.0	11.3	30.6
PE	33:1	702.5074	nd	nd	nd	nd	nd	nd	nd	nd	nd	nd	nd	nd	nd	nd	nd	nd	nd	nd	nd	nd
PE	33:2	700.4918	nd	nd	nd	nd	nd	nd	nd	nd	nd	nd	nd	nd	nd	nd	nd	nd	nd	nd	nd	nd
PE	33:3	698.4761	nd	nd	nd	nd	nd	nd	nd	nd	nd	nd	nd	nd	nd	nd	nd	nd	nd	nd	nd	nd
PE	34:0	718.5387	718.5338	9.17	nd	nd	nd	nd	nd	nd	33	46	nd	16.8	21.5	nd	nd	nd	19.2	2.4	12.3	nd
PE	34:1	716.5230	nd	nd	nd	nd	nd	nd	nd	nd	nd	nd	nd	nd	nd	nd	nd	nd	nd	nd	nd	nd
PE	34:2	714.5074	nd	nd	nd	nd	nd	nd	nd	nd	nd	nd	nd	nd	nd	nd	nd	nd	nd	nd	nd	nd
PE	34:3	712.4918	nd	nd	nd	nd	nd	nd	nd	nd	nd	nd	nd	nd	nd	nd	nd	nd	nd	nd	nd	nd
PE	34:4	710.4761	nd	nd	nd	nd	nd	nd	nd	nd	nd	nd	nd	nd	nd	nd	nd	nd	nd	nd	nd	nd
PE	35:0	732.5543	732.5498	9.98	nd	nd	nd	nd	nd	nd	27	51	nd	13.8	23.9	nd	nd	nd	18.8	5.1	26.8	nd
PE	35:1	730.5387	730.5328	9.01	nd	nd	nd	nd	nd	nd	8	18	nd	4.1	8.4	nd	nd	nd	6.3	2.2	34.8	nd
PE	35:2	728.5230	nd	nd	nd	nd	nd	nd	nd	nd	nd	nd	nd	nd	nd	nd	nd	nd	nd	nd	nd	nd
PE	36:0	746.5700	746.5707	8.60	46	73	nd	21.9	30.9	nd	14	60	92	14.5	30.6	43.1	26.4	4.5	17.0	29.4	11.7	39.8
PE	36:1	744.5543	744.5509	9.51	nd	nd	nd	nd	nd	nd	nd	52	nd	nd	24.4	nd	nd	nd	24.4	0.0	0.0	nd
PE	36:2	742.5387	nd	nd	nd	nd	nd	nd	nd	nd	nd	nd	nd	nd	nd	nd	nd	nd	nd	nd	nd	nd
PE	36:3	740.5230	nd	nd	nd	nd	nd	nd	nd	nd	nd	nd	nd	nd	nd	nd	nd	nd	nd	nd	nd	nd

- Antibody																						
Class	Lipid	Calc. Mass. [M+H] <sup>-</sup>	Found Mass. [M+H] <sup>-</sup>	RT (min)	Area - Atg4B			Conc. (pmol/sample) - Atg4B			Area + Atg4B			Conc. (pmol/sample) + Atg4B			MCF7 pOPIN- GFP-LC3B -Atg4 (n=3)			MCF7 pOPIN- GFP-LC3B +Atg4 (n=3)		
					1	2	3	1	2	3	1	2	3	1	2	3	Mean	SD	%CV	Mean	SD	%CV
PE	36:4	738.5074	nd	nd	nd	nd	nd	nd	nd	nd	nd	nd	nd	nd	nd	nd	nd	nd	nd	nd	nd	nd
PE	36:5	736.4918	nd	nd	nd	nd	nd	nd	nd	nd	nd	nd	nd	nd	nd	nd	nd	nd	nd	nd	nd	nd
PE	36:6	734.4761	nd	nd	nd	nd	nd	nd	nd	nd	nd	nd	nd	nd	nd	nd	nd	nd	nd	nd	nd	nd
PE	38:0	774.6013	774.5952	9.98	28	40	nd	13.3	16.9	nd	nd	nd	49	nd	nd	23.0	15.1	1.8	11.8	23.0	0.0	0.0
PE	38:1	772.5856	nd	nd	nd	nd	nd	nd	nd	nd	nd	nd	nd	nd	nd	nd	nd	nd	nd	nd	nd	nd
PE	38:2	770.5700	nd	nd	nd	nd	nd	nd	nd	nd	nd	nd	nd	nd	nd	nd	nd	nd	nd	nd	nd	nd
PE	38:3	768.5543	nd	nd	nd	nd	nd	nd	nd	nd	nd	nd	nd	nd	nd	nd	nd	nd	nd	nd	nd	nd
PE	38:4	766.5390	nd	nd	nd	nd	nd	nd	nd	nd	nd	nd	nd	nd	nd	nd	nd	nd	nd	nd	nd	nd
PE	38:5	764.5230	nd	nd	nd	nd	nd	nd	nd	nd	nd	nd	nd	nd	nd	nd	nd	nd	nd	nd	nd	nd
PE	38:6	762.5070	nd	nd	nd	nd	nd	nd	nd	nd	nd	nd	nd	nd	nd	nd	nd	nd	nd	nd	nd	nd
PE	38:7	760.4918	nd	nd	nd	nd	nd	nd	nd	nd	nd	nd	nd	nd	nd	nd	nd	nd	nd	nd	nd	nd
PE	40:0	800.6169	800.6202	10.40	nd	10	nd	nd	4.2	nd	nd	nd	15	nd	nd	7.0	4.2	0.0	0.0	7.0	0.0	0.0
PE	40:1	798.6013	nd	nd	nd	nd	nd	nd	nd	nd	nd	nd	nd	nd	nd	nd	nd	nd	nd	nd	nd	nd
PE	40:2	796.5856	nd	nd	nd	nd	nd	nd	nd	nd	nd	nd	nd	nd	nd	nd	nd	nd	nd	nd	nd	nd
PE	40:3	794.5700	794.5654	9.54	nd	nd	nd	nd	nd	nd	nd	24	nd	nd	12.2	nd	nd	nd	nd	12.2	0.0	0.0
PE	40:4	792.5543	nd	nd	nd	nd	nd	nd	nd	nd	nd	nd	nd	nd	nd	nd	nd	nd	nd	nd	nd	nd
PE	40:5	790.5387	790.5346	9.96	nd	77	nd	nd	32.6	nd	nd	nd	nd	nd	nd	nd	32.6	0.0	0.0	nd	nd	nd
PE	40:6	788.5230	nd	nd	nd	nd	nd	nd	nd	nd	nd	nd	nd	nd	nd	nd	nd	nd	nd	nd	nd	nd
PE	40:8	786.5074	nd	nd	nd	nd	nd	nd	nd	nd	nd	nd	nd	nd	nd	nd	nd	nd	nd	nd	nd	nd
PE	44:2	852.6483	nd	nd	nd	nd	nd	nd	nd	nd	nd	nd	nd	nd	nd	nd	nd	nd	nd	nd	nd	nd



- Antibody																						
Class	Lipid	Calc. Mass. [M+H] <sup>-</sup>	Found Mass. [M+H] <sup>-</sup>	RT (min)	Area - Atg4B			Conc. (pmol/sample) - Atg4B			Area + Atg4B			Conc. (pmol/sample) + Atg4B			MCF7 pOPIN-GFP-LC3B -Atg4 (n=3)			MCF7 pOPIN-GFP-LC3B +Atg4 (n=3)		
					1	2	3	1	2	3	1	2	3	1	2	3	Mean	SD	%CV	Mean	SD	%CV
PE	44:12	834.5074	nd	nd	nd	nd	nd	nd	nd	nd	nd	nd	nd	nd	nd	nd	nd	nd	nd	nd	nd	nd

Table 18. Quantified PEs from the immunoprecipitation of HeLa cells employing anti-LC3B antibody followed by treatment with N-(His)<sub>6</sub>-3C-Atg4B.

- Antibody - Atg4B																		
Class	Lipid	Calc. Mass. [M+H] <sup>-</sup>	Found Mass. [M+H] <sup>-</sup>	RT (min)	Area					Conc. (pmol/sample)					HeLa -Atg4 (n=5)			
					1	2	3	4	5	1	2	3	4	5	Mean	SD	%CV	
PE	Std	747.7176	747.7174	9.19	111	138	130	69	90	200.0	200.0	200.0	200.0	200.0	200.0	0.0	0.0	
PE	28:0	634.4448	nd	nd	nd	nd	nd	nd	nd	nd	nd	nd	nd	nd	nd	nd	nd	
PE	30:0	662.4761	662.4777	7.46	nd	nd	nd	nd	nd	nd	nd	nd	nd	nd	nd	nd	nd	
PE	31:0	676.4918	nd	nd	nd	nd	nd	nd	nd	nd	nd	nd	nd	nd	nd	nd	nd	
PE	31:1	674.4761	674.4767	7.21	nd	nd	nd	nd	nd	nd	nd	nd	nd	nd	nd	nd	nd	
PE	32:0	690.5074	nd	nd	nd	nd	nd	nd	nd	nd	nd	nd	nd	nd	nd	nd	nd	
PE	32:1	688.4920	nd	nd	nd	nd	nd	nd	nd	nd	nd	nd	nd	nd	nd	nd	nd	
PE	32:2	686.4760	nd	nd	nd	nd	nd	nd	nd	nd	nd	nd	nd	nd	nd	nd	nd	
PE	32:3	684.4604	nd	nd	nd	nd	nd	nd	nd	nd	nd	nd	nd	nd	nd	nd	nd	
PE	33:0	704.5230	nd	nd	nd	nd	nd	nd	nd	nd	nd	nd	nd	nd	nd	nd	nd	
PE	33:1	702.5074	702.5044	8.78	nd	nd	nd	nd	nd	nd	nd	nd	nd	nd	nd	nd	nd	
PE	33:2	700.4918	nd	nd	nd	nd	nd	nd	nd	nd	nd	nd	nd	nd	nd	nd	nd	
PE	33:3	698.4761	nd	nd	nd	nd	nd	nd	nd	nd	nd	nd	nd	nd	nd	nd	nd	
PE	34:0	718.5387	nd	nd	nd	nd	nd	nd	nd	nd	nd	nd	nd	nd	nd	nd	nd	
PE	34:1	716.5230	716.5234	9.25	nd	35	21	6	6	nd	50.7	32.3	17.4	13.3	28.4	14.7	51.6	
PE	34:2	714.5074	714.5120	8.25	nd	42	21	3	nd	nd	60.9	32.3	8.7	nd	34.0	21.3	62.8	
PE	34:3	712.4918	nd	nd	nd	nd	nd	nd	nd	nd	nd	nd	nd	nd	nd	nd	nd	
PE	34:4	710.4761	nd	nd	nd	nd	nd	nd	nd	nd	nd	nd	nd	nd	nd	nd	nd	
PE	35:0	732.5543	nd	nd	nd	nd	nd	nd	nd	nd	nd	nd	nd	nd	nd	nd	nd	

- Antibody - Atg4B																	
Class	Lipid	Calc. Mass. [M+H]-	Found Mass. [M+H]-	RT (min)	Area					Conc. (pmol/sample)					HeLa -Atg4 (n=5)		
					1	2	3	4	5	1	2	3	4	5	Mean	SD	%CV
PE	35:1	730.5387	730.5403	10.00	nd	nd	nd	nd	nd	nd	nd	nd	nd	nd	nd	nd	nd
PE	35:2	728.5230	728.5215	9.06	nd	nd	nd	nd	nd	nd	nd	nd	nd	nd	nd	nd	nd
PE	36:0	746.5700	nd	nd	nd	nd	nd	nd	nd	nd	nd	nd	nd	nd	nd	nd	nd
PE	36:1	744.5543	744.5572	10.66	11	20	11	nd	3	19.8	29.0	16.9	nd	6.7	18.1	8.0	44.0
PE	36:2	742.5387	742.5330	9.66	59	77	43	nd	9	106.3	111.6	66.2	nd	20.0	76.0	36.8	48.4
PE	36:3	740.5230	740.5198	8.72	nd	14	nd	nd	nd	nd	20.3	nd	nd	nd	20.3	0.0	0.0
PE	36:4	738.5074	738.5082	8.37	nd	13	nd	nd	nd	nd	18.8	nd	nd	nd	18.8	0.0	0.0
PE	36:5	736.4918	nd	nd	nd	nd	nd	nd	nd	nd	nd	nd	nd	nd	nd	nd	nd
PE	36:6	734.4761	nd	nd	nd	nd	nd	nd	nd	nd	nd	nd	nd	nd	nd	nd	nd
PE	38:0	774.6013	nd	nd	nd	nd	nd	nd	nd	nd	nd	nd	nd	nd	nd	nd	nd
PE	38:1	772.5856	nd	nd	nd	nd	nd	nd	nd	nd	nd	nd	nd	nd	nd	nd	nd
PE	38:2	770.5700	770.5665	10.96	nd	nd	nd	nd	nd	nd	nd	nd	nd	nd	nd	nd	nd
PE	38:3	768.5543	nd	nd	nd	nd	nd	nd	nd	nd	nd	nd	nd	nd	nd	nd	nd
PE	38:4	766.5390	nd	nd	nd	nd	nd	nd	nd	nd	nd	nd	nd	nd	nd	nd	nd
PE	38:5	764.5230	nd	nd	nd	nd	nd	nd	nd	nd	nd	nd	nd	nd	nd	nd	nd
PE	38:6	762.5070	nd	nd	nd	nd	nd	nd	nd	nd	nd	nd	nd	nd	nd	nd	nd
PE	38:7	760.4918	nd	nd	nd	nd	nd	nd	nd	nd	nd	nd	nd	nd	nd	nd	nd
PE	40:0	800.6169	nd	nd	nd	nd	nd	nd	nd	nd	nd	nd	nd	nd	nd	nd	nd
PE	40:1	798.6013	798.6042	7.96	62	15	nd	nd	nd	111.7	21.7	nd	nd	nd	66.7	45.0	67.4
PE	40:2	796.5856	nd	nd	nd	nd	nd	nd	nd	nd	nd	nd	nd	nd	nd	nd	nd
PE	40:3	794.5700	nd	nd	nd	nd	nd	nd	nd	nd	nd	nd	nd	nd	nd	nd	nd
PE	40:4	792.5543	nd	nd	nd	nd	nd	nd	nd	nd	nd	nd	nd	nd	nd	nd	nd
PE	40:5	790.5387	nd	nd	nd	nd	nd	nd	nd	nd	nd	nd	nd	nd	nd	nd	nd
PE	40:6	788.5230	788.5245	9.87	nd	nd	nd	nd	nd	nd	nd	nd	nd	nd	nd	nd	nd
PE	40:8	786.5074	nd	nd	nd	nd	nd	nd	nd	nd	nd	nd	nd	nd	nd	nd	nd
PE	44:2	852.6483	nd	nd	nd	nd	nd	nd	nd	nd	nd	nd	nd	nd	nd	nd	nd
PE	44:12	834.5074	nd	nd	nd	nd	nd	nd	nd	nd	nd	nd	nd	nd	nd	nd	nd

- Antibody + Atg4B																	
Class	Lipid	Calc. Mass. [M+H]-	Found Mass. [M+H]-	RT (min)	Area					Conc. (pmol/sample)					HeLa +Atg4 (n=5)		
					1	2	3	4	5	1	2	3	4	5	Mean	SD	%CV
PE	Std	747.7176	747.7174	9.19	76	87	80	100	30	200.0	200.0	200.0	200.0	200.0	200.0	0.0	0.0
PE	28:0	634.4448	nd	nd	nd	nd	nd	nd	nd	nd	nd	nd	nd	nd	nd	nd	nd
PE	30:0	662.4761	662.4777	7.46	7	nd	7	10	nd	18.4	nd	17.5	20.0	nd	18.6	1.0	5.5
PE	31:0	676.4918	nd	nd	nd	nd	nd	nd	nd	nd	nd	nd	nd	nd	nd	nd	nd
PE	31:1	674.4761	674.4767	7.21	nd	nd	nd	7	3	nd	nd	nd	14.0	nd	14.0	0.0	0.0
PE	32:0	690.5074	nd	nd	nd	nd	nd	nd	nd	nd	nd	nd	nd	nd	nd	nd	nd
PE	32:1	688.4920	nd	nd	nd	nd	nd	nd	nd	nd	nd	nd	nd	nd	nd	nd	nd
PE	32:2	686.4760	nd	nd	nd	nd	nd	nd	nd	nd	nd	nd	nd	nd	nd	nd	nd
PE	32:3	684.4604	nd	nd	nd	nd	nd	nd	nd	nd	nd	nd	nd	nd	nd	nd	nd
PE	33:0	704.5230	nd	nd	nd	nd	nd	nd	nd	nd	nd	nd	nd	nd	nd	nd	nd
PE	33:1	702.5074	702.5044	8.78	35	28	27	43	13	92.1	64.4	67.5	86.0	nd	77.5	11.8	15.2
PE	33:2	700.4918	nd	nd	nd	nd	nd	nd	nd	nd	nd	nd	nd	nd	nd	nd	nd
PE	33:3	698.4761	nd	nd	nd	nd	nd	nd	nd	nd	nd	nd	nd	nd	nd	nd	nd
PE	34:0	718.5387	nd	nd	nd	nd	nd	nd	nd	nd	nd	nd	nd	nd	nd	nd	nd
PE	34:1	716.5230	716.5234	9.25	24	30	24	20	7	63.2	69.0	60.0	40.0	46.7	55.8	10.8	19.3
PE	34:2	714.5074	714.5120	8.25	20	23	24	6	nd	52.6	52.9	60.0	12.0	nd	44.4	18.9	42.6
PE	34:3	712.4918	nd	nd	nd	nd	nd	nd	nd	nd	nd	nd	nd	nd	nd	nd	nd
PE	34:4	710.4761	nd	nd	nd	nd	nd	nd	nd	nd	nd	nd	nd	nd	nd	nd	nd
PE	35:0	732.5543	nd	nd	nd	nd	nd	nd	nd	nd	nd	nd	nd	nd	nd	nd	nd
PE	35:1	730.5387	730.5403	10.00	12	13	11	20	nd	31.6	29.9	27.5	40.0	nd	32.2	4.7	14.6
PE	35:2	728.5230	728.5215	9.06	12	6	5	nd	nd	31.6	13.8	12.5	nd	nd	19.3	8.7	45.1
PE	36:0	746.5700	nd	nd	nd	nd	nd	nd	nd	nd	nd	nd	nd	nd	nd	nd	nd
PE	36:1	744.5543	744.5572	10.66	10	14	10	8	nd	26.3	32.2	25.0	16.0	nd	24.9	5.8	23.3
PE	36:2	742.5387	742.5330	9.66	65	68	51	20	nd	171.1	156.3	127.5	40.0	nd	123.7	50.8	41.1
PE	36:3	740.5230	740.5198	8.72	7	nd	nd	nd	nd	18.4	nd	nd	nd	nd	18.4	0.0	0.0
PE	36:4	738.5074	738.5082	8.37	nd	nd	nd	nd	nd	nd	nd	nd	nd	nd	nd	nd	nd
PE	36:5	736.4918	nd	nd	nd	nd	nd	nd	nd	nd	nd	nd	nd	nd	nd	nd	nd
PE	36:6	734.4761	nd	nd	nd	nd	nd	nd	nd	nd	nd	nd	nd	nd	nd	nd	nd
PE	38:0	774.6013	nd	nd	nd	nd	nd	nd	nd	nd	nd	nd	nd	nd	nd	nd	nd
PE	38:1	772.5856	nd	nd	nd	nd	nd	nd	nd	nd	nd	nd	nd	nd	nd	nd	nd

- Antibody + Atg4B																	
Class	Lipid	Calc. Mass. [M+H]-	Found Mass. [M+H]-	RT (min)	Area					Conc. (pmol/sample)					HeLa +Atg4 (n=5)		
					1	2	3	4	5	1	2	3	4	5	Mean	SD	%CV
PE	38:2	770.5700	770.5665	10.96	nd	nd	nd	9	nd	nd	nd	nd	18.0	nd	18.0	0.0	0.0
PE	38:3	768.5543	nd	nd	nd	nd	nd	nd	nd	nd	nd	nd	nd	nd	nd	nd	nd
PE	38:4	766.5390	nd	nd	nd	nd	nd	nd	nd	nd	nd	nd	nd	nd	nd	nd	nd
PE	38:5	764.5230	nd	nd	nd	nd	nd	nd	nd	nd	nd	nd	nd	nd	nd	nd	nd
PE	38:6	762.5070	nd	nd	nd	nd	nd	nd	nd	nd	nd	nd	nd	nd	nd	nd	nd
PE	38:7	760.4918	nd	nd	nd	nd	nd	nd	nd	nd	nd	nd	nd	nd	nd	nd	nd
PE	40:0	800.6169	nd	nd	nd	nd	nd	nd	nd	nd	nd	nd	nd	nd	nd	nd	nd
PE	40:1	798.6013	798.6042	7.96	29	15	nd	nd	nd	76.3	34.5	nd	nd	nd	55.4	20.9	37.8
PE	40:2	796.5856	nd	nd	nd	nd	nd	nd	nd	nd	nd	nd	nd	nd	nd	nd	nd
PE	40:3	794.5700	nd	nd	nd	nd	nd	nd	nd	nd	nd	nd	nd	nd	nd	nd	nd
PE	40:4	792.5543	nd	nd	nd	nd	nd	nd	nd	nd	nd	nd	nd	nd	nd	nd	nd
PE	40:5	790.5387	nd	nd	nd	nd	nd	nd	nd	nd	nd	nd	nd	nd	nd	nd	nd
PE	40:6	788.5230	788.5245	9.87	4	nd	nd	nd	nd	10.5	nd	nd	nd	nd	10.5	0.0	0.0
PE	40:8	786.5074	nd	nd	nd	nd	nd	nd	nd	nd	nd	nd	nd	nd	nd	nd	nd
PE	44:2	852.6483	nd	nd	nd	nd	nd	nd	nd	nd	nd	nd	nd	nd	nd	nd	nd
PE	44:12	834.5074	nd	nd	nd	nd	nd	nd	nd	nd	nd	nd	nd	nd	nd	nd	nd

+ Antibody - Atg4B																	
Class	Lipid	Calc. Mass. [M+H]-	Found Mass. [M+H]-	RT (min)	Area					Conc. (pmol/sample)					HeLa -Atg4 (n=5)		
					1	2	3	4	5	1	2	3	4	5	Mean	SD	%CV
PE	Std	747.7176	747.7184	9.09	91	70	71	99	66	200.0	200.0	200.0	200.0	200.0	200.0	0.0	0.0
PE	28:0	634.4448	634.4416	6.17	nd	nd	nd	nd	nd	nd	nd	nd	nd	nd	nd	nd	nd
PE	30:0	662.4761	662.4763	7.46	nd	nd	nd	nd	nd	nd	nd	nd	nd	nd	nd	nd	nd
PE	31:0	676.4918	nd	nd	nd	nd	nd	nd	nd	nd	nd	nd	nd	nd	nd	nd	nd
PE	31:1	674.4761	674.4784	7.21	nd	nd	nd	nd	nd	nd	nd	nd	nd	nd	nd	nd	nd
PE	32:0	690.5074	690.5013	8.84	nd	nd	nd	nd	nd	nd	nd	nd	nd	nd	nd	nd	nd
PE	32:1	688.4920	688.4920	7.81	nd	nd	nd	2	nd	nd	nd	nd	4.0	nd	4.0	0.0	0.0
PE	32:2	686.4760	nd	nd	nd	nd	nd	nd	nd	nd	nd	nd	nd	nd	nd	nd	nd
PE	32:3	684.4604	nd	nd	nd	nd	nd	nd	nd	nd	nd	nd	nd	nd	nd	nd	nd

+ Antibody - Atg4B																	
Class	Lipid	Calc. Mass. [M+H]-	Found Mass. [M+H]-	RT (min)	Area					Conc. (pmol/sample)					HeLa -Atg4 (n=5)		
					1	2	3	4	5	1	2	3	4	5	Mean	SD	%CV
PE	33:0	704.5230	nd	nd	nd	nd	nd	nd	nd	nd	nd	nd	nd	nd	nd	nd	nd
PE	33:1	702.5074	702.5080	8.78	nd	nd	nd	nd	nd	nd	nd	nd	nd	nd	nd	nd	nd
PE	33:2	700.4918	nd	nd	nd	nd	nd	nd	nd	nd	nd	nd	nd	nd	nd	nd	nd
PE	33:3	698.4761	nd	nd	nd	nd	nd	nd	nd	nd	nd	nd	nd	nd	nd	nd	nd
PE	34:0	718.5387	nd	nd	nd	nd	nd	nd	nd	nd	nd	nd	nd	nd	nd	nd	nd
PE	34:1	716.5230	716.5239	9.31	27	17	15	6	9	59.3	48.6	42.3	12.1	27.3	37.9	16.6	43.7
PE	34:2	714.5074	714.5026	8.31	39	16	12	4	nd	85.7	45.7	33.8	8.1	nd	43.3	28.0	64.6
PE	34:3	712.4918	nd	nd	nd	nd	nd	nd	nd	nd	nd	nd	nd	nd	nd	nd	nd
PE	34:4	710.4761	nd	nd	nd	nd	nd	nd	nd	nd	nd	nd	nd	nd	nd	nd	nd
PE	35:0	732.5543	nd	nd	nd	nd	nd	nd	nd	nd	nd	nd	nd	nd	nd	nd	nd
PE	35:1	730.5387	730.5419	10.03	nd	nd	nd	nd	nd	nd	nd	nd	nd	nd	nd	nd	nd
PE	35:2	728.5230	728.5204	9.09	5	nd	nd	nd	nd	11.0	nd	nd	nd	nd	11.0	0.0	0.0
PE	36:0	746.5700	nd	nd	nd	nd	nd	nd	nd	nd	nd	nd	nd	nd	nd	nd	nd
PE	36:1	744.5543	744.5546	10.60	15	9	7	nd	5	33.0	25.7	19.7	nd	15.2	23.4	6.7	28.6
PE	36:2	742.5387	743.5345	9.56	62	33	29	9	nd	136.3	94.3	81.7	18.2	nd	82.6	42.3	51.2
PE	36:3	740.5230	740.5209	8.78	11	6	nd	nd	nd	24.2	17.1	nd	nd	nd	20.7	3.5	17.0
PE	36:4	738.5074	738.5072	8.41	10	nd	nd	nd	nd	22.0	nd	nd	nd	nd	22.0	0.0	0.0
PE	36:5	736.4918	nd	nd	nd	nd	nd	nd	nd	nd	nd	nd	nd	nd	nd	nd	nd
PE	36:6	734.4761	nd	nd	nd	nd	nd	nd	nd	nd	nd	nd	nd	nd	nd	nd	nd
PE	38:0	774.6013	nd	nd	nd	nd	nd	nd	nd	nd	nd	nd	nd	nd	nd	nd	nd
PE	38:1	772.5856	nd	nd	nd	nd	nd	nd	nd	nd	nd	nd	nd	nd	nd	nd	nd
PE	38:2	770.5700	770.5661	11.13	nd	nd	nd	nd	nd	nd	nd	nd	nd	nd	nd	nd	nd
PE	38:3	768.5543	nd	nd	nd	nd	nd	nd	nd	nd	nd	nd	nd	nd	nd	nd	nd
PE	38:4	766.5390	nd	nd	nd	nd	nd	nd	nd	nd	nd	nd	nd	nd	nd	nd	nd
PE	38:5	764.5230	nd	nd	nd	nd	nd	nd	nd	nd	nd	nd	nd	nd	nd	nd	nd
PE	38:6	762.5070	nd	nd	nd	nd	nd	nd	nd	nd	nd	nd	nd	nd	nd	nd	nd
PE	38:7	760.4918	nd	nd	nd	nd	nd	nd	nd	nd	nd	nd	nd	nd	nd	nd	nd
PE	40:0	800.6169	nd	nd	nd	nd	nd	nd	nd	nd	nd	nd	nd	nd	nd	nd	nd
PE	40:1	798.6013	nd	nd	nd	nd	nd	nd	nd	nd	nd	nd	nd	nd	nd	nd	nd
PE	40:2	796.5856	nd	nd	nd	nd	nd	nd	nd	nd	nd	nd	nd	nd	nd	nd	nd

<b>+ Antibody - Atg4B</b>																	
Class	Lipid	Calc. Mass. [M+H]-	Found Mass. [M+H]-	RT (min)	Area					Conc. (pmol/sample)					HeLa -Atg4 (n=5)		
					1	2	3	4	5	1	2	3	4	5	Mean	SD	%CV
PE	40:3	794.5700	nd	nd	nd	nd	nd	nd	nd	nd	nd	nd	nd	nd	nd	nd	nd
PE	40:4	792.5543	792.5574	8.36	nd	nd	nd	nd	nd	nd	nd	nd	nd	nd	nd	nd	nd
PE	40:5	790.5387	nd	nd	nd	nd	nd	nd	nd	nd	nd	nd	nd	nd	nd	nd	nd
PE	40:6	788.5230	nd	nd	nd	nd	nd	nd	nd	nd	nd	nd	nd	nd	nd	nd	nd
PE	40:8	786.5074	nd	nd	nd	nd	nd	nd	nd	nd	nd	nd	nd	nd	nd	nd	nd
PE	44:2	852.6483	nd	nd	nd	nd	nd	nd	nd	nd	nd	nd	nd	nd	nd	nd	nd
PE	44:12	834.5074	nd	nd	nd	nd	nd	nd	nd	nd	nd	nd	nd	nd	nd	nd	nd

<b>+ Antibody + Atg4B</b>																	
Class	Lipid	Calc. Mass. [M+H]-	Found Mass. [M+H]-	RT (min)	Area					Conc. (pmol/sample)					HeLa +Atg4 (n=5)		
					1	2	3	4	5	1	2	3	4	5	Mean	SD	%CV
PE	Std	747.7176	747.7184	9.09	97	56	86	96	102	200.0	200.0	200.0	200.0	200.0	200.0	0.0	0.0
PE	28:0	634.4448	634.4416	6.17	7	nd	nd	4	5	14.4	nd	nd	8.3	9.8	10.9	2.6	23.9
PE	30:0	662.4761	662.4763	7.46	24	8	nd	12	13	49.5	28.6	nd	25.0	25.5	32.1	10.1	31.5
PE	31:0	676.4918	nd	nd	nd	nd	nd	nd	nd	nd	nd	nd	nd	nd	nd	nd	nd
PE	31:1	674.4761	674.4784	7.21	nd	nd	nd	7	8	nd	nd	nd	14.6	15.7	15.1	0.6	3.6
PE	32:0	690.5074	690.5013	8.84	5	nd	nd	nd	nd	10.3	nd	nd	nd	nd	10.3	0.0	0.0
PE	32:1	688.4920	688.4920	7.81	nd	nd	nd	10	14	nd	nd	nd	20.8	27.5	24.1	3.3	13.7
PE	32:2	686.4760	nd	nd	nd	nd	nd	nd	nd	nd	nd	nd	nd	nd	nd	nd	nd
PE	32:3	684.4604	nd	nd	nd	nd	nd	nd	nd	nd	nd	nd	nd	nd	nd	nd	nd
PE	33:0	704.5230	nd	nd	nd	nd	nd	nd	nd	nd	nd	nd	nd	nd	nd	nd	nd
PE	33:1	702.5074	702.5080	8.78	104	39	52	43	53	214.4	139.3	120.9	89.6	103.9	133.6	43.7	32.7
PE	33:2	700.4918	nd	nd	nd	nd	nd	nd	nd	nd	nd	nd	nd	nd	nd	nd	nd
PE	33:3	698.4761	nd	nd	nd	nd	nd	nd	nd	nd	nd	nd	nd	nd	nd	nd	nd
PE	34:0	718.5387	nd	nd	nd	nd	nd	nd	nd	nd	nd	nd	nd	nd	nd	nd	nd
PE	34:1	716.5230	716.5239	9.31	44	19	29	20	23	90.7	67.9	67.4	41.7	45.1	62.6	17.8	28.5
PE	34:2	714.5074	714.5026	8.31	25	12	23	10	13	51.5	42.9	53.5	20.8	25.5	38.8	13.4	34.4
PE	34:3	712.4918	nd	nd	nd	nd	nd	nd	nd	nd	nd	nd	nd	nd	nd	nd	nd
PE	34:4	710.4761	nd	nd	nd	nd	nd	nd	nd	nd	nd	nd	nd	nd	nd	nd	nd

+ Antibody + Atg4B																	
Class	Lipid	Calc. Mass. [M+H]-	Found Mass. [M+H]-	RT (min)	Area					Conc. (pmol/sample)					HeLa +Atg4 (n=5)		
					1	2	3	4	5	1	2	3	4	5	Mean	SD	%CV
PE	35:0	732.5543	nd	nd	nd	nd	nd	nd	nd	nd	nd	nd	nd	nd	nd	nd	nd
PE	35:1	730.5387	730.5419	10.03	45	15	22	20	25	92.8	53.6	51.2	41.7	49.0	57.6	18.0	31.3
PE	35:2	728.5230	728.5204	9.09	15	nd	9	nd	7	30.9		20.9	nd	13.7	21.9	7.1	32.3
PE	36:0	746.5700	nd	nd	nd	nd	nd	nd	nd	nd	nd	nd	nd	nd	nd	nd	nd
PE	36:1	744.5543	744.5546	10.60	10	8	12	6	nd	20.6	28.6	27.9	12.5	nd	22.4	6.5	29.1
PE	36:2	742.5387	743.5345	9.56	54	32	44	18	23	111.3	114.3	102.3	37.5	45.1	82.1	33.6	41.0
PE	36:3	740.5230	740.5209	8.78	nd	nd	nd	nd	nd	nd	nd	nd	nd	nd	nd	nd	nd
PE	36:4	738.5074	738.5072	8.41	nd	nd	nd	nd	nd	nd	nd	nd	nd	nd	nd	nd	nd
PE	36:5	736.4918	nd	nd	nd	nd	nd	nd	nd	nd	nd	nd	nd	nd	nd	nd	nd
PE	36:6	734.4761	nd	nd	nd	nd	nd	nd	nd	nd	nd	nd	nd	nd	nd	nd	nd
PE	38:0	774.6013	nd	nd	nd	nd	nd	nd	nd	nd	nd	nd	nd	nd	nd	nd	nd
PE	38:1	772.5856	nd	nd	nd	nd	nd	nd	nd	nd	nd	nd	nd	nd	nd	nd	nd
PE	38:2	770.5700	770.5661	11.13	17	nd	nd	nd	7	35.1	nd	nd	nd	13.7	24.4	10.7	43.7
PE	38:3	768.5543	nd	nd	nd	nd	nd	nd	nd	nd	nd	nd	nd	nd	nd	nd	nd
PE	38:4	766.5390	nd	nd	nd	nd	nd	nd	nd	nd	nd	nd	nd	nd	nd	nd	nd
PE	38:5	764.5230	nd	nd	nd	nd	nd	nd	nd	nd	nd	nd	nd	nd	nd	nd	nd
PE	38:6	762.5070	nd	nd	nd	nd	nd	nd	nd	nd	nd	nd	nd	nd	nd	nd	nd
PE	38:7	760.4918	nd	nd	nd	nd	nd	nd	nd	nd	nd	nd	nd	nd	nd	nd	nd
PE	40:0	800.6169	nd	nd	nd	nd	nd	nd	nd	nd	nd	nd	nd	nd	nd	nd	nd
PE	40:1	798.6013	nd	nd	nd	nd	nd	nd	nd	nd	nd	nd	nd	nd	nd	nd	nd
PE	40:2	796.5856	nd	nd	nd	nd	nd	nd	nd	nd	nd	nd	nd	nd	nd	nd	nd
PE	40:3	794.5700	nd	nd	nd	nd	nd	nd	nd	nd	nd	nd	nd	nd	nd	nd	nd
PE	40:4	792.5543	792.5574	8.36	nd	nd	nd	nd	9	nd	nd	nd	nd	17.6	17.6	0.0	0.0
PE	40:5	790.5387	nd	nd	nd	nd	nd	nd	nd	nd	nd	nd	nd	nd	nd	nd	nd
PE	40:6	788.5230	nd	nd	nd	nd	nd	nd	nd	nd	nd	nd	nd	nd	nd	nd	nd
PE	40:8	786.5074	nd	nd	nd	nd	nd	nd	nd	nd	nd	nd	nd	nd	nd	nd	nd
PE	44:2	852.6483	nd	nd	nd	nd	nd	nd	nd	nd	nd	nd	nd	nd	nd	nd	nd
PE	44:12	834.5074	nd	nd	nd	nd	nd	nd	nd	nd	nd	nd	nd	nd	nd	nd	nd

Table 19. Quantified PEs from U87DND shC and shAtg5 cells. The lipids were obtained through precipitation of the proteome, treatment with N-(His)<sub>6</sub>-3C-Atg4B and extraction by organic solvents.

Class	Lipid	Calc. Mass. [M+H] <sup>-</sup>	Found Mass. [M+H] <sup>-</sup>	RT (min)	+ Atg4B																	
					Area shC			Conc. (pmol/sample) shC			Area shAtg5			Conc. (pmol/sample) shAtg5			U87DND shC +Atg4 (n=3)			U87DND shAtg5 +Atg4 (n=3)		
					1	2	3	1	2	3	1	2	3	1	2	3	Mean	SD	%CV	Mean	SD	%CV
PE	Std	747.7176	747.7201	8.83	368	449	376	200.0	200.0	200.0	477	243	377	200.0	200.0	200.0	200.0	0.0	0.0	200.0	0.0	0.0
PE	28:0	634.4448	634.4466	5.95	19	18	17	10.3	8.0	9.0	18	6	15	7.5	4.9	8.0	9.1	0.9	10.3	6.8	1.3	19.6
PE	30:0	662.4761	662.4769	7.17	54	49	53	29.3	21.8	28.2	49	22	43	20.5	18.1	22.8	26.5	3.3	12.5	20.5	1.9	9.4
PE	31:0	676.4918	nd	nd	nd	nd	nd	nd	nd	nd	nd	nd	nd	nd	nd	nd	nd	nd	nd	nd	nd	nd
PE	31:1	674.4761	674.4736	7.04	25	24	24	13.6	10.7	12.8	26	9	21	10.9	7.4	11.1	12.3	1.2	9.9	9.8	1.7	17.4
PE	32:0	690.5074	690.5049	8.55	13	11	13	7.1	4.9	6.9	13	7	12	5.5	5.8	6.4	6.3	1.0	15.7	5.9	0.4	6.5
PE	32:1	688.4920	688.4909	7.67	46	30	31	25.0	13.4	16.5	28	24	26	11.7	19.8	13.8	18.3	4.9	26.9	15.1	3.4	22.5
PE	32:2	686.4760	686.4745	6.73	9	nd	nd	4.9	nd	nd	nd	nd	nd	nd	nd	nd	4.9	0.0	0.0	nd	nd	nd
PE	32:3	684.4604	nd	nd	nd	nd	nd	nd	nd	nd	nd	nd	nd	nd	nd	nd	nd	nd	nd	nd	nd	nd
PE	33:0	704.5230	nd	nd	nd	nd	nd	nd	nd	nd	nd	nd	nd	nd	nd	nd	nd	nd	nd	nd	nd	nd
PE	33:1	702.5074	702.4963	8.52	157	171	189	85.3	76.2	100.5	187	64	151	78.4	52.7	80.1	87.3	10.0	11.5	70.4	12.5	17.8
PE	33:2	700.4918	nd	nd	nd	nd	nd	nd	nd	nd	nd	nd	nd	nd	nd	nd	nd	nd	nd	nd	nd	nd
PE	33:3	698.4761	nd	nd	nd	nd	nd	nd	nd	nd	nd	nd	nd	nd	nd	nd	nd	nd	nd	nd	nd	nd
PE	34:0	718.5387	718.5252	8.61	4	nd	nd	2.2	nd	nd	nd	nd	nd	nd	nd	nd	2.2	0.0	0.0	nd	nd	nd
PE	34:1	716.5230	716.5212	8.99	113	56	55	61.4	24.9	29.3	56	81	53	23.5	66.7	28.1	38.5	16.3	42.2	39.4	19.4	49.1
PE	34:2	714.5074	714.5054	8.05	77	23	25	41.8	10.2	13.3	22	54	23	9.2	44.4	12.2	21.8	14.2	65.3	22.0	15.9	72.6
PE	34:3	712.4918	712.4953	7.19	7	1	3	3.8	0.4	1.6	nd	nd	nd	nd	nd	nd	1.9	1.4	71.5	nd	nd	nd
PE	34:4	710.4761	nd	nd	nd	nd	nd	nd	nd	nd	nd	nd	nd	nd	nd	nd	nd	nd	nd	nd	nd	nd
PE	35:0	732.5543	nd	nd	nd	nd	nd	nd	nd	nd	nd	nd	nd	nd	nd	nd	nd	nd	nd	nd	nd	nd
PE	35:1	730.5387	730.5400	9.77	52	58	56	28.3	25.8	29.8	61	25	60	25.6	20.6	31.8	28.0	1.6	5.8	26.0	4.6	17.7
PE	35:2	728.5230	728.7156	8.77	27	19	17	14.7	8.5	9.0	20	12	16	8.4	9.9	8.5	10.7	2.8	26.1	8.9	0.7	7.6
PE	36:0	746.5700	nd	nd	nd	40	nd	nd	17.8	nd	nd	nd	nd	nd	nd	nd	17.8	0.0	0.0	nd	nd	nd
PE	36:1	744.5543	744.5538	10.40	73	nd	30	39.7	nd	16.0	18	nd	28	7.5	nd	14.9	27.8	11.9	42.6	11.2	3.7	32.6
PE	36:2	742.5387	742.5420	9.62	206	52	51	112.0	23.2	27.1	40	152	49	16.8	125.1	26.0	54.1	41.0	75.7	56.0	49.0	87.6
PE	36:3	740.5230	740.5223	8.46	26	nd	7	14.1	nd	3.7	nd	20	4	nd	16.5	2.1	8.9	5.2	58.3	9.3	7.2	77.2
PE	36:4	738.5074	738.5039	8.08	22	7	7	12.0	3.1	3.7	5	20	7	2.1	16.5	3.7	6.3	4.0	64.3	7.4	6.4	86.5



+ Atg4B																						
Class	Lipid	Calc. Mass. [M+H]-	Found Mass. [M+H]-	RT (min)	Area shC			Conc. (pmol/sample) shC			Area shAtg5			Conc. (pmol/sample) shAtg5			U87DND shC +Atg4 (n=3)			U87DND shAtg5 +Atg4 (n=3)		
					1	2	3	1	2	3	1	2	3	1	2	3	Mean	SD	%CV	Mean	SD	%CV
PE	36:5	736.4918	nd	nd	nd	nd	nd	nd	nd	nd	nd	nd	nd	nd	nd	nd	nd	nd	nd	nd	nd	nd
PE	36:6	734.4761	nd	nd	nd	nd	nd	nd	nd	nd	nd	nd	nd	nd	nd	nd	nd	nd	nd	nd	nd	nd
PE	38:0	774.6013	nd	nd	nd	nd	nd	nd	nd	nd	nd	nd	nd	nd	nd	nd	nd	nd	nd	nd	nd	nd
PE	38:1	772.5856	nd	nd	nd	nd	nd	nd	nd	nd	nd	nd	nd	nd	nd	nd	nd	nd	nd	nd	nd	nd
PE	38:2	770.5700	770.5721	10.87	34	25	25	18.5	11.1	13.3	25	32	29	10.5	26.3	15.4	14.3	3.1	21.5	17.4	6.6	38.1
PE	38:3	768.5543	768.5592	10.34	24	7	9	13.0	3.1	4.8	6	36	8	2.5	29.6	4.2	7.0	4.3	62.1	12.1	12.4	102.2
PE	38:4	766.5390	766.5411	9.49	153	26	36	83.2	11.6	19.1	24	148	40	10.1	121.8	21.2	38.0	32.1	84.6	51.0	50.3	98.5
PE	38:5	764.5230	nd	nd	nd	nd	nd	nd	nd	nd	nd	nd	nd	nd	nd	nd	nd	nd	nd	nd	nd	nd
PE	38:6	762.5070	762.5067	7.92	29	4	5	15.8	1.8	2.7	4	22	nd	1.7	18.1	0.0	6.7	6.4	94.9	6.6	8.2	123.9
PE	38:7	760.4918	nd	nd	nd	nd	nd	nd	nd	nd	nd	nd	nd	nd	nd	nd	nd	nd	nd	nd	nd	nd
PE	40:0	800.6169	nd	nd	nd	nd	nd	nd	nd	nd	nd	nd	nd	nd	nd	nd	nd	nd	nd	nd	nd	nd
PE	40:1	798.6013	798.6068	11.72	7	nd	nd	3.8	nd	nd	nd	nd	nd	nd	nd	nd	3.8	0.0	0.0	nd	nd	nd
PE	40:2	796.5856	nd	nd	nd	nd	nd	nd	nd	nd	nd	nd	nd	nd	nd	nd	nd	nd	nd	nd	nd	nd
PE	40:3	794.5700	nd	nd	nd	nd	nd	nd	nd	nd	nd	nd	nd	nd	nd	nd	nd	nd	nd	nd	nd	nd
PE	40:4	792.5543	792.5526	9.62	25	nd	6	13.6	nd	3.2	nd	33	nd	nd	27.2	nd	8.4	5.2	62.0	27.2	0.0	0.0
PE	40:5	790.5387	790.5397	9.30	25	5	10	13.6	2.2	5.3	5	29	11	2.1	23.9	5.8	7.0	4.8	68.1	10.6	9.5	89.7
PE	40:6	788.5230	nd	nd	nd	nd	nd	nd	nd	nd	nd	nd	nd	nd	nd	nd	nd	nd	nd	nd	nd	nd
PE	40:8	786.5074	nd	nd	nd	nd	nd	nd	nd	nd	nd	nd	nd	nd	nd	nd	nd	nd	nd	nd	nd	nd
PE	44:2	852.6483	nd	nd	nd	nd	nd	nd	nd	nd	nd	nd	nd	nd	nd	nd	nd	nd	nd	nd	nd	nd
PE	44:12	834.5074	nd	nd	nd	nd	nd	nd	nd	nd	nd	nd	nd	nd	nd	nd	nd	nd	nd	nd	nd	nd

Table 20. Quantified PEs from MEF Atg5<sup>-/-</sup> and Atg5<sup>+/+</sup> cells. The lipids were obtained through precipitation of the proteome, treatment with N-(His)<sub>6</sub>-3C-Atg4B and extraction by organic solvents.

Class	Lipid	Calc. Mass. [M+H] <sup>-</sup>	Found Mass. [M+H] <sup>-</sup>	RT (min)	Atg5 <sup>-/-</sup> - Atg4B												Atg5 <sup>-/-</sup> - Atg4 (n=6)		
					Area						Conc. (pmol/sample)						Mean	SD	%CV
					1	2	3	4	5	6	1	2	3	4	5	6			
PE	Std	747.7176	747.7117	8.98	335	197	218	9387	10452	14324	200.0	200.0	200.0	200.0	200.0	200.0	200.0	0.0	0.0
PE	28:0	634.4448	634.4504	6.09	nd	nd	nd	nd	nd	nd	nd	nd	nd	nd	nd	nd	nd	nd	nd
PE	30:0	662.4761	662.4803	7.30	nd	nd	nd	nd	nd	nd	nd	nd	nd	nd	nd	nd	nd	nd	nd
PE	31:0	676.4918	nd	nd	nd	nd	nd	nd	nd	nd	nd	nd	nd	nd	nd	nd	nd	nd	nd
PE	31:1	674.4761	674.4750	7.09	nd	nd	nd	nd	nd	nd	nd	nd	nd	nd	nd	nd	nd	nd	nd
PE	32:0	690.5074	690.5033	8.70	nd	nd	nd	nd	nd	nd	nd	nd	nd	nd	nd	nd	nd	nd	nd
PE	32:1	688.4920	688.4872	7.79	nd	5	15	185	407	nd	nd	5.1	13.8	3.9	7.8	nd	7.6	3.8	49.7
PE	32:2	686.4760	nd	nd	nd	nd	nd	nd	nd	nd	nd	nd	nd	nd	nd	nd	nd	nd	nd
PE	32:3	684.4604	nd	nd	nd	nd	nd	nd	nd	nd	nd	nd	nd	nd	nd	nd	nd	nd	nd
PE	33:0	704.5230	nd	nd	nd	nd	nd	nd	nd	nd	nd	nd	nd	nd	nd	nd	nd	nd	nd
PE	33:1	702.5074	702.5067	8.60	nd	nd	nd	nd	nd	nd	nd	nd	nd	nd	nd	nd	nd	nd	nd
PE	33:2	700.4918	nd	nd	nd	nd	nd	nd	nd	nd	nd	nd	nd	nd	nd	nd	nd	nd	nd
PE	33:3	698.4761	nd	nd	nd	nd	nd	nd	nd	nd	nd	nd	nd	nd	nd	nd	nd	nd	nd
PE	34:0	718.5387	718.5370	10.06	nd	4	9	nd	nd	nd	nd	4.1	8.3	nd	nd	nd	6.2	2.1	34.1
PE	34:1	716.5230	716.5195	9.16	24	33	61	nd	nd	nd	14.3	33.5	56.0	nd	nd	nd	34.6	17.0	49.2
PE	34:2	714.5074	714.5092	8.20	12	13	28	nd	nd	nd	7.2	13.2	25.7	nd	nd	nd	15.4	7.7	50.3
PE	34:3	712.4918	nd	nd	nd	nd	nd	nd	nd	nd	nd	nd	nd	nd	nd	nd	nd	nd	nd
PE	34:4	710.4761	nd	nd	nd	nd	nd	nd	nd	nd	nd	nd	nd	nd	nd	nd	nd	nd	nd
PE	35:0	732.5543	nd	nd	nd	nd	nd	nd	nd	nd	nd	nd	nd	nd	nd	nd	nd	nd	nd
PE	35:1	730.5387	730.5391	9.87	nd	nd	nd	nd	nd	nd	nd	nd	nd	nd	nd	nd	nd	nd	nd
PE	35:2	728.5230	728.5209	8.91	nd	nd	nd	nd	nd	nd	nd	nd	nd	nd	nd	nd	nd	nd	nd
PE	36:0	746.5700	nd	nd	nd	nd	nd	nd	nd	nd	nd	nd	nd	nd	nd	nd	nd	nd	nd
PE	36:1	744.5543	744.5534	10.49	36	51	112	nd	nd	nd	21.5	51.8	102.8	nd	nd	nd	58.7	33.5	57.1
PE	36:2	742.5387	742.5381	9.56	64	76	143	1066	780	705	38.2	77.2	131.2	22.7	14.9	9.8	49.0	42.9	87.6
PE	36:3	740.5230	nd	nd	nd	nd	nd	nd	nd	nd	nd	nd	nd	nd	nd	nd	nd	nd	nd
PE	36:4	738.5074	738.5027	8.26	nd	4	13	nd	nd	nd	nd	4.1	11.9	nd	nd	nd	8.0	3.9	49.2
PE	36:5	736.4918	nd	nd	nd	nd	nd	nd	nd	nd	nd	nd	nd	nd	nd	nd	nd	nd	nd

Atg5 <sup>-/-</sup> - Atg4B																			
Class	Lipid	Calc. Mass. [M+H] <sup>-</sup>	Found Mass. [M+H] <sup>-</sup>	RT (min)	Area						Conc. (pmol/sample)						Atg5 <sup>-/-</sup> - Atg4 (n=6)		
					1	2	3	4	5	6	1	2	3	4	5	6	Mean	SD	%CV
PE	36:6	734.4761	nd	nd	nd	nd	nd	nd	nd	nd	nd	nd	nd	nd	nd	nd	nd	nd	nd
PE	38:0	774.6013	nd	nd	nd	nd	nd	nd	nd	nd	nd	nd	nd	nd	nd	nd	nd	nd	nd
PE	38:1	772.5856	772.5854	10.52	nd	nd	nd	63	nd	nd	nd	nd	nd	1.3	nd	nd	1.3	0.0	0.0
PE	38:2	770.5700	770.5712	10.83	nd	nd	nd	117	111	121	nd	nd	nd	2.5	2.1	1.7	2.1	0.3	15.6
PE	38:3	768.5543	768.5569	10.43	16	21	nd	nd	nd	nd	9.6	21.3	nd	nd	nd	nd	15.4	5.9	38.1
PE	38:4	766.5390	766.5311	9.59	39	51	94	nd	nd	nd	23.3	51.8	86.2	nd	nd	nd	53.8	25.7	47.9
PE	38:5	764.5230	764.5264	8.63	nd	nd	nd	nd	nd	nd	nd	nd	nd	nd	nd	nd	nd	nd	nd
PE	38:6	762.5070	nd	nd	nd	nd	nd	nd	nd	nd	nd	nd	nd	nd	nd	nd	nd	nd	nd
PE	38:7	760.4918	nd	nd	nd	nd	nd	nd	nd	nd	nd	nd	nd	nd	nd	nd	nd	nd	nd
PE	40:0	800.6169	nd	nd	nd	nd	nd	nd	nd	nd	nd	nd	nd	nd	nd	nd	nd	nd	nd
PE	40:1	798.6013	nd	nd	nd	nd	nd	nd	nd	nd	nd	nd	nd	nd	nd	nd	nd	nd	nd
PE	40:2	796.5856	nd	nd	nd	nd	nd	nd	nd	nd	nd	nd	nd	nd	nd	nd	nd	nd	nd
PE	40:3	794.5700	nd	nd	nd	nd	nd	nd	nd	nd	nd	nd	nd	nd	nd	nd	nd	nd	nd
PE	40:4	792.5543	792.5537	9.81	13	nd	32	nd	nd	nd	7.8	nd	29.4	nd	nd	nd	18.6	10.8	58.2
PE	40:5	790.5387	790.5342	9.47	9	16	27	nd	nd	nd	5.4	16.2	24.8	nd	nd	nd	15.5	7.9	51.3
PE	40:6	788.5230	nd	nd	nd	nd	nd	nd	nd	nd	nd	nd	nd	nd	nd	nd	nd	nd	nd
PE	40:8	786.5074	nd	nd	nd	nd	nd	nd	nd	nd	nd	nd	nd	nd	nd	nd	nd	nd	nd
PE	44:2	852.6483	nd	nd	nd	nd	nd	nd	nd	nd	nd	nd	nd	nd	nd	nd	nd	nd	nd
PE	44:12	834.5074	nd	nd	nd	nd	nd	nd	nd	nd	nd	nd	nd	nd	nd	nd	nd	nd	nd

Atg5 <sup>-/-</sup> + Atg4B																			
Class	Lipid	Calc. Mass. [M+H] <sup>-</sup>	Found Mass. [M+H] <sup>-</sup>	RT (min)	Area						Conc. (pmol/sample)						Atg5 <sup>-/-</sup> +Atg4 (n=6)		
					1	2	3	4	5	6	1	2	3	4	5	6	Mean	SD	%CV
PE	Std	747.7176	747.7117	8.98	182	156	238	10295	10623	10426	200.0	200.0	200.0	200.0	200.0	200.0	200.0	0.0	0.0
PE	28:0	634.4448	634.4504	6.09	4	4	3	123	161	180	4.4	5.1	2.5	2.4	3.0	3.5	3.5	1.0	28.4
PE	30:0	662.4761	662.4803	7.30	11	11	14		484	509	12.1	14.1	11.8	nd	9.1	9.8	11.4	1.8	15.6
PE	31:0	676.4918	nd	nd	nd	nd	nd	nd	nd	nd	nd	nd	nd	nd	nd	nd	nd	nd	nd
PE	31:1	674.4761	674.4750	7.09	6	nd	8	nd	275	nd	6.6	nd	6.7	nd	5.2	nd	6.2	0.7	11.4
PE	32:0	690.5074	690.5033	8.70	4	6	5	223	240	258	4.4	7.7	4.2	4.3	4.5	4.9	5.0	1.2	24.3
PE	32:1	688.4920	688.4872	7.79	15	23	10	811	429	462	16.5	29.5	8.4	15.8	8.1	8.9	14.5	7.5	51.9
PE	32:2	686.4760	nd	nd	nd	nd	nd	nd	nd	nd	nd	nd	nd	nd	nd	nd	nd	nd	nd
PE	32:3	684.4604	nd	nd	nd	nd	nd	nd	nd	nd	nd	nd	nd	nd	nd	nd	nd	nd	nd
PE	33:0	704.5230	nd	nd	nd	nd	nd	nd	nd	nd	nd	nd	nd	nd	nd	nd	nd	nd	nd
PE	33:1	702.5074	702.5067	8.60	28	24	31	2177	2661	2744	30.8	30.8	26.1	42.3	50.1	52.6	38.8	10.2	26.3
PE	33:2	700.4918	nd	nd	nd	nd	nd	nd	nd	nd	nd	nd	nd	nd	nd	nd	nd	nd	nd
PE	33:3	698.4761	nd	nd	nd	nd	nd	nd	nd	nd	nd	nd	nd	nd	nd	nd	nd	nd	nd
PE	34:0	718.5387	718.5370	10.06	5	11	3	nd	nd	nd	5.5	14.1	2.5	nd	nd	nd	7.4	4.9	66.6
PE	34:1	716.5230	716.5195	9.16	50	85	23	622	745	737	54.9	109.0	19.3	12.1	14.0	14.1	37.2	35.3	94.8
PE	34:2	714.5074	714.5092	8.20	25	43	8	nd	nd	nd	27.5	55.1	6.7	nd	nd	nd	29.8	19.8	66.6
PE	34:3	712.4918	nd	nd	nd	nd	nd	nd	nd	nd	nd	nd	nd	nd	nd	nd	nd	nd	nd
PE	34:4	710.4761	nd	nd	nd	nd	nd	nd	nd	nd	nd	nd	nd	nd	nd	nd	nd	nd	nd
PE	35:0	732.5543	nd	nd	nd	nd	nd	nd	nd	nd	nd	nd	nd	nd	nd	nd	nd	nd	nd
PE	35:1	730.5387	730.5391	9.87	14	17	23	836	1561	1492	15.4	21.8	19.3	16.2	29.4	28.6	21.8	5.5	25.3
PE	35:2	728.5230	728.5209	8.91	4		6	346	439	468	4.4		5.0	6.7	8.3	9.0	6.7	1.8	26.5
PE	36:0	746.5700	nd	nd	nd	nd	nd	nd	nd	nd	nd	nd	nd	nd	nd	nd	nd	nd	nd
PE	36:1	744.5543	744.5534	10.49	80	127	27	nd	nd	nd	87.9	162.8	22.7	nd	nd	nd	91.1	57.3	62.8
PE	36:2	742.5387	742.5381	9.56	110	181	41	285	659	638	120.9	232.1	34.5	5.5	12.4	12.2	69.6	82.6	118.7
PE	36:3	740.5230	nd	nd	nd	nd	nd	nd	nd	nd	nd	nd	nd	nd	nd	nd	nd	nd	nd
PE	36:4	738.5074	738.5027	8.26	nd	18	nd	nd	nd	nd	nd	23.1	nd	nd	nd	nd	23.1	0.0	0.0
PE	36:5	736.4918	nd	nd	nd	nd	nd	nd	nd	nd	nd	nd	nd	nd	nd	nd	nd	nd	nd
PE	36:6	734.4761	nd	nd	nd	nd	nd	nd	nd	nd	nd	nd	nd	nd	nd	nd	nd	nd	nd
PE	38:0	774.6013	nd	nd	nd	nd	nd	nd	nd	nd	nd	nd	nd	nd	nd	nd	nd	nd	nd
PE	38:1	772.5856	772.5854	10.52	9	nd	nd	nd	nd	nd	9.9	nd	nd	nd	nd	nd	9.9	0.0	0.0

Atg5 <sup>-/-</sup> + Atg4B																			
Class	Lipid	Calc. Mass. [M+H] <sup>-</sup>	Found Mass. [M+H] <sup>-</sup>	RT (min)	Area						Conc. (pmol/sample)						Atg5 <sup>-/-</sup> + Atg4 (n=6)		
					1	2	3	4	5	6	1	2	3	4	5	6	Mean	SD	%CV
PE	38:2	770.5700	770.5712	10.83	27	17	nd	805	1002	829	29.7	21.8	nd	15.6	18.9	15.9	20.4	5.2	25.3
PE	38:3	768.5543	768.5569	10.43	32	56	11	nd	nd	nd	35.2	71.8	9.2	nd	nd	nd	38.7	25.7	66.2
PE	38:4	766.5390	766.5311	9.59	64	123	26	nd	nd	nd	70.3	157.7	21.8	nd	nd	nd	83.3	56.2	67.5
PE	38:5	764.5230	764.5264	8.63	27	60	nd	nd	nd	nd	29.7	76.9	nd	nd	nd	nd	53.3	23.6	44.3
PE	38:6	762.5070	nd	nd	nd	nd	nd	nd	nd	nd	nd	nd	nd	nd	nd	nd	nd	nd	nd
PE	38:7	760.4918	nd	nd	nd	nd	nd	nd	nd	nd	nd	nd	nd	nd	nd	nd	nd	nd	nd
PE	40:0	800.6169	nd	nd	nd	nd	nd	nd	nd	nd	nd	nd	nd	nd	nd	nd	nd	nd	nd
PE	40:1	798.6013	nd	nd	nd	nd	nd	nd	nd	nd	nd	nd	nd	nd	nd	nd	nd	nd	nd
PE	40:2	796.5856	nd	nd	nd	nd	nd	nd	nd	nd	nd	nd	nd	nd	nd	nd	nd	nd	nd
PE	40:3	794.5700	nd	nd	nd	nd	nd	nd	nd	nd	nd	nd	nd	nd	nd	nd	nd	nd	nd
PE	40:4	792.5543	792.5537	9.81	nd	42	nd	nd	nd	nd	nd	53.8	nd	nd	nd	nd	53.8	0.0	0.0
PE	40:5	790.5387	790.5342	9.47	18	34	nd	nd	nd	nd	19.8	43.6	nd	nd	nd	nd	31.7	11.9	37.6
PE	40:6	788.5230	nd	nd	nd	nd	nd	nd	nd	nd	nd	nd	nd	nd	nd	nd	nd	nd	nd
PE	40:8	786.5074	nd	nd	nd	nd	nd	nd	nd	nd	nd	nd	nd	nd	nd	nd	nd	nd	nd
PE	44:2	852.6483	nd	nd	nd	nd	nd	nd	nd	nd	nd	nd	nd	nd	nd	nd	nd	nd	nd
PE	44:12	834.5074	nd	nd	nd	nd	nd	nd	nd	nd	nd	nd	nd	nd	nd	nd	nd	nd	nd

Atg5 <sup>+/+</sup> - Atg4B																			
Class	Lipid	Calc. Mass. [M+H] <sup>-</sup>	Found Mass. [M+H] <sup>-</sup>	RT (min)	Area					Conc. (pmol/sample)					Atg5 <sup>+/+</sup> MEF -Atg4 (n=5)				
					1	2	3	4	5	1	2	3	4	5	Mean	SD	%CV		
PE	Std	747.7176	747.7147	9.07	238	237	294	13133	10022	200.0	200.0	200.0	200.0	200.0	200.0	200.0	200.0	0.0	0.0
PE	28:0	634.4448	634.4359	6.09	nd	nd	nd	nd	nd	nd	nd	nd	nd	nd	nd	nd	nd	nd	nd
PE	30:0	662.4761	662.4799	7.33	nd	nd	nd	nd	nd	nd	nd	nd	nd	nd	nd	nd	nd	nd	nd

Atg5 <sup>+/+</sup> - Atg4B																	
Class	Lipid	Calc. Mass. [M+H] <sup>-</sup>	Found Mass. [M+H] <sup>-</sup>	RT (min)	Area					Conc. (pmol/sample)					Atg5 <sup>+/+</sup> MEF -Atg4 (n=5)		
					1	2	3	4	5	1	2	3	4	5	Mean	SD	%CV
PE	31:0	676.4918	nd	nd	nd	nd	nd	nd	nd	nd	nd	nd	nd	nd	nd	nd	nd
PE	31:1	674.4761	674.4719	7.21	nd	nd	nd	nd	nd	nd	nd	nd	nd	nd	nd	nd	nd
PE	32:0	690.5074	690.5039	8.79	nd	nd	nd	nd	nd	nd	nd	nd	nd	nd	nd	nd	nd
PE	32:1	688.4920	688.4882	7.77	nd	nd	nd	nd	nd	nd	nd	nd	nd	nd	nd	nd	nd
PE	32:2	686.4760	nd	nd	nd	nd	nd	nd	nd	nd	nd	nd	nd	nd	nd	nd	nd
PE	32:3	684.4604	nd	nd	nd	nd	nd	nd	nd	nd	nd	nd	nd	nd	nd	nd	nd
PE	33:0	704.5230	nd	nd	nd	nd	nd	nd	nd	nd	nd	nd	nd	nd	nd	nd	nd
PE	33:1	702.5074	702.5001	8.66	nd	nd	nd	nd	nd	nd	nd	nd	nd	nd	nd	nd	nd
PE	33:2	700.4918	nd	nd	nd	nd	nd	nd	nd	nd	nd	nd	nd	nd	nd	nd	nd
PE	33:3	698.4761	nd	nd	nd	nd	nd	nd	nd	nd	nd	nd	nd	nd	nd	nd	nd
PE	34:0	718.5387	718.5379	10.09	nd	nd	nd	nd	nd	nd	nd	nd	nd	nd	nd	nd	nd
PE	34:1	716.5230	716.5210	9.16	nd	nd	nd	nd	nd	nd	nd	nd	nd	nd	nd	nd	nd
PE	34:2	714.5074	714.5075	8.14	nd	4	nd	nd	nd	nd	3.4	nd	nd	nd	3.4	0.0	0.0
PE	34:3	712.4918	nd	nd	nd	nd	nd	nd	nd	nd	nd	nd	nd	nd	nd	nd	nd
PE	34:4	710.4761	nd	nd	nd	nd	nd	nd	nd	nd	nd	nd	nd	nd	nd	nd	nd
PE	35:0	732.5543	nd	nd	nd	nd	nd	nd	nd	nd	nd	nd	nd	nd	nd	nd	nd
PE	35:1	730.5387	730.5380	9.93	nd	nd	nd	nd	nd	nd	nd	nd	nd	nd	nd	nd	nd
PE	35:2	728.5230	728.5209	8.97	nd	nd	nd	nd	nd	nd	nd	nd	nd	nd	nd	nd	nd
PE	36:0	746.5700	nd	nd	nd	nd	nd	nd	nd	nd	nd	nd	nd	nd	nd	nd	nd
PE	36:1	744.5543	744.5499	10.43	4	nd	nd	nd	nd	3.4	nd	nd	nd	nd	3.4	0.0	0.0
PE	36:2	742.5387	742.5348	9.50	10	nd	nd	nd	nd	8.4	nd	nd	nd	nd	8.4	0.0	0.0
PE	36:3	740.5230	nd	nd	nd	nd	nd	nd	nd	nd	nd	nd	nd	nd	nd	nd	nd
PE	36:4	738.5074	nd	nd	nd	nd	nd	nd	nd	nd	nd	nd	nd	nd	nd	nd	nd
PE	36:5	736.4918	nd	nd	nd	nd	nd	nd	nd	nd	nd	nd	nd	nd	nd	nd	nd
PE	36:6	734.4761	nd	nd	nd	nd	nd	nd	nd	nd	nd	nd	nd	nd	nd	nd	nd
PE	38:0	774.6013	nd	nd	nd	nd	nd	nd	nd	nd	nd	nd	nd	nd	nd	nd	nd
PE	38:1	772.5856	nd	nd	nd	nd	nd	nd	nd	nd	nd	nd	nd	nd	nd	nd	nd
PE	38:2	770.5700	770.5729	11.02	nd	nd	nd	120	142	nd	nd	nd	1.8	2.8	2.3	0.5	21.6
PE	38:3	768.5543	768.5482	10.52	nd	nd	nd	nd	nd	nd	nd	nd	nd	nd	nd	nd	nd
PE	38:4	766.5390	766.5390	9.65	nd	nd	10	nd	nd	nd	nd	6.8	nd	nd	6.8	0.0	0.0

Atg5 <sup>+/+</sup> - Atg4B																	
Class	Lipid	Calc. Mass. [M+H]-	Found Mass. [M+H]-	RT (min)	Area					Conc. (pmol/sample)					Atg5 <sup>+/+</sup> MEF -Atg4 (n=5)		
					1	2	3	4	5	1	2	3	4	5	Mean	SD	%CV
PE	38:5	764.5230	nd	nd	nd	nd	nd	nd	nd	nd	nd	nd	nd	nd	nd	nd	nd
PE	38:6	762.5070	nd	nd	nd	nd	nd	nd	nd	nd	nd	nd	nd	nd	nd	nd	nd
PE	38:7	760.4918	nd	nd	nd	nd	nd	nd	nd	nd	nd	nd	nd	nd	nd	nd	nd
PE	40:0	800.6169	nd	nd	nd	nd	nd	nd	nd	nd	nd	nd	nd	nd	nd	nd	nd
PE	40:1	798.6013	798.6022	12.01	nd	nd	nd	388	377	nd	nd	nd	5.9	7.5	6.7	0.8	12.0
PE	40:2	796.5856	nd	nd	nd	nd	nd	nd	nd	nd	nd	nd	nd	nd	nd	nd	nd
PE	40:3	794.5700	nd	nd	nd	nd	nd	nd	nd	nd	nd	nd	nd	nd	nd	nd	nd
PE	40:4	792.5543	792.5522	9.84	nd	nd	nd	nd	nd	nd	nd	nd	nd	nd	nd	nd	nd
PE	40:5	790.5387	790.5429	9.44	nd	nd	nd	nd	nd	nd	nd	nd	nd	nd	nd	nd	nd
PE	40:6	788.5230	nd	nd	nd	nd	nd	nd	nd	nd	nd	nd	nd	nd	nd	nd	nd
PE	40:8	786.5074	nd	nd	nd	nd	nd	nd	nd	nd	nd	nd	nd	nd	nd	nd	nd
PE	44:2	852.6483	nd	nd	nd	nd	nd	nd	nd	nd	nd	nd	nd	nd	nd	nd	nd
PE	44:12	834.5074	nd	nd	nd	nd	nd	nd	nd	nd	nd	nd	nd	nd	nd	nd	nd

Atg5 <sup>+/+</sup> + Atg4B																	
Class	Lipid	Calc. Mass. [M+H]-	Found Mass. [M+H]-	RT (min)	Area					Conc. (pmol/sample)					Atg5 <sup>+/+</sup> MEF -Atg4 (n=5)		
					1	2	3	4	5	1	2	3	4	5	Mean	SD	%CV
PE	Std	747.7176	747.7147	9.07	245	214	270	10442	11332	200.0	200.0	200.0	200.0	200.0	200.0	0.0	0.0
PE	28:0	634.4448	634.4359	6.09	6	4	6	144	158	4.9	3.7	4.4	2.8	2.8	3.7	0.9	23.1
PE	30:0	662.4761	662.4799	7.33	18	13	17	592	nd	14.7	12.1	12.6	11.3	nd	12.7	1.2	9.8
PE	31:0	676.4918	nd	nd	nd	nd	nd	nd	nd	nd	nd	nd	nd	nd	nd	nd	nd
PE	31:1	674.4761	674.4719	7.21	10	8	11	349	354	8.2	7.5	8.1	6.7	6.2	7.3	0.8	10.5
PE	32:0	690.5074	690.5039	8.79	4	3	6	208	335	3.3	2.8	4.4	4.0	5.9	4.1	1.1	26.4
PE	32:1	688.4920	688.4882	7.77	17	8	13	612	682	13.9	7.5	9.6	11.7	12.0	10.9	2.2	20.1
PE	32:2	686.4760	nd	nd	nd	nd	nd	nd	nd	nd	nd	nd	nd	nd	nd	nd	nd
PE	32:3	684.4604	nd	nd	nd	nd	nd	nd	nd	nd	nd	nd	nd	nd	nd	nd	nd
PE	33:0	704.5230	nd	nd	nd	nd	nd	nd	nd	nd	nd	nd	nd	nd	nd	nd	nd
PE	33:1	702.5074	702.5001	8.66	31	25	43	2688	3897	25.3	23.4	31.9	51.5	68.8	40.2	17.4	43.4
PE	33:2	700.4918	nd	nd	nd	nd	nd	nd	nd	nd	nd	nd	nd	nd	nd	nd	nd

Atg5 <sup>+/+</sup> + Atg4B																	
Class	Lipid	Calc. Mass. [M+H] <sup>-</sup>	Found Mass. [M+H] <sup>-</sup>	RT (min)	Area					Conc. (pmol/sample)					Atg5 <sup>+/+</sup> MEF -Atg4 (n=5)		
					1	2	3	4	5	1	2	3	4	5	Mean	SD	%CV
PE	33:3	698.4761	nd	nd	nd	nd	nd	nd	nd	nd	nd	nd	nd	nd	nd	nd	nd
PE	34:0	718.5387	718.5379	10.09	2	nd	nd	nd	nd	1.6	nd	nd	nd	nd	1.6	0.0	0.0
PE	34:1	716.5230	716.5210	9.16	48	nd	46	794	1049	39.2	nd	34.1	15.2	18.5	26.7	10.1	37.8
PE	34:2	714.5074	714.5075	8.14	22	nd	18	nd	nd	18.0	nd	13.3	nd	nd	15.6	2.3	14.8
PE	34:3	712.4918	nd	nd	nd	nd	nd	nd	nd	nd	nd	nd	nd	nd	nd	nd	nd
PE	34:4	710.4761	nd	nd	nd	nd	nd	nd	nd	nd	nd	nd	nd	nd	nd	nd	nd
PE	35:0	732.5543	nd	nd	nd	nd	nd	nd	nd	nd	nd	nd	nd	nd	nd	nd	nd
PE	35:1	730.5387	730.5380	9.93	22	19	28	nd	384	18.0	17.8	20.7	nd	6.8	15.8	5.3	33.8
PE	35:2	728.5230	728.5209	8.97	nd	nd	6	381	590	nd	nd	4.4	7.3	10.4	7.4	2.4	33.0
PE	36:0	746.5700	nd	nd	nd	nd	nd	nd	nd	nd	nd	nd	nd	nd	nd	nd	nd
PE	36:1	744.5543	744.5499	10.43	87	9	70	nd	nd	71.0	8.4	51.9	nd	nd	43.8	26.2	59.9
PE	36:2	742.5387	742.5348	9.50	135	nd	114	252	475	110.2	nd	84.4	4.8	8.4	52.0	46.3	89.1
PE	36:3	740.5230	nd	nd	nd	nd	nd	nd	nd	nd	nd	nd	nd	nd	nd	nd	nd
PE	36:4	738.5074	nd	nd	nd	nd	nd	nd	nd	nd	nd	nd	nd	nd	nd	nd	nd
PE	36:5	736.4918	nd	nd	nd	nd	nd	nd	nd	nd	nd	nd	nd	nd	nd	nd	nd
PE	36:6	734.4761	nd	nd	nd	nd	nd	nd	nd	nd	nd	nd	nd	nd	nd	nd	nd
PE	38:0	774.6013	nd	nd	nd	nd	nd	nd	nd	nd	nd	nd	nd	nd	nd	nd	nd
PE	38:1	772.5856	nd	nd	nd	nd	nd	nd	nd	nd	nd	nd	nd	nd	nd	nd	nd
PE	38:2	770.5700	770.5729	11.02	39	nd	20	98	120	31.8	nd	14.8	1.9	2.1	12.7	12.2	96.7
PE	38:3	768.5543	768.5482	10.52	22	nd	19	nd	nd	18.0	nd	14.1	nd	nd	16.0	1.9	12.1
PE	38:4	766.5390	766.5390	9.65	50	nd	39	nd	nd	40.8	nd	28.9	nd	nd	34.9	6.0	17.1
PE	38:5	764.5230	nd	nd	nd	nd	nd	nd	nd	nd	nd	nd	nd	nd	nd	nd	nd
PE	38:6	762.5070	nd	nd	nd	nd	nd	nd	nd	nd	nd	nd	nd	nd	nd	nd	nd
PE	38:7	760.4918	nd	nd	nd	nd	nd	nd	nd	nd	nd	nd	nd	nd	nd	nd	nd
PE	40:0	800.6169	nd	nd	nd	nd	nd	nd	nd	nd	nd	nd	nd	nd	nd	nd	nd
PE	40:1	798.6013	798.6022	12.01	11	nd	9	281	315	9.0	nd	6.7	5.4	5.6	6.6	1.4	21.6
PE	40:2	796.5856	nd	nd	nd	nd	nd	nd	nd	nd	nd	nd	nd	nd	nd	nd	nd
PE	40:3	794.5700	nd	nd	nd	nd	nd	nd	nd	nd	nd	nd	nd	nd	nd	nd	nd
PE	40:4	792.5543	792.5522	9.84	9	nd	9	nd	nd	7.3	nd	6.7	nd	nd	7.0	0.3	4.9
PE	40:5	790.5387	790.5429	9.44	17	nd	15	nd	nd	13.9	nd	11.1	nd	nd	12.5	1.4	11.1



Atg5 <sup>+/+</sup> + Atg4B																		
Class	Lipid	Calc. Mass. [M+H] <sup>-</sup>	Found Mass. [M+H] <sup>-</sup>	RT (min)	Area					Conc. (pmol/sample)					Atg5 <sup>+/+</sup> MEF -Atg4 (n=5)			
					1	2	3	4	5	1	2	3	4	5	Mean	SD	%CV	
PE	40:6	788.5230	nd	nd	nd	nd	nd	nd	nd	nd	nd	nd	nd	nd	nd	nd	nd	nd
PE	40:8	786.5074	nd	nd	nd	nd	nd	nd	nd	nd	nd	nd	nd	nd	nd	nd	nd	nd
PE	44:2	852.6483	nd	nd	nd	nd	nd	nd	nd	nd	nd	nd	nd	nd	nd	nd	nd	nd
PE	44:12	834.5074	nd	nd	nd	nd	nd	nd	nd	nd	nd	nd	nd	nd	nd	nd	nd	nd

Table 21. Quantified PEs from the protein N-(His)<sub>6</sub>-3C-Atg4B. The lipids were obtained through incubation of the protein (0, 12.5, 25 and 50 µg) with a mixture of organic solvents at 48 °C for 16h.

0 µg N-(His) <sub>6</sub> -3C-Atg4B																			
Class	Lipid	Calc. Mass. [M+H] <sup>-</sup>	Found Mass. [M+H] <sup>-</sup>	RT (min)	Area						Conc. (pmol/sample)						0 µg Atg4B (n=6)		
					1	2	3	4	5	6	1	2	3	4	5	6	Mean	SD	%CV
PE	Std	749.7332	749.7352	9.22	5050	2706	2602	3317	5410	4084	200	200	200	200	200	200	200	0.0	0.0
PE	28:0	636.4604	nd	nd	nd	nd	nd	nd	nd	nd	nd	nd	nd	nd	nd	nd	nd	nd	nd
PE	30:0	664.4918	nd	nd	nd	nd	nd	nd	nd	nd	nd	nd	nd	nd	nd	nd	nd	nd	nd
PE	31:0	678.5074	nd	nd	nd	nd	nd	nd	nd	nd	nd	nd	nd	nd	nd	nd	nd	nd	nd
PE	31:1	676.4918	676.4919	7.42	nd	nd	nd	nd	nd	nd	nd	nd	nd	nd	nd	nd	nd	nd	nd
PE	32:0	692.5230	692.5181	8.76	nd	nd	nd	nd	nd	nd	nd	nd	nd	nd	nd	nd	nd	nd	nd
PE	32:1	690.5074	690.5031	7.98	nd	nd	nd	nd	nd	nd	nd	nd	nd	nd	nd	nd	nd	nd	nd
PE	32:2	688.4917	nd	nd	nd	nd	nd	nd	nd	nd	nd	nd	nd	nd	nd	nd	nd	nd	nd
PE	32:3	686.4761	nd	nd	nd	nd	nd	nd	nd	nd	nd	nd	nd	nd	nd	nd	nd	nd	nd
PE	33:0	704.5230	704.5254	8.81	nd	nd	nd	nd	nd	nd	nd	nd	nd	nd	nd	nd	nd	nd	nd
PE	33:1	702.5074	nd	nd	nd	nd	nd	nd	nd	nd	nd	nd	nd	nd	nd	nd	nd	nd	nd
PE	33:2	700.4918	nd	nd	nd	nd	nd	nd	nd	nd	nd	nd	nd	nd	nd	nd	nd	nd	nd
PE	34:0	720.5543	nd	nd	nd	nd	nd	nd	nd	nd	nd	nd	nd	nd	nd	nd	nd	nd	nd
PE	34:1	718.5386	718.5408	9.22	nd	nd	nd	nd	nd	nd	nd	nd	nd	nd	nd	nd	nd	nd	nd
PE	34:2	716.5230	716.5248	8.41	nd	nd	nd	nd	nd	nd	nd	nd	nd	nd	nd	nd	nd	nd	nd
PE	34:3	714.5074	nd	nd	nd	nd	nd	nd	nd	nd	nd	nd	nd	nd	nd	nd	nd	nd	nd
PE	34:4	712.4917	712.4919	6.74	nd	nd	nd	nd	nd	nd	nd	nd	nd	nd	nd	nd	nd	nd	nd

0 µg N-(His) <sub>6</sub> -3C-Atg4B																			
Class	Lipid	Calc. Mass. [M+H] <sup>-</sup>	Found Mass. [M+H] <sup>-</sup>	RT (min)	Area						Conc. (pmol/sample)						0 µg Atg4B (n=6)		
					1	2	3	4	5	6	1	2	3	4	5	6	Mean	SD	%CV
PE	35:0	734.5700	nd	nd	nd	nd	nd	nd	nd	nd	nd	nd	nd	nd	nd	nd	nd	nd	nd
PE	35:1	732.5543	732.5551	10.15	nd	nd	nd	nd	nd	nd	nd	nd	nd	nd	nd	nd	nd	nd	nd
PE	35:2	730.5387	730.5364	9.15	nd	nd	nd	nd	nd	nd	nd	nd	nd	nd	nd	nd	nd	nd	nd
PE	36:0	748.5856	nd	nd	nd	nd	nd	nd	nd	nd	nd	nd	nd	nd	nd	nd	nd	nd	nd
PE	36:1	746.5699	nd	nd	nd	nd	nd	nd	nd	nd	nd	nd	nd	nd	nd	nd	nd	nd	nd
PE	36:2	744.5543	744.5507	9.59	nd	nd	nd	nd	nd	nd	nd	nd	nd	nd	nd	nd	nd	nd	nd
PE	36:3	742.5386	nd	nd	nd	nd	nd	nd	nd	nd	nd	nd	nd	nd	nd	nd	nd	nd	nd
PE	36:4	740.5230	nd	nd	nd	nd	nd	nd	nd	nd	nd	nd	nd	nd	nd	nd	nd	nd	nd
PE	36:5	738.5074	nd	nd	nd	nd	nd	nd	nd	nd	nd	nd	nd	nd	nd	nd	nd	nd	nd
PE	36:6	736.4917	nd	nd	nd	nd	nd	nd	nd	nd	nd	nd	nd	nd	nd	nd	nd	nd	nd
PE	38:0	776.6169	nd	nd	nd	nd	nd	nd	nd	nd	nd	nd	nd	nd	nd	nd	nd	nd	nd
PE	38:1	774.6012	nd	nd	nd	nd	nd	nd	nd	nd	nd	nd	nd	nd	nd	nd	nd	nd	nd
PE	38:2	772.5856	772.5859	11.23	nd	nd	nd	nd	nd	nd	nd	nd	nd	nd	nd	nd	nd	nd	nd
PE	38:3	770.5699	nd	nd	nd	nd	nd	nd	nd	nd	nd	nd	nd	nd	nd	nd	nd	nd	nd
PE	38:4	768.5546	nd	nd	nd	nd	nd	nd	nd	nd	nd	nd	nd	nd	nd	nd	nd	nd	nd
PE	38:5	766.5386	nd	nd	nd	nd	nd	nd	nd	nd	nd	nd	nd	nd	nd	nd	nd	nd	nd
PE	38:6	764.5226	nd	nd	nd	nd	nd	nd	nd	nd	nd	nd	nd	nd	nd	nd	nd	nd	nd
PE	38:7	762.5074	nd	nd	nd	nd	nd	nd	nd	nd	nd	nd	nd	nd	nd	nd	nd	nd	nd
PE	40:0	802.6325	nd	nd	nd	nd	nd	nd	nd	nd	nd	nd	nd	nd	nd	nd	nd	nd	nd
PE	40:1	800.6169	nd	nd	nd	nd	nd	nd	nd	nd	nd	nd	nd	nd	nd	nd	nd	nd	nd
PE	40:2	798.6012	nd	nd	nd	nd	nd	nd	nd	nd	nd	nd	nd	nd	nd	nd	nd	nd	nd
PE	40:3	796.5856	nd	nd	nd	nd	nd	nd	nd	nd	nd	nd	nd	nd	nd	nd	nd	nd	nd
PE	40:4	794.5699	nd	nd	nd	nd	nd	nd	nd	nd	nd	nd	nd	nd	nd	nd	nd	nd	nd
PE	40:5	792.5543	nd	nd	nd	nd	nd	nd	nd	nd	nd	nd	nd	nd	nd	nd	nd	nd	nd
PE	40:6	790.5386	nd	nd	nd	nd	nd	nd	nd	nd	nd	nd	nd	nd	nd	nd	nd	nd	nd

0 µg N-(His) <sub>6</sub> -3C-Atg4B																				
Class	Lipid	Calc. Mass. [M+H] <sup>-</sup>	Found Mass. [M+H] <sup>-</sup>	RT (min)	Area						Conc. (pmol/sample)						0 µg Atg4B (n=6)			
					1	2	3	4	5	6	1	2	3	4	5	6	Mean	SD	%CV	
PE	40:8	788.5230	nd	nd	nd	nd	nd	nd	nd	nd	nd	nd	nd	nd	nd	nd	nd	nd	nd	nd

12.5 µg N-(His) <sub>6</sub> -3C-Atg4B																				
Class	Lipid	Calc. Mass. [M+H] <sup>-</sup>	Found Mass. [M+H] <sup>-</sup>	RT (min)	Area						Conc. (pmol/sample)						12.5 µg Atg4B (n=6)			
					1	2	3	4	5	6	1	2	3	4	5	6	Mean	SD	%CV	
PE	Std	749.7332	749.7352	9.22	3502	4648	5717	4923	4954	5163	200	200	200.0	200.0	200.0	200.0	200.0	200.0	0.0	0.0
PE	28:0	636.4604	nd	nd	16	41	nd	nd	nd	nd	0.9	1.8	nd	nd	nd	nd	nd	1.3	0.4	31.8
PE	30:0	664.4918	nd	nd	nd	nd	nd	nd	nd	nd	nd	nd	nd	nd	nd	nd	nd	nd	nd	nd
PE	31:0	678.5074	nd	nd	nd	nd	nd	nd	nd	nd	nd	nd	nd	nd	nd	nd	nd	nd	nd	nd
PE	31:1	676.4918	676.4919	7.42	nd	nd	nd	43	51	41	nd	nd	nd	1.7	2.1	1.6	1.8	0.2	10.9	
PE	32:0	692.5230	692.5181	8.76	30	nd	74	nd	nd	nd	1.7	nd	2.6	nd	nd	nd	2.2	0.4	20.3	
PE	32:1	690.5074	690.5031	7.98	nd	nd	nd	58	63	55	nd	nd	nd	2.4	2.5	2.1	2.3	0.2	7.2	
PE	32:2	688.4917	nd	nd	nd	nd	nd	nd	nd	nd	nd	nd	nd	nd	nd	nd	nd	nd	nd	nd
PE	32:3	686.4761	nd	nd	nd	nd	nd	nd	nd	nd	nd	nd	nd	nd	nd	nd	nd	nd	nd	nd
PE	33:0	704.5230	704.5254	8.81	493	786	720	372	465	368	28.2	33.8	25.2	15.1	18.8	14.3	22.6	7.1	31.6	
PE	33:1	702.5074	nd	nd	nd	nd	nd	nd	nd	nd	nd	nd	nd	nd	nd	nd	nd	nd	nd	nd
PE	33:2	700.4918	nd	nd	nd	nd	nd	nd	nd	nd	nd	nd	nd	nd	nd	nd	nd	nd	nd	nd
PE	34:0	720.5543	nd	nd	nd	nd	nd	nd	nd	nd	nd	nd	nd	nd	nd	nd	nd	nd	nd	nd
PE	34:1	718.5386	718.5408	9.22	870	552	338	123	139	116	49.7	23.8	11.8	5.0	5.6	4.5	16.7	16.2	96.7	
PE	34:2	716.5230	716.5248	8.41	nd	nd	nd	nd	nd	30	nd	nd	nd	nd	nd	1.2	1.2	0.0	0.0	
PE	34:3	714.5074	nd	nd	nd	nd	nd	nd	nd	nd	nd	nd	nd	nd	nd	nd	nd	nd	nd	nd
PE	34:4	712.4917	712.4919	6.74	nd	nd	nd	16	19	20	nd	nd	nd	0.7	0.8	0.8	0.7	0.1	7.8	
PE	35:0	734.5700	nd	nd	nd	nd	nd	nd	nd	nd	nd	nd	nd	nd	nd	nd	nd	nd	nd	nd
PE	35:1	732.5543	732.5551	10.15	nd	nd	nd	156	161	144	nd	nd	nd	6.3	6.5	5.6	6.1	0.4	6.5	
PE	35:2	730.5387	730.5364	9.15	90	102	180	82	92	83	nd	4.4	6.3	3.3	3.7	3.2	4.2	1.1	27.0	
PE	36:0	748.5856	nd	nd	nd	nd	nd	nd	nd	nd	nd	nd	nd	nd	nd	nd	nd	nd	nd	nd
PE	36:1	746.5699	nd	nd	nd	nd	nd	nd	nd	nd	nd	nd	nd	nd	nd	nd	nd	nd	nd	nd
PE	36:2	744.5543	744.5507	9.59	75	104	147	47	59	47	4.3	4.5	5.1	1.9	2.4	1.8	3.3	1.3	40.0	

12.5 µg N-(His) <sub>6</sub> -3C-Atg4B																			
Class	Lipid	Calc. Mass. [M+H] <sup>-</sup>	Found Mass. [M+H] <sup>-</sup>	RT (min)	Area						Conc. (pmol/sample)						12.5 µg Atg4B (n=6)		
					1	2	3	4	5	6	1	2	3	4	5	6	Mean	SD	%CV
PE	36:3	742.5386	nd	nd	nd	nd	nd	nd	nd	nd	nd	nd	nd	nd	nd	nd	nd	nd	nd
PE	36:4	740.5230	nd	nd	nd	nd	nd	nd	nd	nd	nd	nd	nd	nd	nd	nd	nd	nd	nd
PE	36:5	738.5074	nd	nd	nd	nd	nd	nd	nd	nd	nd	nd	nd	nd	nd	nd	nd	nd	nd
PE	36:6	736.4917	nd	nd	nd	nd	nd	nd	nd	nd	nd	nd	nd	nd	nd	nd	nd	nd	nd
PE	38:0	776.6169	nd	nd	nd	nd	nd	nd	nd	nd	nd	nd	nd	nd	nd	nd	nd	nd	nd
PE	38:1	774.6012	nd	nd	nd	nd	nd	nd	nd	nd	nd	nd	nd	nd	nd	nd	nd	nd	nd
PE	38:2	772.5856	772.5859	11.23	158	123	nd	115	99	103	9.0	5.3	nd	4.7	4.0	4.0	5.4	1.9	34.8
PE	38:3	770.5699	nd	nd	nd	nd	nd	nd	nd	nd	nd	nd	nd	nd	nd	nd	nd	nd	nd
PE	38:4	768.5546	nd	nd	nd	nd	nd	nd	nd	nd	nd	nd	nd	nd	nd	nd	nd	nd	nd
PE	38:5	766.5386	nd	nd	nd	nd	nd	nd	nd	nd	nd	nd	nd	nd	nd	nd	nd	nd	nd
PE	38:6	764.5226	nd	nd	nd	nd	nd	nd	nd	nd	nd	nd	nd	nd	nd	nd	nd	nd	nd
PE	38:7	762.5074	nd	nd	nd	nd	nd	nd	nd	nd	nd	nd	nd	nd	nd	nd	nd	nd	nd
PE	40:0	802.6325	nd	nd	nd	nd	nd	nd	nd	nd	nd	nd	nd	nd	nd	nd	nd	nd	nd
PE	40:1	800.6169	nd	nd	nd	nd	nd	nd	nd	nd	nd	nd	nd	nd	nd	nd	nd	nd	nd
PE	40:2	798.6012	nd	nd	nd	nd	nd	nd	nd	nd	nd	nd	nd	nd	nd	nd	nd	nd	nd
PE	40:3	796.5856	nd	nd	nd	nd	nd	nd	nd	nd	nd	nd	nd	nd	nd	nd	nd	nd	nd
PE	40:4	794.5699	nd	nd	nd	nd	nd	nd	nd	nd	nd	nd	nd	nd	nd	nd	nd	nd	nd
PE	40:5	792.5543	nd	nd	nd	nd	nd	nd	nd	nd	nd	nd	nd	nd	nd	nd	nd	nd	nd
PE	40:6	790.5386	nd	nd	nd	nd	nd	nd	nd	nd	nd	nd	nd	nd	nd	nd	nd	nd	nd
PE	40:8	788.5230	nd	nd	nd	nd	nd	nd	nd	nd	nd	nd	nd	nd	nd	nd	nd	nd	nd

25 µg N-(His) <sub>6</sub> -3C-Atg4B																				
Class	Lipid	Calc. Mass. [M+H] <sup>-</sup>	Found Mass. [M+H] <sup>-</sup>	RT (min)	Area						Conc. (pmol/sample)						25 µg Atg4B (n=6)			
					1	2	3	4	5	6	1	2	3	4	5	6	Mean	SD	%CV	
PE	Std	749.7332	749.7336	9.04	3364	7008	7089	3364	7008	7089	200	200	200	200	200	200	200	200	0.0	0.0
PE	28:0	636.4604	636.4588	6.09	98	93	98	98	93	98	5.8	2.7	2.8	5.8	2.7	2.8	3.7	1.5	39.2	
PE	30:0	664.4918	664.4877	7.41	301	292	324	301	292	324	17.9	8.3	9.1	17.9	8.3	9.1	11.8	4.3	36.7	
PE	31:0	678.5074	nd	nd	nd	nd	nd	nd	nd	nd	nd	nd	nd	nd	nd	nd	nd	nd	nd	
PE	31:1	676.4918	676.4943	7.25	325	218	281	325	218	281	19.3	6.2	7.9	19.3	6.2	7.9	11.2	5.8	52.1	
PE	32:0	692.5230	692.5202	8.73	97	197	182	97	197	182	5.8	5.6	5.1	5.8	5.6	5.1	5.5	0.3	4.9	
PE	32:1	690.5074	nd	nd	nd	nd	nd	nd	nd	nd	nd	nd	nd	nd	nd	nd	nd	nd	nd	
PE	32:2	688.4917	nd	nd	nd	nd	nd	nd	nd	nd	nd	nd	nd	nd	nd	nd	nd	nd	nd	
PE	32:3	686.4761	nd	nd	nd	nd	nd	nd	nd	nd	nd	nd	nd	nd	nd	nd	nd	nd	nd	
PE	33:0	704.5230	704.5200	8.67	1501	2356	2394	1501	2356	2394	89.2	67.2	67.5	89.2	67.2	67.5	74.7	10.3	13.8	
PE	33:1	702.5074	nd	nd	nd	nd	nd	nd	nd	nd	nd	nd	nd	nd	nd	nd	nd	nd	nd	
PE	33:2	700.4918	nd	nd	nd	nd	nd	nd	nd	nd	nd	nd	nd	nd	nd	nd	nd	nd	nd	
PE	34:0	720.5543	nd	nd	nd	nd	nd	nd	nd	nd	nd	nd	nd	nd	nd	nd	nd	nd	nd	
PE	34:1	718.5386	718.5387	9.04	570	1082	2610	570	1082	2610	33.9	30.9	73.6	33.9	30.9	73.6	46.1	19.5	42.2	
PE	34:2	716.5230	nd	nd	nd	nd	nd	nd	nd	nd	nd	nd	nd	nd	nd	nd	nd	nd	nd	
PE	34:3	714.5074	nd	nd	nd	nd	nd	nd	nd	nd	nd	nd	nd	nd	nd	nd	nd	nd	nd	
PE	34:4	712.4917	712.4974	6.63	18	19	16	18	19	16	1.1	0.5	0.5	1.1	0.5	0.5	0.7	0.3	39.7	
PE	35:0	734.5700	nd	nd	nd	nd	nd	nd	nd	nd	nd	nd	nd	nd	nd	nd	nd	nd	nd	
PE	35:1	732.5543	732.5499	9.98	5268	2781	1977	5268	2781	1977	313.2	79.4	55.8	313.2	79.4	55.8	149.4	116.2	77.7	
PE	35:2	730.5387	730.5363	8.98	341	565	545	341	565	545	20.3	16.1	15.4	20.3	16.1	15.4	17.3	2.2	12.5	
PE	36:0	748.5856	nd	nd	nd	nd	nd	nd	nd	nd	nd	nd	nd	nd	nd	nd	nd	nd	nd	
PE	36:1	746.5699	nd	nd	nd	nd	nd	nd	nd	nd	nd	nd	nd	nd	nd	nd	nd	nd	nd	
PE	36:2	744.5543	744.5508	9.39	191	481	630	191	481	630	11.4	13.7	17.8	11.4	13.7	17.8	14.3	2.6	18.5	
PE	36:3	742.5386	nd	nd	nd	nd	nd	nd	nd	nd	nd	nd	nd	nd	nd	nd	nd	nd	nd	
PE	36:4	740.5230	nd	nd	nd	nd	nd	nd	nd	nd	nd	nd	nd	nd	nd	nd	nd	nd	nd	
PE	36:5	738.5074	nd	nd	nd	nd	nd	nd	nd	nd	nd	nd	nd	nd	nd	nd	nd	nd	nd	
PE	36:6	736.4917	nd	nd	nd	nd	nd	nd	nd	nd	nd	nd	nd	nd	nd	nd	nd	nd	nd	
PE	38:0	776.6169	nd	nd	nd	nd	nd	nd	nd	nd	nd	nd	nd	nd	nd	nd	nd	nd	nd	
PE	38:1	774.6012	nd	nd	nd	nd	nd	nd	nd	nd	nd	nd	nd	nd	nd	nd	nd	nd	nd	

25 µg N-(His) <sub>6</sub> -3C-Atg4B																			
Class	Lipid	Calc. Mass. [M+H] <sup>-</sup>	Found Mass. [M+H] <sup>-</sup>	RT (min)	Area						Conc. (pmol/sample)						25 µg Atg4B (n=6)		
					1	2	3	4	5	6	1	2	3	4	5	6	Mean	SD	%CV
PE	38:2	772.5856	772.5854	11.08	677	311	585	677	311	585	40.2	8.9	16.5	40.2	8.9	16.5	21.9	13.4	61.1
PE	38:3	770.5699	nd	nd	nd	nd	nd	nd	nd	nd	nd	nd	nd	nd	nd	nd	nd	nd	nd
PE	38:4	768.5546	nd	nd	nd	nd	nd	nd	nd	nd	nd	nd	nd	nd	nd	nd	nd	nd	nd
PE	38:5	766.5386	nd	nd	nd	nd	nd	nd	nd	nd	nd	nd	nd	nd	nd	nd	nd	nd	nd
PE	38:6	764.5226	nd	nd	nd	nd	nd	nd	nd	nd	nd	nd	nd	nd	nd	nd	nd	nd	nd
PE	38:7	762.5074	nd	nd	nd	nd	nd	nd	nd	nd	nd	nd	nd	nd	nd	nd	nd	nd	nd
PE	40:0	802.6325	nd	nd	nd	nd	nd	nd	nd	nd	nd	nd	nd	nd	nd	nd	nd	nd	nd
PE	40:1	800.6169	nd	nd	nd	nd	nd	nd	nd	nd	nd	nd	nd	nd	nd	nd	nd	nd	nd
PE	40:2	798.6012	nd	nd	nd	nd	nd	nd	nd	nd	nd	nd	nd	nd	nd	nd	nd	nd	nd
PE	40:3	796.5856	nd	nd	nd	nd	nd	nd	nd	nd	nd	nd	nd	nd	nd	nd	nd	nd	nd
PE	40:4	794.5699	794.5676	11.02	38	nd	nd	38	nd	nd	2.3	nd	nd	2.3	nd	nd	2.3	0.0	0.0
PE	40:5	792.5543	nd	nd	nd	nd	nd	nd	nd	nd	nd	nd	nd	nd	nd	nd	nd	nd	nd
PE	40:6	790.5386	nd	nd	nd	nd	nd	nd	nd	nd	nd	nd	nd	nd	nd	nd	nd	nd	nd
PE	40:8	788.5230	nd	nd	nd	nd	nd	nd	nd	nd	nd	nd	nd	nd	nd	nd	nd	nd	nd

50 µg N-(His) <sub>6</sub> -3C-Atg4B																				
Class	Lipid	Calc. Mass. [M+H] <sup>-</sup>	Found Mass. [M+H] <sup>-</sup>	RT (min)	Area						Conc. (pmol/sample)						50 µg Atg4B (n=6)			
					1	2	3	4	5	6	1	2	3	4	5	6	Mean	SD	%CV	
PE	Std	749.7332	749.7336	9.04	3874	5766	6073	3874	5766	6073	200	200	200	200	200	200	200	200	0.0	0.0
PE	28:0	636.4604	636.4588	6.09	52	41	46	52	41	46	2.7	1.4	1.5	2.7	1.4	1.5	1.9	0.6	30.7	
PE	30:0	664.4918	664.4877	7.41	162	nd	202	162	nd	202	8.4	nd	6.7	8.4	nd	6.7	7.5	0.9	11.4	
PE	31:0	678.5074	nd	nd	nd	nd	nd	nd	nd	nd	nd	nd	nd	nd	nd	nd	nd	nd	nd	
PE	31:1	676.4918	676.4943	7.25	238	nd	238	238	nd	238	12.3	nd	7.8	12.3	nd	7.8	10.1	2.2	22.1	
PE	32:0	692.5230	692.5202	8.73	nd	nd	141	nd	nd	141	nd	nd	4.6	nd	nd	4.6	4.6	0.0	0.0	

50 µg N-(His) <sub>6</sub> -3C-Atg4B																			
Class	Lipid	Calc. Mass. [M+H] <sup>-</sup>	Found Mass. [M+H] <sup>-</sup>	RT (min)	Area						Conc. (pmol/sample)						50 µg Atg4B (n=6)		
					1	2	3	4	5	6	1	2	3	4	5	6	Mean	SD	%CV
PE	32:1	690.5074	nd	nd	nd	nd	nd	nd	nd	nd	nd	nd	nd	nd	nd	nd	nd	nd	nd
PE	32:2	688.4917	nd	nd	nd	nd	nd	nd	nd	nd	nd	nd	nd	nd	nd	nd	nd	nd	nd
PE	32:3	686.4761	nd	nd	nd	nd	nd	nd	nd	nd	nd	nd	nd	nd	nd	nd	nd	nd	nd
PE	33:0	704.5230	704.5200	8.67	751	862	1725	751	862	1725	38.8	29.9	56.8	38.8	29.9	56.8	41.8	11.2	26.8
PE	33:1	702.5074	nd	nd	nd	nd	nd	nd	nd	nd	nd	nd	nd	nd	nd	nd	nd	nd	nd
PE	33:2	700.4918	nd	nd	nd	nd	nd	nd	nd	nd	nd	nd	nd	nd	nd	nd	nd	nd	nd
PE	34:0	720.5543	nd	nd	nd	nd	nd	nd	nd	nd	nd	nd	nd	nd	nd	nd	nd	nd	nd
PE	34:1	718.5386	718.5387	9.04	522	464	1649	522	464	1649	26.9	16.1	54.3	26.9	16.1	54.3	32.4	16.1	49.5
PE	34:2	716.5230	nd	nd	nd	nd	nd	nd	nd	nd	nd	nd	nd	nd	nd	nd	nd	nd	nd
PE	34:3	714.5074	nd	nd	nd	nd	nd	nd	nd	nd	nd	nd	nd	nd	nd	nd	nd	nd	nd
PE	34:4	712.4917	712.4974	6.63	nd	nd	nd	nd	nd	nd	nd	nd	nd	nd	nd	nd	nd	nd	nd
PE	35:0	734.5700	nd	nd	nd	nd	nd	nd	nd	nd	nd	nd	nd	nd	nd	nd	nd	nd	nd
PE	35:1	732.5543	732.5499	9.98	nd	1226	486	nd	1226	486	nd	42.5	16.0	nd	42.5	16.0	29.3	13.3	45.3
PE	35:2	730.5387	730.5363	8.98	185	245	388	185	245	388	9.6	8.5	12.8	9.6	8.5	12.8	10.3	1.8	17.7
PE	36:0	748.5856	nd	nd	nd	nd	nd	nd	nd	nd	nd	nd	nd	nd	nd	nd	nd	nd	nd
PE	36:1	746.5699	nd	nd	nd	nd	nd	nd	nd	nd	nd	nd	nd	nd	nd	nd	nd	nd	nd
PE	36:2	744.5543	744.5508	9.39	116	200	269	116	200	269	6.0	6.9	8.9	6.0	6.9	8.9	7.3	1.2	16.4
PE	36:3	742.5386	nd	nd	nd	nd	nd	nd	nd	nd	nd	nd	nd	nd	nd	nd	nd	nd	nd
PE	36:4	740.5230	nd	nd	nd	nd	nd	nd	nd	nd	nd	nd	nd	nd	nd	nd	nd	nd	nd
PE	36:5	738.5074	nd	nd	nd	nd	nd	nd	nd	nd	nd	nd	nd	nd	nd	nd	nd	nd	nd
PE	36:6	736.4917	nd	nd	nd	nd	nd	nd	nd	nd	nd	nd	nd	nd	nd	nd	nd	nd	nd
PE	38:0	776.6169	nd	nd	nd	nd	nd	nd	nd	nd	nd	nd	nd	nd	nd	nd	nd	nd	nd
PE	38:1	774.6012	nd	nd	nd	nd	nd	nd	nd	nd	nd	nd	nd	nd	nd	nd	nd	nd	nd
PE	38:2	772.5856	772.5854	11.08	388	272	143	388	272	143	20.0	9.4	4.7	20.0	9.4	4.7	11.4	6.4	56.2
PE	38:3	770.5699	nd	nd	nd	nd	nd	nd	nd	nd	nd	nd	nd	nd	nd	nd	nd	nd	nd
PE	38:4	768.5546	nd	nd	nd	nd	nd	nd	nd	nd	nd	nd	nd	nd	nd	nd	nd	nd	nd
PE	38:5	766.5386	nd	nd	nd	nd	nd	nd	nd	nd	nd	nd	nd	nd	nd	nd	nd	nd	nd
PE	38:6	764.5226	nd	nd	nd	nd	nd	nd	nd	nd	nd	nd	nd	nd	nd	nd	nd	nd	nd

50 µg N-(His) <sub>6</sub> -3C-Atg4B																			
Class	Lipid	Calc. Mass. [M+H] <sup>-</sup>	Found Mass. [M+H] <sup>-</sup>	RT (min)	Area						Conc. (pmol/sample)						50 µg Atg4B (n=6)		
					1	2	3	4	5	6	1	2	3	4	5	6	Mean	SD	%CV
PE	38:7	762.5074	nd	nd	nd	nd	nd	nd	nd	nd	nd	nd	nd	nd	nd	nd	nd	nd	nd
PE	40:0	802.6325	nd	nd	nd	nd	nd	nd	nd	nd	nd	nd	nd	nd	nd	nd	nd	nd	nd
PE	40:1	800.6169	nd	nd	nd	nd	nd	nd	nd	nd	nd	nd	nd	nd	nd	nd	nd	nd	nd
PE	40:2	798.6012	nd	nd	nd	nd	nd	nd	nd	nd	nd	nd	nd	nd	nd	nd	nd	nd	nd
PE	40:3	796.5856	nd	nd	nd	nd	nd	nd	nd	nd	nd	nd	nd	nd	nd	nd	nd	nd	nd
PE	40:4	794.5699	794.5676	11.02	40	69	nd	40	69	nd	2.1	2.4	nd	2.1	2.4	nd	2.2	0.2	7.4
PE	40:5	792.5543	nd	nd	nd	nd	nd	nd	nd	nd	nd	nd	nd	nd	nd	nd	nd	nd	nd
PE	40:6	790.5386	nd	nd	nd	nd	nd	nd	nd	nd	nd	nd	nd	nd	nd	nd	nd	nd	nd
PE	40:8	788.5230	nd	nd	nd	nd	nd	nd	nd	nd	nd	nd	nd	nd	nd	nd	nd	nd	nd

Table 22. Quantified DAGs from the protein N-(His)<sub>6</sub>-3C-Atg4B. The lipids were obtained through incubation of the protein (0, 12.5, 25 and 50 µg) with a mixture of organic solvents at 48 °C for 16h.

0 µg N-(His) <sub>6</sub> -3C-Atg4B																			
Class	Lipid	Calc. Mass. [M-H] <sup>+</sup>	Found Mass. [M-H] <sup>+</sup>	RT (min)	Area						Conc. (pmol/sample)						0 µg Atg4B (n=6)		
					1	2	3	4	5	6	1	2	3	4	5	6	Mean	SD	%CV
DAG	Std	619.6037	619.6093	11.27	29033	15847	22386	13387	23658	19078	166.0	166.0	166.0	166.0	166.0	166.0	166.0	0.0	0.0
DAG	30:0	558.5098	558.5078	8.70	nd	290	142	145	143	125	nd	3.0	1.1	1.8	1.0	1.1	1.6	0.8	48.7
DAG	30:1	556.4942	556.4913	7.76	nd	nd	nd	100	99	88	nd	nd	nd	1.2	0.7	0.8	0.9	0.2	26.9
DAG	30:2	554.4786	nd	nd	nd	nd	nd	nd	nd	nd	nd	nd	nd	nd	nd	nd	nd	nd	nd
DAG	30:3	552.4630	nd	nd	nd	nd	nd	nd	nd	nd	nd	nd	nd	nd	nd	nd	nd	nd	nd
DAG	30:4	550.4474	nd	nd	nd	nd	nd	nd	nd	nd	nd	nd	nd	nd	nd	nd	nd	nd	nd
DAG	32:0	586.5411	586.5417	10.14	nd	4528	135	264	417	191	nd	47.4	1.0	3.3	2.9	1.7	11.3	18.1	160.8
DAG	32:1	584.5255	584.5214	9.32	nd	nd	nd	250	230	245	nd	nd	nd	3.1	1.6	2.1	2.3	0.6	27.0



0 µg N-(His)6-3C-Atg4B																			
Class	Lipid	Calc. Mass. [M-H] <sup>+</sup>	Found Mass. [M-H] <sup>+</sup>	RT (min)	Area						Conc. (pmol/sample)						0 µg Atg4B (n=6)		
					1	2	3	4	5	6	1	2	3	4	5	6	Mean	SD	%CV
DAG	32:2	582.5099	582.5094	8.54	70	52	61	126	134	128	0.4	0.5	0.5	1.6	0.9	1.1	0.8	0.4	49.8
DAG	32:3	580.4943	580.4971	7.50	nd	nd	nd	65	103	92	nd	nd	nd	0.8	0.7	0.8	0.8	0.0	4.9
DAG	32:4	578.4787	nd	nd	nd	nd	nd	nd	nd	nd	nd	nd	nd	nd	nd	nd	nd	nd	nd
DAG	32:5	576.4631	nd	nd	nd	nd	nd	nd	nd	nd	nd	nd	nd	nd	nd	nd	nd	nd	nd
DAG	34:0	614.5724	614.5751	11.39	448	5311	71	241	534	140	2.6	55.6	0.5	3.0	3.7	1.2	11.1	19.9	179.4
DAG	34:1	612.5568	612.5536	10.55	472	453	245	374	413	385	2.7	4.7	1.8	4.6	2.9	3.3	3.4	1.0	31.2
DAG	34:2	610.5412	610.5414	9.64	133	168	78	226	277	247	0.8	1.8	0.6	2.8	1.9	2.1	1.7	0.8	46.6
DAG	34:3	608.5256	608.5240	8.73	11	nd	nd	55	70	60	0.1	nd	nd	0.7	0.5	0.5	0.4	0.2	52.1
DAG	34:4	606.5100	nd	nd	nd	nd	nd	nd	nd	nd	nd	nd	nd	nd	nd	nd	nd	nd	nd
DAG	34:5	604.4944	nd	nd	nd	nd	nd	nd	nd	nd	nd	nd	nd	nd	nd	nd	nd	nd	nd
DAG	34:6	602.4788	nd	nd	nd	nd	nd	nd	nd	nd	nd	nd	nd	nd	nd	nd	nd	nd	nd
DAG	36:0	642.6040	642.6033	12.46	690	3361	467	242	315	124	3.9	35.2	3.5	3.0	2.2	1.1	8.2	12.1	148.9
DAG	36:1	640.5881	640.5902	11.67	303	275	172	573	619	855	1.7	2.9	1.3	7.1	4.3	7.4	4.1	2.4	58.7
DAG	36:2	638.5725	638.5765	10.89	588	584	391	1025	1264	1104	3.4	6.1	2.9	12.7	8.9	9.6	7.3	3.5	48.1
DAG	36:3	636.5569	636.5554	10.01	159	157	nd	194	210	209	0.9	1.6	nd	2.4	1.5	1.8	1.7	0.5	29.4
DAG	36:4	634.5413	634.5409	9.07	29	55	nd	119	153	146	0.2	0.6	nd	1.5	1.1	1.3	0.9	0.5	52.4
DAG	36:5	632.5257	632.5285	8.40	nd	nd	nd	27	51	48	nd	nd	nd	0.3	0.4	0.4	0.4	0.0	9.4
DAG	36:6	630.5101	nd	nd	nd	nd	nd	nd	nd	nd	nd	nd	nd	nd	nd	nd	nd	nd	nd
DAG	38:0	670.6350	670.6370	13.77	nd	nd	nd	nd	nd	nd	nd	nd	nd	nd	nd	nd	nd	nd	nd
DAG	38:1	668.6194	668.6167	12.74	nd	nd	nd	463	440	473	nd	nd	nd	5.7	3.1	4.1	4.3	1.1	25.3
DAG	38:2	666.6038	666.6023	11.96	nd	nd	nd	nd	nd	nd	nd	nd	nd	nd	nd	nd	nd	nd	nd

0 µg N-(His)6-3C-Atg4B																			
Class	Lipid	Calc. Mass. [M-H] <sup>+</sup>	Found Mass. [M-H] <sup>+</sup>	RT (min)	Area						Conc. (pmol/sample)						0 µg Atg4B (n=6)		
					1	2	3	4	5	6	1	2	3	4	5	6	Mean	SD	%CV
DAG	38:3	664.5882	nd	nd	nd	nd	nd	nd	nd	nd	nd	nd	nd	nd	nd	nd	nd	nd	nd
DAG	38:4	662.5726	662.5720	10.64	nd	nd	nd	nd	nd	nd	nd	nd	nd	nd	nd	nd	nd	nd	nd

12.5 µg N-(His)6-3C-Atg4B																			
Class	Lipid	Calc. Mass. [M-H] <sup>+</sup>	Found Mass. [M-H] <sup>+</sup>	RT (min)	Area						Conc. (pmol/sample)						12.5 µg Atg4B (n=6)		
					1	2	3	4	5	6	1	2	3	4	5	6	Mean	SD	%CV
DAG	Standard	619.6037	619.6093	11.27	15666	25964	30665	26339	18508	22146	166.0	166.0	166.0	166.0	166.0	166.0	166.0	0.0	0.0
DAG	30:0	558.5098	558.5078	8.70	1233	2754	598	310	200	270	13.1	17.6	3.2	2.0	1.8	2.0	6.6	6.3	95.6
DAG	30:1	556.4942	556.4913	7.76	nd	nd	nd	100	110	104	nd	nd	nd	0.6	1.0	0.8	0.8	0.1	18.3
DAG	30:2	554.4786	nd	nd	nd	nd	nd	nd	nd	nd	nd	nd	nd	nd	nd	nd	nd	nd	nd
DAG	30:3	552.4630	nd	nd	nd	nd	nd	nd	nd	nd	nd	nd	nd	nd	nd	nd	nd	nd	nd
DAG	30:4	550.4474	nd	nd	nd	nd	nd	nd	nd	nd	nd	nd	nd	nd	nd	nd	nd	nd	nd
DAG	32:0	586.5411	586.5417	10.14	12464	43116	3933	3761	296	2472	132.1	275.7	21.3	23.7	2.7	18.5	79.0	97.8	123.8
DAG	32:1	584.5255	584.5214	9.32	174	1312	1366	292	283	271	1.8	8.4	7.4	1.8	2.5	2.0	4.0	2.8	69.2
DAG	32:2	582.5099	582.5094	8.54	312	386	360	152	161	150	3.3	2.5	1.9	1.0	1.4	1.1	1.9	0.8	43.5
DAG	32:3	580.4943	580.4971	7.50	nd	50	21	109	115	120	nd	0.3	0.1	0.7	1.0	0.9	0.6	0.3	56.7
DAG	32:4	578.4787	nd	nd	nd	nd	nd	nd	nd	nd	nd	nd	nd	nd	nd	nd	nd	nd	nd
DAG	32:5	576.4631	nd	nd	nd	nd	nd	nd	nd	nd	nd	nd	nd	nd	nd	nd	nd	nd	nd
DAG	34:0	614.5724	614.5751	11.39	13383	39878	3276	4731	240	2752	141.8	255.0	17.7	29.8	2.2	20.6	77.8	91.6	117.7
DAG	34:1	612.5568	612.5536	10.55	1338	2314	2098	481	420	497	14.2	14.8	11.4	3.0	3.8	3.7	8.5	5.1	60.0
DAG	34:2	610.5412	610.5414	9.64	419	620	892	307	277	304	4.4	4.0	4.8	1.9	2.5	2.3	3.3	1.1	34.0
DAG	34:3	608.5256	608.5240	8.73	121	166	172	72	81	85	1.3	1.1	0.9	0.5	0.7	0.6	0.8	0.3	32.5
DAG	34:4	606.5100	nd	nd	nd	nd	nd	nd	nd	nd	nd	nd	nd	nd	nd	nd	nd	nd	nd
DAG	34:5	604.4944	nd	nd	nd	nd	nd	nd	nd	nd	nd	nd	nd	nd	nd	nd	nd	nd	nd
DAG	34:6	602.4788	nd	nd	nd	nd	nd	nd	nd	nd	nd	nd	nd	nd	nd	nd	nd	nd	nd
DAG	36:0	642.6040	642.6033	12.46	5381	19119	3201	1629	239	716	57.0	122.2	17.3	10.3	2.1	5.4	35.7	42.8	119.7
DAG	36:1	640.5881	640.5902	11.67	806	1404	1485	802	523	716	8.5	9.0	8.0	5.1	4.7	5.4	6.8	1.8	26.1
DAG	36:2	638.5725	638.5765	10.89	2291	3813	3598	147	1261	1425	24.3	24.4	19.5	0.9	11.3	10.7	15.2	8.4	55.4

12.5 µg N-(His)6-3C-Atg4B																			
Class	Lipid	Calc. Mass. [M-H] <sup>+</sup>	Found Mass. [M-H] <sup>+</sup>	RT (min)	Area						Conc. (pmol/sample)						12.5 µg Atg4B (n=6)		
					1	2	3	4	5	6	1	2	3	4	5	6	Mean	SD	%CV
DAG	36:3	636.5569	636.5554	10.01	406	558	924	256	215	265	4.3	3.6	5.0	1.6	1.9	2.0	3.1	1.3	42.3
DAG	36:4	634.5413	634.5409	9.07	247	400	360	169	161	168	2.6	2.6	1.9	1.1	1.4	1.3	1.8	0.6	33.5
DAG	36:5	632.5257	632.5285	8.40	nd	nd	122	38	48	50	nd	nd	0.7	0.2	0.4	0.4	0.4	0.2	35.6
DAG	36:6	630.5101	nd	nd	nd	nd	nd	nd	nd	nd	nd	nd	nd	nd	nd	nd	nd	nd	nd
DAG	38:0	670.6350	670.6370	13.77	nd	738	199	nd	nd	nd	nd	4.7	1.1	nd	nd	nd	2.9	1.8	62.8
DAG	38:1	668.6194	668.6167	12.74	164	320	245	590	495	404	1.7	2.0	1.3	3.7	4.4	3.0	2.7	1.1	40.9
DAG	38:2	666.6038	666.6023	11.96	28	28	95	nd	nd	nd	0.3	0.2	0.5	nd	nd	nd	0.3	0.1	42.1
DAG	38:3	664.5882	nd	nd	nd	nd	nd	nd	nd	nd	nd	nd	nd	nd	nd	nd	nd	nd	nd
DAG	38:4	662.5726	662.5720	10.64	1	7	6	nd	nd	nd	0.0	0.0	0.0	nd	nd	nd	0.0	0.0	48.3

25 µg N-(His)6-3C-Atg4B																			
Class	Lipid	Calc. Mass. [M-H] <sup>+</sup>	Found Mass. [M-H] <sup>+</sup>	RT (min)	Area						Conc. (pmol/sample)						25 µg Atg4B (n=6)		
					1	2	3	4	5	6	1	2	3	4	5	6	Mean	SD	%CV
DAG	Standard	619.6037	619.6009	11.51	25232	32023	34764	15449	15005	17617	166.0	166.0	166.0	166.0	166.0	166.0	166.0	0.0	0.0
DAG	30:0	558.5098	558.5049	8.97	447	748	809	150	151	202	2.9	3.9	3.9	1.6	1.7	1.9	2.6	2.1	80.5
DAG	30:1	556.4942	556.4924	8.10	nd	nd	nd	108	97	102	nd	nd	nd	1.2	1.1	1.0	1.0	0.2	15.4
DAG	30:2	554.4786	nd	nd	nd	nd	nd	nd	nd	nd	nd	nd	nd	nd	nd	nd	nd	nd	nd
DAG	30:3	552.4630	nd	nd	nd	nd	nd	nd	nd	nd	nd	nd	nd	nd	nd	nd	nd	nd	nd
DAG	30:4	550.4474	nd	nd	nd	nd	nd	nd	nd	nd	nd	nd	nd	nd	nd	nd	nd	nd	nd
DAG	32:0	586.5411	586.5443	10.34	760	4983	5483	241	234	655	5.0	25.8	26.2	2.6	2.6	6.2	16.2	19.2	118.3
DAG	32:1	584.5255	584.5228	950.00	565	1885	1686	307	254	294	3.7	9.8	8.1	3.3	2.8	2.8	4.9	4.4	89.5
DAG	32:2	582.5099	582.5078	8.69	423	509	640	164	157	162	2.8	2.6	3.1	1.8	1.7	1.5	1.8	1.2	63.5
DAG	32:3	580.4943	580.4935	7.48	10	21	22	110	108	105	0.1	0.1	0.1	1.2	1.2	1.0	0.6	0.5	80.4
DAG	32:4	578.4787	nd	nd	nd	nd	nd	nd	nd	nd	nd	nd	nd	nd	nd	nd	nd	nd	nd
DAG	32:5	576.4631	nd	nd	nd	nd	nd	nd	nd	nd	nd	nd	nd	nd	nd	nd	nd	nd	nd
DAG	34:0	614.5724	614.5755	11.54	652	4893	4421	303	250	887	4.3	25.4	21.1	3.3	2.8	8.4	18.1	23.1	127.7
DAG	34:1	612.5568	612.5521	10.67	1614	2710	2941	464	425	428	10.6	14.0	14.0	5.0	4.7	4.0	7.7	5.8	75.1
DAG	34:2	610.5412	610.5370	9.81	777	1264	1437	277	252	279	5.1	6.6	6.9	3.0	2.8	2.6	4.2	2.3	54.7
DAG	34:3	608.5256	608.5234	8.94	201	293	323	82	75	70	1.3	1.5	1.5	0.9	0.8	0.7	1.0	0.6	56.6

25 µg N-(His)6-3C-Atg4B																			
Class	Lipid	Calc. Mass. [M-H] <sup>+</sup>	Found Mass. [M-H] <sup>+</sup>	RT (min)	Area						Conc. (pmol/sample)						25 µg Atg4B (n=6)		
					1	2	3	4	5	6	1	2	3	4	5	6	Mean	SD	%CV
DAG	34:4	606.5100	nd	nd	nd	nd	nd	nd	nd	nd	nd	nd	nd	nd	nd	nd	nd	nd	nd
DAG	34:5	604.4944	nd	nd	nd	nd	nd	nd	nd	nd	nd	nd	nd	nd	nd	nd	nd	nd	nd
DAG	34:6	602.4788	nd	nd	nd	nd	nd	nd	nd	nd	nd	nd	nd	nd	nd	nd	nd	nd	nd
DAG	36:0	642.6040	642.6017	12.66	1095	4208	4050	276	200	336	7.2	21.8	19.3	3.0	2.2	3.2	12.6	16.4	130.1
DAG	36:1	640.5881	640.5910	11.89	1111	1745	1794	826	504	955	7.3	9.0	8.6	8.9	5.6	9.0	15.5	22.0	141.8
DAG	36:2	638.5725	638.5728	11.05	3163	4765	5022	1404	1279	1298	20.8	24.7	24.0	15.1	14.1	12.2	18.1	8.9	49.2
DAG	36:3	636.5569	636.5563	10.21	745	1136	1265	222	230	230	4.9	5.9	6.0	2.4	2.5	2.2	3.5	1.9	54.2
DAG	36:4	634.5413	634.5412	9.28	511	729	750	174	158	163	3.4	3.8	3.6	1.9	1.7	1.5	2.4	1.2	49.5
DAG	36:5	632.5257	632.5262	8.35	90	129	141	55	51	46	0.6	0.7	0.7	0.6	0.6	0.4	0.5	0.3	60.0
DAG	36:6	630.5101	nd	nd	nd	nd	nd	nd	nd	nd	nd	nd	nd	nd	nd	nd	nd	nd	nd
DAG	38:0	670.6350	670.6307	12.88	nd	277	283	nd	nd	nd	nd	1.4	1.4	nd	nd	nd	1.6	0.9	56.6
DAG	38:1	668.6194	668.6189	12.74	262	323	381	427	428	551	1.7	1.7	1.8	4.6	4.7	5.2	3.0	1.8	60.1
DAG	38:2	666.6038	666.6025	11.96	nd	96	111	nd	nd	nd	nd	0.5	0.5	nd	nd	nd	0.3	0.1	39.8
DAG	38:3	664.5882	664.5851	11.21	30	28	39	nd	nd	nd	0.2	0.1	0.2	nd	nd	nd	0.2	0.2	61.8
DAG	38:4	662.5726	662.5693	10.64	6	nd	nd	nd	nd	nd	0.0	nd	nd	nd	nd	nd	0.1	0.0	74.9

50 µg N-(His)6-3C-Atg4B																			
Class	Lipid	Calc. Mass. [M-H] <sup>+</sup>	Found Mass. [M-H] <sup>+</sup>	RT (min)	Area						Conc. (pmol/sample)						50 µg Atg4B (n=6)		
					1	2	3	4	5	6	1	2	3	4	5	6	Mean	SD	%CV
DAG	Standard	619.6037	619.6009	11.51	28312	32247	27822	22920	17012	14851	166.0	166.0	166.0	166.0	166.0	166.0	166.0	0.0	0.0
DAG	30:0	558.5098	558.5049	8.97	147	415	1212	303	174	143	0.9	2.1	7.2	2.2	1.7	1.6	2.6	1.0	36.7
DAG	30:1	556.4942	556.4924	8.10	nd	nd	nd	107	113	98	nd	nd	nd	0.8	1.1	1.1	1.1	0.1	7.7
DAG	30:2	554.4786	nd	nd	nd	nd	nd	nd	nd	nd	nd	nd	nd	nd	nd	nd	nd	nd	nd
DAG	30:3	552.4630	nd	nd	nd	nd	nd	nd	nd	nd	nd	nd	nd	nd	nd	nd	nd	nd	nd
DAG	30:4	550.4474	nd	nd	nd	nd	nd	nd	nd	nd	nd	nd	nd	nd	nd	nd	nd	nd	nd
DAG	32:0	586.5411	586.5443	10.34	658	1152	9069	3932	285	209	3.9	5.9	54.1	28.5	2.8	2.3	11.4	10.4	91.4
DAG	32:1	584.5255	584.5228	950.00	nd	503	2311	332	294	276	nd	2.6	13.8	2.4	2.9	3.1	5.1	2.8	54.8
DAG	32:2	582.5099	582.5078	8.69	45	402	696	174	181	142	0.3	2.1	4.2	1.3	1.8	1.6	2.3	0.6	26.3
DAG	32:3	580.4943	580.4935	7.48	1	18	55	120	116	111	0.0	0.1	0.3	0.9	1.1	1.2	0.6	0.5	85.4

50 µg N-(His)6-3C-Atg4B																			
Class	Lipid	Calc. Mass. [M-H] <sup>+</sup>	Found Mass. [M-H] <sup>+</sup>	RT (min)	Area						Conc. (pmol/sample)						50 µg Atg4B (n=6)		
					1	2	3	4	5	6	1	2	3	4	5	6	Mean	SD	%CV
DAG	32:4	578.4787	nd	nd	nd	nd	nd	nd	nd	nd	nd	nd	nd	nd	nd	nd	nd	nd	nd
DAG	32:5	576.4631	nd	nd	nd	nd	nd	nd	nd	nd	nd	nd	nd	nd	nd	nd	nd	nd	nd
DAG	34:0	614.5724	614.5755	11.54	654	601	10831	4245	355	251	3.8	3.1	64.6	30.7	3.5	2.8	10.9	9.0	83.1
DAG	34:1	612.5568	612.5521	10.67	359	1891	3273	748	489	402	2.1	9.7	19.5	5.4	4.8	4.5	8.7	4.3	49.5
DAG	34:2	610.5412	610.5370	9.81	286	976	1472	490	316	263	1.7	5.0	8.8	3.5	3.1	2.9	4.5	1.8	39.6
DAG	34:3	608.5256	608.5234	8.94	84	200	382	93	90	74	0.5	1.0	2.3	0.7	0.9	0.8	1.1	0.3	31.0
DAG	34:4	606.5100	nd	nd	nd	nd	nd	nd	nd	nd	nd	nd	nd	nd	nd	nd	nd	nd	nd
DAG	34:5	604.4944	nd	nd	nd	nd	nd	nd	nd	nd	nd	nd	nd	nd	nd	nd	nd	nd	nd
DAG	34:6	602.4788	nd	nd	nd	nd	nd	nd	nd	nd	nd	nd	nd	nd	nd	nd	nd	nd	nd
DAG	36:0	642.6040	642.6017	12.66	714	1028	8131	1797	327	147	4.2	5.3	48.5	13.0	3.2	1.6	9.5	8.1	85.3
DAG	36:1	640.5881	640.5910	11.89	389	1102	10831	1062	699	545	2.3	5.7	64.6	7.7	6.8	6.1	8.1	1.3	15.6
DAG	36:2	638.5725	638.5728	11.05	872	3605	5911	2475	1711	1345	5.1	18.6	35.3	17.9	16.7	15.0	18.5	4.9	26.5
DAG	36:3	636.5569	636.5563	10.21	230	850	1199	396	258	224	1.3	4.4	7.2	2.9	2.5	2.5	4.0	1.7	41.7
DAG	36:4	634.5413	634.5412	9.28	284	499	839	224	182	169	1.7	2.6	5.0	1.6	1.8	1.9	2.6	0.9	35.6
DAG	36:5	632.5257	632.5262	8.35	9	72	166	61	51	37	0.1	0.4	1.0	0.4	0.5	0.4	0.6	0.1	13.6
DAG	36:6	630.5101	nd	nd	nd	nd	nd	nd	nd	nd	nd	nd	nd	nd	nd	nd	nd	nd	nd
DAG	38:0	670.6350	670.6307	12.88	nd	134	417	nd	nd	nd	nd	0.7	2.5	nd	nd	nd	1.4	0.0	3.0
DAG	38:1	668.6194	668.6189	12.74	99	241	360	594	578	365	0.6	1.2	2.1	4.3	5.6	4.1	3.3	1.6	47.5
DAG	38:2	666.6038	666.6025	11.96	34	54	85	nd	nd	nd	0.2	0.3	0.5	nd	nd	nd	0.5	0.0	3.2
DAG	38:3	664.5882	664.5851	11.21	19	32	76	nd	nd	nd	0.1	0.2	0.5	nd	nd	nd	0.2	0.0	12.7
DAG	38:4	662.5726	662.5693	10.64	nd	3	18	nd	nd	nd	nd	0.0	0.1	nd	nd	nd	0.0	0.0	0.0

Table 23. Quantified CEs from the protein N-(His)<sub>6</sub>-3C-Atg4B. The lipids were obtained through incubation of the protein (0, 12.5, 25 and 50 µg) with a mixture of organic solvents at 48 °C for 16h.

0 µg N-(His) <sub>6</sub> -3C-Atg4B													
Class	Lipid	Calc. Mass. [M+NH <sub>4</sub> ] <sup>+</sup>	Found Mass. [M+NH <sub>4</sub> ] <sup>+</sup>	RT (min)	Area			Conc. (pmol/sample)			0 µg Atg4B (n=3)		
					1	2	3	1	2	3	Mean	SD	%CV
CE	Std	656.6346	656.6348	17.75	715	1114	1129	188.0	188.0	188.0	188	0	0
CE	14:0	614.5571	nd	nd	nd	nd	nd	nd	nd	nd	nd	nd	nd
CE	15:0	628.5728	nd	nd	nd	nd	nd	nd	nd	nd	nd	nd	nd
CE	16:0	642.6194	nd	nd	nd	nd	nd	nd	nd	nd	nd	nd	nd
CE	16:1	640.6038	640.5974	16.54	185	827	146	48.6	139.6	24.3	71	50	70
CE	16:2	638.5571	nd	nd	nd	nd	nd	nd	nd	nd	nd	nd	nd
CE	17:1	654.5884	nd	nd	nd	nd	nd	nd	nd	nd	nd	nd	nd
CE	18:0	670.6507	nd	nd	nd	nd	nd	nd	nd	nd	nd	nd	nd
CE	18:1	668.6342	668.6298	17.41	323	353	261	84.9	59.6	43.5	63	17	27
CE	18:2	666.6198	666.6144	16.79	128	241	145	33.7	40.7	24.1	33	7	21
CE	18:3	664.6062	nd	nd	nd	nd	nd	nd	nd	nd	nd	nd	nd
CE	20:0	698.6820	nd	nd	nd	nd	nd	nd	nd	nd	nd	nd	nd
CE	20:1	696.6664	696.6631	14.02	166	175	128	43.6	29.5	21.3	31	9	29
CE	20:2	694.6508	694.6487	17.56	143	158	145	37.6	26.7	24.1	29	6	20
CE	20:3	692.6352	692.6367	16.94	143	220	190	37.6	37.1	31.6	35	3	8
CE	20:4	690.6196	690.6161	14.71	37	55	51	9.7	9.3	8.5	9	1	6
CE	20:5	688.6040	nd	nd	nd	nd	nd	nd	nd	nd	nd	nd	nd
CE	20:6	686.5884	nd	nd	nd	nd	nd	nd	nd	nd	nd	nd	nd
CE	22:0	726.7133	nd	nd	nd	nd	nd	nd	nd	nd	nd	nd	nd
CE	22:1	724.6977	724.6983	14.30	310	299	235	81.5	50.5	39.1	57	18	31
CE	22:2	722.6821	nd	nd	nd	nd	nd	nd	nd	nd	nd	nd	nd
CE	22:3	720.6665	720.6664	17.47	20	34	45	5.3	5.7	7.5	6	1	16
CE	22:4	718.6509	nd	nd	nd	nd	nd	nd	nd	nd	nd	nd	nd
CE	22:5	716.6353	nd	nd	nd	nd	nd	nd	nd	nd	nd	nd	nd
CE	22:6	714.6197	nd	nd	nd	nd	nd	nd	nd	nd	nd	nd	nd
CE	24:0	754.7446	nd	nd	nd	nd	nd	nd	nd	nd	nd	nd	nd
CE	24:1	752.7290	nd	nd	nd	nd	nd	nd	nd	nd	nd	nd	nd

0 µg N-(His)6-3C-Atg4B													
Class	Lipid	Calc. Mass. [M+NH4] <sup>+</sup>	Found Mass. [M+NH4] <sup>+</sup>	RT (min)	Area			Conc. (pmol/sample)			0 µg Atg4B (n=3)		
					1	2	3	1	2	3	Mean	SD	%CV
CE	24:2	750.7134	nd	nd	nd	nd	nd	nd	nd	nd	nd	nd	nd
CE	24:3	748.6978	nd	nd	nd	nd	nd	nd	nd	nd	nd	nd	nd
CE	24:4	746.6822	nd	nd	nd	nd	nd	nd	nd	nd	nd	nd	nd
CE	24:5	744.6666	nd	nd	nd	nd	nd	nd	nd	nd	nd	nd	nd
CE	24:6	742.6510	742.6548	15.14	142	287	156	37.3	48.4	26.0	37	9	25

12.5 µg N-(His)6-3C-Atg4B													
Class	Lipid	Calc. Mass. [M+NH4] <sup>+</sup>	Found Mass. [M+NH4] <sup>+</sup>	RT (min)	Area			Conc. (pmol/sample) 12.5			12.5 µg Atg4B (n=3)		
					1	2	3	1	2	3	Mean	SD	%CV
CE	Std	656.6346	656.6348	17.75	1329	1109	1085	188.0	188.0	188.0	188.0	0.0	0.0
CE	14:0	614.5571	nd	nd	nd	nd	nd	nd	nd	nd	nd	nd	nd
CE	15:0	628.5728	nd	nd	nd	nd	nd	nd	nd	nd	nd	nd	nd
CE	16:0	642.6194	nd	nd	nd	nd	nd	nd	nd	nd	nd	nd	nd
CE	16:1	640.6038	640.5974	16.54	705	549	558	99.7	93.1	96.7	96.5	2.7	2.8
CE	16:2	638.5571	nd	nd	nd	nd	nd	nd	nd	nd	nd	nd	nd
CE	17:1	654.5884	nd	nd	nd	nd	nd	nd	nd	nd	nd	nd	nd
CE	18:0	670.6507	nd	nd	nd	nd	nd	nd	nd	nd	nd	nd	nd
CE	18:1	668.6342	668.6298	17.41	194	368	384	27.4	62.4	66.5	52.1	17.5	33.6
CE	18:2	666.6198	666.6144	16.79	275	196	270	38.9	33.2	46.8	39.6	5.6	14.0
CE	18:3	664.6062	nd	nd	nd	nd	nd	nd	nd	nd	nd	nd	nd
CE	20:0	698.6820	nd	nd	nd	nd	nd	nd	nd	nd	nd	nd	nd
CE	20:1	696.6664	696.6631	14.02	161	127	156	22.8	21.5	27.0	23.8	2.4	9.9
CE	20:2	694.6508	694.6487	17.56	182	169	191	25.7	28.6	33.1	29.2	3.0	10.4
CE	20:3	692.6352	692.6367	16.94	210	226	229	29.7	38.3	39.7	35.9	4.4	12.3
CE	20:4	690.6196	690.6161	14.71	62	62	67	8.8	10.5	11.6	10.3	1.2	11.4
CE	20:5	688.6040	nd	nd	nd	nd	nd	nd	nd	nd	nd	nd	nd
CE	20:6	686.5884	nd	nd	nd	nd	nd	nd	nd	nd	nd	nd	nd
CE	22:0	726.7133	nd	nd	nd	nd	nd	nd	nd	nd	nd	nd	nd
CE	22:1	724.6977	724.6983	14.30	319	253	156	45.1	42.9	27.0	38.3	8.1	21.0

12.5 µg N-(His)6-3C-Atg4B													
Class	Lipid	Calc. Mass. [M+NH4] <sup>+</sup>	Found Mass. [M+NH4] <sup>+</sup>	RT (min)	Area			Conc. (pmol/sample) 12.5			12.5 µg Atg4B (n=3)		
					1	2	3	1	2	3	Mean	SD	%CV
CE	22:2	722.6821	nd	nd	nd	nd	nd	nd	nd	nd	nd	nd	nd
CE	22:3	720.6665	720.6664	17.47	24	34	34	3.4	5.8	5.9	5.0	1.1	22.9
CE	22:4	718.6509	nd	nd	nd	nd	nd	nd	nd	nd	nd	nd	nd
CE	22:5	716.6353	nd	nd	nd	nd	nd	nd	nd	nd	nd	nd	nd
CE	22:6	714.6197	nd	nd	nd	nd	nd	nd	nd	nd	nd	nd	nd
CE	24:0	754.7446	nd	nd	nd	nd	nd	nd	nd	nd	nd	nd	nd
CE	24:1	752.7290	nd	nd	nd	nd	nd	nd	nd	nd	nd	nd	nd
CE	24:2	750.7134	nd	nd	nd	nd	nd	nd	nd	nd	nd	nd	nd
CE	24:3	748.6978	nd	nd	nd	nd	nd	nd	nd	nd	nd	nd	nd
CE	24:4	746.6822	nd	nd	nd	nd	nd	nd	nd	nd	nd	nd	nd
CE	24:5	744.6666	nd	nd	nd	nd	nd	nd	nd	nd	nd	nd	nd
CE	24:6	742.6510	742.6548	15.14	205	106	186	29.0	18.0	32.2	26.4	6.1	23.1

25 µg N-(His)6-3C-Atg4B													
Class	Lipid	Calc. Mass. [M+NH4] <sup>+</sup>	Found Mass. [M+NH4] <sup>+</sup>	RT (min)	Area			Conc. (pmol/sample)			25 µg Atg4 (n=3)		
					1	2	3	1	2	3	Mean	SD	%CV
CE	Std	656.6346	656.6370	17.75	1033	1081	1161	188.0	188.0	188.0	188	0	0
CE	14:0	614.5571	nd	nd	nd	nd	nd	nd	nd	nd	nd	nd	nd
CE	15:0	628.5728	nd	nd	nd	nd	nd	nd	nd	nd	nd	nd	nd
CE	16:0	642.6194	nd	nd	nd	nd	nd	nd	nd	nd	nd	nd	nd
CE	16:1	640.6038	640.5980	16.51	nd	800	580	nd	139.1	93.9	117	23	19
CE	16:2	638.5571	nd	nd	nd	nd	nd	nd	nd	nd	nd	nd	nd
CE	17:1	654.5884	nd	nd	nd	nd	nd	nd	nd	nd	nd	nd	nd
CE	18:0	670.6507	nd	nd	nd	nd	nd	nd	nd	nd	nd	nd	nd
CE	18:1	668.6342	668.6380	17.41	282	304	240	51.3	52.9	38.9	48	6	13
CE	18:2	666.6198	666.6225	16.73	197	229	238	35.9	39.8	38.5	38	2	4
CE	18:3	664.6062	nd	nd	nd	nd	nd	nd	nd	nd	nd	nd	nd
CE	20:0	698.6820	nd	nd	nd	nd	nd	nd	nd	nd	nd	nd	nd
CE	20:1	696.6664	696.6614	14.00	161	131	148	29.3	22.8	24.0	25	3	11



25 µg N-(His)6-3C-Atg4B													
Class	Lipid	Calc. Mass. [M+NH4] <sup>+</sup>	Found Mass. [M+NH4] <sup>+</sup>	RT (min)	Area			Conc. (pmol/sample)			25 µg Atg4 (n=3)		
					1	2	3	1	2	3	Mean	SD	%CV
CE	20:2	694.6508	694.6465	17.53	202	162	156	36.8	28.2	25.3	30	5	16
CE	20:3	692.6352	692.6313	16.91	230	202	196	41.9	35.1	31.7	36	4	12
CE	20:4	690.6196	690.6181	14.68	64	57	57	11.6	9.9	9.2	10	1	10
CE	20:5	688.6040	nd	nd	nd	nd	nd	nd	nd	nd	nd	nd	nd
CE	20:6	686.5884	nd	nd	nd	nd	nd	nd	nd	nd	nd	nd	nd
CE	22:0	726.7133	nd	nd	nd	nd	nd	nd	nd	nd	nd	nd	nd
CE	22:1	724.6977	724.6970	14.30	306	nd	264	55.7	nd	42.7	49	6	13
CE	22:2	722.6821	nd	nd	nd	nd	nd	nd	nd	nd	nd	nd	nd
CE	22:3	720.6665	720.6702	17.44	32	54	31	5.8	9.4	5.0	7	2	28
CE	22:4	718.6509	nd	nd	nd	nd	nd	nd	nd	nd	nd	nd	nd
CE	22:5	716.6353	nd	nd	nd	nd	nd	nd	nd	nd	nd	nd	nd
CE	22:6	714.6197	nd	nd	nd	nd	nd	nd	nd	nd	nd	nd	nd
CE	24:0	754.7446	nd	nd	nd	nd	nd	nd	nd	nd	nd	nd	nd
CE	24:1	752.7290	nd	nd	nd	nd	nd	nd	nd	nd	nd	nd	nd
CE	24:2	750.7134	nd	nd	nd	nd	nd	nd	nd	nd	nd	nd	nd
CE	24:3	748.6978	nd	nd	nd	nd	nd	nd	nd	nd	nd	nd	nd
CE	24:4	746.6822	nd	nd	nd	nd	nd	nd	nd	nd	nd	nd	nd
CE	24:5	744.6666	nd	nd	nd	nd	nd	nd	nd	nd	nd	nd	nd
CE	24:6	742.6510	742.6531	15.14	164	130	134	29.8	22.6	21.7	25	4	15

50 µg N-(His)6-3C-Atg4B													
Class	Lipid	Calc. Mass. [M+NH4] <sup>+</sup>	Found Mass. [M+NH4] <sup>+</sup>	RT (min)	Area			Conc. (pmol/sample)			50 µg Atg4 (n=3)		
					1	2	3	1	2	3	Mean	SD	%CV
CE	Std	656.6346	656.6370	17.75	813	1037	1091	188.0	188.0	188.0	188.0	0.0	0.0
CE	14:0	614.5571	nd	nd	nd	nd	nd	nd	nd	nd	nd	nd	nd
CE	15:0	628.5728	nd	nd	nd	nd	nd	nd	nd	nd	nd	nd	nd
CE	16:0	642.6194	nd	nd	nd	nd	nd	nd	nd	nd	nd	nd	nd
CE	16:1	640.6038	640.5980	16.51	735	540	332	170.0	97.9	57.2	108.4	46.6	43.0
CE	16:2	638.5571	nd	nd	nd	nd	nd	nd	nd	nd	nd	nd	nd

50 µg N-(His)6-3C-Atg4B													
Class	Lipid	Calc. Mass. [M+NH4] <sup>+</sup>	Found Mass. [M+NH4] <sup>+</sup>	RT (min)	Area			Conc. (pmol/sample)			50 µg Atg4 (n=3)		
					1	2	3	1	2	3	Mean	SD	%CV
CE	17:1	654.5884	nd	nd	nd	nd	nd	nd	nd	nd	nd	nd	nd
CE	18:0	670.6507	nd	nd	nd	nd	nd	nd	nd	nd	nd	nd	nd
CE	18:1	668.6342	668.6380	17.41	323	365	365	74.7	66.2	62.9	67.9	5.0	7.3
CE	18:2	666.6198	666.6225	16.73	250	253	257	57.8	45.9	44.3	49.3	6.0	12.2
CE	18:3	664.6062	nd	nd	nd	nd	nd	nd	nd	nd	nd	nd	nd
CE	20:0	698.6820	nd	nd	nd	nd	nd	nd	nd	nd	nd	nd	nd
CE	20:1	696.6664	696.6614	14.00	184	189	202	42.5	34.3	34.8	37.2	3.8	10.2
CE	20:2	694.6508	694.6465	17.53	171	183	178	39.5	33.2	30.7	34.5	3.7	10.8
CE	20:3	692.6352	692.6313	16.91	228	243	221	52.7	44.1	38.1	45.0	6.0	13.4
CE	20:4	690.6196	690.6181	14.68	70	64	64	16.2	11.6	11.0	12.9	2.3	17.8
CE	20:5	688.6040	nd	nd	nd	nd	nd	nd	nd	nd	nd	nd	nd
CE	20:6	686.5884	nd	nd	nd	nd	nd	nd	nd	nd	nd	nd	nd
CE	22:0	726.7133	nd	nd	nd	nd	nd	nd	nd	nd	nd	nd	nd
CE	22:1	724.6977	724.6970	14.30	349	471	260	80.7	85.4	44.8	70.3	18.1	25.8
CE	22:2	722.6821	nd	nd	nd	nd	nd	nd	nd	nd	nd	nd	nd
CE	22:3	720.6665	720.6702	17.44	34	35	54	7.9	6.3	9.3	7.8	1.2	15.4
CE	22:4	718.6509	nd	nd	nd	nd	nd	nd	nd	nd	nd	nd	nd
CE	22:5	716.6353	nd	nd	nd	nd	nd	nd	nd	nd	nd	nd	nd
CE	22:6	714.6197	nd	nd	nd	nd	nd	nd	nd	nd	nd	nd	nd
CE	24:0	754.7446	nd	nd	nd	nd	nd	nd	nd	nd	nd	nd	nd
CE	24:1	752.7290	nd	nd	nd	nd	nd	nd	nd	nd	nd	nd	nd
CE	24:2	750.7134	nd	nd	nd	nd	nd	nd	nd	nd	nd	nd	nd
CE	24:3	748.6978	nd	nd	nd	nd	nd	nd	nd	nd	nd	nd	nd
CE	24:4	746.6822	nd	nd	nd	nd	nd	nd	nd	nd	nd	nd	nd
CE	24:5	744.6666	nd	nd	nd	nd	nd	nd	nd	nd	nd	nd	nd
CE	24:6	742.6510	742.6531	15.14	189	257	176	43.7	46.6	30.3	40.2	7.1	17.6

Table 24. Quantified PEs from the delipidated protein N-(His)<sub>6</sub>-3C-Atg4B employing a 0, 2 and 12% of TX114 containing buffer. The lipids were obtained through incubation of the protein with a mixture of organic solvents at 48 °C for 16h.

0% TX114													
Class	Lipid	Calc. Mass. [M+H]-	Found Mass. [M+H]-	RT (min)	Area			Conc. (pmol/sample)			0% TX114 (n=3)		
					1	2	3	1	2	3	Mean	SD	%CV
PE	Std	749.7332	749.7327	9.46	3605	3381	4224	200.0	200.0	200.0	200.0	0.0	0.0
PE	28:0	636.4604	nd	nd	nd	nd	nd	nd	nd	nd	nd	nd	nd
PE	30:0	664.4918	nd	nd	nd	nd	nd	nd	nd	nd	nd	nd	nd
PE	31:0	678.5074	nd	nd	nd	nd	nd	nd	nd	nd	nd	nd	nd
PE	31:1	676.4918	676.4935	7.70	72	nd	65	4.0	nd	3.1	3.5	0.5	13.0
PE	32:0	692.5230	692.5190	9.15	43	35	47	2.4	2.1	2.2	2.2	0.1	5.8
PE	32:1	690.5074	690.5098	8.28	113	85	135	6.3	5.0	6.4	5.9	0.6	10.4
PE	32:2	688.4917	nd	nd	nd	nd	nd	nd	nd	nd	nd	nd	nd
PE	32:3	686.4761	nd	nd	nd	nd	nd	nd	nd	nd	nd	nd	nd
PE	33:0	704.5230	704.5269	9.06	650	509	577	36.1	30.1	27.3	31.2	3.6	11.7
PE	33:1	702.5074	nd	nd	nd	nd	nd	nd	nd	nd	nd	nd	nd
PE	33:2	700.4918	nd	nd	nd	nd	nd	nd	nd	nd	nd	nd	nd
PE	34:0	720.5543	nd	nd	nd	nd	nd	nd	nd	nd	nd	nd	nd
PE	34:1	718.5386	718.5316	9.49	178	144	172	9.9	8.5	8.1	8.8	0.7	8.4
PE	34:2	716.5230	716.5256	8.60	46	37	46	2.6	2.2	2.2	2.3	0.2	7.5
PE	34:3	714.5074	nd	nd	nd	nd	nd	nd	nd	nd	nd	nd	nd
PE	34:4	712.4917	nd	nd	nd	10	nd	nd	0.6	nd	0.6	0.0	0.0
PE	35:0	734.5700	nd	nd	nd	nd	nd	nd	nd	nd	nd	nd	nd
PE	35:1	732.5543	732.5578	10.30	342	273	315	19.0	16.1	14.9	16.7	1.7	10.2
PE	35:2	730.5387	730.5397	9.37	120	91	126	6.7	5.4	6.0	6.0	0.5	8.7
PE	36:0	748.5856	nd	nd	nd	nd	nd	nd	nd	nd	nd	nd	nd
PE	36:1	746.5699	nd	nd	nd	nd	nd	nd	nd	nd	nd	nd	nd
PE	36:2	744.5543	744.5541	9.90	57	39	77	3.2	2.3	3.6	3.0	0.6	18.2
PE	36:3	742.5386	nd	nd	nd	nd	nd	nd	nd	nd	nd	nd	nd
PE	36:4	740.5230	nd	nd	nd	nd	nd	nd	nd	nd	nd	nd	nd
PE	36:5	738.5074	nd	nd	nd	nd	nd	nd	nd	nd	nd	nd	nd
PE	36:6	736.4917	nd	nd	nd	nd	nd	nd	nd	nd	nd	nd	nd

0% TX114													
Class	Lipid	Calc. Mass. [M+H]-	Found Mass. [M+H]-	RT (min)	Area			Conc. (pmol/sample)			0% TX114 (n=3)		
					1	2	3	1	2	3	Mean	SD	%CV
PE	38:0	776.6169	nd	nd	nd	nd	nd	nd	nd	nd	nd	nd	nd
PE	38:1	774.6012	nd	nd	nd	nd	nd	nd	nd	nd	nd	nd	nd
PE	38:2	772.5856	772.5856	11.45	155	118	99	8.6	7.0	4.7	6.8	1.6	23.8
PE	38:3	770.5699	nd	nd	nd	nd	nd	nd	nd	nd	nd	nd	nd
PE	38:4	768.5546	nd	nd	nd	nd	nd	nd	nd	nd	nd	nd	nd
PE	38:5	766.5386	nd	nd	nd	nd	nd	nd	nd	nd	nd	nd	nd
PE	38:6	764.5226	nd	nd	nd	nd	nd	nd	nd	nd	nd	nd	nd
PE	38:7	762.5074	nd	nd	nd	nd	nd	nd	nd	nd	nd	nd	nd
PE	40:0	802.6325	nd	nd	nd	nd	nd	nd	nd	nd	nd	nd	nd
PE	40:1	800.6169	nd	nd	nd	nd	nd	nd	nd	nd	nd	nd	nd
PE	40:2	798.6012	nd	nd	nd	nd	nd	nd	nd	nd	nd	nd	nd
PE	40:3	796.5856	nd	nd	nd	nd	nd	nd	nd	nd	nd	nd	nd
PE	40:4	794.5699	nd	nd	nd	nd	nd	nd	nd	nd	nd	nd	nd
PE	40:5	792.5543	nd	nd	nd	nd	nd	nd	nd	nd	nd	nd	nd
PE	40:6	790.5386	nd	nd	nd	nd	nd	nd	nd	nd	nd	nd	nd
PE	40:8	788.5230	nd	nd	nd	nd	nd	nd	nd	nd	nd	nd	nd

2% TX114													
Class	Lipid	Calc. Mass. [M+H]-	Found Mass. [M+H]-	RT (min)	Area			Conc. (pmol/sample)			2% TX114 (n=3)		
					1	2	3	1	2	3	Mean	SD	%CV
PE	Std	749.7332	749.7327	9.46	5403	6267	4405	200.0	200.0	200.0	200.0	0.0	0.0
PE	28:0	636.4604	nd	nd	nd	nd	nd	nd	nd	nd	nd	nd	nd
PE	30:0	664.4918	nd	nd	nd	nd	nd	nd	nd	nd	nd	nd	nd
PE	31:0	678.5074	nd	nd	nd	nd	nd	nd	nd	nd	nd	nd	nd
PE	31:1	676.4918	676.4935	7.70	nd	nd	nd	nd	nd	nd	nd	nd	nd
PE	32:0	692.5230	692.5190	9.15	nd	nd	nd	nd	nd	nd	nd	nd	nd
PE	32:1	690.5074	690.5098	8.28	nd	46	nd	nd	1.5	nd	1.5	0.0	0.0
PE	32:2	688.4917	nd	nd	nd	nd	nd	nd	nd	nd	nd	nd	nd
PE	32:3	686.4761	nd	nd	nd	nd	nd	nd	nd	nd	nd	nd	nd

2% TX114													
Class	Lipid	Calc. Mass. [M+H]-	Found Mass. [M+H]-	RT (min)	Area			Conc. (pmol/sample)			2% TX114 (n=3)		
					1	2	3	1	2	3	Mean	SD	%CV
PE	33:0	704.5230	704.5269	9.06	26	208	84	1.0	6.6	3.8	3.8	2.3	60.9
PE	33:1	702.5074	nd	nd	nd	nd	nd	nd	nd	nd	nd	nd	nd
PE	33:2	700.4918	nd	nd	nd	nd	nd	nd	nd	nd	nd	nd	nd
PE	34:0	720.5543	nd	nd	nd	nd	nd	nd	nd	nd	nd	nd	nd
PE	34:1	718.5386	718.5316	9.49	nd	60	27	nd	1.9	1.2	1.6	0.3	21.9
PE	34:2	716.5230	716.5256	8.60	nd	nd	nd	nd	nd	nd	nd	nd	nd
PE	34:3	714.5074	nd	nd	nd	nd	nd	nd	nd	nd	nd	nd	nd
PE	34:4	712.4917	nd	nd	nd	nd	nd	nd	nd	nd	nd	nd	nd
PE	35:0	734.5700	nd	nd	nd	nd	nd	nd	nd	nd	nd	nd	nd
PE	35:1	732.5543	732.5578	10.30	nd	434	49	nd	13.9	2.2	8.0	5.8	72.3
PE	35:2	730.5387	730.5397	9.37	nd	40	17	nd	1.3	0.8	1.0	0.3	24.6
PE	36:0	748.5856	nd	nd	nd	nd	nd	nd	nd	nd	nd	nd	nd
PE	36:1	746.5699	nd	nd	nd	nd	nd	nd	nd	nd	nd	nd	nd
PE	36:2	744.5543	744.5541	9.90	nd	41	nd	nd	1.3	nd	1.3	0.0	0.0
PE	36:3	742.5386	nd	nd	nd	nd	nd	nd	nd	nd	nd	nd	nd
PE	36:4	740.5230	nd	nd	nd	nd	nd	nd	nd	nd	nd	nd	nd
PE	36:5	738.5074	nd	nd	nd	nd	nd	nd	nd	nd	nd	nd	nd
PE	36:6	736.4917	nd	nd	nd	nd	nd	nd	nd	nd	nd	nd	nd
PE	38:0	776.6169	nd	nd	nd	nd	nd	nd	nd	nd	nd	nd	nd
PE	38:1	774.6012	nd	nd	nd	nd	nd	nd	nd	nd	nd	nd	nd
PE	38:2	772.5856	772.5856	11.45	nd	39	18	nd	1.2	0.8	1.0	0.2	20.7
PE	38:3	770.5699	nd	nd	nd	nd	nd	nd	nd	nd	nd	nd	nd
PE	38:4	768.5546	nd	nd	nd	nd	nd	nd	nd	nd	nd	nd	nd
PE	38:5	766.5386	nd	nd	nd	nd	nd	nd	nd	nd	nd	nd	nd
PE	38:6	764.5226	nd	nd	nd	nd	nd	nd	nd	nd	nd	nd	nd
PE	38:7	762.5074	nd	nd	nd	nd	nd	nd	nd	nd	nd	nd	nd
PE	40:0	802.6325	nd	nd	nd	nd	nd	nd	nd	nd	nd	nd	nd
PE	40:1	800.6169	nd	nd	nd	nd	nd	nd	nd	nd	nd	nd	nd
PE	40:2	798.6012	nd	nd	nd	nd	nd	nd	nd	nd	nd	nd	nd
PE	40:3	796.5856	nd	nd	nd	nd	nd	nd	nd	nd	nd	nd	nd

2% TX114													
Class	Lipid	Calc. Mass. [M+H]-	Found Mass. [M+H]-	RT (min)	Area			Conc. (pmol/sample)			2% TX114 (n=3)		
					1	2	3	1	2	3	Mean	SD	%CV
PE	40:4	794.5699	nd	nd	nd	nd	nd	nd	nd	nd	nd	nd	nd
PE	40:5	792.5543	nd	nd	nd	nd	nd	nd	nd	nd	nd	nd	nd
PE	40:6	790.5386	nd	nd	nd	nd	nd	nd	nd	nd	nd	nd	nd
PE	40:8	788.5230	nd	nd	nd	nd	nd	nd	nd	nd	nd	nd	nd

12% TX114													
Class	Lipid	Calc. Mass. [M+H]-	Found Mass. [M+H]-	RT (min)	Area			Conc. (pmol/sample)			12% TX114 (n=3)		
					1	2	3	1	2	3	Mean	SD	%CV
PE	Std	749.7332	749.7327	9.46	4901	6605	5594	200.0	200.0	200.0	200.0	0.0	0.0
PE	28:0	636.4604	nd	nd	nd	nd	nd	nd	nd	nd	nd	nd	nd
PE	30:0	664.4918	nd	nd	nd	nd	nd	nd	nd	nd	nd	nd	nd
PE	31:0	678.5074	nd	nd	nd	nd	nd	nd	nd	nd	nd	nd	nd
PE	31:1	676.4918	676.4935	7.70	nd	nd	nd	nd	nd	nd	nd	nd	nd
PE	32:0	692.5230	692.5190	9.15	nd	nd	nd	nd	nd	nd	nd	nd	nd
PE	32:1	690.5074	690.5098	8.28	nd	nd	nd	nd	nd	nd	nd	nd	nd
PE	32:2	688.4917	nd	nd	nd	nd	nd	nd	nd	nd	nd	nd	nd
PE	32:3	686.4761	nd	nd	nd	nd	nd	nd	nd	nd	nd	nd	nd
PE	33:0	704.5230	704.5269	9.06	nd	nd	56	nd	nd	2.0	2.0	0.0	0.0
PE	33:1	702.5074	nd	nd	nd	nd	nd	nd	nd	nd	nd	nd	nd
PE	33:2	700.4918	nd	nd	nd	nd	nd	nd	nd	nd	nd	nd	nd
PE	34:0	720.5543	nd	nd	nd	nd	nd	nd	nd	nd	nd	nd	nd
PE	34:1	718.5386	718.5316	9.49	nd	nd	nd	nd	nd	nd	nd	nd	nd
PE	34:2	716.5230	716.5256	8.60	nd	nd	nd	nd	nd	nd	nd	nd	nd
PE	34:3	714.5074	nd	nd	nd	nd	nd	nd	nd	nd	nd	nd	nd
PE	34:4	712.4917	nd	nd	nd	nd	nd	nd	nd	nd	nd	nd	nd
PE	35:0	734.5700	nd	nd	nd	nd	nd	nd	nd	nd	nd	nd	nd
PE	35:1	732.5543	732.5578	10.30	nd	nd	nd	nd	nd	nd	nd	nd	nd
PE	35:2	730.5387	730.5397	9.37	nd	nd	nd	nd	nd	nd	nd	nd	nd
PE	36:0	748.5856	nd	nd	nd	nd	nd	nd	nd	nd	nd	nd	nd

12% TX114													
Class	Lipid	Calc. Mass. [M+H]-	Found Mass. [M+H]-	RT (min)	Area			Conc. (pmol/sample)			12% TX114 (n=3)		
					1	2	3	1	2	3	Mean	SD	%CV
PE	36:1	746.5699	nd	nd	nd	nd	nd	nd	nd	nd	nd	nd	nd
PE	36:2	744.5543	744.5541	9.90	nd	nd	nd	nd	nd	nd	nd	nd	nd
PE	36:3	742.5386	nd	nd	nd	nd	nd	nd	nd	nd	nd	nd	nd
PE	36:4	740.5230	nd	nd	nd	nd	nd	nd	nd	nd	nd	nd	nd
PE	36:5	738.5074	nd	nd	nd	nd	nd	nd	nd	nd	nd	nd	nd
PE	36:6	736.4917	nd	nd	nd	nd	nd	nd	nd	nd	nd	nd	nd
PE	38:0	776.6169	nd	nd	nd	nd	nd	nd	nd	nd	nd	nd	nd
PE	38:1	774.6012	nd	nd	nd	nd	nd	nd	nd	nd	nd	nd	nd
PE	38:2	772.5856	772.5856	11.45	nd	nd	nd	nd	nd	nd	nd	nd	nd
PE	38:3	770.5699	nd	nd	nd	nd	nd	nd	nd	nd	nd	nd	nd
PE	38:4	768.5546	nd	nd	nd	nd	nd	nd	nd	nd	nd	nd	nd
PE	38:5	766.5386	nd	nd	nd	nd	nd	nd	nd	nd	nd	nd	nd
PE	38:6	764.5226	nd	nd	nd	nd	nd	nd	nd	nd	nd	nd	nd
PE	38:7	762.5074	nd	nd	nd	nd	nd	nd	nd	nd	nd	nd	nd
PE	40:0	802.6325	nd	nd	nd	nd	nd	nd	nd	nd	nd	nd	nd
PE	40:1	800.6169	nd	nd	nd	nd	nd	nd	nd	nd	nd	nd	nd
PE	40:2	798.6012	nd	nd	nd	nd	nd	nd	nd	nd	nd	nd	nd
PE	40:3	796.5856	nd	nd	nd	nd	nd	nd	nd	nd	nd	nd	nd
PE	40:4	794.5699	nd	nd	nd	nd	nd	nd	nd	nd	nd	nd	nd
PE	40:5	792.5543	nd	nd	nd	nd	nd	nd	nd	nd	nd	nd	nd
PE	40:6	790.5386	nd	nd	nd	nd	nd	nd	nd	nd	nd	nd	nd
PE	40:8	788.5230	nd	nd	nd	nd	nd	nd	nd	nd	nd	nd	nd

Table 25. Quantified DAGs from the delipidated protein N-(His)<sub>6</sub>-3C-Atg4B employing a 0, 2 and 12% of TX114 containing buffer. The lipids were obtained through incubation of the protein with a mixture of organic solvents at 48 °C for 16h.

Class	Lipid	Calc. Mass. [M-H] <sup>+</sup>	Found Mass. [M-H] <sup>+</sup>	RT (min)	0% TX114			Conc. (pmol/sample)			0% Atg4 (n=3)					
					Area			1	2	3	1	2	3	Mean	SD	%CV
					1	2	3	1	2	3	1	2	3	Mean	SD	%CV
DAG	Std	619.6037	749.7327	11.73	12088	8364	14620	166.0	166.0	166.0	166.0	0.0	0.0			
DAG	30:0	558.5098	558.5061	9.18	183	199	116	2.5	3.9	1.3	2.6	1.1	41.5			
DAG	30:1	556.4942	nd	nd	nd	nd	nd	nd	nd	nd	nd	nd	nd			
DAG	30:2	554.4786	nd	nd	nd	nd	nd	nd	nd	nd	nd	nd	nd			
DAG	30:3	552.4630	nd	nd	nd	nd	nd	nd	nd	nd	nd	nd	nd			
DAG	30:4	550.4474	nd	nd	nd	nd	nd	nd	nd	nd	nd	nd	nd			
DAG	32:0	586.5411	586.5386	10.54	627	862	207	8.6	17.1	2.4	9.4	6.0	64.6			
DAG	32:1	584.5255	584.5195	9.81	318	306	213	4.4	6.1	2.4	4.3	1.5	34.8			
DAG	32:2	582.5099	582.5086	8.97	137	143	97	1.9	2.8	1.1	1.9	0.7	36.6			
DAG	32:3	580.4943	nd	nd	nd	nd	nd	nd	nd	nd	nd	nd	nd			
DAG	32:4	578.4787	nd	nd	nd	nd	nd	nd	nd	nd	nd	nd	nd			
DAG	32:5	576.4631	nd	nd	nd	nd	nd	nd	nd	nd	nd	nd	nd			
DAG	34:0	614.5724	614.5687	11.82	640	679	168	8.8	13.5	1.9	8.1	4.8	59.0			
DAG	34:1	612.5568	612.5536	11.01	472	532	318	6.5	10.6	3.6	6.9	2.9	41.4			
DAG	34:2	610.5412	610.5399	10.11	237	225	182	3.3	4.5	2.1	3.3	1.0	30.0			
DAG	34:3	608.5256	608.5250	9.21	47	43	41	0.6	0.9	0.5	0.7	0.2	24.2			
DAG	34:4	606.5100	nd	nd	nd	nd	nd	nd	nd	nd	nd	nd	nd			
DAG	34:5	604.4944	nd	nd	nd	nd	nd	nd	nd	nd	nd	nd	nd			
DAG	34:6	602.4788	nd	nd	nd	nd	nd	nd	nd	nd	nd	nd	nd			
DAG	36:0	642.6040	642.6891	12.91	278	343	94	3.8	6.8	1.1	3.9	2.3	60.1			
DAG	36:1	640.5881	640.5860	12.16	1323	1123	746	18.2	22.3	8.5	16.3	5.8	35.5			
DAG	36:2	638.5725	638.5710	11.33	1386	2035	780	19.0	40.4	8.9	22.8	13.1	57.7			
DAG	36:3	636.5569	636.5576	10.49	234	249	177	3.2	4.9	2.0	3.4	1.2	35.5			
DAG	36:4	634.5413	634.5415	nd	nd	105	83	nd	2.1	0.9	1.5	0.6	37.7			
DAG	36:5	632.5257	nd	nd	nd	nd	nd	nd	nd	nd	nd	nd	nd			
DAG	36:6	630.5101	nd	nd	nd	nd	nd	nd	nd	nd	nd	nd	nd			
DAG	38:0	670.6350	nd	nd	nd	nd	nd	nd	nd	nd	nd	nd	nd			



0% TX114													
Class	Lipid	Calc. Mass. [M-H] <sup>+</sup>	Found Mass. [M-H] <sup>+</sup>	RT (min)	Area			Conc. (pmol/sample)			0% Atg4 (n=3)		
					1	2	3	1	2	3	Mean	SD	%CV
DAG	38:1	668.6194	668.6183	7.67	835	767	357	11.5	15.2	4.1	10.2	4.6	45.3
DAG	38:2	666.6038	666.6003	6.77	285	280	220	3.9	5.6	2.5	4.0	1.3	31.3
DAG	38:3	664.5882	nd	nd	nd	nd	nd	nd	nd	nd	nd	nd	nd
DAG	38:4	662.5726	nd	nd	nd	nd	nd	nd	nd	nd	nd	nd	nd

2% TX114													
Class	Lipid	Calc. Mass. [M-H] <sup>+</sup>	Found Mass. [M-H] <sup>+</sup>	RT (min)	Area			Conc. (pmol/sample)			2% Atg4 (n=3)		
					1	2	3	1	2	3	Mean	SD	%CV
DAG	Std	619.6037	749.7327	11.73	20410	20400	15379	166.0	166.0	166.0	166.0	0.0	0.0
DAG	30:0	558.5098	558.5061	9.18	183	325	129	1.5	2.6	1.4	1.8	0.6	30.9
DAG	30:1	556.4942	nd	nd	nd	nd	nd	nd	nd	nd	nd	nd	nd
DAG	30:2	554.4786	nd	nd	nd	nd	nd	nd	nd	nd	nd	nd	nd
DAG	30:3	552.4630	nd	nd	nd	nd	nd	nd	nd	nd	nd	nd	nd
DAG	30:4	550.4474	nd	nd	nd	nd	nd	nd	nd	nd	nd	nd	nd
DAG	32:0	586.5411	586.5386	10.54	2006	5175	266	16.3	42.1	2.9	20.4	16.3	79.7
DAG	32:1	584.5255	584.5195	9.81	229	343	243	1.9	2.8	2.6	2.4	0.4	16.7
DAG	32:2	582.5099	582.5086	8.97	87	136	117	0.7	1.1	1.3	1.0	0.2	22.8
DAG	32:3	580.4943	nd	nd	nd	nd	nd	nd	nd	nd	nd	nd	nd
DAG	32:4	578.4787	nd	nd	nd	nd	nd	nd	nd	nd	nd	nd	nd
DAG	32:5	576.4631	nd	nd	nd	nd	nd	nd	nd	nd	nd	nd	nd
DAG	34:0	614.5724	614.5687	11.82	1891	4014	284	15.4	32.7	3.1	17.0	12.1	71.3
DAG	34:1	612.5568	612.5536	11.01	618	730	412	5.0	5.9	4.4	5.1	0.6	12.0
DAG	34:2	610.5412	610.5399	10.11	269	370	190	2.2	3.0	2.1	2.4	0.4	17.5
DAG	34:3	608.5256	608.5250	9.21	38	68	45	0.3	0.6	0.5	0.4	0.1	22.9
DAG	34:4	606.5100	nd	nd	nd	nd	nd	nd	nd	nd	nd	nd	nd
DAG	34:5	604.4944	nd	nd	nd	nd	nd	nd	nd	nd	nd	nd	nd
DAG	34:6	602.4788	nd	nd	nd	nd	nd	nd	nd	nd	nd	nd	nd
DAG	36:0	642.6040	642.6891	12.91	757	1902	154	6.2	15.5	1.7	7.8	5.8	74.1
DAG	36:1	640.5881	640.5860	12.16	698	811	657	5.7	6.6	7.1	6.5	0.6	9.1

2% TX114													
Class	Lipid	Calc. Mass. [M-H] <sup>+</sup>	Found Mass. [M-H] <sup>+</sup>	RT (min)	Area			Conc. (pmol/sample)			2% Atg4 (n=3)		
					1	2	3	1	2	3	Mean	SD	%CV
DAG	36:2	638.5725	638.5710	11.33	1628	1906	851	13.2	15.5	9.2	12.6	2.6	20.7
DAG	36:3	636.5569	636.5576	10.49	301	316	172	2.4	2.6	1.9	2.3	0.3	13.6
DAG	36:4	634.5413	634.5415	nd	105	124	83	0.9	1.0	0.9	0.9	0.1	7.1
DAG	36:5	632.5257	nd	nd	nd	nd	nd	nd	nd	nd	nd	nd	nd
DAG	36:6	630.5101	nd	nd	nd	nd	nd	nd	nd	nd	nd	nd	nd
DAG	38:0	670.6350	nd	nd	nd	nd	nd	nd	nd	nd	nd	nd	nd
DAG	38:1	668.6194	668.6183	7.67	636	464	335	5.2	3.8	3.6	4.2	0.7	16.7
DAG	38:2	666.6038	666.6003	6.77	292	190	227	2.4	1.5	2.5	2.1	0.4	19.3
DAG	38:3	664.5882	nd	nd	nd	nd	nd	nd	nd	nd	nd	nd	nd
DAG	38:4	662.5726	nd	nd	nd	nd	nd	nd	nd	nd	nd	nd	nd

12% TX114													
Class	Lipid	Calc. Mass. [M-H] <sup>+</sup>	Found Mass. [M-H] <sup>+</sup>	RT (min)	Area			Conc. (pmol/sample)			12% Atg4 (n=3)		
					1	2	3	1	2	3	Mean	SD	%CV
DAG	Std	619.6037	749.7327	11.73	18909	22627	22413	166.0	166.0	166.0	166.0	0.0	0.0
DAG	30:0	558.5098	558.5061	9.18	263	516	175	2.3	3.8	1.3	2.5	1.0	41.5
DAG	30:1	556.4942	nd	nd	nd	nd	nd	nd	nd	nd	nd	nd	nd
DAG	30:2	554.4786	nd	nd	nd	nd	nd	nd	nd	nd	nd	nd	nd
DAG	30:3	552.4630	nd	nd	nd	nd	nd	nd	nd	nd	nd	nd	nd
DAG	30:4	550.4474	nd	nd	nd	nd	nd	nd	nd	nd	nd	nd	nd
DAG	32:0	586.5411	586.5386	10.54	3559	9327	261	31.2	68.4	1.9	33.9	27.2	80.3
DAG	32:1	584.5255	584.5195	9.81	259	479	370	2.3	3.5	2.7	2.8	0.5	18.0
DAG	32:2	582.5099	582.5086	8.97	112	188	162	1.0	1.4	1.2	1.2	0.2	13.6
DAG	32:3	580.4943	nd	nd	nd	nd	nd	nd	nd	nd	nd	nd	nd
DAG	32:4	578.4787	nd	nd	nd	nd	nd	nd	nd	nd	nd	nd	nd
DAG	32:5	576.4631	nd	nd	nd	nd	nd	nd	nd	nd	nd	nd	nd
DAG	34:0	614.5724	614.5687	11.82	3946	7535	258	34.6	55.3	1.9	30.6	22.0	71.8
DAG	34:1	612.5568	612.5536	11.01	599	1062	577	5.3	7.8	4.3	5.8	1.5	25.7
DAG	34:2	610.5412	610.5399	10.11	247	438	277	2.2	3.2	2.1	2.5	0.5	21.1

12% TX114													
Class	Lipid	Calc. Mass. [M-H] <sup>+</sup>	Found Mass. [M-H] <sup>+</sup>	RT (min)	Area			Conc. (pmol/sample)			12% Atg4 (n=3)		
					1	2	3	1	2	3	Mean	SD	%CV
DAG	34:3	608.5256	608.5250	9.21	49	82	91	0.4	0.6	0.7	0.6	0.1	18.0
DAG	34:4	606.5100	nd	nd	nd	nd	nd	nd	nd	nd	nd	nd	nd
DAG	34:5	604.4944	nd	nd	nd	nd	nd	nd	nd	nd	nd	nd	nd
DAG	34:6	602.4788	nd	nd	nd	nd	nd	nd	nd	nd	nd	nd	nd
DAG	36:0	642.6040	642.6891	12.91	1662	3409	229	14.6	25.0	1.7	13.8	9.5	69.3
DAG	36:1	640.5881	640.5860	12.16	800	1163	834	7.0	8.5	6.2	7.2	1.0	13.4
DAG	36:2	638.5725	638.5710	11.33	1790	2381	1437	15.7	17.5	10.6	14.6	2.9	19.8
DAG	36:3	636.5569	636.5576	10.49	275	423	256	2.4	3.1	1.9	2.5	0.5	20.0
DAG	36:4	634.5413	634.5415	nd	111	163	133	1.0	1.2	1.0	1.1	0.1	9.7
DAG	36:5	632.5257	nd	nd	nd	nd	nd	nd	nd	nd	nd	nd	nd
DAG	36:6	630.5101	nd	nd	nd	nd	nd	nd	nd	nd	nd	nd	nd
DAG	38:0	670.6350	nd	nd	nd	nd	nd	nd	nd	nd	nd	nd	nd
DAG	38:1	668.6194	668.6183	7.67	507	286	534	4.5	2.1	4.0	3.5	1.0	28.9
DAG	38:2	666.6038	666.6003	6.77	204	441	235	1.8	3.2	1.7	2.3	0.7	30.7
DAG	38:3	664.5882	nd	nd	nd	nd	nd	nd	nd	nd	nd	nd	nd
DAG	38:4	662.5726	nd	nd	nd	nd	nd	nd	nd	nd	nd	nd	nd

Table 26. Quantified CEs from the delipidated protein N-(His)<sub>6</sub>-3C-Atg4B employing a 0, 2 and 12% of TX114 containing buffer. The lipids were obtained through incubation of the protein with a mixture of organic solvents at 48 °C for 16h.

0% TX114													
Class	Lipid	Calc. Mass. [M+NH4] <sup>+</sup>	Found Mass. [M+NH4] <sup>+</sup>	RT (min)	Area			Conc. (pmol/sample)			0% TX114 (n=3)		
					1	2	3	1	2	3	Mean	SD	%CV
CE	Standard	656.6346	656.6336	17.78	810	805	1353	188.0	188.0	188.0	188.0	0.0	0.0
CE	14:0	614.5571	nd	nd	nd	nd	nd	nd	nd	nd	nd	nd	nd
CE	15:0	628.5728	nd	nd	nd	nd	nd	nd	nd	nd	nd	nd	nd
CE	16:0	642.6194	nd	nd	nd	nd	nd	nd	nd	nd	nd	nd	nd
CE	16:1	640.6038	640.6028	16.54	nd	236	228	nd	55.1	31.7	43.4	11.7	27.0
CE	16:2	638.5571	nd	nd	nd	nd	nd	nd	nd	nd	nd	nd	nd

0% TX114													
Class	Lipid	Calc. Mass. [M+NH4] <sup>+</sup>	Found Mass. [M+NH4] <sup>+</sup>	RT (min)	Area			Conc. (pmol/sample)			0% TX114 (n=3)		
					1	2	3	1	2	3	Mean	SD	%CV
CE	17:1	654.5884	nd	nd	nd	nd	nd	nd	nd	nd	nd	nd	nd
CE	18:0	670.6507	nd	nd	nd	nd	nd	nd	nd	nd	nd	nd	nd
CE	18:1	668.6342	668.6318	17.44	189	195	299	43.9	45.5	41.5	43.7	1.6	3.8
CE	18:2	666.6198	666.6141	16.79	471	28	154	109.3	6.5	21.4	45.8	45.4	99.1
CE	18:3	664.6062	nd	nd	nd	nd	nd	nd	nd	nd	nd	nd	nd
CE	20:0	698.6820	nd	nd	nd	nd	nd	nd	nd	nd	nd	nd	nd
CE	20:1	696.6664	696.6655	14.12	212	134	66	49.2	31.3	9.2	29.9	16.4	54.8
CE	20:2	694.6508	694.6496	17.56	81	57	64	18.8	13.3	8.9	13.7	4.1	29.6
CE	20:3	692.6352	692.6345	16.94	73	56	86	16.9	13.1	11.9	14.0	2.1	15.3
CE	20:4	690.6196	690.6222	14.68	nd	nd	20	nd	nd	2.8	2.8	0.0	0.0
CE	20:5	688.6040	nd	nd	nd	nd	nd	nd	nd	nd	nd	nd	nd
CE	20:6	686.5884	nd	nd	nd	nd	nd	nd	nd	nd	nd	nd	nd
CE	22:0	726.7133	nd	nd	nd	nd	nd	nd	nd	nd	nd	nd	nd
CE	22:1	724.6977	724.7010	14.34	275	316	72	63.8	73.8	10.0	49.2	28.0	56.9
CE	22:2	722.6821	nd	nd	nd	nd	nd	nd	nd	nd	nd	nd	nd
CE	22:3	720.6665	720.6682	17.44	10	28	14	2.3	6.5	1.9	3.6	2.1	57.8
CE	22:4	718.6509	nd	nd	nd	nd	nd	nd	nd	nd	nd	nd	nd
CE	22:5	716.6353	nd	nd	nd	nd	nd	nd	nd	nd	nd	nd	nd
CE	22:6	714.6197	nd	nd	nd	nd	nd	nd	nd	nd	nd	nd	nd
CE	24:0	754.7446	nd	nd	nd	nd	nd	nd	nd	nd	nd	nd	nd
CE	24:1	752.7290	nd	nd	nd	nd	nd	nd	nd	nd	nd	nd	nd
CE	24:2	750.7134	nd	nd	nd	nd	nd	nd	nd	nd	nd	nd	nd
CE	24:3	748.6978	nd	nd	nd	nd	nd	nd	nd	nd	nd	nd	nd
CE	24:4	746.6822	nd	nd	nd	nd	nd	nd	nd	nd	nd	nd	nd
CE	24:5	744.6666	nd	nd	nd	nd	nd	nd	nd	nd	nd	nd	nd
CE	24:6	742.6510	742.6524	15.14	nd	nd	295	nd	nd	41.0	41.0	0.0	0.0

2% TX114													
Class	Lipid	Calc. Mass. [M+NH4] <sup>+</sup>	Found Mass. [M+NH4] <sup>+</sup>	RT (min)	Area			Conc. (pmol/sample)			2% TX114 (n=3)		
					1	2	3	1	2	3	Mean	SD	%CV
CE	Standard	656.6346	656.6336	17.78	923	779	1065	188.0	188.0	188.0	188.0	0.0	0.0
CE	14:0	614.5571	nd	nd	nd	nd	nd	nd	nd	nd	nd	nd	nd
CE	15:0	628.5728	nd	nd	nd	nd	nd	nd	nd	nd	nd	nd	nd
CE	16:0	642.6194	nd	nd	nd	nd	nd	nd	nd	nd	nd	nd	nd
CE	16:1	640.6038	640.6028	16.54	593	399	177	120.8	96.3	31.2	82.8	37.8	45.6
CE	16:2	638.5571	nd	nd	nd	nd	nd	nd	nd	nd	nd	nd	nd
CE	17:1	654.5884	nd	nd	nd	nd	nd	nd	nd	nd	nd	nd	nd
CE	18:0	670.6507	nd	nd	nd	nd	nd	nd	nd	nd	nd	nd	nd
CE	18:1	668.6342	668.6318	17.44	298	331	387	60.7	79.9	68.3	69.6	7.9	11.3
CE	18:2	666.6198	666.6141	16.79	233	130	300	47.5	31.4	53.0	43.9	9.2	20.8
CE	18:3	664.6062	nd	nd	nd	nd	nd	nd	nd	nd	nd	nd	nd
CE	20:0	698.6820	nd	nd	nd	nd	nd	nd	nd	nd	nd	nd	nd
CE	20:1	696.6664	696.6655	14.12	174	167	119	35.4	40.3	21.0	32.3	8.2	25.4
CE	20:2	694.6508	694.6496	17.56	69	55	81	14.1	13.3	14.3	13.9	0.4	3.2
CE	20:3	692.6352	692.6345	16.94	86	68	89	17.5	16.4	15.7	16.5	0.7	4.5
CE	20:4	690.6196	690.6222	14.68	23	20	21	4.7	4.8	3.7	4.4	0.5	11.3
CE	20:5	688.6040	nd	nd	nd	nd	nd	nd	nd	nd	nd	nd	nd
CE	20:6	686.5884	nd	nd	nd	nd	nd	nd	nd	nd	nd	nd	nd
CE	22:0	726.7133	nd	nd	nd	nd	nd	nd	nd	nd	nd	nd	nd
CE	22:1	724.6977	724.7010	14.34	269	287	126	54.8	69.3	22.2	48.8	19.7	40.3
CE	22:2	722.6821	nd	nd	nd	nd	nd	nd	nd	nd	nd	nd	nd
CE	22:3	720.6665	720.6682	17.44	12	7	13	2.4	1.7	2.3	2.1	0.3	15.2
CE	22:4	718.6509	nd	nd	nd	nd	nd	nd	nd	nd	nd	nd	nd
CE	22:5	716.6353	nd	nd	nd	nd	nd	nd	nd	nd	nd	nd	nd
CE	22:6	714.6197	nd	nd	nd	nd	nd	nd	nd	nd	nd	nd	nd
CE	24:0	754.7446	nd	nd	nd	nd	nd	nd	nd	nd	nd	nd	nd
CE	24:1	752.7290	nd	nd	nd	nd	nd	nd	nd	nd	nd	nd	nd
CE	24:2	750.7134	nd	nd	nd	nd	nd	nd	nd	nd	nd	nd	nd
CE	24:3	748.6978	nd	nd	nd	nd	nd	nd	nd	nd	nd	nd	nd
CE	24:4	746.6822	nd	nd	nd	nd	nd	nd	nd	nd	nd	nd	nd

2% TX114													
Class	Lipid	Calc. Mass. [M+NH4] <sup>+</sup>	Found Mass. [M+NH4] <sup>+</sup>	RT (min)	Area			Conc. (pmol/sample)			2% TX114 (n=3)		
					1	2	3	1	2	3	Mean	SD	%CV
CE	24:5	744.6666	nd	nd	nd	nd	nd	nd	nd	nd	nd	nd	nd
CE	24:6	742.6510	742.6524	15.14	318	246	197	64.8	59.4	34.8	53.0	13.1	24.6

12% TX114													
Class	Lipid	Calc. Mass. [M+NH4] <sup>+</sup>	Found Mass. [M+NH4] <sup>+</sup>	RT (min)	Area			Conc. (pmol/sample)			12% TX114 (n=3)		
					1	2	3	1	2	3	Mean	SD	%CV
CE	Standard	656.6346	656.6336	17.78	815	547	1387	188.0	188.0	188.0	188.0	0.0	0.0
CE	14:0	614.5571	nd	nd	nd	nd	nd	nd	nd	nd	nd	nd	nd
CE	15:0	628.5728	nd	nd	nd	nd	nd	nd	nd	nd	nd	nd	nd
CE	16:0	642.6194	nd	nd	nd	nd	nd	nd	nd	nd	nd	nd	nd
CE	16:1	640.6038	640.6028	16.54	259	590	194	59.7	202.8	26.3	96.3	76.5	79.5
CE	16:2	638.5571	nd	nd	nd	nd	nd	nd	nd	nd	nd	nd	nd
CE	17:1	654.5884	nd	nd	nd	nd	nd	nd	nd	nd	nd	nd	nd
CE	18:0	670.6507	nd	nd	nd	nd	nd	nd	nd	nd	nd	nd	nd
CE	18:1	668.6342	668.6318	17.44	326	316	206	75.2	108.6	27.9	70.6	33.1	46.9
CE	18:2	666.6198	666.6141	16.79	107	210	120	24.7	72.2	16.3	37.7	24.6	65.3
CE	18:3	664.6062	nd	nd	nd	nd	nd	nd	nd	nd	nd	nd	nd
CE	20:0	698.6820	nd	nd	nd	nd	nd	nd	nd	nd	nd	nd	nd
CE	20:1	696.6664	696.6655	14.12	173	173	140	39.9	59.5	19.0	39.4	16.5	41.9
CE	20:2	694.6508	694.6496	17.56	72	85	119	16.6	29.2	16.1	20.7	6.1	29.3
CE	20:3	692.6352	692.6345	16.94	81	71	144	18.7	24.4	19.5	20.9	2.5	12.1
CE	20:4	690.6196	690.6222	14.68	20	17	35	4.6	5.8	4.7	5.1	0.6	10.9
CE	20:5	688.6040	nd	nd	nd	nd	nd	nd	nd	nd	nd	nd	nd
CE	20:6	686.5884	nd	nd	nd	nd	nd	nd	nd	nd	nd	nd	nd
CE	22:0	726.7133	nd	nd	nd	nd	nd	nd	nd	nd	nd	nd	nd
CE	22:1	724.6977	724.7010	14.34	323	328	130	74.5	112.7	17.6	68.3	39.1	57.2
CE	22:2	722.6821	nd	nd	nd	nd	nd	nd	nd	nd	nd	nd	nd
CE	22:3	720.6665	720.6682	17.44	9	6	18	2.1	2.1	2.4	2.2	0.2	8.0
CE	22:4	718.6509	nd	nd	nd	nd	nd	nd	nd	nd	nd	nd	nd

12% TX114													
Class	Lipid	Calc. Mass. [M+NH4] <sup>+</sup>	Found Mass. [M+NH4] <sup>+</sup>	RT (min)	Area			Conc. (pmol/sample)			12% TX114 (n=3)		
					1	2	3	1	2	3	Mean	SD	%CV
CE	22:5	716.6353	nd	nd	nd	nd	nd	nd	nd	nd	nd	nd	nd
CE	22:6	714.6197	nd	nd	nd	nd	nd	nd	nd	nd	nd	nd	nd
CE	24:0	754.7446	nd	nd	nd	nd	nd	nd	nd	nd	nd	nd	nd
CE	24:1	752.7290	nd	nd	nd	nd	nd	nd	nd	nd	nd	nd	nd
CE	24:2	750.7134	nd	nd	nd	nd	nd	nd	nd	nd	nd	nd	nd
CE	24:3	748.6978	nd	nd	nd	nd	nd	nd	nd	nd	nd	nd	nd
CE	24:4	746.6822	nd	nd	nd	nd	nd	nd	nd	nd	nd	nd	nd
CE	24:5	744.6666	nd	nd	nd	nd	nd	nd	nd	nd	nd	nd	nd
CE	24:6	742.6510	742.6524	15.14	187	233	123	43.1	80.1	16.7	46.6	26.0	55.8

# ARTICLES






 Cite this: *Med. Chem. Commun.*,  
2016, 7, 550

# Squaramides with cytotoxic activity against human gastric carcinoma cells HGC-27: synthesis and mechanism of action†‡

 Mireia Quintana,<sup>§a</sup> Juan V. Alegre-Requena,<sup>§ab</sup> Eugenia Marqués-López,<sup>b</sup>  
Raquel P. Herrera<sup>\*b</sup> and Gemma Triola<sup>\*a</sup>

 Received 6th November 2015,  
Accepted 22nd February 2016

DOI: 10.1039/c5md00515a

[www.rsc.org/medchemcomm](http://www.rsc.org/medchemcomm)

A series of squaramates and squaramides have been synthesized and their cytotoxic activity has been investigated in different cancer cell lines. Among the studied compounds, squaramide **34** showed a potent and selective cytotoxicity against the human gastric cancer cell line HGC-27. Studies directed to elucidate the mechanism of induced cell death were performed. Cell cycle distribution analysis and cell death studies showed that compound **34** induces cell cycle arrest at the G<sub>1</sub> phase and caspase-dependent apoptosis. In conclusion, squaramide **34** can be considered a potential anticancer agent for gastric carcinoma.

## 1. Introduction

The field of squaramides has experienced an extraordinary growth since the work reported by Rawal and co-workers in 2008,<sup>1</sup> where these molecules were used as organocatalysts. Their promising properties also make them appealing for diverse areas of research beyond organocatalysis.<sup>2–4</sup>

Their unique structural features are believed to have an effect on the biological activity of these substrates; squaramide structures present a planar aromatic framework<sup>5</sup> bearing two adjacent carbonyl acceptor groups and two NH donor sites that are able to establish multiple hydrogen bond interactions.<sup>6</sup> In this sense, due to their important ability to selectively bind through cooperative hydrogen bonds, squaramides have received special attention in medicinal chemistry since they may be able to interact with biological targets *via* specific molecular recognition.<sup>7</sup>

This has promoted recent interest of medicinal chemists in considering squaramide motifs as promising candidates for drug design and interesting tools as bioisosteres of ureas, guanidines or phosphates, among others.<sup>8–16</sup> Moreover, squaramides exhibit an interesting dual behaviour, as they are able to act as good hydrogen bond acceptors and hydrogen bond donors, which make them suitable for both cation

and anion recognition. This could be crucial for the success of cell internalization of these compounds, one of the most important issues in drug design.

In spite of the increasing number of bioactive squaramide-based compounds found in the literature, their application as anticancer agents has not yet been intensively explored and no exhaustive studies in different cancer cells have been previously reported.<sup>17,18</sup> In addition, some squaramides have been shown to selectively bind protein kinases<sup>18</sup> or the CXCR2 receptor,<sup>19</sup> thus indicating that this class of compounds may exert their function by selectively binding to cellular targets. Hence, this interesting behaviour suggests that squaramides may serve as a good starting point to identify molecules that can specifically target cancer cells. This, together with the interest in searching for new anticancer agents, prompted us to evaluate the antitumor activity of a variety of squaramides synthesized following a protocol recently published by us.<sup>20–22</sup>

Based on these precedents, we envisioned that the ability of squaramides to generate hydrogen bonds and electrostatic interactions could be an interesting option to design specific recognition systems with potential antitumor effects. Herein, we present a series of squaramides and squaramates and the study of their activity against different cancer cells that confirms the antitumor properties of this family of promising drug candidates.

## 2. Results and discussion

Firstly, following our optimized reaction conditions,<sup>20,22</sup> a series of differently substituted squaramates **1–14** and squaramides **15–39** were synthesized (Charts 1 and 2). Substituents with different stereoelectronic properties and

<sup>a</sup> Biomedical Chemistry Department, Institute of Advanced Chemistry of Catalonia (IQAC), CSIC, E-08034, Barcelona, Spain.  
E-mail: gemma.triola@iqac.csic.es

<sup>b</sup> Laboratorio de Organocatálisis Asimétrica, Departamento de Química Orgánica, Instituto de Síntesis Química y Catálisis Homogénea (ISQCH), CSIC-Universidad de Zaragoza, E-50009 Zaragoza, Spain. E-mail: raquelph@unizar.es

† The authors declare no competing interests.

‡ Electronic supplementary information (ESI) available. See DOI: 10.1039/c5md00515a

§ These authors equally contributed to this manuscript.



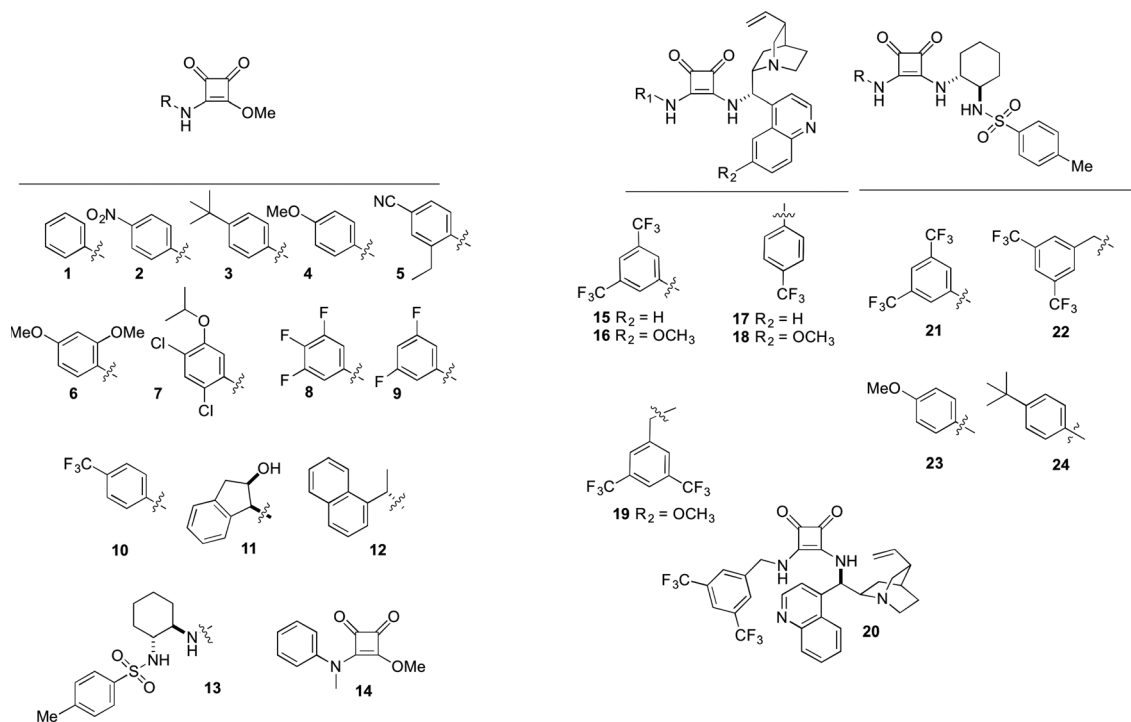


Chart 1 Squaramates and squaramides evaluated.

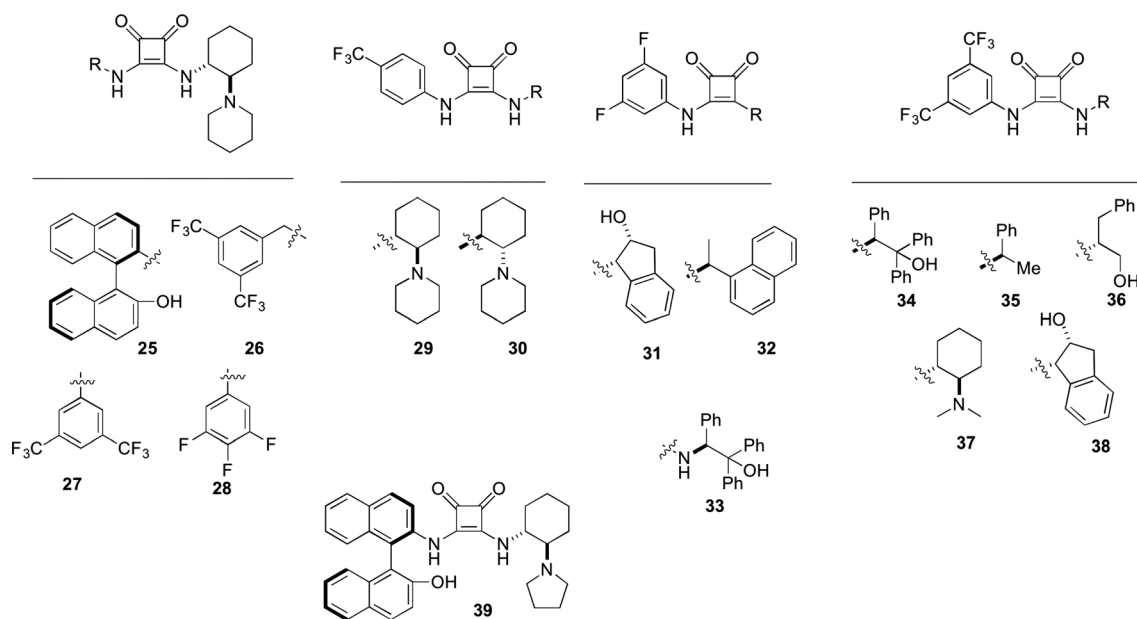


Chart 2 Squaramides evaluated.

lipophilicities were incorporated with the aim of investigating if their biological activity may correlate with the presence of different NH amide-type donor sites.

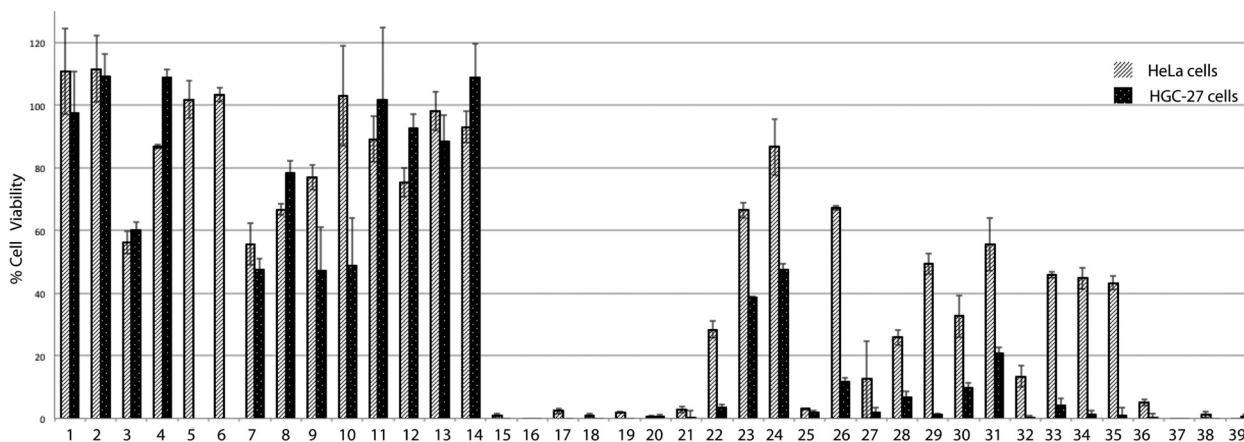
### 2.1. Cell-type specific cytotoxic effect of squaramides

The effect of squaramides on cell viability was initially evaluated on different tumor cell lines (HeLa, cervical carcinoma,

and HGC-27, gastric carcinoma) using an MTT assay after 24 h of treatment at 100  $\mu$ M (Fig. 1).

As shown in Fig. 1, treatment with some of the compounds resulted in significant loss of cell viability. Some structure–activity relationships can be disclosed from this initial screening. Hence, squaramates 1–14 (Chart 1) showed no remarkable activity in any of the cases, thus indicating that the second NH amide bond is required for activity.





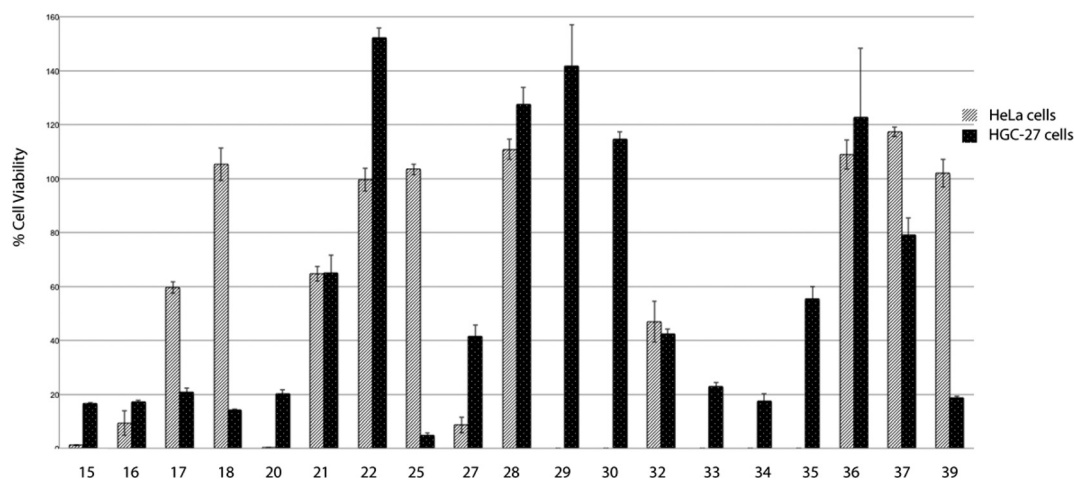
**Fig. 1** Percentage of cell viability after 24 h of treatment with a concentration of 100  $\mu\text{M}$  as measured by an MTT assay. The cells were grown on a 96-well plate and treated with the squaramides or DMSO (vehicle group). After 24 h of treatment, cell viability was evaluated using an MTT assay, as described in the Experimental section. Cell viability is represented in relation to the vehicle group. Data are the average  $\pm$  SD of three experiments.

Substantial inhibition can be seen for compounds 15–20 all of them sharing a cinchona-based substituent. Interestingly, the presence of a 3,5-bis(trifluoromethyl)phenyl moiety confers almost in all the cases inhibition of cell viability (15, 16, 21, 27, 34–38), irrespective of the other substituent present at the second amide. Similarly, 3,5-bis(trifluoromethyl)benzyl substituted squaramides 22 and 26 also show good activities in HGC-27 cells, whereas they are less active in HeLa cells.

After this initial screening, the most potent compounds were selected and were further evaluated at 20  $\mu\text{M}$  (Fig. 2). Interesting information was revealed from this second screening. In general, HGC-27 cells seem to be more sensitive than HeLa cells to the effect of the tested squaramides, except for compound 27 which shows a more potent cell viability inhibitory activity in HeLa cells than in HGC-27. This cell-type specificity may discard a general non-specific cytotoxic effect exerted by the squaramides. Again, the cinchona-based

compounds 15–20 showed good inhibitory activities, independently of the substituents present at the other point of diversity. Squaramides containing bulky and chiral substituents at both sites (25, 39) are more potent than the corresponding *p*-trifluoromethylphenyl analogues (29, 30). The 3,5-bis(trifluoromethyl)phenyl substituted squaramides 34–38 displayed different potencies depending on their substitution pattern, with the highly lipophilic 33 and 34 being the most potent compounds. As a result of this second screening, squaramides 21, 22, 28–30, 32 and 35–37 were discarded due to the low potency displayed at 20  $\mu\text{M}$  and, consequently,  $\text{IC}_{50}$  values were measured for the remaining compounds (Table 1).

The increased sensitivity of HGC-27 cells compared to HeLa cells was again proven, showing in all the cases  $\text{IC}_{50}$  values in the low micromolar range for all the tested squaramides. Interestingly, squaramide 34, bearing a 1,1,2-triphenylethanol and a 3,5-trifluoromethylphenyl substituent,



**Fig. 2** Percentage of cell viability after 24 h of treatment with a concentration of 20  $\mu\text{M}$  as measured by an MTT assay. The cells were grown on a 96-well plate and treated with the squaramides or DMSO (vehicle group). After 24 h of treatment, cell viability was evaluated using an MTT assay, as described in the Experimental section. Cell viability is represented in relation to DMSO. Data are the average  $\pm$  SD of three experiments. Note: compounds 29, 30 and 33–35 were not investigated in HeLa cells at 20  $\mu\text{M}$ .



**Table 1** Effect of squaramides on cell viability against HeLa and HGC-27 cell lines as measured by an MTT assay. Cisplatin and doxorubicin were added as a positive control. IC<sub>50</sub> values are indicated as the average ± SD of three experiments

Compound	Mean IC <sub>50</sub> (95% CI) in μM	
	HeLa cells	HGC-27 cells
15	11.26 (10.33–12.2)	8.12 (7.14–9.24)
16	15.17 (13.2–17.4)	8.21 (7.68–8.78)
17	10.79 (9.49–12.26)	4.53 (3.83–5.36)
18	>20	12.76 (11.84–13.7)
20	12.08 (11.37–3.93)	3.01 (2.26–5.02)
25	>20	11.11 (10.51–11.74)
33	>20	3.39 (2.85–4.04)
34	34.63 (27.97–42.87)	1.81 (1.47–2.23)
39	>20	10.79 (10.30–11.20)
Cisplatin	—	20.44 (19.84–22.18)
Doxorubicin	—	37.40 (30.63–45.67)

was found to be one of most potent and selective compounds tested, showing an IC<sub>50</sub> value of 34.63 μM in HeLa cells and 1.81 μM in HGC-27 cells. Analogously, squaramide 33, where the 3,5-bis(trifluoromethyl)phenyl had been replaced by 3,5-difluorophenyl, displayed a similar activity pattern. Moreover, this low micromolar IC<sub>50</sub> decreased further to nanomolar values (660 nM, Table 2) when HGC-27 cells were exposed to compound 34 for 48 h.

With these promising results in hand regarding the activity and selectivity of squaramide 34, we decided next to explore the activity profile of 34 on different cell lines. Hence, cell viability studies were extended to the glioblastoma cells lines, T98 and U87 (the most aggressive type of primary brain tumor) and the non-cancer cells HEK293, MDCK (Madin-Darby Canine Kidney Epithelial cells) and the Vero cell line (African green monkey kidney cell line). The results are displayed in Table 2 and confirm certain cell-dependent toxicity (IC<sub>50</sub> values of 60.25 μM and 7.15 μM for the glioblastoma cell lines U87 and T98, respectively, 9.03 μM for the HEK293 cells, 70.20 μM for the MDCK cells and 33.40 μM for the Vero cells).

Gastric cancer accounts for 8% of the total cases of cancers and 10% of total deaths. The survival for patients with this type of cancer has improved only modestly over the last 50 years. Consequently, there is still a clear need for the development of more efficient treatments. Moreover, gastric cancer presents high molecular heterogeneity, which prevents the uniform application of specific targeted agents,<sup>23</sup> and therefore the identification of novel targets or novel com-

pounds active on gastric cancer cells is of great interest.<sup>23,24</sup> With this aim, and due to the high potency displayed by 34 in the gastric cancer cells HGC-27 together with its interesting selectivity profile observed in the other cell lines, we aimed to further examine the molecular mechanisms underlying 34-mediated cell death in HGC-27 cells.

## 2.2. Apoptotic cell death study

The MTT assay reflects viable cells but cannot be employed as a marker of cell proliferation. A decrease in the number of viable cells can be attributed to cell cycle arrest and/or cell death. To determine whether 34-induced decrease in cell viability in HGC-27 cells was accompanied by alterations in cell cycle distribution, the percentage of cells in the different stages of the cell cycle was analysed by flow cytometry. As shown in Fig. 3, treatment with 34 for 24 h induced a significant accumulation of G<sub>0</sub>/G<sub>1</sub> cells associated with a decrease in the S–G<sub>2</sub>/M cell population, suggesting that cell cycle arrest at the G<sub>0</sub>/G<sub>1</sub> phase contributes to the observed effect, whereas treatment of cells with doxorubicin, included as a positive control, resulted in G<sub>2</sub>/M arrest.

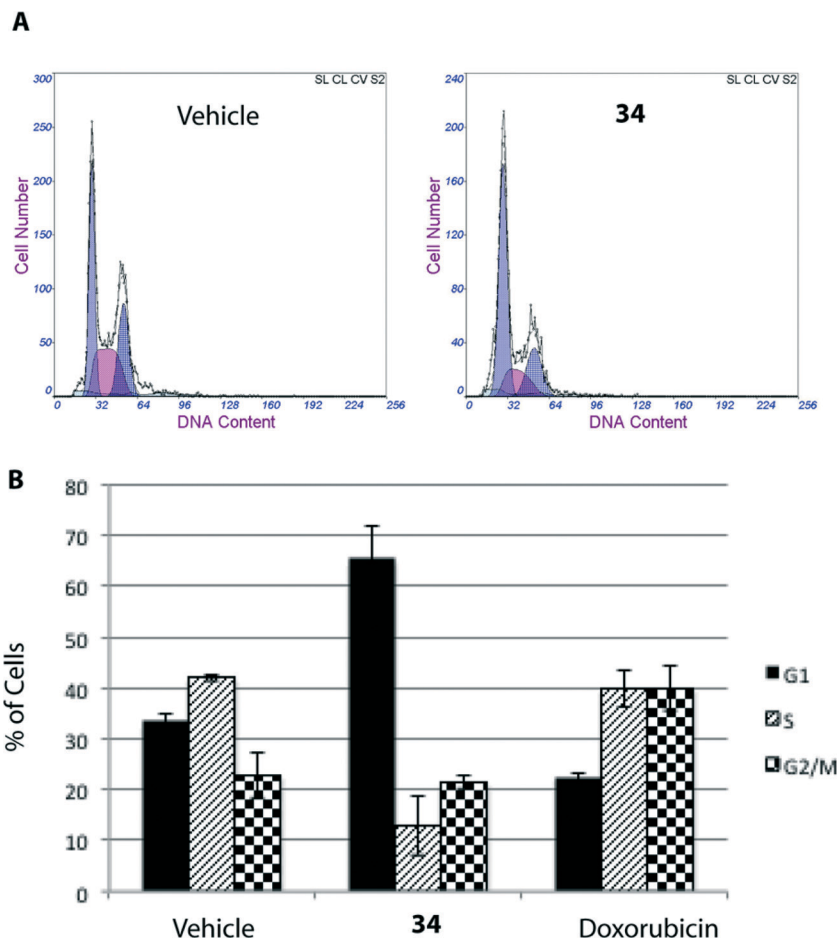
Cell death can be controlled by several mechanisms or pathways.<sup>25</sup> Therefore, we decided to quantify the cell death caused by 34 as well as determine the specific cell death modality, which is mainly apoptosis, necrosis or autophagy that may be prevalent in these cells. With this aim, we evaluated the apoptotic effect of 34 on HGC-27 cells using an Annexin V-FITC/PI staining assay and analysed the stained cells by flow cytometry.<sup>26</sup> Briefly, loss of plasma membrane integrity is indicative of cell death and this can be assessed using cell-impermeable dyes that are able to enter the cell once the integrity of the plasma membrane is lost, such as propidium iodide (PI). Moreover, apoptotic cells expose phosphatidylserine (PS) before membrane rupture, whereas in necrotic cells PS exposure and membrane disruption occur simultaneously, thus discriminating early and late apoptotic cells as well as necrotic cells. To study the effect of 34 on HGC-27 cells, cells were treated with the vehicle alone as control or with 34 at three different concentrations (1, 2.5 and 8 μM). After 24 hours, the samples were double stained with Annexin V-FITC and PI and the percentage of cells was analysed. As shown in Fig. 4, compound 34 induced cell apoptosis in a concentration-dependent manner. In the case of 1 μM, 2.5 μM and 8 μM treated HGC-27 cells, the total percentage of early and late apoptotic cells were 2.4%, 24.7%,

**Table 2** Effect of squaramide 34 on cell viability against various human cancer cell lines as measured by an MTT assay. IC<sub>50</sub> values are indicated as the mean ± SD of three experiments

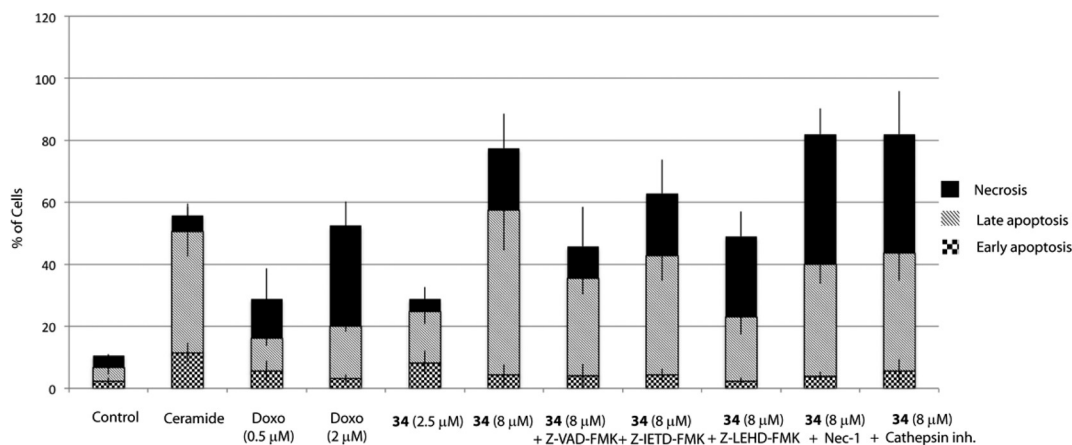
Compound	Mean IC <sub>50</sub> (95% CI) in μM						
	HeLa	HGC-27	T98	U87	HEK293	MDCK	Vero
34	34.63 (27.97–42.87)	1.81 (1.47–2.23) 0.66 <sup>a</sup> (0.57–0.76)	7.15 (6.12–8.34)	60.25 (41.52–87.42)	9.03 (7.07–11.54)	70.20 (50.58–97.43)	33.40 (27.96–39.90)

<sup>a</sup> IC<sub>50</sub> measured after 48 h of treatment.





**Fig. 3** Cell cycle distribution of HGC-27 cells with or without treatment of compound **34** at 5  $\mu\text{M}$  in DMSO for 24 h. Doxorubicin (500 nM) was included as a positive control. The cells were collected and processed for cell cycle analysis. A) Representative cell cycle histograms obtained from HGC-27 cells after 24 h of exposure to vehicle or **34**. B) Quantification of the relative number of cells in each stage of the cell cycle (Multicycle AV software). Data are the average  $\pm$  SD of three experiments.



**Fig. 4** Apoptotic effect of squaramide **34** on HGC-27 cells. Cells were treated with DMSO (vehicle group) or **34** alone or together with Z-VAD-FMK (20  $\mu\text{M}$ ), Z-IETD-FMK (20  $\mu\text{M}$ ), Z-LEHD-FMK (20  $\mu\text{M}$ ), Nec-1 (10  $\mu\text{M}$ ) or cathepsin inhibitor III (10  $\mu\text{M}$ ). Cells were pre-treated for 1 h with Z-VAD-FMK, Z-IETD-FMK, Z-LEHD-FMK and cathepsin inhibitor III and 3 h with Nec-1 before adding **34**. C8-ceramide (20  $\mu\text{M}$ ) was added as a positive control. After 24 h of treatment, the cells were double-stained with Annexin V and PI and analysed. The percentage of apoptotic and necrotic cells upon incubation with **34** were quantified by flow cytometry as described in the Experimental section (live cells (bottom left quadrant), early apoptotic cells (bottom right quadrant), late apoptotic cells (upper right quadrant) and necrotic cells (upper left quadrant)). The graph shows the quantitative analysis of necrosis and early and late apoptosis in treated cells. The data were obtained from three independent experiments.





and 60.1%, respectively. In contrast, only 6.7% of the early and late apoptotic cells were detected in the control, which revealed that compound 34 efficiently induces apoptosis in HGC-27 cells (Fig. 4). Doxorubicin and cisplatin have been used for the treatment of gastric cancer, usually in combination with other anticancer agents. Therefore, the effect of doxorubicin in HGC-27 cells was also investigated, resulting in dose-dependent induction of apoptosis. HGC-27 cells treated with a concentration of 2  $\mu\text{M}$  of doxorubicin<sup>27</sup> presented 3.2% of early apoptotic cells, 16.7% of late apoptotic cells and 32.4% of necrotic cells, thus showing a slightly less potent effect than squaramide 34.

To explain the high doses required to detect cell death compared to the  $\text{IC}_{50}$  values obtained in the MTT assays, we measured the effect of these compounds on cell viability by an alternative assay based on the quantification of cellular ATP levels. Indeed, although  $\text{IC}_{50}$  values resulting from these studies were in a similar range, the dose-dependent curve obtained in the ATP-based analysis was in agreement with concentrations required in cells to cause an apoptotic effect (Fig. S1†). Alternatively, a sulforhodamine B (SRB) assay was employed to investigate the cytotoxicity of 34. SRB is a dye that binds proteins under mild acidic conditions, and the amount of detected dye can be correlated with the cell mass.<sup>28</sup> Hence, the SRB assay is independent of the mitochondrial function. In this case, an  $\text{IC}_{50}$  of 9.74  $\mu\text{M}$  was obtained for squaramide 34 in HGC-27 cells (vs. 149  $\mu\text{M}$  and 73.85  $\mu\text{M}$  in MDCK and Vero cells, respectively). In contrast to the MTT assay that requires cellular metabolic activity and therefore only stains viable cells, SRB stains viable and dead cells, thus giving generally slightly higher  $\text{IC}_{50}$  values.<sup>28</sup>

### 2.3. Squaramide 34 induces caspase-dependent cell death

Apoptosis can be triggered through caspase-dependent or independent mechanisms. To explore whether 34 induces cell death through a caspase-dependent mechanism, Z-VAD-FMK, a pan-caspase inhibitor was employed. Hence, pre-treatment of cells with Z-VAD-FMK (20  $\mu\text{M}$ ) for 1 h partially prevented 34-induced cell death, thus suggesting that a caspase-dependent mechanism may be involved (Fig. 4).

Apoptosis may be initiated by the extrinsic or the intrinsic signaling pathway. The extrinsic signaling pathway involves death receptors located at the membrane, such as FasL/FasR and TNF- $\alpha$ /TNFR1, the transmission of the signal from the cell surface to intracellular signaling pathways and the implication of caspase-8. The intrinsic pathway is the mitochondrial pathway and may be caused by different stimuli including free radicals, toxins, or hypoxia, and involves the activation of caspase-9. The extrinsic pathway and the intrinsic pathway converge on the final execution phase, mediated by the effector caspase-3.<sup>29</sup> Hence, we next investigated the implication of both pathways by pre-treatment of the cells with a caspase-8 (Z-IETD-FMK) or a caspase-9 (Z-LEHD-FMK) inhibitor. Interestingly, the percentage of apoptotic cells decreased markedly upon treatment with the caspase-9 inhibi-

tor Z-LEHD-FMK, compared to the results obtained with the other caspase inhibitors, thus suggesting the implication of the mitochondrial pathway (Fig. 4). A smaller decrease in apoptosis rate was also observed when cells were treated with the caspase inhibitor Z-IETD-FMK, which could be due to the described cross reactivity for these inhibitors.<sup>30</sup>

### 2.4. Alternative cell death mechanism

**Cathepsin-dependent cell death.** Cell death can also be mediated by lysosomal cathepsin proteases in the so-called lysosomal cell death (LCD), consisting of lysosomal membrane permeabilization (LMP) and subsequent release of lysosomal proteases to the cytosol.<sup>31</sup> Extensive LMP leads to uncontrolled necrosis, whereas limited LMP can activate caspase-dependent or independent pathways,<sup>32</sup> resulting in a cell death that can be prevented upon cathepsin inhibition. Hence, to elucidate whether part of the cell death observed in 34-treated cells was due to a cathepsin-mediated process, cells were incubated with 34, with or without a cathepsin inhibitor cocktail (cathepsin inhibitor III, EMD Millipore) which primarily targets cathepsin B, and the extent of cell death was then measured by an Annexin V-FITC/PI staining assay. As shown in Fig. 4, the presence of the cathepsin inhibitor did not have any effect on the percentage of live cells but on the contrary it did dramatically induce necrosis on HGC-27 cells. Treatment of HGC-27 cells with cathepsin inhibitor III alone did not have remarkable apoptotic effects (not shown). The obtained results discard the involvement of LCD in the molecular mechanism responsible for 34 effects.

**Necrosis.** Initial cell death analysis by flow cytometry studies revealed that 34 also causes a significant increase in the number of necrotic cells (Fig. 4). Necrosis may be primary or secondary. Secondary necrotic cells follow apoptosis, whereas primary necrosis, also termed necroptosis, is a non-apoptotic programmed cell death that is mediated by kinases of the receptor interacting protein (RIP) family.<sup>33</sup> Hence, we then investigated if necroptosis could contribute to the caspase-independent cell death. With this aim, HGC-27 cells were pre-treated with Necrostatin-1 (Nec-1), an RIP1 inhibitor that blocks this pathway. Interestingly, the necrosis induced by 34 turned out to be not Nec-1 sensitive, thus discarding the involvement of necroptosis as a cell death method, and suggesting that the necrotic cells observed in the flow cytometry analysis are probably post-apoptotic cells.

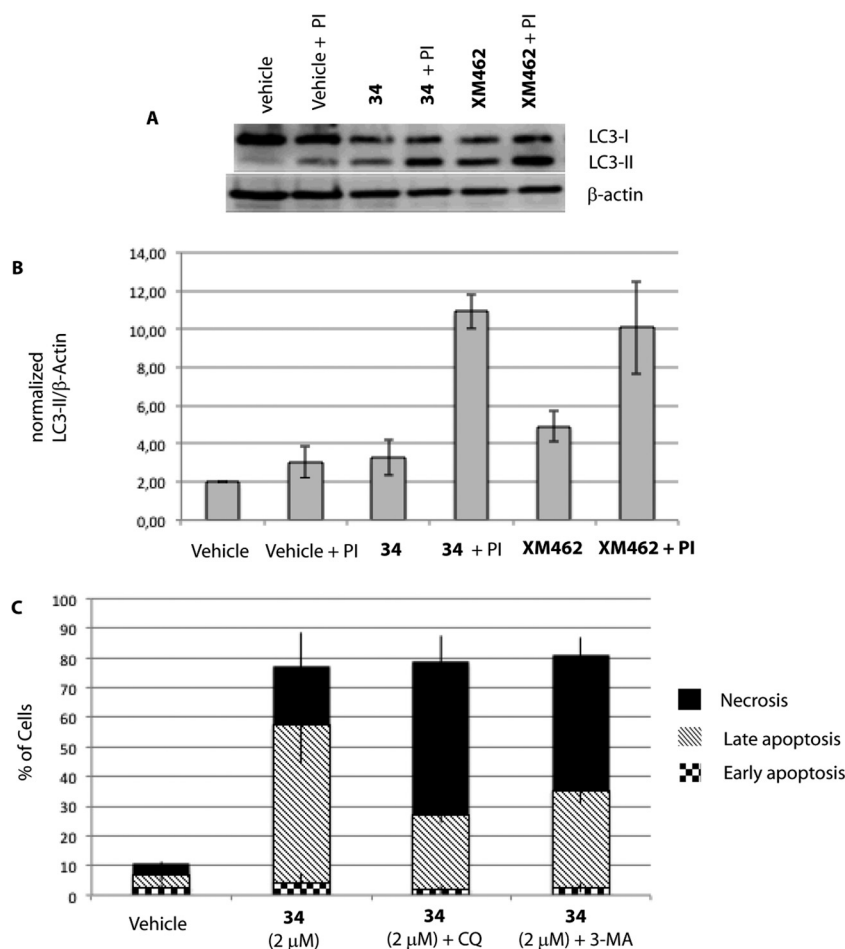
**Autophagy.** Apart from apoptosis or necrosis, another mechanism of programmed cell death is associated with excessive levels of autophagy in a process known as autophagic cell death (ACD).<sup>34</sup> Considering that an autophagic pathway could play a role in the 34-mediated effect, we determine whether this compound induces autophagy in HGC-27 cells and how this process may impact the cellular fate. Therefore, we evaluated the effects of squaramide 34 on autophagy by assessing a key marker of this process, LC3-II. During autophagosome formation, microtubule-associated protein 1 light chain 3 (LC3-I) gets lipidated at the C-terminus with a



phosphatidylethanolamine unit (LC3-II) and subsequently associated with the autophagosome membrane. Since the amount of LC3-II correlates well with the number of autophagosomes, it has been widely employed to monitor autophagy. Hence, HGC-27 cells were treated with **34** for 24 h, and the cell lysates were subjected to Western blotting to determine the changes in expression of LC3-II. As shown in Fig. 5, Western blot analysis revealed a minor increase in this specific autophagic marker after squaramide **34** treatment. Because autophagy is a dynamic process, LC3 accumulation can occur as a result of autophagy induction or due to impairment of the lysosomal function. Moreover, certain cells present a high basal autophagic flux, and as a consequence, autophagy induction is not always correlated with a clear LC3-II accumulation.<sup>35</sup> To discard these possibilities, LC3-II levels were also measured upon inhibition of the lysosomal function. Indeed, these studies revealed a pronounced accu-

mulation of LC3-II in **34**-treated cells, indicating a correct autophagic flux, an unmasked LC3-II accumulation probably due to its rapid turnover and confirming an important autophagy induction.

Although it has been proven that autophagy can contribute to cell death,<sup>36</sup> there is still a controversy whether it is a cell death caused by autophagy, or a cell death accompanied by induction of autophagy that may exert a survival or cytoprotective effect.<sup>37,38</sup> To determine how this autophagy induction impacts the cell fate, we aimed to test if autophagy plays a causative role in preventing **34**-induced cell death by employing autophagy inhibitors. Herein, we used two autophagy inhibitors, chloroquine (CQ), a lysosomotropic agent that impairs the lysosomal function, and 3-methyladenine (3-MA), a pan inhibitor of the lipid kinase phosphatidylinositol 3-kinase (PI3K), involved in the first steps of autophagosome formation, and the percentage of apoptotic/



**Fig. 5** HGC-27 cells were exposed to **34** for 24 h. A) Levels of LC3-II were assessed by Western blotting of cell lysates as described in the Experimental procedures. XM462 (10  $\mu$ M), a known autophagy inducer in HGC-27 cells, was used as a positive control.<sup>47</sup> The images shown are representative of three independent experiments with similar results. B) Quantified LC3-II levels with respect to  $\beta$ -actin. C) Effect of autophagy inhibition on apoptosis/necrosis of treated HGC-27 cells. Cells were treated with DMSO (vehicle group), **34** alone, chloroquine (CQ, 50  $\mu$ M in EtOH) or 3-methyladenine (3-MA, 2 mM in DMSO). The cells were pre-treated for 2 h with CQ or 3 h with 3-MA before adding **34**. After 24 h of treatment, the cells were double-stained with Annexin V and PI and analysed. The percentage of apoptotic and necrotic cells upon incubation with **34** were quantified by flow cytometry as described in the Experimental section (live cells (bottom left quadrant), early apoptotic cells (bottom right quadrant), late apoptotic cells (upper right quadrant) and necrotic cells (upper left quadrant)). The graph shows the quantitative analysis of necrosis and early and late apoptosis in cells treated with **34**. The data were obtained from three independent experiments.





necrotic and live cells upon autophagy inhibition was analysed. As shown in Fig. 5, co-treatment of 34 with autophagy inhibitors such as CQ or 3-MA did not increase the number of live cells, but on the contrary significantly increased the number of necrotic cells. Taken all together, all data described above suggest that autophagy is triggered by 34 exposure to HGC-27 cells as a protective response to alleviate its cytotoxicity. Moreover, the fact that cathepsin inhibition, which causes lysosomal dysfunction, results also in increased cell death may underscore the pro-survival function of autophagy, which requires a correct lysosomal function to take place (Fig. 4).<sup>39</sup>

## 2.5. Mitochondria and ROS

MTT assays measure the activity of succinate dehydrogenase, a mitochondrial enzyme, hence reflecting the activity status of this organelle and suggesting that the differences observed in both cell viability methods employed above (MTT vs. ATP-based assay) may occur due to mitochondrial damage, which would be in agreement with the increased viability upon treatment with the caspase-9 inhibitor, a marker of the intrinsic mitochondrial pathway.

If the intrinsic mitochondrial pathway is activated, there are alterations in the inner mitochondrial membrane, resulting in changes in transmembrane potential, loss of membrane permeability and activation of caspase. Therefore, we next investigated the mitochondrial membrane potential in HGC-27 cells treated with squaramide 34. JC-1 accumulates as aggregates in the mitochondria (orange color) and the color changes from orange to green fluorescence in apoptotic cells with depolarization of mitochondrial membrane potential, where JC-1 exists in the monomeric form.<sup>40</sup> Therefore, JC-1 has been widely used to detect mitochondrial depolarization during apoptosis. The results showed that 34 efficiently caused mitochondrial membrane depolarization. When  $\Delta\Psi_m$  levels were assessed quantitatively by the ratio of orange/green fluorescence intensity, there was a significant reduction of  $\Delta\Psi_m$  in HGC-27 cells compared to control cells after a 2  $\mu\text{M}$  and 8  $\mu\text{M}$  treatment for 24 h (Fig. 6), which indicates that compound 34 induces  $\Delta\Psi_m$  changes in HGC-27 cells during apoptosis. These results confirmed the implication of the intrinsic pathway in the 34-mediated cell death.

Reactive oxygen species (ROS) are known triggers of the intrinsic apoptotic cascade.<sup>41</sup> Therefore, oxidative damage caused by the generation of ROS may be one of the underlying mechanisms of 34-mediated cell death. To elucidate whether oxidative stress mediated by ROS generation plays a critical role in the onset of cell death caused by 34, we determined the changes in the intracellular redox potential upon treatment with 34 by employing the fluorescent probe 2',7'-dichlorofluorescein diacetate (DCFH-DA), which is converted to highly fluorescent dichlorofluorescein (DCF) in the presence of intracellular ROS. However, although a remarkable increase in ROS formation was detected when  $\text{H}_2\text{O}_2$  was employed as a positive control, no signs of ROS production

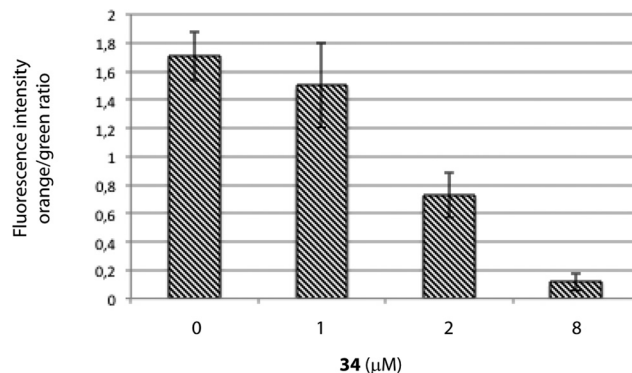


Fig. 6 Mitochondrial membrane potential in 34-treated HGC-27 cells evaluated by JC-1 staining and flow cytometry analysis. Quantification of the orange/green ratio. Data are the average  $\pm$  SD of three experiments.

could be detected in HGC-27 treated cells, thus discarding the implication of oxidative damage in the molecular mechanism responsible for 34-mediated cell death (Fig. S2 $\ddagger$ ).

## Summary and conclusions

In this study, it has been shown that substituted squaramide 34 effectively inhibited the proliferation of HGC-27 cells in a concentration-dependent manner. These inhibitory effects were associated with the cell cycle arrest and induction of apoptosis dependent of caspases that implicates the activation of the intrinsic pathway and the subsequent mitochondrial membrane depolarization. The implication of ROS as stimuli for the activation of the intrinsic pathway has been discarded, suggesting that other stimuli or pro-apoptotic proteins may be involved in the activation of the intrinsic pathway. Apart from the observed caspase-dependent apoptosis, no signs of cathepsin-mediated cell death or necroptosis have been detected. Moreover, the cell death caused by 34 is accompanied by autophagy induction having a protective effect. These overall results indicate that the decrease in cell viability caused by squaramide 34 is most likely mediated by  $G_0/G_1$  cell cycle arrest and caspase-mediated apoptosis. Since the identification of compounds inducing a specific cell death subroutine is preferred to avoid side-effects and nonspecific cytotoxic effects, squaramide 34 can be considered a promising agent for the treatment of gastric carcinoma. Moreover, although 34 presents an specific effect on HGC-27 cells vs. HeLa, U87 and T98 cells, similar anti-tumor effects on other epithelial tumor types, particularly those of the GI tract, cannot be discarded and will be characterized in future studies.

## Experimental section

### Materials

Minimum essential medium eagle, fetal bovine serum, non-essential amino acids, 3-[4,5-dimethylthiazol-2-yl]-2,5-diphenyltetrazolium bromide (MTT), BSA, NADH, Tween 20, trypsin-EDTA, chloroquine diphosphate, 3-methyladenine, necrostatin-1, pepstatin A, C8-ceramide, doxorubicin, 2',7'-



dichlorofluorescein diacetate and protease inhibitors were obtained from Sigma. Laemmli buffer and acrylamide were procured from BioRad, SDS from Fluka, and the microBCA protein assay kit from Thermo Scientific. The protease inhibitor cocktail contained  $2 \mu\text{g ml}^{-1}$  aprotinin,  $5 \mu\text{g ml}^{-1}$  leupeptin, and  $1 \text{ mM}$  phenylmethylsulphonyl fluoride. Z-VAD-FMK and E-64-D were acquired from Enzo Life Science. Z-IEDT-FMK and Z-LEHD-FMK were purchased from Alfa Aesar and cathepsin inhibitor III from CalBioChem. Annexin V-FITC early apoptosis detection kit was obtained from Cell Signaling. Antibodies: microtubule-associated protein 1-light chain 3 (LC3) II (rabbit) was obtained from Abcam, and  $\beta$ -actin (mouse) was purchased from Sigma. HRP secondary antibodies were acquired from GE Healthcare.

### General experimental methods

Purification of reaction products was carried out either by filtration or by flash chromatography using silica gel (0.063–0.200 mm). Analytical thin layer chromatography was performed on 0.25 mm silica gel 60-F plates. The ESI ionization method and a mass analyzer type MicroToF-Q were used for ESI measurements.  $^1\text{H-NMR}$  spectra were recorded at 300 and 400 MHz;  $^{13}\text{C-NMR-APT}$  spectra were recorded at 75 and 100 MHz;  $\text{CDCl}_3$  and  $\text{DMSO-}d_6$  were used as solvents. Chemical shifts were reported in the  $\delta$  scale relative to residual  $\text{CHCl}_3$  (7.26 ppm) and  $\text{DMSO}$  (2.50 ppm) for  $^1\text{H-NMR}$  and to the central line of  $\text{CDCl}_3$  (77 ppm) and  $\text{DMSO-}d_6$  (39.43 ppm) for  $^{13}\text{C-NMR-APT}$ . All commercially available solvents and reagents were used as received.

### Representative procedure for the synthesis of squaramates and squaramides

To a mixture of 3,4-dimethoxy-3-cyclobutene-1,2-dione (0.2 mmol) in MeOH (0.75–1.5 ml), appropriate amine (0.2 mmol) was added at room temperature. After the appropriate reaction time, the corresponding squaramate was purified either by filtration, washing with MeOH at  $-25 \text{ }^\circ\text{C}$ , or column chromatography (see the ESI $\ddagger$ ). Squaramate 1 is commercially available. The  $^1\text{H}$  and  $^{13}\text{C-NMR}$  spectral data for squaramates 2,<sup>42</sup> 3,<sup>10</sup> 4,<sup>42</sup> 9,<sup>42</sup> and 10,<sup>42</sup> are consistent with values previously reported in the literature. For spectral and analytical data for all new squaramates (5–8 and 11–14), see the ESI $\ddagger$ .

Squaramides 15–39 were synthesized following our own reported procedure.<sup>20,22</sup> The  $^1\text{H}$  and  $^{13}\text{C-NMR}$  spectral data for squaramides 15–18,<sup>43</sup> 19,<sup>44</sup> 20,<sup>1</sup> 21,<sup>20</sup> 22,<sup>20</sup> 23,<sup>20</sup> 24,<sup>20</sup> 25,<sup>20</sup> 26,<sup>1</sup> 27,<sup>45</sup> 28,<sup>20</sup> 29,<sup>46</sup> 30,<sup>43</sup> 31,<sup>20</sup> 32,<sup>20</sup> 33,<sup>20</sup> 34,<sup>20</sup> 35,<sup>20</sup> 36,<sup>20</sup> 37,<sup>45</sup> 38,<sup>20</sup> and 39,<sup>20</sup> are consistent with values previously reported in the literature.

### Cell culture

The human gastric cancer cell line HGC-27 was cultured at  $37 \text{ }^\circ\text{C}$  in 5%  $\text{CO}_2$  in minimum essential medium supplemented with 10% fetal bovine serum and 1% nonessential amino acids. Cells were routinely grown at 80% maximum confluence. Glioblastoma cells T98G and U87 as well as

HEK293 and HeLa cells were maintained at  $37 \text{ }^\circ\text{C}$  in 5%  $\text{CO}_2$  in Dulbecco's modified Eagle's medium supplemented with 10% fetal bovine serum and  $100 \text{ ng ml}^{-1}$  each of penicillin and streptomycin.

### Cell viability assay

To determine cell viability, the colorimetric MTT metabolic activity assay was employed. Cells were seeded at a density of  $0.1 \times 10^6 \text{ cells ml}^{-1}$ , 0.1 ml per well (96-well plates) and cultured at  $37 \text{ }^\circ\text{C}$  and 5%  $\text{CO}_2$ . Twenty-four hours after seeding, cells were exposed to varying concentrations of the investigated compounds and viability was determined 24 h or 48 h later. The control culture was prepared by addition of culture medium (cell viability control) or DMSO (vehicle control) in the absence of treatment. The stock solution of doxorubicin was prepared in water. After 24 h or 48 h of treatment, MTT solution ( $10 \mu\text{l}$  at  $5 \text{ mg ml}^{-1}$  in PBS) was added to each well and the cells were incubated for another 3 h. The solution was removed from the precipitate and the resulting formazan crystals were dissolved in DMSO ( $100 \mu\text{l}$ ) and the absorbance intensity was measured using a microplate reader (Molecular Devices, SpectramaxM5) at 570 nm. All experiments were performed in triplicate, and the relative cell viability (%) is expressed as the percentage of cell viability relative to the cells treated with DMSO (0.1%, vehicle group).

### SRB assay

Cells were seeded at a density of  $0.1 \times 10^6 \text{ cells per ml}$ , 0.1 ml per well (96-well plates) and cultured at  $37 \text{ }^\circ\text{C}$  and 5%  $\text{CO}_2$ . Twenty-four hours after seeding, cells were exposed to varying concentrations of 34 and viability was determined after 24 h. The control culture was prepared by addition of DMSO (vehicle control) in the absence of treatment. After 24 h,  $50 \mu\text{l}$  of TCA (50% w/v) and  $200 \mu\text{l}$  of PBS were added to each well and the cells were incubated for 1 h at  $4 \text{ }^\circ\text{C}$ . The solution was then removed and the plate was washed with Milli-Q water four times. After that,  $100 \mu\text{l}$  per well of SRB solution (0.4% sulforhodamine B w/v in 0.1% acetic acid) was added and the samples were incubated for another 30 min at room temperature. The plate was then washed with 1% acetic acid five times and  $200 \mu\text{l}$  of a 10 mM Tris solution (pH 10.5) were added to each well. After 30 min of incubation at room temperature, the absorbance intensity was measured using a microplate reader (Molecular Devices, SpectramaxM5) at 564 nm. All experiments were performed in triplicate, and the relative cell viability (%) is expressed as the percentage of cell viability relative to the cells treated with DMSO (0.1%, vehicle group).

### Cell cycle analysis

Cells were seeded at 150 000 cells per ml in 6-well plates (1 ml per well). Cells were allowed to adhere for 24 h, and then they were treated with the vehicle (0.1% ethanol) or 34. After exposure for 24 h, cell media were discarded and cells were washed with  $400 \mu\text{l}$  of PBS-EDTA (1% BSA) and



harvested with 400  $\mu\text{l}$  of trypsin-EDTA (1% BSA) (37 °C per 2 min). Cells were pulled down by centrifugation at 1300 rpm per 3 min; the cell pellet was washed once with 400  $\mu\text{l}$  of PBS-EDTA (1% BSA) and again centrifuged at the same speed/time. Cells were fixed by -20 °C overnight incubation with 70% ethanol (9.5 ml) in 1  $\times$  PBS solution (0.5 ml). Fixed cells were pulled down, washed once with PBS-EDTA (1% BSA) and stained at 37 °C for 2 h with propidium iodide solution (0.1 mg ml<sup>-1</sup> in PBS) and RNase, DNase-free (10  $\mu\text{g}$  ml<sup>-1</sup>). Stained cells were analyzed by using a Guava EasyCyte™ flow cytometer (Merck Millipore, Billerica, MA). Data analysis was performed using the program Multicycle AV (Phoenix Flow Systems, San Diego, CA).

### Apoptosis assay

HGC-27 cells were plated in 6-well plates (100 000 cells per ml per well) and were treated with compound 34; 0.1% DMSO was used as a vehicle control. After induction for 24 h, both treated and untreated cells were collected (trypsin and PBS with 5% BSA) and the cells were washed with PBS containing 5% BSA. The percentages of apoptotic cells were estimated by staining with Annexin-V-FITC and PI (Annexin-V-FITC apoptosis detection kit, Cell Signaling). Almost 10 000 events were collected for each sample and analyzed by flow cytometry. In brief, cells were incubated with 96  $\mu\text{l}$  of binding buffer, 1  $\mu\text{l}$  of Annexin V-FITC and 12.5  $\mu\text{l}$  of PI solution at room temperature for 10 min in the dark. After a final addition of 150  $\mu\text{l}$  of PBS, HGC-27 cells were immediately analyzed on a Guava EasyCyte™ single sample flow cytometer. Samples were excited by a light wavelength of 488 nm with barrier filters of 525 nm and 575 nm for FITC fluorescence and PI detection, respectively. Data were analyzed by InCyte Software and plotted for Annexin V-FITC and PI in a two-way dot plot. Live, early apoptotic, late apoptotic and necrotic cells are designed as Annexin-/PI-, Annexin+/PI-, and Annexin+/PI+, respectively. Results are shown as the percentage of cells.

### Western blotting

For protein analysis, 1  $\times$  10<sup>5</sup> cells were plated in 6-well plates and were allowed to adhere for 24 h. In the samples containing protease inhibitors, cells were treated with protease inhibitors, 1  $\mu\text{l}$  of pepstatin A at a concentration of 1 mg ml<sup>-1</sup> in 9:1 of methanol and acetic acid (1%), and 1  $\mu\text{l}$  of E-64-D at a concentration of 10 mg ml<sup>-1</sup> in ethanol. After 2 h of incubation, HGC-27 cells were treated with 34 (2  $\mu\text{M}$ ) or DMSO (0.1%) for 24 h, collected with trypsin, and then the pellets were washed twice with cold PBS. Cell lysis was performed with 30  $\mu\text{l}$  of lysis buffer (50 mM Tris-Cl (pH 7.5), 150 mM NaCl, 0.5% Triton X-100, 2  $\mu\text{g}$  ml<sup>-1</sup> aprotinin, 5  $\mu\text{g}$  ml<sup>-1</sup> leupeptin and 1 mM PMSF) by five cycles of bath sonication (20 s)/rest on ice (20 s). Then samples were kept on ice for 30 min and centrifuged for 3 min at 10 000 rpm. Supernatants were collected and protein determination was performed using the Micro BCA™ protein assay kit. Supernatants

were combined with Laemmli sample buffer and boiled for 5 min. Equal amounts of proteins (20  $\mu\text{g}$ ) were loaded onto a 15% polyacrylamide gel, separated by electrophoresis at 140 V per 60 min, and transferred onto a polyvinylidene fluoride (PVDF) membrane (100 V/1 h). PVDF membranes were then cut to separate LC3B and  $\beta$ -actin bands. Unspecific binding sites were then blocked with 5% milk in TBS with 0.1% Tween 20 (TBST) in the case of the LC3B membrane and with 3% BSA in TBST in the case of the anti- $\beta$ -actin antibody. The anti-LC3B antibody was diluted 1:1000 in 5% milk in TBST, and the anti- $\beta$ -actin antibody was diluted 1:2000 in 3% BSA in TBST. Membranes were incubated overnight at 4 °C under gentle agitation. After washing with TBST, membranes were probed with the corresponding secondary antibody for 1 h at 25 °C (LC3B: 1:1000 dilution in 3% BSA in TBST; actin: 1:10 000 dilution in 5% milk in TBST). Antibody excess was eliminated by washing with TBST and protein detection was carried out using ECL and membrane scanning with a LI-COR C-DiGit® blot scanner. Band intensities were quantified by LI-COR Image Studio Lite Software. All experiments were performed in triplicate and band intensities were expressed as the relation of the samples with the control.

### Mitochondrial membrane potential

HGC-27 cells were seeded at a density of 100 000 cells per ml (1 ml per well) in 6-well plates, cultured at 37 °C and 5% CO<sub>2</sub>, and allowed to adhere for 24 h. Cells were treated with 34 at various concentrations (1  $\mu\text{M}$ , 2  $\mu\text{M}$ , 8  $\mu\text{M}$  in DMSO) or DMSO (0.2%) as negative control (vehicle group). After 24 h of incubation, cells were collected (trypsin with 5% BSA) and washed with PBS containing 5% BSA. The cell pellet was then resuspended in 200  $\mu\text{l}$  of medium and seeded in a 96-well plate (1 sample per well). 4  $\mu\text{l}$  of a previously prepared 50 $\times$  solution of JC-1 and 7-AAD were added to each well and cells were incubated for 30 min at 37 °C and 5% CO<sub>2</sub>. Finally, cells were collected in Eppendorf flasks and analysed on a Guava EasyCyte™ Single Sample Flow Cytometer. Data were analyzed by InCyte Software and plotted for orange (JC-1 aggregates) and green fluorescence (JC-1 monomers).

### ROS detection

The oxidative metabolism was examined in triplicate samples by using 2',7'-dichlorofluorescein diacetate, a non-fluorescent membrane-permeable compound which can be oxidised to 2',7'-dichlorofluorescein in case the cell has high levels of reactive oxygen species.

HGC-27 cells were seeded at a density of 0.1  $\times$  10<sup>6</sup> cells per ml, 0.1 ml per well (96-well plates), cultured at 37 °C and 5% and allowed to adhere for 24 h. 2',7'-Dichlorofluorescein diacetate (25  $\mu\text{M}$ ) in DMSO was then added and incubated for 1 h. Compound 34 was then added at various concentrations (24 to 1.40  $\mu\text{M}$ ). DMSO and H<sub>2</sub>O<sub>2</sub> were added too as a negative and positive control, respectively. After 5 h of incubation, fluorescence was measured by a microplate reader





(Spectramax) at an excitation wavelength of 485 nm and an emission wavelength of 538 nm.

## Acknowledgements

Funding from the Marie Curie Career Integration Grants (Grant PCIG12-GA-2012-333835), the Max Planck Society (Partner Groups), the Ministerio de Economía y Competitividad (Grant CTQ2013-44334-P), the University of Zaragoza (JIUZ-2014-CIE-07), the High Council of Scientific Investigation (CSIC) (PIE-201580I010) and Government of Aragon DGA (Research Group E-104) is gratefully acknowledged. J. V. A.-R. thanks the DGA for his predoctoral contract. G. T. thanks all the members of the RUBAM group for their helpful and generous support.

## Notes and references

- J. P. Malerich, K. Hagihara and V. H. Rawal, *J. Am. Chem. Soc.*, 2008, **130**, 14416–14417.
- P. Chauhan, S. Mahajan, U. Kaya, D. Hack and D. Enders, *Adv. Synth. Catal.*, 2015, **357**, 253–281.
- J. V. Alegre-Requena, *Synlett*, 2014, **25**, 298–300.
- J. Aleman, A. Parra, H. Jiang and K. A. Jørgensen, *Chem. – Eur. J.*, 2011, **17**, 6890–6899.
- D. Quiñero, C. Garau, A. Frontera, P. Ballester, A. Costa and P. M. Deya, *Chem. – Eur. J.*, 2002, **8**, 433–438.
- C. Rotger, B. Soberats, D. Quiñero, A. Frontera, P. Ballester, J. Benet-Buchholz, P. M. Deyà and A. Costa, *Eur. J. Org. Chem.*, 2008, 1864–1868.
- R. I. Storer, C. Aciro and L. H. Jones, *Chem. Soc. Rev.*, 2011, **40**, 2330–2346.
- E. T. Burman, M. A. Foulk, N. Gao, V. A. Laganas, D. C. McKinney, D. T. Moustakas, J. A. Rose, A. B. Shapiro and P. R. Fleming, *J. Bacteriol.*, 2012, **194**, 5504–5512.
- T. S. Elliott, A. Slowey, Y. Ye and S. J. Conway, *MedChemComm*, 2012, **3**, 735–751.
- P. M. Gloria, J. Gut, L. M. Gonçalves, P. J. Rosenthal, R. Moreira and M. M. Santos, *Bioorg. Med. Chem.*, 2011, **19**, 7635–7642.
- S. P. Kumar, P. M. Gloria, L. M. Gonçalves, J. Gut, P. J. Rosenthal, R. Moreira and M. M. Santos, *MedChemComm*, 2012, **3**, 489.
- S. K. Narasimhan, P. Sejwal, S. Zhu and Y. Y. Luk, *Bioorg. Med. Chem.*, 2013, **21**, 2210–2216.
- F. Olmo, C. Rotger, I. Ramirez-Macias, L. Martinez, C. Marin, L. Carreras, K. Urbanova, M. Vega, G. Chaves-Lemaur, A. Sampedro, M. J. Rosales, M. Sanchez-Moreno and A. Costa, *J. Med. Chem.*, 2014, **57**, 987–999.
- C. Schieber, A. Bestetti, J. P. Lim, A. D. Ryan, T. L. Nguyen, R. Eldridge, A. R. White, P. A. Gleeson, P. S. Donnelly, S. J. Williams and P. Mulvaney, *Angew. Chem., Int. Ed.*, 2012, **51**, 10523–10527.
- Q. Zhang, Z. Xia, M. J. Mitten, L. M. Lasko, V. Klinghofer, J. Bouska, E. F. Johnson, T. D. Penning, Y. Luo, V. L. Giranda, A. R. Shoemaker, K. D. Stewart, S. W. Djuric and A. Vasudevan, *Bioorg. Med. Chem. Lett.*, 2012, **22**, 7615–7622.
- X. Zhang, Z. Zuo, J. Tang, K. Wang, C. Wang, W. Chen, C. Li, W. Xu, X. Xiong, K. Yuntai, J. Huang, X. Lan and H. B. Zhou, *Bioorg. Med. Chem. Lett.*, 2013, **23**, 3793–3797.
- J. W. Janetka and S. Ashwell, *Expert Opin. Ther. Pat.*, 2009, **19**, 165–197.
- P. Villalonga, S. Fernandez de Mattos, G. Ramis, A. Obrador-Hevia, A. Sampedro, C. Rotger and A. Costa, *ChemMedChem*, 2012, **7**, 1472–1480.
- M. P. Dwyer, Y. Yu, J. Chao, C. Aki, J. Chao, P. Biju, V. Girijavallabhan, D. Rindgen, R. Bond, R. Mayer-Ezel, J. Jakway, R. W. Hipkin, J. Fossetta, W. Gonsiorek, H. Bian, X. Fan, C. Terminelli, J. Fine, D. Lundell, J. R. Merritt, L. L. Rokosz, B. Kaiser, G. Li, W. Wang, T. Stauffer, L. Ozgur, J. Baldwin and A. G. Taveras, *J. Med. Chem.*, 2006, **49**, 7603–7606.
- J. V. Alegre-Requena, E. Marqués-López and R. P. Herrera, *RSC Adv.*, 2015, **5**, 33450–33462.
- J. V. Alegre-Requena, E. Marqués-López, P. J. Sanz Miguel and R. P. Herrera, *Org. Biomol. Chem.*, 2014, **12**, 1258–1264.
- E. Marqués-López, J. V. Alegre-Requena and R. P. Herrera, *Eu. Pat. EP14382260.*, 2014.
- A. Cervantes, D. Roda, N. Tarazona, S. Rosello and J. A. Perez-Fidalgo, *Cancer Treat. Rev.*, 2013, **39**, 60–67.
- A. Jemal, F. Bray, M. M. Center, J. Ferlay, E. Ward and D. Forman, *CA Cancer J. Clin.*, 2011, **61**, 69–90.
- O. Kepp, L. Galluzzi, M. Lipinski, J. Yuan and G. Kroemer, *Nat. Rev. Drug Discovery*, 2011, **10**, 221–237.
- G. Liu, J. K. Lynch, J. Freeman, B. Liu, Z. Xin, H. Zhao, M. D. Serby, P. R. Kym, T. S. Suhar, H. T. Smith, N. Cao, R. Yang, R. S. Janis, J. A. Krauser, S. P. Cepa, D. W. Beno, H. L. Sham, C. A. Collins, T. K. Surowy and H. S. Camp, *J. Med. Chem.*, 2007, **50**, 3086–3100.
- H. G. Yu, Y. W. Ai, L. L. Yu, X. D. Zhou, J. Liu, J. H. Li, X. M. Xu, S. Liu, J. Chen, F. Liu, Y. L. Qi, Q. Deng, J. Cao, S. Q. Liu, H. S. Luo and J. P. Yu, *Int. J. Cancer*, 2008, **122**, 433–443.
- V. Vichai and K. Kirtikara, *Nat. Protoc.*, 2006, **1**, 1112–1116.
- S. Elmore, *Toxicol. Pathol.*, 2007, **35**, 495–516.
- A. B. Berger, K. B. Sexton and M. Bogyo, *Cell Res.*, 2006, **16**, 961–963.
- S. Aits and M. Jaattela, *J. Cell Sci.*, 2013, **126**, 1905–1912.
- T. Kirkegaard and M. Jaattela, *Biochim. Biophys. Acta, Gen. Subj.*, 2009, **1793**, 746–754.
- H. Sawai and N. Domae, *Biochem. Biophys. Res. Commun.*, 2011, **411**, 569–573.
- G. Triola, *Tetrahedron*, 2015, **71**, 387–406.
- R. Castino, I. Fiorentino, M. Cagnin, A. Giovia and C. Isidoro, *Toxicol. Sci.*, 2011, **123**, 523–541.
- M. Elgendy, C. Sheridan, G. Brumatti and S. J. Martin, *Mol. Cell*, 2011, **42**, 23–35.
- M. Katayama, T. Kawaguchi, M. S. Berger and R. O. Pieper, *Cell Death Differ.*, 2007, **14**, 548–558.
- G. Kroemer and B. Levine, *Nat. Rev. Mol. Cell Biol.*, 2008, **9**, 1004–1010.
- M. Jung, J. Lee, H. Y. Seo, J. S. Lim and E. K. Kim, *PLoS One*, 2015, **10**, e0116972.
- J. D. Ly, D. R. Grubb and A. Lawen, *Apoptosis*, 2003, **8**, 115–128.



- 41 Y. Tsujimoto and S. Shimizu, *Apoptosis*, 2007, **12**, 835–840.
- 42 M. C. Brezak Pannetier and A. Bourgouin, *Pat. WO2009/034258 A1*, 2009.
- 43 W. Yang and D. M. Du, *Adv. Synth. Catal.*, 2011, **353**, 1241–1246.
- 44 H. Jiang, M. W. Paixao, D. Monge and K. A. Jørgensen, *J. Am. Chem. Soc.*, 2010, **132**, 2775–2783.
- 45 H. Konishi, T. Y. Lam, J. P. Malerich and V. H. Rawal, *Org. Lett.*, 2010, **12**, 2028–2031.
- 46 Y. Zhu, J. P. Malerich and V. H. Rawal, *Angew. Chem., Int. Ed.*, 2010, **49**, 153–156.
- 47 P. Signorelli, J. M. Munoz-Olaya, V. Gagliostro, J. Casas, R. Ghidoni and G. Fabrias, *Cancer Lett.*, 2009, **282**, 238–243.





## Research paper

Identification of benzo[*cd*]indol-2(1*H*)-ones as novel Atg4B inhibitors via a structure-based virtual screening and a novel AlphaScreen assayMireia Quintana<sup>1</sup>, Ana Bilbao<sup>1</sup>, Júlia Comas-Barceló, Jordi Bujons, Gemma Triola\*

Department of Biological Chemistry, Institute of Advanced Chemistry of Catalonia, IQAC-CSIC, Barcelona, Spain

## ARTICLE INFO

## Article history:

Received 2 April 2019

Received in revised form

20 May 2019

Accepted 29 May 2019

Available online 5 June 2019

## Keywords:

Atg4B

LC3

Autophagy

AlphaScreen

## ABSTRACT

Targeting autophagy is a promising therapeutic strategy for cancer treatment. As a result, the identification of novel autophagy inhibitors is an emerging field of research. Herein, we report the development of a novel AlphaScreen HTS assay that combined with a MS-based assay and a structure-based high-throughput virtual screening have enabled the identification of benzo[*cd*]indol-2(1*H*)-one as a novel scaffold that targets Atg4B. Thus, an initial screening campaign led to the identification of **NSC126353** and **NSC611216** bearing a chlorohydrin moiety. Structural-activity relationship analysis of the initial hits provided an optimized lead, compound **33**, bearing a 7-aminobenzo[*cd*]indol-2-[1*H*]-one scaffold and a propyl group replacing the chlorine. Inhibition of autophagy was also investigated in cells by measuring LC3-II and p62 protein levels. Moreover, the synergistic effect of **33** combined with oxaliplatin resulted in an enhanced cell death in the human colorectal adenocarcinoma cell line HT-29. We are convinced that the developed AlphaScreen and MS-based assays can be key tools enabling the high-throughput identification of novel Atg4B inhibitors. Moreover, the aminobenzo[*cd*]indol-2-[1*H*]-one scaffold represents a novel chemotype for the further development of small molecule inhibitors of Atg4B.

© 2019 Elsevier Masson SAS. All rights reserved.

## 1. Introduction

Autophagy is an evolutionarily conserved pathway of lysosomal degradation and recycling of obsolete organelles, long-lived proteins and the clearance of protein aggregates and pathogens. This process starts with the formation of a double-membrane phagophore which is then elongated and it eventually closes, engulfing the cargo to be degraded, to form the autophagosome. The final step is the fusion of the autophagosome with the lysosome and the enzymatic digestion of the cargo by lysosomal hydrolases.

This recycling mechanism is involved in several essential processes including cellular development, differentiation, survival and homeostasis [1]. As a result, excessive or deficient levels of autophagy are strongly associated with several pathologies, such as neurodegeneration and cancer [2,3]. Thus, autophagy activators are expected to be potential therapies for neurodegenerative disorders [4], whereas autophagy inhibitors can prevent tumor growth, particularly in nutrient deprived and hypoxic environments or in some types of cancer resistance to chemotherapeutic agents [5,6].

The combination of chemotherapy and autophagy inhibition has already shown promising results in the treatment of several types of cancer [5,7–9].

In the last decade, autophagy has become an emerging field of research. Hence, there is a great demand of small-molecule autophagy modulators that can aid to decipher the underlying molecular mechanism regulating this process, to understand the relevance between autophagy and disease and to offer new opportunities for drug discovery [10–12]. Despite this growing interest, chemical modulators of autophagy are limited and in most cases act non-specifically [13]. One relevant example are lysosomotropic agents such as chloroquine and derivatives. These compounds act as autophagy inhibitors by preventing lysosomal acidification and blocking the function of pH-dependent lysosomal hydrolases and proteases [14]. Another interesting target for autophagy inhibition is the class III phosphoinositide-3-kinase complex (PI3K), involved in autophagosome initiation. Wortmannin and 3-methyladenine belong to this compound class. However, both are considered non-selective inhibitors because they target all isoforms of the PI3K family [15]. More recently, potent and selective inhibitors of the class III PI3K vacuolar protein sorting 34 (Vps34) have been reported [16,17]. These compounds can effectively block cellular autophagy but also alter endosomal trafficking.

\* Corresponding author.

E-mail address: [gemma.triola@iqac.csic.es](mailto:gemma.triola@iqac.csic.es) (G. Triola).<sup>1</sup> These authors contributed equally.

Substantial progress has been made in recent years with the identification of more than 36 autophagy-related proteins (Atgs). These proteins are responsible for the core machinery of autophagosome formation, thereby serving as starting point for the development of specific inhibitors. One of the best-characterized Atg proteins is the autophagy marker MAP1A/B/LC3 (microtubule-associated proteins 1 A/B/LC3 (light chain 3)) together with GABARAP ( $\gamma$ -aminobutyric acid receptor-associated protein), the other mammal homolog of the yeast Atg8, which is recruited to autophagosomal membranes after conjugation with phosphatidylethanolamine. The conversion of proLC3 into LC3-I and the subsequent delipidation of LC3-II to LC3-I requires the activity of the cysteine protease Atg4. There is only one Atg4 protein in yeast [18], but four homologs (Atg4A, Atg4B, Atg4C, Atg4D) in mammals [19] with different substrate specificity [20]. However, Atg4B seems to be the principal homolog in mammals as it can cleave both the LC3 and the GABARAP subfamily [21]. Moreover, its genetic deletion results in notable defects in autophagy [22,23] and inhibits tumor growth in cancer cells [7,24]. Thus Atg4B can be considered as a promising target for the identification of selective autophagy modulators.

A number of small-molecule compounds with moderate inhibitory activity against Atg4B have been previously reported, including peptidic and covalent active-site directed inhibitors equipped with halomethyl moieties [25,26], and polyphenolic structures (Fig. 1). More recently, compound **S130** [27], the anti-fungal drug tioconazole [28] and the quinoline **LV-320** [29] have been identified as Atg4B inhibitors. However, most of the identified compounds are known promiscuous inhibitors lacking the necessary drug-like properties for lead optimization, and the identification of novel chemotypes for Atg4B still remains an urgent need. Here, we report the development of a novel HTS assay that together with a structure-based virtual screening, a medicinal chemistry optimization and biological evaluation led us to the discovery of the benzo[*cd*]indol-2(1*H*)-one scaffold as a new class of Atg4B inhibitor.

## 2. Results and discussion

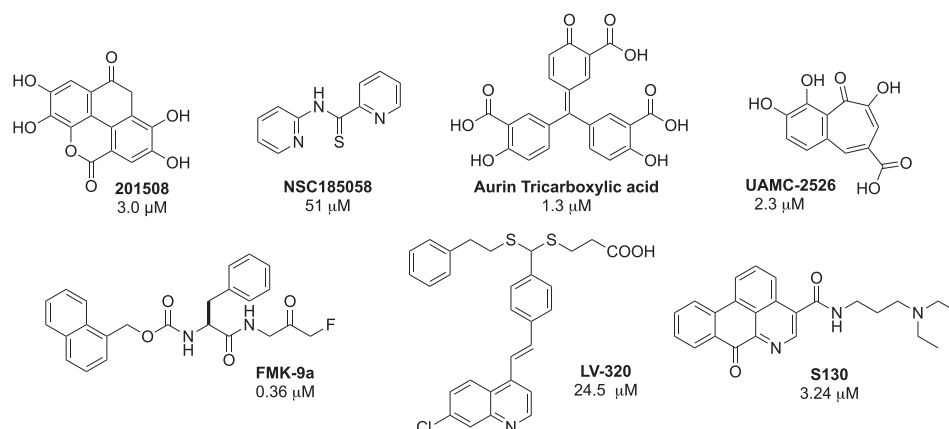
### 2.1. Assay development

During the past years a limited number of protocols for assaying small-molecule Atg4B inhibitors have been described. One of the major limitations is that Atg4B requires full length protein substrates since short peptides spanning the natural pro-LC3B cleavage site cannot be efficiently processed by the enzyme [20,32,33] or

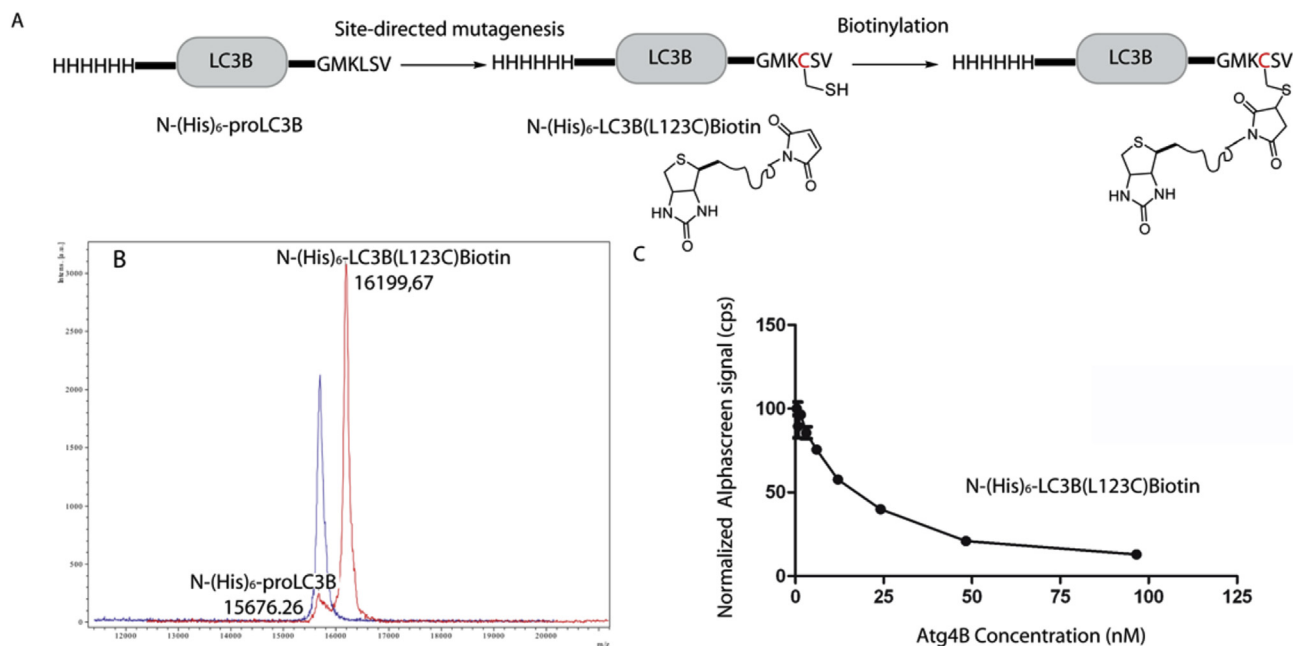
present moderate  $K_m$  values [35]. The existing assays include the electrophoretic separation of a cleaved LC3B-GST protein [20,33], and an indirect assay based on a LC3-PLA<sub>2</sub> fusion protein [30]. However, the first approach is not suitable for high-throughput screening (HTS) and the second assay requires a counterscreen to eliminate compounds directly inhibiting PLA<sub>2</sub>. A doubly fluorescence LC3B protein has been also employed in a fluorescence resonance energy transfer (FRET)-based assay [32,36] but it presented significant donor-acceptor emission overlap and fluorescence photobleaching. More recently, a TR-FRET assay has been developed employing a doubly-tagged GATE-16 as substrate because LC3B could not be efficiently processed under the same conditions [26].

Our initial aim was to develop an AlphaScreen-based assay and to optimize the assay conditions for future HTS applications. AlphaScreen technology offers important advantages. It provides a luminescent readout based on transfer within 200 nm of singlet oxygen molecules, thereby overcoming the Förster radius constraints of FRET assays [37]. Another important feature is a low background caused by a time-resolved readout and an emission wavelength lower than the excitation wavelength, which reduces interferences from other assay components, resulting in excellent signal-to-noise ratios [38]. To set up a robust assay to identify Atg4B inhibitors, we decided to apply a substrate depletion approach employing a doubly tagged substrate. Thus, the intact substrate would yield a high signal and the cleavage of the tagged protein by Atg4B would result in a loss of signal that could be prevented by compounds inhibiting Atg4B activity. To generate an appropriate substrate, a proLC3B protein was fused at the N-terminus with a (His)<sub>6</sub>-tag, that binds nickel chelate acceptor beads, and a biotin moiety, that binds streptavidin donor beads, was incorporated at the C-terminus. Site-selective modification was achieved by the introduction of a cysteine residue (L123C) into proLC3B by site-directed mutagenesis, followed by a coupling reaction with a maleimide-containing biotin. The strategy for large-scale production and purification of the resulting N-(His)<sub>6</sub>-LC3B(L123C)Biotin is illustrated in Fig. 2 and involves the expression and site-specific modification of the (His)<sub>6</sub>-tagged protein (N-(His)<sub>6</sub>-LC3B(L123C)). Identity and purity of the modified protein were assessed by SDS-PAGE followed by Coomassie staining and Western-Blot of the gel (Fig. S2) and MALDI-TOF mass analysis (Fig. 2B). Atg4B was initially expressed as a N-(His)<sub>6</sub>-tagged protein but the tag was cleaved to prevent interference with the assay components (Fig. S1).

We next explored if the doubly tagged protein was an appropriate substrate for Atg4B. To this end, the modified protein was



**Fig. 1.** Structures of the Atg4B inhibitors **201508** [30], **NSC185058** [31], **Aurin tricarboxylic acid** [32], **UAMC-2526** [33,34], **FMK-9a** [26], **LV-320** [29] and **S130** [27] and their reported IC<sub>50</sub> values.



**Fig. 2.** A) L123C mutation was introduced in (His)<sub>6</sub>-tagged proLC3B by mutagenesis. The resulting protein was treated with a maleimide-containing Biotin to generate a doubly labeled proLC3B with a (His)<sub>6</sub>-tag at the N-terminus and a Biotin at the C-terminus (N-(His)<sub>6</sub>-LC3B(L123C)Biotin). B) Purity and identity of the modified protein was confirmed by MALDI-TOF. C) Titration curve of N-(His)<sub>6</sub>-LC3B(L123C)Biotin treated with increasing concentrations of Atg4B. Upon incubation with a range of concentrations of Atg4B, N-(His)<sub>6</sub>-LC3B(L123C)Biotin is cleaved at Gly120 releasing the biotinylated peptide. The increase in the distance between donor and acceptor results in a loss of AlphaScreen signal that can be monitored, thus enabling the detection of Atg4B inhibitors.

incubated with Atg4B, thus generating the (His)<sub>6</sub>-tagged LC3B-I and a biotinylated peptide. Substrate cleavage was verified by mass spectrometry (MS) analysis by UPLC-TOF. Thus, Atg4B was shown to cleave (His)<sub>6</sub>-proLC3B-Biotin yielding the corresponding biotinylated peptide (Fig. S3).

Then we set out to develop an HTS assay based on this substrate. First, optimal assay conditions were determined. Stability of the signal was investigated using different buffer solutions, pH, salt concentration, DMSO content and additives. The use of 25 mM Hepes buffer resulted in protein aggregation and high signal due to non-specific interactions. Addition of detergents and bovine serum albumin (BSA) minimized this effect resulting in a dose-dependent increase of the signal, whereas similar conditions employing a Tris buffered solution resulted in a complete loss of signal. However, the 25 mM Hepes buffer showed a loss of 90% signal after 1 h incubation which was not compatible with assay conditions (Fig. S4A). To improve this performance, the stability of the protein solution over time was improved by increasing the ionic strength (NaCl) and glycerol concentration of the buffer solution. The strongest and most stable LC3B signal was obtained using the following assay buffer: 25 mM Hepes pH 8 containing 150 mM NaCl, 0.5% Triton X-100, 0.1% BSA, 1% glycerol and 1 mM TCEP (Fig. S3B).

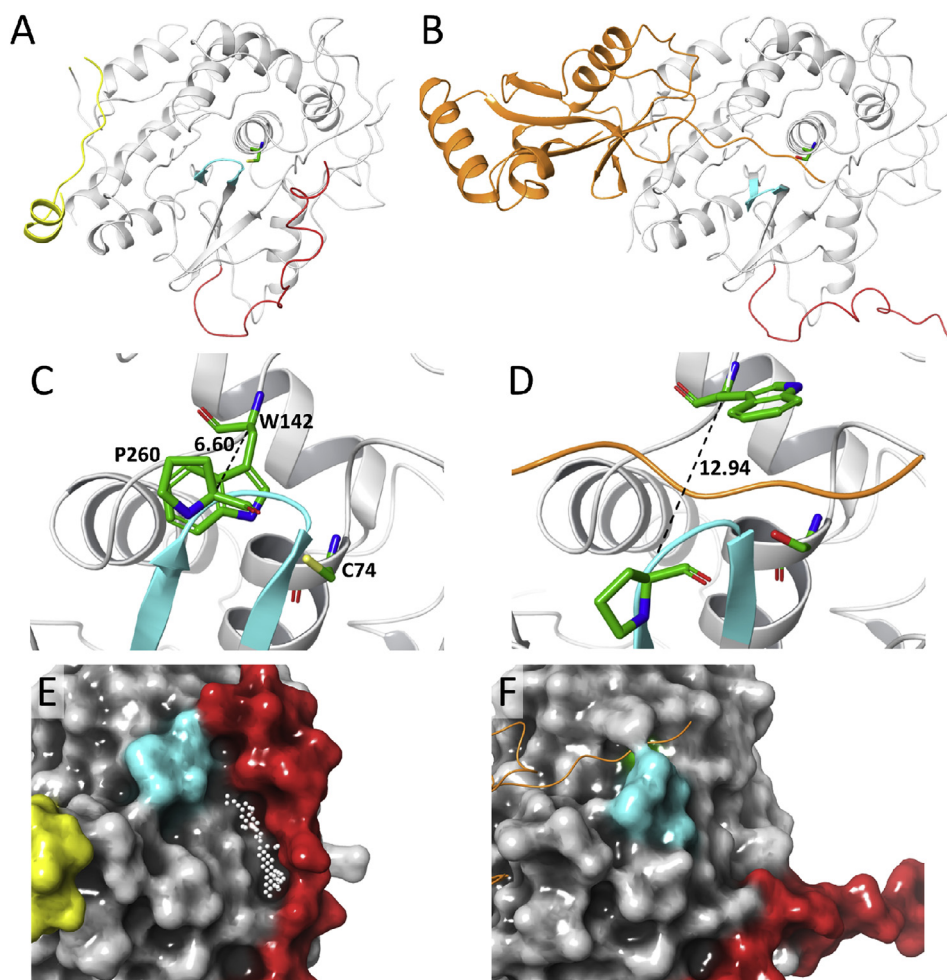
Next, the optimal enzyme concentration to achieve a robust assay signal was investigated. Thirty minutes at 37 °C was chosen as an incubation period for this assay to accommodate future automation on a large scale. In addition, Atg4B was activated by pre-incubation for 1 h with a suitable reducing agent (TCEP) and reactions were eventually run at pH 8.0, which has been previously reported to be optimal for enzyme activity [39]. Then, the N-(His)<sub>6</sub>-LC3B(L123C)Biotin protein was titrated with increasing concentrations of Atg4B (Fig. 2C). Substrate depletion measurements are based on signal changes from a high baseline value. Hence, to obtain a sufficient assay window, the substrate turnover may need to be close to 50% or higher [40,41]. As a result, a 25 nM concentration of enzyme was chosen showing a S/B ratio ~ 3 (Fig. 2C).

Most of compound collections are stored in DMSO solutions. Hence, the effect of DMSO on enzyme activity and assay performance was determined by incubating the assay mixture with increasing concentrations of DMSO. No significant differences were observed in any case, indicating that the assay can tolerate up to 5% DMSO (not shown). With the optimized assay conditions (25 mM Hepes buffer pH 8, containing 150 mM NaCl, 0.5% Triton X-100, 0.1% BSA, 1% glycerol and 1 mM TCEP), good assay stability and consistency could be achieved with a Z' factor of 0.52 (Fig. S4C). The established HTS assay was then employed to search for Atg4B inhibitors. Using this assay, we validate the effect of Z-L-Phe-chloromethyl ketone (Z-L-PheCMK) showing a concentration-dependent inhibition with an IC<sub>50</sub> of 38 μM [32,33]. Thus, the assay can quantitatively determine the effects of small molecule modulators of Atg4B. As a second positive control, we tested compound NSC185058 identified by Akin et al. as Atg4B inhibitor [31]. However, in this case we could only confirm a slight inhibitory activity at concentrations up to 200 μM (11% inhibition). This lack of activity has been also reported by other authors [29,33]. The observed discrepancies may be attributed to different assay conditions.

## 2.2. Computational structural analysis

There are a few crystal structures reported for human Atg4B in the literature [42–44] which show the existence of two structurally different forms of the enzyme: the form found when there is no substrate bound, where a regulatory loop (residues 258–263) masks the entrance to the active site, i.e. the “closed” form, and that found when the LC3 substrate is bound, where the regulatory loop is displaced from its original location, i.e. the “open” form. PDB structure 2CY7 [44] is representative of the closed Atg4B (Fig. 3A,C,E), and structure 2ZZP [43], corresponding to the complex of the inactive Atg4B C74S mutant with a bound LC3 substrate, is representative of the open form (Fig. 3B,D,F). Aside from the differences in the conformation of this regulatory loop, comparison of





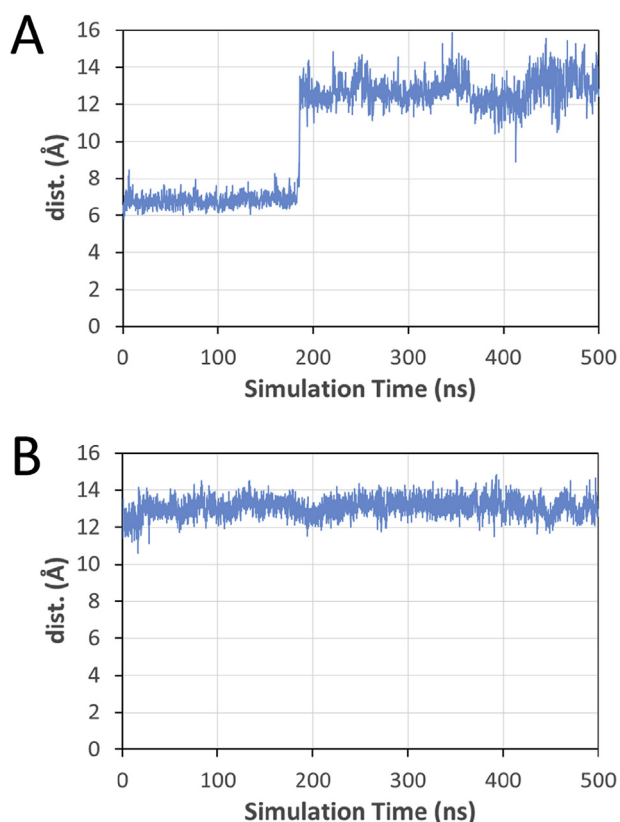
**Fig. 3.** Crystal structure of (A) free Atg4B (PDB 2CY7) and (B) the LC3-Atg4B C74S complex (PDB 2ZZP), showing the N-terminal tail (residues 5–26) in red, the C-terminal tail (355–377) in yellow (A), the regulatory loop (258–263) in cyan, the LC3 substrate in orange (B), and the catalytic cysteine (C74, A) or the mutationally introduced serine (S74, B) with green C-atoms. Detailed view of the active center of (C) free Atg4B, showing the distance between the  $C_{\alpha}$ -atoms of residues W142 and P260, and (D) the same for the LC3-Atg4B C74S complex. Surface representation of Atg4B in 2CY7 (E) and 2ZZP (F) showing the region close to residues D278 and H280, where a potential ligand binding site present only in the closed form is highlighted with white spheres. Surface coloring is the same as in panels A–B. (For interpretation of the references to color in this figure legend, the reader is referred to the Web version of this article.)

the two forms of the enzyme makes evident that binding of LC3 produces additional conformational changes in the structure of Atg4B. In particular, the N-terminal tail, located at the exit of the active site in the free Atg4B form, is detached from the enzyme core when LC3 is bound. Furthermore, the C-terminal tail is also displaced from its location upon complex formation [43]. Finally, a large loop located far from the active site of Atg4B (residues 186–218) and several additional residues are unresolved in all reported structures (see Materials and Methods). All of this reveals a high conformational flexibility of different regions of the protein.

In order to get insight into the conformational mobility of Atg4B and, specifically, to determine if the open form of the protein is only accessible when the LC3 substrate is bound, molecular dynamics studies on the open and closed forms of Atg4B were undertaken. For that purpose and given the high number of unresolved residues on the crystal structures of the protein, a model of the closed form was obtained from the ModBase database of comparative protein structure models [45,46] which comprises the full structure of residues 5–377, and we called it 2CY7\_full since it was based on the 2CY7 structure. Furthermore, based on 2CY7\_full and on the 2ZZP structure, we also built a structural model of the full Atg4B C74S sequence between residues 6–354 complexed to LC3, which we

called 2ZZP\_full. These two models were submitted to molecular dynamics (500 ns) in explicit solvent. The results from these simulations showed that while the LC3-Atg4B complex is mostly stable through all the simulation, i.e. the LC3 substrate and the regulatory loop remain in place, in the structure of the free Atg4B the regulatory loop fluctuates between two conformations corresponding to the closed and open states of the protein (Fig. S7). This is clear when analyzing the distance between the  $C_{\alpha}$ -atoms of residues W142 and P260 of Atg4B, which on the closed form interact and fix the conformation of the regulatory loop, i.e. distance ( $C_{\alpha}^{142} - C_{\alpha}^{260}$ )  $\sim$  6.6 Å, while on the open form both residues are set apart and the distance ( $C_{\alpha}^{142} - C_{\alpha}^{260}$ ) increases to  $\sim$  13 Å (Fig. 3C and D). In the simulation of 2ZZP\_full this distance remains essentially unperturbed and close to 13 Å during the whole simulation, whereas for 2CY7\_full that distance remains close to 7 Å for the initial 180 ns but then it increases to about 13 Å and remains like that during the rest of the simulation (Fig. 4A and B). This suggests that the presence of the LC3 substrate is not required to reach the open form of Atg4B, and that potential ligands could bind into the active site of the protease, directly interfering with the binding of the natural substrate.

An alternative potential binding site close to residues D278 and



**Fig. 4.** Results from molecular dynamics simulations: Time dependence of the distance between the  $C_{\gamma}$ -atoms of residues W142 and P260 of Atg4B from the simulations of (A) 2CY7\_full and (B) 2ZZP\_full.

H280, at the interface between the detachable N-terminal tail and the core of the closed form of the protein, has also been proposed as target to identify compounds which could lock Atg4B in its closed-inactive form [31]. This site is depicted in Fig. 3E and the results of MD show that, although with small changes in shape, it perdures during the whole simulation (Fig. S7A). On the contrary and as mentioned above, binding of LC3 induces a change in the conformation of the N-terminal tail that removes this site (Fig. 3F) and it is not restored during the simulation (Fig. S7B). Thus, the Atg4B structure from 2ZZP\_full was chosen to identify ligands that could bind into the active site while that from 2CY7\_full would allow to identify ligands that could target the second alternative site.<sup>2</sup>

### 2.3. High throughput virtual screening (HTVS)

Virtual screening was performed employing the National Cancer Institute (NCI) Open Database as source of potential ligands

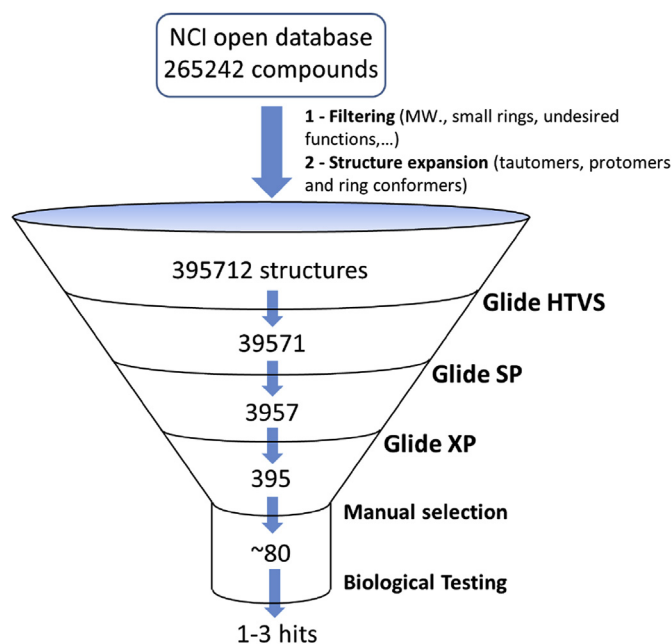
<sup>2</sup> During the preparation of this manuscript, a paper appeared reporting the use of structural data and the program PocketFinder to identify four pockets located on the surface of Atg4B as potential binding sites for ligands [29]. In the open Atg4B form, one of the identified pockets corresponds to the active site (Open#1 pocket), which we also explored, while a second one appears to be at the LC3-interface (Open#2 pocket). However, it is uncertain if this second site is available for ligand binding when LC3 is not bound, since it could be masked by the flexible C-terminal tail that is not solved on the 2ZZP X-ray structure, as our MD study reveals (Fig. S7A). On the other hand, on the closed Atg4B form, another identified site (Closed#1 pocket) is adjacent and partially overlaps the D278/H280 site shown in Fig. 3E, which again we explored, while the fourth site (Closed#2 site) is at the hinge of the mobile N-terminus, far from the active site, which we have not explored in our work.

(265242 compounds) and the two Atg4B structures, 2CY7\_full (closed form) and 2ZZP\_full (open form). This collection of compounds has already been used by other authors to search for Atg4B inhibitors [47–50]. At variance with these other studies, which apparently used the structures deposited in the Protein Data Bank without adding the fragments that were not defined in the crystal structures (see Materials and Methods), here we used the mostly complete protein sequence to avoid artifacts due to the absence of those fragments. In addition, among the large number of docking programs that can be used for virtual screening, we chose Glide [47–50] as it is one of the best recognized high throughput docking softwares available at the moment [51,52].

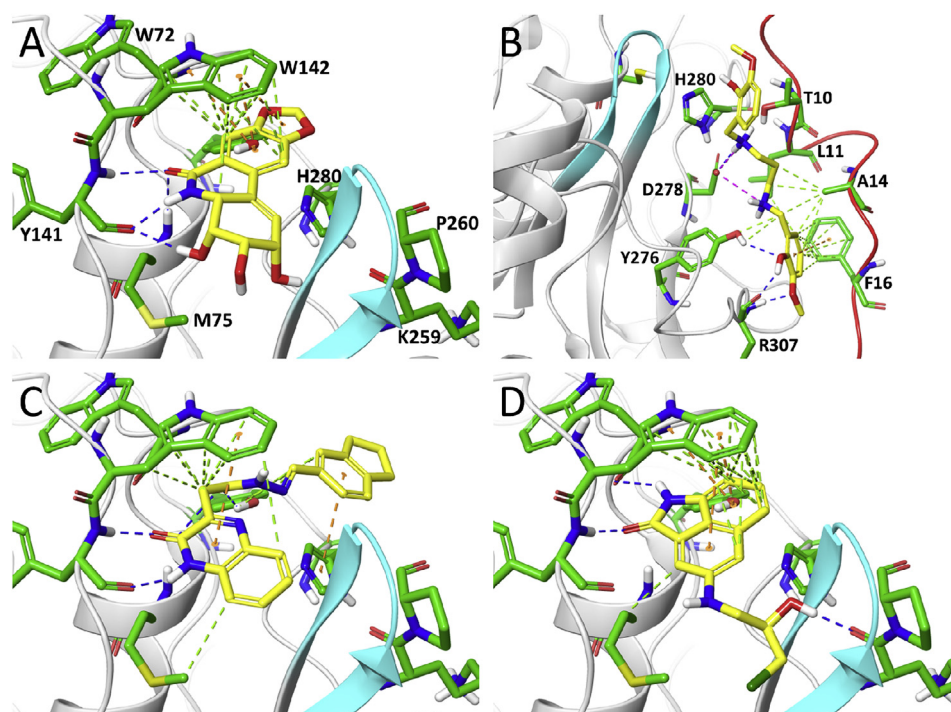
As preliminary control, we run a small docking test using the 2CY7\_full structure as target, in order to check the binding of two compounds, NSC185058 [27] and S130 [27], that were identified as inhibitors of Atg4B. The results obtained (Fig. S8) showed that both compounds could bind with similar poses to those previously reported, although with moderate docking scores ( $>-6$  kcal/mol). This discrepancy relative to the reported results could arise from the fact that the protein structures used for docking are not the same, as well as the different docking methods employed in each case.

Thus, starting with the full NCI database and after an initial filtering to remove compounds with undesired properties and a structure expansion step to generate different tautomers, protomers, and ring conformers of each compound (see Materials and Methods), a total of 395712 structures resulted which were submitted to HTVS against the two Atg4B target sites. For that purpose, a virtual screening workflow [53] that uses the docking software Glide [47–50] to perform the flexible docking of the ligand structures at different levels of accuracy was employed (Fig. 5).

The results of this virtual screening showed that many of the best hits at the AtgB4 active site were mainly stabilized by hydrophobic contacts and  $\pi$ -stacking interactions with residue W142, (Fig. 6A,C,D). This residue has been shown to be crucial for the processing activity of Atg4B since it acts as a clamp to keep residues F119 and G120 of the natural LC3 substrate in place, previous to the cleavage of the contiguous peptide scissile-bond [43]. On the other



**Fig. 5.** Screening funnel to identify binders against each of the two Atg4B target sites.



**Fig. 6.** Docked poses for the best hits from HTVS against (A) the active site of Atg4B (**NSC349155**) and (B) the second alternative site (**NSC86286**). These compounds could not be tested biologically because they were not available from the NCI. Docked poses for the two best Atg4B inhibitors determined by biological testing, (C) **NSC126353** and (D) **NSC611216**. Ligands are shown with yellow C-atoms and protein residues with green C-atoms. The regulatory loop is highlighted in cyan and the N-terminal tail in red. Interactions are depicted with dashed lines: Hydrogen bonds in blue, salt bridges in magenta, hydrophobic in green and  $\pi$ -stacking in orange. (For interpretation of the references to color in this figure legend, the reader is referred to the Web version of this article.)

hand, common features of the best hits from screening at the second site were the presence of at least one cationic group (i.e. protonated amine), that could establish electrostatic interactions with residue D278 of Atg4B, and an extended structure that allowed them to occupy the relatively narrow groove at the interface between the N-terminal tail and the Atg4B core, making hydrophobic contacts with residues L11, A14 and F16 (Fig. 6B). The top scored compounds from virtual screening at the two Atg4B sites were visually inspected and, once promiscuous and non-specific compounds were discarded [54] and availability was checked, 75 compounds were selected as potential binders against the Atg4B active site and 81 against the second alternative site (Tables S2 and S3). These compounds were obtained from the NCI for biological testing.

#### 2.4. Biological screening

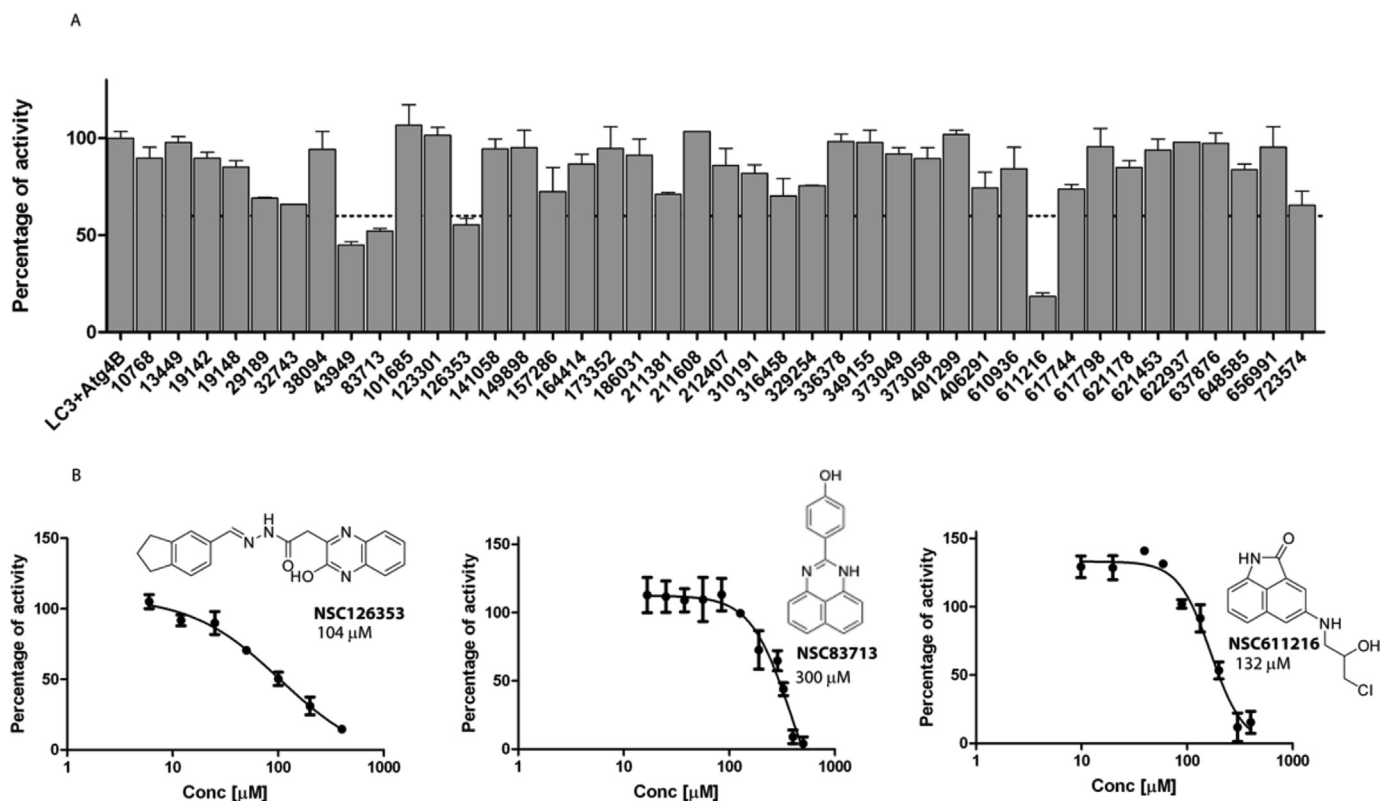
Among the 75 active-site directed hits tested, three compounds (**NSC83713**, **NSC126353** and **NSC611216**) showed around 50% or better inhibition in a preliminary single concentration assay (200  $\mu$ M concentration), while only one (**NSC43949**) of the 81 hits against the second binding site showed >50% inhibition (Fig. 7). All active hits, except the commercially available **NSC126353**, were resynthesized to confirm the identity of the library samples and their inhibitory activity. Moreover, purity and identity of the active library samples and the synthesized compounds were checked by Mass Spectrometry (MS). These validation assays discarded **NSC43949**, that did not fulfill the analysis requirements, and corrected the structure of **NSC83713** that corresponded to the depicted analog (Fig. 7). Half-maximal inhibitory concentrations ( $IC_{50}$ ) were then determined for these initial hits in concentration response studies. The compounds showed promising dose-dependent

inhibition of Atg4B with  $IC_{50}$  values ranging from 104 to 300  $\mu$ M. The inhibitory profiles of these three compounds with an unambiguous dose-dependent effect are shown in Fig. 7.

To identify compounds that specifically interfere with Atg4B activity and do not act as pan assay interference compounds (PAINS) [55], hits were also evaluated in two different counter-screen assays. An AlphaScreen assay employing a (His)<sub>6</sub>-tagged biotinylated peptide as substrate was applied to discard false positives or target-independent hits such as oxygen quenchers, color quenchers, biotin mimetics, and nickel chelate competitors. The tested compounds did not show inhibition of the AlphaScreen signal when employing the (His)<sub>6</sub>-tagged biotinylated peptide.

In addition, an orthogonal MS-based assay was used to measure the cleavage of proLC3B and the concomitant release of the corresponding C-terminal peptide. This assay employed the full length protein proLC3 as a substrate and Atg4B and it is based on the MS detection of the cleaved peptide. First, (His)<sub>6</sub>-Atg4B was shown to cleave the N-(His)<sub>6</sub>-LC3B-L123C and convert it to LC3-I, together with the release of the corresponding C-terminal peptide with an observed molecular mass of 567.2643 Da that matches its calculated monoisotopic mass (Fig. S5). Next, a calibration curve for the cleaved peptide was established by injecting serially diluted samples of N-(His)<sub>6</sub>-LC3B-L123C (18  $\mu$ M) fully cleaved by incubation with 100 nM of Atg4B at 37 °C for 2 h. Complete reaction was confirmed by disappearance of N-(His)<sub>6</sub>-LC3B-L123C and formation of LC3B-I. Linearity of the signal-concentration relationship was confirmed in all the range of concentrations investigated (Fig. S6A). Then, varying concentrations of N-(His)<sub>6</sub>-Atg4B (0–100 nM) were titrated to a fixed protein substrate concentration (18  $\mu$ M) and the mixture was incubated at 37 °C during 30 min. The amount of formed peptide was quantified and changes in peak areas were used to calculate the rate of the cleavage by comparison with the





**Fig. 7.** A) Preliminary in vitro validation of hit compounds on Atg4B. The hit molecules identified through virtual screening were investigated using the developed HTS assay at 200  $\mu\text{M}$  concentration. Representative results including 41 of the tested compounds and DMSO control are shown. Values shown are mean of two replicates and results are expressed as percentage of activity compared to vehicle control. The dotted line indicates 40% inhibition. B) Atg4B concentration-response curves of hit molecules **NSC126353**, **NSC83713** and **NSC611216**. Values shown are means of 3 experiments performed in duplicate.

calibration curve. (Fig. S6B). Based on these results, a 10 nM concentration of NHis-Atg4B was chosen. Once established, the MS-based assay was employed to validate and confirm the activity of the hits detected in the AlphaScreen assay.

Thus, all compounds were found to inhibit the activity of Atg4B with similar or slightly better  $\text{IC}_{50}$  values when employing the LC-MS-based assay (**NSC126353** ~ 79  $\mu\text{M}$ , **NSC83713** ~ 150  $\mu\text{M}$ , **NSC611216** ~ 97  $\mu\text{M}$ ). The MS-based assay employs higher substrate and lower enzyme concentrations, what can explain the better  $\text{IC}_{50}$  values obtained.

### 2.5. Synthesis and testing of new Atg4B inhibitors

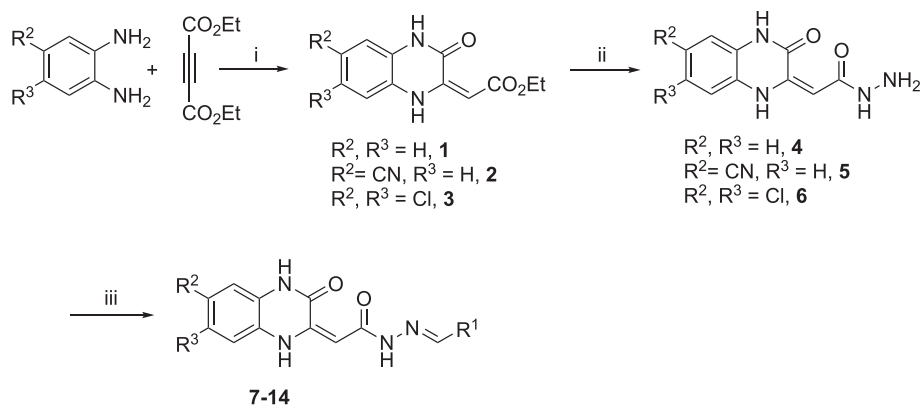
Focused libraries based on the more potent scaffolds **NSC611216** and **NSC126353** were next designed and synthesized. Quinoxaline derivatives are privileged scaffolds with a wide array of biological activities [56,57]. Hence, a series of **NSC126353** derivatives were designed to explore the chemical space for affinity improvement (Scheme 1). The results of virtual screening suggest that the quinoxaline of **NSC126353** could occupy the active site cavity of Atg4B (Fig. 6C), with its heterocyclic ring establishing hydrogen bonds with the backbone of residue Y143 as well as a  $\pi$ -stacking interaction with W142, and leaving little available space in the cavity. At the other end of the molecule, the bicyclic substituent is placed in a more exposed region, with its aromatic moiety making a  $\pi$ -stacking interaction with H280. Thus, we preferentially evaluated modifications of the benzene ring of the quinoxaline with small hydrophobic substituents ( $\text{R}^2$ ,  $\text{R}^3 = \text{H}$ , Cl, CN) and variations on the substituent linked to the hydrazine moiety ( $\text{R}^1 = \text{Pr}$ , Ph, Py, ...) (Table 1). Induced fit docking results suggested that these

modifications were compatible with binding at the Atg4B active site with similar affinity to the parent **NSC126353** (Fig. S9).

Briefly, condensation of phenylenediamines with diethylacetylenedicarboxylate proceeded in acetonitrile at room temperature with good yields to yield 3-ethoxycarbonylmethylquinoxalin-2(1H)-ones **1–3**, which were then converted to 3-hydrazinocarbonylmethylquinoxalin-2(1H)-one (**4–6**) by reaction with a 10-fold excess of hydrazine hydrate [58]. Finally, reaction with aliphatic aldehydes, substituted benzaldehydes and heteroaryl aldehydes afforded 2-hydroxyquinoxalines (**7–14**). Activities were then investigated using the established assays. Unfortunately, none of the synthesized compounds lead to inhibitors showing higher potency. Only Compound **14** (Table 1) bearing a dichlorohydroxyquinoxaline scaffold and a hydroxybenzene moiety showed moderate response. However, with a 3-fold decrease in activity compared to **NSC126353**, it was less potent than the parent compound thereby suggesting that the presence of the indane ring is important for compound activity.

We then focused on **NSC611216**. The benzo[*cd*]indol-2(1H)-one scaffold has attracted increasing attention in the last years. Thus, 5,6-disubstituted derivatives have been shown to be effective thymidylate synthase inhibitors, [59] 5-sulfonamide derivatives have been described as BET bromodomain inhibitors [60] phosphodiesterase 2A inhibitors [61] and protein kinase FGFR1 inhibitors, [62] and 3-pyrrolyl derivatives substituted at the 5,6-position have also showed CDK2 inhibitory activity [63]. However, 7-amino-benzo[*cd*]indol-2(1H)-ones derivatives represent a novel class of inhibitors with no biological activity associated.

The synthesis of **NSC611216** was performed as depicted in Scheme 2. Briefly, 3-nitro-1,8-naphthalic anhydride was reacted with hydroxylamine hydrochloride and *p*-toluenesulfonyl chloride

**Scheme 1.** Synthesis of compounds **7–14**.

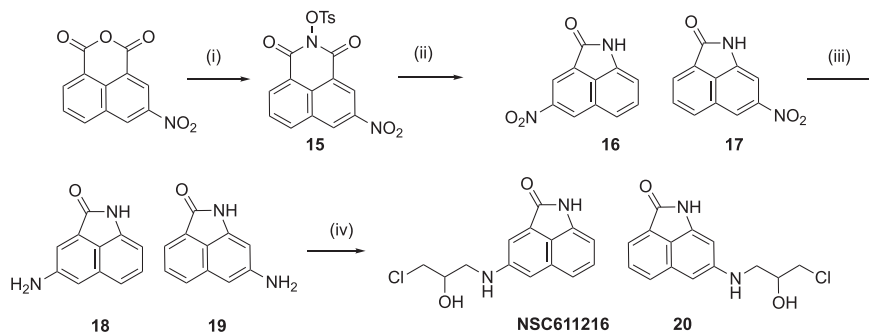
Reagents and conditions: (i)  $\text{CH}_3\text{CN}$ ; (ii)  $\text{N}_2\text{H}_4 \cdot \text{H}_2\text{O}$ , EtOH, reflux 3–6 h; (iii)  $\text{R}^1\text{-CHO}$ , EtOH, reflux, 3–6 h.

**Table 1**

Residual activities (Act. %) of Atg4B compared to control with no inhibitor present<sup>a</sup> and  $\text{IC}_{50}$  values of the most active compounds.

Compound	$\text{R}^1$	$\text{R}^2$	$\text{R}^3$	Act. (%)	$\text{IC}_{50}$ ( $\mu\text{M}$ )
<b>NSC126353</b>		–	–	55	104 (87–125)
<b>4</b>	–	H	H	76	–
<b>5</b>	–	CN	H	N.A.	–
<b>6</b>	–	Cl	Cl	N.A.	–
<b>7</b>		H	H	74	–
<b>8</b>	–	H	H	71	–
<b>9</b>		CN	H	78	–
<b>10</b>	–	Cl	Cl	70	–
<b>11</b>		H	H	93	–
<b>12</b>	–	Cl	Cl	64	–
<b>13</b>		H	H	61	–
<b>14</b>	–	Cl	Cl	51	315 (292–337)

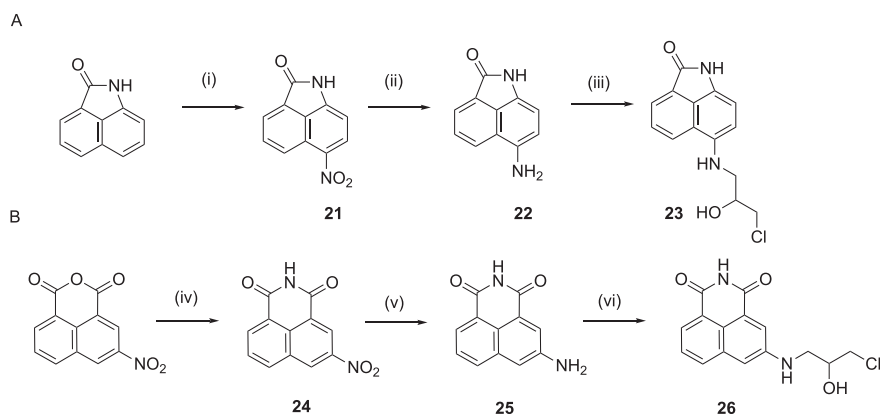
<sup>a</sup> Residual activities are mean values of three independent experiments performed in duplicate. Assay conditions as in Fig. 1A.  $\text{IC}_{50}$  values were calculated from AlphaScreen assay and validated with the MS-based assay (95% confidence intervals). N.A.: not active.

**Scheme 2.** Synthesis of benzo[cd]indol-2(1H)-one derivatives **NSC611216** and **20**.

Reagents and conditions: (i)  $\text{NH}_2\text{OH} \cdot \text{HCl}$ , pyridine, reflux, 1 h, then *p*-TsCl, reflux, 2 h; (ii) NaOH in  $\text{H}_2\text{O}/\text{EtOH}$ , reflux 1 h, then HCl; (iii)  $\text{SnCl}_2$ ,  $\text{H}_2\text{O}/\text{HCl}$ , 50 °C, 4 h. (iv) epichlorohydrin,  $\text{LiClO}_4$ ,  $\text{CH}_3\text{CN}$ , mw, 150 °C, 150 W, 60 min.

in the presence of pyridine to yield compound **15** that could be easily isolated after crystallization in excellent yields. Lossen rearrangement of the imidate to the lactam was accomplished in two steps. First, treatment with ethanolic NaOH was the

intermediate aminocarboxylic acid that was converted upon treatment with hot water acidified to pH 2–3 to the desired lactams **4**–(**16**) and 7-nitrobenzo[cd]indol-2-(1H)-one (**17**) in a 2:1 ratio, that were not easily separable by column chromatography. Finally, reduction of



**Scheme 3.** A) Synthesis of 6-amino-benzo[cd]indol-2(1H)-one derivative **23**. B) Synthesis of the 1,8-naphthalimide derivative **26**.

Reagents and conditions: (i) HNO<sub>3</sub> in glacial acetic acid, 50 °C, 1.5 h; (ii) SnCl<sub>2</sub>, H<sub>2</sub>O/HCl, 50 °C, 4 h; (iii) epichlorohydrin, LiClO<sub>4</sub>, EtOH, 80 °C, 14 h; (iv) NH<sub>4</sub>OH, H<sub>2</sub>O, reflux, 4 h; (v) SnCl<sub>2</sub>, H<sub>2</sub>O/HCl, 50 °C; (vi) epichlorohydrin, LiBr, DMF, 100 °C, 14 h.

the aromatic nitro compounds to aniline was performed with SnCl<sub>2</sub> and hydrochloric acid. Epoxide ring opening of (±)-epichlorohydrin with the poorly nucleophilic aromatic amines was facilitated by the presence of LiClO<sub>4</sub> [64], owing to the coordination of the lithium ion with the oxygen atom of the epoxide. The ring opening of the terminal epoxide is completely regioselective due to the attack of the amine nucleophile at the less hindered site of the oxirane moiety. The reaction was promoted by microwave irradiation yielding the expected β-amino alcohols (**NSC611216** and **20**) with moderate yields. Typically, a 4-fold excess of lithium perchlorate and equivalent amounts of amine and epoxide were used in this procedure. Large excess of amines was avoided due to their costly preparation.

Then, based on their similar binding mode and docking scores (Fig. S9) we decided to explore several modifications on the benzo[cd]indol-2(1H)-one scaffold and on the exocyclic substituents. As a first attempt, we kept the benzo[cd]indol-2(1H)-one core and change the position of the amino group. The synthesis of the 6-amino-benzo[cd]indol-2(1H)-one derivative (**23**) was more straightforward and started with the nitration of the commercially available benzo[cd]indol-2(1H)-one to yield the known 6-nitrobenzo[cd]indol-2(1H)-one (**21**, Scheme 3A) [59]. Reduction and subsequent alkylation of the aniline nitrogen in refluxing ethanol provided the desired compound **23**. The activity of the synthesized analogues was then evaluated. Hence, the resynthesized 4-(3-chloro-2-hydroxypropylamino)benzo[cd]indol-2(1H)-one exhibited similar potency to the parent compound **NSC611216** (126 μM vs 132 μM), whereas the 7-substituted analog (**20**) showed a potency enhancement of about two-fold (69 μM, Table 2).

However, the 6-substituted analog (**23**) exhibited a significant decrease in potency (Table 2). The moderate potency gain of analog **20** relative to **NSC611216** was compatible with the similar binding modes of both compounds (Figs. 6D and 8A and S9). Thus, despite having the acyclic substituent at a different position of the main core, the results from Induced Fit Docking suggest that **20** could adopt a disposition at the Atg4B active site inverted 180° relative to that of **NSC611216**, that allows it to keep the main interactions of the benzo[cd]indol-2(1H)-one core with residue W142, as well as the hydrogen bonds established by the endocyclic amide group. On the other hand, the decreased potency of compound **23** correlates with a binding mode where the exocyclic chain is placed at the other end of the active site cavity, more exposed to the bulk solvent (Fig. S9).

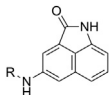
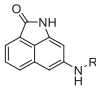
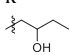
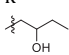
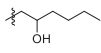
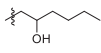
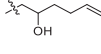
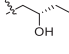
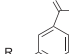

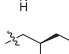
The benzo[cd]indol-2(1H)-one core was then replaced by a 1,8-naphthalimide scaffold. This class of compounds has gained attention as anticancer and antiviral agents. Amonafide, with activity as DNA intercalating agent and topoisomerase II inhibitor [65], has entered into phase II clinical trials for prostate cancer, and sulfonated derivatives of 1,8-naphthalimides can block viral expression in HIV-infected human peripheral blood mononuclear cells by inhibiting reverse transcriptase [66]. Hence, synthesis of naphthalimide derivative **26** started with the reaction of the commercially available of 3-nitro-1,8-naphthalic anhydride with concentrated ammonium hydroxide. Subsequent reduction of the nitro group with SnCl<sub>2</sub> and monoalkylation of the resulting aniline afforded compound **26** (Scheme 3B), which unfortunately did not show activity as Atg4B inhibitor (Table 2).

**Table 2**  
Activities of compounds **NSC611216**, **20**, **23** and **26**.<sup>a</sup>

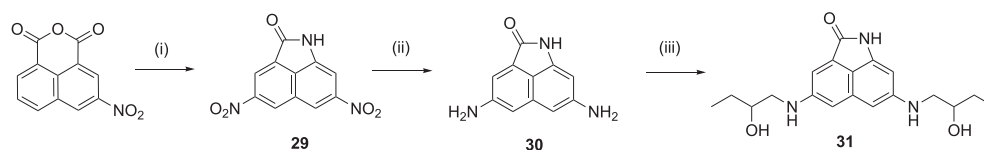
Compound	IC <sub>50</sub> (μM)	Compound	IC <sub>50</sub> (μM)
<b>NSC611216</b>	132 (99–163)	<b>20</b>	69 (55–84)
<b>23</b>	>300	<b>26</b>	N. A.

<sup>a</sup> IC<sub>50</sub> values were calculated from AlphaScreen assay and validated with the MS-based assay (95% confidence intervals). Data from at least three independent experiments performed in duplicate. N. A.: not active.

**Table 3**  
Activities of compounds 27–36.<sup>a</sup>

Scaffold		Scaffold			
Compound 27	R: 	IC <sub>50</sub> (μM)	Compound 28	R: 	IC <sub>50</sub> (μM)
27		111 (76–161)	28		29 (15–56)
32		235 (195–284)	33		12 (6–18)
34		N. A.	Scaffold		
35		113 (92–138)	31		68 (47–88)
36		119 (98–145)			

<sup>a</sup> IC<sub>50</sub> (μM, 95% confidence intervals) values were calculated from AlphaScreen assay and validated with the MS-based assay. Data from at least three independent experiments performed in duplicate. N. A.: not active.

**Scheme 4.** Synthesis of the disubstituted derivative **31**

Reagents and conditions: (i) H<sub>2</sub>SO<sub>4</sub>, HNO<sub>3</sub>, 60 °C, 1.5 h; then NH<sub>2</sub>OH·HCl, pyridine, reflux, 1 h; then *p*-TsCl, reflux, 2 h; NaOH in H<sub>2</sub>O/EtOH, reflux 1 h, then HCl (ii) SnCl<sub>2</sub>, H<sub>2</sub>O/HCl, 50 °C, 4 h; (iii) epichlorohydrin, LiClO<sub>4</sub>, EtOH, mw, 150 °C, 150 W, 60 min.

Based on the previous experimental results, we selected **NSC611216** and **20** for further structural modification. We kept the 4-amino and 7-aminobenzo[*cd*]indol-2-[1*H*]-one core and focused on modifications on the alkyl group. Different substituent groups were attached to the aniline nitrogen to explore their effect on the inhibition.  $\alpha$ -chlorohydrins are moderately reactive alkylating agents that can covalently react with proteins, thereby causing its inactivation. To explore if this effect was the cause of the observed inhibition, two analogues in which the chlorine was replaced by a methyl group (**27**) and (**28**) were prepared. These compounds were prepared by aminolysis under refluxing ethanol of (*R,S*)-( $\pm$ )-1,2-epoxybutane in the presence of LiClO<sub>4</sub> as a catalyst, affording the corresponding  $\beta$ -amino alcohols **27** and **28** in good yields (Table 3). The presence of the methyl group improved the inhibition and the effect was more pronounced in (**28**) which exhibited a more than two-fold increase in potency relative to **20**. To explore the structure-activity relationship (SAR), the 4,7-diaminobenzo[*cd*]indol-2(1*H*)-one scaffold was also prepared starting by nitration of the commercially available 3-nitro-1,8-naphthalic anhydride [67], followed by Lossen rearrangement to afford 4,7-dinitrobenzo[*cd*]indol-2(1*H*)-one (**29**). Reduction to the corresponding dianiline followed by double amine alkylation with (*R,S*)-( $\pm$ )-1,2-epoxybutane yielded disubstituted **31** in moderate yields. However, the 4,7-dialkylated lactam (**31**) exhibited an intermediated potency, with an IC<sub>50</sub> of 68 μM (Scheme 4, Table 3). Extension of the alkyl chain was also explored. Hence, reaction with (*R,S*)-( $\pm$ )-1,2-epoxyhexane gave different results depending on the regioisomers. Thus, whereas the 7-aminobenzo[*cd*]indol-2-[1*H*]-one derivative (**33**) showed an improved IC<sub>50</sub> of 12 μM, the activity of the 4-aminobenzo[*cd*]indol-2-[1*H*]-one derivative (**32**) dropped significantly (Table 3). Similarly, reaction of the 4-aminobenzo[*cd*]indol-2-[1*H*]-one with 1,2-epoxy-5-hexene afforded compound **34**,

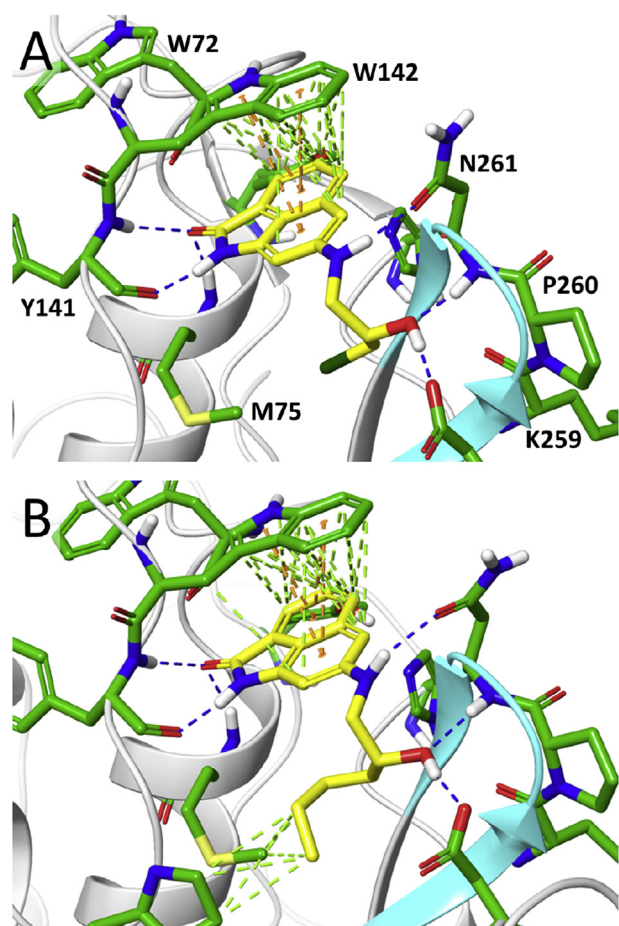
which showed an even lower activity than **32**. The activity of compound **33** could be rationalized on the basis of its binding to Atg4B which is similar to that of analog **20** (Fig. 8A). However, the longer hydrophobic chain of **33** allows it to establish new hydrophobic interactions with residues M75, P145 and A263, which could explain the improved activity observed (Fig. 8B).

We next explored if chirality played a role in the biological activity of **27**. With this aim, enantiomerically pure  $\beta$ -amino alcohols were prepared from epoxide ring opening of (*S*)-(-)-1,2-epoxybutane and (*R*)-(+)-1,2-epoxybutane. However, no substantial differences were detected and the resulting compounds **35** and **36** showed essentially the same activity than the racemic mixture **27**.

Atg4B shows the highest structural similarity to papain and its homologous proteases [44]. Thus to evaluate the selectivity over other cysteine proteases, we tested whether **NSC611216** and compound **33** could also inhibit papain activity. Neither **NSC611216** nor **33** inhibited the activity of this cysteine protease thus suggesting certain selectivity for Atg4B, whereas chymostatin completely block the activity and substantial inhibition was observed with Z<sub>1</sub>-PheCMK (Fig. 9A).

Based on the structure-activity relationship (SAR) investigation, compound **33** was chosen for further in-depth characterization. Thus, we next studied if the treatment of cells with **33** resulted in changes cellular autophagy. To do this, autophagy was induced by amino acid deprivation (Earle's Balanced Salt Solution, EBSS) and the levels of the autophagy markers LC3-II and p62 were examined by immunoblotting. Typically, the chemical and genetic inhibition of Atg4B leads to accumulation of LC3-II and increased levels of the cargo adaptor of proteins p62 due to its decreased clearance [29]. Moreover, as differences in the protein levels can be caused by both modulation in autophagy or changes in lysosomal degradation of





**Fig. 8.** Best poses from Induced Fit Docking of (A) (S)-**20**, (B) (R)-**33**. Ligands are shown with yellow C-atoms and protein residues with green C-atoms. The regulatory loop is highlighted in cyan. Interactions are depicted with dashed lines: Hydrogen bonds in blue, hydrophobic in green and  $\pi$ -stacking in orange. Similar binding modes were observed for the alternative enantiomers of **20** and **33** (Fig. S9). (For interpretation of the references to color in this figure legend, the reader is referred to the Web version of this article.)

the proteins, these studies were performed in the presence lysosomal inhibitors to estimate the overall autophagic flux [68]. As depicted in Fig. 9, **33** resulted in an increase of LC3-II in starved HT-29 cells comparable to Chloroquine (CQ). Autophagy flux analysis indicated that **33** enhanced the LC3-II accumulation induced by protease inhibitors (Fig. 9B and C). In addition, treatment with **33** decreased the autophagy-induced degradation of p62. The observed changes support an impairment of autophagy and suggest an inhibition of autophagic flux.

Oxaliplatin is a drug commonly used for the treatment of colorectal cancer. Its mechanism of action is mediated by the formation of inter-strand and intra-strand crosslinks with DNA, thereby inhibiting DNA replication and resulting in apoptosis. It has been reported that compounds which inhibit autophagy can sensitize cancer cells to oxaliplatin, and Beclin1 knockdown enhances oxaliplatin sensitivity in colon cancer cells under normoxic and hypoxic conditions [69]. Hence, we next investigated the antitumor activity of **33** against HT-29 cells in the presence and absence of oxaliplatin. As depicted in Fig. 9D cell viability inhibition by oxaliplatin was markedly enhanced in the presence of a non-toxic concentration of **33**, thus indicating that autophagy inhibition may result in an additive or synergic anticancer effect. However, it cannot be discarded an additional effect of **33** on other

cellular targets such as kinases, thereby contributing to the final outcome [63]. Interestingly, a recent work has described that benzo[cd]indol-2-[1H]-ones bearing a polyamine tail on the lactam ring inhibit tumor growth probably via activation of autophagy and apoptosis. These results can be caused by its specific lysosomal localization probably mediated by the polyamine tail, but it may also indicate that the substitution pattern may play a role on the activity of benzo[cd]indol-2-[1H]-ones [70].

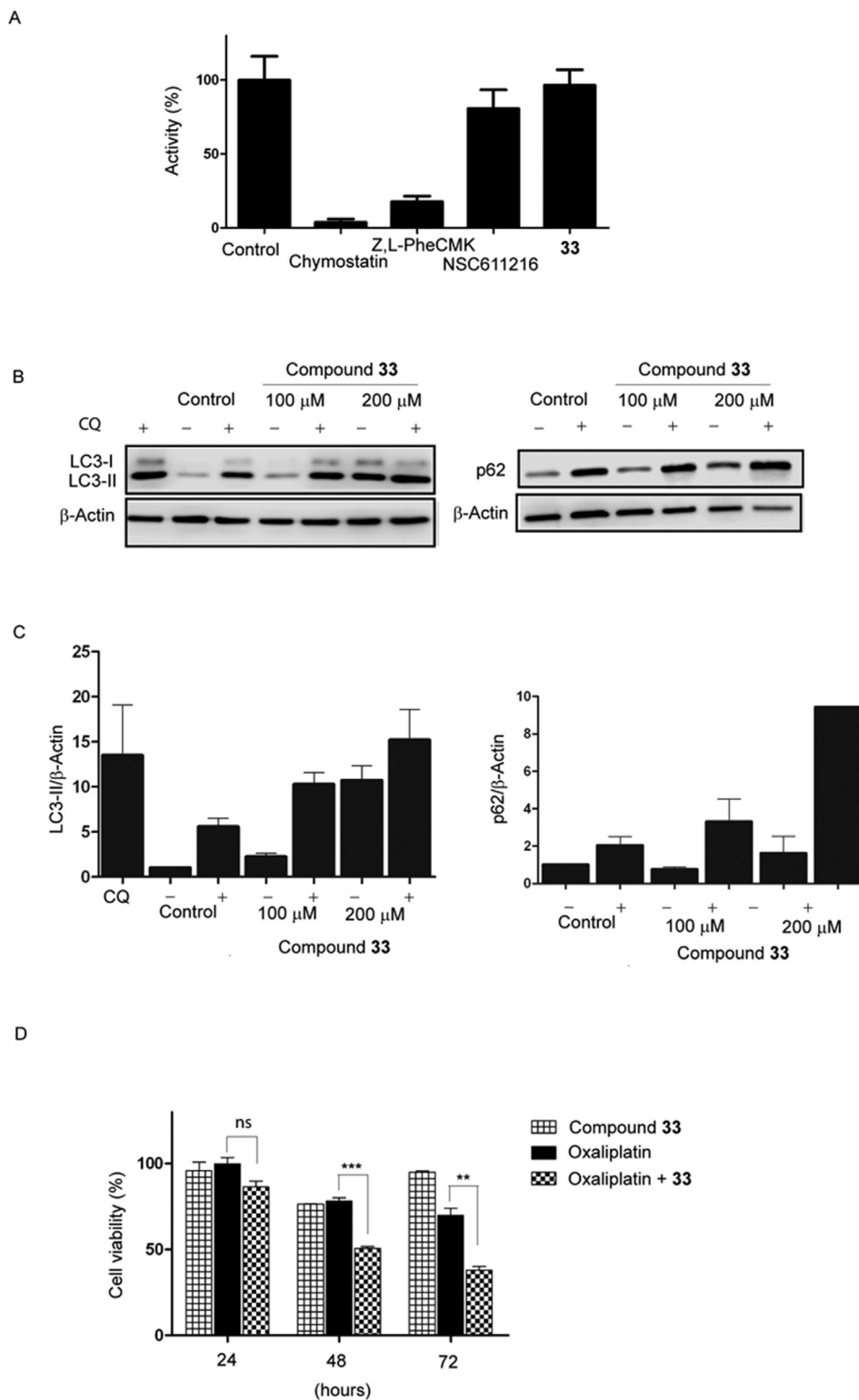
### 3. Conclusions

In summary, we report the development and optimization of a novel AlphaScreen-based assay for measuring the catalytic activity of the cysteine protease Atg4B that combined with a structure-based high-throughput virtual screening of a library of about 265242 compounds yielded a series of novel autophagy inhibitors. Medicinal chemistry optimization of the initial hit **NSC611216** provided insight into the structural requirements for the inhibition of Atg4B. The most potent compound **33** shows a 10-fold improvement relative to the parent hit and in vitro activities in the range or better than inhibitors previously identified. This compound also demonstrated a good cytotoxicity profile while maintaining autophagy inhibition, as measured by LC3-II and p62 protein levels. Moreover, the synergistic effect of **33** combined with oxaliplatin resulted in an enhanced cell death in the human colorectal adenocarcinoma cell line HT-29. All in all, the developed AlphaScreen and MS-based assays can be key tools enabling the high-throughput identification of novel Atg4B inhibitors. Moreover, the aminobenzo[cd]indol-2-[1H]-one scaffold represents a novel chemotype for the further development of small molecule inhibitors of Atg4B. We are convinced that these results will contribute to expand the toolbox used to study autophagy in mammal cells and to unravel the role of Atg4B in cancer treatment.

### 4. Experimental section

**Chemistry.** All commercially available compounds were used as provided without further purifications. Chemicals and solvents were purchased from Sigma Aldrich, Alfa Aesar, Acros Organics, Merck Chemicals, Life Technologies, Santa Cruz Biotechnology, TCI and Fisher Scientific. Analytical thin-layer chromatography (TLC) was performed on ALUGRAM SIL G/UV<sub>254</sub> precoated aluminum sheets (Macherey–Nagel). Compounds were visualized by UV light, or stained with potassium permanganate, 5% (w/v) ethanolic solution of phosphomolybdic acid, or ninhydrin solution. Flash chromatographic purifications were performed on silica gel Acros 60 Å (particle size 0.035–0.070 mm) or using a Biotage Isolera Prime purification system with a cartridge and solvent gradient as indicated. Dry solvents were obtained by passing through an activated alumina column on a Solvent Purification System (SPS). NMR experiments were carried out on a Varian Mercury 400 instrument (400 MHz for <sup>1</sup>H and 101 MHz for <sup>13</sup>C). Chemical shifts ( $\delta$ ) are reported in part per million (ppm) referenced to the residual solvent. Signal characterization is described using the following abbreviations: s (singlet), d (doublet), dd (doublet of doublets), t (triplet), q (quartet), m (multiplet), br (broad signal) and app (apparent). Spin-spin coupling constant (*J*) are reported in Hertz (Hz). 2D-NMR experiments COSY, HSQC and HMBC were used where necessary for assigning NMR spectra. High resolution mass spectra (HRMS) were recorded on an Acquity UPLC system coupled to a LCT Premier orthogonal accelerated time-of-flight mass spectrometer (Waters) using electrospray ionization (ESI) technique and an Acquity UPLC<sup>®</sup> BEH C18 1.7 mm, 2.1 × 100 mm column; flow rate: 0.3 mL/min, mobile phase: water with 20 mM formic acid and acetonitrile with 20 mM formic acid.





**Fig. 9.** (A) Effect of **NSC611216** and **33** on papain activity. The enzyme (0.6  $\mu$ g) was incubated with the substrate (0.22 mM) in the absence (Control) or presence of Chymostatin (10  $\mu$ M) and the test compounds (50  $\mu$ M). Absorbance was determined at 410 nm after 30 min. Chymostatin was used as positive control of inhibition of papain activity. (B) Analysis of autophagy inhibition in nutrient deprived HT-29 cells, treated with **33** (or vehicle) for 16 h and subjected to western blotting to assess LC3-II and p62 expression.  $\beta$ -Actin served as a loading control. Representative blots from 3 independent experiments are shown. (C) Bar graph shows LC3-II and p62 expression normalized to  $\beta$ -actin loading control (fold change); mean  $\pm$  SEM; n = 3; (D) Sensitization of HT-29 cells by **33** to the cytotoxic effects of oxaliplatin. Cell viability was determined by an MTT assay after treatment with oxaliplatin (30  $\mu$ M) for 24, 48 and 72 h in the absence or presence of **33** (75  $\mu$ M).

Reactions under microwave irradiation were carried out in a CEM Discover Focused™ Microwave reactor. The instrument consist on a continuous focused microwave power delivery system with operator selectable power output from 0 to 300 W. Reactions were performed in glass vessels of 10 mL sealed with septum. The temperature of the content of the vessel was monitored using an IR sensor and the indicated temperature corresponds to the maximal temperature reached during each experiment. The content of the vessels are stirred by means of rotating magnetic plate located below the floor of the microwave cavity and a Teflon coated magnetic stir bar in the vessel. The specified time corresponds to the total irradiation time. Efficient cooling is accomplished by means of pressurized air during the entire experiment. Temperature, pressure and power profiles were monitored using commercially available software provided by the microwave manufacturer. Purities of all final compounds were determined to be  $\geq 95\%$  by analytical HPLC analysis.

**4-(2,3-dihydro-1H-perimidin-2-yl)phenol.** To a stirred solution of 1,8-diaminonaphthalene (300 mg, 1.90 mmol) in methanol, 4-hydroxybenzaldehyde (281 mg, 2.30 mmol) and zinc acetate (3.5 mg, 0.02 mmol) were added and the mixture was left to stir at room temperature for 16 h. The crude was filtered and washed with methanol affording the desired product (94 mg, 19% yield). Further purification was achieved by recrystallisation from hot dichloromethane.  $^1\text{H}$  NMR (DMSO- $d_6$ , 400 MHz):  $\delta$  9.55 (s, br, 1H), 7.40 (d,  $J = 8.5$  Hz, 2H), 7.13 (t,  $J = 8.0$  Hz, 2H), 6.96 (d,  $J = 8.0$  Hz, 2H), 6.81 (d,  $J = 8.5$  Hz, 2H), 6.60 (s, 1H), 6.48 (d,  $J = 7.0$  Hz, 2H), 5.24 (s, 1H).  $^{13}\text{C}$  NMR (DMSO- $d_6$ , 101 MHz):  $\delta$  157.8, 143.4, 134.4, 131.9, 129.1, 126.8, 115.1, 114.8, 112.4, 104.2, 66.3. HRMS: ( $m/z$ ) calcd. for  $\text{C}_{17}\text{H}_{14}\text{N}_2\text{O}$  [ $\text{M} + \text{H}^+$ ]: 263.1184, found: 263.1185.

**4-(1H-perimidin-2-yl)phenol (NSC83713).** To a stirred solution of 4-(2,3-dihydro-1H-perimidin-2-yl)phenol (498 mg, 1.90 mmol) in a 1:3 water-ethanol mixture, sodium disulfite (361 mg, 1.90 mmol) was added and the mixture was left to stir at reflux temperature for 4 h. The hot crude mixture was filtered and the filtrate was diluted with cold water in order to precipitate the desired product (203 mg, 41% yield).  $^1\text{H}$  NMR (DMSO- $d_6$ , 400 MHz):  $\delta$  10.54 (s, br, 1H), 10.06 (s, 1H), 7.89 (d,  $J = 8.5$  Hz, 2H), 7.14 (t,  $J = 8.0$  Hz, 2H), 7.01 (d,  $J = 8.0$  Hz, 2H), 6.89 (d,  $J = 8.5$  Hz, 2H), 6.59 (d,  $J = 7.5$  Hz, 2H).  $^{13}\text{C}$  NMR (DMSO- $d_6$ , 101 MHz):  $\delta$  160.1, 152.4, 135.0, 128.6, 128.4 (br, x2C), 123.8, 121.2, 118.1 (br, x2C), 115.1. HRMS: ( $m/z$ ) calcd. for  $\text{C}_{17}\text{H}_{12}\text{N}_2\text{O}$  [ $\text{M} + \text{H}^+$ ]: 261.1028, found: 261.1005.

**General procedure for the preparation of oxo-dihydroquinoxaline derivatives.** To a stirred solution of the corresponding diamine (1 eq.) in acetonitrile, diethyl acetylenedicarboxylate (1 eq.) was added and the mixture was left to stir at room temperature for the designed period of time. The reaction was partitioned with ethyl acetate and water, extracted with ethyl acetate, dried over  $\text{MgSO}_4$  and concentrated in vacuo. Purification by recrystallisation from hot dichloromethane afforded the desired products after filtration.

**Ethyl 2-(3-oxo-3,4-dihydroquinoxalin-2(1H)-ylidene)acetate (1).** Following the general procedure using *o*-phenylenediamine (600 mg, 0.94 mmol) with a reaction time of 4 h, the desired product could be isolated (1.15 g, 89% yield).  $^1\text{H}$  NMR (DMSO- $d_6$ , 400 MHz):  $\delta$  11.73 (s, 1H), 11.05 (s, 1H), 7.41–7.35 (m, 1H), 7.09–6.96 (m, 3H), 5.49 (s, 1H), 4.15 (q,  $J = 7.0$  Hz, 2H), 1.24 (t,  $J = 7.0$  Hz, 3H).  $^{13}\text{C}$  NMR (DMSO- $d_6$ , 101 MHz):  $\delta$  169.2, 155.6, 144.0, 125.1, 124.8, 123.4, 122.5, 115.4, 115.2, 83.7, 59.1, 14.3. HRMS: ( $m/z$ ) calcd. for  $\text{C}_{12}\text{H}_{13}\text{N}_2\text{O}_3$  [ $\text{M} + \text{H}^+$ ]: 233.0926, found: 233.0929.

**Ethyl 2-(6-cyano-3-oxo-3,4-dihydroquinoxalin-2(1H)-ylidene)acetate (2).** Following the general procedure using 3,4-diaminobenzonitrile (125 mg, 0.92 mmol) with a reaction time of 5 h, the desired product could be isolated (155 mg, 65% yield).

$^1\text{H}$  NMR (DMSO- $d_6$ , 400 MHz):  $\delta$  12.02 (s, 1H), 11.05 (s, 1H), 7.98

(d,  $J = 1.5$  Hz, 1H), 7.43 (dd,  $J = 8.5, 1.5$  Hz, 1H), 7.14 (d,  $J = 8.5$  Hz, 1H), 5.55 (s, 1H), 4.17 (q,  $J = 7.0$  Hz, 2H), 1.25 (t,  $J = 7.0$  Hz, 3H).  $^{13}\text{C}$  NMR (DMSO- $d_6$ , 101 MHz):  $\delta$  168.6, 155.8, 143.0, 129.3, 126.2, 125.6, 119.0, 118.9, 115.9, 105.0, 85.7, 59.4, 14.3. HRMS: ( $m/z$ ) calcd. for  $\text{C}_{13}\text{H}_{11}\text{N}_3\text{O}_3$  [ $\text{M} + \text{H}^+$ ]: 258.0879, found: 258.0861.

**Ethyl 2-(6,7-dichloro-3-oxo-3,4-dihydroquinoxalin-2(1H)-ylidene)acetate (3).** Following the general procedure using 4,5-dichlorobenzene-1,2-diamine (177 mg, 1.0 mmol) with a reaction time of 20 h, the desired product could be isolated (203 mg, 67% yield).  $^1\text{H}$  NMR (DMSO- $d_6$ , 400 MHz):  $\delta$  11.81 (s, 1H), 10.96 (s, 1H), 7.80 (s, 1H), 7.12 (s, 1H), 5.52 (s, 1H), 4.14 (q,  $J = 7.0$  Hz, 2H), 1.24 (t,  $J = 7.0$  Hz, 3H).  $^{13}\text{C}$  NMR (DMSO- $d_6$ , 101 MHz):  $\delta$  168.5, 155.4, 142.7, 125.4, 125.3, 124.8, 123.4, 116.8, 115.8, 85.9, 59.3, 30.68, 14.3. HRMS: ( $m/z$ ) calcd. for  $\text{C}_{12}\text{H}_{10}\text{Cl}_2\text{N}_2\text{O}_3$  [ $\text{M} + \text{H}^+$ ]: 301.0147, found: 301.0124.

**General Procedure for the preparation of oxo-dihydroquinoxaline acetohydrazide derivatives.** To a stirred solution of the corresponding 3-oxo-3,4-dihydroquinoxalin-2(1H)-ylidene ester (1 eq.) in ethanol, hydrazine hydrate (10 eq.) was added dropwise and the mixture was heated to reflux under an inert atmosphere and left to stir for 3–6 h. Upon cooling, the crude mixture was filtered, washed with ethanol and dried affording the desired product.

**2-(3-Oxo-3,4-dihydroquinoxalin-2(1H)-ylidene)acetohydrazide (4).** Following the general procedure using ethyl 2-(3-oxo-3,4-dihydroquinoxalin-2(1H)-ylidene)acetate (1) (400 mg, 1.72 mmol), the desired product was obtained (297 mg, 79% yield) as a mixture of tautomers, being the tautomeric ratio(enamine-imine) = 1:6. Spectroscopic data refers to major compound.  $^1\text{H}$  NMR (DMSO- $d_6$ , 400 MHz):  $\delta$  11.62 (s, 1H), 9.14 (s, 1H), 7.10 (d,  $J = 8.0$  Hz, 1H), 6.98 (t,  $J = 8.0$  Hz, 2H), 6.89 (t,  $J = 7.5$  Hz, 1H), 5.58 (s, 1H), 4.30 (s, br, 2H), 4.23 (s, br, 1H).  $^{13}\text{C}$  NMR (DMSO- $d_6$ , 101 MHz):  $\delta$  168.6, 156.5, 140.1, 125.7, 124.7, 123.4, 121.1, 115.1, 114.1, 86.8. HRMS: ( $m/z$ ) calcd. for  $\text{C}_{10}\text{H}_{10}\text{N}_4\text{O}_2$  [ $\text{M} + \text{H}^+$ ]: 219.0882, found: 219.0853.

**2-(6-Cyano-3-oxo-3,4-dihydroquinoxalin-2(1H)-ylidene)acetohydrazide (5).** Following the general procedure using ethyl 2-(6-cyano-3-oxo-3,4-dihydroquinoxalin-2(1H)-ylidene)acetate (2) (100 mg, 0.39 mmol), the desired product was obtained (74 mg, 78% yield) as a mixture of tautomers, being the tautomeric ratio(enamine-imine) = 9:1. Spectroscopic data refers to major compound.  $^1\text{H}$  NMR (DMSO- $d_6$ , 400 MHz):  $\delta$  11.61 (s, 1H), 9.25 (s, 1H), 7.69 (s, 1H), 7.31 (d,  $J = 8.0$  Hz, 1H), 7.06 (d,  $J = 8.0$  Hz, 1H), 5.65 (s, 1H), 4.35 (s, br, 2H).  $^{13}\text{C}$  NMR (DMSO- $d_6$ , 101 MHz):  $\delta$  167.9, 156.6, 138.9, 128.9, 126.5, 125.0, 119.0, 117.5, 115.7, 105.0, 88.8. HRMS: ( $m/z$ ) calcd. for  $\text{C}_{11}\text{H}_9\text{N}_5\text{O}_2$  [ $\text{M} + \text{H}^+$ ]: 244.0835, found: 244.0825.

**2-(6,7-Dichloro-3-oxo-3,4-dihydroquinoxalin-2(1H)-ylidene)acetohydrazide (6).** Following the general procedure using ethyl 2-(6,7-dichloro-3-oxo-3,4-dihydroquinoxalin-2(1H)-ylidene)acetate (3) (600 mg, 2.00 mmol), the desired product was obtained (467 mg, 82% yield) as a mixture of tautomers, being the tautomeric ratio(enamine-imine) = 4:1. Spectroscopic data refers to major compound.  $^1\text{H}$  NMR (DMSO- $d_6$ , 400 MHz):  $\delta$  11.56 (s, 1H), 9.24 (s, 1H), 7.59 (s, 1H), 7.09 (s, 1H), 5.65 (s, 1H), 4.34 (s, br, 2H), 4.17 (s, br, 1H).  $^{13}\text{C}$  NMR (DMSO- $d_6$ , 101 MHz):  $\delta$  167.9, 156.3, 138.8, 126.2, 125.2, 124.7, 121.9, 115.8, 115.5, 88.9. HRMS: ( $m/z$ ) calcd. for  $\text{C}_{10}\text{H}_8\text{Cl}_2\text{N}_4\text{O}_2$  [ $\text{M} + \text{H}^+$ ]: 287.0103, found: 287.0072.

**General procedure for the preparation of *N'*-substituted oxo-dihydroquinoxaline acetohydrazide derivatives.** To a stirred solution of the corresponding 3-oxo-3,4-dihydroquinoxalin-2(1H)-ylidene acetohydrazide (1 eq.) in ethanol, the corresponding aldehyde (1 eq.) was added dropwise and the mixture was heated to reflux under an inert atmosphere and left to stir for 3–6 h. Upon cooling, the crude mixture was filtered and crude was washed with ethanol and dried affording the desired product. The desired products were obtained as mixtures of both the enamine and the

imine tautomer of the *E* and the *Z* hydrazone regioisomers respectively, affording complex NMR spectra containing 4 different species. Due to this high complexity, the chemical shift values for these compounds are not quoted below.

***N'*-Butylidene-2-(3-oxo-3,4-dihydroquinoxalin-2(1*H*)-ylidene)acetohydrazide (7).** Following the general procedure using 2-(3-oxo-3,4-dihydroquinoxalin-2(1*H*)-ylidene)acetohydrazide (**4**) (60 mg, 0.29 mmol) and butyraldehyde (0.03 mL, 0.29 mmol), the desired product was obtained (35 mg, 44% yield). HRMS: (*m/z*) calcd. for C<sub>14</sub>H<sub>16</sub>N<sub>4</sub>O<sub>2</sub> [M + H]<sup>+</sup>: 273.1352, found: 273.1339.

***N'*-Benzylidene-2-(3-oxo-3,4-dihydroquinoxalin-2(1*H*)-ylidene)acetohydrazide (8).** Following the general procedure using 2-(3-oxo-3,4-dihydroquinoxalin-2(1*H*)-ylidene)acetohydrazide (**4**) (100 mg, 0.46 mmol) and benzaldehyde (0.05 mL, 0.46 mmol), the desired product was obtained (99 mg, 70% yield). HRMS: (*m/z*) calcd. for C<sub>17</sub>H<sub>14</sub>N<sub>4</sub>O<sub>2</sub>: 307.1195, found: 307.1167.

***N'*-Benzylidene-2-(6-cyano-3-oxo-3,4-dihydroquinoxalin-2(1*H*)-ylidene)acetohydrazide (9).** Following the general procedure using 2-(6-cyano-3-oxo-3,4-dihydroquinoxalin-2(1*H*)-ylidene)acetohydrazide (**5**) (50 mg, 0.21 mmol) and salicylaldehyde (0.02 mL, 0.21 mmol), the desired product was obtained (35 mg, 50% yield). HRMS: (*m/z*) calcd. for C<sub>18</sub>H<sub>13</sub>N<sub>5</sub>O<sub>2</sub> [M + H]<sup>+</sup>: 332.1147, found: 332.1140.

***N'*-Benzylidene-2-(6,7-dichloro-3-oxo-3,4-dihydroquinoxalin-2(1*H*)-ylidene)acetohydrazide (10).** Following the general procedure using 2-(6,7-dichloro-3-oxo-3,4-dihydroquinoxalin-2(1*H*)-ylidene)acetohydrazide (**6**) (100 mg, 0.35 mmol) and benzaldehyde (0.04 mL, 0.35 mmol), the desired product was obtained (71 mg, 54% yield). HRMS: (*m/z*) calcd. for C<sub>17</sub>H<sub>12</sub>Cl<sub>2</sub>N<sub>4</sub>O<sub>2</sub> [M + H]<sup>+</sup>: 375.0416, found: 375.0399.

**2-(3-Oxo-3,4-dihydroquinoxalin-2(1*H*)-ylidene)-*N'*-(pyridin-2-ylmethylene)acetohydrazide (11).** Following the general procedure using 2-(3-oxo-3,4-dihydroquinoxalin-2(1*H*)-ylidene)acetohydrazide (**4**) (100 mg, 0.46 mmol) and 2-pyridinecarboxaldehyde (0.04 mL, 0.46 mmol), the desired product was obtained (129 mg, 91% yield). HRMS: (*m/z*) calcd. for C<sub>16</sub>H<sub>13</sub>N<sub>5</sub>O<sub>2</sub> [M + H]<sup>+</sup>: 308.1147, found: 308.1136.

**2-(6,7-Dichloro-3-oxo-3,4-dihydroquinoxalin-2(1*H*)-ylidene)-*N'*-(pyridin-2-ylmethylene)acetohydrazide (12).** Following the general procedure using 2-(6,7-dichloro-3-oxo-3,4-dihydroquinoxalin-2(1*H*)-ylidene)acetohydrazide (**6**) (100 mg, 0.35 mmol) and 2-pyridinecarboxaldehyde (0.03 mL, 0.35 mmol), the desired product was obtained (102 mg, 78% yield). HRMS: (*m/z*) calcd. for C<sub>16</sub>H<sub>11</sub>Cl<sub>2</sub>N<sub>5</sub>O<sub>2</sub> [M + H]<sup>+</sup>: 376.0368, found: 376.0370.

***N'*-(2-Hydroxybenzylidene)-2-(3-oxo-3,4-dihydroquinoxalin-2(1*H*)-ylidene)acetohydrazide (13).** Following the general procedure using 2-(3-oxo-3,4-dihydroquinoxalin-2(1*H*)-ylidene)acetohydrazide (**4**) (100 mg, 0.46 mmol) and salicylaldehyde (0.05 mL, 0.46 mmol), the desired product was obtained (126 mg, 85% yield). HRMS: (*m/z*) calcd. for C<sub>17</sub>H<sub>14</sub>N<sub>4</sub>O<sub>3</sub> [M + H]<sup>+</sup>: 323.1144, found: 323.1128.

**2-(6,7-Dichloro-3-oxo-3,4-dihydroquinoxalin-2(1*H*)-ylidene)-*N'*-(2-hydroxybenzylidene)acetohydrazide (14).** Following the general procedure using 2-(6,7-dichloro-3-oxo-3,4-dihydroquinoxalin-2(1*H*)-ylidene)acetohydrazide (**6**) (100 mg, 0.35 mmol) and salicylaldehyde (0.04 mL, 0.35 mmol), the desired product was obtained (130 mg, 95% yield). HRMS: (*m/z*) calcd. for C<sub>17</sub>H<sub>12</sub>Cl<sub>2</sub>N<sub>4</sub>O<sub>2</sub> [M + H]<sup>+</sup>: 391.0365, found: 391.0356.

**5-nitro-1,3-dioxo-1*H*-benzo[*de*]isoquinolin-2(3*H*)-yl *p*-toluenesulfonate (15).** 3-nitro-1,8-naphthalic anhydride (500 mg, 2.06 mmol) and hydroxylamine hydrochloride (142.9 mg, 2.06 mmol) were dissolved in pyridine (7 mL) and the resulting reaction mixture was heated to reflux for 1 h. Then, the reaction was cooled to 80 °C and *p*-toluenesulfonyl chloride (784 mg, 4.11 mmol) was added. The reaction mixture was heated to reflux

for 2 additional hours and after this time, it was cooled to room temperature and it was poured into ice water (50 mL) and stirred. The resulting precipitate was filtered and rinsed with additional cold water and saturated NaHCO<sub>3</sub> to yield the desired compound (830 mg, 2.06 mmol, quantitative yield). <sup>1</sup>H NMR (400 MHz, CDCl<sub>3</sub>) δ (ppm): 9.30 (s, 1H), 9.19 (s, 1H), 8.81 (d, *J* = 8.4 Hz, 1H), 8.52 (d, *J* = 8.3 Hz, 1H), 8.0 (m, 3H), 7.44 (m, 2H), 2.52 (s, 3H). <sup>13</sup>C NMR (101 MHz, CDCl<sub>3</sub>) δ (ppm): 159.3, 158.7, 147.3, 146.8, 137.24, 136.0, 134.0, 132.3, 131.8, 130.5, 130.4, 130.0, 129.8, 125.7, 124.8, 123.2, 22.41. HRMS: (*m/z*) calcd. for C<sub>19</sub>H<sub>12</sub>N<sub>2</sub>O<sub>7</sub>S [M+H]<sup>+</sup>: 413.0443, found 413.0409.

**4-nitrobenzo[*cd*]indol-2(1*H*)-one (16) and 7-nitrobenzo[*cd*]indol-2(1*H*)-one (17).** Compound **15** (778 mg, 1.89 mmol) was dissolved in ethanol (5 mL) and water (4 mL) and an aqueous solution of sodium hydroxide (2.7 M, 3 mL) was added at room temperature. The resulting mixture was heated to reflux temperature for 1 h while distilling the ethanol. When TLC showed the completeness of the reaction, the mixture was cooled to 75 °C and concentrated hydrochloric acid was added dropwise until a yellow precipitate was formed. After cooling at room temperature, the precipitate was collected by filtration and washed with water, yielding a mixture of 4- and 7-nitrobenzo[*cd*]indol-2(1*H*)-one (390 mg, 1.82 mmol, 97%) in a 2:1 ratio. **4-Nitrobenzo[*cd*]indol-2(1*H*)-one (16)** <sup>1</sup>H NMR (400 MHz, DMSO-*d*<sub>6</sub>) δ (ppm): 11.14 (s, 1H), 9.21 (d, *J* = 1.6 Hz, 1H), 8.59 (d, *J* = 1.6 Hz, 1H), 7.86 (d, *J* = 8.5 Hz, 1H), 7.67 (dd, *J* = 8.5, 7.2 Hz, 1H), 7.19 (d, *J* = 7.1 Hz, 1H); **7-Nitrobenzo[*cd*]indol-2(1*H*)-one (17).** <sup>1</sup>H NMR (400 MHz, DMSO-*d*<sub>6</sub>) δ (ppm): 11.14 (s, 1H), 8.73 (d, *J* = 1.5 Hz, 1H), 8.48 (d, *J* = 8.1 Hz, 1H), 8.24 (d, *J* = 7.0 Hz, 1H), 7.98 (dd, *J* = 8, 7.5 Hz, 1H), 7.58 (d, *J* = 1.6 Hz, 1H). HRMS: (*m/z*) calcd. for C<sub>11</sub>H<sub>6</sub>N<sub>2</sub>O<sub>3</sub> [M - H]<sup>-</sup>: 213.0300, found 213.0344.

**4-aminobenzo[*cd*]indol-2(1*H*)-one (18) and 7-aminobenzo[*cd*]indol-2(1*H*)-one (19).** SnCl<sub>2</sub> (2.6 g, 13.89 mmol) was mixed with HCl (37%, 14 mL) and water (5 mL). To this solution, a mixture of 4-nitrobenzo[*cd*]indol-2(1*H*)-one (**16**) and 7-nitrobenzo[*cd*]indol-2(1*H*)-one (**17**) (700 mg, 3.27 mmol) was slowly added under stirring. The mixture was heated at 50 °C for 4 h until TLC showed completion of the reaction. After cooling the mixture to 0 °C, the reaction was basified to pH 10 by adding a solution of 6 M NaOH. The reaction mixture was then extracted with ethyl acetate (x3). The combined organic layers were then dried (MgSO<sub>4</sub>) and concentrated under reduced pressure to afford a 2:1 mixture of 4- and 7-aminobenzo[*cd*]indol-2(1*H*)-one (540 mg) that was separated by flash chromatography (Isolera Biotage, SNAP Cartridge KP-Sil 25 g, eluent CH<sub>2</sub>Cl<sub>2</sub>/MeOH (from 98:2 to 97:3), yielding pure **18** (103.6 mg, 0.56 mmol) and **19** (56.2 mg, 0.31 mmol), together with a mixed fraction of both (369.1 mg, 2.00 mmol) with an overall yield of 88%. **4-aminobenzo[*cd*]indol-2(1*H*)-one (18).** <sup>1</sup>H NMR (400 MHz, CD<sub>3</sub>OD) δ (ppm): 7.50 (d, *J* = 1.6 Hz, 1H), 7.31 (m, 2H), 7.23 (d, *J* = 1.5 Hz, 1H), 6.73 (dd, *J* = 6.0, 1.4 Hz, 1H). <sup>13</sup>C NMR (101 MHz, CD<sub>3</sub>OD) δ (ppm): 170.9, 149.6, 137.2, 130.7, 128.6, 127.5, 119.6, 118.5, 114.4, 111.9, 103.2. HRMS: (*m/z*) calcd. for C<sub>11</sub>H<sub>8</sub>N<sub>2</sub>O [M+H]<sup>+</sup>: 185.0715, found 185.0702; **7-aminobenzo[*cd*]indol-2(1*H*)-one (19).** <sup>1</sup>H NMR (400 MHz, CD<sub>3</sub>OD) δ (ppm): 7.75 (d, *J* = 8.0 Hz, 1H), 7.67 (d, *J* = 6.8 Hz, 1H), 7.57 (dd, *J* = 8.1, 7.1 Hz, 1H), 6.65 (d, *J* = 1.4 Hz, 1H), 6.62 (d, *J* = 1.4 Hz, 1H). <sup>13</sup>C NMR (101 MHz, CD<sub>3</sub>OD) δ (ppm): 172.8, 150.4, 139.5, 132.3, 129.7, 129.5, 127.3, 122.3, 120.0, 101.6, 99.9. HRMS: (*m/z*) calcd. for C<sub>11</sub>H<sub>8</sub>N<sub>2</sub>O [M+H]<sup>+</sup>: 185.0715, found: 185.0712.

**4-((3-chloro-2-hydroxypropyl)amino)benzo[*cd*]indol-2(1*H*)-one (NSC611216) and 7-((3-chloro-2-hydroxypropyl)amino)benzo[*cd*]indol-2(1*H*)-one (20).** To a solution of LiClO<sub>4</sub> (101.7 mg, 0.96 mmol) and epichlorohydrin (22.1 mg, 0.24 mmol) in acetonitrile (2 mL), a mixture of anilines **18** and **19** (44 mg, 0.24 mmol) was added and stirred under microwave irradiation for 60 min

(T = 150 °C, P = 150 PSI, P = 150 W). The reaction mixture was diluted with water and extracted with ethyl acetate (x3). The combined organic layers were dried over MgSO<sub>4</sub>, filtered, and concentrated in vacuo, giving a crude product which was purified by flash chromatography using CH<sub>2</sub>Cl<sub>2</sub>/MeOH (100:0 + 1% NEt<sub>3</sub> to 95:5 + 1% NEt<sub>3</sub>) to afford **NSC611216** (18 mg, 28%) and **20** (10 mg, 15%). **NSC611216**: <sup>1</sup>H NMR (400 MHz, CD<sub>3</sub>OD) δ (ppm): = 7.53 (d, J = 1.7 Hz, 1H), 7.39–7.30 (m, 2H), 7.14 (d, J = 1.7 Hz, 1H), 6.73 (dd, J = 5.3, 2.2 Hz, 1H), 4.09 (m, 1H), 3.77–3.64 (dq, J = 11.2 Hz, 3.2 Hz, 2H), 3.51 (dd, J = 7.6 Hz, 5.2 Hz, 1H), 3.33 (m, 1H). <sup>13</sup>C NMR (101 MHz, CD<sub>3</sub>OD) δ (ppm): 175.5, 151.6, 138.7, 132.3, 130.1, 129.0, 120.7, 120.1, 115.4, 109.3, 104.5, 70.8, 48.3, 48.1. HRMS: (m/z) calcd for C<sub>14</sub>H<sub>13</sub>ClN<sub>2</sub>O<sub>2</sub> [M+H]<sup>+</sup>: 277.0587, found 277.0280; **20**: <sup>1</sup>H NMR (400 MHz, CD<sub>3</sub>OD) δ (ppm): = 7.38 (d, J = 1.0 Hz, 1H), 7.31 (d, J = 1.7 Hz, 1H), 6.96 (d, J = 1.7 Hz, 1H), 6.77 (dd, J = 5.9, 1.7 Hz, 2H), 4.59 (br s, 1H), 4.31 (m, 1H), 3.80–3.64 (m, 2H), 3.51 (dd, J = 13.4, 5.2 Hz, 1H), 3.35 (m, 1H). <sup>13</sup>C NMR (101 MHz, CD<sub>3</sub>OD) δ (ppm): 172.3, 151.6, 138.7, 131.8, 130.3, 128.9, 125.7, 112.3, 110.5, 104.9, 63.0, 48.3, 48.1. HRMS: (m/z) calcd for C<sub>14</sub>H<sub>13</sub>ClN<sub>2</sub>O<sub>2</sub> [M+H]<sup>+</sup>: 277.0744, found 277.0765.

**6-nitrobenz[cd]indol-2(1H)-one (21)**. To a solution of benzo[cd]indol-2(1H)-one (500 mg, 3 mmol) in 5 mL of glacial acetic acid, a solution of 70% nitric acid (171 μL, 3.84 mmol) was added dropwise. The reaction mixture was heated to 50 °C for 1.5 h and then cooled to room temperature. The resulting greenish suspension was filtered, washed with 50% aqueous acetic acid, and dried. The solid obtained was refluxed in 7 mL MeOH during 4 h (the solution turned orange) and then cooled to 0 °C. Finally, the mixture was filtered, washed with cold MeOH and dried under reduced pressure to afford a wet orange filter cake (700 mg) which was carried into the next reaction without further manipulation [59]. <sup>1</sup>H NMR (400 MHz, DMSO-*d*<sub>6</sub>) δ (ppm): 9.07 (d, J = 8.5 Hz, 1H), 8.62 (d, J = 8.1 Hz, 1H), 8.18 (d, J = 7.0 Hz, 1H), 7.98 (dd, J = 8.6, 7.0 Hz, 1H), 7.02 (d, J = 8.0 Hz, 1H); HRMS: (m/z) calcd for C<sub>11</sub>H<sub>6</sub>N<sub>2</sub>O<sub>3</sub> [M – H]<sup>-</sup>: 213.0300 found 213.0341.

**6-aminobenzo[cd]indol-2(1H)-one (22)**. Compound **21** (171 mg, 0.8 mmol) was slowly added as a solid under stirring to a solution of SnCl<sub>2</sub> (645 mg, 3.40 mmol) in HCl (37%, 4 mL) and water (1.5 mL). The reaction mixture was stirred at 50 °C for 4 h. Then it was cooled to 0 °C and basified to pH 10 by adding an aqueous solution of NaOH (6 M). The crude was then extracted with ethyl acetate (x3) and the combined organic layers were dried over MgSO<sub>4</sub> and concentrated under reduced pressure and filtered through Celite<sup>®</sup> to afford the desired compound (147 mg, 0.798 mmols, quantitative yield). <sup>1</sup>H NMR (400 MHz, DMSO-*d*<sub>6</sub>) δ (ppm): 10.87 (br s, 1H), 8.32 (d, J = 8.2 Hz, 1H), 8.09 (d, J = 6.9 Hz, 1H), 7.91 (dd, J = 8.3, 7.0 Hz, 1H), 7.41 (d, J = 7.4 Hz, 1H), 6.97 (d, J = 7.5 Hz, 1H). <sup>13</sup>C NMR (101 MHz, DMSO-*d*<sub>6</sub>) δ (ppm): 168.6, 137.2, 131.5, 129.4, 127.1, 125.9, 124.8, 123.4, 123.3, 122.2, 105.9; HRMS: (m/z) calcd. for C<sub>11</sub>H<sub>8</sub>N<sub>2</sub>O [M+H]<sup>+</sup>: 185.0715, found 185.0689.

**6-((3-chloro-2-hydroxypropyl)amino)benzo[cd]indol-2(1H)-one (23)**. To a solution of LiClO<sub>4</sub> (76.7 mg, 0.72 mmol) and epichlorohydrin (20 mg, 0.22 mmol) in ethanol (2 mL) the aniline **22** (40 mg, 0.22 mmol) was added dropwise and the mixture was heated at 80 °C overnight. After this time another equivalent of epichlorohydrin was added and the reaction was heated again for 24 h. Water (2 mL) was added, and the reaction mixture was extracted with ethyl acetate (3 × 5 mL). The combined organic phases were washed with brine and concentrated in vacuo. The residue was then purified by flash chromatography on silica gel (CH<sub>2</sub>Cl<sub>2</sub>/MeOH, gradient from 0 to 10% of MeOH) to obtain compound **23** (12.6 mg, 0.045 mmol, 21%) together with unreacted starting material (22.4 mg, 0.122 mmol, 54%). <sup>1</sup>H NMR (400 MHz, CD<sub>3</sub>OD) δ (ppm): 8.33 (d, J = 8.2 Hz, 1H), 8.05 (d, J = 7.0 Hz, 1H), 7.72 (dd, J = 8.2, 7.0 Hz, 1H), 6.89 (d, J = 7.7 Hz, 1H), 6.52 (d, J = 7.6 Hz,

1H), 4.17 (m, 1H), 3.51–3.99 (m, 4H), 3.36 (s, OH). <sup>13</sup>C NMR (101 MHz, CD<sub>3</sub>OD) δ (ppm): 171.5, 165.0, 128.31, 128.1, 127.5, 125.3, 123.3, 110.4, 105.7, 105.0, 70.5, 49.3, 48.2. HRMS: (m/z) calcd. for C<sub>14</sub>H<sub>13</sub>ClN<sub>2</sub>O<sub>2</sub> [M+H]<sup>+</sup>: 277.0744, found 277.0737 [M+H].

**5-Nitro-1H-benzo[de]isoquinoline-1,3(2H)-dione (24)**. To a solution of commercial available 3-nitro-1,8-naphthalic anhydride (560 mg, 2.30 mmol) in H<sub>2</sub>O (10 mL) ammonium hydroxide (448 μL) was added and the reaction mixture was heated at reflux for 4 h. The mixture was then cooled to 0 °C, and the resulting precipitate was collected by filtration and washed with cold water and ethanol. The solid was dried under vacuum to give the expected product that was used without further purification (486.7 mg, 2.01 mmol, 87%). <sup>1</sup>H NMR (400 MHz, DMSO-*d*<sub>6</sub>) δ (ppm): 12.03 (br s, 1H), 9.43 (d, J = 2.4 Hz, 1H), 8.87 (d, J = 2.3 Hz, 1H), 8.74 (d, J = 8.3 Hz, 1H), 8.60 (dd, J = 7.2, 1.1 Hz, 1H), 8.02 (t, J = 7.5 Hz, 1H). <sup>13</sup>C NMR (101 MHz, CD<sub>3</sub>OD) δ (ppm): 163.5, 162.9, 145.8, 136.3, 133.1, 131.1, 130.8, 129.7, 129.1, 124.5, 123.0, 122.2. HRMS: (m/z) calcd. for C<sub>12</sub>H<sub>6</sub>N<sub>2</sub>O<sub>4</sub> [M – H]<sup>-</sup>: 241.0249, found 241.0219.

**5-Amino-1H-benzo[de]isoquinoline-1,3(2H)-dione (25)**. Compound **24** (300 mg, 1.24 mmol) was slowly added as a solid under stirring to a solution of SnCl<sub>2</sub> (998 mg, 5.26 mmol) in HCl (37%, 12 mL) and water (5 mL). The resulting reaction mixture was heated at 50 °C until completeness of the reaction. After cooling the mixture to 0 °C, the reaction was basified to pH 10 by adding a solution of 6 M NaOH. The desired amine was extracted with ethyl acetate (x3). The combined organic extracts were dried (MgSO<sub>4</sub>) and concentrated under vacuum to afford compound **25** (283 mg, quantitative yield). <sup>1</sup>H NMR (400 MHz, DMSO-*d*<sub>6</sub>) δ (ppm): 11.51 (br s, 1H), 8.0 (d, J = 7.7 Hz, 2H), 7.89 (d, J = 2.3 Hz, 1H), 7.58 (t, J = 7.7 Hz, 1H), 7.26 (d, J = 2.3 Hz, 1H), 5.95 (s, 2H). <sup>13</sup>C NMR (101 MHz, DMSO-*d*<sub>6</sub>) δ (ppm): 164.5, 164.3, 147.8, 133.8, 131.5, 126.8, 124.7, 123.1, 122.2, 121.8, 121.0, 111.7. HRMS: (m/z) calcd. for C<sub>12</sub>H<sub>8</sub>N<sub>2</sub>O<sub>2</sub> [M+H]<sup>+</sup>: 213.0664, found 213.0647.

**5-((3-chloro-2-hydroxypropyl)amino)-1H-benzo[de]isoquinoline-1,3(2H)-dione (26)**.

Epichlorohydrin (36.8 μL, 0.47 mmol) was dissolved in DMF (1 mL) and LiBr (5% mol, 0.0235 mmol) was added followed by aniline **25** (100 mg, 0.47 mmol). The mixture was heated at 100 °C overnight. After this time, the reaction mixture was diluted with water and extracted with ethyl acetate (x3). The combined organic layers were dried over MgSO<sub>4</sub>, filtered and concentrated in vacuo to give a crude product, which was purified by flash chromatography (Isolera Biotage, SNAP Cartridge KP-C18-HS 12 g, SNAP Flash, using water + 0.1% HCOOH/ACN + 0.1% HCOOH (from 90:10 to 80:20) as eluent, to afford the desired compound (16 mg, 0.057 mmol) with a 12% yield. <sup>1</sup>H NMR (400 MHz, CD<sub>3</sub>OD) δ (ppm): 8.20 (dd, J = 7.1, 0.8 Hz, 1H), 8.04 (d, J = 2.3 Hz, 1H), 7.99 (d, J = 8.0 Hz, 2H), 7.60 (t, J = 7.5 Hz, 1H), 7.37 (d, J = 2.2 Hz, 1H), 4.45–4.37 (m, 1H), 4.26–4.15 (m, 2H), 3.72–3.57 (ddd, J = 30.6, 11.3, 4.2 Hz, 2H). <sup>13</sup>C NMR (101 MHz, CD<sub>3</sub>OD) δ (ppm): 166.5, 166.2, 148.9, 135.3, 133.1, 128.0, 127.7, 124.1, 123.4, 123.3, 123.1, 114.7, 70.3, 48.5, 44.6. HRMS: (m/z) calcd. for C<sub>15</sub>H<sub>13</sub>ClN<sub>2</sub>O<sub>3</sub> [M+H]<sup>+</sup>: 305.0693, found 305.0613.

**General procedure for the synthesis of aminobenz[cd]indol-2(1H)-one derivatives**. A solution of LiClO<sub>4</sub> (4 eq) and the corresponding epoxide (1.5 eq) in EtOH was added to a 2:1 mixture of 4- and 7-aminobenzo[cd]indol-2(1H)-one (**18** and **19**, 1 eq) and the reaction mixture was heated to reflux (80 °C) overnight. The solvent was then eliminated under reduced pressure and the residue was purified by flash chromatography using CH<sub>2</sub>Cl<sub>2</sub>/MeOH as eluent. Alternatively, the reaction mixture was heated under microwave irradiation for 60 min (T = 150 °C, P = 150 W), then diluted with water and extracted with ethyl acetate (x3). The organic layer was dried over MgSO<sub>4</sub> and concentrated under reduced pressure, giving a crude which was purified by flash chromatography using mixture of CH<sub>2</sub>Cl<sub>2</sub>/MeOH as eluent.

**4-((2-hydroxybutyl)amino)benzo[*cd*]indol-2(1*H*)-one (27) and 7-((2-hydroxybutyl)amino)benzo[*cd*]indol-2(1*H*)-one (28).**

General procedure was applied to 40 mg, (0.22 mmol) of a mixture 2:1 of 4- and 7-aminobenzo[*cd*]indol-2(1*H*)-one and (*R,S*)-( $\pm$ )-1,2-epoxybutane to yield 29 mg of **27** (0.113 mmol, 52%), 8.4 mg of **28** (0.033 mmol, 15%) together with 10.6 mg (0.061 mmols, 28%) of unreacted anilines. (**27**)  $^1\text{H}$  NMR (400 MHz,  $\text{CD}_3\text{OD}$ )  $\delta$  (ppm): 7.50 (d,  $J = 1.6$  Hz, 1H), 7.32 (m, 1H), 7.07 (d,  $J = 1.6$  Hz, 1H), 6.71 (dd,  $J = 5$ , 2.5 Hz, 1H), 3.76 (m, 1H), 3.32 (dd,  $J = 13.5$ , 4.3 Hz), 3.14 (dd,  $J = 13$ , 7.3 Hz), 1.70 (m, 1H), 1.54 (m, 1H), 1.04 (t,  $J = 7.5$  Hz, 3H).  $^{13}\text{C}$  NMR (101 MHz,  $\text{CD}_3\text{OD}$ )  $\delta$  (ppm): 172.4, 151.8, 138.6, 132.3, 130.0, 128.8, 120.5, 120.1, 115.4, 109.2, 104.4, 72.3, 51.0, 29.0, 10.4. HRMS: ( $m/z$ ) calcd. for  $\text{C}_{15}\text{H}_{16}\text{N}_2\text{O}_2$  [ $\text{M}+\text{H}$ ] $^+$ : = 257.1290, found 257.1306. (**28**)  $^1\text{H}$  NMR (400 MHz,  $\text{CD}_3\text{OD}$ )  $\delta$  (ppm): 7.78 (d,  $J = 8.0$  Hz, 1H), 7.64 (d,  $J = 6.8$  Hz, 1H), 7.57 (dd,  $J = 8.1$ , 7.1 Hz, 1H), 6.61 (d,  $J = 1.5$  Hz, 1H), 6.46 (d,  $J = 1.5$ , 1H), 3.80 (m, 1H), 3.28 (m,  $J =$ , 1H), 3.15 (dd,  $J = 12.8$ , 7.1 Hz, 1H), 1.68 (m, 1H), 1.55 (m, 1H), 1.05 (t,  $J = 7.4$  Hz, 3H).  $^{13}\text{C}$  NMR (101 MHz,  $\text{CD}_3\text{OD}$ )  $\delta$  (ppm): 173.1, 151.5, 139.5, 132.9, 130.0, 129.7, 129.6, 127.4, 119.6, 101.6, 95.5, 72.2, 50.8, 29.1, 10.4. HRMS: ( $m/z$ ) calcd. for  $\text{C}_{15}\text{H}_{16}\text{N}_2\text{O}_2$  [ $\text{M}+\text{H}$ ] $^+$ : 257.1290, found [ $\text{M}+\text{H}$ ] $^+$  257.1292.

**4,7-dinitrobenzo[*cd*]indol-2(1*H*)-one (29).** 3-nitro-1,8-naphthalic anhydride (1.2 g, 4.9 mmol) was placed in a flask which contained sulphuric acid (4 mL, 73.3 mmol). The resulting mixture was cooled to 5 °C in an ice bath and nitric acid (905  $\mu\text{L}$ , 21.7 mmol) was added dropwise. The reaction mixture was stirred at 60 °C for 90 min and then diluted by addition of water, neutralized with a saturated aqueous solution of  $\text{NaHCO}_3$  and extracted with dichloromethane (x3). The combined organic layers were dried ( $\text{MgSO}_4$ ) and concentrated under vacuum to afford 3,6-Dinitro-1,8-naphthalic anhydride (673 mg, 2.3 mmol, 47%) [67].  $^1\text{H}$  NMR (400 MHz, acetone- $d_6$ )  $\delta$  (ppm): 9.76 (d,  $J = 2.1$  Hz, 2H), 9.24 (d,  $J = 2.1$  Hz, 2H).

3,6-Dinitro-1,8-naphthalic anhydride (1.3 g, 4.51 mmol) and hydroxylamine hydrochloride (313 mg, 4.51 mmol) were then dissolved in pyridine (13 mL) and the resulting mixture was heated under reflux for 1 h and cooled to 80 °C. After that, *p*-toluenesulfonyl chloride (1.7 g, 9 mmol) was added and the reaction was heated to reflux for 2 additional hours. After this time, the reaction mixture was cooled to room temperature, poured into ice-water (50 mL) and stirred. The brown precipitate was filtered and rinsed with cold water and saturated solution of  $\text{NaHCO}_3$  to give the expected compound 5,8-dinitro-1,3-dioxo-1*H*-benzo[*de*]isoquinolin-2(3*H*)-yl *p*-toluenesulfonate (1.5 g, 3.40 mmol, 84%). The resulting compound was then dissolved in ethanol (6 mL) and water (5 mL) and an aqueous solution of sodium hydroxide (2.7 M, 4 mL) was then added at room temperature. The resulting mixture was heated to reflux temperature for 3 h while distilling the ethanol. When TLC showed the completeness of the reaction, the mixture was cooled, an aqueous solution of hydrochloric acid (37%) was added dropwise and a precipitate was formed. After cooling, the precipitate was collected by filtration and washed with water yielding 4,7-dinitrobenzo[*cd*]indol-2(1*H*)-one (**29**) (700 mg, 2.70 mmol, 77%) that was used in the next reaction without further purification.  $^1\text{H}$  NMR (400 MHz, acetone- $d_6$ )  $\delta$  (ppm): 10.41 (s, 1H), 9.45 (s, 1H), 8.91 (s, 1H), 8.82 (s, 1H), 7.85 (s, 1H).  $^{13}\text{C}$  NMR (101 MHz, acetone- $d_6$ )  $\delta$  (ppm): 166.9, 150.9, 150.6, 140.2, 130.7, 130.2, 128.9, 127.2, 121.5, 119.0, 103.1. HRMS: ( $m/z$ ) calcd. for  $\text{C}_{11}\text{H}_5\text{N}_3\text{O}_5$  [ $\text{M}+\text{H}$ ] $^+$ : 258.0151, found 258.0194.

**4,7-diaminobenzo[*cd*]indol-2(1*H*)-one (30).**  $\text{SnCl}_2$  (1.6 g, 8.81 mmol) was mixed with an aqueous solution of HCl (37%, 16 mL) and water (6 mL). 4,7-dinitrobenzo[*cd*]indol-2(1*H*)-one (**29**) (537 mg, 2.07 mmol) was slowly added under stirring to this solution and the resulting solution was heated at 50 °C for 4 h until TLC showed completion of the reaction. After cooling the mixture to 0 °C, the reaction was basified to pH 10 by adding a solution of

$\text{NaOH}$  6 M. The reaction mixture was then extracted with ethyl acetate (x3). The combined organic layers were dried ( $\text{MgSO}_4$ ) and concentrated under reduced pressure to afford the desired compound (142 mg, 0.71 mmol, 34%).  $^1\text{H}$  NMR (400 MHz, acetone- $d_6$ )  $\delta$  (ppm): 9.25 (br s, 1H), 7.08 (d,  $J = 1.6$  Hz, 1H), 6.86 (d,  $J = 1.6$  Hz, 1H), 6.32 (d,  $J = 1.4$  Hz, 1H), 6.31 (d,  $J = 1.3$  Hz, 1H), 2.89 (br s, 4H).  $^{13}\text{C}$  NMR (101 MHz, acetone- $d_6$ )  $\delta$  (ppm): 170.8, 151.0, 150.7, 133.5, 128.7, 116.9, 112.6, 109.5, 109.4, 97.7, 97.1. HRMS: ( $m/z$ ) calcd. for  $\text{C}_{11}\text{H}_9\text{N}_3\text{O}$  [ $\text{M}+\text{H}$ ] $^+$ : 200.0824, found 200.0819 [ $\text{M}+\text{H}$ ] $^+$ .

**4,7-bis((2-hydroxybutyl)amino)benzo[*cd*]indol-2(1*H*)-one (31).** Compound **31** was prepared following the general procedure for amine alkylation. 50 mg (0.25 mmol) of **30** were stirred with (*R,S*)-( $\pm$ )-1,2-epoxybutane in the presence of  $\text{LiClO}_4$  under microwave irradiation for 60 min. The reaction mixture was then diluted with water and extracted with ethyl acetate. The organic layer was dried over  $\text{MgSO}_4$  and concentrated under reduced pressure, giving a crude compound which was purified by flash chromatography using a mixture of  $\text{CH}_2\text{Cl}_2/\text{MeOH}/\text{Et}_3\text{N}$  [(98/2/1 to 96/4/1)] as eluent to afford the desired compound **31** with a 29% yield (25 mg, 0.073 mmol), together with unreacted starting material (9.2 mg, 0.05 mmol, 18%), monoalkylated (7.58 mg, 0.028 mmol) and trialkylated side-products (10.72 mg, 0.026 mmol).  $^1\text{H}$  NMR (400 MHz,  $\text{CD}_3\text{OD}$ )  $\delta$  (ppm): 7.11 (d,  $J = 1.6$  Hz, 1H), 6.84 (d,  $J = 1.6$  Hz, 1H), 6.29 (m, 1H), 3.77 (ddd,  $J = 12.3$ , 4.6, 3.1 Hz, 2H), 3.32 (br s, 1H), 3.31–3.08 (m, 4H), 1.74–1.40 (m, 4H), 1.04 (t,  $J = 7.5$  Hz, 6H).  $^{13}\text{C}$  NMR (101 MHz,  $\text{CD}_3\text{OD}$ )  $\delta$  (ppm): 173.4, 152.2, 151.6, 139.2, 133.8, 128.3, 116.3, 109.6, 108.3, 98.3, 72.4, 72.3, 51.2, 50.9, 29.1, 29.0, 10.4. HRMS: ( $m/z$ ) calcd. for  $\text{C}_{19}\text{H}_{25}\text{N}_3\text{O}_3$  [ $\text{M}+\text{H}$ ] $^+$ : 344.1974, found 344.1964.

**4-((2-hydroxyhexyl)amino)benzo[*cd*]indol-2(1*H*)-one (32) and 7-((2-hydroxyhexyl)amino)benzo[*cd*]indol-2(1*H*)-one (33).** The general procedure was applied to.

168 mg, (0.91 mmol) of a 2:1 mixture of 4- and 7-aminobenzo[*cd*]indol-2(1*H*)-one using (*R,S*)-( $\pm$ )-1,2-epoxyhexane to yield 52.8 mg of (**32**) (0.19 mmol, 20%), 20.9 mg of (**33**) (0.07 mmol, 14%) together with 33 mg (0.18 mmol, 20%) of unreacted starting material. (**32**)  $^1\text{H}$  NMR (400 MHz,  $\text{CD}_3\text{OD}$ )  $\delta$  (ppm): 7.50 (d,  $J = 1.7$  Hz, 1H), 7.31 (m, 2H), 7.07 (d,  $J = 1.6$  Hz, 1H), 6.71 (dd,  $J = 5.1$ , 2.4 Hz, 1H), 3.85 (m, 1H), 3.28 (m, 1H), 3.17 (dd,  $J = 12.9$ , 7.4 Hz, 1H), 1.63 (m, 2H), 1.53 (m, 2H), 1.39 (m, 2H), 0.95 (t,  $J = 7.1$  Hz, 3H).  $^{13}\text{C}$  NMR (101 MHz,  $\text{CD}_3\text{OD}$ )  $\delta$  (ppm): 172.4, 151.9, 138.6, 132.3, 130.0, 128.8, 120.5, 120.1, 115.4, 109.2, 104.4, 70.9, 51.4, 36.0, 29.0, 23.8, 14.4. HRMS: ( $m/z$ ) calcd. for  $\text{C}_{17}\text{H}_{20}\text{N}_2\text{O}_2$  [ $\text{M}+\text{H}$ ] $^+$ : 285.1603, found 285.1608; (**33**)  $^1\text{H}$  NMR (400 MHz,  $\text{CD}_3\text{OD}$ )  $\delta$  (ppm): 7.78 (d,  $J = 7.9$  Hz, 1H), 7.64 (d,  $J = 7.0$  Hz, 1H), 7.57 (dd,  $J = 8.3$ , 7.7 Hz, 1H), 6.61 (d,  $J = 1.3$  Hz, 1H), 6.46 (d,  $J = 1.2$  Hz, 1H), 3.87 (m, 1H), 3.30 (m, 1H), 3.15 (dd,  $J = 12.9$ , 7.4 Hz, 1H), 1.55 (m, 2H), 1.42 (m, 2H), 1.30 (m, 2H), 0.96 (t, 7.2 Hz, 3H).  $^{13}\text{C}$  NMR (101 MHz,  $\text{CD}_3\text{OD}$ )  $\delta$  (ppm): 173.1, 151.5, 139.5, 132.9, 130.0, 129.7, 127.4, 122.9, 119.6, 101.6, 95.5, 70.8, 51.2, 36.0, 29.0, 23.9, 14.4. HRMS: ( $m/z$ ) calcd. for  $\text{C}_{17}\text{H}_{20}\text{N}_2\text{O}_2$  [ $\text{M}+\text{H}$ ] $^+$ : 285.1603, found 285.1592.

**4-((2-hydroxyhex-5-en-1-yl)amino)benzo[*cd*]indol-2(1*H*)-one (34).** General procedure promoted by microwave irradiation was applied to 4-aminobenzo[*cd*]indol-2(1*H*)-one (23 mg, 0.13 mmol) and 1,2-epoxy-5-hexene. The crude was purified by column chromatography on silica gel using  $\text{CH}_2\text{Cl}_2/\text{MeOH}$  (99:1) as eluent to yield compound **33** (30 mg, 0.106 mmol, 85% yield) together with recovered starting material (4 mg, 0.021 mmols, 17%).  $^1\text{H}$  NMR (400 MHz,  $\text{CD}_3\text{OD}$ )  $\delta$  (ppm) = 7.48 (d,  $J = 1.6$  Hz, 1H), 7.30 (m, 2H), 7.06 (d,  $J = 1.6$  Hz, 1H), 6.69 (dd,  $J = 5.2$ , 2.3 Hz, 1H), 5.85 (m, 1H), 5.04 (dq,  $J = 17.2$ , 1.7 Hz, 1H), 4.94 (ddd,  $J = 10.2$ , 2.2, 1.1 Hz, 1H), 3.85 (m, 1H), 3.29 (m, 1H), 3.17 (dd,  $J = 13.0$ , 7.3 Hz, 1H), 2.27 (m, 1H), 2.17 (m, 1H), 1.71 (m, 1H), 1.59 (m, 1H).  $^{13}\text{C}$  NMR (101 MHz,  $\text{CD}_3\text{OD}$ )  $\delta$  (ppm): 172.4, 151.9, 139.6, 138.7, 132.3, 130.0, 128.9, 120.5, 120.1, 115.4, 115.2, 109.2, 104.4, 70.2, 51.4, 35.5, 31.0. HRMS: ( $m/z$ )



calcd. for  $C_{17}H_{18}N_2O_2 [M+H]^+$  283.1447, found 283.1455.

**(S)-4-((2-hydroxybutyl)aminobenzo[cd]indol-2(1H)-one (35).** Compound **35** was prepared under microwave irradiation applying the general procedure to 100 mg (0.54 mmol) of a 2:1 mixture of 4- and 7-aminobenzo[cd]indol-2(1H)-one. The crude was purified by flash column chromatography ( $CH_2Cl_2/MeOH$  99:1), yielding 48.5 mg of **35** (0.18 mmol, 33%) and 62.6 mg (0.25 mmol, 47%) of a mixture of unreacted anilines.  $^1H$  NMR (400 MHz,  $CD_3OD$ )  $\delta$  (ppm): 7.48 (d,  $J = 1.7$  Hz, 1H), 7.29 (m, 2H), 7.05 (d,  $J = 1.7$  Hz, 1H), 6.69 (dd,  $J = 4.7, 2.8$  Hz, 1H), 3.77 (m, 1H), 3.28 (m, 1H), 3.15 (dd,  $J = 12.9, 7.4$  Hz, 1H), 1.67 (m, 1H), 1.55 (m, 1H), 1.03 (t,  $J = 7.5$  Hz, 3H).  $^{13}C$  NMR (101 MHz,  $CD_3OD$ )  $\delta$  (ppm): 172.3, 151.8, 138.6, 132.2, 130.0, 128.8, 120.5, 120.1, 115.4, 109.2, 104.4, 72.3, 51.0, 29.0, 10.4. HRMS: ( $m/z$ ) calcd. for  $C_{15}H_{16}N_2O_2 [M+H]^+$  257.1290, found  $[M+H]^+$  257.1286.

**(R)-4-((2-hydroxybutyl)amino)benzo[cd]indol-2(1H)-one (36).** Compound **36** was prepared under microwave irradiation applying the general procedure to 100 mg (0.54 mmol) of a 2:1 mixture of 4- and 7-aminobenzo[cd]indol-2(1H)-one. The crude was purified by flash column chromatography ( $CH_2Cl_2/MeOH$  98:2), yielding 48.3 mg of **36** (0.19 mmol, 35%) together with 44.9 mg (0.24 mmol, 44%) of unreacted starting material.  $^1H$  NMR (400 MHz,  $CD_3OD$ )  $\delta$  (ppm): 7.50 (d,  $J = 1.5$  Hz, 1H), 7.32 (m, 2H), 7.07 (d,  $J = 1.5$  Hz, 1H), 6.71 (dd,  $J = 4.9, 2.3$  Hz, 1H), 3.78 (m, 1H), 3.32 (m, 1H), 3.17 (dd,  $J = 12.9, 7.4$  Hz, 1H), 1.67 (m, 1H), 1.54 (m, 1H), 1.04 (t,  $J = 7.5$  Hz, 3H).  $^{13}C$  NMR (101 MHz,  $CD_3OD$ )  $\delta$  (ppm): 172.4, 151.9, 138.6, 132.3, 130.0, 128.3, 120.5, 120.1, 115.4, 109.2, 104.4, 72.3, 51.0, 29.8, 10.4. HRMS: ( $m/z$ ) calcd. for  $C_{15}H_{16}N_2O_2 [M+H]^+$ : 257.1290, found 257.1271.

## 5. Computational methods

**Molecular Modeling.** All the computational work was carried out with the Schrödinger Suite 2016 [71], through its graphical interface Maestro [72]. Coordinates of wild-type Atg4B alone (PDB 2CY7 [44]) and of the inactive mutant C74S in complex with the LC3 natural substrate (PDB 2ZZP [43]) were obtained from the Protein Data Bank [73] at Brookhaven National Laboratory. Structure 2CY7 is representative of the closed form of the enzyme, while chain A of structure 2ZZP is representative of the open form. Since structures 2CY7 and 2ZZP have multiple Atg4B residues that are incomplete (2CY7: 5, 7, 21, 141, 189, 217, 259, 287, 312, 334, 337, 340–342, 350, 373, 375, 376; 2ZZP, chain A: 12, 21, 101, 102, 120, 177, 181, 185, 186, 237, 261, 287, 338, 340, 342) or missing (2CY7: 1–4, 190–216, 288–290, 343–346, 356–361, 378–393; 2ZZP, chain A: 1–5, 187–217, 289–293, 343–344, 355–393), a model of the full structure between residues 5–377 was obtained from the ModBase database of comparative protein structure models (Database ID Q53NU4) [45,46]. This structure had been built based on the 2CY7 structure and it is essentially identical to that one (RMSD  $\sim 0.5$  Å) but includes the previously unresolved residues, except for the N- and C-terminal tails (residues 1–4 and 378–393, respectively), thus we called it 2CY7\_full. The Protein Preparation Wizard [74,75] included in Maestro was used to add hydrogens to the 2CY7\_full structure and setting the protonation state of its ionizable residues based on PROPKA [76]. Next, the unresolved residues in 2ZZP were built based on 2CY7\_full, using the program Prime [77–79] with default settings to minimize the energy of the resulting 2ZZP\_full model structure, which includes the LC3 substrate (residues 4–122) and residues 6–354 of Atg4B.

**Molecular Dynamics Simulations.** Molecular simulations on structures 2CY7\_full and 2ZZP\_full were performed with the program Desmond [80,81] included in the Schrödinger Suite 2016 [71], using the OPLS3 force field [82]. Simulation systems were built using the System Builder of the Maestro-Desmond interface [83], which automatically assigned parameters to every atom, added

enough  $Na^+$  ions to achieve neutralization, and solvated everything with an orthorhombic box of TIP3P water that extended at least 15 Å from any protein atom. Systems were relaxed stepwise with the default relaxation protocol: (1) 100 ps Brownian Dynamics (PBC (periodic boundary conditions), NVT ensemble) at 10 K with 1 fs timestep and restraints (50 kcal/mol Å<sup>-2</sup>) on solute heavy atoms; (2) 12 ps MD (PBC, NVT) at 10 K, with 1 fs timestep and restraints on solute heavy atoms, using a Berendsen thermostat; (3) 12 ps MD (PBC, NPT) at 10 K and 1.0 bar, with 2 fs timestep and restraints on solute heavy atoms, using a Berendsen thermostat and barostat; (4) 12 ps MD (PBC, NPT) at 300 K and 1.0 bar, with 2 fs timestep and restraints on solute heavy atoms, using a Berendsen thermostat and barostat; (5) 24 ps MD (PBC, NPT) at 300 K and 1.0 bar, with 2 fs timestep and no restraints, using a Berendsen thermostat and barostat. Production MD simulations (500 ns, 2 fs timestep) were performed under the same conditions of the last equilibration step (PBC, NPT ensemble, 300 K and 1.0 bar) using the Nose-Hoover thermostat method [84,85] with a relaxation time of 1.0 ps and the Martyna-Tobias-Klein barostat method [86] with isotropic coupling and a relaxation time of 2 ps. Integration was carried out with the RESPA integrator [87] using time steps of 2.0, 2.0, and 6.0 fs for the bonded, short range and long range interactions, respectively. A cut-off of 9.0 Å was applied to van der Waals and short-range electrostatic interactions, while long-range electrostatic interactions were computed using the smooth particle mesh Ewald method, with an Ewald tolerance of  $10^{-9}$  [88,89]. Bond lengths to hydrogen atoms were constrained using the Shake algorithm [90]. Coordinates were saved every 100 ps, hence 5000 snapshots (frames) were obtained from each simulation. The Simulation Event Analysis application included in the Desmond-Maestro interface was used to analyze the simulations results.

**Virtual Screening.** The source of ligand structures for virtual screening was the downloadable National Cancer Institute Open Database [91], which contains 265242 structures in SDF format. The database was filtered to remove compounds too big ( $MW \geq 1000$ ) or too small ( $MW \leq 100$ ), compounds including rings of more than 9 atoms, compounds with elements other than C, H, N, O, S, P, F, Cl, Br and I, or compounds with undesired groups (eg. polyfluorinated, thiols, sulfur acids, ...). Ligands were set up with the LigPrep module [92] included in Maestro to generate ionization states, tautomers, and ring conformers, as well as for geometry optimization. Generation of stereoisomers was not considered to avoid an extremely large number of resulting structures, therefore all compounds were assumed to have the stereochemistry that appeared in the downloaded NCI database. With this protocol, a total of 395712 structures ready for docking were generated which were challenged against the 2CY7\_full and 2ZZP\_full (without the LC3 substrate) Atg4B structures. In particular, a groove at the interface between the N-terminal tail and the core structure of 2CY7\_full (residues 10, 11, 14–17, 261, 264, 276, 278, 280, 306 and 307) and the Atg4B active site cavity of 2ZZP\_full were the target regions selected for screening. For that purpose, the Virtual Screening Workflow [53] implemented in the Schrödinger Suite was used. This workflow uses the docking program Glide [47–50] at different levels of accuracy to successively filter the compounds according to their predicted binding potency. Thus, initially all the compounds in the database were docked at the high throughput (HTVS) level, then the best 10% was subjected to a second round of docking at the standard precision (SP) level, and finally the best 10% was submitted to a third round of docking at the extra precision (XP) level and ligands were ranked according to their docking scores. Among the final hits from screening against both target sites, compounds that exhibited scores better than  $-9$  kcal/mol, for screening against 2ZZP\_full, or  $-7$  kcal/mol, for screening against 2CY7\_full, were considered as positive hits. Selected ligands were docked using the

Induced Fit Docking Protocol [93] of the Schrodinger Suite, which uses Glide XP [50] to perform the docking phase and takes into consideration the flexibility of the protein residues within a given distance (5 Å) from the bound ligands to refine the geometries of the docked poses.

## Contributions

The manuscript was written through contributions of all authors. All authors have given approval to the final version of the manuscript.

## Acknowledgment

We would like to thank Karel Hernandez and Roman Bonet for his support in the expression and purification of recombinant proteins and Kristina Lang for her help in the preparation of N-(His)<sub>6</sub>-LC3B-L123C. We are grateful to the Ministerio de Economía and Competitividad for supporting this work with a research grant CTQ2013-44334-P) and FPI fellowship to A.B.G (BES-2014-070026).

## Appendix A. Supplementary data

Supplementary data to this article can be found online at <https://doi.org/10.1016/j.ejmech.2019.05.086>.

## References

- [1] P. Boya, F. Reggiori, P. Codogno, Emerging regulation and functions of autophagy, *Nat. Cell Biol.* 15 (2013) 713–720.
- [2] D.C. Rubinsztein, G. Marino, G. Kroemer, Autophagy and aging, *Cell* 146 (2011) 682–695.
- [3] D.J. Metcalf, M. Garcia-Arencibia, W.E. Hochfeld, D.C. Rubinsztein, Autophagy and misfolded proteins in neurodegeneration, *Exp. Neurol.* 238 (2012) 22–28.
- [4] E. Wong, A.M. Cuervo, Autophagy gone awry in neurodegenerative diseases, *Nat. Neurosci.* 13 (2010) 805–811.
- [5] F. Janku, D.J. McConkey, D.S. Hong, R. Kurzrock, Autophagy as a target for anticancer therapy, *Nat. Rev. Clin. Oncol.* 8 (2011) 528–539.
- [6] J.D. Mancias, A.C. Kimmelman, Targeting autophagy addiction in cancer, *Oncotarget* 2 (2011) 1302–1306.
- [7] S. Bortnik, C. Choutka, H.M. Horlings, S. Leung, J.H. Baker, C. Lebovitz, W.H. Dragowska, N.E. Go, M.B. Bally, et al., Identification of breast cancer cell subtypes sensitive to ATG4B inhibition, *Oncotarget* 7 (2016) 66970–66988.
- [8] K. Rothe, H. Lin, K.B. Lin, A. Leung, H.M. Wang, M. Malekesmaeil, R.R. Brinkman, D.L. Forrest, S.M. Gorski, et al., Identification of the Core Autophagy Protein ATG4B as a Potential Biomarker and Therapeutic Target in CML Stem/progenitor Cells, *Blood*, 2014.
- [9] A. Apel, I. Herr, H. Schwarz, H.P. Rodemann, A. Mayer, Blocked autophagy sensitizes resistant carcinoma cells to radiation therapy, *Cancer Res.* 68 (2008) 1485–1494.
- [10] S. He, Q. Li, X. Jiang, X. Lu, F. Feng, W. Qu, Y. Chen, H. Sun, Design of small molecule autophagy modulators: a promising druggable strategy, *J. Med. Chem.* 61 (2018) 4656–4687.
- [11] D.C. Rubinsztein, P. Codogno, B. Levine, Autophagy modulation as a potential therapeutic target for diverse diseases, *Nat. Rev. Drug Discov.* 11 (2012) 709–730.
- [12] A. Fleming, T. Noda, T. Yoshimori, D.C. Rubinsztein, Chemical modulators of autophagy as biological probes and potential therapeutics, *Nat. Chem. Biol.* 7 (2011) 9–17.
- [13] G. Triola, Chemical tools for modulating autophagy, *Tetrahedron* 71 (2015) 387–406.
- [14] T. Wang, M.L. Goodall, P. Gonzales, M. Sepulveda, K.R. Martin, S. Gately, J.P. MacKeigan, Synthesis of improved lysosomotropic autophagy inhibitors, *J. Med. Chem.* 58 (2015) 3025–3035.
- [15] Y.T. Wu, H.L. Tan, G.H. Shui, C. Bauvy, Q. Huang, M.R. Wenk, C.N. Ong, P. Codogno, H.M. Shen, Dual role of 3-methyladenine in modulation of autophagy via different temporal patterns of inhibition on class I and III phosphoinositide 3-kinase, *J. Biol. Chem.* 285 (2010) 10850–10861.
- [16] B. Pasquier, Y. El-Ahmad, B. Filoche-Romme, C. Dureau, F. Fassy, P.Y. Abecassis, M. Mathieu, T. Bertrand, T. Benard, et al., Discovery of (2S)-8-[(3R)-3-methylmorpholin-4-yl]-1-(3-methyl-2-oxobutyl)-2-(trifluoromethyl)-3,4-dihydro-2H-pyrimido[1,2-a]pyrimidin-6-one: a novel potent and selective inhibitor of Vps34 for the treatment of solid tumors, *J. Med. Chem.* 58 (2015) 376–400.
- [17] L. Robke, L. Lاراia, M.A. Carnero Corrales, G. Konstantinidis, M. Muroi, A. Richters, M. Winzker, T. Engbring, S. Tomassi, et al., Phenotypic identification of a novel autophagy inhibitor chemotype targeting lipid kinase VPS34, *Angew. Chem. Int. Ed. Engl.* 56 (2017) 8153–8157.
- [18] T. Kirisako, Y. Ichimura, H. Okada, Y. Kabeya, N. Mizushima, T. Yoshimori, M. Ohsumi, T. Takao, T. Noda, et al., The reversible modification regulates the membrane-binding state of Atg8/Aut7 essential for autophagy and the cytoplasm to vacuole targeting pathway, *J. Cell Biol.* 151 (2000) 263–275.
- [19] G. Marino, J.A. Uria, X.S. Puente, V. Quesada, J. Bordallo, C. Lopez-Otin, Human autophagins, a family of cysteine proteinases potentially implicated in cell degradation by autophagy, *J. Biol. Chem.* 278 (2003) 3671–3678.
- [20] M. Li, Y.F. Hou, J.S. Wang, X.Y. Chen, Z.M. Shao, X.M. Yin, Kinetics comparisons of mammalian Atg4 homologues indicate selective preferences toward diverse Atg8 substrates, *J. Biol. Chem.* 286 (2011) 7327–7338.
- [21] I. Tanida, Y.S. Sou, J. Ezaki, N. Minematsu-Ikeguchi, T. Ueno, E. Kominami, HsAtg4B/HsApg4B/autophagin-1 cleaves the carboxyl termini of three human Atg8 homologues and delipidates microtubule-associated protein light chain 3- and GABAA receptor-associated protein-phospholipid conjugates, *J. Biol. Chem.* 279 (2004) 36268–36276.
- [22] H. Nakatogawa, J. Ishii, E. Asai, Y. Ohsumi, Atg4 recycles inappropriately lipidated Atg8 to promote autophagosome biogenesis, *Autophagy* 8 (2012) 177–186.
- [23] Z.Q. Yu, T. Ni, B. Hong, H.Y. Wang, F.J. Jiang, S. Zou, Y. Chen, X.L. Zheng, D.J. Klionsky, et al., Dual roles of Atg8-PE deconjugation by Atg4 in autophagy, *Autophagy* 8 (2012) 883–892.
- [24] P.F. Liu, C.M. Leung, Y.H. Chang, J.S. Cheng, J.J. Chen, C.J. Weng, K.W. Tsai, C.J. Hsu, Y.C. Liu, et al., ATG4B promotes colorectal cancer growth independent of autophagic flux, *Autophagy* 10 (2014) 1454–1465.
- [25] Z. Qiu, B. Kuhn, J. Aebi, X. Lin, H. Ding, Z. Zhou, Z. Xu, D. Xu, L. Han, et al., Discovery of fluoromethylketone-based peptidomimetics as covalent ATG4B (Autophagin-1) inhibitors, *ACS Med. Chem. Lett.* 7 (2016) 802–806.
- [26] D. Xu, Z. Xu, L. Han, C. Liu, Z. Zhou, Z. Qiu, X. Lin, G. Tang, H. Shen, et al., Identification of new ATG4B inhibitors based on a novel high-throughput screening platform, *J. Biomol. Screen* 22 (2017) 338–347.
- [27] Y. Fu, L. Hong, J. Xu, G. Zhong, Q. Gu, Q. Gu, Y. Guan, X. Zheng, Q. Dai, et al., Discovery of a small molecule targeting autophagy via ATG4B inhibition and cell death of colorectal cancer cells in vitro and in vivo, *Autophagy* (2018) 1–17.
- [28] P.F. Liu, K.L. Tsai, C.J. Hsu, W.L. Tsai, J.S. Cheng, H.W. Chang, C.W. Shiau, Y.G. Goan, H.H. Tseng, et al., Drug repurposing screening identifies tioconazole as an ATG4 inhibitor that suppresses autophagy and sensitizes cancer cells to chemotherapy, *Theranostics* 8 (2018) 830–845.
- [29] D. Bosc, L. Vezenkov, S. Bortnik, J. An, J. Xu, C. Choutka, A.M. Hannigan, S. Kovacic, S. Loo, et al., A new quinoline-based chemical probe inhibits the autophagy-related cysteine protease ATG4B, *Sci. Rep.* 8 (2018) 11653.
- [30] C.W. Shu, C. Madiraju, D. Zhai, K. Welsh, P. Diaz, E. Sergienko, R. Sano, J.C. Reed, High-throughput fluorescence assay for small-molecule inhibitors of autophagins/Atg4, *J. Biomol. Screen* 16 (2011) 174–182.
- [31] D. Akin, S.K. Wang, P. Habibzadegah-Tari, B. Law, D. Ostrov, M. Li, X.M. Yin, J.S. Kim, N. Horenstein, et al., A novel ATG4B antagonist inhibits autophagy and has a negative impact on osteosarcoma tumors, *Autophagy* (2014) 10.
- [32] T.G. Nguyen, N.S. Honson, S. Arns, T.L. Davis, S. Dhe-Paganon, S. Kovacic, N.S. Kumar, T.A. Pfeifer, R.N. Young, Development of fluorescent substrates and assays for the key autophagy-related cysteine protease enzyme, ATG4B, *Assay Drug Dev. Technol.* 12 (2014) 176–189.
- [33] M. Cleenewerck, M.O.J. Grootaert, R. Gladysz, Y. Adriaenssens, R. Roelandt, J. Joossens, A.M. Lambeir, G.R.Y. De Meyer, W. Declercq, et al., Inhibitor screening and enzymatic activity determination for autophagy target Atg4B using a gel electrophoresis-based assay, *Eur. J. Med. Chem.* 123 (2016) 631–638.
- [34] A. Kurdi, M. Cleenewerck, C. Vangestel, S. Lyssens, W. Declercq, J.P. Timmermans, S. Stroobants, K. Augustyns, G.R.Y. De Meyer, et al., ATG4B inhibitors with a benzotropolone core structure block autophagy and augment efficiency of chemotherapy in mice, *Biochem. Pharmacol.* 138 (2017) 150–162.
- [35] L. Vezenkov, N.S. Honson, N.S. Kumar, D. Bosc, S. Kovacic, T.G. Nguyen, T.A. Pfeifer, R.N. Young, Development of fluorescent peptide substrates and assays for the key autophagy-initiating cysteine protease enzyme, ATG4B, *Bioorg. Med. Chem.* 23 (2015) 3237–3247.
- [36] M. Li, X. Chen, Q.Z. Ye, A. Vogt, X.M. Yin, A high-throughput FRET-based assay for determination of Atg4 activity, *Autophagy* 8 (2012) 401–412.
- [37] P. Wu, L. Brand, Resonance energy transfer: methods and applications, *Anal. Biochem.* 218 (1994) 1–13.
- [38] J.F. Glickman, X. Wu, R. Mercuri, C. Illy, B.R. Bowen, Y. He, M. Sills, A comparison of ALPHAScreen, TR-FRET, and TRF as assay methods for FXR nuclear receptors, *J. Biomol. Screen* 7 (2002) 3–10.
- [39] C.W. Shu, M. Drag, M. Bekes, D. Zhai, G.S. Salvesen, J.C. Reed, Synthetic substrates for measuring activity of autophagy proteases: autophagins (Atg4), *Autophagy* 6 (2010) 936–947.
- [40] G. Wu, Y. Yuan, C.N. Hodge, Determining appropriate substrate conversion for enzymatic assays in high-throughput screening, *J. Biomol. Screen* 8 (2003) 694–700.
- [41] M.G. Acker, D.S. Auld, Considerations for the design and reporting of enzyme assays in high-throughput screening applications, *Perspect. Sci.* 1 (2014) 56–73.
- [42] T. Kumanomidou, T. Mizushima, M. Komatsu, A. Suzuki, I. Tanida, Y. Sou, T. Ueno, E. Kominami, K. Tanaka, et al., The crystal structure of human Atg4b, a

- processing and de-conjugating enzyme for autophagosome-forming modifiers, *J. Mol. Biol.* 355 (2006) 612–618.
- [43] K. Sato, N.N. Noda, H. Kumeta, Y. Fujioka, N. Mizushima, Y. Ohsumi, F. Inagaki, The structure of Atg4B-LC3 complex reveals the mechanism of LC3 processing and delipidation during autophagy, *EMBO J.* 28 (2009) 1341–1350.
- [44] K. Sugawara, N.N. Suzuki, Y. Fujioka, N. Mizushima, Y. Ohsumi, F. Inagaki, Structural basis for the specificity and catalysis of human Atg4B responsible for mammalian autophagy, *J. Biol. Chem.* 280 (2005) 40058–40065.
- [45] ModBase: Database of Comparative Protein Structure Models: <https://modbase.compbio.ucsf.edu/modbase/cgi/index.cgi>.
- [46] U. Pieper, B.M. Webb, D.T. Barkan, D. Schneidman-Duhovny, A. Schlessinger, H. Braberg, Z. Yang, E.C. Meng, E.F. Pettersen, et al., ModBase, a database of annotated comparative protein structure models, and associated resources, *Nucleic Acids Res.* 39 (2011) D465–D474.
- [47] R.A. Friesner, J.L. Banks, R.B. Murphy, T.A. Halgren, J.J. Klicic, D.T. Mainz, M.P. Repasky, E.H. Knoll, M. Shelley, et al., Glide: a new approach for rapid, accurate docking and scoring. 1. Method and assessment of docking accuracy, *J. Med. Chem.* 47 (2004) 1739–1749.
- [48] T.A. Halgren, R.B. Murphy, R.A. Friesner, H.S. Beard, L.L. Frye, W.T. Pollard, J.L. Banks, Glide: a new approach for rapid, accurate docking and scoring. 2. Enrichment factors in database screening, *J. Med. Chem.* 47 (2004) 1750–1759.
- [49] Schrödinger, Release 2016-4: Glide, Schrödinger, LLC, New York, NY, 2016.
- [50] R.A. Friesner, R.B. Murphy, M.P. Repasky, L.L. Frye, J.R. Greenwood, T.A. Halgren, P.C. Sanschagrin, D.T. Mainz, Extra precision glide: docking and scoring incorporating a model of hydrophobic enclosure for protein-ligand complexes, *J. Med. Chem.* 49 (2006) 6177–6196.
- [51] Z. Wang, H. Sun, X. Yao, D. Li, L. Xu, Y. Li, S. Tian, T. Hou, Comprehensive evaluation of ten docking programs on a diverse set of protein-ligand complexes: the prediction accuracy of sampling power and scoring power, *Phys. Chem. Chem. Phys.* 18 (2016) 12964–12975.
- [52] N.S. Pagadala, K. Syed, J. Tuszynski, Software for molecular docking: a review, *Biophys. Rev.* 9 (2017) 91–102.
- [53] Schrödinger, Release 2016-4: Virtual Screening Workflow, Schrödinger, LLC, New York, NY, 2016.
- [54] J.B. Baell, G.A. Holloway, New substructure filters for removal of pan assay interference compounds (PAINS) from screening libraries and for their exclusion in bioassays, *J. Med. Chem.* 53 (2010) 2719–2740.
- [55] C. Aldrich, C. Bertozzi, G.I. Georg, L. Kießling, C. Lindsley, D. Liotta, K.M. Merz Jr., A. Schepartz, S. Wang, The ecstasy and agony of assay interference compounds, *J. Med. Chem.* 60 (2017) 2165–2168.
- [56] M.A. Shaaban, O.M. Khalil, K.R. Ahmed, P.F. Lamie, Synthesis and antibacterial activity of novel quinoxalinone derivatives, *J. Chem. Res.* (2009) 574–578.
- [57] S. Tariq, K. Somakala, M. Amir, Quinoxaline: an insight into the recent pharmacological advances, *Eur. J. Med. Chem.* 143 (2018) 542–557.
- [58] Y. Kurasawa, M.Y. T. Ebukuro, A. Takada, Synthesis and reactions of 3-(1,3,4-Oxadiazol-yl)methylene-2-oxo-1,2,3,4-tetrahydroquinoxalines, *Chem. Pharm. Bull. (Tokyo)* 31 (1983) 3897–3901.
- [59] M.D. Varney, G.P. Marzoni, C.L. Palmer, J.G. Deal, S. Webber, K.M. Welsh, R.J. Bacquet, C.A. Bartlett, C.A. Morse, et al., Crystal-structure-based design and synthesis of benz[cd]indole-containing inhibitors of thymidylate synthase, *J. Med. Chem.* 35 (1992) 663–676.
- [60] X. Xue, Y. Zhang, Z. Liu, M. Song, Y. Xing, Q. Xiang, Z. Wang, Z. Tu, Y. Zhou, et al., Discovery of benzo[cd]indol-2(1H)-ones as potent and specific BET bromodomain inhibitors: structure-based virtual screening, optimization, and biological evaluation, *J. Med. Chem.* 59 (2016) 1565–1579.
- [61] C. Zhang, L.J. Feng, Y. Huang, D. Wu, Z. Li, Q. Zhou, Y. Wu, H.B. Luo, Discovery of novel phosphodiesterase-2a inhibitors by structure-based virtual screening, structural optimization, and bioassay, *J. Chem. Inf. Model.* 57 (2017) 355–364.
- [62] A.A. Gryshchenko, K.V. Levchenko, V.G. Bdzhola, T.P. Ruban, L.L. Lukash, S.M. Yarmoluk, Design, synthesis and biological evaluation of naphthostyryl derivatives as novel protein kinase FGFR1 inhibitors, *J. Enzym. Inhib. Med. Chem.* 30 (2015) 126–132.
- [63] J.J. Liu, A. Dermatakis, C. Lukacs, F. Konzelmann, Y. Chen, U. Kammlott, W. Depinto, H. Yang, X. Yin, et al., 3,5,6-Trisubstituted naphthostyryls as CDK2 inhibitors, *Bioorg. Med. Chem. Lett.* 13 (2003) 2465–2468.
- [64] M. Chini, P. Crotti, M.F. Metal Salts as new catalysts for mild and efficient aminolysis of oxiranes, *Tetrahedron Lett.* 31 (1990) 4661–4664.
- [65] Y.H. Hsiang, J.B. Jiang, L.F. Liu, Topoisomerase II-mediated DNA cleavage by amonafide and its structural analogs, *Mol. Pharmacol.* 36 (1989) 371–376.
- [66] D. Rideout, R. Schinazi, C.D. Pauza, K. Lovelace, L.C. Chiang, T. Calogeropoulou, M. McCarthy, J.H. Elder, Derivatives of 4-amino-3,6-disulfonato-1,8-naphthalimide inhibit reverse transcriptase and suppress human and feline immunodeficiency virus expression in cultured cells, *J. Cell. Biochem.* 51 (1993) 446–457.
- [67] S. Girouard, M.H. Houle, A. Grandbois, J.W. Keillor, S.W. Michnick, Synthesis and characterization of dimaleimide fluorogens designed for specific labeling of proteins, *J. Am. Chem. Soc.* 127 (2005) 559–566.
- [68] D.J. Klionsky, K. Abdelmohsen, A. Abe, M.J. Abedin, H. Abeliovich, A. Acevedo Arozena, H. Adachi, C.M. Adams, P.D. Adams, et al., Guidelines for the use and interpretation of assays for monitoring autophagy, *Autophagy* 12 (2016) 1–22, third ed.
- [69] M. Selvakumaran, R. Amaravadi, I.A. Vasilevska, P.J. O'Dwyer, Autophagy inhibition sensitizes colon cancer cells to anti-angiogenic and cytotoxic therapy, *Clin. Cancer Res.* 19 (2013) 2995–3007.
- [70] J. Li, R. Tian, C. Ge, Y. Chen, X. Liu, Y. Wang, Y. Yang, W. Luo, F. Dai, et al., Discovery of the polyamine conjugate with benzo[cd]indol-2(1H)-one as a lysosome-targeted antimetastatic agent, *J. Med. Chem.* 61 (2018) 6814–6829.
- [71] Schrödinger, Release 2016-4, Schrödinger, LLC, New York, NY, 2016.
- [72] Schrödinger, Release 2016-4, Maestro, Schrödinger, LLC, New York, NY, 2016.
- [73] H.M. Berman, J. Westbrook, Z. Feng, G. Gilliland, T.N. Bhat, H. Weissig, I.N. Shindyalov, P.E. Bourne, The protein Data Bank, *Nucleic Acids Res.* 28 (2000) 235–242.
- [74] G.M. Sastry, M. Adzhigirey, T. Day, R. Annabhimoju, W. Sherman, Protein and ligand preparation: parameters, protocols, and influence on virtual screening enrichments, *J. Comput. Aided Mol. Des.* 27 (2013) 221–234.
- [75] Schrödinger, Release 2016-4: Protein Preparation Wizard, Epik, Impact, Prime, Schrödinger, LLC, New York, NY, 2016.
- [76] M.H.M. Olsson, C.R. Søndergaard, M. Rostkowski, J.J.H. PROPKA3: consistent treatment of internal and surface residues in empirical pKa predictions, *J. Chem. Theory Comput.* 7 (2011) 525–537.
- [77] M.P. Jacobson, R.A. Friesner, Z. Xiang, B. Honig, On the role of the crystal environment in determining protein side-chain conformations, *J. Mol. Biol.* 320 (2002) 597–608.
- [78] M.P. Jacobson, D.L. Pincus, C.S. Rapp, T.J. Day, B. Honig, D.E. Shaw, R.A. Friesner, A hierarchical approach to all-atom protein loop prediction, *Proteins* 55 (2004) 351–367.
- [79] Schrödinger, Release 2016-4: Prime, Schrödinger, LLC, New York, NY, 2016.
- [80] K.J. Bowers, E. Chow, H. Xu, R.O. Dror, M.P. Eastwood, B.A. Gregersen, J.L. Klepeis, I. Kolossváry, M.A. Moraes, et al., Scalable algorithms for molecular dynamics simulations on commodity clusters, in: Proceedings of the ACM/IEEE Conference on Supercomputing, (SC06)Tampa, Florida, 2006.
- [81] Schrödinger, Release 2016-4: Desmond Molecular Dynamics System, D. E. Shaw Research, New York, NY, 2016.
- [82] E. Harder, W. Damm, J. Maple, C. Wu, M. Reboul, J.Y. Xiang, L. Wang, D. Lupyan, M.K. Dahlgren, et al., OPLS3: a force field providing broad coverage of drug-like small molecules and proteins, *J. Chem. Theory Comput.* 12 (2016) 281–296.
- [83] Schrödinger, Release 2016-4: Maestro-Desmond Interoperability Tools, D. E. Shaw Research, New York, NY, 2016.
- [84] D.J. Evans, B.L. Holian, The nose–hoover thermostat, *J. Chem. Phys.* 83 (1985) 4069–4074.
- [85] G.J. Martyna, M.L. Klein, M. Tuckerman, Nosé–Hoover chains: the canonical ensemble via continuous dynamics, *J. Chem. Phys.* 97 (1992) 2635–2643.
- [86] G.J. Martyna, D.J. Tobias, M.L. Klein, Constant pressure molecular dynamics algorithms, *J. Chem. Phys.* 101 (1994) 4177–4189.
- [87] M. Tuckerman, B.J. Berne, G.J. Martyna, Reversible multiple time scale molecular dynamics, *J. Chem. Phys.* 97 (1992) 1990–2001.
- [88] T. Darden, D. York, L. Pedersen, Particle mesh Ewald: an N·log(N) method for Ewald sums in large systems, *J. Chem. Phys.* 98 (1993) 10089–10092.
- [89] U. Essmann, L. Perera, M.L. Berkowitz, T. Darden, H. Lee, L.G. Pedersen, A smooth particle mesh Ewald method, *J. Chem. Phys.* 103 (1995) 8577–8593.
- [90] V. Krättinger, W.F. van Gunsteren, P.H. Hünenberger, A fast SHAKE algorithm to solve distance constraint equations for small molecules in molecular dynamics simulations, *J. Comput. Chem.* 22 (2001) 501–508.
- [91] NCI Open Database. <https://cactus.nci.nih.gov/download/nci>.
- [92] Schrödinger, Release 2016-4, LigPrep, Schrödinger, LLC, New York, NY, 2016.
- [93] Schrödinger, Induced Fit Docking Protocol 2016-4, Schrödinger, LLC, New York, NY, 2016.